Structural Performance of Reinforced Concrete Beams Subjected to Service Loads Coupled with Corrosion of Flexural Reinforcement

by

Abdullah Al-Bayti

Thesis submitted to the University of Ottawa
in partial Fulfillment of the requirements for the
Doctor of Philosophy in Civil Engineering

Department of Civil Engineering
Faculty of Engineering
University of Ottawa

Abstract

Corrosion of steel reinforcement has been identified as one of the major problems facing many existing reinforced concrete structures including bridges. The exposure to aggressive environmental conditions such as those with high concentrations of chloride ions due to the use of de-icing salt in cold regions or high concentrations of carbon dioxide due to increased greenhouse gas emissions, accelerate the initiation process of corrosion. As corrosion initiates, the structural performance in terms of load-carrying capacity, ductility, and service life deteriorate over time. Coupling the effect of reinforcement corrosion with service loads may further weaken the structural performance of reinforced concrete bridges due to the presence of transverse load-induced cracks. Accordingly, a research program was conducted to evaluate the structural performance of reinforced concrete beams subjected to coupled effects of service loads and reinforcement corrosion. The research project consisted of combined experimental and numerical investigations.

The experimental phase consisted of tests of nine small-scale beams and six large-scale beams. The beams were designed, constructed, instrumented, and loaded under a four-point load test. The primary test variables were the applied corrosion current density, level of corrosion, and level of sustained loading as percentage of beam ultimate capacity (0% P_u, 40% P_u, and 60% P_u). The corrosion level of steel reinforcement was quantitatively assessed using gravimetric weight measurements and three-dimensional laser scanner technique. Test results indicated that failure of corroded RC beams was brittle due to premature rupture of corroded steel bars, which was attributed to the development of localized corrosion at the sections with flexural cracks in beams. Furthermore, it was found that beams subjected to higher levels of service loads, experienced further reductions in ultimate load capacity and ductility.

In addition, tensile tests were used to evaluate the effect of corrosion on the mechanical performance of steel bars retrieved from the corroded beams. It was found that the tensile strength of corroded steel bars, based on nominal sectional area, was reduced with the increase of corrosion levels. In contrast, the tensile strength, based on minimum sectional area, was not influenced by the non-uniform distribution and localization of corrosion. In fact, there was a slight increase in strength with the increase of corrosion levels.

The numerical phase consisted of finite element analyses of beams using DIANA FE analysis software. A simplified approach was implemented to introduce the damage induced by corrosion into two-dimensional nonlinear FE models, based on the experimental testing of corroded beams and corroded steel bars. The analyses were reasonably accurate in predicting cracking patterns, residual load capacity, residual ductility, and failure modes of corroded beams. Subsequently, the validated model was used to conduct a parametric study on the level of service loads, level of corrosion, strength of concrete, and tensile reinforcement ratio. It was found that the FE model of corroded beams was strongly influenced by the level of service loads, level of corrosion, and tensile reinforcement ratio.

Acknowledgments

I would like to express my deepest gratitude to my supervisors, Dr. Husham Almansour and Dr. Murat Saatcioglu, for their encouragement, patience, guidance, and invaluable knowledge that helped me in all phases of this research project.

My sincere thanks also go to the team of the Construction Research Centre of the National Research Council Canada for their assistance throughout this research project. Thank you to Dr. Bessam Kadhom, Mr. Roger Smith, Mr. Dennis Krys, Mr. Antal Prigli, Mr. Bruce Baldock, Mr. Alex Wang, Mr. Joe Hum, and Ms. Kerri Henriques. Special thanks to Mr. Dennis Kyrs for writing the MATLAB code for the laser scanner.

I would also like to thank the staff and colleagues of the Civil Engineering Department at the University of Ottawa for their support over the last four years.

The financial and academic support provided by the National Research Council Canada and the University of Ottawa are greatly acknowledged.

Last but not least, without the encouragement and support of my family and friends, this work would not be possible. Thank you very much to everyone.

Table of Content

List of Tables

List of Figures

List of Abbreviations

A_0	Cross-sectional area of non-corroded steel bars
A_c	Cross-sectional area of corroded steel bars
$A_{c,avg}$	Average cross-sectional area of corroded steel bars
$A_{c,min}$	Minimum cross-sectional area of corroded steel bars
$B(\%)$	Percentage of flexural strength of control beam
b_o	Original width of beam
D_o	Nominal diameter of steel bars
D	Diameter of steel bars
E_s	Modulus of elasticity of steel bars
F	Faraday's constant
F_0	Load capacity of non-corroded steel bars
f_0	Strength of non-corroded steel bars
F_c	Load capacity of corroded steel bars
f_c	Strength of corroded steel bars
F_{u0}	Ultimate load capacity of non-corroded steel bars
f_{u0}	Ultimate strength of non-corroded steel bars
F_{uc}	Ultimate load capacity of corroded steel bars
f_{uc}	Ultimate strength of corroded steel bars
F_{y0}	Yield load capacity of non-corroded steel bars
f_{y0}	Yield strength of non-corroded steel bars
F_{yc}	Yield load capacity of corroded steel bars
f_{yc}	Yield strength of corroded steel bars
f_c'	Compressive strength of non-corroded concrete
$f_c^{c\prime}$	Compressive strength of corroded concrete
f_t	Tensile strength of non-corroded concrete
f_t^c	Tensile strength of corroded concrete
G_c	Compressive fracture energy
G_t	Tensile fracture energy

h	Characteristic element length of concrete
I_{cor}	Current of corrosion
i_{corr}	Corrosion current density
k	Coefficient that accounts for the roughness and diameter of steel bars
M	Atomic mass of iron
m_0	Mass of non-corroded steel bars after cleaning
m_c	Mass of corroded steel bars after cleaning
n	Number of steel bars in compression
$p(T)_{general}$	Depth of generalized corrosion attack at time T
$p(T)_{pit}$	Depth of pit corrosion attack at time T
P_{cr}	Cracking load of reinforced concrete beams
P_R	Residual capacity ratio
P_u	Ultimate load of reinforced concrete beams
P_u^{EXP}	Experimental load at ultimate
P_u^{FEA}	Finite element analysis load at ultimate
P_y	Yield load of reinforced concrete beams
R	Ratio between the depth of pit and generalized corrosion attacks
T	Time of corrosion
t	Duration of corrosion exposure
v_c	Poisson's ratio
v_{rs}	Ratio of volume expansion of corrosive by-products relative to non-corroded steel
X	Penetration depth of corrosion
Z	Valence electrons of iron
α_1	Coefficients for the reduction in ultimate strain of corroded steel bars
α_u	Coefficients for the reduction in ultimate strength of corroded steel bars
α_y	Coefficients for the reduction in yield strength of corroded steel bars
β	Correction factor that accounts for the loss in bond and other factors
ε_o	Strain of concrete at maximum compressive strength
ε_1	Average tensile strain of concrete perpendicular to compression

ε_{r0}	Rupture strain of non-corroded steel bars
ε_{u0}	Ultimate strain of non-corroded steel bars
ε_{uc}	Ultimate strain of corroded steel bars
$\eta_{avg,m}$	Average mass loss of corroded steel bars
η_{3D}	Area loss of corroded steel bars
$\eta_{avg,3D}$	Average sectional area loss of corroded steel bars
$\eta_{crit,3D}$	Critical sectional area loss of corroded steel bars
$\eta_{crit,mean}$	Maximum sectional area loss of steel bars according to mean predictions
$\eta_{crit,upper}$	Maximum sectional area loss of steel bars according to upper bound predictions
Δ_{cr}	Displacement at the cracking load of reinforced concrete beams
Δ_R	Residual ductility ratio
Δ_u	Displacement at the ultimate load of reinforced concrete beams
Δ_u^{EXP}	Experimental displacement at ultimate
Δ_u^{FEA}	Finite element analysis displacement at ultimate
Δ_y	Displacement at the yield load of reinforced concrete beams

Chapter One : Introduction

1.1 General

Reinforced concrete (RC) is a composite material that is widely used in the construction of important civil structures including, tunnels, buildings, and bridges. Over the past several decades, corrosion of steel reinforcement had been identified as one of the major problems facing existing reinforced concrete structures. Globally, the economic losses due to corrosion are approximately US2.5 trillion dollars, corresponding to 3.4% of the global gross domestic product (Koch et al., 2016). The cost includes, maintenance, rehabilitation or replacement of damaged structures.

It is well-known that climate change has a strong influence on the environmental conditions, causing an increase of temperatures, frequency and intensity of extreme events. Reinforced concrete structures are constantly exposed to high concentrations of carbon dioxide due to increased gas emissions, and increased temperatures and humidity associated with climate change. These in turn, increase the risks of concrete carbonation. Furthermore, the increase of sea water levels due to thermal expansion of water, melting of ice sheets and glaciers caused by global warming exposes reinforced concrete structures in coastal regions to increased rates of chloride ingress. Initially, the embedded steel reinforcement in concrete structures is protected from corrosion by a thin passive film layer formed during the early stages of cement hydration. However, the exposure to aggressive environmental conditions such as those with high concentrations of carbon dioxide or chloride ions can damage the protective layer, which in turn accelerates the initiation process of corrosion.

1.2 Problem Statement

Field and experimental investigations had shown that the progression of corrosion has severe adverse effects on the performance of reinforced concrete structures. This is attributed to loss of reinforcement area, reduction of reinforcement ductility (Du et al., 2005), and deterioration of concrete due to the volume growth of corrosion by-products (Cabrera, 1996). Furthermore, the mechanical interlock between the corroded steel reinforcement and surrounding concrete worsen at high levels of corrosion (Almusallam et al., 1996). The combined effect of these impairments

reduces the load-carrying capacity, ductility and service life of corroded reinforced concrete structures.

In engineering practice, corrosion of steel reinforcement in concrete structures is coupled with the effect of service loads, which may potentially cause more adverse effects on the structural response. Reinforced concrete bridge beams/girders are structural elements that are particularly vulnerable to this coupling effect. Previously, numerous research studies were devoted to understand the effect of reinforcement corrosion on the structural behavior of reinforced concrete beams. However, most studies did not simulate in-service conditions and the presence of loads while corroding the beams (Rodriguez et al., 1997; Mangat and Elgarf, 1999; Azad et al., 2007; Du et al., 2007; Torres-Acosta et al., 2007; Azam et al., 2016). Studying of the structural behavior and damage mechanisms of reinforced concrete beams under the coupled effects of reinforcement corrosion and service loads is essential to evaluate the residual load capacity, ductility and serviceability of damaged beams due to corrosion.

In the last two decades, several researchers examined the coupled effects of reinforcement corrosion and service loads (Yoon et al., 2000; Ballim and Reid, 2003; El Maaddawy and Topper, 2005; Malumbela et al., 2009; Hariche et al., 2012; Li et al., 2018; Zhang et al., 2018). However, limited research attempts were conducted to examine the structural behavior and failure mechanisms at the end of service life of corroded reinforced concrete beams. Reinforced concrete beams are designed to carry a specified service load over their service life. As corrosion initiates, the ultimate load capacity is reduced over time up until the occurrence of failure under service loads, as illustrated in Figure 1.1. As a result, the service life of corroded reinforced concrete beams is also reduced.

Investigating the interaction between corrosion of longitudinal tensile steel reinforcement and different levels of service loads is of a particular interest, primarily due to the presence of transverse load-induced cracks. The development of flexural cracks under different service loads could have a significant influence on the degradation rates of load-carrying capacity, ductility and service life of corroded reinforced concrete beams. This current research project, undertaken between the University of Ottawa and the National Research Council Canada aims to examine the flexural behavior of small-scale and large-scale reinforced concrete beams subjected to reinforcement corrosion and different service loads.

1.3 Objective

The primary objective of this research project is to evaluate the structural performance of reinforced concrete beams subjected to the coupled effects of service loads and reinforcement corrosion through combined experimental and analytical research. A particular attention is given to reinforced concrete beams designed to perform predominantly in the flexure mode of behavior. The objective also includes the development of a simplified procedure to simulate the corrosion process as a function of time under service loads to predict the response of corroded reinforced concrete beams. The results of this research will help engineers to better understand and assess the effect of reinforcement corrosion on the serviceability of damaged reinforced concrete bridge beams/girders.

1.4 Scope

The research project consists of combined experimental and numerical investigations. The following forms the scope of the research project:

- Review of previous experimental tests and analytical modeling tools of damaged reinforced concrete beams due to corrosion. An emphasis will be placed on reviewing the behavior of reinforced concrete beams which were corroded in the presence or absence of service loads.
- Construct, prepare and test small-scale and large-scale reinforced concrete beam specimens designed to perform predominantly in the flexure mode of behavior. The tests in this task include the following:
    - Test to failure two small-scale and two large-scale beams without reinforcement corrosion to establish their load-carrying capacity and ductility.
    - Test to failure seven additional small-scale beams subjected to different levels of service loads coupled with corrosion of the main flexural reinforcement.
    - Test to failure four additional large-scale beams subjected to different levels of service loads coupled with corrosion of the main flexural reinforcement.
- Extract the corroded steel reinforcement from the beams tested in the previous task to evaluate the patterns and distribution of corrosion along the corroded region of beams using three-dimensional laser scanner.

- Experimentally investigate the effect of corrosion on the mechanical performance of corroded steel reinforcement retrieved from the beams.
- Propose a simplified approach to predict the load-carrying capacity and ductility of corroded reinforced concrete beams when subjected to the coupled effects of reinforcement corrosion and service loads.
- Incorporate the simplified approach into finite element analyses to develop and validate finite element models using DIANA software to predict the response of flexural-dominant corroded reinforced concrete beams.
- Conduct an extensive parametric investigation to expand test data for cases that have not been covered experimentally, including different levels of service loads, levels of corrosion, strengths of concrete and percentages of reinforcement.

1.5 Original Contributions

The research project is conducted in the field of reinforced concrete beams under the coupled effects of reinforcement corrosion and service loads. The following original contributions resulted from this combined experimental and analytical investigations:

- Unlike previous research conducted on the coupled effects of reinforcement corrosion and service loads, the current test program included beams under sustained loading up to failure. This is important in assessing the damage and failure mechanisms, as well as the service life of existing bridge beams/girders in an aggressive corrosive environment.
- Highlighted the interaction between flexural cracks and corrosion of reinforcement in concrete beams with different percentages of longitudinal reinforcement when subjected to different levels of service loads.
- Investigated the mechanical properties of corroded reinforcement in concrete beams under different levels of service loads as affected by the presence of flexural concrete cracks.
- Developed a simplified approach to incorporate the damage induced by corrosion into finite element analysis to predict failure modes, residual capacity and ductility of reinforced concrete beams under the coupled effects of reinforcement corrosion and service loads without the complexities associated with modeling the corrosion process.

1.6 Thesis Organization

The thesis consists of seven chapters, where chapters 3 to 6 are written in a journal article format. In addition to the thesis chapters, two appendices are included to provide a comprehensive presentation of the experimental test data. A brief description of each chapter is summarized in the following:

- **Chapter 1** presents background information of the problem, objective and scope of the research project.
- **Chapter 2** provides a comprehensive review of the corrosion phenomena in reinforced concrete structures, corrosion-induced damage, previous experimental and analytical investigations on the flexural behavior of corroded reinforced concrete beams, including those which were corroded in the presence or absence of service loads.
- **Chapter 3** investigates the effect of different levels of service loads on the structural behavior of small-scale reinforced concrete beams when coupled with reinforcement corrosion. This chapter provides a description of the experimental testing program, specimens preparation, material properties, accelerated corrosion and mechanical test setup, test results and discussion.
- **Chapter 4** investigates the structural behavior of large-scale reinforced concrete beams when subjected to the coupled effects of reinforcement corrosion and service loads. Four of the small-scale beams reported in Chapter 3 are also included to assess the effects of percentage and number of reinforcing bars. This chapter provides a description of the experimental testing program, specimens preparation, material properties, accelerated corrosion and mechanical test setup, test results and discussion.
- **Chapter 5** investigates the effect of corrosion on the mechanical performance of steel reinforcement. This chapter provides a description of the experimental methodology, including the techniques employed; (i) to measure the corrosion level, and (ii) to perform the tensile testing of corroded steel bars. Test results are also presented and discussed.
- **Chapter 6** presents the proposed simplified approach implemented into finite element models using DIANA software to predict the response of corroded reinforced concrete beams. Modeling approach, validation of the proposed models, and results of the parametric investigation are presented and discussed.

- **Chapter 7** summarizes the conclusions obtained from this research project and provides recommendations for future research.
- **Appendix A** provides supplementary materials for the experimental testing of small-scale reinforced concrete beams. This includes: test images, corrosion level measurements, voltage measurements, applied loads, displacements, and strains readings.
- **Appendix B** provides supplementary materials for the experimental testing of large-scale reinforced concrete beams. This includes: test images, corrosion level measurements, voltage measurements, applied loads, displacements, and strains readings.

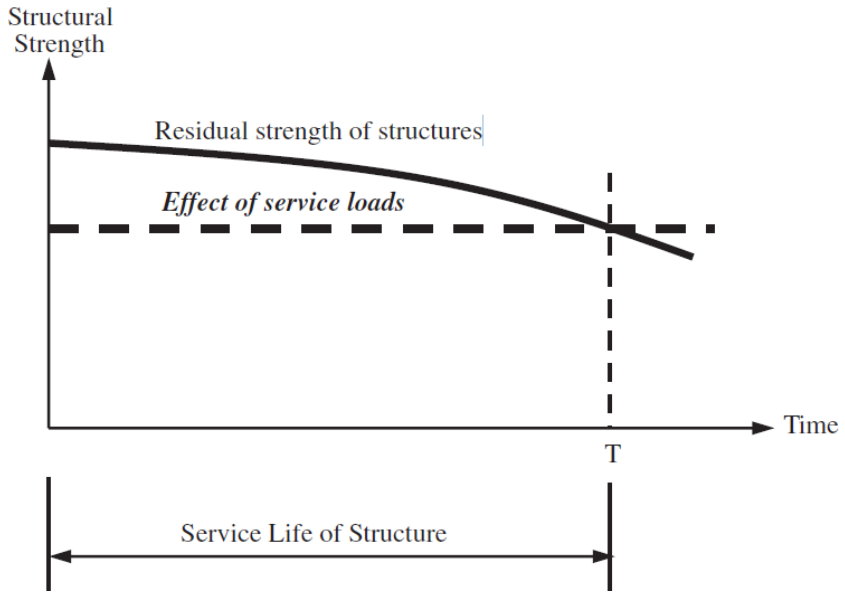

Figure 1.1: Response of structures when subjected to service loads over time (Du et al., 2013)

1.7 References

Almusallam, A. A., Al-Gahtani, A. S., Aziz, A. R., and Rasheeduzzafar. (1996). Effect of reinforcement corrosion on bond strength. Construction and Building Materials, 10(2), 123-129.

Azad, A. K., Ahmad, S., and Azher, S. A. (2007). Residual strength of corrosion-damaged reinforced concrete beams. ACI Materials Journal, 104(1), 40-47.

Azam, R., El-Sayed, A. K., and Soudki, K. (2016). Behaviour of reinforced concrete beams without stirrups subjected to steel reinforcement corrosion. Journal of Civil Engineering and Management, 22(2), 146-153.

Ballim, Y., and Reid, J. C. (2003). Reinforcement corrosion and the deflection of RC beams – an experimental critique of current test methods. Cement and Concrete Composites, 25(6), 625-632.

Cabrera, J. G. (1996). Deterioration of concrete due to reinforcement steel corrosion. Cement and Concrete Composites, 18(1), 47-59.

Du, Y. G., Clark, L. A., and Chan A. H. C. (2005). Effect of corrosion on ductility of reinforcing bars. Magazine of Concrete Research, 57(7), 407-419.

Du, Y., Clark, L. A., and Chan, A. H. C. (2007). Impact of reinforcement corrosion on ductile behavior of reinforced concrete beams. ACI Structural Journal, 104(3), 285-293.

Du, Y., Cullen, M., and Li, C. (2013). Structural performance of RC beams under simultaneous loading and reinforcement corrosion. Construction and Building Materials, 38, 472-481.

El Maaddawy, T., Soudki, K., and Topper, T. (2005). Long-term performance of corrosion damaged reinforced concrete beams. ACI Structural Journal, 102(5), 649-656.

Hariche, L., Ballim, Y., Bouhicha, M., and Kenai, S. (2012). Effects of reinforcement configuration and sustained load on the behaviour of reinforced concrete beams affected by reinforcing steel corrosion. Cement and Concrete Composites, 34(10), 1202-1209.

Koch, G., Varney, J., Thompson, N., Moghissi, O., Gould, M., and Payer, J. (2016). International measures of prevention, application, and economics of corrosion technologies study. NACE International IMPACT, Houston, Texas, USA.

Li, H., Li, B., Jin, R., Li, S., and Yu, J.-G. (2018). Effects of sustained loading and corrosion on the performance of reinforced concrete beams. Construction and Building Materials, 169, 179-187.

Malumbela, G., Moyo, P., and Alexander, M. (2009). Behaviour of RC beams corroded under sustained service loads. Construction and Building Materials, 23(11), 3346-3351.

Mangat, P. S., and Elgarf, M. S. (1999). Flexural strength of concrete beams with corroding reinforcement. ACI Structural Journal, 96(1), 149-158.

Rodriguez, J., Ortega, L. M., and Casal, J. (1997). Load carrying capacity of concrete structures with corroded reinforcement. Construction and Building Materials, 11(4), 239-248.

Torres-Acosta, A. A., Navarro-Gutierrez, S., and Terán-Guillén, J. (2007). Residual flexure capacity of corroded reinforced concrete beams. Engineering Structures, 29(6), 1145-1152.

Yoon, S., Wang, K., Weiss, W. J., and Shah, S. P. (2000). Interaction between loading, corrosion, and serviceability of reinforced concrete. ACI Materials Journal, 97(6), 637-644.

Zhang, W., Zhang, H., Gu, X., and Liu, W. (2018). Structural behavior of corroded reinforced concrete beams under sustained loading. Construction and Building Materials, 174, 675-683.

Chapter Two : Literature Review

2.1 General

This chapter provides a discussion on previous literature, covering reinforcement corrosion in concrete structures, corrosion-induced damage, and previous experimental research on the flexural behavior of corroded reinforced concrete beams. The emphasis is placed on reviewing the behavior of reinforced concrete beams under the coupled and separate effects of reinforcement corrosion and service loads. The literature review also presents previous numerical research on the behavior of damaged reinforced concrete beams due to corrosion. Finally, a discussion on existing research gaps is presented.

2.2 Corrosion in Reinforced Concrete Structures

2.2.1 Corrosion Phenomena

Concrete is known to be a highly alkaline material with an approximate pH level of 12.6 (Richardson, 2002). During the early stages of cement hydration, a thin passive film layer forms around embedded steel reinforcement at such high pH level. The passive film layer protects steel reinforcement from corrosion. Depassivation of steel reinforcement occurs as a result of concrete carbonation or chloride ingress. Breakage of the protective layer combined with the availability of oxygen and water triggers the initiation process of corrosion in reinforced concrete structures.

Corrosion of steel reinforcement occurs as a result of an electrochemical reaction process, in which electrons migrate from the anodic site to cathodic site, as illustrated in Figure 2.1. The anodic and cathodic reactions are expressed in the following:

$$Fe \rightarrow Fe^{2+} + 2e^{-} \qquad \text{(anodic reaction)} \tag{2.1}$$

$$\frac{1}{2}O_2 + H_2O + 2e^{-} \rightarrow 2(OH)^{-} \qquad \text{(cathodic reaction)} \tag{2.2}$$

Ferrous hydroxide $Fe(OH)_2$ is formed on the surface of steel reinforcement with the flow of ions from the cathodic site to the anodic site, as expressed in the following:

$$Fe^{2+} + 2OH \rightarrow Fe(OH)_2 \quad (2.3)$$

Ferrous hydroxide reacts with oxygen, resulting in the formation of rust products, as expressed by the following reaction:

$$4Fe(OH)_2 + O_2 + 2H_2O \rightarrow 4Fe(OH)_3 \quad (2.4)$$

Depending on the environmental conditions, other types of rust are formed in subsequent secondary reactions (Richardson, 2002). These reactions are expressed in the following:

$$2Fe(OH)_2 + O_2 \rightarrow FeOOH \quad (2.5)$$

$$2FeOOH \rightarrow \alpha Fe_2O_3 + H_2O \quad (2.6)$$

$$4Fe(OH)_3 \rightarrow 3Fe_2O_3.H_2O + 4H_2O \quad (2.7)$$

2.2.2 Corrosion Accelerators

As mentioned previously, carbonation of concrete and chloride ingress are the leading cause of accelerating the corrosion process of steel reinforcement.

2.2.2.1 Carbonation-Induced Corrosion

Carbonation-induced corrosion is caused by the presence of high levels of carbon dioxide CO_2 and other gases in the atmosphere due to increased greenhouse gas emissions. Dissolved carbon dioxide in water reacts with calcium dioxide $Ca(OH)_2$, which is present in the cementitious paste of concrete, producing calcium carbonate $CaCO_3$, as presented in the following reactions (Richardson, 2002):

$$CO_2 + H_2O \rightarrow H_2CO_3 \quad (2.8)$$

$$H_2CO_3 + Ca(OH)_2 \rightarrow CaCO_3 + 2H_2O \quad (2.9)$$

The outcome of these reactions reduces the alkalinity of concrete. With reduced pH levels, the passive layer around the embedded steel reinforcement can be broken down easily, and hence the initiation of corrosion becomes possible. Typically, carbonation of concrete causes a uniform loss of reinforcement sectional area, along the entire affected region.

2.2.2.2 Chloride-Induced Corrosion

Chloride-induced corrosion is caused by the exposure to high concentrations of chloride ions Cl^-, which is typically found in marine environments, where concrete structures are exposed to splashed seawater. It can be also present in the form of de-icing salt which is usually applied on roadways in cold regions. Chloride ions penetrate to the surface of steel reinforcement through the voids and cracks of the surrounding concrete, as illustrated in Figure 2.2. The passive film layer around the embedded steel reinforcement can be broken down when sufficient chlorides are present. This in turn, accelerates the corrosion process of steel reinforcement and leads to the development of a localized loss of reinforcement sectional area (i.e., pit corrosion). This type of corrosion can be present in various shapes, resulting in different cross-sectional area losses, as illustrated in Figure 2.3.

2.3 Corrosion-Induced Damage

There are several consequences associated with the progression of corrosion in reinforced concrete structures, including (i) cracking and spalling of concrete surrounding the corroded steel reinforcement, (ii) loss of reinforcement sectional area, (iii) degradation of the mechanical properties of corroded steel reinforcement, and (iv) impairment or complete loss of bond at the interface between the corroded steel reinforcement and concrete.

2.3.1 Deterioration of Concrete

Corrosion is considered to be one of the leading causes of deterioration mechanisms in reinforced concrete structures. As mentioned previously, corrosion initiates with the breakage of the passive layer around reinforcing bars, together with the availability of oxygen and water. Rust products are formed during this process, replacing the passive layer around steel reinforcement. The density of rust products is lower than that of steel, and hence it occupies a larger volume than the corroded steel. Volume occupancy of different forms of corrosive by-products relative to the original volume of steel reinforcement is shown in Figure 2.4.

The low tensile capacity of concrete makes it susceptible to cracking due to the volumetric expansion of corrosion by-products, which increases in the radial direction around the corroded steel reinforcement. This leads to the development of longitudinal cracks at the level of steel reinforcement. Furthermore, spalling of the corroded concrete region occurs if corrosion-induced

cracks are able to propagate to the outer surface of concrete (Richardson 2002), as illustrated in Figure 2.5.

2.3.2 Loss of Reinforcement Area

Depending on the exposure condition in natural environments (i.e., carbonation of concrete or chloride ingress), two types of corrosion can be identified on the surface of steel reinforcement in concrete structures namely, generalized corrosion and localized corrosion. Generalized corrosion causes a uniform loss of cross-sectional area along the entire length of steel reinforcement. The average loss of reinforcement sectional area (i.e., average mass loss) caused by generalized corrosion attack can be evaluated using Faraday's law. In this law, the loss of reinforcement sectional area is dependent on the current density of corrosion, as expressed in the following:

$$\eta_{avg,m} = \frac{MI_{cor}t}{ZF} \tag{2.10}$$

where, $\eta_{avg,m}$ is the average mass loss of corroded steel bar (g), M is the atomic mass of iron ($= 55.85\ g/mol$), I_{cor} is the current of corrosion (A), t is the duration of corrosion exposure (s), Z is the valence electrons of iron ($= 2$), and F is Faraday's constant ($= 96{,}500\ A.s$). Alternatively, the expression given in Eq. (2.10) can be rewritten in terms of the depth of generalized corrosion attack, $p(T)_{general}$ in (mm), which is expressed in the following:

$$p(T)_{general} = 0.0116Ti_{corr} \tag{2.11}$$

where, T is the time of corrosion (year), and i_{corr} is the current density of corrosion ($\mu A/cm^2$). On the other hand, pit corrosion is a localized form of corrosion that develops at random sites along the corroded steel reinforcement. This type of corrosion is found in various shapes, causing difficulties in assessing the localized corrosion level. In order to simplify the complex geometries associated with pit corrosion, Val et al. (2007) assumed that the configuration shape of pit corrosion is hemispherical, as shown in Figure 2.6. The depth of pit corrosion attack, $p(T)_{pit}$ in (mm), is related to the depth of generalized corrosion attack using the following expression:

$$p(T)_{pit} = p(T)_{general}R \tag{2.12}$$

where, R is the ratio between the maximum depth of pit corrosion and average depth of generalized corrosion. González et al. (1995) reported R values in the range of 4 – 8 in natural corrosion

environment and R values in the range of 5 – 13 in accelerated corrosion testing. Further details on estimating the residual cross-sectional area of corroded steel bars due to pit corrosion are presented in Val et al. (2007).

2.3.3 Mechanical Performance of Corroded Steel Reinforcement

Over the past few decades, there have been many experimental research studies that investigated the influence of corrosion on the mechanical properties of steel reinforcement. These studies revealed that corrosion had a little to no effect on the tensile strength of steel reinforcement, however the ductility of reinforcement was significantly reduced due to the localized effect of pit corrosion.

Almusallam (2001) carried out an experimental investigation to examine the influence of corrosion on the mechanical properties of steel reinforcement. Reinforcing steel bars were embedded in concrete samples. Diameter of steel bars was either 6 mm or 12 mm. Corrosion of steel bars was accelerated using the direct impressed current technique with a current density of 2,000 $\mu A/cm^2$.

Figure 2.7 shows the influence of corrosion on the ultimate tensile strength of steel reinforcement. In this figure, the strength was calculated using the residual sectional area (i.e., corroded area) of steel bars. It can be clearly seen that corrosion had a slight effect on the ultimate strength of steel reinforcement. In contrast to this observation, the author had noted that the strength of some corroded steel bars was below code requirements, when the nominal sectional area was used to calculate the strength instead of the residual sectional area.

Cairns et al. (2005) investigated the effect of localized corrosion on the mechanical properties of steel reinforcement. Localized pit corrosion was simulated in two different methods. In the first method, the area of a small portion along the reinforcement was artificially removed to achieve a sectional area loss of either 5%, 10%, 20%, 30%, 40%, or 50%. In the second method, the direct impressed current technique was employed to accelerate the corrosion process of steel reinforcement using various current densities in the range of 50 – 500 $\mu A/cm^2$.

Figure 2.8(a) shows the effect of corrosion on the yield and ultimate tensile strength of steel reinforcement, where the strength was calculated using the residual corroded sectional area of steel reinforcement. The authors indicated that the yield strength remained unchanged, while the

ultimate strength was slightly increased with the increase of sectional area loss of steel reinforcement. Furthermore, the ductility of steel reinforcement was reduced significantly, as illustrated in Figure 2.8(b), due to the localized effect of corrosion.

Du et al. (2005) examined the influence of corrosion on the mechanical properties of bare steel reinforcement and embedded steel reinforcement in concrete samples. Test parameters of this experimental study included: type of steel reinforcement, diameter of steel reinforcement, and level of corrosion. Type of reinforcement was either plain or ribbed steel bar. Diameter of steel reinforcement was either 8 mm, 16 mm, or 32 mm. Steel bars were corroded using the impressed current technique with different current densities of 500 μA/cm^2, 1,000 μA/cm^2, and 2,000 μA/cm^2 in order to achieve different corrosion levels. Level of corrosion was either 5%, 10%, 15%, or 20%.

Figure 2.9(a) shows the yield and ultimate tensile strengths of plain bars (R and RC series) and ribbed bars (T and TC series) as a function of the level of corrosion. Test results showed that both yield and ultimate strengths of corroded steel bars were reduced with the increase of corrosion levels. Figure 2.9(b) shows the effect of corrosion on the ultimate strain ratio (defined as the ultimate strain of corroded steel bar relative to that of control steel bar). It can be clearly seen that there was a drastic reduction in ultimate strain ratio with the increase of corrosion levels. The researchers attributed this reduction to the non-uniform distribution of cross-sectional area along the corroded steel reinforcement.

In addition, the researchers performed a regression analysis of their experimental data to develop a relationship between the residual strength/ductility of steel reinforcement and the level of corrosion. The proposed linear relationships are expressed in the following:

$$f_{yc} = \left[1 - \alpha_y \eta_{avg}\right] f_{y0} \tag{2.13}$$

$$f_{uc} = \left[1 - \alpha_u \eta_{avg}\right] f_{u0} \tag{2.14}$$

$$\varepsilon_{uc} = \left[1 - \alpha_1 \eta_{avg}\right] \varepsilon_{u0} \tag{2.15}$$

where, $f_{yc}, f_{uc}, \varepsilon_{uc}$ are the yield strength, ultimate strength, and ultimate strain of corroded steel bars, respectively, $f_{y0}, f_{u0}, \varepsilon_{u0}$ are yield strength, ultimate strength, and ultimate strain of non-corroded steel bars, respectively, $\alpha_y, \alpha_u, \alpha_1$ are empirical coefficients for the reduction rates of

yield strength, ultimate strength, and ultimate strain of corroded steel bars, respectively. All coefficients are presented in Du et al. (2005).

Ou et al. (2016) investigated the influence of corrosion on the mechanical properties of naturally and artificially corroded steel reinforcement. Natural corroded steel bars were extracted from beams, columns, and walls of a residential building constructed in the 1970s. The deformed bars from these structural elements had a diameter of either 13 mm, 16 mm, or 19 mm. Artificial corroded steel bars were retrieved from beams that were corroded using the direct impressed current technique, with an applied corrosion current density of 600 $\mu A/cm^2$. The deformed bars had a diameter of either 13 mm or 29 mm.

Figure 2.10 and Figure 2.11 show the effect of corrosion on the mechanical properties of naturally and artificially corroded steel bars, respectively. The researchers indicated that the reductions in yield and ultimate strength ratios of artificially corroded steel bars were similar to those of naturally corroded steel bars. However, the reduction in ultimate strain ratio of artificially corroded steel bars was more than that of naturally corroded steel bars. This was explained by the observed corrosion patterns, as artificially corroded steel bars had more non-uniform corrosion than those which were corroded naturally.

2.3.4 Bond Strength

The transfer mechanism of forces between steel reinforcement and the surrounding concrete is strongly influenced by corrosion, mainly due to the combined effects of loss of reinforcement sectional area and the volumetric expansion of corrosion by-products that leads to the development of corrosion cracks. Over the past few decades, numerous experimental studies were carried out to examine the characteristics of bond at the interface between the corroded steel reinforcement and concrete. It was shown that small amounts of corrosion resulted in a slight increase in bond strength due to increased friction caused by the expansion of corrosion by-products. However, the bond mechanism weakens with increased corrosion levels due to the development of longitudinal corrosion cracks and reduced height of ribs along the corroded reinforcement.

Al-Sulaimani et al. (1990) studied the influence of corrosion on the bond behavior between steel reinforcement and concrete. In this study, concrete blocks with dimensions of 150 x 150 x 150 mm were constructed. Test specimens were reinforced with a single steel bar that had a diameter of either 10 mm, 14 mm, or 20 mm. The ratio between the embedment length and diameter of steel

bar was equal to 4.0. The corrosion process of steel bars was accelerated using the direct impressed current technique with a current density of 2,000 $\mu A/cm^2$.

Figure 2.12 shows results of the pullout test for the various bar sizes considered in this study. It can be clearly seen that all steel bar sizes exhibited an increase in bond strength at low corrosion levels. This was followed by a sudden drastic reduction in bond strength with increased corrosion levels. The researchers attributed the initial increase in bond strength to the formation of corrosion by-products which enhanced the roughness of steel reinforcement at low levels of corrosion. The reduction in bond strength was explained by worsening of the interlock between the ribs of reinforcement and concrete.

Almusallam et al. (1996) carried out an experimental study to investigate the influence of corrosion on the bond behavior in reinforced concrete. In this study, the cantilever bond test was used to evaluate the bond characteristics of the corroded specimens. The specimens had dimensions of 152 x 254 x 279 mm. All specimens were reinforced with a single 12 mm steel bar. Corrosion of steel reinforcement was accelerated using the direct impressed current technique using a constant voltage of 0.4 V.

The researchers indicated that the bond strength at the interface between steel reinforcement and concrete increased prior to the development of corrosion cracks and at corrosion levels less than 4%, as illustrated in Figure 2.13. This increase in bond strength was explained by the increase in the confinement of concrete surrounding the corroded reinforcement due to the volumetric expansion of corrosion by-products. It was also explained by the increase of frictional forces at the interface due to enhancement of reinforcement roughness. At higher corrosion levels (i.e., greater than 4%), there was a drastic reduction in bond strength due to the development of cracks in the cover of concrete.

Other experimental studies that examined the influence of corrosion on the bond strength in reinforced concrete, such as those conducted by Wei-liang and Yu-xi (2001) and Fang et al. (2004), had similar conclusions to those discussed in this section.

2.4 Simulation of Reinforcement Corrosion

It is well-known that corrosion of reinforcement is a slow process that takes many years in natural environments. Typically, on-site measurements of corrosion rate in concrete structures range

between 0.1–1.0 μA/cm^2, while corrosion rates exceeding 1.0 μA/cm^2 are rarely measured (Andrade and Alonso, 2001). Previously, numerous research studies examined the structural behavior of different corroded reinforced concrete members. Several techniques were employed to simulate reinforcement corrosion in these studies, including (i) exposure to natural environment, (ii) artificial corrosion using chloride spray (dry/wet cycles), and (iii) accelerated corrosion using impressed current.

In the majority of previous studies, corrosion of steel reinforcement was accelerated using the impressed current technique. In this technique, the duration of testing is controlled by the applied current density. Applying higher values of current densities can decrease the duration of experimental testing from years to months/days, however proper selection of the current density is critical in simulating the observed corrosion damage in the field. Based on a review conducted by El Maaddawy and Soudki (2003), the applied current density adopted by other researchers had a minimum value of 45 μA/cm^2, maximum of value of 10,400 μA/cm^2, and average value ranging between 200 and 3,000 μA/cm^2. A summary of tests conducted using the impressed current technique along the applied current density is presented in Table 2.1. Clearly, there is a wide range of current densities adopted by other researchers, which in turn may influence the behavior of corroded reinforced concrete members.

Nguyen and Lambert (2018) carried out an experimental study to investigate the influence of current density on the structural performance of corroded reinforced concrete beams. A total of 20 beams with dimensions of 100 x 150 x 900 mm were constructed and divided into four groups. All beams were reinforced with 10 mm non-deformed steel bars, serving as the main tensile reinforcement. The beams in groups one, two, three and four were corroded over different durations to achieve targeted corrosion levels of 0.5%, 1.0%, 2.5%, and 5.0%, respectively. In each group, one beam served as control beam without reinforcement corrosion, while the remaining four beams were corroded using a current density of either 250 μA/cm^2, 500 μA/cm^2, 1,000 μA/cm^2, or 2,000 μA/cm^2. The beams were placed in a water tank containing sodium chloride solution (3.5% NaCl) during the corrosion exposure. After achieving the targeted corrosion level, the beams were loaded using a four-point bending test.

After extracting and cleaning the corroded steel bars, the researchers observed that steel bars from beams that were corroded with a targeted corrosion level of 5% using current densities of 1,000

$\mu A/cm^2$ and 2,000 $\mu A/cm^2$, had more and larger localized corrosion sites when compared to steel bars that were corroded using current densities of 250 $\mu A/cm^2$ and 500 $\mu A/cm^2$. In terms of structural performance, the researchers indicated that the applied current density had a small effect on the load-displacement relationships of beams with the same corrosion level (i.e., corroded beams within the same group), as shown in Figure 2.14. As a result, the effect of applied current density on the ultimate load capacity of beams that were corroded within the same group was also very small, as shown in Figure 2.15. Based on the results of this study, the researchers indicated that the use of a current density of 1,000 $\mu A/cm^2$ is appropriate to accelerate the corrosion process in reinforced concrete.

2.5 Flexural Behavior of Corroded Reinforced Concrete Beams

In the past, extensive research efforts were devoted to understand the flexural behavior of reinforced concrete beams with corroded reinforcement. As mentioned previously, there are several consequences associated with the initiation and progression of corrosion in reinforced concrete beams, including loss of reinforcement sectional area, degradation of mechanical performance of corroded reinforcement, cracking and spalling of concrete surrounding the corroded reinforcement, and loss of bond strength at the interface between the corroded reinforcement and concrete. Consequently, the ultimate load capacity and ductility of reinforced concrete beams are influenced by corrosion.

The main focus of previous experimental research was the flexural behavior of corroded reinforced concrete beams without considering the effect of service loads (i.e., beams were corroded first and then loaded to failure). Afterward, the focus of research shifted towards understanding the flexural behavior of reinforced concrete beams under the coupled effects of reinforcement corrosion and loads, to simulate in-service conditions. In this section, previous experimental research studies that examined the flexural behavior of corroded reinforced concrete beams in the absence and presence of service loads are presented.

2.5.1 Corroded Reinforced Concrete Beams without the Effect of Loads

Rodriguez et al. (1997) carried out an experimental study to investigate the behavior of reinforced concrete beams with corroded longitudinal and transverse reinforcement. A total of thirty-one beams with dimensions of 150 x 200 x 2300 mm were constructed. The beams had different

reinforcement detailing in terms of longitudinal (tensile/compressive) and transverse reinforcement ratios. Corrosion of steel reinforcement was accelerated using the direct impressed current technique with a constant current density of 100 μA/cm^2. The beams were corroded over various durations, ranging between 100 and 200 days to achieve different levels of corrosion. Reinforcement corrosion was further accelerated by adding calcium chloride (3% by weight of cement) in the concrete mix in some beams. All beams were loaded using a four-point bending test after reaching the desired level of corrosion. Loads were first applied up to the service level, and then up to the failure of beams.

Test results showed that the deflections and width of cracks in corroded reinforced concrete beams were increased at the service level. The observed failure modes of control and corroded reinforced concrete beams are shown in Figure 2.16. Control and corroded beams with low tensile reinforcement ratio exhibited Type 1 flexural failure. Control beams with high tensile reinforcement ratio and corroded beams with high shear reinforcement ratio exhibited Type 2 crushing of concrete failure. Corroded beams with high tensile reinforcement ratio and widely spaced stirrups exhibited Type 3 shear failure. Control and corroded beams with curtailed bottom tensile reinforcement exhibited Type 4 combined shear/anchorage failure. The researchers indicated that corrosion of steel reinforcement reduced the ultimate load capacity of beams. It also changed the flexural response of some beams to undesired shear failure.

Mangat and Elgarf (1999) investigated the effect of corrosion on the flexural capacity of reinforced concrete beams. A total of 111 beams with dimensions of 100 x 150 x 910 mm were constructed and tested. All beams were reinforced with either two 8 mm diameter steel bars or two 10 mm diameter steel bars. Corrosion of reinforcement was accelerated using the direct impressed current technique with a current density of either 1,000 μA/cm^2, 2,000 μA/cm^2, 3,000 μA/cm^2, or 4,000 μA/cm^2, while placing the beams in a sodium chloride solution (5% NaCl). Reinforcement corrosion was further accelerated by adding sodium chloride (1% by weight of cement) in the concrete mix. The beams were loaded using a four-point bending test.

Test results indicated that the corrosion current density did not have an influence on the load-displacement relationship of beams with corrosion level of 2.5%, as shown Figure 2.17(a). However, the load-displacement relationship of beams was strongly influenced by the current density at corrosion level of 7.5%, as can be clearly seen in Figure 2.17(b). For that reason, the

researchers suggested using the smallest current density to simulate corrosion of steel reinforcement in concrete beams. Furthermore, the ultimate load capacity of beams was reduced with the increase of corrosion levels, as shown in Figure 2.18. This reduction was attributed to the loss of bond strength at the interface between steel reinforcement and concrete. The researchers also indicated that the loss of reinforcement area had insignificant effect on the ultimate load capacity of corroded beams.

In order to estimate the residual capacity of corroded reinforced concrete beams, the researchers developed a predictive model based on a regression analysis of their experimental data. In this model, the residual flexural strength of beams was correlated with the diameter of reinforcement, corrosion current density, and duration of corrosion exposure. The predictive model is expressed in the following:

$$B(\%) = \left[1 - sin^2\left(2.312\frac{T}{D}i_{corr}LNi_{corr}\right)\right]100 \tag{2.16}$$

where, $B(\%)$ is a percentage of flexural strength of control beam, T is duration of corrosion exposure (in years), D is the diameter of reinforcement (in mm), and i is the current density of corrosion (in μA/cm^2). Figure 2.19 shows a good agreement between the predictive model and experimental data up to a corrosion level of 3.75%. At higher levels of corrosion, the predictive model gave a conservative estimation of the flexural capacity of beams.

Azad et al. (2007) completed an experimental study that investigated the flexural behavior of corroded reinforced concrete beams. A total of fifty-six beams with dimensions of 150 x 150 x 1100 mm were constructed and tested. All beams were reinforced with either two 10 mm diameter steel bars or two 12 mm diameter steel bars, serving as the main flexural reinforcement. Concrete cover was either 25 mm or 40 mm. The beams were placed in a water tank containing sodium chloride solution (5% NaCl) during the corrosion exposure. Steel bars were corroded using the direct impressed current technique with a constant current density of either 2,000 μA/cm^2 or 3,000 μA/cm^2, which was applied over a duration of either 4 days, 6 days, or 8 days. At the end of the corrosion phase, all beams were loaded to failure using a four-point bending test.

Test results showed that the residual flexural capacity of corroded beams was reduced with increased corrosion activity index, as shown in Figure 2.20. In this figure, the corrosion activity index $I_{corr}T$ is defined as the corrosion current density multiplied by duration of corrosion

exposure. The researchers indicated that the residual flexural capacity of corroded beams could be estimated using the residual sectional area of corroded steel bars at low values of corrosion activity index. However, at high values of corrosion activity index, other factors such as loss of bond should be taken into consideration.

In order to predict the residual capacity of corroded reinforced concrete beams, the researchers proposed a two-step approach based on their experimental data. In the first step, the moment capacity of corroded beams is computed using the residual cross-sectional area of steel bars. In the second step, the moment capacity is multiplied by a correction factor β to account for the loss of bond and other factors that may contribute to the loss of flexural capacity in corroded beams. The correction factor was established by a regression analysis of the experimental test data, which is expressed in the following:

$$\beta = \frac{14.7}{D(i_{corr}T)^{0.15}} \leq 1.0 \tag{2.17}$$

Du et al. (2007) conducted an experimental study to examine the influence of corrosion on the ductility of reinforced concrete beams. A total of nineteen beams with dimensions of 150 x 200 x 2100 mm were constructed and tested in this study. The beams were designed to be in one of the following categories: very under-reinforced, under-reinforced, balanced, or over-reinforced. The direct impressed current technique was utilized to accelerate the corrosion process of either the tensile longitudinal reinforcement, compressive longitudinal reinforcement, or transverse reinforcement. Current densities in the range of 250 – 900 μA/cm^2 were applied over durations in the range of 60 – 120 days. At the end of the corrosion phase, all beams were loaded using a four-point bending test.

Figure 2.21 shows the influence of reinforcement corrosion on the ductile response of beams with different longitudinal tensile reinforcement ratios. Test results of previous studies were also included in this figure for comparison. The researchers found that under-reinforced beams with corrosion levels exceeding 10%, could exhibit rupturing of the corroded longitudinal tensile reinforcement (i.e., reduction in ductility). Furthermore, reinforcement corrosion could shift the brittle response of over-reinforced concrete beams with low corrosion levels to a more ductile response (i.e., increase in ductility).

Torres-Acosta et al. (2007) carried out an experimental study to investigate the effect of reinforcement corrosion on the flexural capacity of concrete beams. Twelve beams with dimensions of 100 x 150 x 1500 mm were designed and constructed for this purpose. All beams were reinforced with a single 10 mm steel bar. Steel bars were corroded using the direct impressed current technique with a current density of 80 $\mu A/cm^2$, applied over a duration of either 40 days, 80 days, or 200 days. The corrosion process was further accelerated by adding calcium chloride in the concrete mix. After attaining the desired level of corrosion, all beams were loaded to failure using a three-point bending test.

The researchers indicated that corroding reinforced concrete beams in a wet humid environment, enhanced the formation of pit corrosion when compared to those which were corroded in a dry environment. Furthermore, it was found that the maximum depth of pit corrosion attack had a better correlation with the residual flexural capacity of corroded beams than the average depth of generalized corrosion attack. Figure 2.22(a) shows the empirical relation between the residual capacity ratio 'RLC_{COR}' and maximum pit depth 'PIT_{max}'. Similar correlation was also found using previous experimental data, as shown in Figure 2.22(b).

Azam et al. (2016) experimentally investigated the effect of corrosion in reinforced concrete beams without transverse shear reinforcement. A total of seven beams with dimensions of 150 x 250 x 1100 mm were constructed and tested in this investigation. The beams had a tensile reinforcement ratio of either 0.91%, 1.21%, or 1.82%. All corroded beams were constructed with salted concrete in the bottom 100 mm and non-salted concrete in the top 50 mm. Corrosion of steel reinforcement was accelerated using the direct impressed current technique with a constant current density of 200 $\mu A/cm^2$ to achieve a targeted corrosion level of either 3% or 10%. The beams were loaded using a three-point bending test.

The researchers showed that the beam with the highest tensile reinforcement ratio experienced less corrosion level than the beam with the lowest tensile reinforcement ratio. This was attributed to the formation of corrosion by-products, which quickly filled up the voids and cracks of the beam with high tensile reinforcement ratio, resulting in a slowing down the corrosion process. Figure 2.23 compares the ultimate load capacity of control and corroded beams with different tensile reinforcement ratios. Clearly, the beam with the highest tensile reinforcement ratio experienced

the least reduction in ultimate load capacity. Furthermore, the results of this study revealed that corrosion of steel reinforcement shifted the shear failure of beams without stirrups to bond failure.

2.5.2 Corroded Reinforced Concrete Beams with the Effect of Loads

Yoon et al. (2000) carried out an experimental investigation aimed at the response of corroded reinforced concrete beams under loads. A total of ten beams with dimensions of 100 x 150 x 1170 mm were constructed and tested. All beams were reinforced with a single 19 mm steel bar. Table 2.2 presents a summary of the experimental testing program. Two loading protocols were adopted to examine the presence of flexural cracks on the response of corroded beams. In the first protocol (i.e., preload), the beams were first loaded to either 45% or 75% of the beam ultimate load capacity. Then, loads were removed while corroding the longitudinal steel reinforcement. In the second protocol (i.e., sustained), the beams were first loaded to either 20%, 45%, 60%, or 75% of the beam ultimate load capacity. Then, loads were sustained while corroding the longitudinal steel reinforcement. The beams were corroded in two different stages. In the first stage, the beams were either placed in 3% NaCl solution (4 days wet/ 3 days dry) or left in air-dry environment. In the second stage, an external current was applied to corrode steel reinforcement using constant increments of voltage. The beams were then loaded to failure using a four-point bending test.

Test results revealed that reinforcement corrosion initiated faster in beams which were subjected to higher levels of loading, which was likely due to the presence of flexural cracks that provided a clear path for chloride ions and water to reach the surface of steel reinforcement. The researchers also indicated that corroded beams under sustained loads exhibited higher corrosion levels and lower residual flexural capacities in comparison to corroded beams which were only preloaded. Figure 2.24 shows the failure modes and residual flexural capacities of control and corroded beams. It can be clearly seen that increasing the level of corrosion had a significant influence on the residual capacity of beams, shifting the shear failure of control beams to bond splitting failure in the corroded beams.

Ballim and Reid (2003) conducted an experimental investigation to examine the behavior of reinforced concrete beams under the coupled effects of reinforcement corrosion and loads. A total of twelve beams with dimensions of 100 x 160 x 1500 mm were cast and tested in this investigation. The beams were divided into two series. Series 1 beams were subjected to sustained loads equivalent to 23% of the beam ultimate load capacity for a duration of 30 days, while Series

2 beams were subjected to sustained loads equivalent to 46% of the beam ultimate load capacity for a duration of 35 days. Tensile longitudinal reinforcement were depassivated by carbonation of concrete. Furthermore, tensile longitudinal reinforcement were subjected to a constant current density of 400 $\mu A/cm^2$. All beams were loaded using a four-point bending test. It is worth noting that the researchers reported corrosion of the supports in Series 1 beams, which contributed to increasing the deflections of supports.

Test results showed that beams subjected to the coupling effects of reinforcement corrosion and loads experienced an increase in deflections with increased corrosion levels (i.e., over time), as shown in Figure 2.25. The initial high rate of increase in deflections was explained by the propagation of transverse load-induced cracks and volumetric expansion of corrosion by-products. In order to demonstrate the significance of the coupling effects of reinforcement corrosion and loads, the results of this study were compared with previous experimental study of reinforced concrete beams which were corroded without the effect of loads, as shown in Figure 2.26. In this figure, the deflection ratio is defined as the deflection of corroded beams relative to that of the control beam. The researchers showed that corroded beams under loads had higher deflection ratios than those which were corroded under no loads.

El Maaddawy and Topper (2005) performed an experimental study to examine the behavior of corroded reinforced concrete beams in the presence and absence of loads. A total of nine beams with dimensions of 152 x 254 x 3200 mm were designed and employed in the experimental program. The bottom portion of beams (1400 mm length x 100 mm depth) was cast with salted concrete. Longitudinal tensile reinforcement were subjected to a direct current of 215 mA. Furthermore, the beams were placed in a compressed air nozzle that sprays mist to further accelerate the corrosion process. One beam served as control specimen without reinforcement corrosion. Four beams were corroded for a duration of either 50 days, 110 days, 210 days, or 310 days under no loads. The remaining four beams were corroded for a duration of either 50 days, 110 days, 210 days, or 310 days under sustained loads equivalent to 60% of the beam yield capacity. All beams were loaded using a four-point bending test.

The researchers found that the presence of loads accelerated the initiation and development of corrosion cracks since more oxygen and moisture were able to penetrate to the surface of steel reinforcement. Table 2.3 presents key results from the tests of beams, where Group A beams were

corroded under no loads, while Group B beams were corroded under loads. The beams that were corroded under loads for durations of 50 days and 110 days, experienced higher reductions in ultimate load capacity in comparison to the beams which were corroded under no loads. The researchers attributed the further reduction in capacity to the increase of corrosion levels in corroded beams under loads. However, unlike the reduction in ultimate load capacity at 50 days and 110 days, there was no additional reduction in capacity when comparing Group A and B beams at 210 days and 310 days. This was primarily attributable to the fact that the level of corrosion in both groups was similar. In terms of ductility, it was found that beams with corrosion levels exceeding 15% exhibited a reduced ductility, as shown in Figure 2.27.

Malumbela et al. (2009) carried out experimental tests to investigate the influence of corrosion on the depth of neutral axis and curvature in reinforced concrete beams under the coupling effects of reinforcement corrosion and loads. A total of four beams with dimensions of 153 x 254 x 3000 mm were constructed and tested for this purpose. The middle portion of beams (700 mm length x 50 mm depth) was placed in a sodium chloride solution (5% NaCl). All beams were exposed to cycles of wet environment over four days and air-dry environment over two days. Longitudinal tensile reinforcement were subjected to a current density of 189 $\mu A/cm^2$ during the wet cycles. Two beams were corroded under loads equivalent to either 1% (i.e., beam 1) or 8% (i.e., beam 2) of the beam ultimate load capacity, which corresponded to loads that did not induce flexural cracks. One beam was corroded under loads equivalent to 12% (i.e., beam 3) of the beam ultimate load capacity, which corresponded to a load that led to the development of flexural cracks. The last beam was loaded to 12% (i.e., beam 4) of the beam ultimate load capacity without reinforcement corrosion. Longitudinal strains were measured at different positions within the corroded region of beams. Strain gauges were installed on the tensile face of concrete and at 30 mm away from the compressive face of concrete. All beams were loaded using a four-point bending test.

Figure 2.28 shows the average strain measurements from the gauges installed on the beams. It is clear that the progression of tensile strains over time in the corroded beam with flexural cracks (i.e., beam 3) was higher than that of corroded beams without flexural cracks (i.e., beams 1 and 2). The researchers attributed this increase to the loss of reinforcement sectional area, loss of bond at the interface between steel reinforcement and concrete, lateral tensile strain induced by the expansion of corrosion by-products, and to the strains generated by the applied loads. Furthermore, the researchers evaluated the variation of neutral axis depth by assuming a linear relationship

between the tensile and compressive strains within the corroded region of beams. According to Figure 2.29, it was indicated that the depth of natural axis of the corroded beam with flexural cracks (i.e., beam 3) decreased with the increase of corrosion levels, while that of the corroded beam without flexural cracks (i.e., beam 2) was not influenced by corrosion.

Hariche et al. (2012) investigated the influence of reinforcement configuration and loading levels on the flexural behavior of reinforced concrete beams under the coupled effects of reinforcement corrosion and loads. Test setup and size of beams employed by Ballim and Reid (2003) were also used in this study. A total of twenty-four beams were constructed and divided into four groups. The beams in the first three groups had longitudinal tensile reinforcement in the form of either 2Y12, 1Y16, or 3Y10. These beams were subjected to sustained loads of 20 kN. Group four beams had the same reinforcement detailing as Group one beams (i.e., 2Y12), however they were subjected to sustained loads of 30 kN. Corrosion of steel reinforcement was accelerated using a current density of 150 $\mu A/cm^2$ which was applied over a duration in the range of 30 – 48 days. The beams were also placed in a sodium chloride solution (3% NaCl). At the end of the corrosion phase, all beams were loaded to failure using a four-point bending test.

Test results showed that the deflection ratios of corroded beams were increased during the early stages of testing, as shown in Figure 2.30. However, as corrosion progressed, the rate of increase in deflection ratios was reduced. In addition, the researchers indicated that corroded beams with two or three steel bars, serving as the main tensile reinforcement, performed better than those which were reinforced with a single steel bar. In terms of ultimate load capacity, the researchers established a linear relationship between the residual flexural capacity of beams and the level of corrosion, as shown in Figure 2.31.

Du et al. (2013) conducted an experimental study to examine the structural performance of reinforced concrete beams under the coupled effects of reinforcement corrosion and loads. A total of five beams with dimensions of 100 x 150 x 1300 mm were constructed and tested. All beams were reinforced with longitudinal tensile reinforcement in the form of two 8 mm steel bars. Corrosion of steel reinforcement was accelerated using the direct impressed current technique with an applied constant current density of 250 $\mu A/cm^2$ during the first two weeks of testing and 500 $\mu A/cm^2$ during the remaining six weeks of testing. The beams were exposed to cycles of wet environment over 2 hours and air-dry environment over 22 hours. Besides, the corrosion process

was further accelerated by adding calcium chloride (3.5% by weight of cement) in the concrete mix. One beam served as a control beam (beam CB5) without reinforcement corrosion. Two beams were corroded within the middle portion over a length of either 150 mm (beam CB1) or 500 mm (beam CB2). The remaining two beams were corroded at the end region over a length of either 300 mm (beam CB3) or 650 mm (beam CB4), as shown in Figure 2.32. All beams were loaded to 60% of the beam ultimate load capacity using a three-point bending test.

Figure 2.33 shows the effect of corrosion on the time-dependent deflections and load-deflection relationships of beams. It is clear that the rate of increase in deflections of corroded beams was more than that of the control beam. The researchers indicated that beams with a short length of corroded tensile reinforcement (i.e., beams CB1, CB2 and CB3) failed at the sustained loading level in brittle manner due to the rupture of corroded reinforcement. The remaining beam (beam CB4) failed due to increased loads in a slightly more ductile manner when compared to other beams, however it also failed due to the rupture of corroded steel reinforcement.

Furthermore, the researchers investigated the presence of loads while corroding the beams by comparing their results with the experimental results in Du et al. (2007), in which the beams were corroded under no loads. There were several differences between the two experimental studies, including size of the beam, reinforcement area ratio, strength of concrete, applied current density, and length of corroded region. Therefore, the comparison was completed for beams which were corroded in the mid-span region only. Also, the results were compared in terms of percentages of reductions in load capacity and deflection, as shown in Figure 2.34. It can be clearly seen that the reduction rates in capacity and deflection were more drastic in the beams which were corroded under service loads (i.e., simultaneous) than those which were corroded under no loads (i.e., separate).

Liu et al. (2016) performed an experimental investigation to examine the performance of reinforced concrete beams under the coupled effects of reinforcement corrosion and different levels of loading. A total of twelve beams with dimensions of 150 x 250 x 2000 mm were tested in this study. Corrosion of steel reinforcement was accelerated by applying an external current by setting the voltage at a maximum value of 25 V and the current at a maximum value of 2.5 A. Two beams served as control specimens without reinforcement corrosion. Eight beams were corroded over a duration of 10 days under different levels of sustained loads equivalent to either 0%, 50%,

65%, or 80% of the beam ultimate load capacity. The remaining two beams were corroded over a duration of 15 days and sustained loads equivalent to 80% of the beam ultimate load capacity. All beams were loaded under a four-point bending test.

Test results revealed that the stiffness and ductility ratio of corroded beams were reduced due to the coupled effects of reinforcement corrosion and sustained loads, as shown in Figure 2.35. Furthermore, the researchers observed an increase in the level of corrosion in beams subjected to higher levels of sustained loading. Based on their results, the researchers indicated that the reduction in ultimate load capacity of corroded beams under service loads is dependent on the level of corrosion and level of sustained loading.

Li et al. (2018) carried out an experimental investigation to study the behavior of reinforced concrete beams under the coupled effects of reinforcement corrosion and different levels of loading. A total of thirteen beams with dimensions of 120 x 200 x 1700 mm were constructed and tested for this purpose. The beams were corroded using the direct impressed current technique with a current density of 1,000 $\mu A/cm^2$. The beams were exposed to cycles of wet environment for durations of 24 hours and air-dry environment for durations of 24 hours. The middle portion of beams with a total length of 1450 mm was placed in a sodium chloride solution (5% NaCl). The beams were corroded for a duration of either 5 days, 10 days, or 20 days. Sustained loads were equivalent to either 0%, 15%, 30%, or 60% of the beam ultimate loading capacity. All beams were loaded using a four-point bending test.

The researchers suggested using sectional area loss instead of mass loss to assess the level of corrosion in beams with pit corrosion attack. Accordingly, the relationship between sectional area loss and level of loading is shown in Figure 2.36(a). Clearly, the level of corrosion (i.e., sectional loss) increased with the increase of loading level. It can be also seen that, as the loading level increased from 30% to 60% of the beam ultimate loading capacity, the rate of increase in sectional loss was reduced in comparison to the increase of loading levels from 15% to 30% of the beam ultimate loading capacity. The researchers indicated that such behavior is likely due to the fact that the width of flexural cracks did not increase when loading levels increased from 30% to 60% of the beam ultimate loading capacity. In addition, the researchers did not observe a change in the width of corrosion cracks with the increase of loading levels. In terms of structural performance,

the ultimate load capacity of corroded beams was further reduced with the increase of loading levels, as illustrated in Figure 2.36(b).

Zhang et al. (2018) performed an experimental investigation to examine the structural behavior of reinforced concrete beams subjected to the coupled effects of reinforcement corrosion and loads. A total of eight beams with dimensions of 150 x 200 x 2200 mm were constructed and tested. Three beams served as control specimens without reinforcement corrosion, and they were loaded to either 17%, 33%, or 50% of the beam ultimate load capacity. Three beams were subjected to sustained loads equivalent to 33% of the beam ultimate load capacity while corroding the reinforcement using a current density of either 25 $\mu A/cm^2$, 50 $\mu A/cm^2$, or 100 $\mu A/cm^2$. Two beams were subjected to sustained loads equivalent to either 17% or 50% of the beam ultimate load capacity while corroding the reinforcement using a current density of 50 $\mu A/cm^2$. All beams were loaded using a four-point bending test.

Test results revealed that the coupling effects of reinforcement corrosion and loads had a slight influence on the width of flexural cracks of beams. Figure 2.37 compares the time-dependent deflections of control and corroded beams under sustained loads. The researchers indicated that deflections increased rapidly after the development of corrosion cracks, however the rate of increase slowed down when the cracks were filled up with corrosion by-products. Figure 2.38 shows the influence of corrosion current density on the time-dependent deflections of corroded beams subjected to loads equivalent to 33% of the beam ultimate load capacity. The researchers indicated that the use of higher current densities delayed the development of corrosion cracks due to more insufficient oxidization and less expansion of corrosion by-products.

2.6 Modeling of Corroded Reinforced Concrete Beams

Lundgren (2002) developed a three-dimensional finite element (FE) model using DIANA software to simulate reinforcement corrosion in concrete structures. Concrete and steel reinforcement were modeled using solid elements. Modeling corrosion of steel reinforcement and the bond behavior at the interface between steel reinforcement and concrete were combined into one interface element layer around the embedded reinforcement. This was incorporated into the FE models using a user-supplied subroutine. A frictional model was adopted to simulate the bond between the reinforcement and concrete. The corrosion model was developed to account for the expansion of corrosion by-products, as illustrated in Figure 2.39, in order to simulate splitting bond

failure. The volume expansion of rust was taken as two times the volume of steel reinforcement. The author assumed that the properties of the rust layer is similar to that of a granular material. The results of the FE model were in good agreement with the experimental results of pull-out tests as it was able to predict the degradation of bond strength due to reinforcement corrosion.

Dekoster et al. (2003) employed FE analysis to simulate the structural response of corroded reinforced concrete beams using CASTEM 2000 software. Concrete section was modeled using three-node triangular elements. Two material models were adopted to simulate the constitutive behavior of concrete, which were an elastic-plastic model based on a smeared crack approach and a damage model based on thermodynamics irreversible process. Steel reinforcement was modeled using two-node elements, with an elastic-plastic material model. The interface between steel reinforcement and concrete was modeled using rust elements. Rust section was modeled using three-node triangular elements with modified sectional properties, as illustrated in Figure 2.40. The properties of rust elements were influenced by the expansion of corrosion by-products. The researchers concluded by indicating that the effect of corrosion can be modeled by reducing the area of steel reinforcement, adopting a damage approach to simulate the material behavior of concrete, and incorporating the rust element in the FE model.

Coronelli and Gambarova (2004) developed a numerical procedure using FE analysis to evaluate the structural response of corroded reinforced concrete beams. Concrete section was modeled using four-node plane stress elements, while steel reinforcement was modeled using two-node truss elements. The bond between steel reinforcement and concrete was modeled using link elements. A schematic illustration of the two-dimensional FE model is shown in Figure 2.41. The effects of corrosion were modeled by: i) reducing the geometrical properties of concrete and steel reinforcement elements, and ii) modifying the material properties of concrete, reinforcement, and link elements.

Corrosion-induced cracks and deterioration of concrete cover were modeled by reducing the compressive strength of the affected elements. A previously developed model by Vecchio and Collins (1986) for cracked concrete elements was used for this purpose. The reduced compressive of corroded concrete $f_c^{c\prime}$ is expressed in the following:

$$f_c^{c\prime} = \frac{f_c'}{1 + k\,\varepsilon_1/\varepsilon_o} \tag{2.18}$$

where, f_c' is the compressive strength of non-corroded concrete, k is a coefficient that accounts for the roughness and diameter of reinforcing bars, ε_o is the strain of concrete at maximum compressive strength, and ε_1 is the average tensile strain of concrete perpendicular to compression, which is expressed in the following:

$$\varepsilon_1 = \frac{2\pi n(v_{rs} - 1)X}{b_o} \tag{2.19}$$

where, n is the number of reinforcing bars in compression, v_{rs} is the ratio of volume expansion of corrosion by-products relative to the non-corroded steel, X is the penetration depth of corrosion, and b_o is the original width of the beam.

Generalized corrosion was modeled by reducing the cross-sectional area of steel reinforcement, while pit corrosion was modeled by reducing the ultimate strain of steel reinforcement. The local bond-slip relationship between steel reinforcement and concrete was modeled by assuming a brittle post peak behavior to simulate splitting bond failure caused by corrosion. Figure 2.42 shows the modifications that were applied to the material properties of concrete, steel reinforcement, and bond in the FE model. The results of FE analysis were compared and verified with previous experimental studies. The researchers indicated that it is important to account for the bond between the corroded reinforcement and concrete, in order to evaluate the failure modes, ultimate load capacity, and ductility of corroded reinforced concrete beams.

Kallias and Rafiq (2010) modeled the behavior of corroded reinforced concrete beams using DIANA FE analysis software. Concrete was modeled using four-node plane stress elements, while steel reinforcement was modeled using two-node truss elements. To simulate the deterioration of concrete in the compressed cover of corroded beams, the compressive strength of concrete was reduced according to the expression proposed by Coronelli and Gambarova (2004). Generalized corrosion was modeled by reducing the area of steel reinforcement, while pit corrosion was modeled by reducing the yield strength of steel reinforcement. The bond between the corroded reinforcement and concrete was modeled using two-dimensional interface elements. The effect of corrosion on bond strength was modeled according to the expression proposed by El Maaddawy (2005). Figure 2.43 illustrates of modifications that were applied to the material properties of corroded beams.

The results of the FE models were verified and compared with corroded reinforced concrete beams available in the literature. The researchers indicated that loss of reinforcement area and deterioration of concrete were the main contributing parameters in the simulation of corroded reinforced concrete beams using FE analysis. It was also indicated that loss of bond did not influence the load-displacement relationship of corroded beams, and hence it can be ignored if longitudinal steel reinforcement are properly anchored.

Hanjari et al. (2011) employed FE analysis to predict the response of corroded reinforced concrete beams. The effects of corrosion were integrated into two-dimensional FE models. Generalized and pit corrosion were modeled by reducing the area of steel reinforcement. Specifically, pit corrosion was modeled by randomly distributing localized elements along the length of stirrups. The length of each element was assumed to be equal to twice the diameter of stirrup. In addition, the ductility of steel bars was reduced due to corrosion. Spalling of corroded concrete was modeled by removing concrete elements from the affected zone in the FE models. Tensile behavior of cracked concrete due to corrosion was modeled by reducing the tensile strength of concrete using the same proportions as those used to reduce the compressive strength of corroded concrete in accordance with expression proposed by Coronelli and Gambarova (2004). The reduced tensile strength of corroded concrete f_t^c is expressed in the following:

$$f_t^c = \frac{f_c^{c\prime}}{f_c^{\prime}} f_t \tag{2.20}$$

where, f_t is the tensile strength of non-corroded concrete. Figure 2.44 shows the discretized FE model of beams, along with the modified stress-strain curves of the corroded concrete in tension and compression. The effect of corrosion on bond strength was modeled by shifting the local bond-slip relationship based on the level of corrosion. The results of the FE models were in good agreement with experimental results available in the literature. The researchers indicated that both types of corrosion (i.e., generalized and pit) should be considered while modeling the response of corroded reinforced concrete beams.

Ou and Nguyen (2014) investigated the influence of corrosion on the plastic hinge length of reinforced concrete beams using FE analysis. Concrete section was modeled using four-node plane stress elements, while the material behavior of concrete was modeled using the total strain crack model with rotating cracks. Deterioration of concrete due to corrosion was modeled by reducing

the compressive strength of concrete according to the expression proposed by Coronelli and Gambarova (2004). Steel reinforcement was modeled using two-node truss elements, while its behavior was modeled using Mander material model. Generalized corrosion was modeled by reducing the area of steel reinforcement. Pit corrosion was modeled by reducing the mechanical properties of steel reinforcement. The effect of corrosion on bond strength between steel reinforcement and concrete was modeled according to the expression proposed by El Maaddawy (2005). Figure 2.45 illustrates the modifications that were implemented in modeling the corroded beams.

The predictions of the FE model were validated with previous experimental studies. The verified model was then employed to conduct a parametric study to examine the effect of corrosion level, compressive strength of concrete, tensile reinforcement ratio, and shear span on the plastic hinge length of reinforced concrete beams. The results revealed that the plastic hinge length of corroded beams was influenced by the level of corrosion and shear span. It was also found that the compressive strength of concrete and tensile reinforcement ratio did not influence the plastic hinge length of corroded beams.

Al-Sakkaf (2016) developed a three-dimensional FE model using ABAQUS software to simulate the behavior of corroded reinforced concrete beams. Concrete and steel reinforcement were modeled using eight-node solid elements. The concrete damaged plasticity model was used to simulate the material behavior of concrete. An elastic-plastic model was used to simulate the material behavior of steel reinforcement. Compressive and tensile strength of concrete were reduced using the proposed expression by Coronelli and Gambarova (2004) in order to simulate corrosion-induced cracking. Generalized corrosion was modeled by reducing the area of steel reinforcement, while pit corrosion was modeled by reducing the mechanical properties of steel reinforcement. The bond strength between the corroded reinforcement and concrete was modeled using the expression proposed by El Maaddawy (2005).

The predictions of the FE model were compared and verified with previous experimental studies of corroded reinforced concrete beams. Figure 2.46 shows that the predictions by the FE analysis were in good agreement with the experimental load-displacement curves of the control and corroded beams.

Jnaid and Aboutaha (2016) carried out FE analysis and analytical investigations to predict the residual capacity of corroded reinforced concrete beams. Three-dimensional FE model was developed using ANSYS software. Concrete was modeled using three-dimensional solid elements with Willam and Warnke's material model. Steel reinforcement was modeled using three-dimensional link elements with an elastic-plastic material model. Corrosion of steel reinforcement was modeled by reducing the cross-sectional area and yield strength of steel bars within the corroded region only. Loss of bond between steel reinforcement and concrete within the corroded region of beams was modeled using spring elements, as illustrated in Figure 2.47. The researchers assumed a complete loss of bond within the corroded region of beams.

The predictions of the FE analysis were verified with previous experimental studies of corroded reinforced concrete beams. After verifying the FE model, the researchers developed detailed and simplified analytical modeling tools to predict the residual flexural capacity of corroded reinforced concrete beams. The researchers indicated that the reduction in ultimate load capacity of corroded beams with high levels of corrosion is primarily attributable to the loss of steel reinforcement area and strength.

2.7 Summary of Previous Studies and Research Gaps

A review of previous research studies revealed that there are several consequences associated with corrosion of reinforcement in concrete beams. It was reported that corrosion of reinforcement can change an anticipated flexure response of beams to a brittle failure (Rodriguez et al., 1997). Although numerous experimental research projects were devoted to understand the flexural behavior of corroded reinforced concrete beams, the majority did not consider the existence of service loads while corroding the beams. Corroding the beams under loads is a more realistic representation of in-service conditions since it simulates the interaction between the presence of flexural cracks and the initiation/progression phases of corrosion. It was reported that the deflections of beams subjected to the simultaneous effects of reinforcement corrosion and service loads were increased with the increase of corrosion levels (Ballim and Reid, 2003). Furthermore, it was reported that increasing the level of loading caused a further reduction in the ultimate load capacity of corroded beams (Li et al., 2018).

While there is a number of research studies that examined the coupled effects of reinforcement corrosion and service loads, limited research attempts were conducted to examine the damage and

failure mechanisms of reinforced concrete beams at the end of their service life. As corrosion initiates, the ultimate load capacity and ductility of corroded reinforced concrete beams are reduced over time, resulting in a reduced service life. Du et al. (2013) conducted an experimental study to examine the behavior of corroded beams at the end of their service life, however the main focus of their work was on the effect of location and length of the corroded region within the beams.

The main objective of this research project is to increase understanding of the flexural behavior of reinforced concrete beams subjected to the coupled effects of reinforcement corrosion and service loads. A particular attention is given to the coupling effects of reinforcement corrosion and different levels of service loads for small-scale and large-scale reinforced concrete beams. This will address the interaction between the presence of flexural cracks and serviceability of corroded beams.

In addition, the review of previous experimental research studies on the influence of corrosion on the mechanical properties of steel bars revealed that the majority of test coupons were either corroded bare steel bars or corroded bars embedded in concrete samples. However, the presence of flexural cracks in reinforced concrete beams subjected to service loads, may change the distribution of corrosion and the sectional loss of reinforcement area along the affected region. It is well-established that the ductility of corroded steel bars is strongly influenced by the non-uniform distribution of corrosion (Du et al., 2005). Therefore, the presence of flexural cracks will be addressed by retrieving the corroded steel bars from corroded beams under service loads.

Finally, the review of previous numerical research studies revealed that FE analysis can be implemented to simulate the response of corroded reinforced concrete beams. A simplified approach can be adopted to incorporate corrosion-induced damage in the FE models to predict the failure modes, ultimate load capacity, and ductility of corroded beams. However, simulating the presence of service loads in corroded reinforced concrete beams using FE analysis is scarce in the literature. Experimentally, it was reported that the ultimate load capacity of corroded beams is dependent on the levels of corrosion and sustained loading (Liu et al., 2016). Therefore, the simultaneous presence of service loads and corrosion of reinforcement will be addressed in this research project to ensure accurate predictions of ultimate load capacity and ductility of corroded reinforced concrete beams.

Table 2.1: Summary of current densities adopted in previous research studies

Study	Current density (μA/cm^2)	Test type
Zhang et al. (2021)	600	tensile test–embedded bars
Zhang et al. (2018)	25 / 50 / 100	flexure–beams
Li et al. (2018)	1,000	flexure–beams
Sun et al. (2018)	400	tensile test–embedded bars
Azam et al. (2016)	200	flexure–beams
Ou et al. (2016)	600	tensile test–embedded bars
Tang et al. (2014)	80 – 220	tensile test–embedded bars
Du et al. (2013)	250	flexure–beams
Hariche et al. (2012)	150	flexure–beams
Zhang et al. (2012)	100	tensile test–embedded bars
Malumbela et at. (2009)	189	flexure–beams
Torres-Acosta et al. (2007)	80	flexure–beams
Azad et al. (2007)	2,000 / 3,000	flexure– beams
Du et al. (2007)	250 – 900	flexure–beams
Du et al. (2005)	500 / 1,000 / 2,000	tensile test–embedded bars
Cairns et al. (2005)	50 – 500	tensile test–embedded bars
Ballim and Reid (2003)	400	flexure–beams
Almusallam (2001)	2,000	tensile test–embedded bars
Mangat and Elgarf (1999)	1,000 / 2,000 / 3,000 / 4,000	flexure–beams
Rodriguez et al. (1997)	100	flexure–beams
Al-Sulaimani et al. (1990)	2,000	pullout test–reinforced concrete

Table 2.2: Experimental test program by Yoon et al. (2000)

Beam	% of ultimate load	Ponding stage	Current stage
AP00	0	NA	NA
AS45	45% Sustanied	NA	NA
AS75	75% Sustanied	NA	NA
NP45	45% Preload	NaCl	50 days after ponding
NP75	75% Preload	NaCl	50 days after ponding
NS45	45% Sustanied	NaCl	50 days after ponding
NS75	75% Sustanied	NaCl	50 days after ponding
NS00	0	NaCl	After moist curing
NS20	20% Sustanied	NaCl	After moist curing
NS60	60% Sustanied	NaCl	After moist curing

Table 2.3: Experimental results of RC beams tested by El Maaddawy and Topper (2005)

Group	Beam	Crack		Yield		Ultimate		Corrosion level (%)
		P_{cr}, kN	Δ_{cr}, mm	P_y, kN	Δ_y, mm	P_u, kN	Δ_u, mm	
Control	Virgin	10.79	0.92	67.20	15.63	75.00	73.33	NA
A	CN-50	11.02	1.07	61.71	14.39	70.22	88.96	8.9
	CN-110	11.87	1.16	57.39	13.91	66.76	78.39	14.2
	CN-210	11.28	1.25	50.74	12.96	60.02	62.38	22.2
	CN-310	11.06	1.35	44.16	11.74	53.27	58.96	31.6
B	CS-50	NA	NA	59.88	12.34	66.08	73.41	9.7
	CS-110	NA	NA	55.10	8.93	64.59	85.86	15.4
	CS-210	NA	NA	50.10	8.41	64.18	79.90	22.8
	CS-310	NA	NA	46.14	7.42	56.87	66.82	30.0

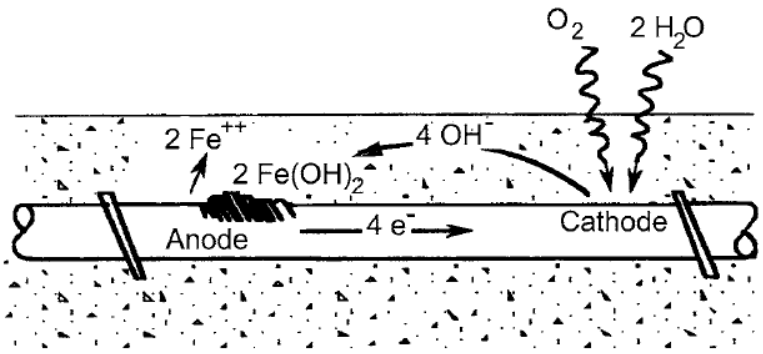

Figure 2.1: Corrosion of embedded steel reinforcement in concrete structures (Richardson, 2002)

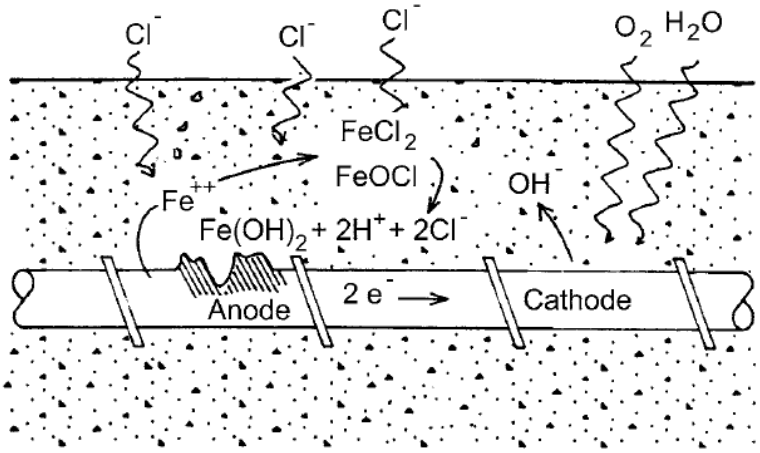

Figure 2.2: Chloride-induced corrosion (Richardson, 2002)

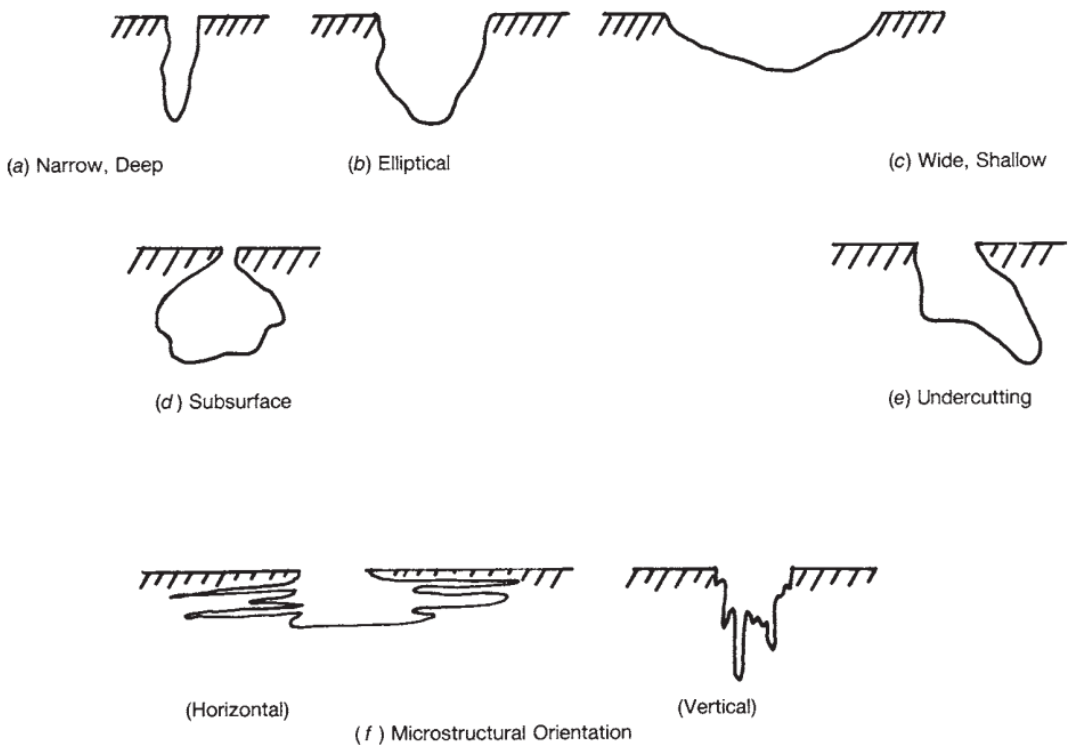

Figure 2.3: Cross-sectional area of different pit shapes (ASTM, 2005)

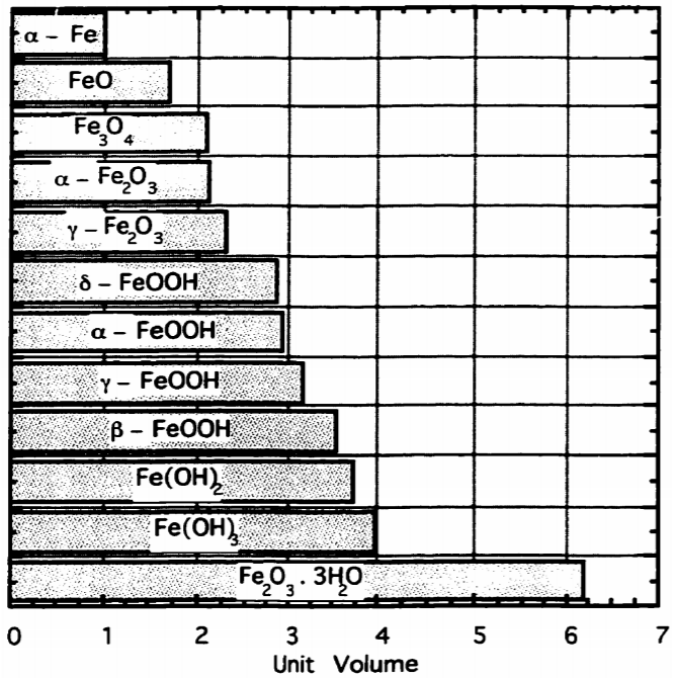

Figure 2.4: Relative volume of corrosive by-products (taken from Marcotte, 2001)

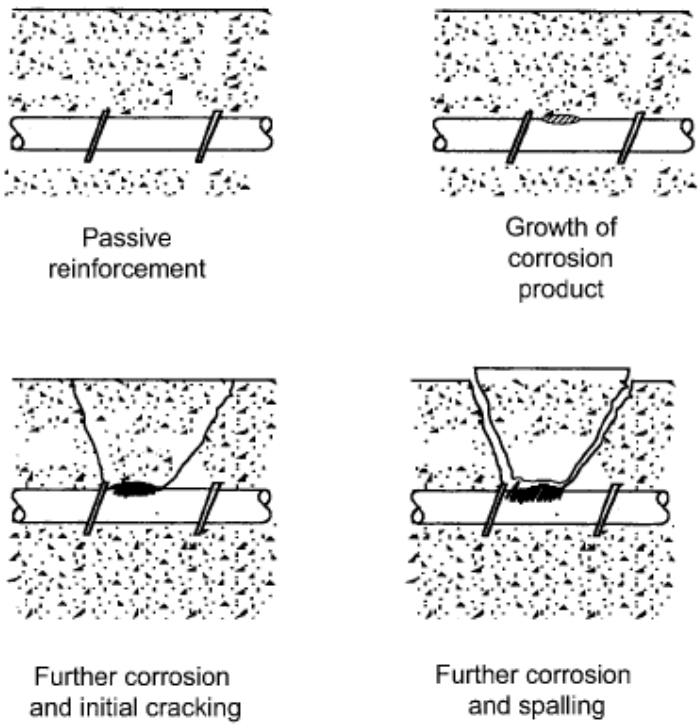

Figure 2.5: Progression of corrosion in reinforced concrete structures (Richardson, 2002)

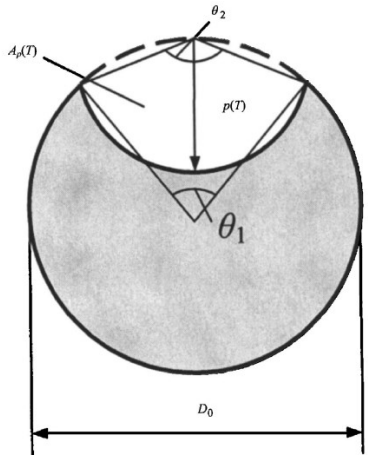

Figure 2.6: Assumption of the configuration shape of pit corrosion (Val et al., 2007)

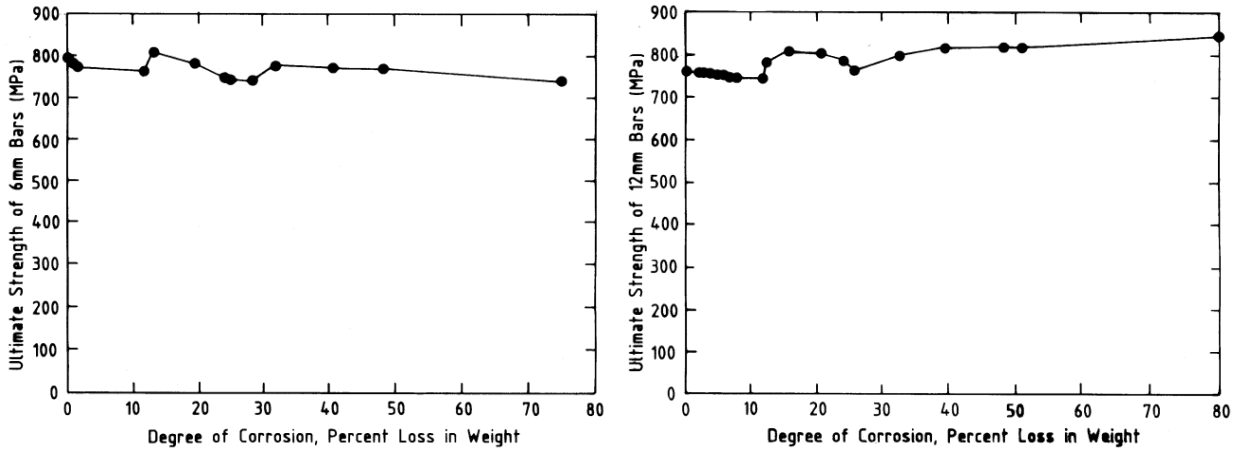

(a) 6 mm (b) 12 mm

Figure 2.7: Effect of corrosion on the ultimate tensile strength of steel bars tested by Almusallam (2001)

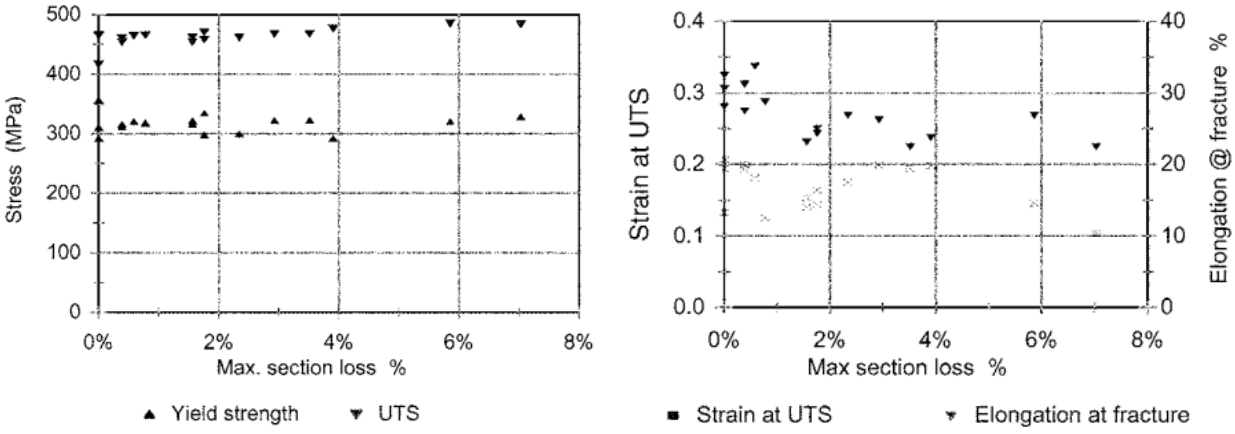

(a) strength (b) ultimate strain

Figure 2.8: Effect of localized corrosion on the mechanical properties of steel bars tested by Cairns et al. (2005)

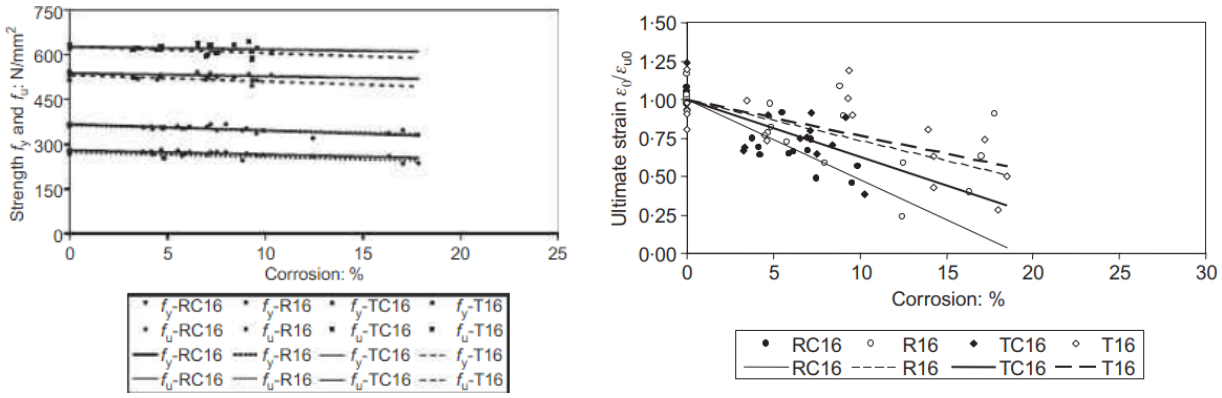

(a) strength (b) ductility

Figure 2.9: Effect of corrosion on the mechanical properties of steel bars tested by Du et al. (2005)

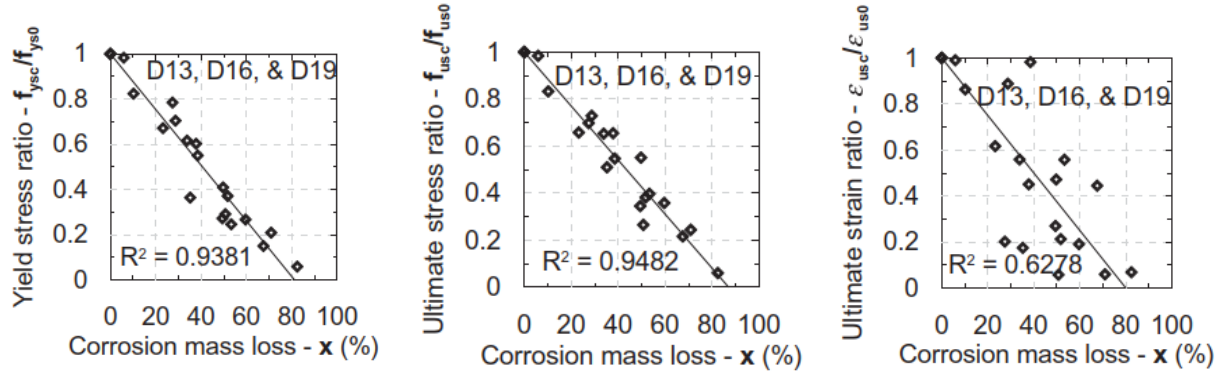

(a) yield strength (b) ultimate strength (c) ultimate strain

Figure 2.10: Mechanical properties of naturally corroded steel bars tested by Ou et al. (2016)

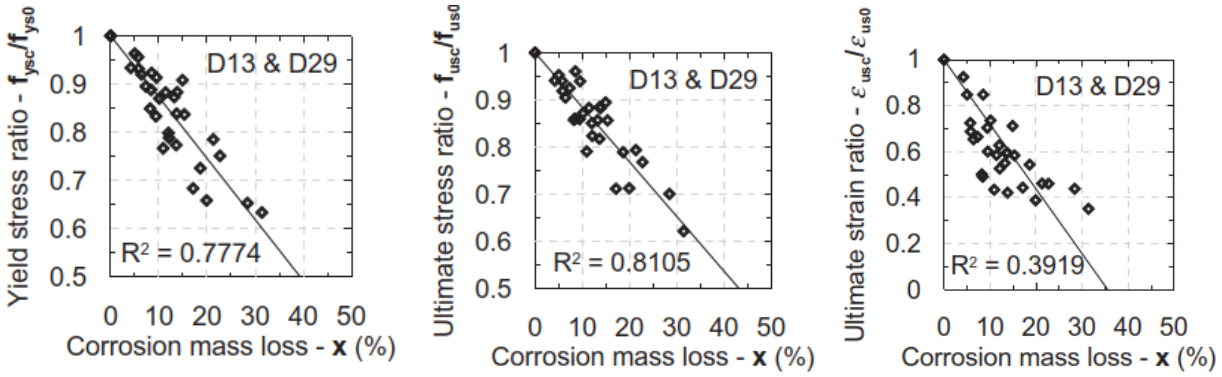

(a) yield strength (b) ultimate strength (c) ultimate strain

Figure 2.11: Mechanical properties of artificially corroded steel bars tested by Ou et al. (2016)

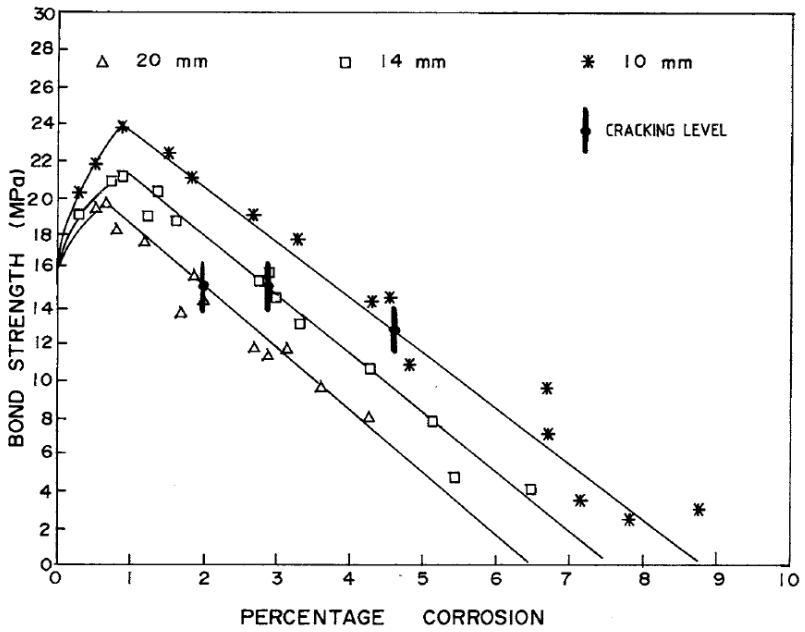

Figure 2.12: Effect of corrosion on the bond strength of reinforced concrete samples tested by Al-Sulaimani et al. (1990)

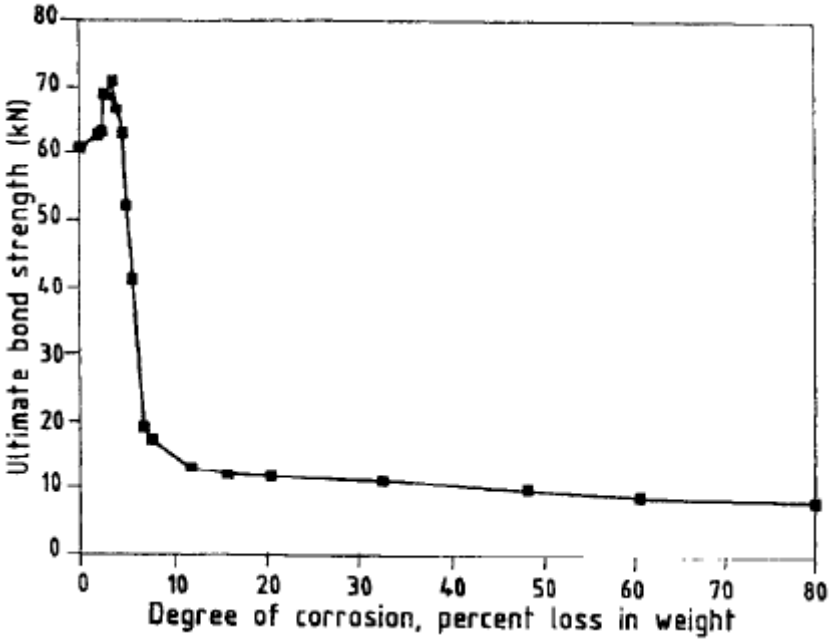

Figure 2.13: Effect of corrosion on the bond strength of reinforced concrete samples tested by Almusallam et al. (1996)

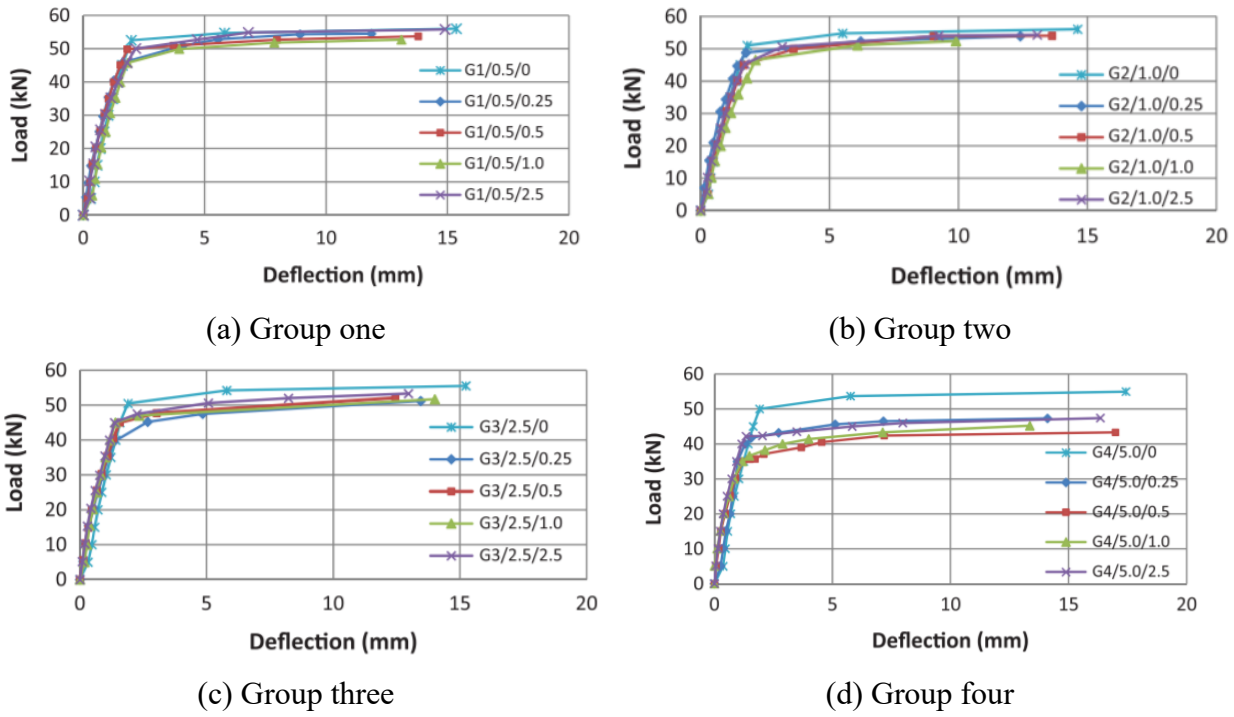

(a) Group one

(b) Group two

(c) Group three

(d) Group four

Figure 2.14: Effect of current density on the load-displacement relationship of corroded RC beams tested by Nguyen and Lambert (2018)

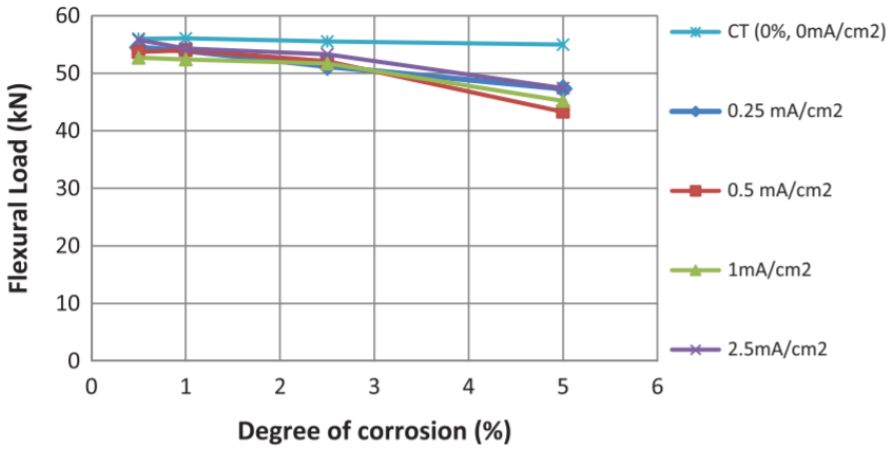

Figure 2.15: Effect of current density on the ultimate load capacity of corroded RC beams test by Nguyen and Lambert (2018)

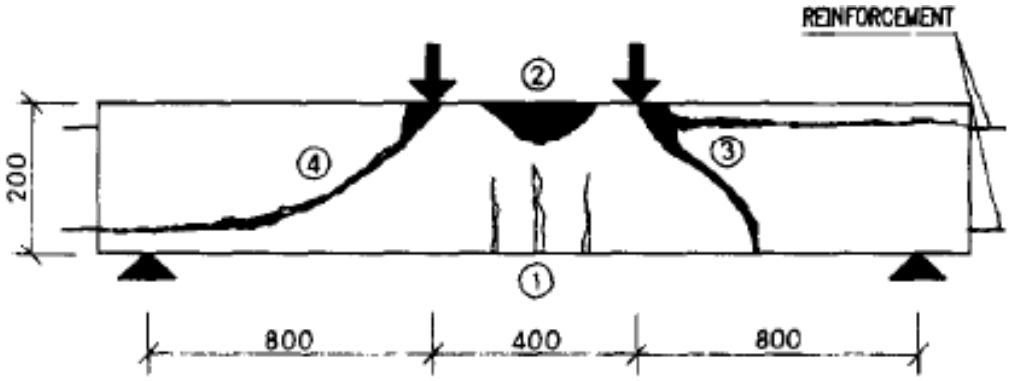

Figure 2.16: Failure modes of non-corroded and corroded RC beams tested by Rodriguez et al. (1997)

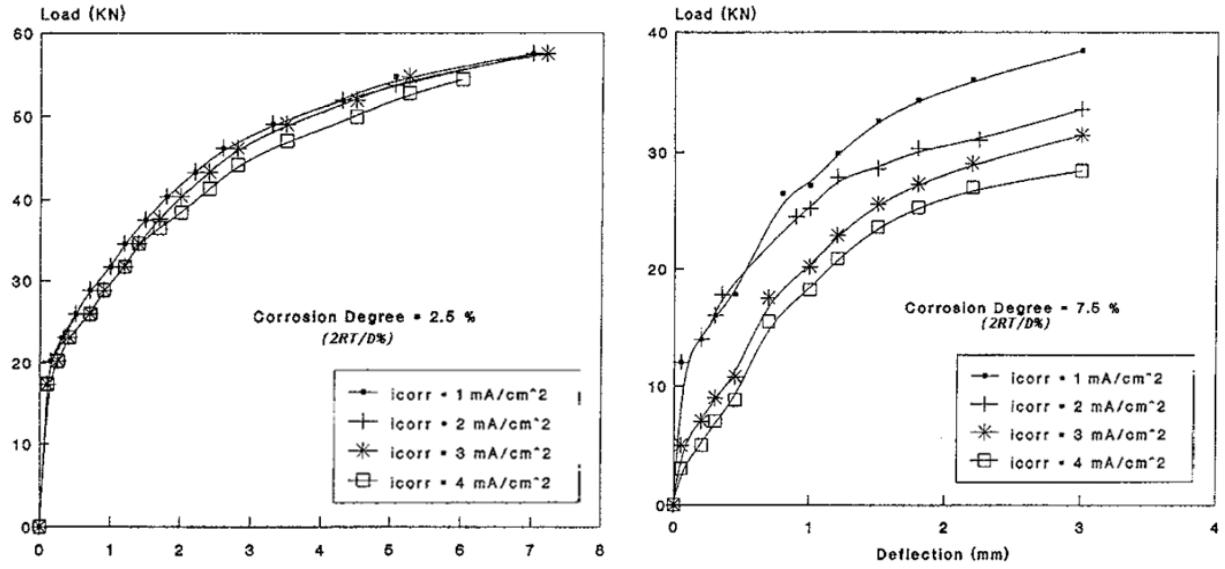

(a) Corrosion level of 2.5% (b) Corrosion level of 7.5%

Figure 2.17: Load-displacement relationship of corroded RC beams tested by Mangat and Elgarf (1999)

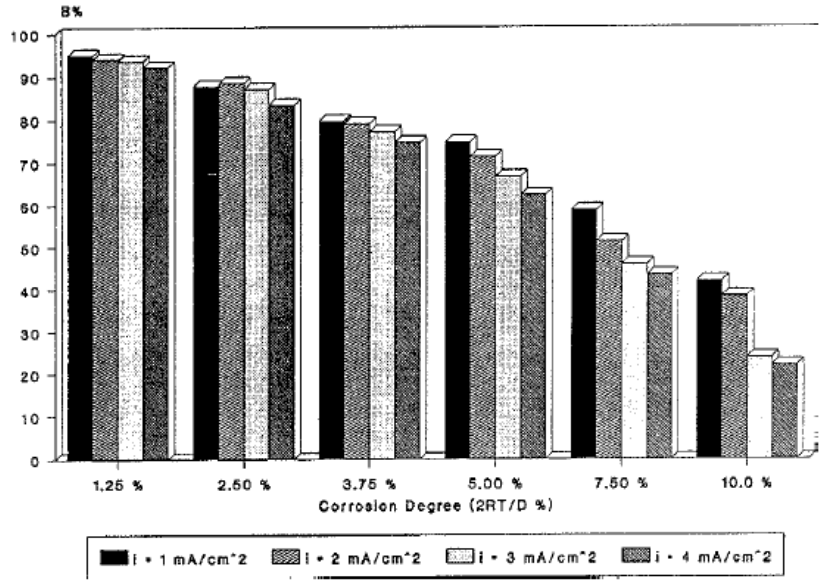

Figure 2.18: Effect of corrosion level on the flexural capacity of RC beams tested by Mangat and Elgarf (1999)

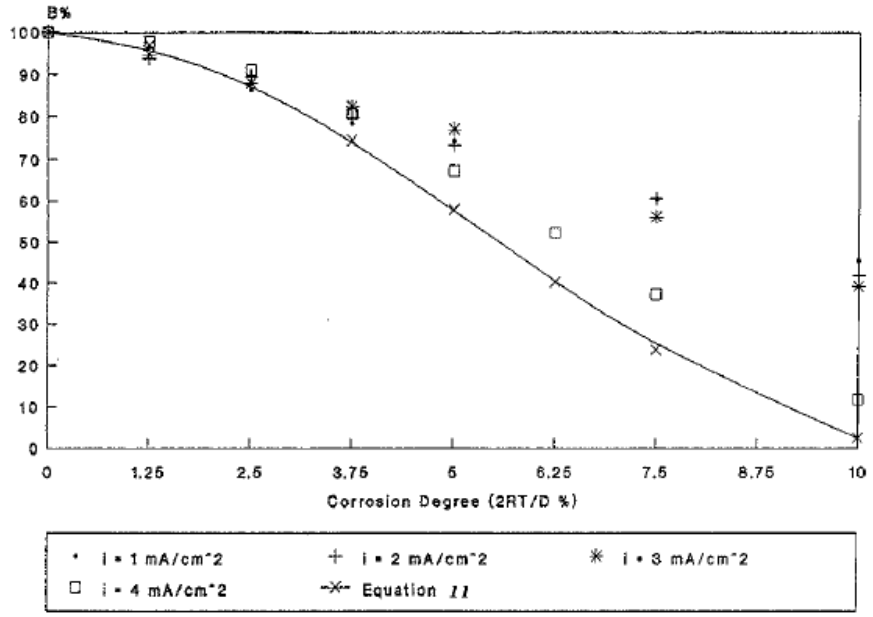

Figure 2.19: Predictive results of the model developed by Mangat and Elgarf (1999)

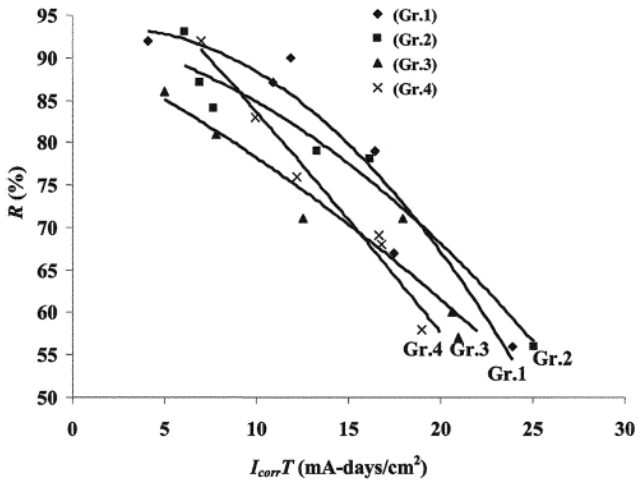

Figure 2.20: Relationship between residual flexural capacity and corrosion activity index of corroded RC beams tested by Azad et al. (2007)

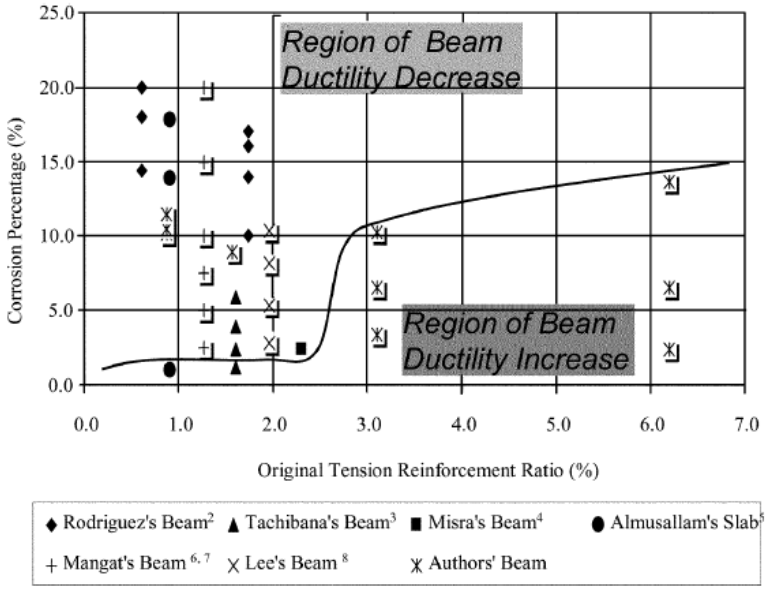

Figure 2.21: Effect of corrosion on the ductile behavior of RC beams tested by Du et al. (2007)

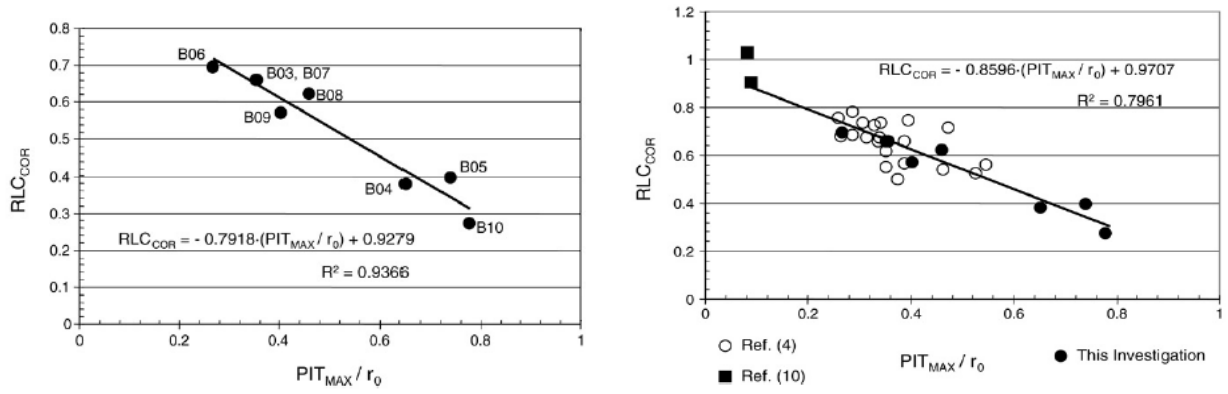

(a) Torres-Acosta et al. (2007) (b) Comparison with other studies

Figure 2.22: Correlation between residual flexural capacity ratio and maximum pit depth of corroded RC beams (Torres-Acosta et al., 2007)

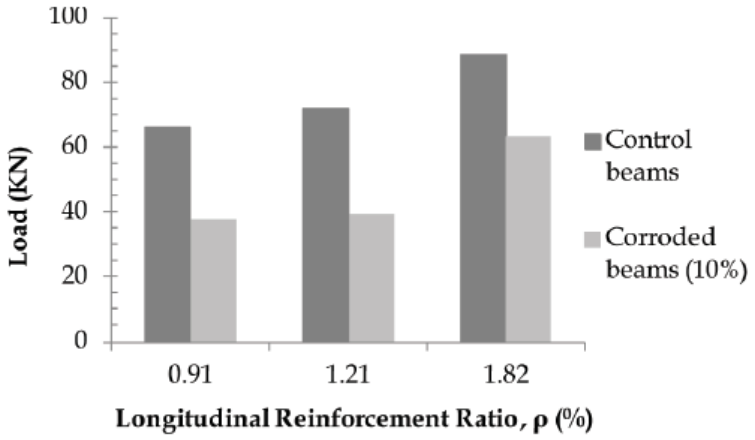

Figure 2.23: Effect of corrosion on ultimate load capacity of RC beams tested by Azam et al. (2016)

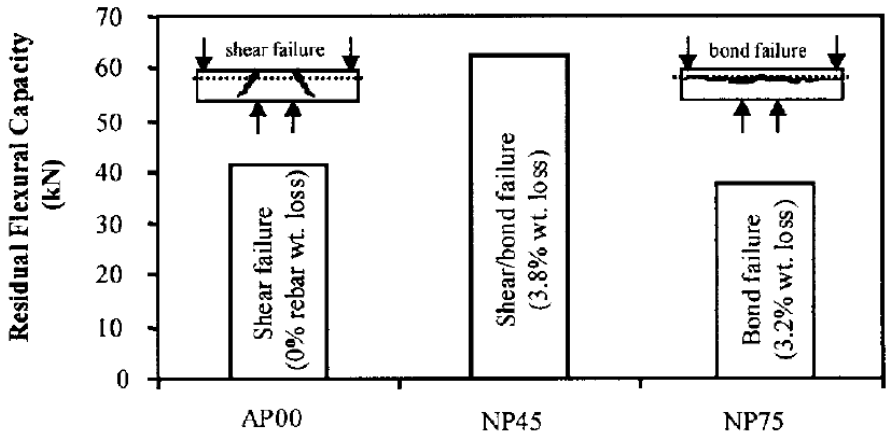

(a) Preloaded beams

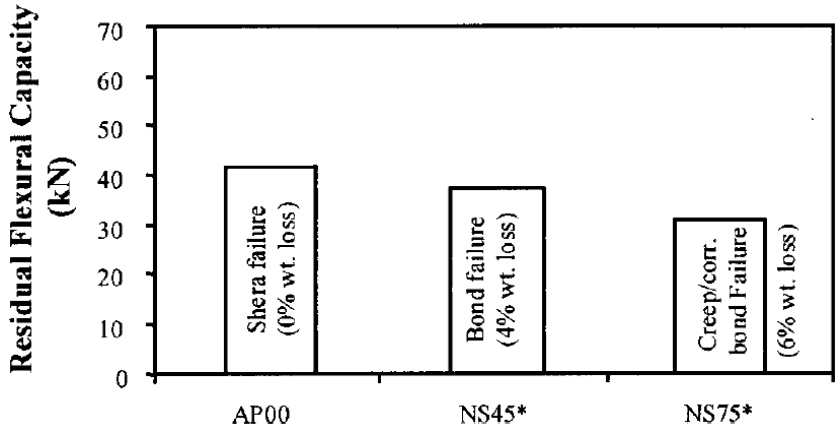

(b) Beams subjected to sustained loads with current being applied 50 days after ponding

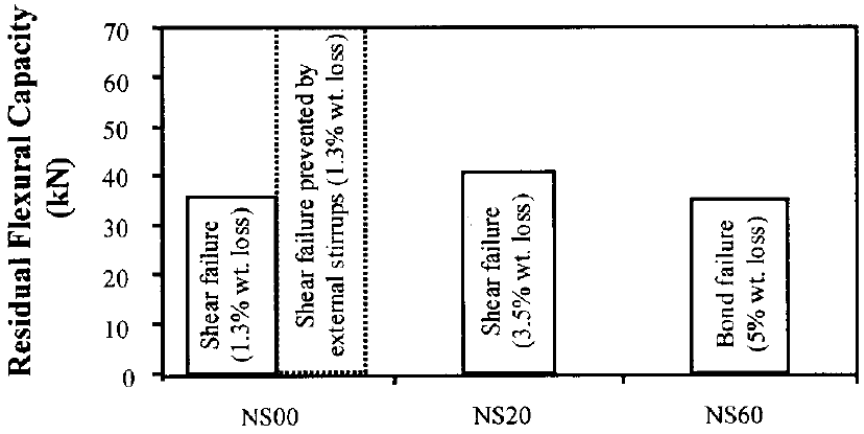

(c) Beams subjected to sustained loads with current being applied after moist curing

Figure 2.24: Failure modes and residual flexural capacities of corroded RC beams tested by Yoon et al. (2000)

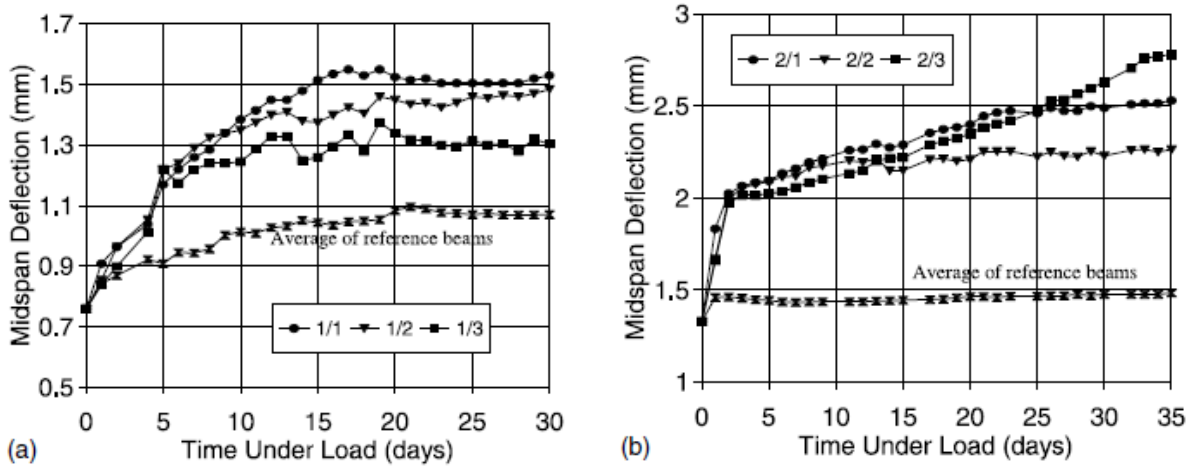

(a) Series 1 beams (b) Series 2 beams

Figure 2.25: Mid-span deflections of RC beams tested by Ballim and Reid (2003)

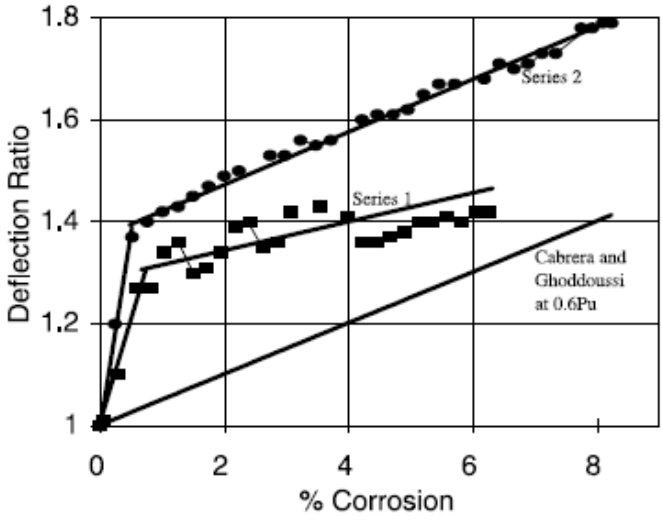

Figure 2.26: Relationship between deflection ratio and level of corrosion (Ballim and Reid, 2003)

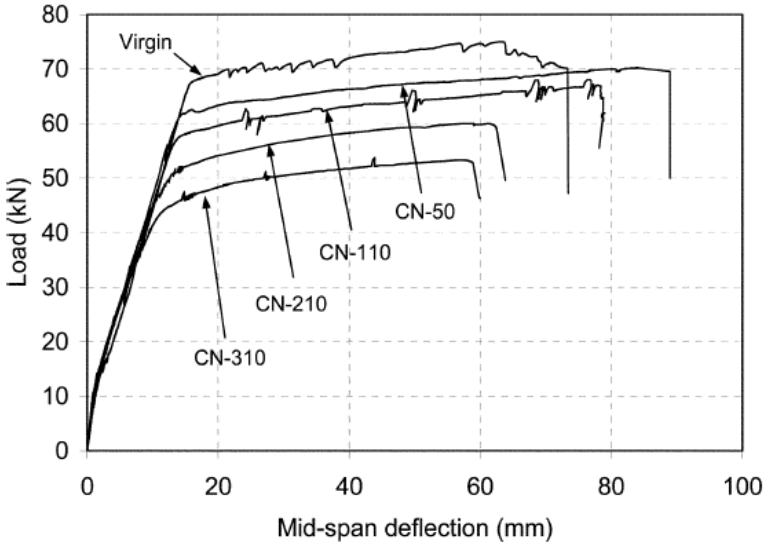

(a) Group A – beams under no loads

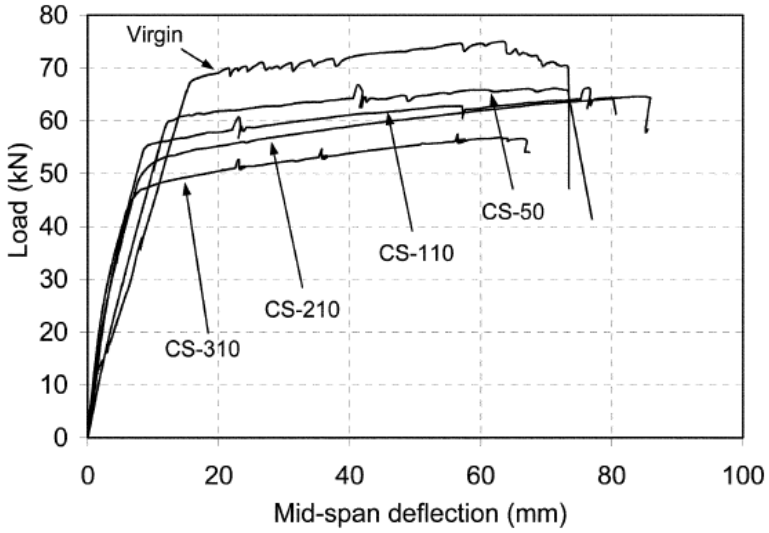

(b) Group B – beams under loads

Figure 2.27: Load-displacement relationship of RC beams tested by El Maaddawy and Topper (2005)

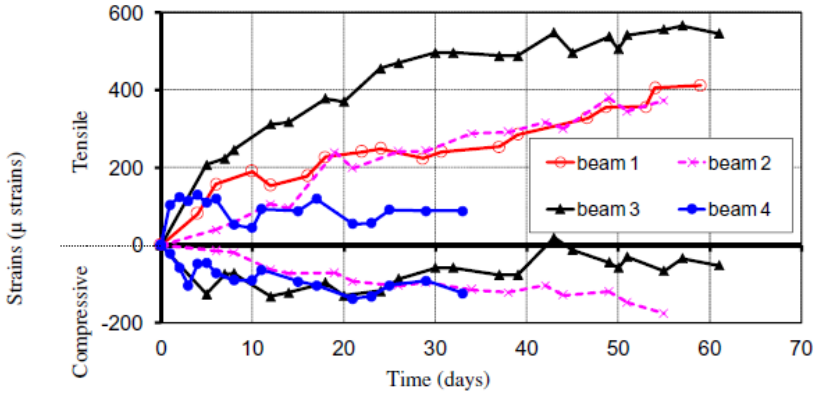

Figure 2.28: Longitudinal tensile and compressive strains readings of RC beams tested by Malumbela et al. (2009)

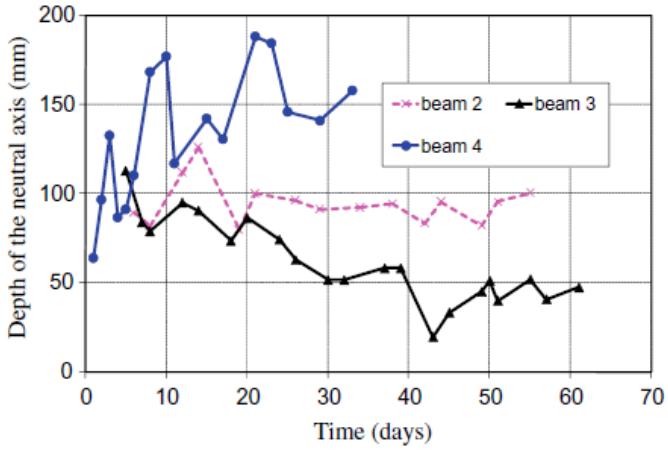

Figure 2.29: Depth of neutral axis of RC beams tested by Malumbela et al. (2009)

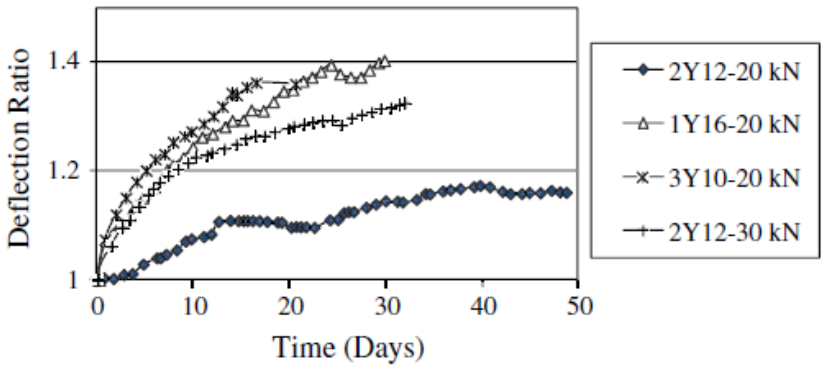

Figure 2.30: Deflection ratio of corroded RC beams tested by Hariche et al. (2012)

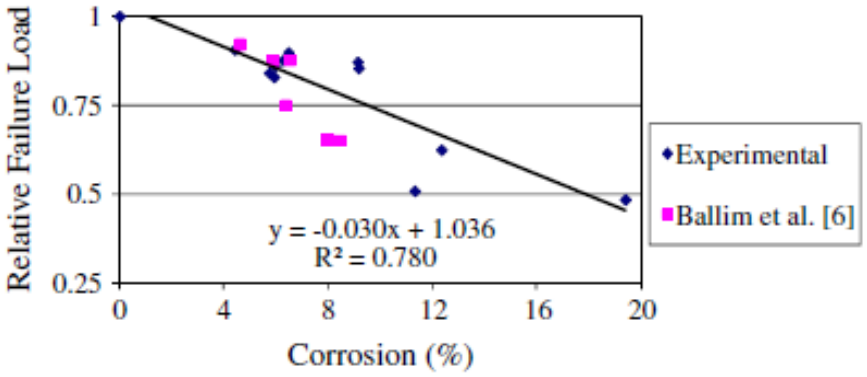

Figure 2.31: Correlation between relative failure load and corrosion level of RC beams tested by Hariche et al. (2012)

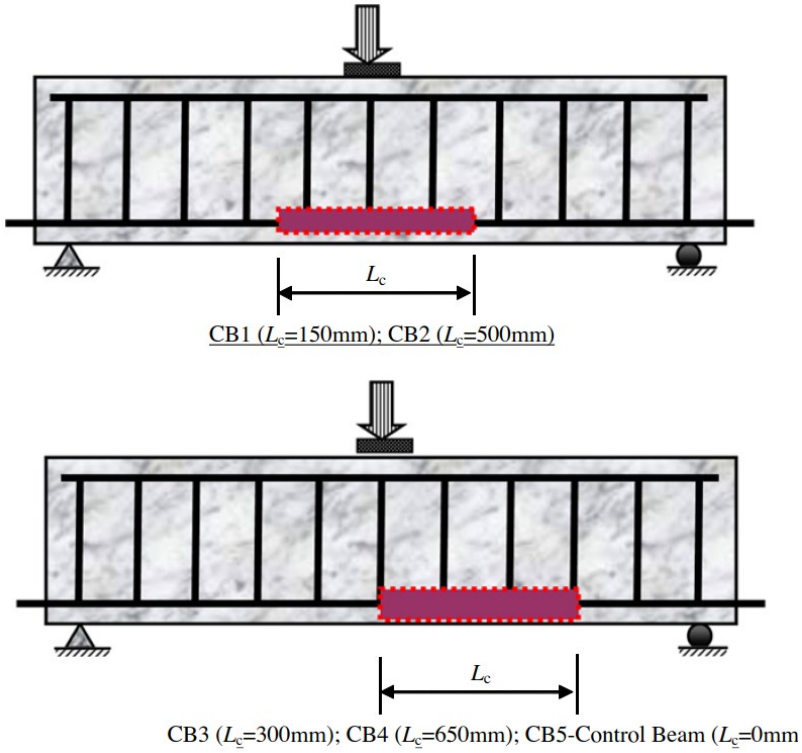

Figure 2.32: Test parameters and setup by Du et al. (2013)

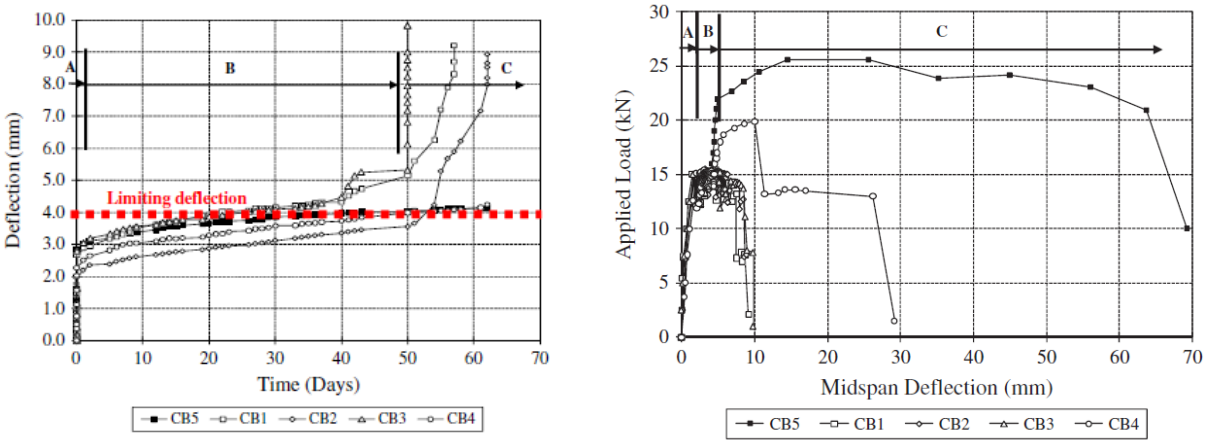

(a) Time-dependent deflections (b) Load-deflection relationships

Figure 2.33: Effect of reinforcement corrosion on the behavior of RC beams tested by Du et al. (2013)

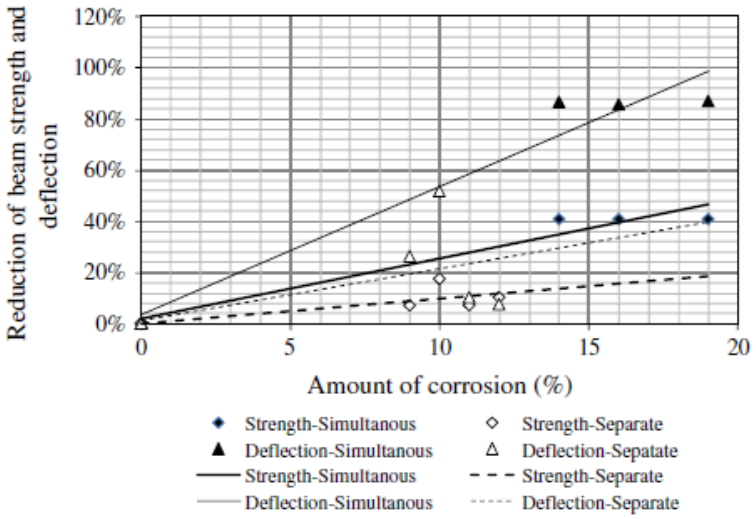

Figure 2.34: Comparison between the simultaneous and separate effects of reinforcement corrosion and loads by Du et al. (2013)

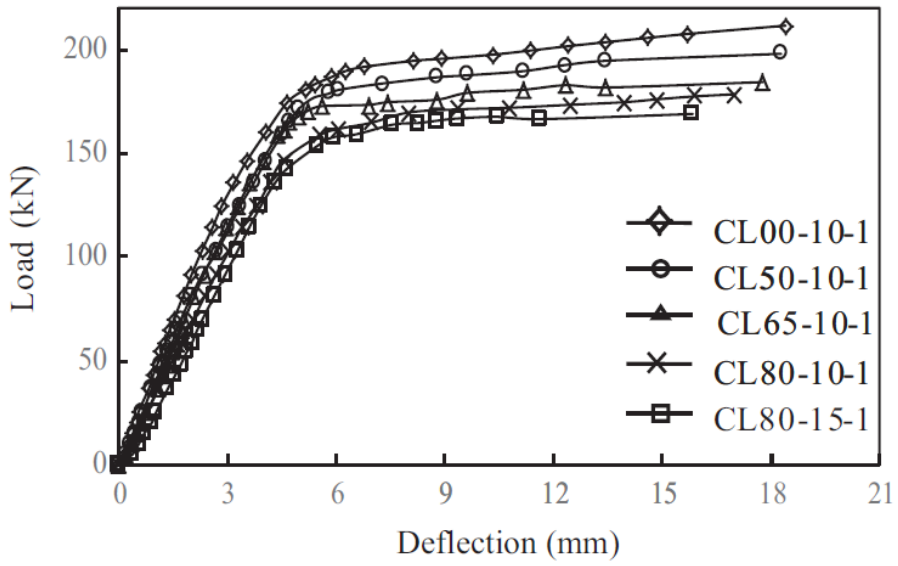

(a)

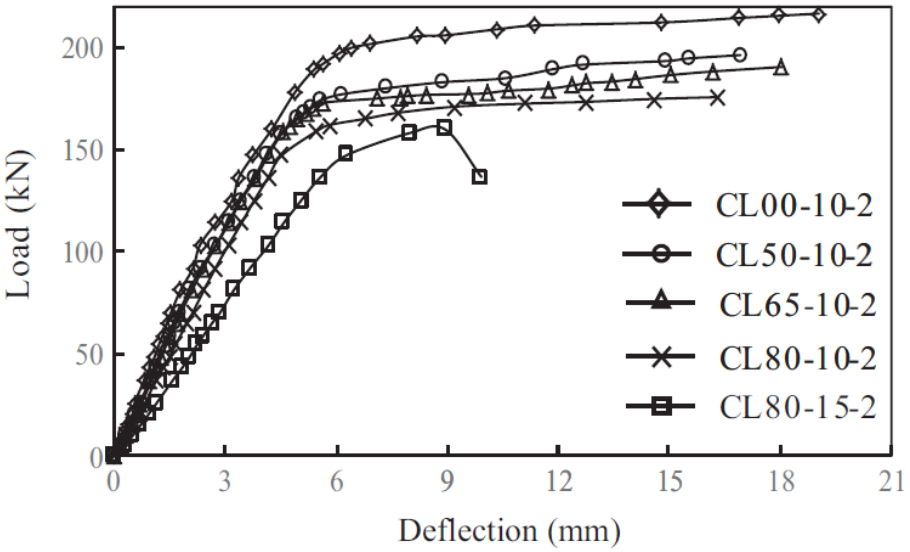

(b)

Figure 2.35: Load-deflection relationships of corroded RC beams tested by Liu et al. (2016)

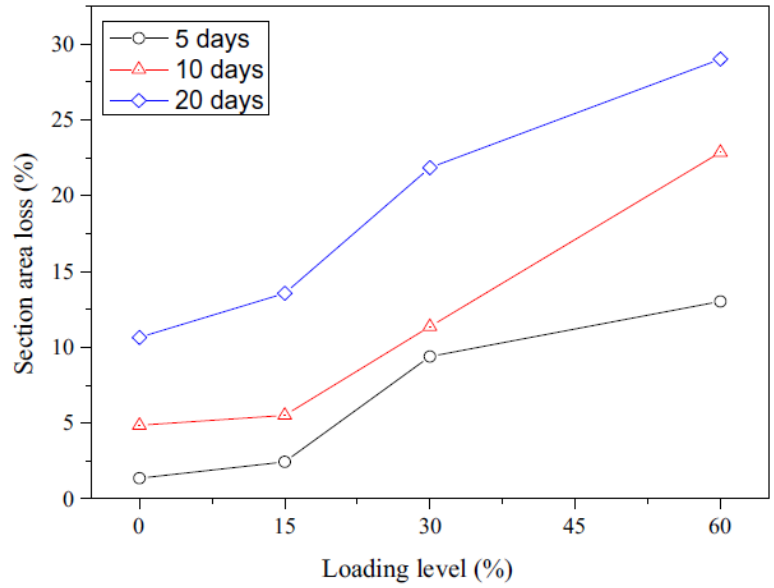

(a) Sectional area loss

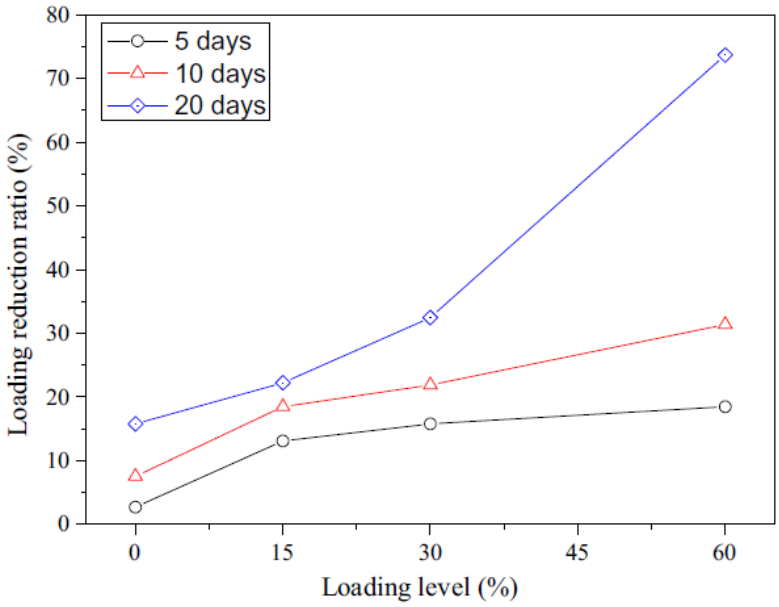

(b) Ultimte load capacity

Figure 2.36: Effect of loading level on the behavior of corroded RC beams tested by Li et al. (2018)

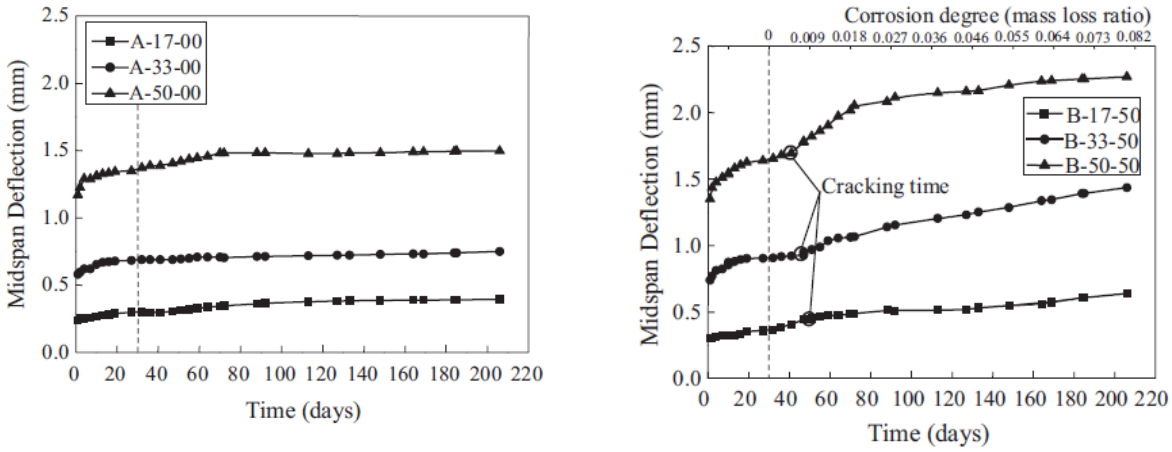

(a) Control beams (b) Corroded beams

Figure 2.37: Effect of loading level on the time-dependent deflections of RC beams tested by Zhang et al. (2018)

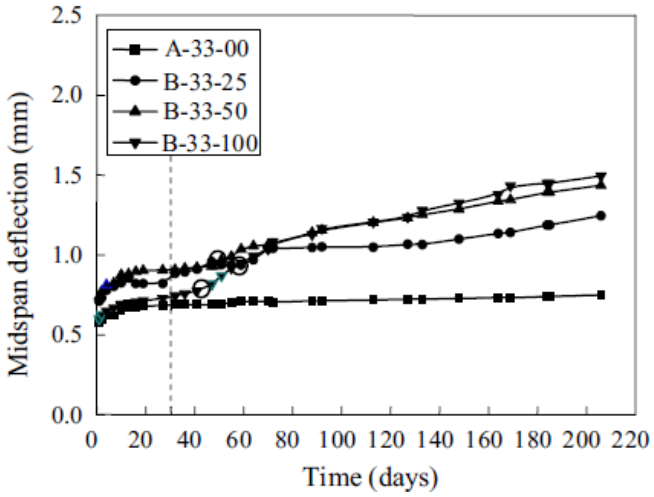

Figure 2.38: Effect of current density on the time-dependent deflections of RC beams tested by Zhang et al. (2018)

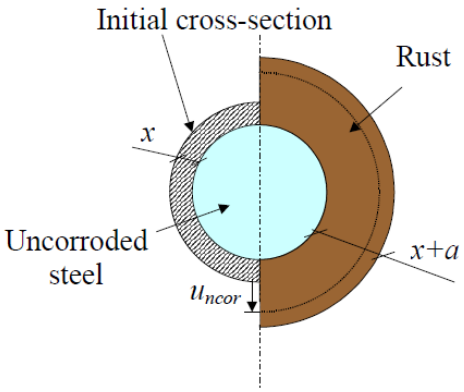

Figure 2.39: A schematic illustration of the corrosion model by Lundgren (2002)

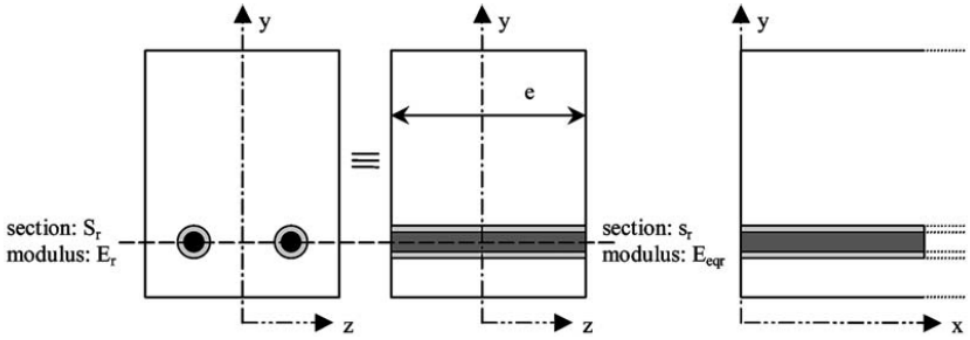

Figure 2.40: A schematic illustration of the modified sectional properties of rust elements by Dekoster et al. (2003)

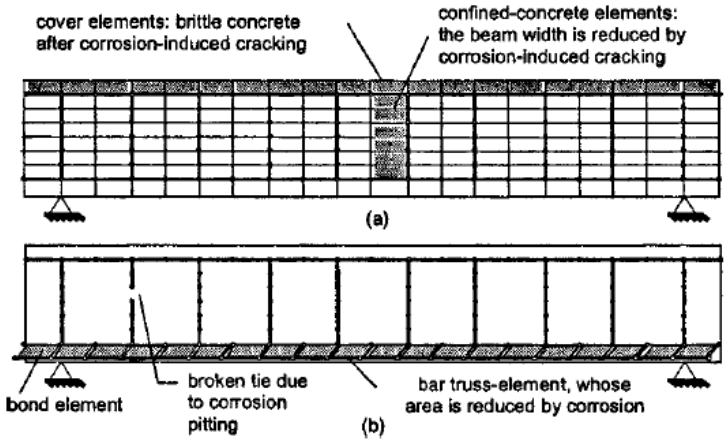

Figure 2.41: A schematic illustration of the finite element model developed by Coronelli and Gambarova (2004)

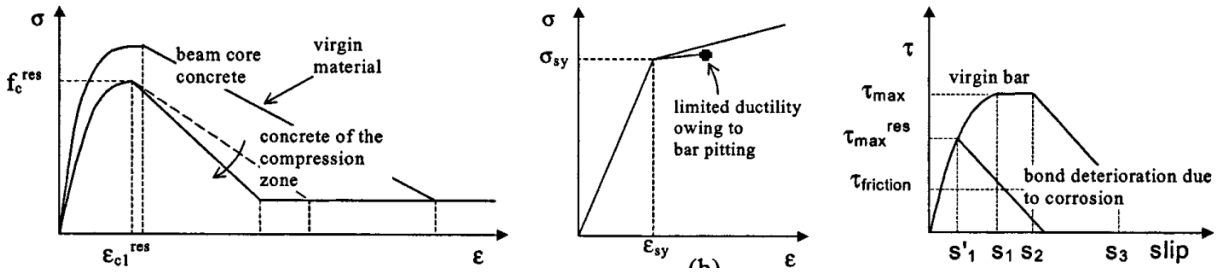

(a) Concrete (b) Reinforcement (c) Local bond-slip

Figure 2.42: Material properties of non-corroded and corroded finite element models by Coronelli and Gambarova (2004)

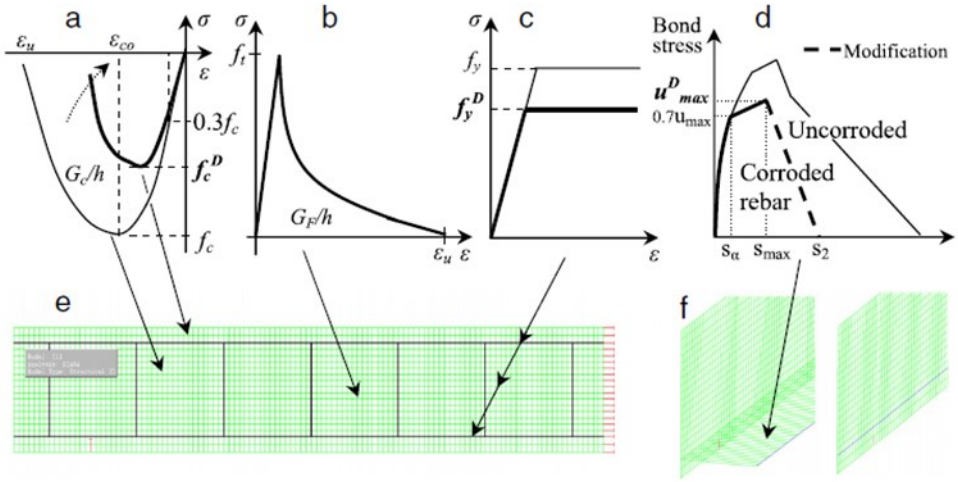

Figure 2.43: Finite element model: (a) material model of concrete in compression (b) material model of concrete in tension (c) material model of reinforcement (d) bond-slip relationship (e) boundary conditions (f) interface element (Kallias and Rafiq, 2010)

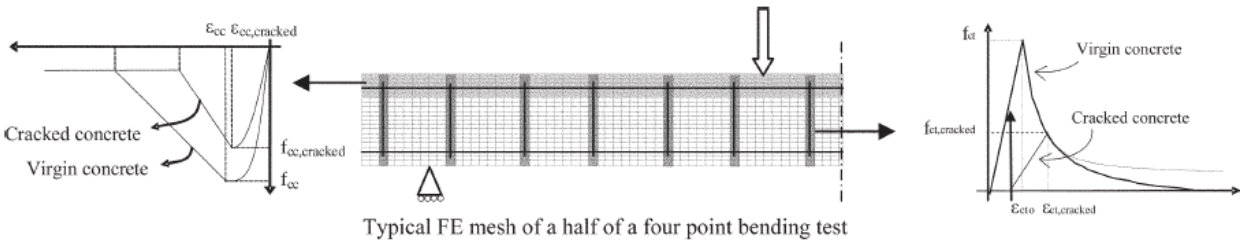

Figure 2.44: Discretized finite element model of control and corroded RC beams investigated by Hanjari et al. (2011)

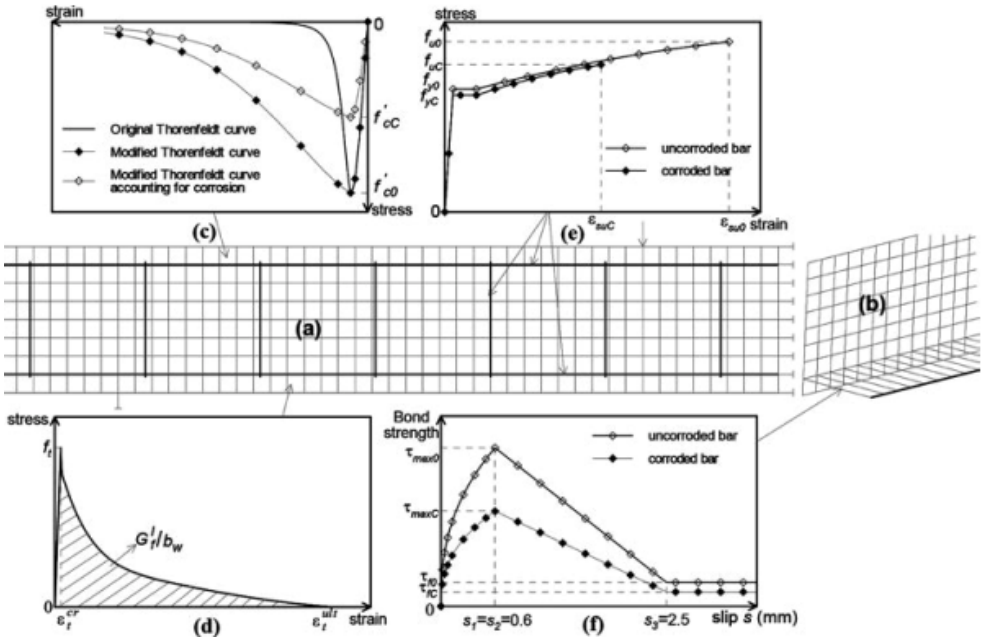

Figure 2.45: Finite element model: (a) mesh (b) bond (c) material model of concrete in compression (d) material model of concrete in tension (e) material model of reinforcement (f) bond-slip relationship (Ou and Nguyen, 2014)

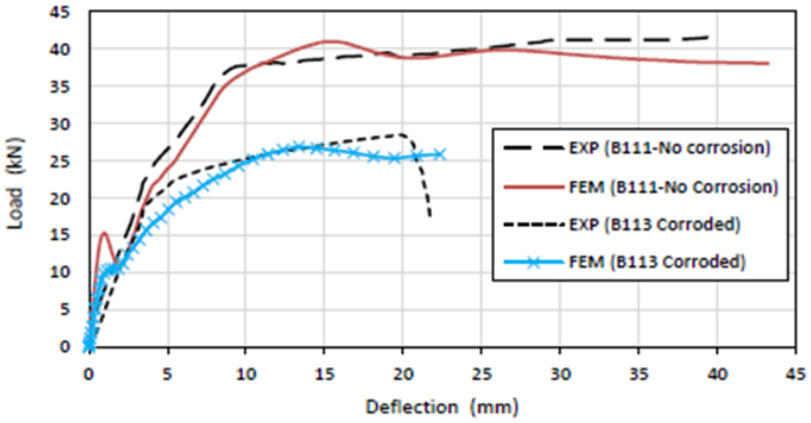

(a) Comparison between FE analyses and experimental load-deflection curves

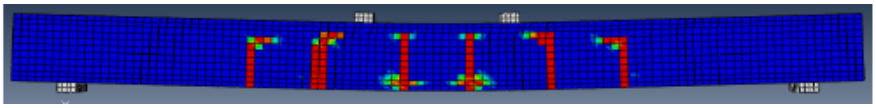

(b) Damage in control RC beam

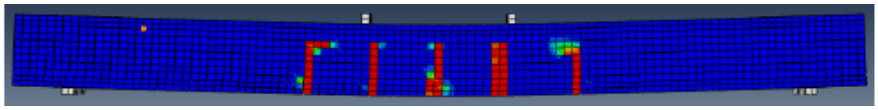

(c) Damage in corroded RC beam

Figure 2.46: Predictions of finite element analysis by Al-Sakkaf (2016)

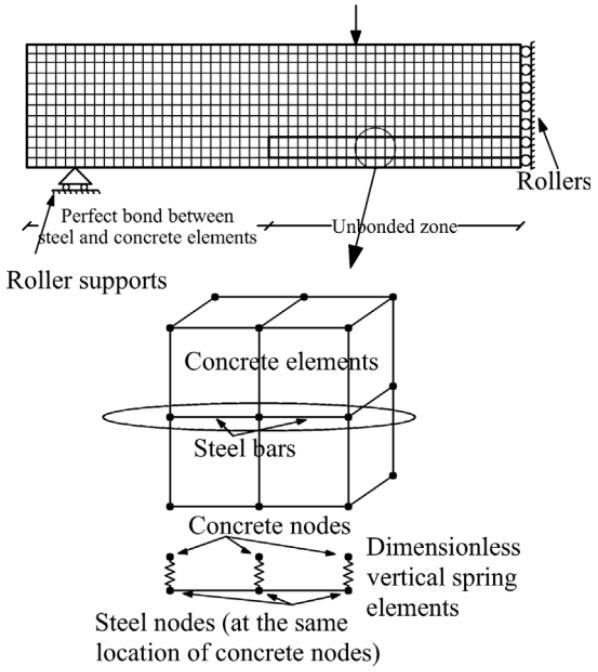

Figure 2.47: A schematic illustration of spring elements adopted by Jnaid and Aboutaha (2016)

2.8 References

Almusallam, A. A., Al-Gahtani, A. S., Aziz, A. R., and Rasheeduzzafar. (1996). Effect of reinforcement corrosion on bond strength. Construction and Building Materials, 10(2), 123-129.

Almusallam, A. A. (2001). Effect of degree of corrosion on the properties of reinforcing steel bars. Construction and Building Materials, 15(8), 361-368.

Andrade, C., and Alonso, C. (2001). On-site measurements of corrosion rate of reinforcements. Construction and Building Materials, 15(2-3), 141-145.

Al-Sakkaf, H. A. (2016). Modelling of corroded reinforced concrete beams. MASc Thesis, King Fahd University of Petroleum & Minerals, Dhahran, Saudi Arabia.

Al-Sulaimani, G. J., Kaleemullah, M., Basunbul, I. A., and Rasheeduzzafar. (1990). Influence of corrosion and cracking on bond behavior and strength of reinforced concrete members. ACI Structural Journal, 87(2), 220-231.

ASTM G46-94. (2005). Standard guide for examination and evaluation of pitting corrosion. ASTM International, West Conshohocken, Pennsylvania, USA.

Azad, A. K., Ahmad, S., and Azher, S. A. (2007). Residual strength of corrosion-damaged reinforced concrete beams. ACI Materials Journal, 104(1), 40-47.

Azam, R., El-Sayed, A. K., and Soudki, K. (2016). Behaviour of reinforced concrete beams without stirrups subjected to steel reinforcement corrosion. Journal of Civil Engineering and Management, 22(2), 146-153.

Ballim, Y., and Reid, J. C. (2003). Reinforcement corrosion and the deflection of RC beams – an experimental critique of current test methods. Cement and Concrete Composites, 25(6), 625-632.

Cairns, J., Plizzari, G. A., Du, Y., Law, D. W., and Franzoni, C. (2005). Mechanical properties of corrosion-damaged reinforcement. ACI Materials Journal, 102(4), 256-264.

Coronelli, D., and Gambarova, P. (2004). Structural assessment of corroded reinforced concrete beams: Modeling guidelines. ASCE Journal of Structural Engineering, 130(8), 1214-1224.

Dekoster, M., Buyle-Bodin, F., Maurel, O., and Delmas, Y. (2003). Modelling of the flexural behaviour of RC beams subjected to localised and uniform corrosion. Engineering Structures, 25(10), 1333-1341.

Du, Y. G., Clark, L. A., and Chan A. H. C. (2005). Residual capacity of corroded reinforcing bars. Magazine of Concrete Research, 57(3), 135-147.

Du, Y. G., Clark, L. A., and Chan A. H. C. (2005). Effect of corrosion on ductility of reinforcing bars. Magazine of Concrete Research, 57(7), 407-419.

Du, Y., Clark, L. A., and Chan, A. H. C. (2007). Impact of reinforcement corrosion on ductile behavior of reinforced concrete beams. ACI Structural Journal, 104(3), 285-293.

Du, Y., Cullen, M., and Li, C. (2013). Structural performance of RC beams under simultaneous loading and reinforcement corrosion. Construction and Building Materials, 38, 472-481.

El Maaddawy, T. A., and Soudki, K. A. (2003). Effectiveness of impressed current technique to simulate corrosion of steel reinforcement in concrete. ASCE Journal of Material in Civil Engineering, 15(1), 41-47.

El Maaddawy, T., Soudki, K., and Topper, T. (2005). Long-term performance of corrosion damaged reinforced concrete beams. ACI Structural Journal, 102(5), 649-656.

El Maaddawy, T., Soudki, K., and Topper, T. (2005). Analytical Model to Predict Nonlinear Flexural Behavior of Corroded Reinforced Concrete Beams. ACI Structural Journal, 102(4), 550-559.

Fang, C., Lundgren, K., Chen, L., and Zhu, C. (2004). Corrosion influence on bond in reinforced concrete. Cement and Concrete Research, 34(11), 2159-2167.

González, J. A., Andrade, C., Alonso, C., and Feliu, S. (1995). Comparison of rates of general corrosion and maximum pitting penetration on concrete embedded steel reinforcement. Cement and Concrete Research, 25(2), 257-264.

Hanjari, K. Z., Kettil, P., and Lundgren, K. (2011). Analysis of mechanical behavior of corroded reinforced concrete structures. ACI Structural Journal, 108(5), 532-541.

Hariche, L., Ballim, Y., Bouhicha, M., and Kenai, S. (2012). Effects of reinforcement configuration and sustained load on the behaviour of reinforced concrete beams affected by reinforcing steel corrosion. Cement and Concrete Composites, 34(10), 1202-1209.

Jnaid, F., and Aboutaha, R. S. (2016). Residual flexural strength of corroded reinforced concrete beams. Engineering Structures, 119, 198-216.

Kallias, A. N., and Rafiq, M. I. (2010). Finite element investigation of the structural response of corroded RC beams. Engineering Structures, 32(9), 2984-2994.

Li, H., Li, B., Jin, R., Li, S., and Yu, J.-G. (2018). Effects of sustained loading and corrosion on the performance of reinforced concrete beams. Construction and Building Materials, 169, 179-187.

Liu, Y., Jiang, N., Deng, Y., Ma, Y., Zhang, H., and Li, M. (2016). Flexural experiment and stiffness investigation of reinforced concrete beam under chloride penetration and sustained loading. Construction and Building Materials, 117, 302-310.

Lundgren, K. (2001). Bond between corroded reinforcement and concrete. Report No. 00:3, Chalmers University of Technology. Göteborg, Sweden.

Malumbela, G., Moyo, P., and Alexander, M. (2009). Behaviour of RC beams corroded under sustained service loads. Construction and Building Materials, 23(11), 3346-3351.

Mangat, P. S., and Elgarf, M. S. (1999). Flexural strength of concrete beams with corroding reinforcement. ACI Structural Journal, 96(1), 149-158.

Marcotte, T. D. (2001). Characterization of chloride-induced corrosion products that form in steel-reinforced cementitious materials. PhD Thesis. University of Waterloo, Ontario, Canada.

Nguyen, C. V., and Lambert, P. (2018). Effect of current density on accelerated corrosion of reinforcing steel bars in concrete. Structure and Infrastructure Engineering, 14(11), 1535-1546.

Ou, Y.-C., and Nguyen, N. D. (2014). Plastic hinge length of corroded reinforced concrete beams. ACI Structural Journal, 111(5), 1049-1058.

Ou, Y.-C., Susanto, Y. T. T., and Roh, H. (2016). Tensile behavior of naturally and artificially corroded steel bars. Construction and Building Materials, 103, 93-104.

Richardson, M. G. (2002). Fundamentals of durable reinforced concrete. Spon Press, Taylor & Francis Group, London and New York.

Rodriguez, J., Ortega, L. M., and Casal, J. (1997). Load carrying capacity of concrete structures with corroded reinforcement. Construction and Building Materials, 11(4), 239-248.

Sun, X., Kong, H., Wang, H., and Zhang, Z. (2018). Evaluation of corrosion characteristics and corrosion effects on the mechanical properties of reinforcing steel bars based on three-dimensional scanning. Corrosion Science, 142, 284-294.

Tang, F., Lin, Z., Chen, G., and Yi, W. (2014). Three-dimensional corrosion pit measurement and statistical mechanical degradation analysis of deformed steel bars subjected to accelerated corrosion. Construction and Building Materials, 70, 104-117.

Torres-Acosta, A. A., Navarro-Gutierrez, S., and Terán-Guillén, J. (2007). Residual flexure capacity of corroded reinforced concrete beams. Engineering Structures, 29(6), 1145-1152.

Val, D. V. (2007). Deterioration of strength of RC beams due to corrosion and its influence on beam reliability. ASCE Journal of Structural Engineering, 133(9), 1297-1306.

Vecchio, F. J., and Collins, M. P., 1986. The modified-compression field theory for reinforced concrete elements subjected to shear. ACI Journal Proceedings, 83(2), 219-231.

Wei-liang, J., Yu-xi, Z. (2001). Effect of corrosion on bond behavior and bending strength of reinforced concrete beams. Journal of Zhejiang University (SCIENCE), 2(3), 298-308.

Yoon, S., Wang, K., Weiss, W. J., and Shah, S. P. (2000). Interaction between loading, corrosion, and serviceability of reinforced concrete. ACI Materials Journal, 97(6), 637-644.

Zhang, J., Huang, J., Fu, C., Huang, L., and Ye, H. (2021). Characterization of steel reinforcement corrosion in concrete using 3D laser scanning techniques. Construction and Building Materials, 270, 121402.

Zhang, W., Song, X., Gu, X., and Li, S. (2012). Tensile and fatigue behavior of corroded rebars. Construction and Building Materials, 34, 409-417.

Zhang, W., Zhang, H., Gu, X., and Liu, W. (2018). Structural behavior of corroded reinforced concrete beams under sustained loading. Construction and Building Materials, 174, 675-683.

Chapter 3: Tests of Reinforced Concrete Beams under Coupled Effects of Variable Service Loads and Reinforcement Corrosion

Abstract

This paper presents results of an experimental study aimed to investigate the structural behavior of reinforced concrete (RC) beams subjected to service loads coupled with corrosion of the main tensile steel reinforcement. The experimental program consisted of tests of nine small-scale beams with dimensions of 145 x 250 x 1800 mm. The simply-supported beams were loaded under a four-point bending test. The main test variables were corrosion current density and level of service loading. The beams were loaded to either 60%, 40%, or 0% of the beam ultimate load capacity. Applied loads and corrosion of steel reinforcement were sustained up until the failure of beams. Test results indicated that the failure of corroded RC beams was brittle caused by the premature rupture of corroded steel bars. This behavior was attributed to the development of localized corrosion at the sections with flexural cracks in beams. Furthermore, it was found that beams subjected to higher levels of service loading experienced further reductions in ultimate load capacity and ductility.

Keywords: corrosion of steel reinforcement, reinforced concrete beams, service loads, structural behavior, flexural cracks, experimental, ultimate load capacity, ductility.

3.1 Introduction

Corrosion is considered to be one of the leading causes of deterioration mechanisms in reinforced concrete (RC) structures. RC bridges are essential structures that are particularly exposed to corrosion of steel reinforcement, causing safety concerns. Corrosion in RC structures is a slow process that takes many years, however this process is accelerated due to chloride penetration and/or carbonation of concrete. The use of de-icing salts on roadways in cold regions, exposure to marine environments, air pollution and greenhouse gases are instances where corrosion of steel reinforcement occurs in RC bridges. Once corrosion initiates, the structural performance in terms of load-carrying capacity and ductility degrades over time, costing billions of dollars in order to maintain and rehabilitate damaged bridges.

Numerous researchers employed an accelerated approach to simulate field corrosion in laboratory environments to shorten the duration of research activities. The most commonly adopted technique is known as the direct impressed current, in which current is impressed between the anode to cathode using an external power supply. In this technique, corrosion rate is controlled by the supplied current. A review conducted by El Maaddawy and Soudki (2003) revealed that corrosion current density used in previous research projects was widely varied, with a minimum value of 45 $\mu A/cm^2$, maximum value of 10,400 $\mu A/cm^2$, and average value ranging between 200 and 3,000 $\mu A/cm^2$. Proper selection of the current density is critical in simulating the damage induced by corrosion in laboratory settings within a short period of time, but also with corrosion products and damage similar to those observed in the field.

There are several adverse effects associated with reinforcement corrosion which influence the structural response of RC beams. This includes: loss of steel reinforcement area, degradation of mechanical properties of corroded steel reinforcement (Cairns et al. 2005), cracking and/or spalling of concrete surrounding the corroded steel reinforcement (Cabrera, 1996), and deterioration of bond at the interface between the corroded steel reinforcement and concrete (Almusallam et al. 1996). Many researchers investigated the effect of corrosion on the overall structural behavior of corroded RC beams (Rodriguez et al., 1997; Mangat and Elgarf, 1999; Azad et al., 2007; Du et al., 2007; Torres-Acosta et al., 2007; Azam et al., 2016). Rodriguez et al. (1997) indicated that reinforcement corrosion might alter a flexural mode of behavior of RC beams to a

shear failure. Mangat and Elgarf (1999) correlated the residual flexural capacity of corroded beams with the diameter of reinforcement, current density, and duration of corrosion exposure.

In above-mentioned studies, all beams were corroded under no loads (i.e., beams were loaded at the end of the corrosion phase). However, in engineering practice, RC bridge beams/girders are subjected to the coupled effects of reinforcement corrosion and service loads. The presence of flexural cracks due to loads may accelerate the degradation rates of load-carrying capacity and ductility in RC beams. A number of studies were conducted to investigate this coupling effect (Yoon et al., 2000; Du et al., 2013; Liu et al., 2016; Li et al., 2018; Zhang et al., 2018). Yoon et al. (2000) noted that corrosion of steel reinforcement initiated faster in beams subjected to higher levels of loading. Zhang et al. (2018) reported a delay in the initiation and propagation of corrosion-induced cracks in beams subjected to lower levels of sustained loading. Du et al. (2013) reported that the ultimate load capacity of beams under the coupled effects of reinforcement corrosion and loads is dependent on corrosion level, location and length of the corroded region. Liu et al. (2016) showed that the stiffness and ductility ratio of corroded beams were reduced due to the coupled effects of corrosion and sustained loads. Li et al. (2018) indicated that increasing sustained loads caused a further loss of the ultimate load capacity in corroded beams.

While there are many studies that investigated the coupling effects of reinforcement corrosion and loads, limited research attempts were carried out to examine the structural performance of RC beams under different service loads. Although the studies conducted by Liu et al. (2016) and Li et al. (2018) examined the response of corroded beams under different loads, the beams were corroded for specified duration, selected based on a targeted corrosion level. In both studies, the maximum level of corrosion was approximately 10%. It is important to recognize that the duration of corrosion or level of corrosion that causes beam failure under service loads is an unknown parameter, which is linked to the service life of beams.

The main objective of this research paper is to investigate the response of RC beams subjected to the coupled effects of reinforcement corrosion and different levels of service loads. A particular attention is given to understand the behavior and failure mechanisms of beams with corrosion levels that result in their failure under the applied service loads. Three different loading levels equivalent to 60%, 40%, and 0% of the beam ultimate load capacity were selected. These levels are considered representative of in-service conditions. Applied loads are sustained up until the

simultaneous failure of beams under corrosion and loads. The results of this study would help engineers to better understand and assess the effect of reinforcement corrosion on the serviceability of RC beams.

3.2 Experimental Program

3.2.1 Program Description

The intent of this experimental program is to study the flexural performance of RC beams subjected to the coupled effects of reinforcement corrosion and various service loads. Under-reinforced concrete beams were designed with anticipated flexural failure. Table 3.1 provides a summary of the experimental testing program. Group 1 beams (SS-1.1 and SS-1.2) served as control beams without corrosion. The main reason for testing two beams is to examine the influence of using epoxy-coated reinforcement in the shear span regions outside the corroded moment region (as in beam SS-1.2). These two beams were loaded to failure to determine their ultimate load capacities.

A successful experimental study related to reinforcement corrosion in concrete structures should demonstrate a satisfactory reproduction of the corrosion damage observed in the field. This includes the formation of corrosion by-products, propagation of corrosion and development of cracks, and loss of reinforcement sectional area. Since the applied current density controls the simulation of corrosion in laboratory environments, Group 2 and 3 beams were tested to address this parameter. This was accomplished by corroding Group 2 beams (SS-2.1 and SS-2.2) with a constant current density of 100 $\mu A/cm^2$ for 35 days before increasing it to 300 $\mu A/cm^2$ for the remaining duration until failure. This staged approach, with a low current density in the early stages of testing, permits proper reproduction of corrosion in concrete structures when exposed to aggressive environmental conditions. In this way, the development of corrosion-related cracks is ensured prior to a further acceleration of the corrosion process. In contrast, Group 3 beams (SS-3.1 and SS-3.2) were corroded using an accelerated approach over the entire duration of testing using a constant current density of 300 $\mu A/cm^2$. In both Groups 2 and 3 beams, the sustained loading level was equivalent to 60% of the beam ultimate load capacity.

Groups 3 to 5 beams were tested to address the coupled effects of reinforcement corrosion and different service loads. Two beams in Group 3 (SS-3.1 and SS-3.2) were corroded under 60% of

the beam ultimate load capacity, representing beams under maximum service loads. Two beams in Group 4 (SS-4.1 and SS-4.2) were corroded under 40% of the beam ultimate load capacity, representing beams under lower levels of service loads, however flexural cracks are still induced by the applied loads. One beam in Group 5 (SS-5.1) was corroded under no loads, representing the case where the beam is subjected to its self-weight only, without any transverse cracks. All these beams were corroded using a constant current density of 300 $\mu A/cm^2$.

3.2.2 Specimen Preparation

A total of nine small-scale RC beams with dimensions of 145 x 250 x 1800 mm were constructed and tested in this research program. Longitudinal reinforcement were in the form of 2-10M deformed steel bars placed at the bottom to serve as the main tensile reinforcement, while transverse reinforcement were in the form of 10M U-stirrups spaced at 110 mm c/c. The top of the beams had also 2-10M deformed steel bars which served as detailing reinforcement. Clear concrete cover to stirrups was 15 mm. Figure 3.1 shows the dimension of beams, reinforcement layout and detailing.

The beams were loaded under a four-point bending test. Loads were applied in such a way to generate a constant moment region of 500 mm within the middle portion of beams. The bottom longitudinal steel bars of control beam SS-1.1 were left uncoated. In the remaining eight beams, the bottom longitudinal steel bars were covered with an epoxy-coated layer in the regions outside the constant moment region. This would ensure the formation of corrosion damage is limited to the constant moment region. Prior to casting, all bottom longitudinal steel bars were connected with wires intended for current supply during the corrosion stage of testing.

3.2.3 Material Properties

Normal strength concrete was supplied by a local ready-mix concrete company and used to construct the beams. The concrete mix had a water-to-cement (w/c) ratio of 0.5 and a maximum aggregate size of 14 mm. Concrete cylinders with a diameter of 100 mm and a height of 200 mm were prepared. All cylinders were tested according to ASTM C39 “Standard Test Method for Compressive Strength of Cylindrical Concrete Specimens” at different times during the experimental program. The average 28-day compressive strength of concrete was equal to 38.0 MPa.

Steel reinforcement properties were evaluated using a direct tensile test in accordance with ASTM A370 “Standard Test Methods and Definitions for Mechanical Testing of Steel Products”. The average yield and ultimate strengths of 10M reinforcing bars were 445 MPa and 591 MPa, respectively. The elongation of the reinforcing bar at failure was 18%.

3.2.4 Accelerated Corrosion

In this study, corrosion of steel reinforcement was accelerated using the direct impressed current technique. Figure 3.2 shows a schematic illustration of the accelerated corrosion test setup. A direct current (DC) power supply with a maximum voltage capacity of 20 V and a maximum current capacity of 150 mA was used to connect the anode and cathode. In this experiment, the bottom longitudinal reinforcement served as the anode, while a 20 Gauge 316 LN stainless steel sheet served as the cathode. A styrofoam tray was attached to the bottom middle portion of beams. The 20 Gauge 316 LN stainless steel sheet was placed inside this tray. The tray was filled with an electrolyte solution in the form sodium chloride (5% NaCl) to help in depassivating steel reinforcement and further accelerate the corrosion process. The level of solution in the tray was maintained at 25 mm to ensure adequate saturation of the concrete surrounding steel reinforcement. Details of the supplied current during the corrosion stage of testing are discussed in the experimental program description.

3.2.5 Test Setup, Instrumentation, and Loading Procedure

Figure 3.3 shows the frames that were used to conduct the mechanical testing of small-scale beams under the coupled effects of reinforcement corrosion and loads. The loading system consisted of self-supporting frames with beams that span the columns in both directions. Test specimens were placed on two steel plates that react on the bottom beam. The steel plates were designed to simulate simple supports with a span length of 1500 mm. Loads were applied using hydraulic jacks that react on the top beam. The loading jacks were placed to generate a constant moment region within the middle portion of beams with a length of 500 mm. Prior to testing, a thin layer of dental plaster was added at the interface between the beam and its supports to smoothen the surface of concrete and ensure a uniform load transfer between the plates and the beam.

Group 1 control beams were loaded at a rate of 3.5 kN/min up until failure. In Groups 2 to 4 beams, loads were first increased to the desired level of service loading. For Groups 2 and 3, this load was

equal to 60 kN, which is equivalent to approximately 60% of the beam ultimate load capacity, while in Group 4 beams, this load was equal to 40 kN, which is equivalent to approximately 40% of the beam ultimate load capacity. These loads were then sustained, and the corrosion process of the bottom longitudinal reinforcement was activated. The simultaneous exposure to corrosion and loads was sustained until failure, and hence test duration was dependent on when the beams failed. Finally, Group 5 beam was corroded under its self-weight only. The corrosion process of this beam was conducted in parallel with beam SS-4.2 (i.e., both tests started and ended at the same time). At the end of the corrosion process, loads were applied and increased up until the failure of the beam. A typical test setup from one of the corroded beams is shown in Figure 3.4.

Linear variable differential transformers (LVDTs) were used to measure the displacements during the test. Test data were collected by a computerized data acquisition system. Prior to testing, the pressure sensors, LVDTs, strain gauges, and corrosion wires were connected to the data acquisition system. The data acquisition system was set to capture measurements at a sampling rate of 50 Hz during the loading stage of testing, and 1 Hz during the simultaneous exposure to corrosion and loads.

3.2.6 Level of Corrosion

After the failure of RC beams, the corroded longitudinal steel bars were carefully retrieved from the middle portion of the beams. Reinforcing bars were then screened visually to check for different types of corrosion. Next, the corroded steel bars were cleaned in accordance with the procedure outlined in ASTM G1-03 "Standard Practice for Preparing, Cleaning, and Evaluation Corrosion Test Specimens". After cleaning, the weight of each bar was documented. The level of corrosion was assessed using the gravimetric method according to the following expression:

$$\eta_{avg,m}(\%) = \frac{m_0 - m_c}{m_0} \times 100\% \tag{3.1}$$

where, $\eta_{avg,m}$ is the average mass loss of steel bars due to corrosion, m_0 and m_c are the weights of non-corroded and corroded steel bars, respectively. It should be noted that the gravimetric method measures average mass loss which may lead to a less accurate assessment of the corrosion level in the presence of non-uniform corrosion along steel reinforcement. In this study, a three-dimensional (3D) laser scanner was also employed to assess the localized corrosion level by estimating the residual cross-sectional area distribution along the length of the corroded

reinforcement. Further details of this technique are discussed in a companion study (Al-Bayti et al., 2022a). The maximum sectional loss is estimated using the following expression:

$$\eta_{crit,3D}(\%) = \frac{A_0 - A_{c,min}}{A_0} \times 100\% \tag{3.2}$$

where, $\eta_{crit,3D}$ is the critical cross-sectional area loss of steel bar due to corrosion, A_0 and $A_{c,min}$ are the cross-sectional areas of non-corroded and corroded steel bars, respectively.

3.3 Results and Discussion

3.3.1 Corrosion-Induced Cracks

Figure 3.5 shows a typical illustration of the initiation and propagation of corrosion in one of the beams that was corroded under service loads (beam SS-2.2). Initially, it can be observed that the electrolyte solution penetrated into the concrete, particularly through the opening of flexural cracks during the early stages of testing (day 1). This was followed by the formation of corrosion stains at the crack opening (day 14). Then, the accumulation of corrosion by-products was detected at the crack opening as well as the surrounding region (day 42). Afterward, the accumulation of products became more apparent across the entire corroded region of the beam (day 82). These observations highlight the influence of flexural crack presence on the distribution of damage induced by corrosion, as the opening of cracks provides a clear pathway for chloride solution and oxygen to penetrate to the surface of the embedded steel reinforcement. It is important to note that such behavior was only observed in corroded beams with flexural cracks (i.e., Groups 2 to 4 beams). The self-weight of the beam was not enough to induce transverse cracks, and hence the accumulation of corrosion by-products described above was not observed in Group 5 beam.

The volumetric expansion of corrosion by-products led to the development of internal cracks in the concrete surrounding the corroded reinforcement. The cracks were able to propagate and extend to the outer surface of beams as illustrated in Figure 3.6. These longitudinal cracks were typically found on the bottom face and/or sides of beams.

3.3.2 Corrosion of Steel Reinforcement

Figure 3.7 shows a typical illustration of the extent of corrosion damage in the corroded portion of the beams. It was found that the bottom portion of the rebar (i.e., facing concrete cover) had more

corrosion damage than the top portion of the rebar (i.e., facing inner core of concrete), as demonstrated in the corrosion pattern shown in Figure 3.8. This was expected since the bottom region of beams was immersed in chloride solution, increasing the exposure likelihood and corrosion level in the bottom portion of the rebar. The effectiveness of the use of epoxy-coated reinforcement against corrosion is demonstrated in Figure 3.9. Clearly, the right portion of this coupon, which was initially covered with an epoxy-coated layer, did not experience any corrosion when compared to the left portion of the coupon.

Figure 3.10 shows the types of corrosion that were detected after cleaning the corroded steel bars. As shown in the figure, three distinct types were identified; (i) generalized corrosion, (ii) pit corrosion, and (iii) localized crack corrosion. Generalized corrosion which primarily affects the ribs of steel reinforcement, was found to be very noticeable in the corroded bars that were retrieved from Groups 4 and 5 beams. Pit corrosion which causes a localized loss of steel area at random sites along the reinforcement, was identified in the corroded bars that were retrieved from Groups 2 to 5 beams. Localized crack corrosion, is also another form of localized loss, however this type of corrosion was only detected at the locations where flexural cracking occurred in beams. For that reason, it was only detected in Groups 2 to 4 beams. It should be noted that localization of this type of corrosion was not limited at the exact width of flexural crack opening, but it extended a few millimeters beyond the crack, as can be clearly seen in Figure 3.10(c).

The corrosion level of steel reinforcement was quantitatively assessed using the average mass loss $\eta_{avg,m}$ and localized sectional area loss $\eta_{crit,3D}$. Table 3.2 presents a summary of corrosion levels for each steel bar retrieved from the corroded beams. It should be noted that all beams failed due to rupture of steel reinforcement (which will be discussed in the next section), and hence the maximum sectional loss at the failure point includes the total loss due to corrosion and necking. Therefore, $\eta_{crit,3D}$ values reported in the table corresponds to any location with a peak loss other than those at the failure point.

As expected, increasing the duration of corrosion exposure increased the achieved mass loss when the current density was kept the same, as can be seen when comparing Group 3 to 5 beams. However, this relation does not apply when comparing Groups 2 and 3 beams due to the use of a low current density for a portion of the test in Group 2 beams, increasing the duration of corrosion exposure that led to the failure of beams. It is worth noting that the average mass losses of

individual steel bars within each beam were slightly different. However, the difference in beam SS-4.2 steel bars was quite high, despite the fact that each rebar had its own power supply during the test. This indicates that there might have been a loss of current which could occur if there is a slight connection between the longitudinal and transverse reinforcement. In this study, insulation layers were provided at the interfaces between longitudinal and transverse reinforcement, however this layer could have been damaged while casting the beams.

Figure 3.11 shows a typical profile of the distribution of cross-sectional area loss along the corroded portion of steel reinforcement in beam SS-3.2. It is very clear that distribution of corrosion is non-uniform mainly due to the presence of flexural cracks, causing a further loss of reinforcement sectional area. This effect can be clearly seen at the crack located near the center (i.e., at approximately 220 mm). It important to note that the loss of reinforcement sectional area at approximately 155 mm is due to pit corrosion. In the absence of transverse cracks as in beam SS-5.1, the non-uniform distribution of sectional area loss is only attributed to the spatial variability of pit corrosion.

3.3.3 Failure of RC Beams

Figure 3.12 shows the propagation of cracks and patterns at failure of the control and corroded RC beams. It can be observed that both control beams in Group 1 exhibited a ductile response characterized by the development of transverse cracks on the tensile side prior to crushing of top concrete at the center of the beams, while all corroded beams in Groups 2 to 5 exhibited a brittle failure due to the rupture of corroded tensile steel bars.

Theoretically, the failure of beams could take place at any section within the constant moment region. In the beams that were corroded under loads (i.e., Groups 2 to 4 beams), the critical section is located at the cracked sections of beams (i.e., due to flexural cracking), since these sections exhibited a significant loss of reinforcement sectional area when compared to other positions along the constant moment region of beams, as discussed previously. The exact location of the critical section where the failure occurred is subjected to the variability associated with the position, spacing, and width of flexural cracks, as they have a strong influence on the non-uniform distribution of corrosion in cracked beams under loads. In particular, the width of flexural cracks is believed to be a key parameter that can accelerate the corrosion rate since increasing the crack width is associated with ease in chloride penetration to the surface of steel reinforcement. For that

reason, the rupture of reinforcement could take place at any crack within the corroded portion of beams. For example, beams SS-2.1/SS-3.1/SS-4.2 failed at the crack close to the mid-span, while beams SS-2.2/SS-3.2/SS-4.1 failed at the crack close to the end of the corroded region. In contrast to the corroded beams under loads, the failure of the beam under no loads SS-5.1, was subjected to spatial variability of pit corrosion due to the absence of transverse cracks.

3.3.4 Flexural Behavior of RC Beams

Figure 3.13 compares the load and mid-span displacement relationships of all beams, while Figure 3.14 shows the displacement time histories of the beams that were corroded under loads. Table 3.3 summarizes key findings from the experimental testing program.

The overall response of control beams SS-1.1 (without epoxy-coated reinforcement) and SS-1.2 (with epoxy-coated reinforcement) was almost identical. Flexural cracks were first initiated at a load of approximately 26 kN. As the applied loads continued to increase, the beams started to yield at a load of approximately 82 kN. Afterward, the beams exhibited a large amount of deformation prior to their failure due to the crushing of concrete. The ultimate load capacity of the beams was approximately 106 kN. At the end of testing, displacements of beam SS-1.1 were higher than beam SS-1.2 because loading in beam SS-1.1 was continued beyond failure. Evidently, the results of these tests indicate that the use of epoxy-coated reinforcement in regions outside the constant moment region did not influence the flexural response of beams.

In contrast, the response of Groups 2 to 5 beams was significantly influenced by corrosion of the main flexural reinforcement, especially the beams which were corroded under loads (i.e., Groups 2 to 4). These beams experienced significant reductions in ultimate load capacity and ductility due to premature rupture of corroded steel bars. In these beams, applied loads and corrosion of reinforcement were sustained until failure, and hence the loading capacity degraded over time due to the initiation and propagation of corrosion. The deflections were also increased over time, as shown in Figure 3.14. At first, the deflections increased at a slow rate for a long period of time before increasing sharply in the last few days of testing. This sudden increase in deflections can be explained by yielding of the bottom tensile steel bars since applied loads were kept constant. Eventually, the continuous reduction in ultimate load capacity led to the failure of beams under their service capacity. As anticipated, all beams that were corroded under 40% and 60% of the beam ultimate load capacity, failed at ultimate load capacities of approximately 40 kN and 60 kN,

respectively. It should be noted that the beams did not fail exactly at the expected service loads due to slight fluctuations in laboratory temperatures. In the absence of loads, Group 5 beam showed a better performance in comparison to Groups 2 to 4 beams. This beam exhibited corrosion cracks prior to the loading stage, and hence the load-displacement relationship does not display the cracking stage. At the end of testing, the ultimate load capacity of the beam was approximately 72.8 kN.

In order to examine the influence of corrosion on the ductility of the beams, the residual ductility ratio 'defined as the ratio between ultimate displacement of corroded beams and ultimate displacement of control beam' was adopted. This ratio was used as a substitute to the well-known ratio between the ultimate and yield displacements, due to the difficulty in quantifying the ductility of beams when both yield and ultimate displacements are influenced by corrosion. This was also pointed out by Dang and François (2014). Besides, due to the methodology adopted to test the beams, displacements at yield cannot be directly obtained from load-displacements curves. Therefore, for consistency and comparison purposes, the residual ductility ratio was used. Accordingly, the residual ductility ratio of Group 3 beams (i.e., under 60% of the beam ultimate load capacity) was either 0.28 or 0.35, while that in Group 4 beams (i.e., under 40% of the beam ultimate load capacity) was either 0.19 or 0.24. This indicates that beams, which were corroded under 40% of the beam ultimate load capacity exhibited a further reduction in ductility, which can be explained by their lengthy corrosion exposure. Increasing the duration of exposure is directly related to increasing the loss of reinforcement area and reducing the ductility of steel reinforcement.

3.3.5 Influence of Parameters

3.3.5.1 Influence of Current Density

The effect of corrosion current density is examined by comparing Group 2 beams which were corroded using a staged approach (100 to 300 $\mu A/cm^2$) and Group 3 beams which were corroded using an accelerated approach (300 $\mu A/cm^2$). The main aspects that were examined are corrosion-induced cracks and the level of corrosion, as well as their impact on the overall behavior of the beams.

A comparison between the observed longitudinal corrosion cracks in beams SS-2.2 and SS-3.2 (shown in Figure 3.6), does not display differences in the damage produced by employing the two

approaches. However, images are only able to detect cracks that extend to the outer surface of beams. In order to examine the development of internal concrete damage caused by corrosion cracking, the fluctuations of voltage were monitored during the test. According to Ohm's law, a decrease in voltage indicates that the resistance is also reduced when the current is kept constant. In this study, the current was kept constant, and hence the drop in voltage indicates that the electrical resistance is also reduced, which could be attributed to the formation of corrosion-related cracks within the concrete surrounding the corroded steel bars that permits the access of chloride solution. It should be noted that the electrical resistance can also increase once the existing cracks are filled up with corrosion by-products that limits the access of chloride solution. This concept is also explained by Smith (2007).

Figure 3.15 compares the voltage time histories of all corroded beams. The sudden increase in voltage of Group 2 beams on the 35th day is due to increasing the current density during the second stage of testing. As shown in the figure, the fluctuations in the voltage in Group 2 and 3 beams were almost identical, indicating that adopting the accelerated approach did not have a significant influence on the formation of corrosion-related cracks in the corroded concrete. The same concept can be also applied to compare the extent of corrosion damage in Groups 3 to 5 beams that were corroded under different levels of service loads. Clearly, Groups 4 and 5 beams displayed voltage fluctuations characterized by sudden voltage drops when compared to Group 3 beams. This indicates that Groups 4 and 5 beams exhibited more cracking due to the expansion of corrosion by-products, which is expected due to their lengthy corrosion exposure. Furthermore, the increase in the resistance is clearly observed on the 122nd day of beam SS-5.1 testing, as the corrosion by-products had sufficient time to fill up the existing cracks, preventing the access of chloride solution.

The effect of current density on the level of corrosion (i.e., measured using mass loss) is examined by comparing beams that failed near the center (SS-2.1 and SS-3.1), and beams that failed near the end of the corroded region (SS-2.2 and SS-3.2), separately. The average mass loss of beams SS-2.1 and SS-3.1 were 13.7% and 12.9%, respectively, while the average mass loss of beams SS-2.2 and SS-3.2 were 18.7% and 19.0%, respectively. In general, test data show that the achieved corrosion levels using both approaches were very similar.

The similarities of both approaches with respect to the development of corrosion cracks and the achieved corrosion levels resulted in a similar behavior of the beams in Groups 2 and 3, as shown previously in the load-deflection curves (see Figure 3.13). Although there was a slight difference in the ultimate displacement at failure mainly due to the slight difference in the achieved corrosion levels, all beams experienced a brittle failure due to rupture of corroded steel bars at the locations where flexural cracks were present. Therefore, the use of the staged approach is not justified since it increased the experimental duration significantly. Also, the accelerated corrosion approach adopted in this study is a suitable technique that can be used to investigate the behavior of corroded beams under different service loads.

3.3.5.2 Influence of the Coupling Effects of Reinforcement Corrosion and Loads

The effect of loading presence is examined by comparing beams SS-4.2 and SS-5.1 which were corroded over the same duration, however beam SS-4.2 was corroded under loads while beam SS-5.1 was corroded under no loads. Figure 3.16 compares the residual ultimate load capacity and ductility ratios of both beams relative to the control beam. It can be observed that beam SS-4.2 exhibited a further reduction in ultimate load capacity by approximately 47% relative to beam SS-5.1, even though the mass loss of beam SS-4.2 (=29.7%) was slightly lower than beam SS-5.1 (=32.9%). This can be attributed to the presence of flexural cracks in beam SS-4.2 which permits a further loss of reinforcement sectional area due to the localization of corrosion at the position of cracks in beams. Furthermore, the presence of flexural cracks allows in a simultaneous localization of corrosion in the adjacent steel bars at the cracked sections of beams, while in the absence of cracks, the likelihood that pit corrosion is developed in both steel bars at a specific section of the beam is lower.

Furthermore, it can be observed that the reduction in ductility was more drastic than the loading capacity. The ductility of beam SS-4.2 was reduced by approximately 68% relative to beam SS-5.1. This substantial reduction in ductility of the corroded beam under loads can be attributed to the non-uniform distribution of corrosion caused by the loss of reinforcement sectional area at the cracks. Based on the above observations, it can be concluded that the coupling effects of reinforcement corrosion and service loads is an important parameter that should be taken into consideration when evaluating the flexural behavior of RC beams.

3.3.5.3 Influence of Service Loads

The effect of different levels of service loads on the behavior of corroded RC beams is demonstrated in Figure 3.17. It is clear that increasing the level of service loading is associated with increasing the rates of reduction in ultimate load capacity and ductility. As discussed previously, the reductions in ultimate load capacity and ductility when service loads were increased from 0% to 40% of the beam ultimate load capacity, is attributed to the presence of flexural cracks. However, the reductions in ultimate load capacity and ductility when service loads were increased from 40% to 60% of the beam ultimate load capacity, are rather related to the increase in flexural crack width. Increasing the width of crack openings would make the access of chloride ions and oxygen to the surface of steel reinforcement considerably easier.

Furthermore, increasing the levels of service loads reduced the service life of beams due to increased rate of reduction in ultimate load capacity. In this study, the laboratory service life is defined as the duration from initial corrosion exposure until the simultaneous failure of beams due to reinforcement corrosion and service loads. The average laboratory service life in Group 3 beams which were corroded under 60% of the beam ultimate load capacity was equal to 45 days, while the average laboratory service life in Group 4 beams which were corroded under 40% of the beam ultimate load capacity was equal to 160 days. This indicates that the service life of the beam was reduced by almost 3.5 times, by just increasing service loads from 40% to 60% of the beam ultimate load capacity.

3.4 Conclusions

This paper investigated the coupling effects of reinforcement corrosion and service loads on the flexural behavior of RC beams. The experimental testing of beams was mainly focused on the effect of different levels of service loads. In addition, the experimental program included beams which were corroded using different levels of accelerated corrosion (i.e., corrosion current density). The following conclusions can be drawn from the current investigation:

1) The use of an accelerated corrosion approach with a current density of 300 $\mu A/cm^2$ to corrode the longitudinal tensile reinforcement in RC beams instead of a staged approach with a slow rate of 100 $\mu A/cm^2$ for a portion of the test prior to further accelerating the rate to 300 $\mu A/cm^2$ had only a slight influence on damage induced by corrosion, and hence the

effect of current density on the overall behavior of beams was concluded to be minimal for the range considered.

2) Corrosion of reinforcement had a significant influence on the flexural response of RC beams when coupled with service loads. The ductile failure of non-corroded beams was replaced by a brittle failure caused by the rupture of corroded tensile steel bars. At failure, the ultimate load capacity and ductility were reduced significantly.
3) The presence of flexural cracks caused by service loads opened up a clear pathway for the chloride ions to reach the surface of embedded steel reinforcement, causing a localization of corrosion at the cracked sections of beams. This in turn resulted in a further loss of reinforcement area. Loss of reinforcement area combined with the presence of non-uniform corrosion along the corroded portion of steel bars were the main contributing factors to degrading the load capacity and ductility of beams.
4) The degradation rates of ultimate load capacity and ductility were more drastic for corroded beams under high service loads. This could be attributed to the increase in crack width openings under higher levels of service loads, allowing in a further localization of corrosion at the positions of cracks. This effect was clearly evident when comparing the beams which were corroded under 40% and 60% of the beam ultimate load capacity.
5) The coupling effect is an important parameter that should be taken into consideration while evaluating the load-carrying capacity and ductility of damaged RC beams due to corrosion. According to the results of this study, the presence of service loads that induces transverse cracks coupled with corrosion of the main flexural reinforcement, caused further reductions in ultimate load capacity and ductility by approximately 47% and 68%, respectively, when compared to the beam that was corroded without being subjected to service loads.

Table 3.1: Experimental testing program

	Beam designation	Loading type	Current density ($\mu A/cm^2$)	Corrosion duration
Group 1	SS-1.1 (uncoated rebars)	Monotonic to failure	NA	NA
	SS-1.2 (coated rebars)	Monotonic to failure	NA	NA
Group 2	SS-2.1 / SS-2.2	Sustained load (i.e., 60% of ultimate) coupled with corrosion of reinforcement	Stage 1:100 Stage 2: 300	35 days up to failure
Group 3	SS-3.1 / SS-3.2	Sustained load (i.e., 60% of ultimate) coupled with corrosion of reinforcement	300	up to failure
Group 4	SS-4.1 / SS-4.2	Sustained load (i.e., 40% of ultimate) coupled with corrosion of reinforcement	300	up to failure
Group 5	SS-5.1	Stage 1: Sustained load (i.e., 0% of ultimate) coupled with corrosion of reinforcement Stage 2: Monotonic to failure	300	same as SS-4.2

Table 3.2: Corrosion level of steel reinforcement

Beam	Time (days)	$\eta_{avg,m}$ (%)*			$\eta_{crit,3D}$ (%)**		
		R1	R2	Avg.	R1	R2	Avg.
SS-2.1	73	11.9	15.5	13.7		NA***	
SS-2.2	82	19.5	17.9	18.7	38.0	37.9	38.0
SS-3.1	37	12.0	13.8	12.9	45.9	33.9	39.9
SS-3.2	52	17.6	20.3	19.0	56.9	51.3	54.1
SS-4.1	152	31.8	48.4	40.1	54.1	71.3	62.7
SS-4.2	167	26.5	32.8	29.7	61.3	53.9	57.6
SS-5.1	167	36.1	29.6	32.9	56.6	49.9	53.3

*Mass loss was evaluated according ASTM G1-03.

**Maximum sectional area loss was evaluated using a 3D laser scanner.

***Coupons retrieved from beam SS-2.1 were short.

Table 3.3: Summary of key experimental findings

Beam	Displacement at failure (mm)	Load at failure (kN)	Residual ductility ratio*	Residual capacity ratio*
SS-1.1	33.72	107.84		
SS-1.2	27.22	106.00	1.00	1.00
SS-2.1	9.35	58.65	0.34	0.55
SS-2.2	9.45	57.85	0.35	0.55
SS-3.1	7.53	58.35	0.28	0.55
SS-3.2	8.63	59.55	0.32	0.56
SS-4.1	6.44	38.06	0.24	0.36
SS-4.2	5.27	38.25	0.19	0.36
SS-5.1	16.34	72.77	0.60	0.69

*Residual ductility and capacity ratios were calculated relative to control beam SS-1.2.

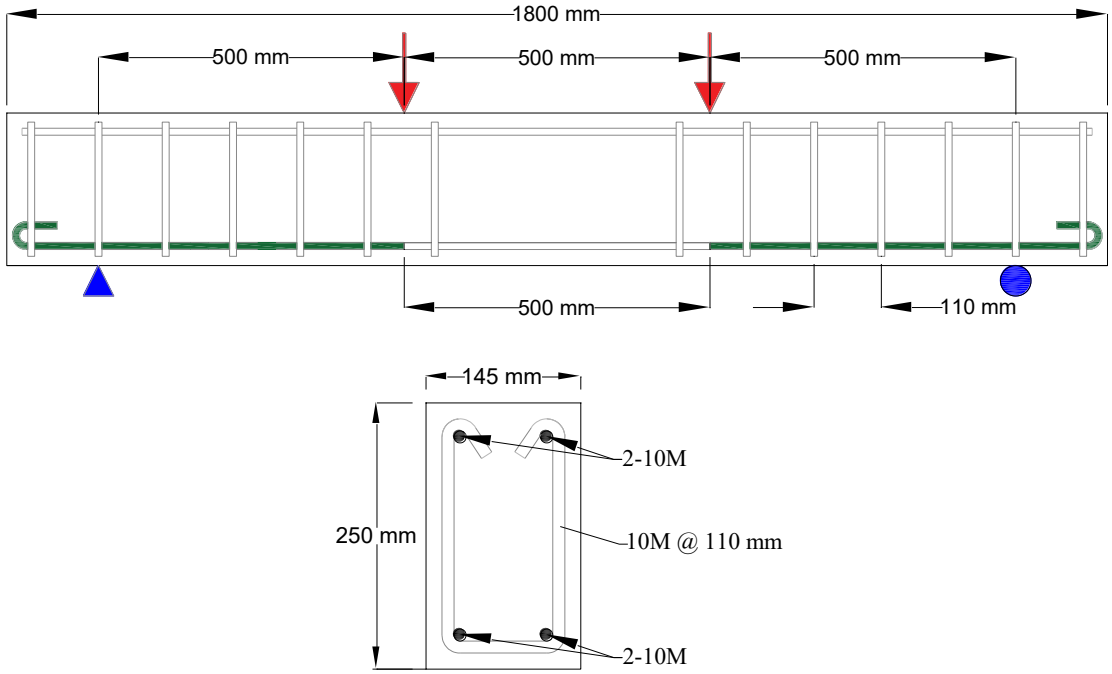

Figure 3.1: Dimension of beams and reinforcement detailing

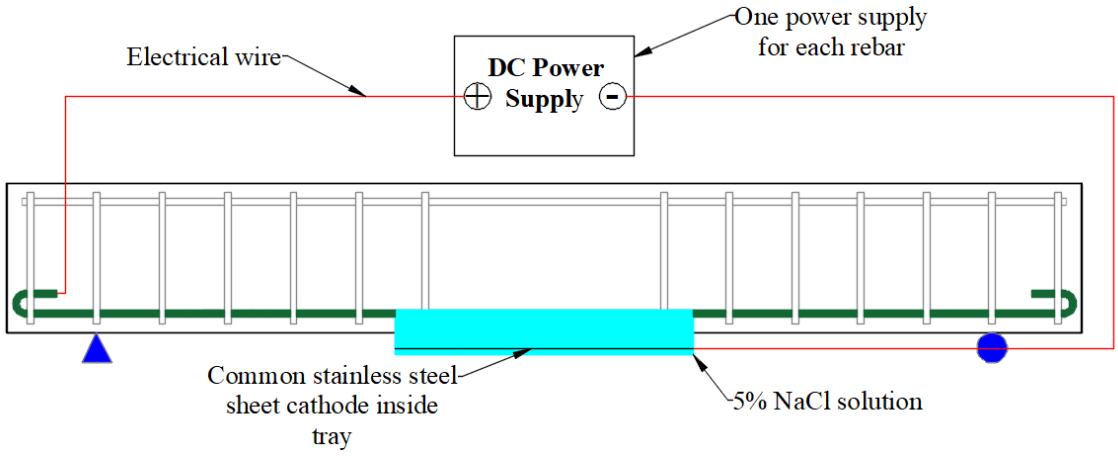

Figure 3.2: Schematic illustration of the accelerated corrosion setup

Figure 3.3: Testing frames for small-scale RC beams

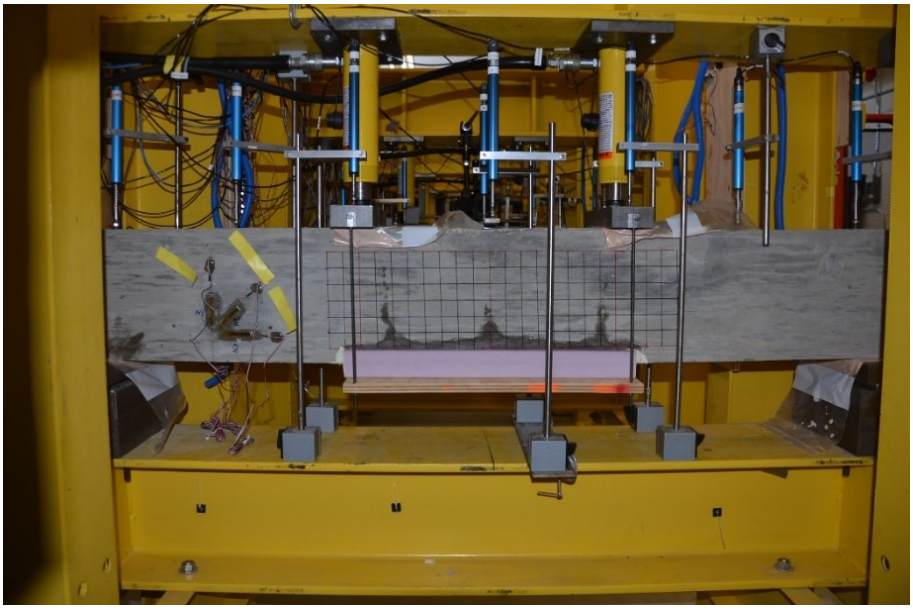

Figure 3.4: Test setup of accelerated corrosion and sustained loads



Day 1 Day 14 Day 42

Day 82

Figure 3.5: Initiation and progression of corrosion in beam SS-2.2

(a) Beam SS-2.2

(b) Beam SS-3.2

Figure 3.6: Corrosion-induced cracks after the failure of beams

(a) (b)

Figure 3.7: Corrosion damage: (a) across the entire length of the affected zone (b) cross-sectional

(a)

(b)

Figure 3.8: Corrosion pattern on the longitudinal steel bar facing: (a) concrete cover (b) inner core concrete

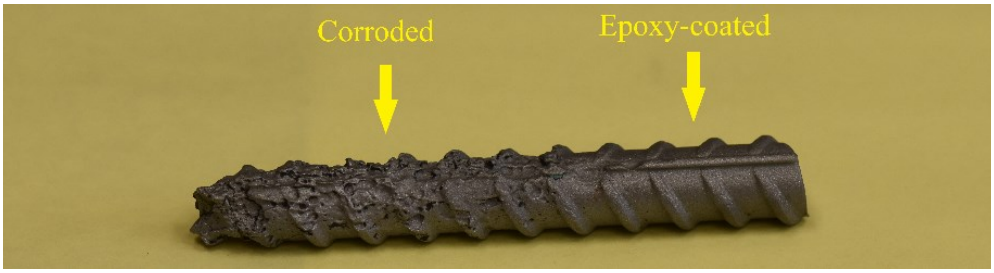

Figure 3.9: Effectiveness of epoxy-coated reinforcement against corrosion

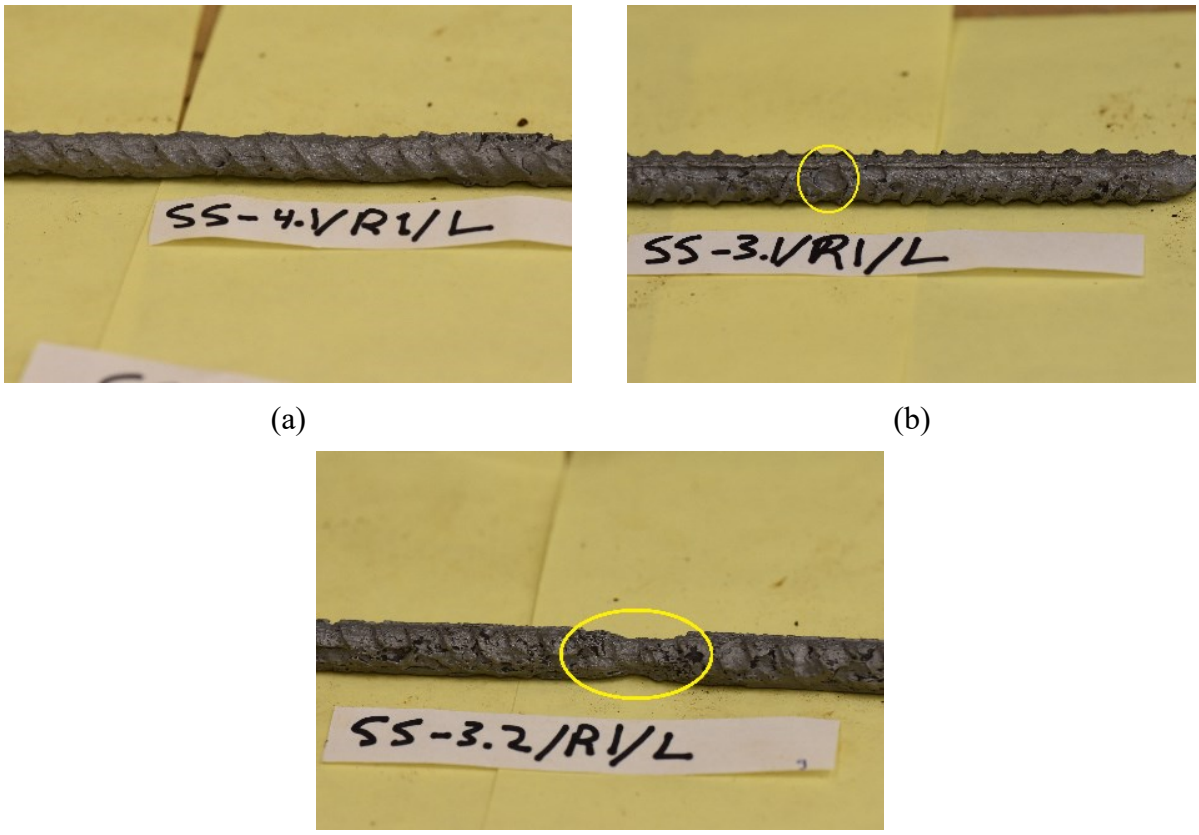

(a) (b)

(c)

Figure 3.10: Corrosion types: (a) generalized corrosion (b) pit corrosion (c) localized crack corrosion

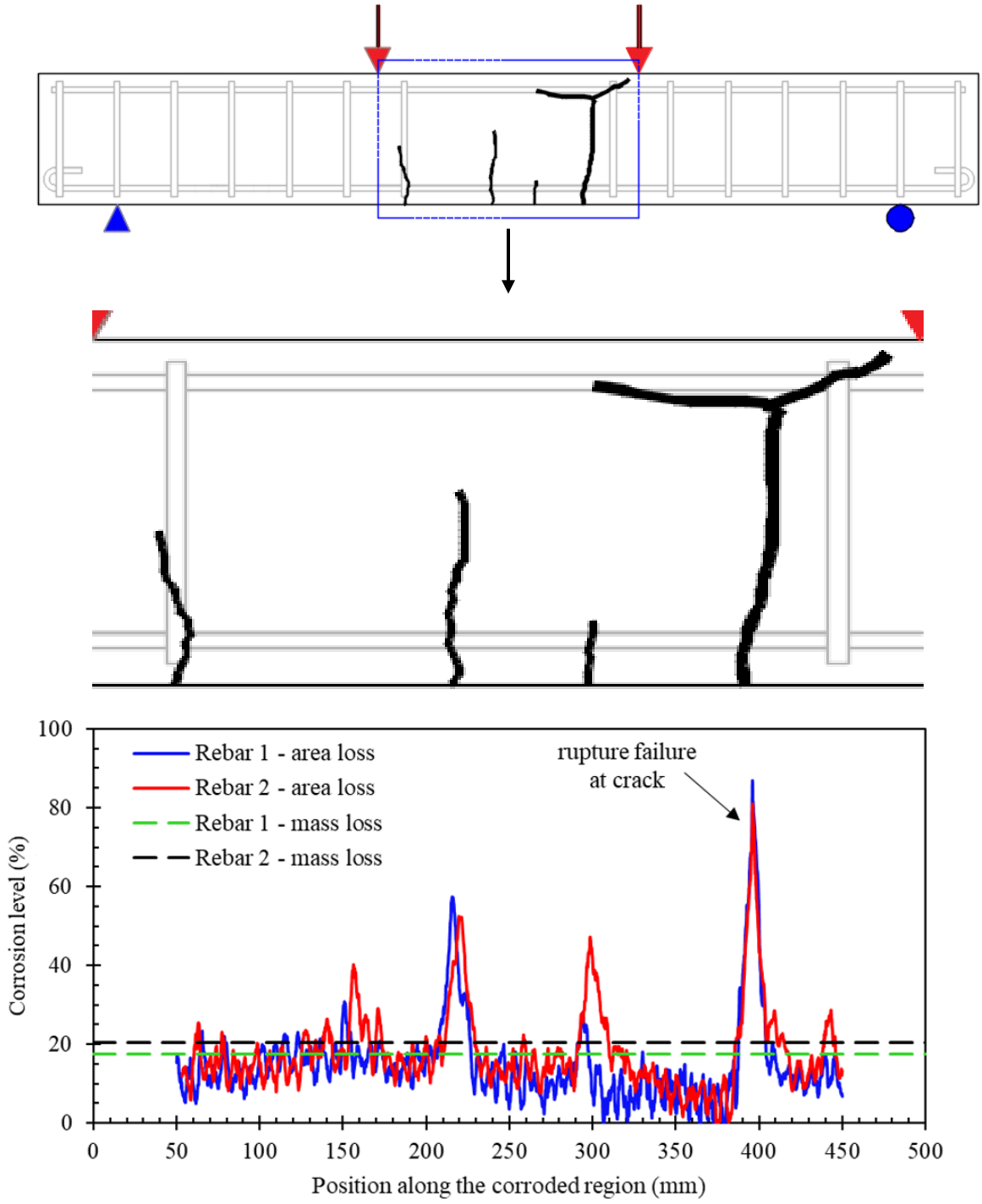

Figure 3.11: Distribution of reinforcement sectional area loss along the corroded zone of beam SS-3.2

(a) SS-1.1

(b) SS-1.2

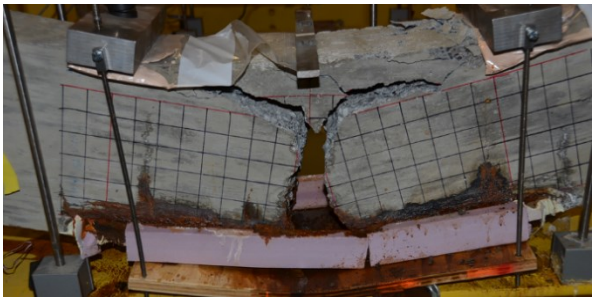

(c) SS-2.1

(d) SS-2.2

(e) SS-3.1

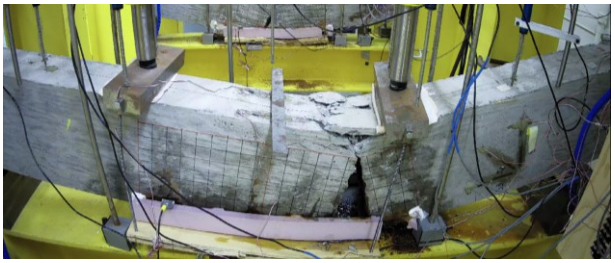

(f) SS-3.2

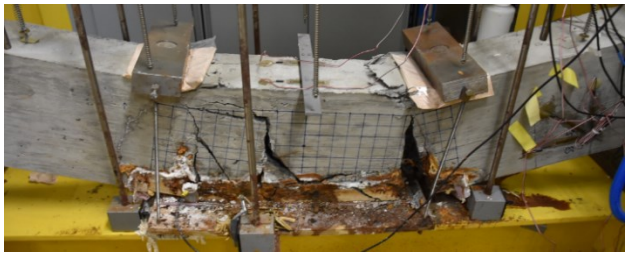

(g) SS-4.1

(h) SS-4.2

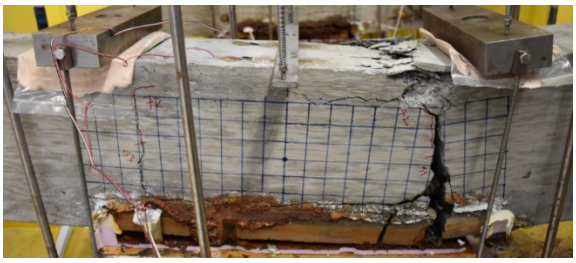

(i) SS-5.1

Figure 3.12: Crack patterns of RC beams at failure

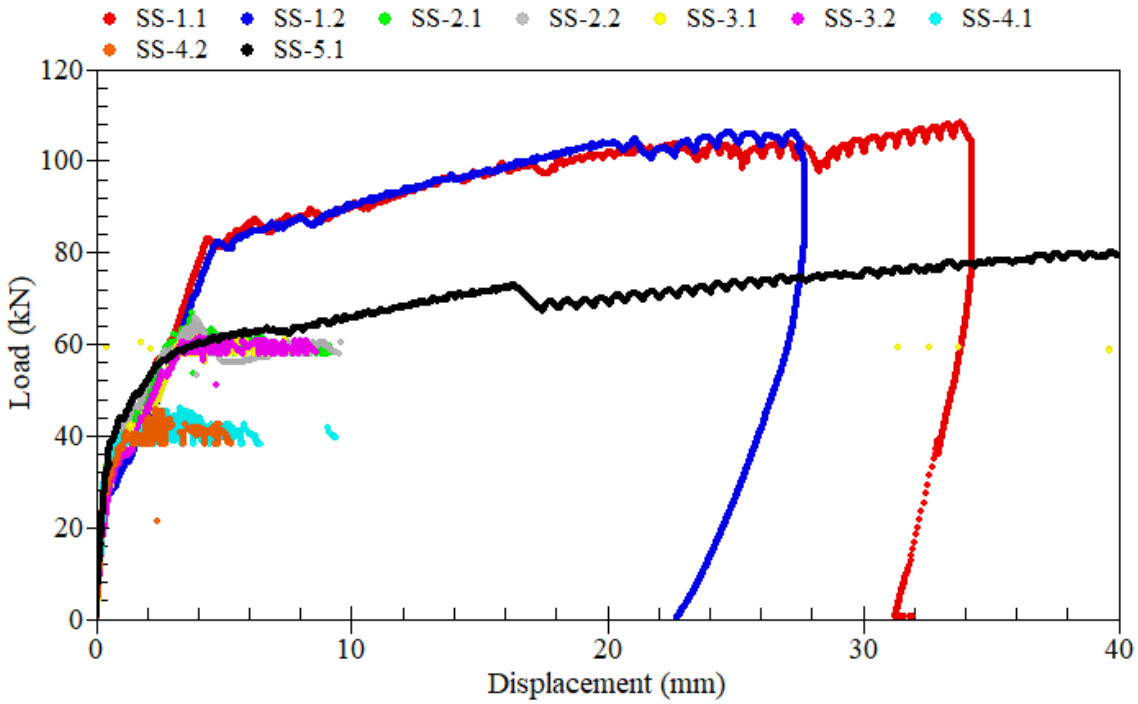

Figure 3.13: Load-displacement relationships of RC beams

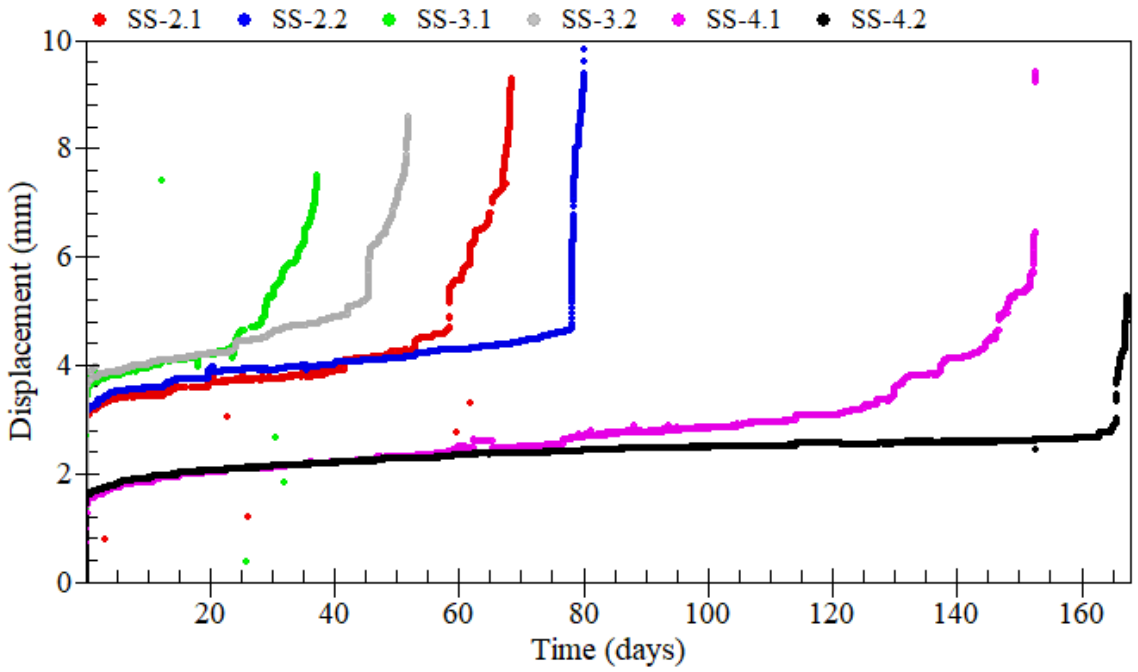

Figure 3.14: Displacement-time histories of corroded beams under service loads

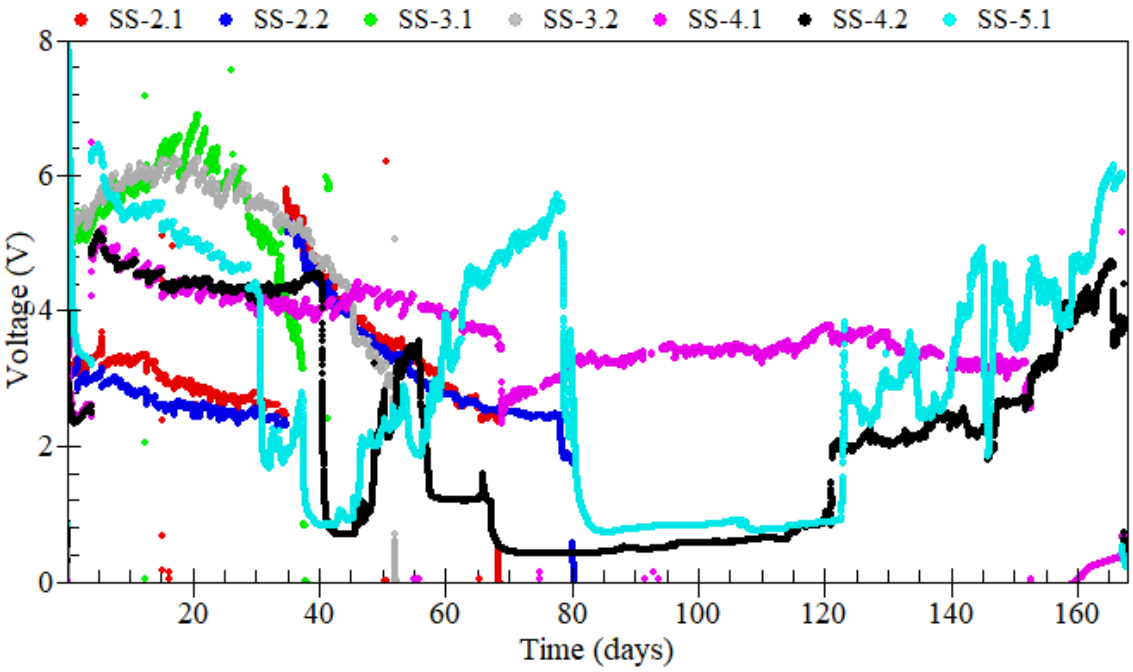

Figure 3.15: Voltage-time histories of corroded beams

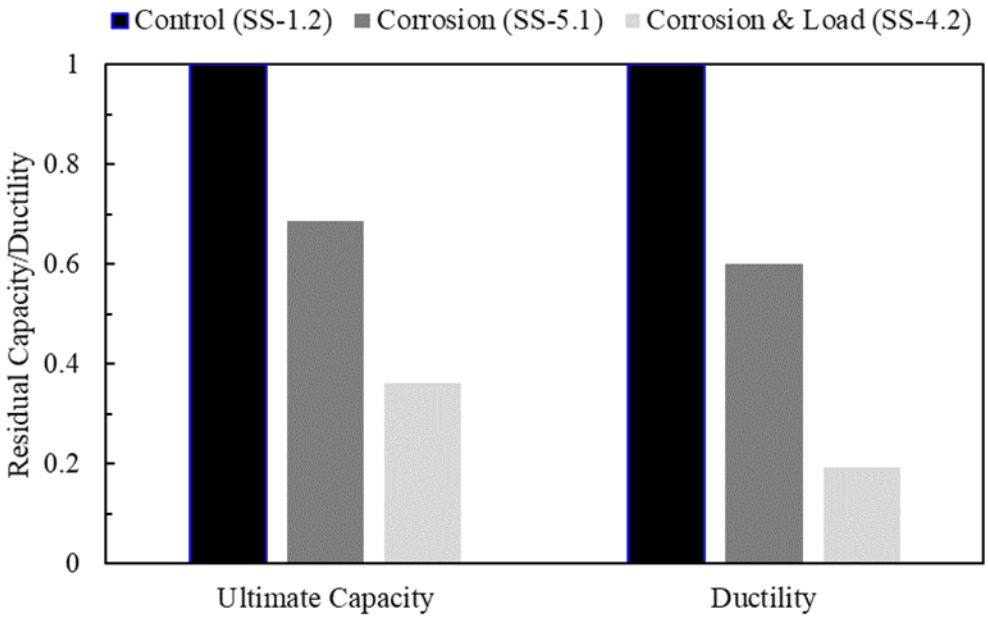

Figure 3.16: Influnce of the coupling effects of reinforcement corrosion and loading on the response of beams

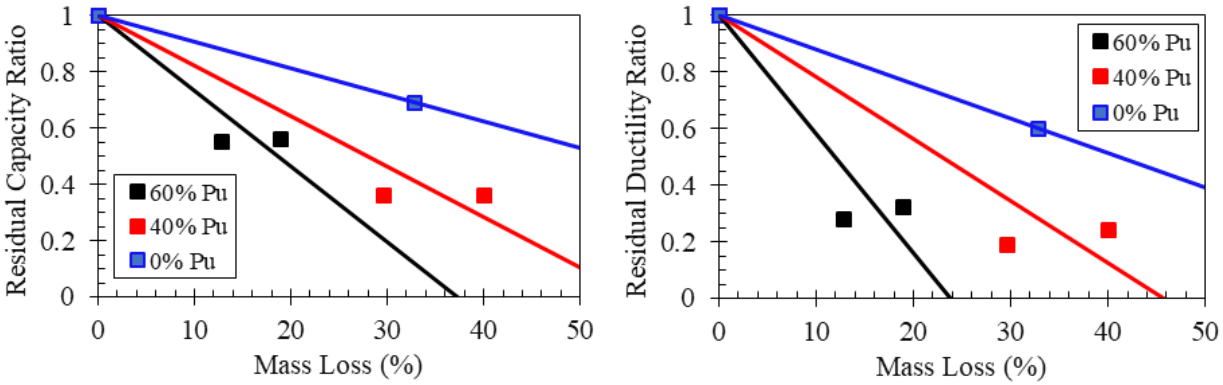

(a) Residual capacity ratio

(b) Residual ductiltiy ratio

Figure 3.17: Effect of different levels of service loads on the behavior of corroded RC beams

3.5 References

Al-Bayti, A., Almansour, H., Saatcioglu, M. (2022a). Influence of Corrosion on the Mechanical Performance of Steel Reinforcement. To be submitted for publication.

Almusallam, A. A., Al-Gahtani, A. S., Aziz, A. R., and Rasheeduzzafar. (1996). Effect of reinforcement corrosion on bond strength. Construction and Building Materials, 10(2), 123-129.

ASTM C39 / C39M. (2016). Standard test method for compressive strength of cylindrical concrete specimens. ASTM International, West Conshohocken, Pennsylvania, USA.

ASTM A370. (2017). Standard test methods and definitions for mechanical testing of steel products. ASTM International, West Conshohocken, Pennsylvania, USA.

ASTM G1-03. (2017)e1. Standard practice for preparing, cleaning, and evaluation corrosion test specimens. ASTM International, West Conshohocken, Pennsylvania, USA.

Azad, A. K., Ahmad, S., and Azher, S. A. (2007). Residual strength of corrosion-damaged reinforced concrete beams. ACI Materials Journal, 104(1), 40-47.

Azam, R., El-Sayed, A. K., and Soudki, K. (2016). Behaviour of reinforced concrete beams without stirrups subjected to steel reinforcement corrosion. Journal of Civil Engineering and Management, 22(2), 146-153.

Cabrera, J. G. (1996). Deterioration of concrete due to reinforcement steel corrosion. Cement and Concrete Composites, 18(1), 47-59.

Cairns, J., Plizzari, G. A., Du, Y., Law, D. W., and Franzoni, C. (2005). Mechanical properties of corrosion-damaged reinforcement. ACI Materials Journal, 102(4), 256-264.

Dang, V. H., and François, R. (2014). Prediction of ductility factor of corroded reinforced concrete beams exposed to long term aging in chloride environment. Cement and Concrete Composites, 53, 136-147.

Du, Y., Clark, L. A., and Chan, A. H. C. (2007). Impact of reinforcement corrosion on ductile behavior of reinforced concrete beams. ACI Structural Journal, 104(3), 285-293.

Du, Y., Cullen, M., and Li, C. (2013). Structural performance of RC beams under simultaneous loading and reinforcement corrosion. Construction and Building Materials, 38, 472-481.

El Maaddawy, T. A., and Soudki, K. A. (2003). Effectiveness of impressed current technique to simulate corrosion of steel reinforcement in concrete. ASCE Journal of Material in Civil Engineering, 15(1), 41-47.

Li, H., Li, B., Jin, R., Li, S., and Yu, J.-G. (2018). Effects of sustained loading and corrosion on the performance of reinforced concrete beams. Construction and Building Materials, 169, 179-187.

Liu, Y., Jiang, N., Deng, Y., Ma, Y., Zhang, H., and Li, M. (2016). Flexural experiment and stiffness investigation of reinforced concrete beam under chloride penetration and sustained loading. Construction and Building Materials, 117, 302-310.

Mangat, P. S., and Elgarf, M. S. (1999). Flexural strength of concrete beams with corroding reinforcement. ACI Structural Journal, 96(1), 149-158.

Rodriguez, J., Ortega, L. M., and Casal, J. (1997). Load carrying capacity of concrete structures with corroded reinforcement. Construction and Building Materials, 11(4), 239-248.

Smith, R. W. (2007). The effects of corrosion on the performance of reinforced concrete beams. MASc Thesis. Ryerson University, Ontario, Canada.

Torres-Acosta, A. A., Navarro-Gutierrez, S., and Terán-Guillén, J. (2007). Residual flexure capacity of corroded reinforced concrete beams. Engineering Structures, 29(6), 1145-1152.

Yoon, S., Wang, K., Weiss, W. J., and Shah, S. P. (2000). Interaction between loading, corrosion, and serviceability of reinforced concrete. ACI Materials Journal, 97(6), 637-644.

Zhang, W., Zhang, H., Gu, X., and Liu, W. (2018). Structural behavior of corroded reinforced concrete beams under sustained loading. Construction and Building Materials, 174, 675-683.

Chapter 4: Tests of Reinforced Concrete Beams under Coupled Effects of Maximum Service Loads and Variable Reinforcement Corrosion

Abstract

An experimental study was carried out to examine the time-dependent flexural behavior of reinforced concrete (RC) beams subjected to service loads coupled with corrosion of the main flexural reinforcement. The experimental program consisted of tests of six simply supported large-scale beams with dimensions of 200 x 300 x 3400 mm. The beams were under-reinforced, with approximately 29% of balanced section reinforcement. Two beams were loaded to failure using a four-point bending test, serving as control specimens. Two beams were first loaded to 60% of the beam ultimate load capacity, and then the corrosion process of the longitudinal tensile reinforcement was accelerated using the direct impressed current technique while sustaining the applied service loads. Similarly, one beam was corroded under service loads, but for a shorter duration to examine the influence of different corrosion levels. The remaining beam specimen was corroded with no service loads. Test results indicated that corrosion of the main flexural reinforcement resulted in significant reductions in ultimate load capacity and ductility of RC beams. Test results were also compared with those of the companion small-scale beams with smaller percentage of steel and fewer bars, tested earlier. The results indicated that the reduction rates in ultimate load capacity and ductility associated with corrosion in reinforced concrete beams under service loads were accelerated when smaller percentage of steel with fewer number of bars were used.

Keywords: reinforcement corrosion, reinforced concrete beams, service loads, flexural behavior, experimental, small-scale beam, large-scale beam, ultimate load capacity, ductility.

4.1 Introduction

Corrosion of steel reinforcement causes major concerns on the durability of reinforced concrete (RC) that is widely used in the construction of important civil infrastructures including bridges. Initially, steel reinforcement is protected from corrosion by a thin passive layer which is formed around the embedded reinforcement during the early stages of cement hydration. However, corrosion of reinforcement is accelerated due to the use of de-icing salts or exposure to chlorides in coastal regions. High concentrations of chloride ions penetrating through the voids and cracks of concrete can break down the passive protective layer. As corrosion progresses, the load-carrying capacity of existing RC structures is reduced over time, causing safety concerns and huge economic losses used for maintenance and rehabilitation.

Field inspections and experimental investigations had shown that corrosion causes loss of reinforcement sectional area which can be present in a generalized or localized form. The localized form of corrosion impairs the mechanical performance of steel reinforcement. In addition, the volumetric expansion of corrosion by-products leads to the development of cracks in the concrete surrounding the corroded reinforcement (Cabrera, 1996). The combined effects of reduction in reinforcement sectional area and cracking of concrete weakens the bond strength at the interface between steel reinforcement and concrete. For these reasons, the load-carrying capacity, ductility, and service life of corroded RC structures are also reduced.

Extensive experimental research efforts were devoted to understand the flexural behavior of corroded RC beams (Rodriguez et al., 1997; Mangat and Elgarf, 1999; Du et al., 2007; Torres-Acosta et al., 2007; Azam et al., 2016). Rodriguez et al. (1997) observed an increase in crack widths at the service limit state. Also, the researchers had noted that corrosion of steel reinforcement may shift an anticipated flexural failure of beams to a shear failure. Du et al. (2007) reported that under-reinforced beams with corrosion levels exceeding 10% could fail due to the rupture of steel reinforcement. Mangat and Elgarf (1999) correlated the residual strength of corroded reinforced concrete beams with the diameter of reinforcement, corrosion current density, and duration of corrosion exposure. Torres-Acosta et al. (2007) correlated the residual strength of corroded reinforced concrete beams with the maximum pit depth. Although these studies highlight the effect of corrosion in reinforced concrete beams, the presence of service loads during the initiation of propagation phases of corrosion was not considered.

A number of researchers had experimentally coupled the effects of reinforcement corrosion and service loads to better understand the behavior of reinforced concrete beams (Yoon et al., 2000; Ballim and Reid, 2003; El Maaddawy and Topper, 2005; Malumbela et al., 2009; Hariche et al., 2012; Du et al., 2013; Li et al., 2018; Zhang et al., 2018). Ballim and Reid (2003) indicated that beams subjected to this coupling effect experienced an increase in deflections with increased corrosion levels. El Maaddawy and Topper (2005) observed an increase in the degradation of loading capacity in beams subjected to this coupling effect when compared to beams which were corroded under no loads. This was explained by the increase of corrosion levels in beams subjected to service loads. However, the researchers did not observe this increase when corrosion exposures were further increased in the beams subjected to service loads, and hence the coupling effect did not increase the reduction in ultimate load capacity. Zhang et al. (2018) indicated that the coupling effect had a slight influence on the width of flexural cracks, and no influence on their spacing. Li et al. (2018) showed that corroded beams subjected to higher levels of sustained loads experienced a further reduction in ultimate load capacity. The majority of these studies examined the response of beams at a certain point during the service life of beams (i.e., beams were tested with a targeted corrosion level). However, the response and failure mechanisms of beams at the end of their service life are not well investigated, as also pointed out by Du et al. (2013), in which the researchers investigated the influence of length and location of the corroded region at the end of service life of reinforced concrete beams.

The intent of this paper is to increase understanding of the time-dependent flexural behavior of RC beams under the coupled effects of reinforcement corrosion and service loads. A particular attention is given to the response and failure mechanisms of beams during and at the end of their service life. The response of corroded beams was examined by constant monitoring of deflections, tensile and compressive strains of longitudinal steel reinforcement, and concrete strains over the entire duration under the simultaneous exposure to corrosion and service loads. As part of the experimental study, large-scale beams were designed, cast and tested. The structural performance of large-scale beams was also compared with that of small-scale beams which were tested in a companion study (Al-Bayti et al. 2022b), in order to examine the effects of percentage of steel and number of bars.

4.2 Experimental Methodology

4.2.1 Experimental Program

The primary objective of this experimental program is to study the flexural behavior of RC beams under the coupled effects of reinforcement corrosion and service loads. The beams were designed with anticipated flexural failure. The experimental program consisted of tests of six large-scale beams. Four other small-scale beams, tested in the first phase of the experimental program, are also included for comparison. Small-scale beams had a tensile reinforcement ratio close to the minimum code requirement, while large-scale beams were reinforced with a higher tensile reinforcement ratio.

Two beams in each category served as control beams without reinforcement corrosion. The control small-scale beams were referred to as SS-1.1 and SS-1.2, while control large-scale beams were referred to as LS-1.1 and LS-1.2. All control beams were tested to failure to evaluate their ultimate load capacities. In addition, two beams in each category were subjected to the coupled effects of reinforcement corrosion and service loads equivalent to 60% of the beam ultimate load capacity. In this category, small-scale beams were referred to as SS-3.1 and SS-3.2, while large-scale beams were referred to as LS-2.1 and LS-2.2. These beams were corroded until the simultaneous failure due to reinforcement corrosion and service loads (i.e., up until the end of their service life). The remaining two large-scale beams were tested to examine the influence of corrosion level as beam LS-2.3 and the absence of service loads as beam LS-2.4. Table 4.1 provides the details of the tests considered.

The direct impressed current technique was employed to accelerate the corrosion process of the main flexural reinforcement. Small-scale beams SS-3.1 and SS-3.2 were corroded using a constant current density of 300 $\mu A/cm^2$ up until failure. This current density is considered to be within the average range between 200 and 3,000 $\mu A/cm^2$ reported in previous studies (El Maaddawy and Soudki, 2003). Likewise, large-scale beam LS-2.1 was corroded using a constant current density of 300 $\mu A/cm^2$ for 135 days, however it was increased to 1,000 $\mu A/cm^2$ during the last 15 days of testing. It should be noted that the influence of increasing the density to 1,000 $\mu A/cm^2$ is slight since the damage induced by corrosion had sufficient time to develop in this beam (i.e., the corrosion process using a current density of 300 $\mu A/cm^2$ was 90% of entire test duration). In

contrast, beam LS-2.2 was corroded using a current density of 500 μA/cm^2 until the development of first corrosion-related crack (cracking occurred on day 33), which was then increased to 1,000 μA/cm^2. This staged approach with a relatively low current density in the beginning of the test would ensure the formation of corrosion is more distributed as the development of corrosion cracks opens new pathways for chloride ions to penetrate to the surface of steel reinforcement. Based on the test results of beams LS-2.1 and LS-2.2 (which will be discussed later), beams LS-2.3 and LS-2.4 were corroded using a constant current density of 300 μA/cm^2.

4.2.2 Specimen Preparation

All small-scale beams had a rectangular cross-section of 145 x 250 mm and an overall length of 1800 mm. Each beam was longitudinally reinforced with 2-10M steel bars in tension and 2-10M steel bars in compression. The provided tensile reinforcement ratio is 0.63% while minimum code requirement is 0.33% ($A_{s,prov.}/A_{s,min.}$=1.91). The beams were also transversely reinforced with 10M U-stirrups spaced at 110 mm c/c. The thickness of concrete cover was 15 mm. On the other hand, all large-scale beams had a rectangular cross-section of 200 x 300 mm and an overall length of 3400 mm. Each beam was longitudinally reinforced with of 3-15M steel bars in tension and 2-10M steel bars in compression. The provided tensile reinforcement ratio is 1.17% while minimum code requirement is 0.42% ($A_{s,prov.}/A_{s,min.}$=2.82). The beams were also transversely reinforced with 10M U-stirrups spaced at 150 mm c/c. The thickness of concrete cover was 25 mm. The dimension of beams, reinforcement layout and detailing are shown in Figure 4.1.

A four-point bending test was used to load the small-scale and large-scale beams that had constant moment regions of 500 mm and 1000 mm, respectively. In order to examine the pure flexural behavior of beams, the bottom longitudinal steel bars were only corroded within the middle constant moment region. For that reason, the bottom longitudinal steel bars were covered with an epoxy-coated layer in the regions outside the constant moment zone. In addition, the stirrups were covered with an electrical tape at the points of contact with the longitudinal reinforcement, to prevent them from corroding. All bottom longitudinal steel bars were connected with wires used for power supply during the corrosion phase of testing.

4.2.3 Material Properties

All beams were constructed with a normal strength concrete that was supplied by a ready-mix concrete company. Small scale and large-scale beams were cast using the same concrete batch that had a water-to-cement (w/c) ratio of 0.5 and a maximum aggregate size of 14 mm. The compressive strength of concrete was evaluated by testing standard cylinders with a diameter of 100 mm and a height of 200 mm, in accordance with ASTM C39 "Standard Test Method for Compressive Strength of Cylindrical Concrete Specimens". The average compressive strength of concrete at 28 days was equal to 38.0 MPa.

Steel reinforcement properties were evaluated in accordance with ASTM A370 "Standard Test Methods and Definitions for Mechanical Testing of Steel Products". The direct tensile test was conducted using MTS universal testing machine. Three coupons were tested for each reinforcing bar size. The average yield and ultimate strengths of 10M deformed steel bars were 445 MPa and 591 MPa, respectively, while those of 15M deformed steel bars were 404 MPa and 605 MPa, respectively.

4.2.4 Accelerated Corrosion

As mentioned previously, corrosion of steel reinforcement was accelerated using the direct impressed current technique. Figure 4.2 shows a schematic illustration of the accelerated corrosion test setup. As shown in the figure, a direct current was impressed between the bottom longitudinal steel bars which served as the anode and a 20 Gauge 316 LN stainless steel sheet which served as the cathode. The flow of current between the anode and cathode was monitored through the use of separate power supply for each steel bar. The power supplies that were used to corroded the small-scale beams had a maximum voltage capacity of 20 V and a maximum current capacity of 150 mA, while those for large-scale beams had a maximum voltage capacity of 30 V and a maximum current capacity of 3 A. The cathode was placed inside the styrofoam tray that was attached to the middle bottom portion of beams. In order to depassivate the steel bars, an electrolyte solution in the form sodium chloride (5% NaCl) was added to the tray. The corrosion process was activated by applying a constant current based on the current densities discussed in the experimental testing program.

4.2.5 Instrumentation

Ten electrical strain gauges were attached at select positions on the bottom and top longitudinal steel bars as shown in Figure 4.3. The positions of internal strain gauges were carefully selected for a better understanding of the behavior of compression struts between loads and supports. All strain gauges were covered with three protection layers to prevent them from being damaged due to moisture or while casting the beams. Furthermore, external rosette strain gauges were attached on the side and top faces of beams as shown in Figure 4.4. The position and number of rosette strain gauges were selected to capture the change in strut angle during the experimental testing of beams.

Linear variable differential transformers (LVDT) were used to measure the displacements at the center of beams. Test data were collected by a computerized data acquisition system. Prior to testing, the pressure sensors, LVDTs, strain gauges and corrosion wires were connected to the data acquisition system. All measurements were captured at a sampling rate of 50 Hz during the loading stage of testing, and 1 Hz during the sustained exposure to corrosion and service loads stage of testing.

4.2.6 Test Setup and Loading Protocol

A four-point bending test was performed using the steel frames shown in Figure 4.5. The frames that were used to test the small-scale and large-scale beams were designed in a similar fashion. The systems consisted of self-supported frames with beams that span the columns in both directions. Test specimens were placed on two steel plates that react on the bottom beam. The steel plates were designed to simulate simple supports with span lengths of 1500 mm and 3000 mm for small-scale and large-scale beam testing, respectively. Loads were applied using hydraulic jacks that react on the top beam. The load jacks were placed in such a way to generate constant moment regions with lengths of 500 mm and 1000 mm within the middle of portion of small-scale and large-scale beams, respectively. Prior to testing, a thin layer of dental plaster was added at interfaces between the beam and steel plates to ensure a uniform transfer in forces. Figure 4.6 shows a typical test setup from one of the corroded small-scale and large-scale beams.

Testing of control beams (SS-1.1/SS-1.2 and LS-1.1/LS-1.2) was initiated by increasing the applied loads at a rate of 3.5 kN/min up until the failure of beams, to establish their ultimate load

capacities. For the corroded beams, loads were first increased to 60% of the beam ultimate load capacity. This load was equivalent to approximately 60 kN and 80 kN for the small-scale and large-scale beams, respectively. Next, this load was sustained and the corrosion process of the bottom longitudinal steel bars was activated. As mentioned previously, testing of beams SS-2.1/SS-2.2 and LS-2.1/LS-2.2 was not limited to a targeted mass loss, and hence corrosion of reinforcement and applied loads were sustained until the failure of beams. For that reason, the duration of test (i.e., equivalent to the laboratory service life of beams) was dependent on the failure of beams. Likewise, the test of beam LS-2.3 was conducted in a similar way as beam LS-2.1, however the corrosion process was stopped after 61 days (i.e., equivalent to 41% of the laboratory service life of the large-scale beam), and then loads were further increased from the service baseline up until the failure of the beam. Lastly, testing of beam LS-2.4 was conducted in a similar way as beam LS-2.1, however the beam was corroded under its self-weight only (i.e., without added loads). The corrosion process of this beam was stopped after 103 days, and then loads were applied up until the failure of the beam.

4.2.7 Level of Corrosion

Upon the completion of testing, the corroded longitudinal steel bars were extracted from the corroded portion of beams. The corroded steel bars were then cleaned from adhering mortar and corrosion by-products in accordance with ASTM G1-03 "Standard Practice for Preparing, Cleaning, and Evaluation Corrosion Test Specimens". The corrosion level of steel bars was assessed quantitatively using the gravimetric measurements and localized sectional area loss. In the gravimetric method, the corrosion level is expressed in the following:

$$\eta_{avg,m}(\%) = \frac{m_0 - m_c}{m_0} \times 100\% \tag{4.1}$$

where, $\eta_{avg,m}$ is the average mass loss of steel bars due to corrosion, m_0 and m_c are the weights of non-corroded and corroded steel bars, respectively. In order to assess the localized corrosion level, a three-dimensional (3D) laser scanner was used to estimate the sectional loss of steel reinforcement along the corroded portion of beams. Further details with regards to the scanner can be found in a companion study (Al-Bayti et al., 2022a). The corrosion level in terms of sectional area loss is expressed in the following:

$$\eta_{3D}(\%) = \frac{A_0 - A_c}{A_0} \times 100\% \quad (4.2)$$

where, η_{3D} is the cross-sectional area loss of steel bars due to corrosion, A_0 and A_c are the cross-sectional areas of non-corroded and corroded steel bars, respectively.

4.3 Results and Discussion

4.3.1 Corrosion Level

After the failure of RC beams, the corroded steel bars were extracted and cleaned as shown in Figure 4.7. The average mass loss for each corroded beam is presented in Table 4.2. A qualitative assessment through visual inspection revealed that there was a loss of reinforcement area due to both forms of corrosion (i.e., generalized and pit corrosion attacks). It was also observed that there was a significant loss of reinforcement area at the cracked sections of beams caused by bending loads. In order to quantitatively demonstrate the influence of flexural crack presence on the distribution of corrosion along the affected region of beams, the spatial distribution of the loss in reinforcement sectional area within the corroded portions of beams SS-3.1 and LS-2.1 are shown in Figure 4.8 and Figure 4.9, respectively. Clearly, the sectional loss of steel reinforcement at the cracked sections of beams was significantly more than other locations within the corroded portion of beams. This can be explained by the fact that the tensile longitudinal steel bars were directly exposed to chloride ions through flexural crack openings. It is important to note that large-scale beams had more flexural cracks within the constant moment region when compared to small-scale beams, and hence large-scale beams experienced more localized sectional area reductions.

4.3.2 Cracking and Failure Patterns

Figure 4.10 shows the cracking patterns at the failure of all control and corroded RC beams. It was found that all control small-scale beams (SS-1.1/1.2) and large-scale beams (LS-1.1/1.2) failed as anticipated in flexure, which can be characterized by a significant amount of deformations prior to crushing of top compression concrete. In contrast, small-scale beams (SS-3.1/3.2) and large-scale beams (LS-2.1/2.2) which were corroded until the end of their service life (i.e., until the failure under service loads), exhibited a brittle failure characterized by a sudden rupture of the corroded longitudinal steel bars. In these beams, it was observed that there was a localization of corrosion at the cracked sections (as discussed previously), and hence the rupture of steel bars took place at

one of the flexural cracks formed within the constant moment region of beams. It is noted that the rupture failure did not always take place at the center of beams (see beams SS-3.2 and LS-2.1 failures), which could be attributed to the further reduction in reinforcement sectional area at one of the adjacent cracks rather than the one located close to the center. Prior to their failure, it was observed that the critical flexural crack became wide, and started to further extend towards the top of beams, however its propagation was prevented by the top longitudinal steel bars. In contrast to the brittle failures of large-scale beams LS-2.1 and LS-2.2, the remaining corroded large-scale beams LS-2.3 and LS-2.4 failed in flexure. Both beams displayed a ductile response characterized by the development and widening of flexural cracks prior to crushing of top compression concrete. Figure 4.11 shows a typical illustration of concrete crushing and brittle failures observed in the testing of corroded large-scale beams.

At the end of testing, corrosion-induced cracks were mainly observed on the bottom face of RC beams. Figure 4.12 shows a typical illustration of the longitudinal corrosion cracks developed in small scale-beam SS-3.1 and large-scale beam LS-2.1. This type of cracking occurred due to the volumetric expansion of corrosion by-products around the embedded corroded steel bars, resulting in the generation of internal pressures greater than the tensile capacity of concrete. This in turn, resulted in weakening of bond characteristics at the interface between the corroded reinforcement and concrete. However, the loss in bond was localized, as evidenced by the reasonably intact cover concrete observed at the end of the test, except for the main crack that led to failure. Indeed, the removal of concrete cover to access the corroded steel bars for further examination created a challenge, and could not be removed without using a jack hammer. It is believed that, any loss in bond and associated bar slippage outside of the main crack region resulted in redistribution of stresses without affecting the load-displacement relationship recorded.

4.3.3 Structural Performance of RC Beams

4.3.3.1 General Behavior

Figure 4.13 displays the load and mid-span displacement relationships of small-scale and large-scale beams. Table 4.2 summarizes key findings from the experimental testing program; where, P_u is the ultimate load, Δ_u is the ultimate displacement, P_R is the residual capacity ratio defined as the ultimate load capacity of the corroded beam relative to the ultimate load capacity of the control beam, Δ_R is the residual ductility ratio defined as the ultimate displacement of the corroded beam

relative to the ultimate displacement of the control beam. It is important to emphasize that some beams were corroded until their failure under service loads, and hence the displacement at yield cannot be established from the load-displacement curves of beams. For that reason, the influence of corrosion on the ductility of beams was quantified using the residual ductility ratio. This ratio was also adopted by other researchers (Dang and François, 2014). The residual capacity and ductility ratios of corroded small-scale and large-scale beams were calculated relative to control beams SS-1.2 and LS-1.1, respectively.

Small-scale beams:

As shown in Figure 4.13(a), the overall behavior of control small-scale beams SS-1.1 and SS-1.2 was almost identical. It can be observed that both beams exhibited the expected ductility prior to their ultimate crushing of top concrete, as typically observed in flexure-dominant reinforced concrete beams. At the end of the test, displacements of beam SS-1.1 were higher than SS-1.2 because loading in beam SS-1.1 was continued after the crushing failure. In contrast, the corroded small-scale beams experienced significant reductions in their ultimate load capacities in comparison to control beams. It is worth noting that loads were sustained up until the failure of beams, and hence beams SS-3.1 and SS-3.2 had residual capacity ratios of 0.55 and 0.56, respectively. In terms of ductility, corroded beams SS-3.1 and SS-3.2 had residual ductility ratios of 0.28 and 0.32, respectively. This drastic reduction in ductility can be explained by the non-uniform distribution of reinforcement sectional area along the corroded portion of beams caused by the added loss of reinforcement at the positions of cracks or due to pit corrosion.

Large-scale beams:

Similar to small-scale beams, control large-scale beams LS-1.2 and LS-2.2 exhibited the expected ductility prior to their flexural failure. The overall behavior of both beams was similar, however beam LS-1.2 had a slightly softer response. The corroded large-scale beams LS-2.1 and LS-2.2 had residual capacity ratios of 0.59 and 0.56, respectively, as anticipated, since service loads were sustained up until their failure. It was also found that both beams experienced significant reductions in ductility, with beams LS-2.1 and LS-2.2 having residual ductility ratios of 0.39 and 0.40, respectively. In contrast to the beams which were loaded until the end of their service life, large-scale beams LS-2.3 and LS-2.4 displayed a better performance in terms of ultimate load

capacity and ductility. Large-scale beams LS-2.3 and LS-2.4 had residual capacity ratios of 0.89 and 0.87, respectively, and residual ductility ratios of 1.09 and 0.87, respectively.

4.3.3.2 Time-Dependent Behavior

Figure 4.14 shows the displacement time histories of the corroded beams under 60% of the beam ultimate load capacity. It should be noted that the initial increase in deflections during the first hour of testing is caused by the application of sustained loads. After that, it can be observed that there was an increase in deflections under the simultaneous exposure to reinforcement corrosion and service loads, which can be divided into two stages. In the first stage, the increase in deflections occurred at a steady slow rate which is primarily attributable to the damage induced by corrosion and the creep effect of sustained loading. In the second stage, the increase in deflections was more rapid and occurred over a shorter period of time when compared to the previous stage. This sudden increase in defections can be attributed to yielding of corroded tensile steel bars at the critical flexural crack. The continuous loss of reinforcement area, especially at the critical crack, coupled with the sustained service load led to the rupture of the corroded steel bars.

To better comprehend the response of corroded beams under 60% of the beam ultimate load capacity, strains in the bottom and top longitudinal steel bars, as well as concrete strains are plotted in Figure 4.15. Prior to the failure of beams, strains in top concrete at the mid-span of beams SS-3.1/3.2 and LS-2.1/2.2, shown in Figure 4.15(a), were well-below the crushing limit of 3500 μm/m, which confirms that crushing of concrete did not occur in all these beams. Strains in top longitudinal steel bars at mid-span, shown in Figure 4.15(b), indicate that these bars were initially in compression, however they became in tension with the progression of corrosion over time. Strains in bottom longitudinal steel bars at 275 mm (for small-scale) and 600 mm (for large-scale) away from the left support, shown in Figure 4.15(c), show that there was a slight increase in strains over the service life of beams.

A typical distribution profile of the increase in strains due to corrosion for beams SS-3.1 and LS-2.1 is shown in Figure 4.16. In this figure, the increase in strains is calculated by subtracting strains after loading the beams to the desired service level from strains at the failure. It is noted that all strain values are expressed in μm/m. It can be observed that there was a slight increase in strains over time. This indicates that corrosion of longitudinal steel bars within the constant moment region of beams, had a slight influence on the transfer and redistribution of strains/stresses to the

adjacent shear spans. Accordingly, the degradation of bond strength within the corroded portion of beams did not increase the demands at the beams ends. Such behavior describes a typical beam action response, and hence the tied-arch mechanism explained in Coronelli and Gambarova (2004) was not activated. The beam action behavior can be also verified using concrete strains from the external triaxial rosettes attached on the side face of beams SS-3.1 and LS-2.1, as shown in Figure 4.17. It is clear that the strains were relatively small, and their change over time was also small.

4.4 Influence of Parameters

4.4.1 Influence of Current Density

The influence of corrosion current density is examined by comparing large-scale beam LS-2.1 (corroded using a current density of 300 $\mu A/cm^2$ for 90% of test duration) and beam LS-2.2 (corroded using a current density of 1000 $\mu A/cm^2$ for 83% of test duration). As shown earlier, both beams had an almost identical response in terms of ultimate load capacity and ductility at the end of their service life. However, the failure time of beam LS-2.2 (191 days) was longer than beam LS-2.1 (150 days), which in turn contributed to a higher achieved corrosion level in beam LS-2.2 (25.1%) in comparison to beam LS-2.1 (21.1%). This increase in duration to cause the failure of beam LS-2.2 might be attributed to the accelerated approach employed to corrode the beam. The use of such high current density would initially accelerate the corrosion process of steel bars. However, as the corrosion by-products starts to build-up and quickly fill the voids and cracks around the embedded steel bars, their presence could block chloride ions from reaching the surface of steel bars, which slows down the corrosion process. This phenomena was also explained by Azam et al. (2016). Based on the results of both tests, the behavior of the remaining large-scale beams (LS-2.3 and LS-2.4) was assessed using a constant current density of 300 $\mu A/cm^2$.

4.4.2 Influence of Corrosion Level

The influence of corrosion level on the structural performance of large-scale beams is shown in Figure 4.18. This figure examines beam LS-1.1 (no corrosion), beam LS-2.3 (41% of the beam service life), and beam LS-2.1 (at end of the beam service life). Clearly, both yield and ultimate load capacity ratios were reduced with increased corrosion levels. However, the decline rates are faster after achieving a corrosion level of 15.5%. Besides, it is interesting to note that the reduction in ultimate load capacity was less than that of yield load capacity. This can be explained by the

added tensile capacity provided by the increase in stress levels in the longitudinal tensile steel bars, exhibiting strain hardening at ultimate. In terms of ductility, it is evident that the ductility was improved at a corrosion level of 15.5% which could be explained by the decrease in tensile reinforcement ratio due to the corrosion and/or the variability of concrete material that has a significant impact on concrete crushing failure at this corrosion level since this beam behaved in flexure. At a corrosion level of 21.1%, the beam exhibited a drastic reduction in ductility (i.e., rupture of steel bars) due to the non-uniform distribution of corrosion. Finally, it should be noted that increasing the level of corrosion is not directly related to time, since beam LS-2.3 was corroded for a duration equivalent to 41% of beam LS-2.1, however beam LS-2.3 achieved a corrosion level of approximately 73% of that in beam LS-2.1.

4.4.3 Influence of Loading Presence

The influence of loading presence while corroding the beams is examined by comparing beams LS-2.1 and LS-2.4 which were corroded under 60% and 0% of the beam ultimate load capacity, respectively. Beam LS-2.1 was corroded over a longer duration than beam LS-2.4, resulting in a slightly more corrosion level in beam LS-2.1 (21.1%) when compared to beam LS-2.4 (20.2%). That being said, the achieved corrosion level in beam LS-2.4 is approximately 97% of that in beam LS-2.1, and hence a direct comparison between both beams is appropriate. Figure 4.19 compares the flexural performance of both beams relative to the control beam. It can be observed that, in the presence of service loads, beam LS-2.1 exhibited further reductions by approximately 36% in yield load capacity, 32% in ultimate load capacity, and 55% in ductility relative to beam LS-2.4 which was corroded under no loads. These amplified reductions in load capacities and ductility for beams which were corroded under loads were also found by other researchers (Al-Bayti et al., 2022b; Du et al., 2013). These observations highlight the influence of flexural crack presence and its impact on the localization of corrosion at the cracked sections of corroded beams under service loads.

4.4.4 Influence of Percentage Steel and Number of Bars

The influences of percentage of steel and number of bars are examined by comparing the flexural behavior of small-scale (SS-3.1/3.2) and large-scale (LS-2.1/2.2) beams. There are two key parameters that could have contributed to the difference in the response of beams. These are the tensile reinforcement ratio and the number of longitudinal tensile steel bars. As described previously, small-scale beams had a tensile reinforcement ratio of 0.63% ($A_{s,prov.}/A_{s,min.}$=1.91) in

the form of 2-10M steel bars, while large-scale beams had a tensile reinforcement ratio of 1.17% ($A_{s,prov.}/A_{s,min.}$=2.82) in the form of 3-15M steel bars. However, both beams were corroded under the coupled effects of reinforcement corrosion and service loads equivalent to 60% of the beam ultimate load capacity.

As shown in Figure 4.20, the residual capacity and ductility ratios of small-scale beams decreased more rapidly than large-scale beams with increased corrosion levels. The reductions in load capacity and ductility are closely related to the loss of reinforcement area at the transverse flexure cracks of the beams. Small-scale beams had wider flexural cracks than large-scale beams since they were reinforced with a lower tensile reinforcement ratio. This increase in crack width creates an easier pathway for chloride ions to reach the exposed surface of tensile steel bars, which in turn accelerates the degradation of load capacity in small-scale beams. Due to the rapid reduction in load capacity, the laboratory service life of small-scale beams was also reduced drastically. For example, the average laboratory service life of small-scale beams was approximately 3.8 times lower than that of large-scale beams.

Furthermore, the number of longitudinal steel bars used in tension might have contributed to the response of beams. In large-scale beams, the failure of one steel bar (i.e., rupture) might not result in a beam failure as the remaining two steel bars could potentially generate enough resistance to withstand service loads. This is possible in large-scale beams since they had a relatively good ratio between the provided tensile reinforcement and minimum code requirements. In contrast, the failure of one steel bar in small-scale beams could potentially lead to collapse as the remaining corroded steel bar is likely to rupture too, since small-scale beams had a tensile reinforcement ratio close to minimum code requirement. Accordingly, the tensile reinforcement ratio and number of steel bars have strong influences on the response of the two different beam scales subjected to a similar corrosion exposure and service loading levels.

4.4.5 Practical Implications

The results of this study has practical importance in assessing the behavior of damaged RC bridge beams/girders due to corrosion. As demonstrated previously, the serviceability of beams is strongly influenced by the interaction of service loads and corrosion of the main flexural reinforcement. The presence of transverse cracks, induced by service loads, combined with chloride penetration, would accelerate the response of RC beams/girders beyond their

serviceability. Under high service loads, the beams could exhibit premature brittle failures with limited ductility due to the non-uniform distribution of corrosion and the additional loss of reinforcement steel at crack openings. In such cases, there are no warning signs that can be observed before the failure of beams, other than the formation of corrosion by-products and the development of longitudinal cracks in the affected region. As such, it is important to address the presence of high service loads in RC bridge beam/girders by either reducing traffic loads and/or fixing the existing cracks (due to either loads or shrinkage) in the critical flexural zones.

In addition, providing a higher amount of reinforcement above the minimum code requirements (but less than the balanced ratio) could slow down the degradation rates of load capacity and ductility in corroded RC beams, which in turn increases their service life. As a result, it is recommended to provide RC beams/girders located in critical flexure regions with higher amounts of reinforcement above the minimum required to ensure the safety of bridge structures over their life span.

4.5 Conclusions

An experimental program was carried out to examine the time-dependent structural behavior of small-scale and large-scale RC beams under the coupled effects of reinforcement corrosion and service loads. The following conclusions can be drawn from this study:

1) The presence of flexural cracks in beams subjected to the coupled effects of reinforcement corrosion and service loads of 60% of the beam ultimate load capacity led to a localized loss of reinforcement sectional area at the cracked sections of beams. This in turn, resulted in a sudden rupture of corroded tensile steel bars through crack openings at the end of service life of beams. These beams exhibited significant reductions in ultimate load capacity and ductility by more than 40% and 60%, respectively.
2) Test results showed that the degradation of bond strength at the interface between the corroded steel bars and concrete due to increased corrosion levels, had a minimal impact on the response of the corroded beams considered in this study. This was explained by the slight redistribution in strains/stresses from the corroded constant moment region to the adjacent shear-dominant regions in corroded beams.
3) The presence of service loads is an important parameter that should be taken into consideration when assessing in-service corroded RC beams. In this study, the large scale

beam under service loads, experienced further reductions by approximately 36% in yield load capacity, 32% in ultimate load capacity, and 55% in ductility when compared to the beam that was corroded under no loads. This behavior is only expected in corroded beams with load-induced bending cracks.

4) Small-scale beams experienced more rapid decline in loading capacity than large-scale beams, which could be attributed to the increase of flexural crack width in small-scale beams because of the low percentage of steel used. Increasing the width of flexure cracks creates a clear and easy pathway for the chloride ions to reach the exposed tensile steel bars, and hence increasing the localized effect of corrosion.
5) The provided tensile reinforcement area ratio relative to minimum code requirement is a key parameter that contributes to the response of corroded RC beams of different sizes. It is recommended to provide a higher tensile reinforcement ratio and the use of multiple steel bars for enhanced redundancy to ensure that there are multiple paths for the beam to withstand service loads in the case where one steel bar ruptures due to corrosion.
6) At the end of service life, the overall behavior of large-scale beams that were corroded using different current densities was almost identical. However, the use of a very high current density delayed the failure of the beam due to the fast build-up of corrosion by-products around the embedded steel bars, which filled up the voids and cracks of concrete, slowing down the corrosion process of steel bars.

Table 4.1: Experimental testing program

Beam size	Beam designation	Loading type	Current density ($\mu A/cm^2$)	Corrosion duration
Small-scale	SS-1.1/SS-1.2	Monotonic to failure	NA	NA
	SS-3.1/ SS-3.2	Sustained load (i.e., 60% of ultimate) coupled with corrosion of reinforcement	300	up to failure
Large-scale	LS-1.1/LS-1.2	Monotonic to failure	NA	NA
	LS-2.1	Sustained load (i.e., 60% of ultimate) coupled with corrosion of reinforcement	Stage 1:300 Stage 2:1000	135 days up to failure
	LS-2.2	Sustained load (i.e., 60% of ultimate) coupled with corrosion of reinforcement	Stage 1:500 Stage 2:1000	33 days up to failure
	LS-2.3	Stage 1: Sustained load (i.e., 60% of ultimate) coupled with corrosion of reinforcement Stage 2: Monotonic to failure	300	61 days (~41% of LS-2.1)
	LS-2.4	Stage 1: Sustained load (i.e., 0% of ultimate) coupled with corrosion of reinforcement Stage 2: Monotonic to failure	300	103 days (~70% of LS-2.1)

Table 4.2: Summary of key experimental findings

	Beam	Duration (days)	$\eta_{avg,m}$ (%)	P_u (kN)	Δ_u (mm)	P_R	Δ_R	Failure mode
Small-scale	SS-1.1	NA	0	107.84	33.72	-	-	Flexure
	SS-1.2	NA	0	106.00	27.22	1.00	1.00	Flexure
	SS-3.1	37	12.90	58.35	7.53	0.55	0.28	Brittle
	SS-3.2	52	18.98	59.55	8.63	0.56	0.32	Brittle
Large-scale	LS-1.1	NA	0	139.1	51.54	1.00	1.00	Flexure
	LS-1.2	NA	0	131.1	51.44	-	-	Flexure
	LS-2.1	150	21.13	82.10	20.00	0.59	0.39	Brittle
	LS-2.2	204*	25.06	79.65	20.45	0.57	0.40	Brittle
	LS-2.3	61	15.45	123.80	56.43	0.89	1.09	Flexure
	LS-2.4	103	20.20	120.50	44.73	0.87	0.87	Flexure

*beam LS-2.2 experienced an electrical shutdown which started on day 168 and lasted for 13 days. The total duration of corrosion exposure was 191 days.

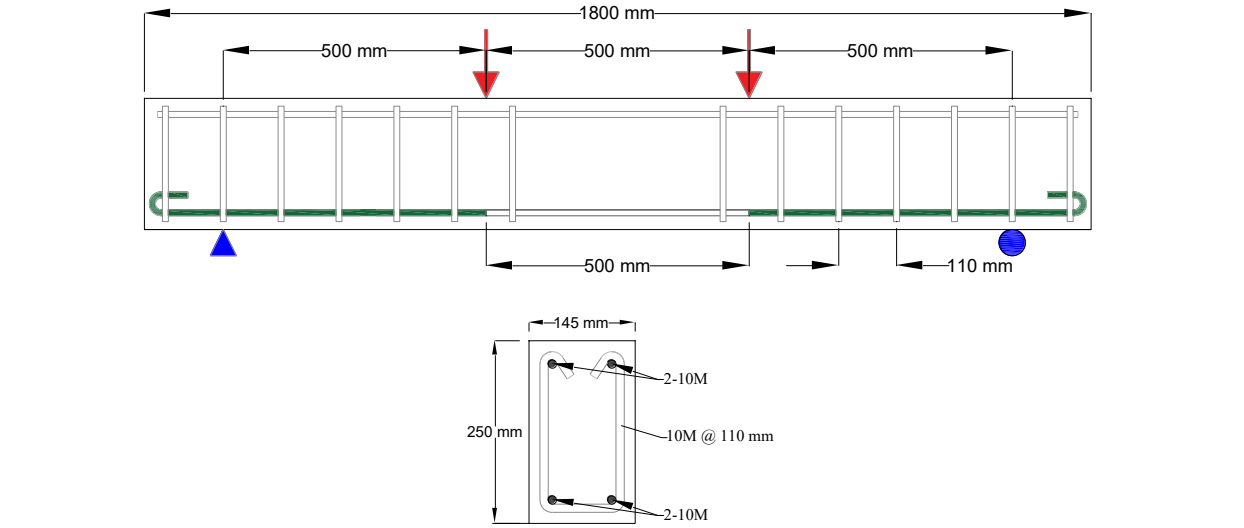

(a) Small-scale

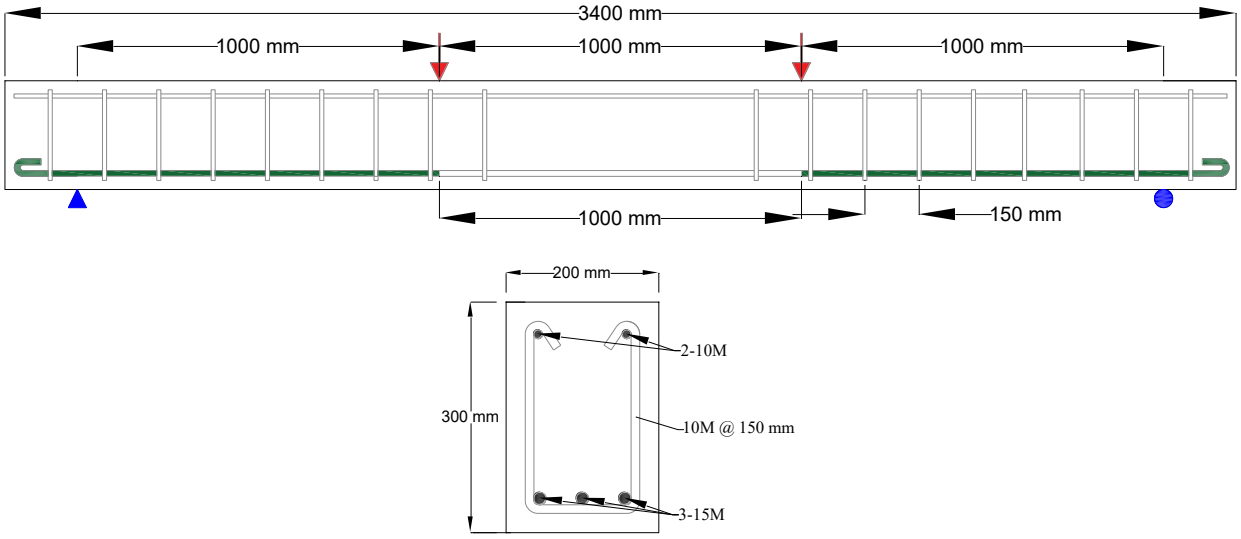

(b) Large-scale

Figure 4.1: Dimension of beams and reinforcement detailing

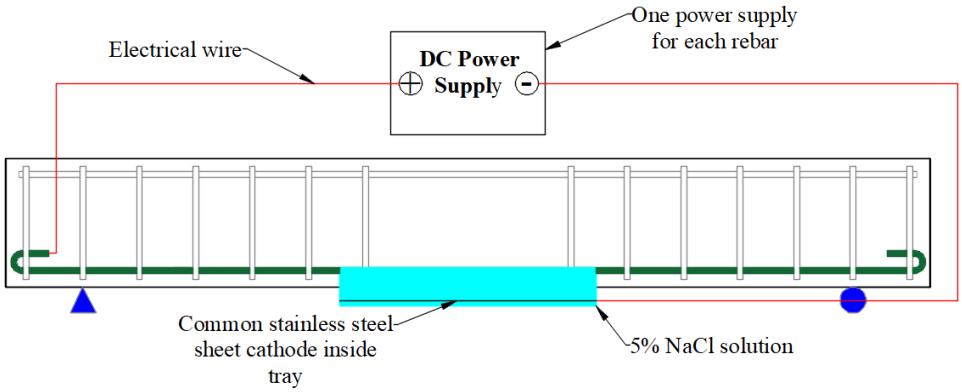

Figure 4.2: Schematic illustration of the accelerated corrosion setup

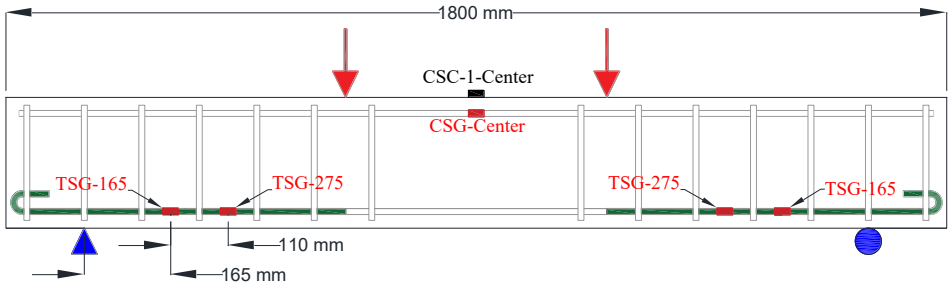

(a) Small-scale beam

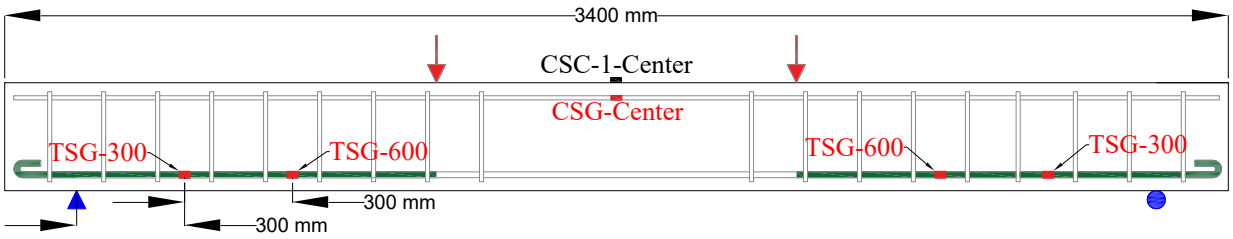

(b) Large-scale beam

Figure 4.3: Position of internal strain gauges

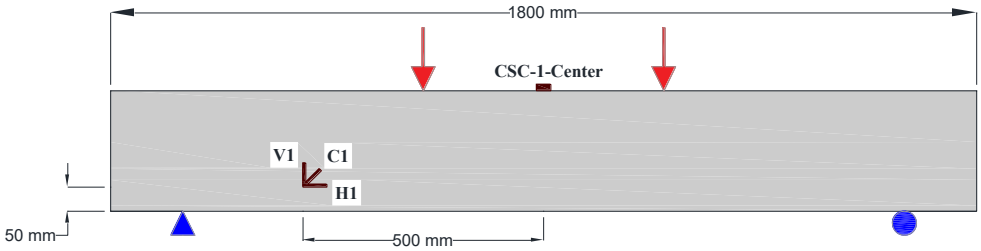

(a) Small-scale beam

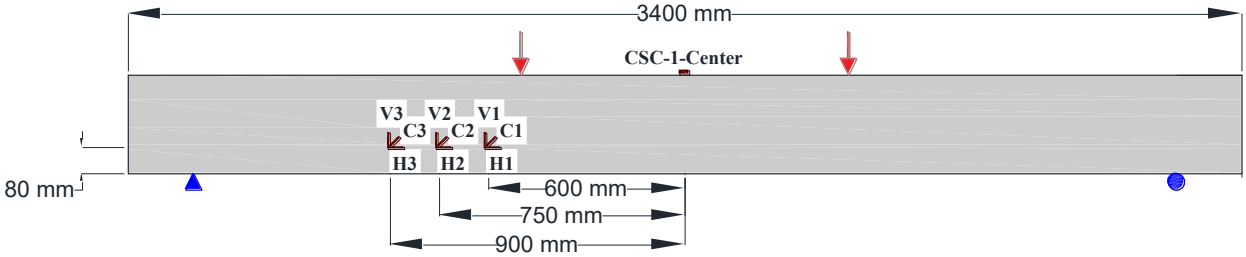

(b) Large-scale beam

Figure 4.4: Position of external strain gauges

(a)

(b)

Figure 4.5: Testing frames for: (a) small-scale beams (b) large-scale beams

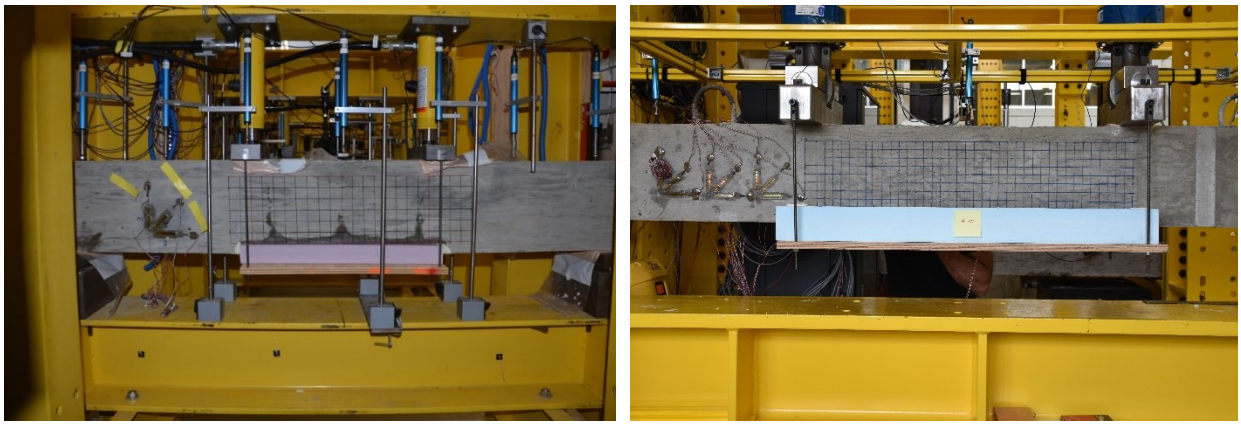

(a) (b)

Figure 4.6: Test setup of: (a) small-scale beams (b) large-scale beams

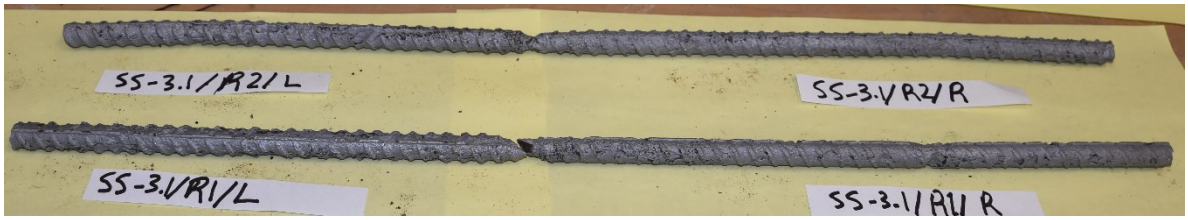

(a) beam SS-3.1

(b) beam LS-2.1

Figure 4.7: Typical illustration of the clean corroded steel bars

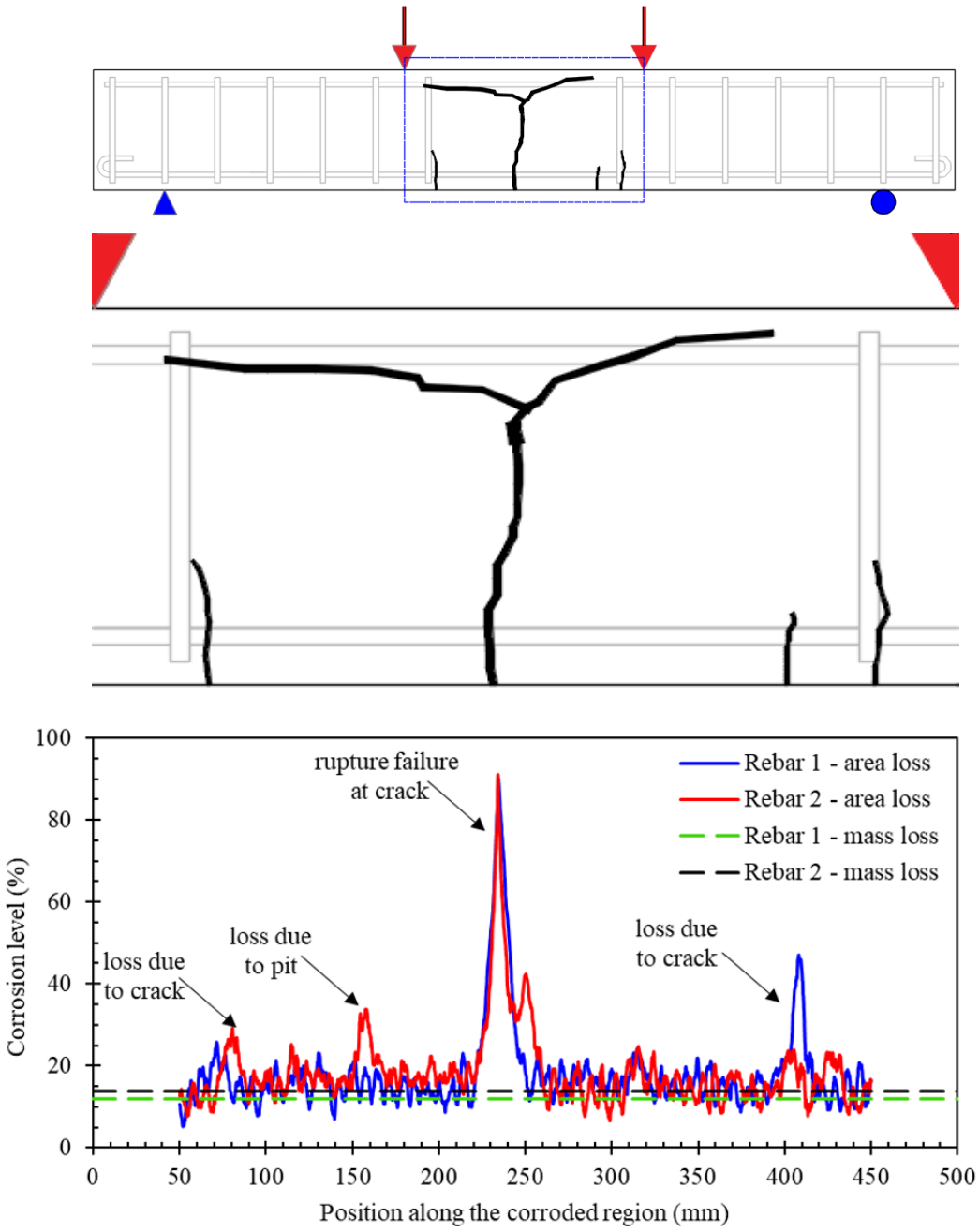

Figure 4.8: Distribution of reinforcement sectional area loss along the corroded zone of beam SS-3.1

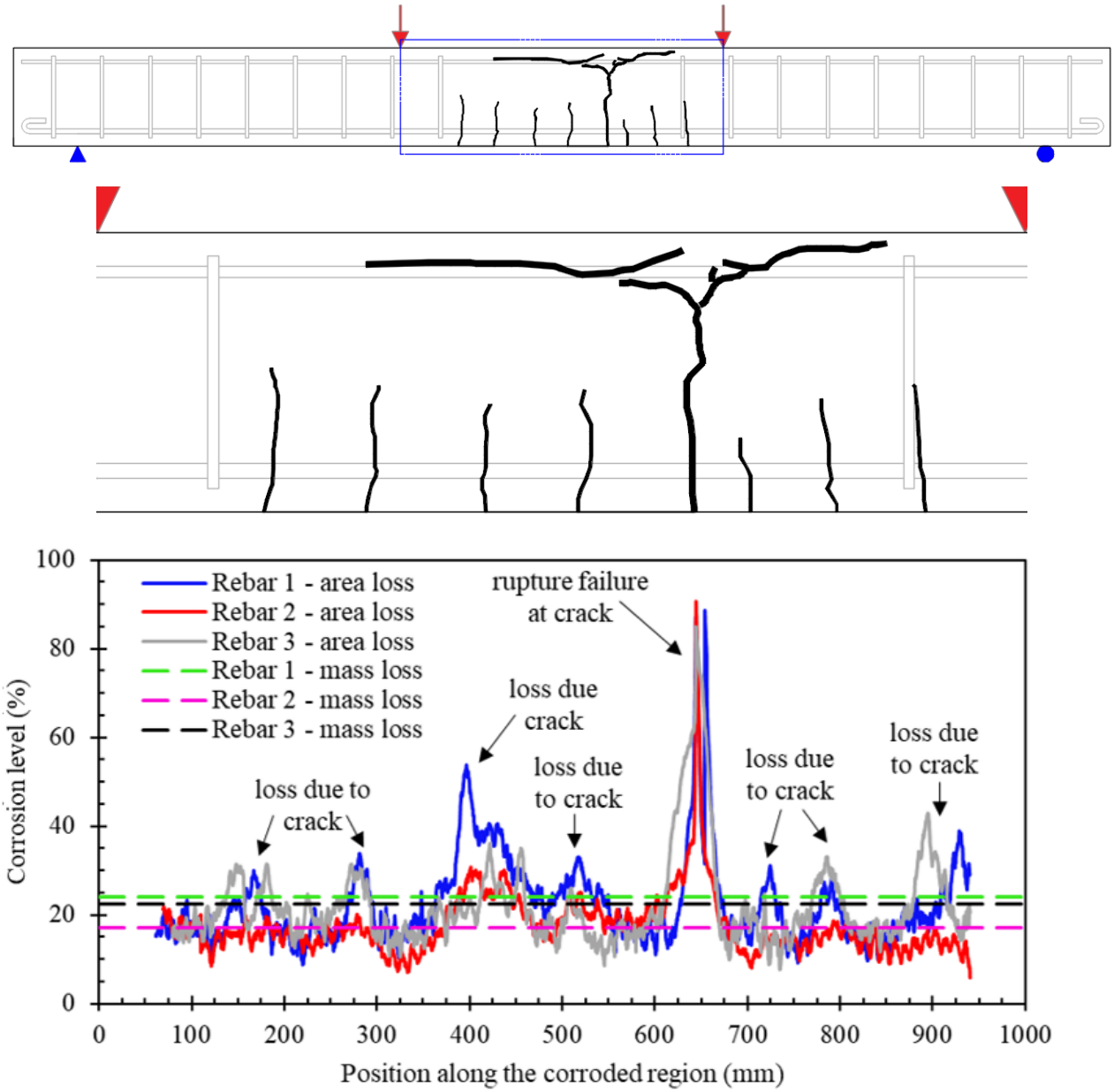

Figure 4.9: Distribution of reinforcement sectional area loss along the corroded zone of beam LS-2.1

(a) SS-1.1

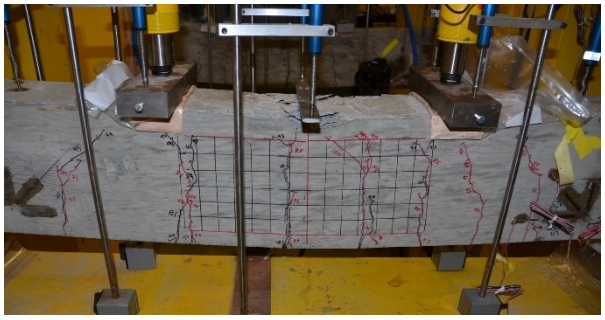

(b) SS-1.2

(c) SS-3.1

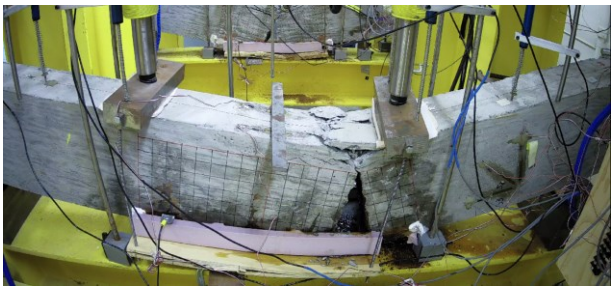

(d) SS-3.2

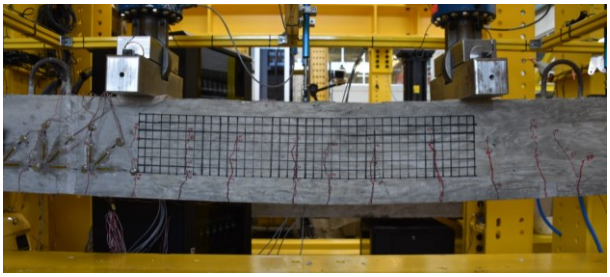

(e) LS-1.1

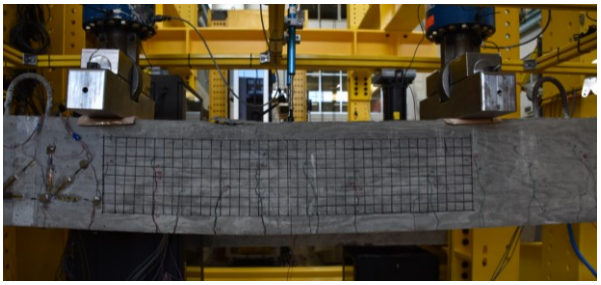

(f) LS-1.2

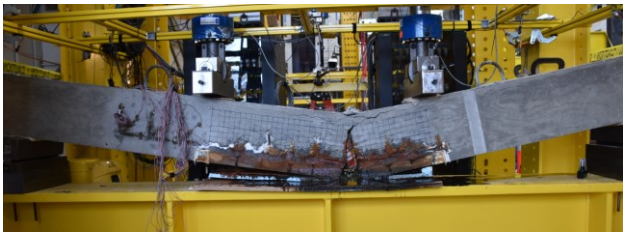

(g) LS-2.1

(h) LS-2.2

(i) LS-2.3

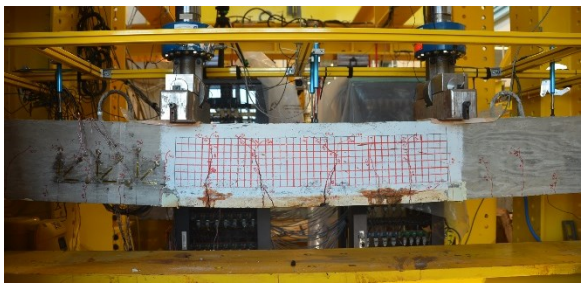

(j) LS-2.4

Figure 4.10: Cracking patterns at failure of RC beams

(a) LS-2.1

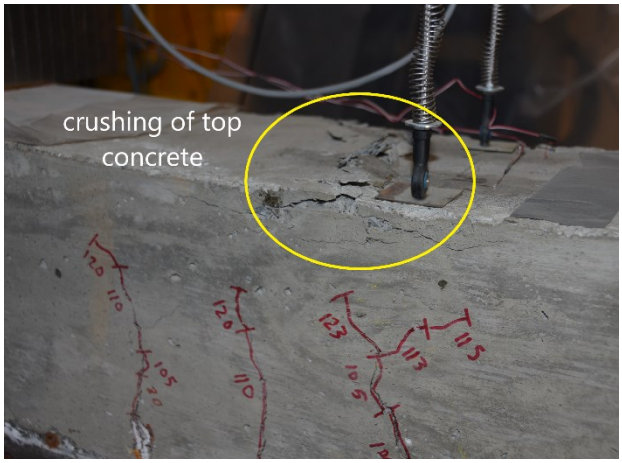

(b) LS-2.3

Figure 4.11: Failure modes of RC beams

(a) SS-3.1

(b) LS-2.1

Figure 4.12: Corrosion-induced cracks on the bottom face of corroded RC beams

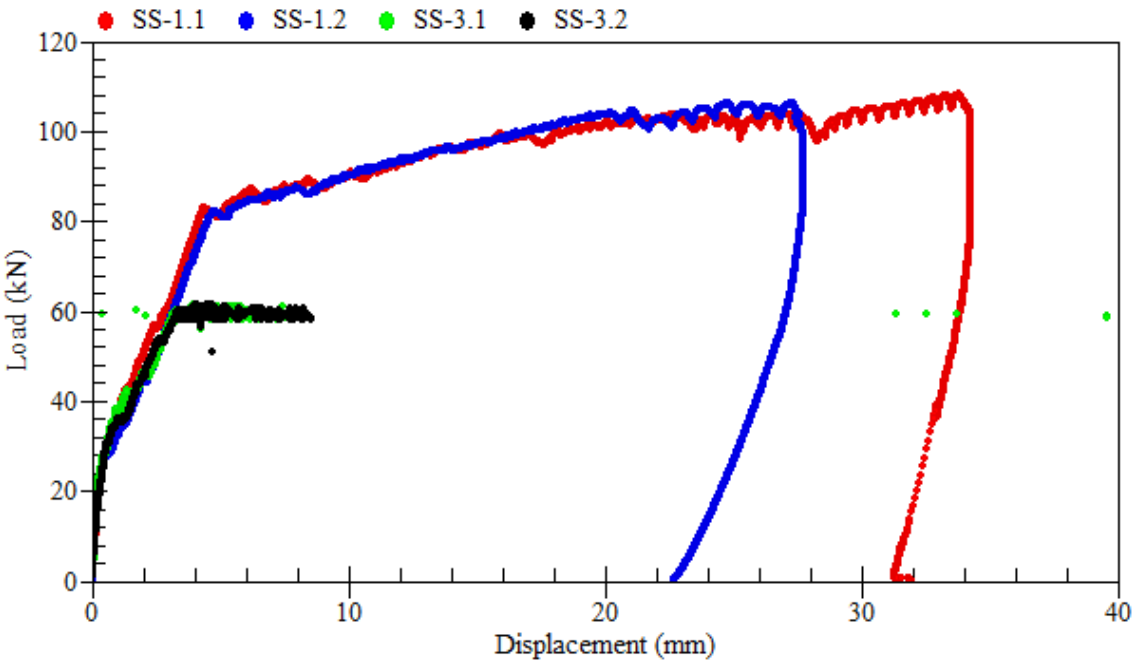

(a) Small-scale beams

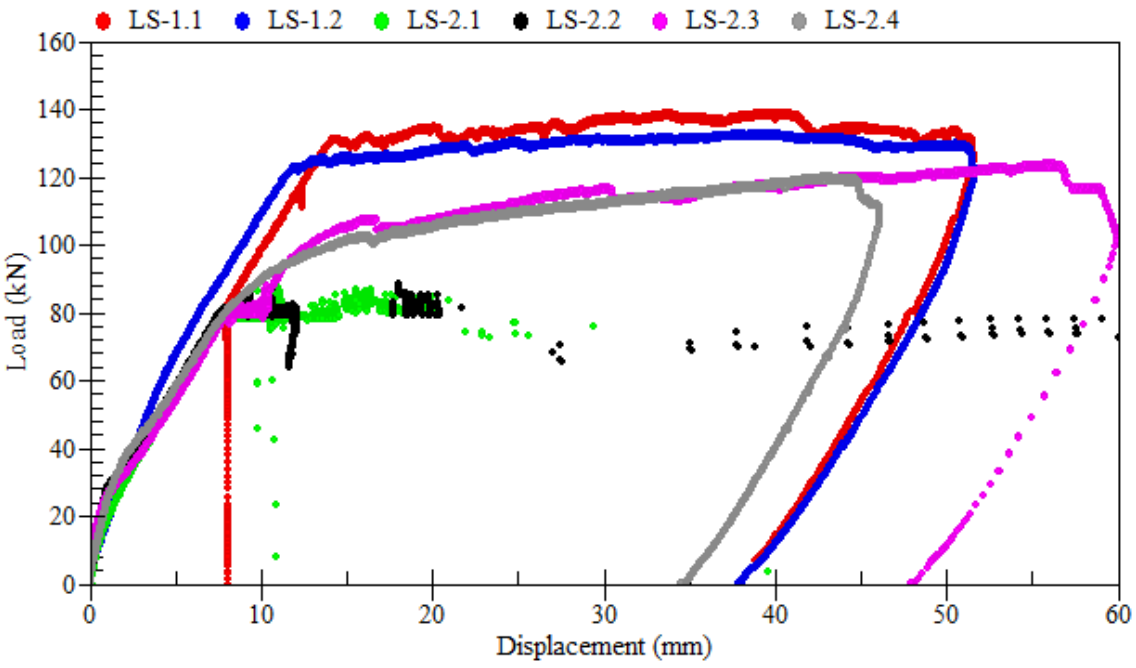

(b) Large-scale beams

Figure 4.13: Load-displacement relationships of RC beams

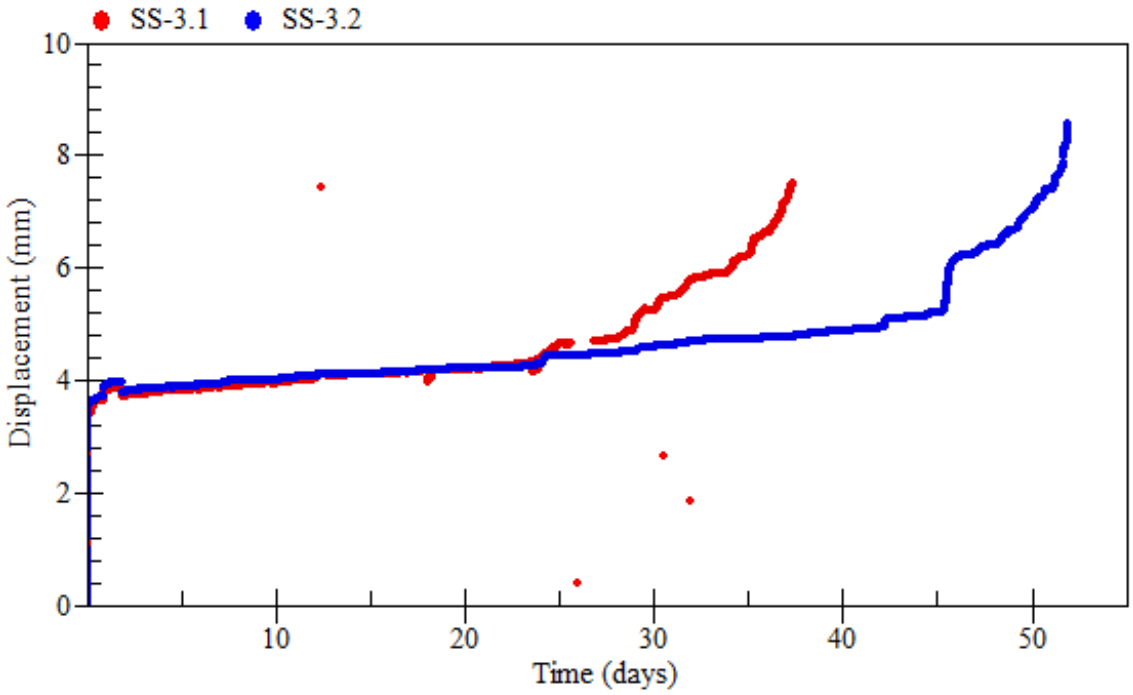

(a) Small-scale beams

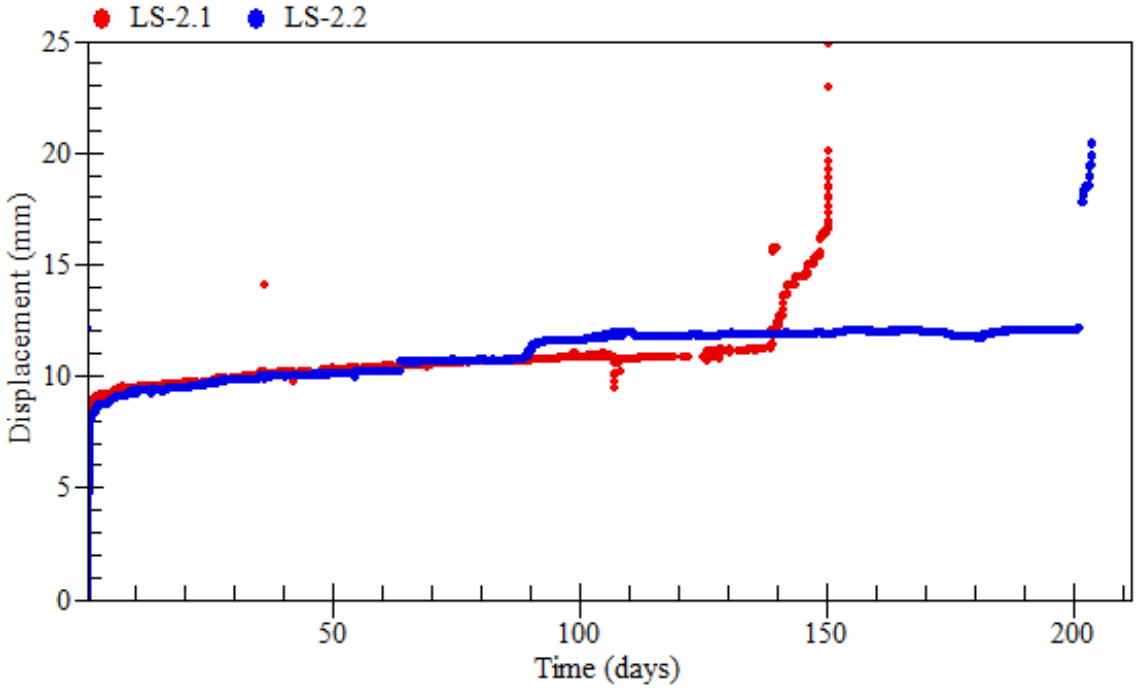

(b) Large-scale beams

Figure 4.14: Displacement-time histories of corroded beams under service loads

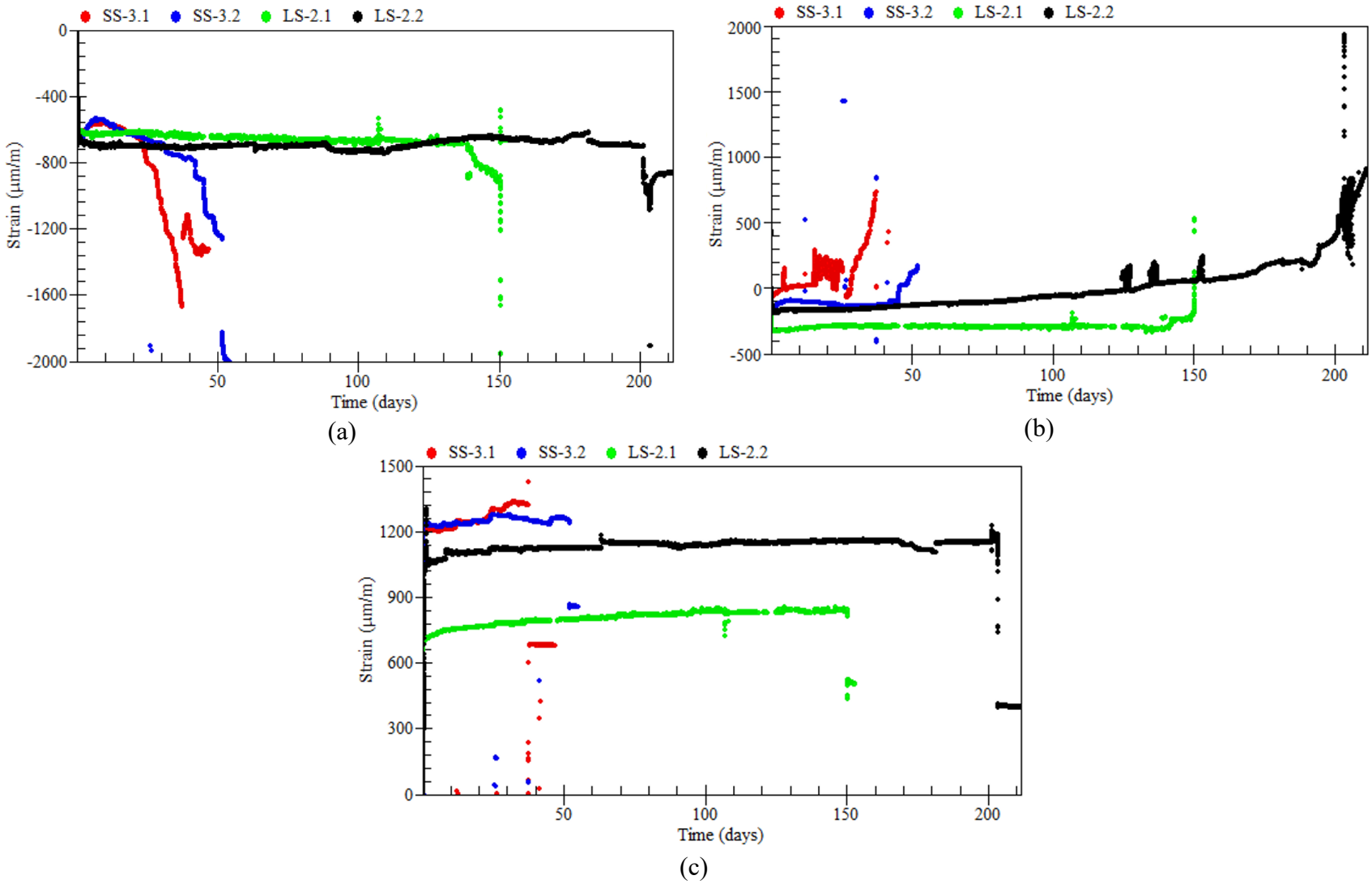

Figure 4.15: Strain measurement from: (a) CSC-1-Center (b) CSG-Center (c) TSG-275 mm (small-scale) and TSG-600 (large-scale) (refer to Figure 6.3 for location of gauges)

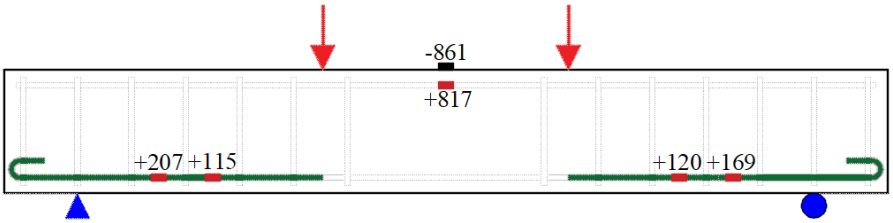

(a) Beam SS-3.1

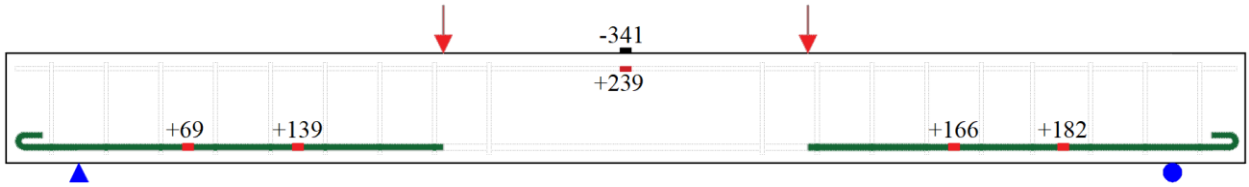

(b) Beam LS-2.1

Figure 4.16: Development of strains in beams subjected to reinforcement corrosion and service loads

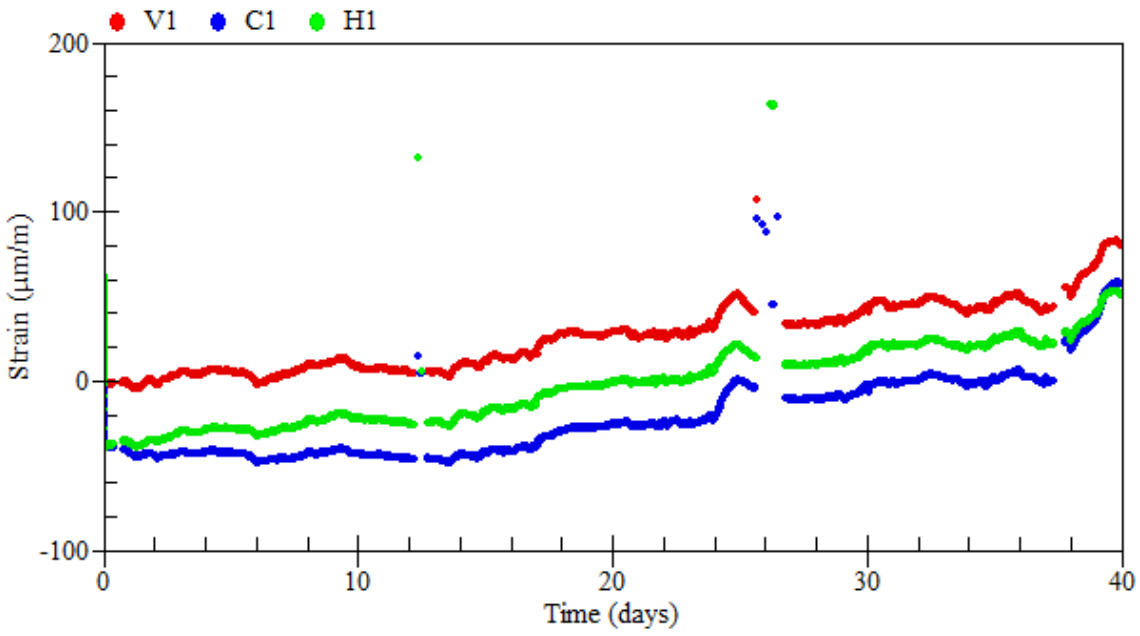

(a) Beam SS-3.1

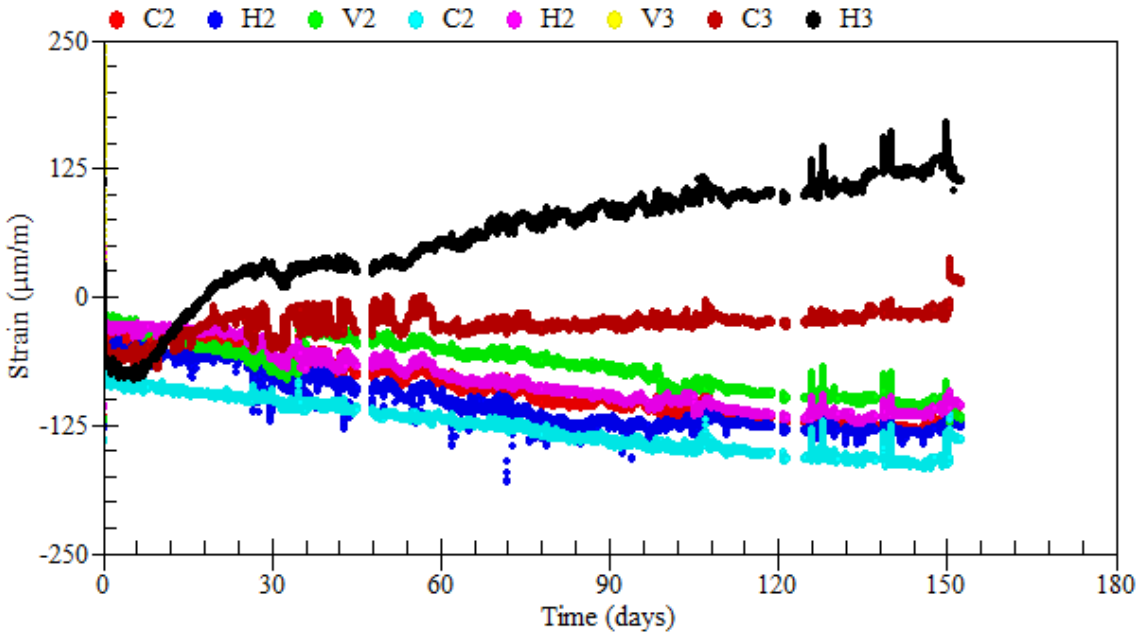

(b) Beam LS-2.1

Figure 4.17: Strain readings from the external triaxial rosette

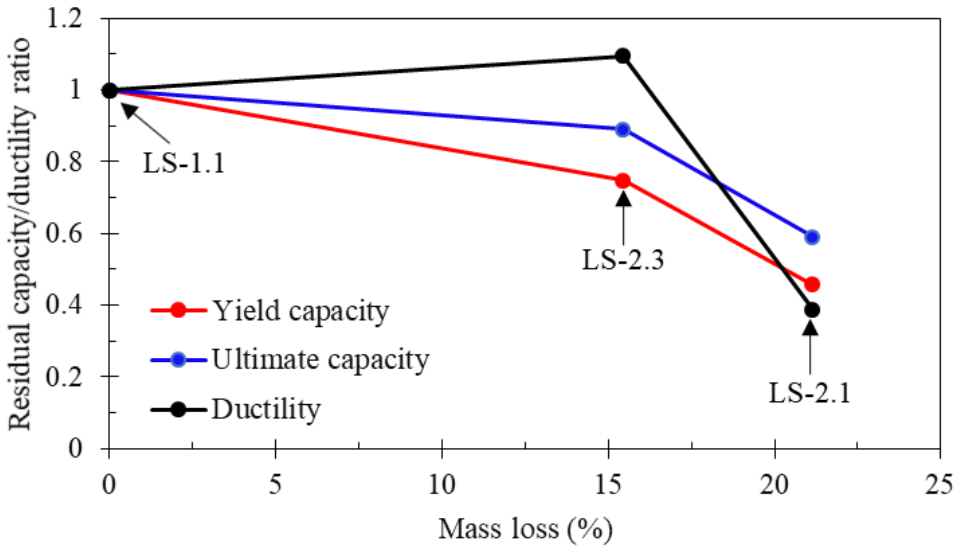

Figure 4.18: Effect of corrosion level on the response of large-scale beams

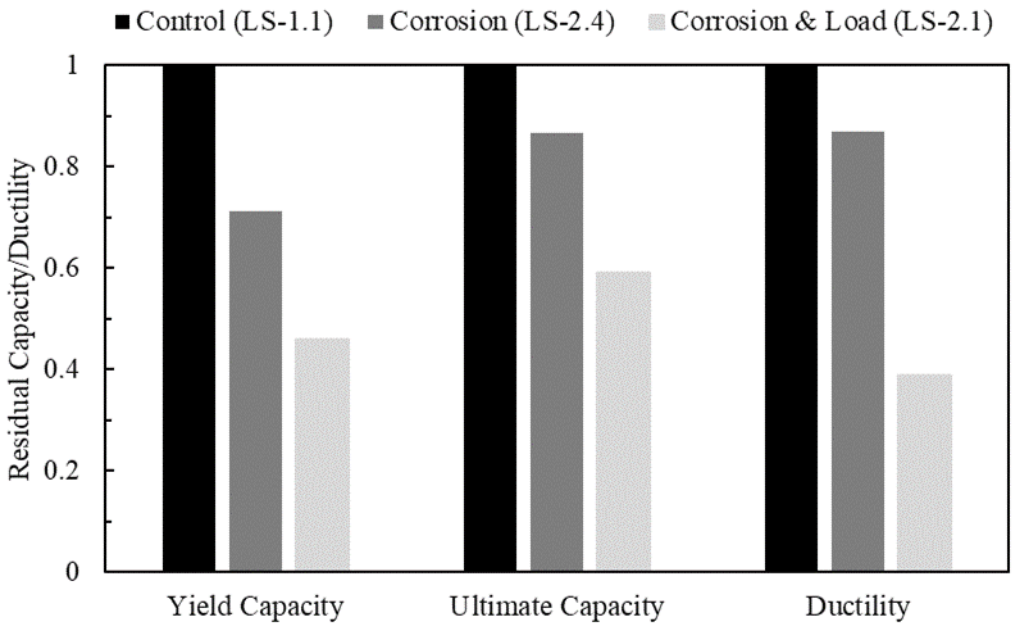

Figure 4.19: Effect of loading presence on the behavior of corroded large-scale beams

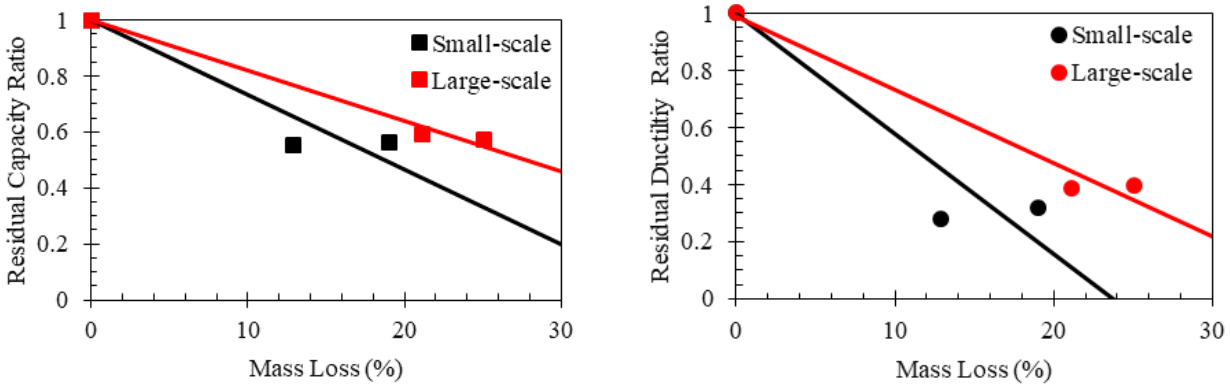

(a) (b)

Figure 4.20: Comparison between small-scale and large-scale beams in terms of: (a) residual capacity ratio (b) residual ductility ratio

4.6 References

Al-Bayti, A., Almansour, H., Saatcioglu, M. (2022a). Influence of Corrosion on the Mechanical Performance of Steel Reinforcement. To be submitted for publication.

Al-Bayti, A., Almansour, H., Saatcioglu, M. (2022b). Tests Reinforced Concrete Beams under Coupled Effects of Variable Service Loads and Reinforcement Corrosion. To be submitted for publication.

ASTM C39 / C39M. (2016). Standard test method for compressive strength of cylindrical concrete specimens. ASTM International, West Conshohocken, Pennsylvania, USA.

ASTM A370. (2017). Standard test methods and definitions for mechanical testing of steel products. ASTM International, West Conshohocken, Pennsylvania, USA.

ASTM G1-03. (2017)e1. Standard practice for preparing, cleaning, and evaluation corrosion test specimens. ASTM International, West Conshohocken, Pennsylvania, USA.

Azam, R., El-Sayed, A. K., and Soudki, K. (2016). Behaviour of reinforced concrete beams without stirrups subjected to steel reinforcement corrosion. Journal of Civil Engineering and Management, 22(2), 146-153.

Ballim, Y., and Reid, J. C. (2003). Reinforcement corrosion and the deflection of RC beams – an experimental critique of current test methods. Cement and Concrete Composites, 25(6), 625-632.

Cabrera, J. G. (1996). Deterioration of concrete due to reinforcement steel corrosion. Cement and Concrete Composites, 18(1), 47-59.

Coronelli, D., and Gambarova, P. (2004). Structural assessment of corroded reinforced concrete beams: Modeling guidelines. ASCE Journal of Structural Engineering, 130(8), 1214-1224.

Dang, V. H., and François, R. (2014). Prediction of ductility factor of corroded reinforced concrete beams exposed to long term aging in chloride environment. Cement and Concrete Composites, 53, 136-147.

Du, Y., Clark, L. A., and Chan, A. H. C. (2007). Impact of reinforcement corrosion on ductile behavior of reinforced concrete beams. ACI Structural Journal, 104(3), 285-293.

Du, Y., Cullen, M., and Li, C. (2013). Structural performance of RC beams under simultaneous loading and reinforcement corrosion. Construction and Building Materials, 38, 472-481.

El Maaddawy, T. A., and Soudki, K. A. (2003). Effectiveness of impressed current technique to simulate corrosion of steel reinforcement in concrete. ASCE Journal of Material in Civil Engineering, 15(1), 41-47.

El Maaddawy, T., Soudki, K., and Topper, T. (2005). Long-term performance of corrosion damaged reinforced concrete beams. ACI Structural Journal, 102(5), 649-656.

Hariche, L., Ballim, Y., Bouhicha, M., and Kenai, S. (2012). Effects of reinforcement configuration and sustained load on the behaviour of reinforced concrete beams affected by reinforcing steel corrosion. Cement and Concrete Composites, 34(10), 1202-1209.

Li, H., Li, B., Jin, R., Li, S., and Yu, J.-G. (2018). Effects of sustained loading and corrosion on the performance of reinforced concrete beams. Construction and Building Materials, 169, 179-187.

Malumbela, G., Moyo, P., and Alexander, M. (2009). Behaviour of RC beams corroded under sustained service loads. Construction and Building Materials, 23(11), 3346-3351.

Mangat, P. S., and Elgarf, M. S. (1999). Flexural strength of concrete beams with corroding reinforcement. ACI Structural Journal, 96(1), 149-158.

Rodriguez, J., Ortega, L. M., and Casal, J. (1997). Load carrying capacity of concrete structures with corroded reinforcement. Construction and Building Materials, 11(4), 239-248.

Torres-Acosta, A. A., Navarro-Gutierrez, S., and Terán-Guillén, J. (2007). Residual flexure capacity of corroded reinforced concrete beams. Engineering Structures, 29(6), 1145-1152.

Yoon, S., Wang, K., Weiss, W. J., and Shah, S. P. (2000). Interaction between loading, corrosion, and serviceability of reinforced concrete. ACI Materials Journal, 97(6), 637-644.

Zhang, W., Zhang, H., Gu, X., and Liu, W. (2018). Structural behavior of corroded reinforced concrete beams under sustained loading. Construction and Building Materials, 174, 675-683.

Chapter 5: Influence of Corrosion on the Mechanical Performance of Steel Reinforcement

Abstract

An experimental study was carried out to examine the influence of corrosion on the mechanical performance of steel reinforcement. A total of 9 small-scale and 6 large-scale reinforced concrete (RC) beams were tested under the coupled effects of reinforcement corrosion and service loads. The corrosion process of longitudinal steel bars was accelerated using the direct impressed current technique. The corroded steel bars were retrieved from the critical flexure regions of 7 small-scale and 2 large-scale reinforced concrete beams after the tests. A three-dimensional (3D) laser scanner was employed to assess the non-uniform distribution of corrosion along the steel bars. Subsequently, a direct tensile test was conducted to evaluate mechanical properties of corroded steel bars. Then, the load capacity, strength, and ductility were correlated with the level of corrosion. Test results indicated that the nominal strength and ductility of steel bars were reduced with increased corrosion levels. However, the reduction in ductility was more drastic than that of nominal strength due to the non-uniform distribution of corrosion. This non-uniform distribution of corrosion was primarily attributable to the presence of transverse cracks in concrete beams, allowing in a further localization of corrosion and loss of reinforcement sectional area at crack locations. As a result, the corroded steel bars developed rupturing failure at crack locations.

Keywords: mechanical performance, steel bars, experimental, non-uniform corrosion, laser scanner, transverse cracks, load capacity, strength, ductility.

5.1 Introduction

Reinforcement corrosion has been recognized as a major deterioration problem in many aged reinforced concrete (RC) structures, resulting in huge economic losses to maintain and/or rehabilitate such vulnerable structures. Corrosion of steel reinforcement is accelerated due to carbonation of concrete or chloride ingress. Carbonation of concrete is caused by air pollution, and causes a uniform loss of sectional area along the entire surface of reinforcement. Chloride ingress is caused by the use of de-icing salt, and causes a localized loss of reinforcement sectional area. However, both types of corrosion can coexist in RC structures. As corrosion progresses, the structural performance is adversely influenced by the damage associated with reinforcement corrosion, which includes: (i) loss of reinforcement sectional area, (ii) degradation in the mechanical performance of corroded steel reinforcement, (iii) deterioration of concrete surrounding the corroded steel reinforcement caused by the volumetric expansion of corrosion by-products, and (iv) impairment or complete loss of bond at the interface between steel reinforcement and concrete.

Investigating the tensile behavior of corroded steel bars is of particular interest due to their critical role in resisting service loads in RC structures. Numerous research studies were devoted to examine the influence of corrosion on the mechanical performance of steel bars (Almusallam, 2001; Palsson and Mirza, 2002; Cairns et al. 2005; Du et al., 2005; Apostolopoulos and Papadakis, 2008; Xia et al., 2013; Zhu and François, 2013; Ou et al., 2016; Sun et al., 2018; Fernandez and Berrocal, 2019; Chen et al., 2020; Zhang et al., 2021). In these studies, several techniques were adopted to simulate the corrosion process of steel bars, including (i) natural corrosion in RC structures (Palsson and Mirza, 2002; Ou et al., 2016; Fernandez and Berrocal, 2019), (ii) artificial corrosion using wet/dry cycles of chlorides (Lu et al., 2016; Chen et al., 2020), (iii) accelerated corrosion using the direct impressed current technique (Almusallam, 2001; Du et al., 2005; Zhang et al., 2021), and (iv) simulated corrosion by the removal of a small portion of steel bars (Carin et al., 2005). Subsequently, tensile tests were conducted to correlate the residual capacity and ductility of steel bars with the level of corrosion. Different decay laws were proposed based on test results to provide engineers with tools to assess the influence of corrosion on steel reinforcement.

Based on a comprehensive literature review, it was found that the tensile strength of corroded steel bars was evaluated using either the nominal non-corroded sectional area, average corroded sectional area, or actual corroded sectional area of steel bars. For that reason, there were some differences in the observations noted by previous researchers with respect to the influence of corrosion on the tensile strength of steel bars. Du et al. (2005), and Apostolopoulos and Papadakis (2008) showed that increasing the level of corrosion resulted in a decrease of strength when computed based on average corroded sectional area. Almusallam (2001) indicated that strength computed based on actual corroded sectional area was slightly influenced by corrosion. Cairns et al. (2005) observed a slight increase in ultimate strength when computed using actual corroded sectional area, while Tang et al. (2014) observed the same increase for both yield and ultimate strengths. Fernandez and Berrocal (2019) found that increasing the level of corrosion resulted in a decrease of strength when computed based on nominal or average sectional areas, however a slight increase of strength was observed when the actual corroded sectional area was used. In all of the above-mentioned studies, it was reported that steel bars exhibited reduced ductility with the increase of corrosion levels.

It can be seen that there is some degree of discrepancy in the conclusions drawn by previous researchers, in particular relative to the effect of corrosion on the actual tensile strength of steel bars. This can be attributed to the accuracy of techniques employed to measure the level of corrosion, especially in the presence of localized corrosion attack, since it is associated with complex irregular geometries. In previous studies, localized corrosion level was assessed using: (i) vernier caliper to measure the diameter of corroded steel bars (Lu et al., 2016), (ii) gravimetric measurement to obtain the mass loss of a small portion of the corroded steel bar at the failure point (Zhu and François, 2013), and (iii) three-dimensional laser scanner to generate the surface morphology of corroded steel bars. The latter technique had shown its capability in estimating the residual cross-sectional area caused by localized corrosion attacks (Tang et al., 2014; Fernandez and Berrocal, 2019).

An important aspect that needs to be taken into consideration while investigating the influence of corrosion on the mechanical performance of steel bars is the presence of cracks in concrete structures. Lu et al. (2016) employed an artificial method using cycles of dry and wet environments with sodium chloride solution (5% NaCl) to corrode the steel bars in concrete elements with pre-cracks. The results of their study revealed that there is an increase in the loss of reinforcement

sectional area at the position of cracks relative to other positions along the steel bars. This non-uniform loss of sectional area caused by localization of corrosion may significantly impact the mechanical response of corroded steel bars. Therefore, further investigation is needed.

The main objective of this paper is to investigate the effect of corrosion on the mechanical performance of steel reinforcement. The corroded steel bars were retrieved from corroded RC beams which were tested in companion experimental investigations (Al-Bayti et al. 2022b and 2022c). A total of 9 small-scale beams (145 x 250 x 1800 mm) and 6 large scale beams (200 x 300 x 3400 mm) were subjected to the coupled effects of reinforcement corrosion and service loads. The corroded steel bars were retrieved from the critical flexure regions of 7 small-scale and 2 large-scale reinforced concrete beams subjected to different levels of service loads, to examine the influence of flexural crack presence on the capacity and ductility of corroded steel bars. A three-dimensional laser scanner was employed to assess the distribution of corrosion and residual cross-sectional area along steel bars. The findings of this paper may provide engineers with tools to estimate the capacity and ductility of corroded steel bars in aged bridge RC structures.

5.2 Experimental Methodology

5.2.1 Reference Study

An experimental investigation was carried out by Al-Bayti et al. (2022b, 2022c) to examine the behavior of RC beams under service loads coupled with corrosion of the main flexural reinforcement. As part of the experimental program, small-scale and large-scale beams were designed, constructed, and tested. The main test variables were the level of service loads and size of beams. All small-scale beams had dimensions of 145 x 250 x 1800 mm, and were longitudinally reinforced with 2-10M, serving as the main tensile steel reinforcement. The large-scale beams, on the other hand, had dimensions of 200 x 300 x 3400 mm, and were longitudinally reinforced with 3-15M, serving as the main tensile steel reinforcement. Dimension of beams, reinforcement layout and detailing are shown in Figure 5.1.

All simply-supported beams were tested under a four-point bending setup. Load cells were positioned in a way to generate a constant moment region with a length of either 500 mm in the small-scale beams or 1000 mm in the large-scale beams. Testing started by loading the beams to the desired service level. For small scale beams, this load was equivalent to either 0%, 40%, or

60% of the beam ultimate load capacity, while large-scale beams were subjected to 60% of the beam ultimate load capacity. The corrosion process of longitudinal tensile steel bars was then activated while sustaining the applied loads. The direct impressed current technique was employed to accelerate the corrosion process of steel bars. In addition, the bottom middle portion of the beams was submerged in sodium chloride solution (5% NaCl) to help in depassivating the steel bars. All beams were tested until the simultaneous failure due to corrosion and sustained loads, and hence the duration of corrosion exposure was different for each beam. However, the corrosion process of the small-scale beam that was corroded under no service loads (i.e., SS-5.1) was intentionally stopped after a certain duration, and then loads were applied and increased until the failure of the beam.

After the failure of RC beams, the corroded steel bars were retrieved from the constant moment regions of beams. These regions had flexural cracks of different widths and spacing, depending on the size of the beam and the level of applied loads. Table 5.1 presents a summary of test coupons that were retrieved from the beams along with the primary test parameters. The location of corroded steel bars was selected to ensure that steel bars had a direct exposure to chlorides through flexural crack opening, as illustrated for each beam in Figure 5.2. It should be noted that the coupons were taken away from the position of failure in the corroded beams, and it is believed that the corroded coupons did not yield. The corroded steel bars were then cleaned in accordance with ASTM standards. A three-dimensional laser scanner was used to analyze the distribution of corrosion along the steel bars. Subsequently, tensile tests were conducted to evaluate the mechanical performance of corroded steel bars.

5.2.2 Corrosion Level

Upon the completion of testing, all beams were carefully demolished using a jack hammer to retrieve the corroded steel bars. Steel bars were then screened visually for different types of corrosion attacks. After that, the cleaning process was conducted in accordance with the procedure outlined in the ASTM G1-03 “Standard Practice for Preparing, Cleaning, and Evaluation Corrosion Test Specimens”.

All corroded bars were first cleaned with a non-metallic bristle brush to remove the adhering mortar, as shown in Figure 5.3(a). This was followed by immersing the corroded bars in hydrochloric acid solution for 10 min, as shown in Figure 5.3(b). Then, the corroded steel bars

were left in air-dry environment for 24 hours. The remaining mortar and corrosion by-products in the heavily corroded coupons were removed through surface treatment by sandblasting. This methodology was proven to be effective and efficient (Fernandez et al., 2018). The corroded bars were placed inside the sandblasting pressure cabinet, and then the surface treatment was performed by blasting the corroded bars with fine silica sand. After that, the corrosion level of each bar was quantitatively assessed using gravimetric measurements and three-dimensional laser scanner.

5.2.2.1 Gravimetric Measurement

After completing the cleaning process of non-corroded and corroded steel bars, the bars were weighed using an electronic scale with a precision of 0.01g. The mass loss of each bar was evaluated using the following expression:

$$\eta_{avg,m}(\%) = \frac{m_0 - m_c}{m_0} \times 100\% \tag{5.1}$$

where, $\eta_{avg,m}$ is the average mass loss of steel bars due to corrosion, m_0 and m_c are the weights of non-corroded and corroded steel bars after cleaning, respectively.

5.2.2.2 Laser Scanner

A three-dimensional laser scanner was used to assess the distribution and localization of corrosion along steel bars. This technique provides an improved assessment of the level of corrosion in steel bars with localized sectional loss when compared to other techniques such as gravimetric weight measurements or vernier caliper. The former works well only in steel bars with a uniform sectional loss, while the latter lacks accuracy in steel bars with irregular corroded sectional shapes or with different rib patterns. In this study, the corroded steel bars were scanned using Roland PICZA 3D Laser Scanner LPX-600, which is capable of generating detailed 3D models with high resolution. The laser scanner was used to generate three-dimensional data points of the visible surfaces of steel bars as shown in Figure 5.4(a). Afterward, the surface morphology of steel bars was constructed using a polygon mesh as shown in Figure 5.4(b-c). The point cloud data generated by the scanner were then exported for further analysis using MATLAB software to examine the variation of cross-sectional area along the corroded steel bars. In order to enhance the accuracy of the scanner outcome, the cross-sectional area was obtained at short intervals of 0.2 mm. The cross-sectional area loss due to corrosion was evaluated using the following expressions:

$$\eta_{avg,3D}(\%) = \frac{A_0 - A_{c,avg}}{A_0} \times 100\% \quad (5.2)$$

$$\eta_{crit,3D}(\%) = \frac{A_0 - A_{c,min}}{A_0} \times 100\% \quad (5.3)$$

where, $\eta_{avg,3D}$ and $\eta_{crit,3D}$ are the average and critical cross-sectional area losses of steel bars due to corrosion, respectively, A_0 is the cross-sectional area of non-corroded steel bars, $A_{c,avg}$ is the average cross-sectional area of corroded steel bars, and $A_{c,min}$ is the minimum cross-sectional area of corroded steel bars.

5.2.3 Tensile Test Setup

A total of 17 corroded steel bars (8-10M and 9-15M) were examined using a direct tensile test. In addition, a total of 6 non-corroded steel bars (3-10M and 3-15M) were included in the test program to serve as control coupons. Tensile tests were conducted using MTS universal testing machine, shown in Figure 5.5(a). Prior to testing, the location with the critical cross-sectional area along the corroded steel bars was identified using the distribution of corrosion obtained by the laser scanner. In this study, the critical section is defined as the section with least area along the corroded steel bars, however when the least section was in the grip locations of the machine, the section with the next least area was assumed as the critical section. The extensometer with a gauge length of 45 mm was positioned around the critical section during the test, shown in Figure 5.5(b), to capture the local deformations and necking stage where the failure is expected. The steel bars were placed in between the grips, and then loads were applied using a displacement control method until the rupture of steel bars. Loads were applied at a slow rate in initial stages of testing (i.e., prior to the yielding of steel bars). Test data in terms of applied loads and deformations were captured using a data acquisition system.

The mechanical performance of steel bars was evaluated in terms of load capacity and strength at both yield and ultimate, as well as the elongation at ultimate. In this study, ultimate strain is defined as the elongation corresponding to the ultimate strength, while rupture strain is the elongation corresponding to the rupture strength.

5.3 Experimental Results

Table 5.2 summarizes key experimental data, including mass loss ($\eta_{avg,m}$), critical cross-sectional area loss ($\eta_{crit,3D}$), yield load capacity (F_y), ultimate load capacity (F_u), and ultimate strain (ε_u) of all corroded steel bars.

5.3.1 Level of Corrosion

5.3.1.1 Gravimetric Measurements

Figure 5.6 shows all types of corrosion that were visually identified on the clean surface of the corroded steel bars. As shown in the figure, corrosion of reinforcement in cracked concrete can be classified into three categories: generalized corrosion, localized pit corrosion, and localized crack corrosion. Generalized corrosion was noticeable in the heavily corroded steel bars, while localized pit corrosion was detected in various shapes at random sites along all corroded steel bars. Crack corrosion, on the other hand, is another form of localized corrosion, however it was only detected at the locations where flexural cracks were present. This type of corrosion developed as a result of the presence of flexural cracks in reinforced concrete beams under service loads, creating a clear pathway for chloride ions to attack the exposed embedded steel bars.

5.3.1.2 Three-Dimensional Laser Scanner

Figure 5.7 shows illustrative 3D images generated by the scanner for steel bars with different levels of corrosion. The images of corroded bars SS-3.2-R1-L ($\eta_{avg,m}$=17.6%) and LS-2.1-R1-L-1 ($\eta_{avg,m}$=26.7%) display a significant loss of reinforcement area due to localized pit and crack corrosion attacks at various positions along the steel bars. In the severely corroded bar SS-5.1-R1-L ($\eta_{avg,m}$=36.1%), the image clearly shows the prevalence of generalized corrosion, where the ribs were almost vanished. Besides, it shows the presence of deep pit corrosion attack that was well-captured by the scanner. The distribution of sectional area loss along the corroded steel bars SS-3.2-R1-L and LS-2.1-R1-L-1 are shown in Figure 5.8 and Figure 5.9, respectively. It can be observed that the distribution of sectional area loss was not uniform. Clearly, the presence of flexural cracks resulted in a localized loss of reinforcement area where the cracks were formed. It should be noted that the localization of sectional area loss extended a few millimeters beyond the opening of flexural cracks.

The reliability and accuracy of the laser scanner were confirmed by comparing the average cross-sectional area loss obtained by the laser scanner $\eta_{avg,3D}$ with the average mass loss obtained by the gravimetric weight measurements $\eta_{avg,m}$, as shown in Figure 5.10. It should be noted that all steel bars retrieved from the corroded regions of beams were included in this figure. Clearly, the laser scanner was able to predict the loss of reinforcement sectional area with a reasonable accuracy since all data points were scattered within a 5% interval. The difference in the estimation of corrosion levels using the two approaches is primarily attributable to the scanner approximation of sectional losses at intervals of 0.2 mm which may reduce its precision. Another possible explanation for the difference is the complexity and irregularity of pit corrosion attack. For example, the scanner cannot accurately model the presence of subsurface corrosion since the laser cannot penetrate into the interior hidden faces of such complex pit shapes. This was also pointed out in another study that examined the use of 3D laser scanner (Tahershamsi et al., 2017). Nevertheless, the overall reliability and accuracy of the laser scanner is considered; (i) exceptional in predicting the distribution of corrosion along steel bars, and (ii) satisfactory in approximating the residual cross-sectional area of corroded steel bars.

In practice, loss of reinforcement area due to generalized corrosion might be approximated using Faraday's law, however maximum sectional loss of reinforcement area due to localized corrosion is not readily available. For that reason, it is important to obtain a relationship between the loss of reinforcement area due to generalized and localized corrosion attacks. However, there are a lot of variations and uncertainties associated with the loss of reinforcement area due to pit corrosion attack since it is linked to various complex cross-sectional shapes. Likewise, loss of reinforcement area caused by localized crack corrosion is subjected to the variations in the width of flexural cracks. This in turn, is influenced by many factors, including level of service loads, reinforcement area ratio, and uncertainties in the material of concrete. The combination of all these factors has a significant influence on the concentration of chloride ions that reaches the surface of steel bars, resulting in variance of corrosion levels.

A relationship between mass loss $\eta_{avg,m}$ and maximum sectional loss $\eta_{crit,3D}$ of all retrieved corroded steel bars is plotted in Figure 5.11. As expected, the data is scattered due to all the above-mentioned factors, influencing the localization of corrosion. Regardless, the line of best fit (i.e., mean curve) using a power-law function is proposed (shown in black). Clearly, the rate of increase

in maximum sectional loss is reduced with the increase of mass loss. The high rate of sectional area loss at low mass loss levels is attributed to the fact that the corroded steel bars were extracted from beams under high service loads, and hence wider flexural cracks, resulting in a further loss of reinforcement sectional area. As mass loss increases, the rate of increase in maximum sectional loss is reduced since the corroded steel bars were extracted from beams under lower levels of service loads or from beams with higher percentages of steel (i.e., lesser crack widths), resulting in a less localization of sectional area loss. It is important to note that the loss of reinforcement area due to localized corrosion can be underestimated when the mean curve is used, due to the large scatter in data. Accordingly, an upper bound curve (shown in blue) is also proposed to ensure that the capacity of corroded steel bars is not overestimated. The proposed relationships are expressed in the following:

$$\eta_{crit,3D} = \begin{cases} 4.68\,{\eta_{avg,m}}^{0.69} & \text{(mean curve)} \\ 12.07\,{\eta_{avg,m}}^{0.50} & \text{(upper curve)} \end{cases} \tag{5.4}$$

A summary of previous experimental research studies that employed a 3D laser scanner to obtain the maximum sectional loss as a function of the average sectional loss is presented in Table 5.3, while Figure 5.12 shows how the findings of this study compares with previous studies. In this comparison, the mean curve was used to ensure consistency between all studies. In general, at low levels of mass loss, the empirical relation of this study predicted a higher loss of reinforcement area when compared to other studies. Yet again, this is mainly due to the presence of wide flexural cracks under high service loads, resulting in a further loss of reinforcement sectional area. The predictions by Fernandez et al. (2019) are closely comparable to the relationship in this study. This could be attributed to the fact that the corroded steel bars in Fernandez et al. (2019) were retrieved from an actual bridge edge girder, and hence the girder could have been cracked within the corroded region, however the researchers did not indicate if this was the case. In contrast, the empirical relations by Sun et al. (2018) for corroded bare steel bars and Zhang et al. (2021) for embedded corroded steel bars in concrete blocks, had the lowest predictions of the reduction in reinforcement area since cracks were not present.

5.3.2 Tensile Test Results

5.3.2.1 General Behavior of Corroded Steel Bars

Figure 5.13 shows typical rupture failures of corroded steel bars at the end of the tensile test. All corroded steel bars failed at the position with critical sectional area loss, corresponding to the location with localized crack corrosion. With the exception of corroded bar SS-5.1-R1-L, the failure took place at one of the pit sites along the reinforcement since this coupon was retrieved from a beam that was corroded under no loads (i.e., without transverse cracks).

Load-strain relationships obtained from the tensile tests of 10M and 15M steel bars are shown in Figure 5.14. As shown in the figure, the load capacity of corroded steel bars was reduced in comparison to non-corroded steel bars. It can be also observed that the characteristics of yielding were significantly influenced by corrosion. The non-corroded steel bars had a clear well-defined yield point. In contrast, the yield point in the majority of corroded coupons was not well-defined, however few coupons had a very short yield plateau stage prior to exhibiting strain hardening. In this study, the yield point was taken as the point at which the rate of change in strains was increased substantially, as visually observed. Furthermore, the ductility of steel bars was strongly influenced by corrosion. The ultimate strain of corroded steel bars (corresponds to ultimate load) was reduced. It should be noted that the majority of corroded steel bars exhibited necking prior to their rupturing failures. At failure, the corroded steel bars were ruptured at relatively lower strains when compared with non-corroded steel bars.

5.3.2.2 Influence of Corrosion on the Load Capacity of Steel Bars

The influence of corrosion on the load capacity of steel bars is examined using the ratio between the load capacity of corroded steel bars and non-corroded steel bars at yield (F_{yc}/F_{y0}) and ultimate (F_{uc}/F_{u0}). In this way, it is possible to directly assess different reinforcing bar sizes (i.e., 10M and 15M). Figure 5.15 shows the load capacity ratio of steel bars as a function of the corrosion level. In this figure, the corrosion level is presented using both average sectional area loss (gravimetric measurements) and critical sectional area loss (3D laser scanner). It is very clear that the load capacity ratios of steel bars were reduced with the increase of corrosion levels. Besides, the relationship between the load capacity ratios and critical sectional area loss (red line) were

stronger than those with the average sectional area loss (black line). This indicates that the loss of load capacity in corroded steel bars is closely related to the loss of reinforcement area.

To further demonstrate this point, the residual area ratio, defined as the ratio between critical cross-sectional area of corroded steel bars and cross-sectional area of non-corroded steel bars (A_c/A_0) is also added to Figure 5.15 (blue line). Theoretically, the residual area ratio is equivalent to the load capacity ratio if the loss of strength in corroded steel bars is only attributed to the loss of area. In other words, the tensile strength of steel bars is not influenced by corrosion (i.e., $f_c = f_0$), as demonstrated in the following expressions:

$$f_o = \frac{F_0}{A_0} \;\&\; f_c = \frac{F_c}{A_c} \qquad \text{if} \quad f_c = f_0 \quad \rightarrow \quad \frac{A_c}{A_0} = \frac{F_c}{F_0} \tag{5.5}$$

where, f_0 and f_c are the strengths of non-corroded and corroded steel bars, respectively, F_0 and F_c are the load capacities of non-corroded and corroded steel bars, respectively. The relation above can be applied at both yield and ultimate. As demonstrated in Figure 5.15, it is evident that the loss of load capacity (red line) is close to the loss of area (blue line).

5.3.2.3 Influence of Corrosion on the Strength of Steel Bars

The effect of corrosion on the tensile strength of steel bars is examined by expressing the strength in two ways; (i) nominal strength – by dividing the load capacity by the non-corroded area of steel bars, and (ii) effective strength – by dividing the load capacity by the residual corroded area of steel bars prior to failure.

It should be noted that the nominal strength ratios of corroded steel bars at yield (f_{yc}/f_{yo}) and ultimate (f_{uc}/f_{uo}) are equivalent to the load capacity ratios of corroded steel bars at yield (F_{yc}/F_{yo}) and ultimate (F_{uc}/F_{uo}), respectively. This due to the use of nominal areas when computing the strengths of steel bars, resulting in identical expressions. As shown in Figure 5.15, the nominal strength ratio was correlated with the corrosion level using a linear trend-line. It was found that the correlation at ultimate was stronger than that at yield. Similar observation was noted in Xia et al. (2013). This could be attributed to the methodology adopted to identify the yield point of corroded steel bars that did not exhibit plateaued yielding. The nominal strength capacity of corroded steel bars is expressed in the following:

$$f_{yc}/f_{y0} = [1 - \alpha_y \eta] \tag{5.6}$$

$$f_{uc}/f_{u0} = [1 - \alpha_u \eta] \tag{5.7}$$

where, f_{yc} and f_{uc} are the yield and ultimate strengths of corroded steel bars, respectively, f_{y0} and f_{u0} are the yield and ultimate strengths of non-corroded steel bars, respectively, α_y and α_u are regression factors for reductions in yield and ultimate strengths, respectively. In the case where critical sectional area loss is used to assess the level of corrosion, the regression factors at yield, α_y and at ultimate, α_u are equal to 0.0084 and 0.0086, respectively. In the case where average sectional area loss is used to assess the level of corrosion, the regression factors at yield, α_y and at ultimate, α_u are equal to 0.0141 and 0.0147, respectively.

The empirical relationship between the nominal strength ratio and level of corrosion is compared with the relationships acquired in previous experimental research studies in Table 5.4. In all these studies, a linear relationship was established between the nominal strength ratio and level of corrosion. Therefore, Table 5.4 included the regression factors at yield and ultimate along with key experimental parameters such as corrosion technique, steel bar size, and the range of achieved corrosion levels. It can be observed that the majority of studies used the average mass loss to assess the level of corrosion, yet few studies adopted the critical sectional loss. For that reason, the findings of this study is compared with previous studies using average mass loss and localized sectional loss at yield and ultimate, as shown in Figure 5.16. Cleary, the results of this study compares very well with previous research at both yield and ultimate.

The effect of corrosion on the effective strength ratio of steel bars at yield (f_{yc}/f_{y0}) and ultimate (f_{uc}/f_{u0}) is examined in Figure 5.17. As stated earlier, the effective strength is computed by dividing the load capacity by the critical corroded section area of steel bars. It can be observed that the data is largely scattered, however the linear trend-line indicates that there is a slight increase of effective strength ratio (at yield and ultimate) with increased corrosion levels. Similar observations were also noted in (Cairns et al., 2005; Tang et al., 2014). Such behavior can be explained by the sudden loss of reinforcement area at the location where corroded steel bars were ruptured, resulting in high localization of stresses.

5.3.2.4 Influence of Corrosion on the Ductility of Steel Bars

The effect of corrosion on the ductility of steel bars is examined by adopting; (i) the ratio between ultimate strain of corroded steel bars and non-corroded steel bars ($\varepsilon_{uc}/\varepsilon_{u0}$) as an indicator of the reduction in ductility due to corrosion, and (ii) the ratio between ultimate and yield strengths of corroded steel bars (f_{uc}/f_{yc}) as an indicator of the reinforcement ability to develop inelastic rotations.

The ultimate strain ratio of steel bars is plotted as a function of the corrosion level in Figure 5.18. Clearly, there is a drastic reduction in the ultimate strain ratio of steel bars with the increase of corrosion levels, due to non-uniformity in the distribution of corrosion caused by localized corrosion attacks. This has huge implications on damaged reinforced concrete structures due to corrosion, where a relatively low amounts of corrosion could result in a severe reduction in ductility, causing premature failure. The ultimate strain ratio was correlated with the level of corrosion in terms of average mass loss and critical sectional loss using a 2nd degree polynomial. Yet again, the ultimate strain ratio is better correlated with the critical sectional loss than average mass loss. The ultimate strain ratio is expressed in the following:

$$\frac{\varepsilon_{uc}}{\varepsilon_{u0}} = \left[3.05(10^{-4})\eta_{avg,m}{}^2 - 3.02(10^{-2})\eta_{avg,m} + 1.00\right] \tag{5.8}$$

$$\frac{\varepsilon_{uc}}{\varepsilon_{u0}} = \left[1.11(10^{-4})\eta_{crit,3D}{}^2 - 1.76(10^{-2})\eta_{crit,3D} + 1.00\right] \tag{5.9}$$

Table 5.5 presents a summary of empirical relations between the ultimate strain ratio and level of corrosion acquired in previous research studies, while Figure 5.19 shows how the findings of this study compare with previous research. As shown in the figure, the results of this study compares well with other studies, however the majority of previous studies predicted higher reductions in ultimate strain ratio. The study conducted by Ou et al. (2016) for naturally corroded steel bars was the only exception. The main finding of their study was that the reduction in ultimate strain ratio of artificially corroded steel bars was higher than that of naturally corroded steel bars, which can be also interpreted from Figure 5.19(a). Such behavior was explained by the more non-uniform distribution of corrosion in steel bars that were artificially corroded. This concept can be also applied to explain the reason behind the increase in the reduction in ultimate strain ratio found in previous studies when compared to this study, as the use of higher current densities (i.e., 400 –

1,000 μA/cm^2) in previous research studies relative to that used to corrode the majority of steel bars in this study (i.e., 300 μA/cm^2), could have contributed to more non-uniformity in the distribution of corrosion along the steel bars, and hence further reductions in the ultimate strain ratios.

Figure 5.20 shows the ratio between ultimate and yield strengths (f_u/f_y) of non-corroded and corroded steel bars as a function of the level of corrosion. It can be seen that there is no clear relationship between this ratio and the level of corrosion. Nevertheless, this ratio can be used to check the reinforcement ability to development inelastic rotations. According to ACI 318-14, the ratio between ultimate and yield strengths of steel bars should be at least 1.25. The non-corroded 10M and 15M steel bars had ratios of 1.33 and 1.50, respectively. Likewise, the majority of corroded steel bars satisfied this requirement, however few coupons were below the limit. This could have a detrimental effect on the integrity of existing reinforced concrete structures in developing inelastic rotations.

5.4 Conclusions

An experimental investigation was carried out to examine the influence of corrosion on the tensile behavior of steel bars retrieved from RC beams subjected to the coupled effects of reinforcement corrosion and service loads. The corroded steel bars had a direct exposure to chlorides through flexural crack openings. The non-uniform distribution of corrosion and loss of reinforcement sectional area were assessed using a three-dimensional laser scanner. The following conclusions can be drawn from the current investigation:

1) The non-uniform distribution of corrosion in cracked reinforced concrete beams was influenced by the presence of transverse cracks since crack openings allowed chloride ions to ingress to the exposed surface of steel bars, resulting in a further loss of reinforcement area. Pit corrosion at random sites along steel bars was the other contributor to the non-uniform distribution of corrosion.
2) The loss of reinforcement area due to localized corrosion was increased with the increase of corrosion levels (i.e., mass loss). However, the rate of increase in the loss of reinforcement area was reduced with the increase of corrosion levels, for the corroded steel bars considered in this study. This was attributed to the reduction in flexural crack widths since the corroded steel bars were retrieved from beams subjected to lower levels of service

loads or from beams with higher percentage of steel, and hence the access of chlorides to the surface of steel bars was limited.

3) At the end of the tensile tests, all the corroded steel bars retrieved from the cracked reinforced concrete beams were ruptured at the location with the critical sectional loss, corresponding to the location where flexural cracks were present. For the corroded steel bar in un-cracked reinforced concrete beam, the location of reinforcement rupture was subjected to the spatial variability of pit corrosion.
4) The majority of corroded steel bars did not exhibit plateauing of yield (i.e., no transition from yielding stage to strain hardening stage). However, few corroded steel bars exhibited a short yield plateau stage relative to that exhibited by the control steel bars.
5) The tensile strength of steel bars, based on critical sectional area, was not influenced by the presence of localized corrosion attack. In fact, there was a slight increase in strength with increased corrosion levels. For that reason, the load capacity of corroded steel bars can be conservatively estimated using the maximum sectional loss of steel bars.
6) The ductility of steel bars was strongly influenced by the non-uniform distribution of corrosion. There was a drastic reduction in ultimate strain of steel bars as the level of corrosion was increased. In addition, few corroded bars did not satisfy ACI 318-14 minimum code requirement for the ratio between ultimate and yield strengths.

Table 5.1: Test coupons retrieved from corroded RC beams

Beam size	Beam designation	Sustained load (% of ultimate)	Corrosion density ($\mu A/cm^2$)	Duration (days)	# of coupons	Coupon designation
Small-scale	SS-2.2	60%	Stage 1: 100	35	1	SS-2.2-R1-L
			Stage 2: 300	47		
	SS-3.1	60%	300	37	1	SS-3.1-R1-R
	SS-3.2	60%	300	52	2	SS-3.2-R1-L
						SS-3.2-R2-L
	SS-4.1	40%	300	152	2	SS-4.1-R1-L
						SS-4.1-R2-R
	SS-4.2	40%	300	167	1	SS-4.2-R1-R
	SS-5.1	0%	300	167	1	SS-5.1-R1-L
Large-scale	LS-2.1	60%	Stage 1: 300	135	5	LS-2.1-R1-L-1
			Stage 2:1000	15		LS-2.1-R1-R
						LS-2.1-R2-L-1
						LS-2.1-R3-L-1
						LS-2.1-R3-R
	LS-2.2	60%	Stage 1: 500	33	4	LS-2.2-R1-L-1
			Stage 2:1000	158		LS-2.2-R1-L-2
						LS-2.2-R2-R
						LS-2.2-R3-L-1

Table 5.2: Summary of key experimental findings

Bar size	Coupon	$\eta_{avg,m}$ (%)	$\eta_{crit,3D}$ (%)	F_y (kN)	F_u (kN)	ε_u (mm/mm)
10M	Control*	0.00	0.00	44.47	59.08	0.1430
	SS-2.2-R1-L	19.47	37.95	30.86	38.71	0.0807
	SS-3.1-R1-R	13.17	45.86	25.27	37.48	0.0647
	SS-3.2-R1-L	17.61	56.91	22.32	31.31	0.0410
	SS-3.2-R2-L	20.35	51.33	26.30	32.44	0.0506
	SS-4.1-R1-L	31.78	54.11	28.31	35.85	0.0444
	SS-4.1-R2-R	48.36	68.31	12.88	16.15	0.0387
	SS-4.2-R1-R	28.31	61.32	16.17	25.29	0.0726
	SS-5.1-R1-L	36.10	56.60	32.80	33.90	0.0090
15M	Control*	0.00	0.00	80.87	121.05	0.1510
	LS-2.1-R1-L-1	26.71	53.81	42.09	64.49	0.1031
	LS-2.1-R1-R	22.29	30.01	63.23	92.95	0.0552
	LS-2.1-R2-L-1	20.56	29.26	64.32	90.68	0.0685
	LS-2.1-R3-L-1	21.42	34.98	48.71	77.19	0.1001
	LS-2.1-R3-R	23.17	33.10	53.05	86.55	0.1139
	LS-2.2-R1-L-1	26.64	33.69	56.03	85.79	0.0794
	LS-2.2-R1-L-2	26.60	43.96	49.83	78.54	0.0734
	LS-2.2-R2-R	16.89	30.26	68.61	96.08	0.0851
	LS-2.2-R3-L-1	29.49	41.78	62.00	84.21	0.0407

*Properties of 10M and 15M control steel bars were evaluated using the average of three coupons.

Table 5.3: Previous empirical relationships between average and maximum sectional losses

Study	Corrosion technique*	Specimen type	Corrosion level	η_{crit} (%)
This Study	Direct current (300–1000 μA/cm^2)	Embedded bars	$\eta_{avg,m}$= 0-48%	4.677 $\eta_{avg,m}^{0.6925}$
Zhang et al. (2021)	Direct current (600 μA/cm^2)	Eembedded bars	$\eta_{avg,m}$= 0-20.3%	0.02 + 1.4 $\eta_{avg,m}$
Fernandez et al. (2019)	Natural exposure	Embedded bars	$\eta_{avg,m}$= 0-18.6%	1.3 $\eta_{avg,m}^{0.8}$
Sun et al. (2018)	Direct current (400 μA/cm^2)	Bare bars	$\eta_{avg,m}$= 0-10.9%	1.6867 $\eta_{avg,m}$

*Corrosion technique was either;

(i) Direct current: corrosion of steel bars was accelerated using direct impressed current technique.

(ii) Natural exposure: corroded steel bars were retrieved from RC structures.

Table 5.4: Previous experimental studies with strength reduction factors

Study	Corrosion technique*	Bar size (P/R**)	Corrosion level	α_y	α_u
This Study	Direct current (300–1000 μA/cm^2)	11.3, 16 mm (R)	$\eta_{avg,m}$= 0-48.0%	0.0141	0.0147
			$\eta_{crit,3D}$= 0-68.0%	0.0084	0.0086
Zhang et al. (2021)	Direct current (600 μA/cm^2)	8, 10 mm (P) 12, 14, 16, 18 mm (R)	$\eta_{avg,m}$= 0-20.3%	0.0136	0.0141
Chen et al. (2020)	Artificial (16.5% NaCl)	10 mm (R)	$\eta_{crit,3D}$= 0-33.7%	0.0087	0.0105
Fernandez et al. (2019)	Natural exposure	16 mm (R)	$\eta_{avg,m}$= 0-19.2%	0.0136	0.0143
Sun et al. (2018)	Direct current (400 μA/cm^2)	14, 16 mm (R)	$\eta_{avg,m}$= 0-10.9%	0.0110	0.0130
			$\eta_{crit,3D}$= 0-15.6%	0.0058	0.0072
Lu et al. (2016)	Artificial (5% NaCl)	16 mm (R)	$\eta_{avg,m}$= 0-6.0%	0.0195	0.0231
Ou et al. (2016)	Natural exposure	13, 16, 19 mm (R)	$\eta_{avg,m}$= 6-82.0%	0.0123	0.0130
	Direct current (600 μA/cm^2)	13, 29 mm (R)	$\eta_{avg,m}$= 0-31.0%	0.0127	0.0116
Tang et al. (2014)	Direct current (80–220 μA/cm^2)	19.1 mm (R)	$\eta_{avg,m}$= 0-29.0%	0.0170	0.0170
			$\eta_{crit,3D}$= 0-63.0%	0.0090	0.0090
Zhang et al. (2012)	Natural exposure – carbonation	6.5 mm (P)	$\eta_{avg,m}$= 0-31.2%	0.0112	0.0136
	Direct current (100 μA/cm^2)	12 mm (R)	$\eta_{avg,m}$= 0-39.7%	0.0110	0.0122
Cairns et al. (2005)	Direct current (10–50 μA/cm^2)	16 mm (P) 20 mm (R)	$\eta_{avg,m}$= 0-30.0%	0.0120	0.0110
Du et al. (2005)	Direct current (1,000 μA/cm^2)	16 mm (P&R)	$\eta_{avg,m}$= 0-18.0%	0.0140	0.0140

*Corrosion technique was either;

(i) Direct current: corrosion of steel bars was accelerated using direct impressed current technique.

(ii) Natural exposure: corroded steel bars were retrieved from RC structures

(iii) Artificial: corrosion of steel bars was accelerated using wet/dry cycles with chlorides solution.

**P/R refers to plain bar/ribbed bar.

Table 5.5: Previous experimental studies with ductility reduction relationships

Study	Corrosion technique*	Bar size (P/R**)	$\varepsilon_{uc}/\varepsilon_{u0}$
This Study	Direct current (300-1000 μA/cm^2)	11.3, 16 mm (R)	$3.05(10^{-4})\eta_{avg,m}{}^2 - 3.02(10^{-2})\eta_{avg,m} + 1.00$
			$1.11(10^{-4})\eta_{crit,3D}{}^2 - 1.76(10^{-2})\eta_{crit,3D} + 1.00$
Zhang et al. (2021)	Direct current (600 μA/cm^2)	8, 10 mm (P)	$-0.287 + 1.251e^{-0.0349\eta_{avg,m}}$
			$-0.046 + 1.032e^{-0.0367\eta_{crit,3D}}$
Sun et al. (2018)	Direct current (400 μA/cm^2)	14, 16 mm (R)	$1 - 0.04127\eta_{crit,3D}$
Ou et al. (2016)	Nnatural exposure	13, 16, 19 mm (R)	$1 - 0.0125\eta_{avg,m}$
	Direct current (600 μA/cm^2)	13, 29 mm (R)	$1 - 0.0281\eta_{avg,m}$
Du et al. (2005)	Ddirect current (1,000 μA/cm^2)	16 mm (P&R)	$1 - 0.044\eta_{avg,m}$

*Corrosion technique was either;

(i) Direct current: corrosion of steel bars was accelerated using direct impressed current technique.

(ii) Natural exposure: corroded steel bars were retrieved from RC structures

(iii) Artificial: corrosion of steel bars was accelerated using wet/dry cycles with chlorides solution.

**P/R refers to plain bar/ribbed bar.

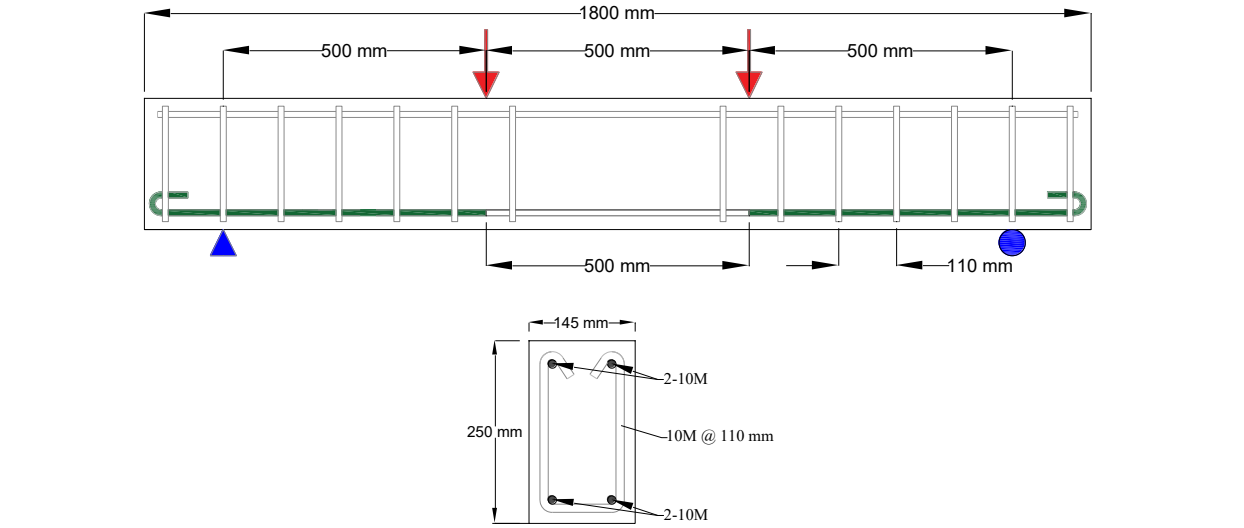

(a) Small-scale beam

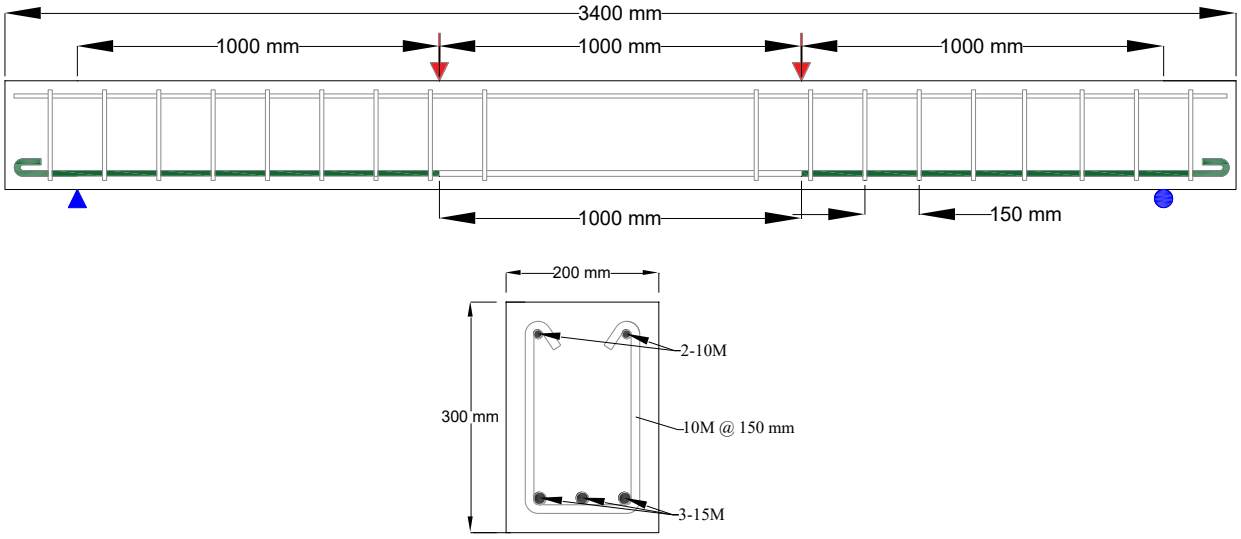

(b) Large-scale beam

Figure 5.1: Dimension of RC beams and reinforcement detailing

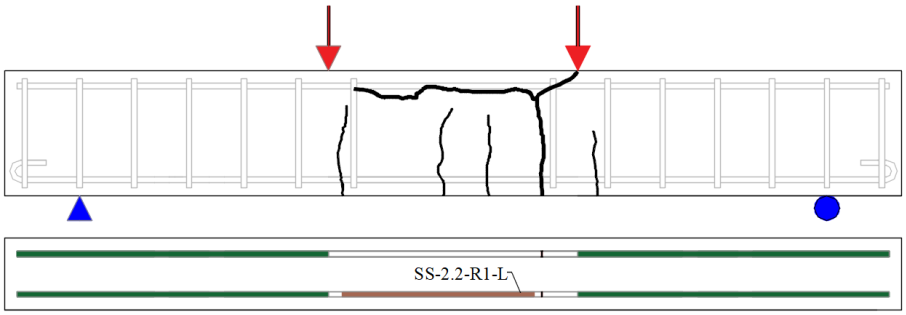

(a) SS-2.2

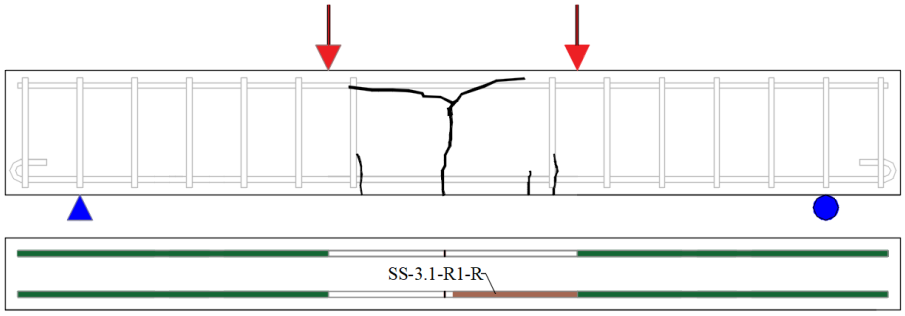

(b) SS-3.1

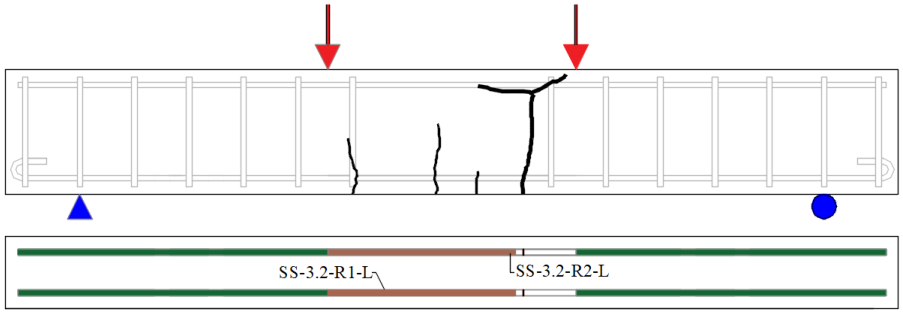

(c) SS-3.2

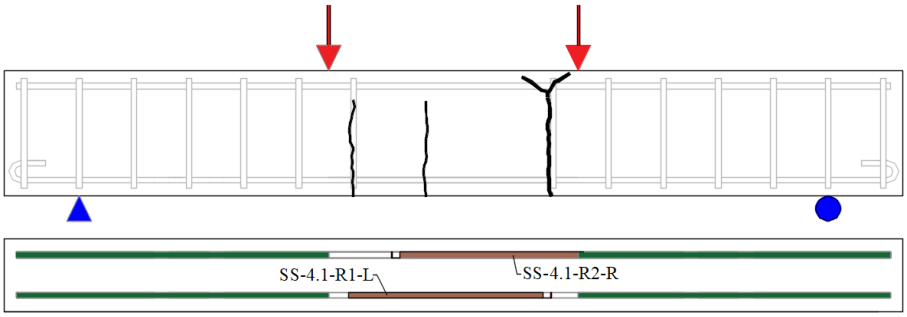

(d) SS-4.1

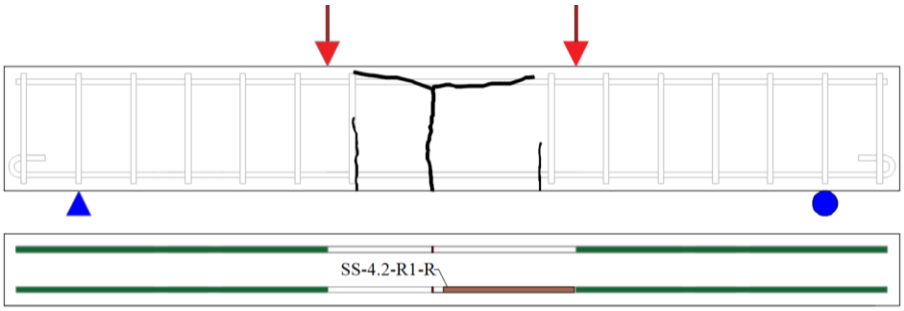

(e) SS-4.2

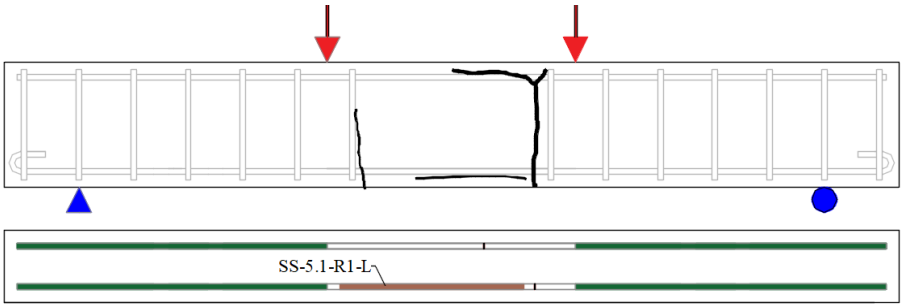

(f) SS-5.1

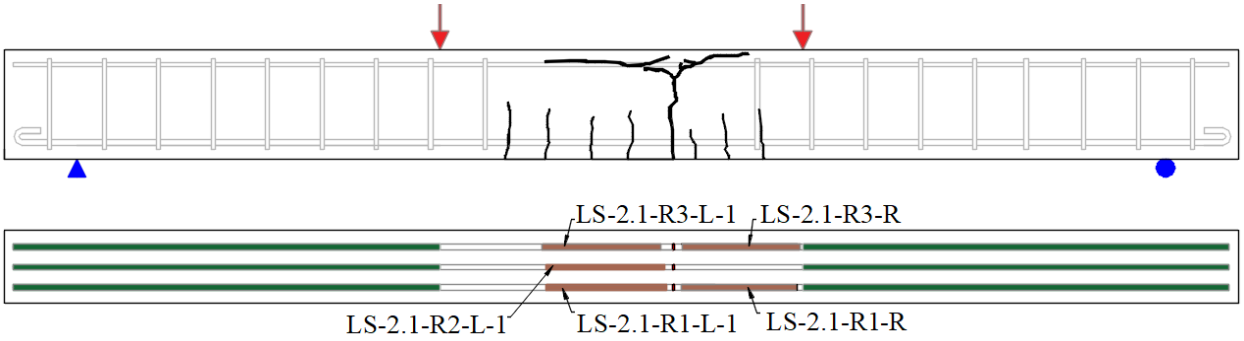

(g) LS-2.1

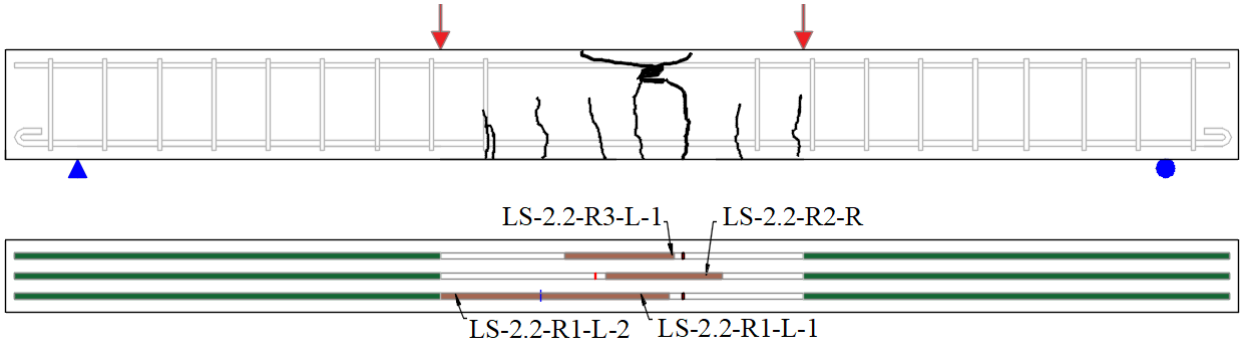

(h) LS-2.2

Figure 5.2: Location of the retrieved corroded steel bar coupons from RC beams

(a) After the removal from beams

(b) During the chemical cleaning process

Figure 5.3: Corroded steel bars

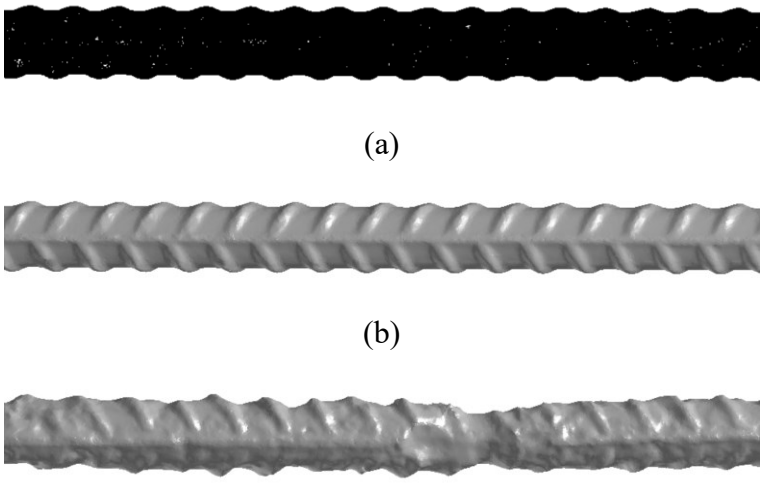

(a)

(b)

(c)

Figure 5.4: Typical illustration of: (a) point cloud data (b) generated mesh of control steel bar (c) generated mesh of corroded steel bar

(a) Univeral testing machine

(b) Close up at the failure

Figure 5.5: Tensile test setup

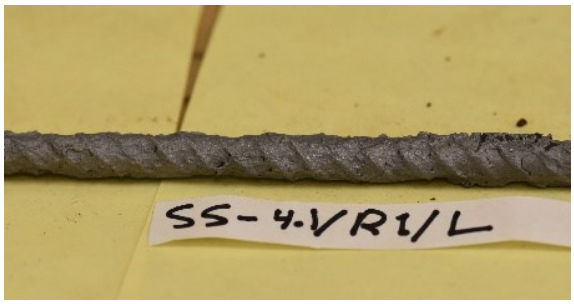

(a) Generalized corrosion

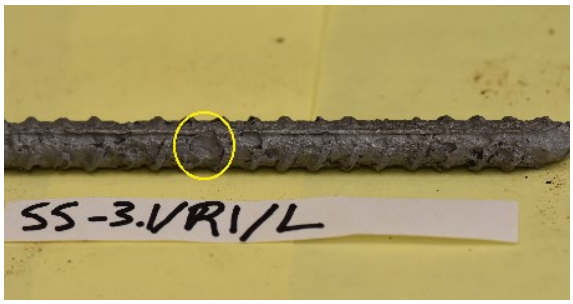

(b) Localized pit corrosion

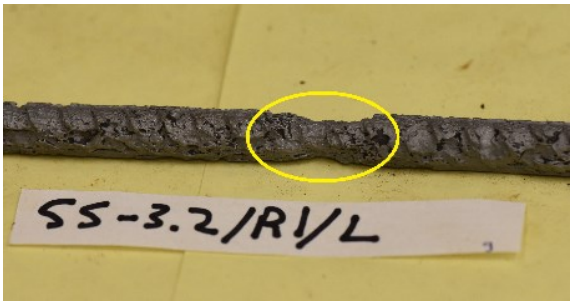

(c) Localized crack corrosion

Figure 5.6: Types of corrosion on the clean surface of steel bars

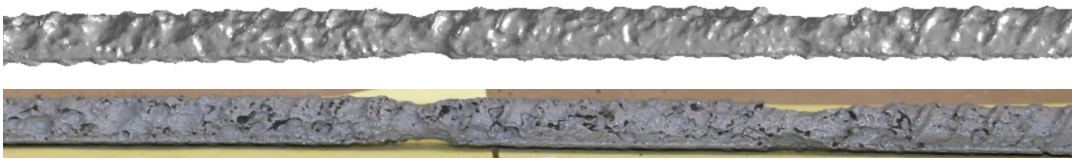

(a) SS-3.2-R1-L ($\eta_{avg,m}$=17.6%)

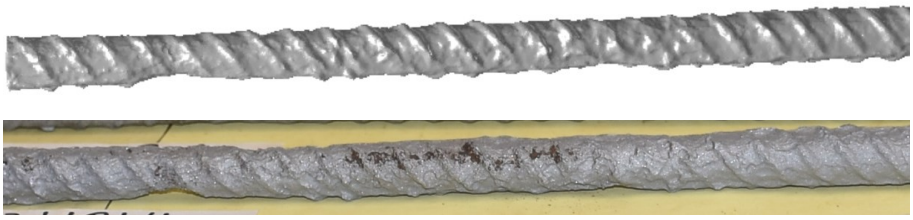

(b) LS-2.1-R1-L-1 ($\eta_{avg,m}$=26.7%)

(c) SS-5.1-R1-L ($\eta_{avg,m}$=36.1%)

Figure 5.7: Illustrative 3D images of the corroded steel bars

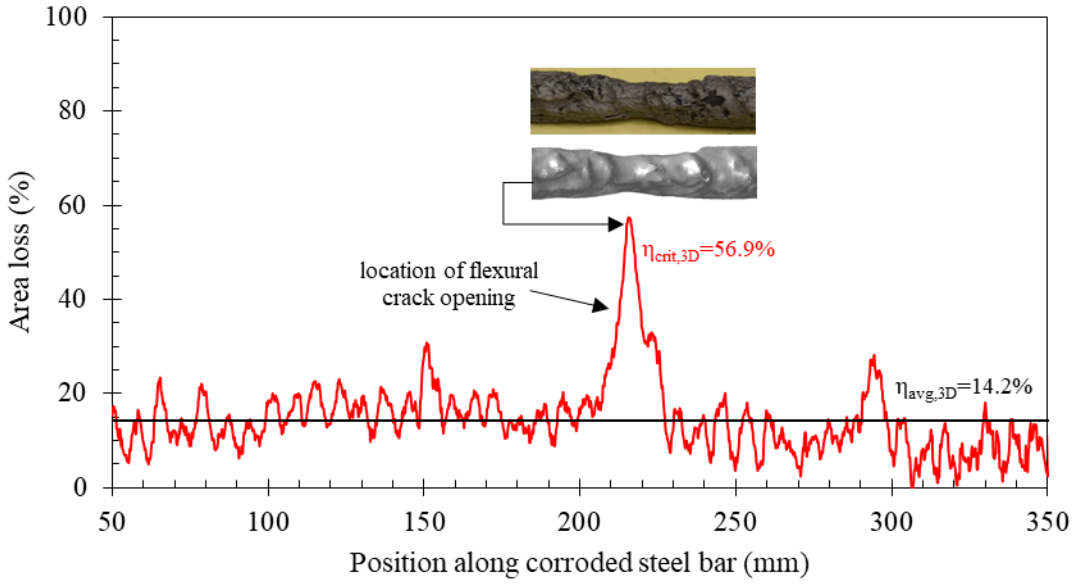

(a) Longitudinal distribution of cross-sectional area loss along steel bar

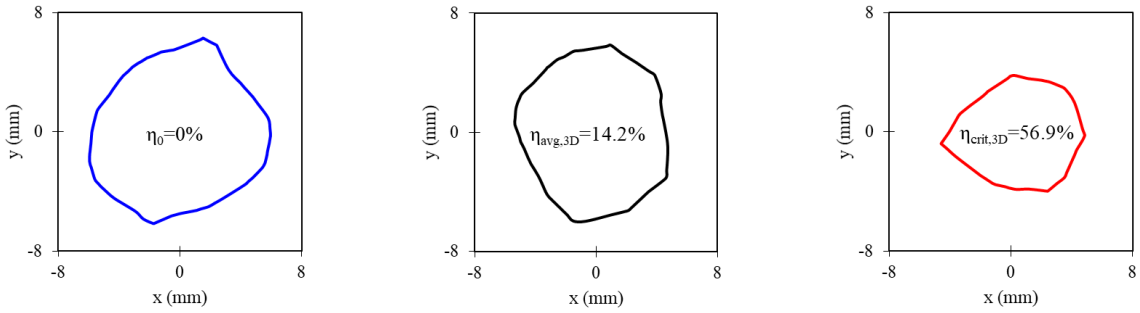

(a) Cross-sectional view at different sections

Figure 5.8: Distribution of corrosion along steel bar SS-3.2-R1-L

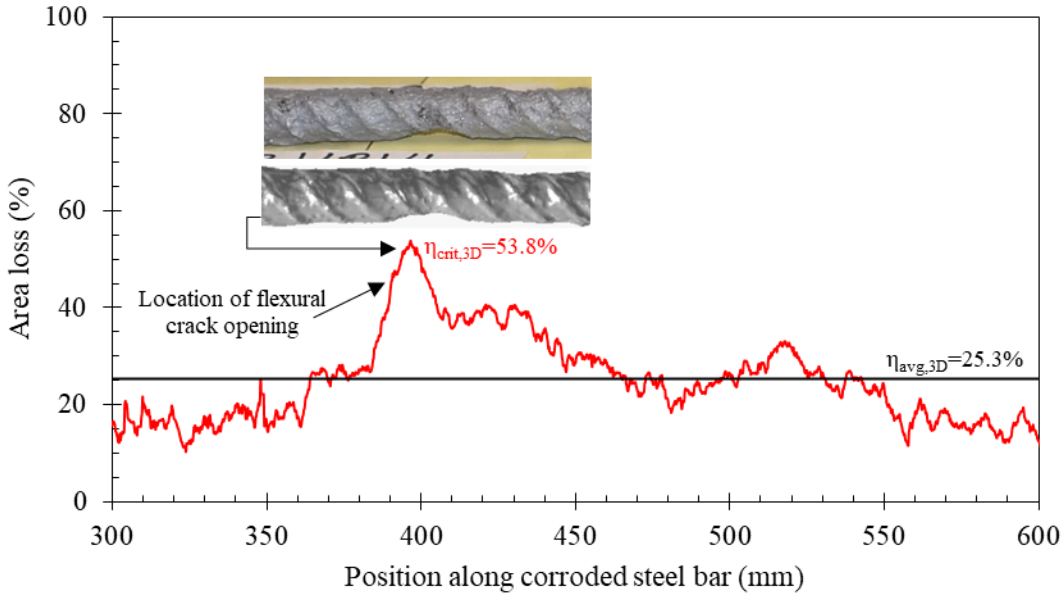

(a) Longitudinal distribution of cross-sectional area loss along steel bar

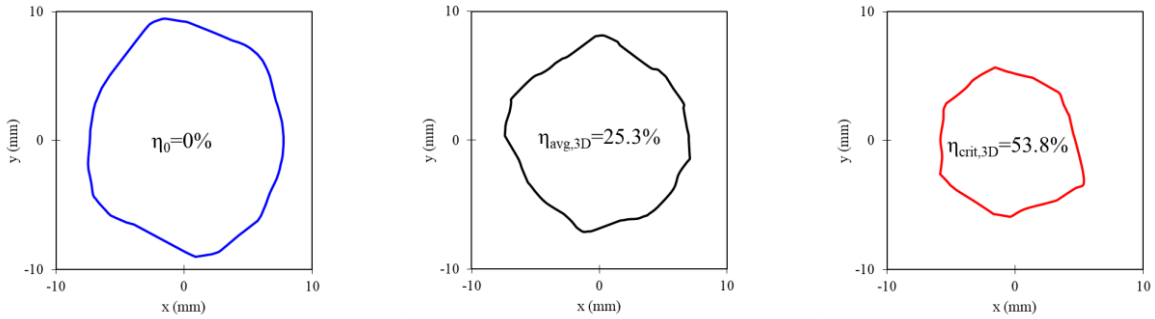

(b) Cross-sectional view at different sections

Figure 5.9: Distribution of corrosion along steel bar LS-2.1-R1-L-1

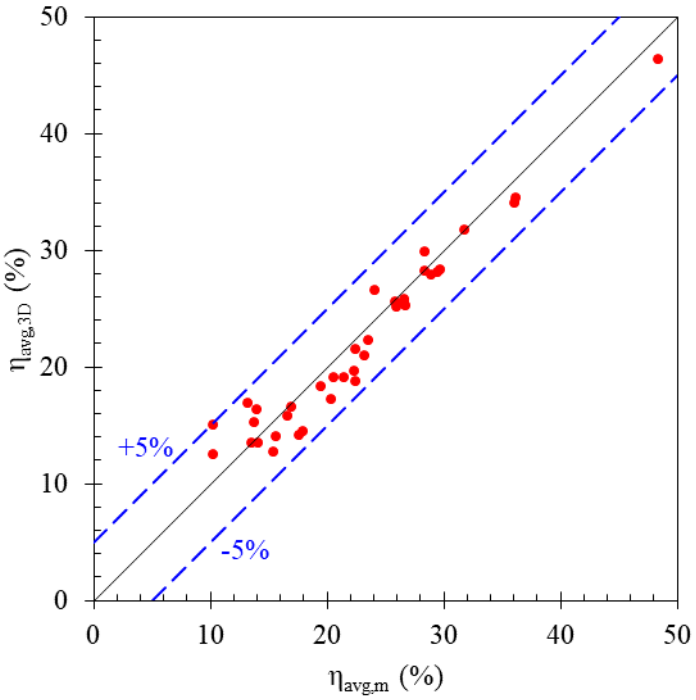

Figure 5.10: Reliability and accuracy of three-dimensional laser scanner

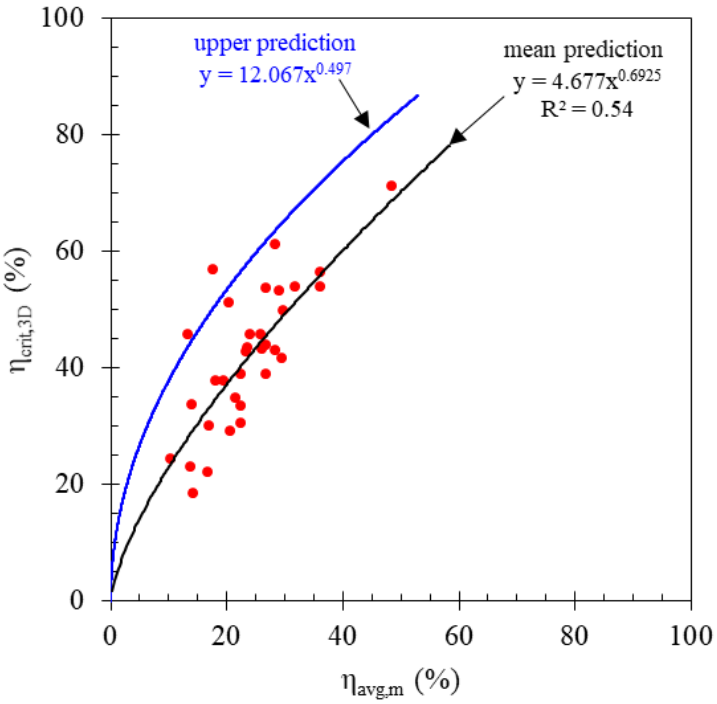

Figure 5.11: Relationship between average mass loss and maximum sectional loss

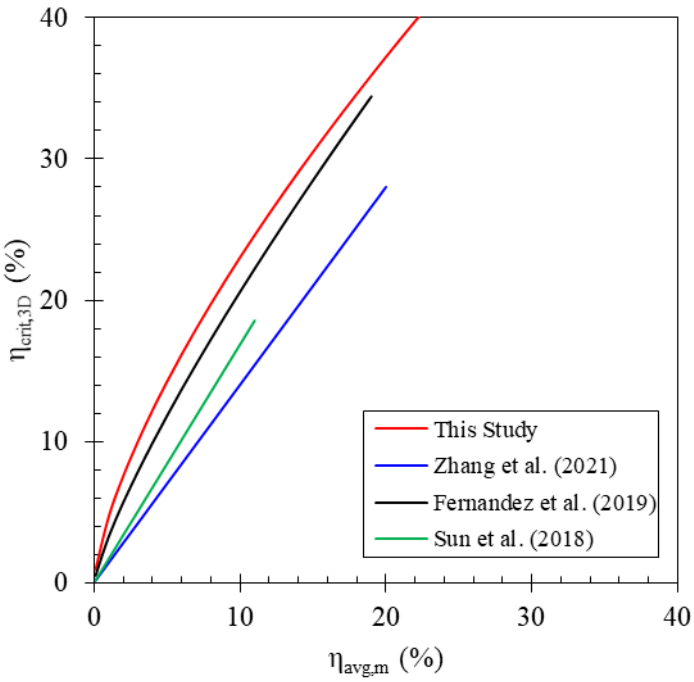

Figure 5.12: Comparison of the empirical relationship between average and maximum sectional losses with previous studies

SS-3.1-R2-L

SS-5.1-R1-L

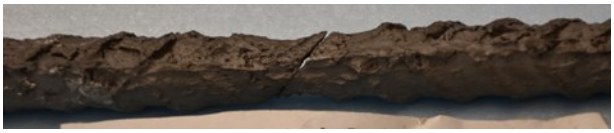

LS-2.1-R1-R

Figure 5.13: Failure of corroded steel bars

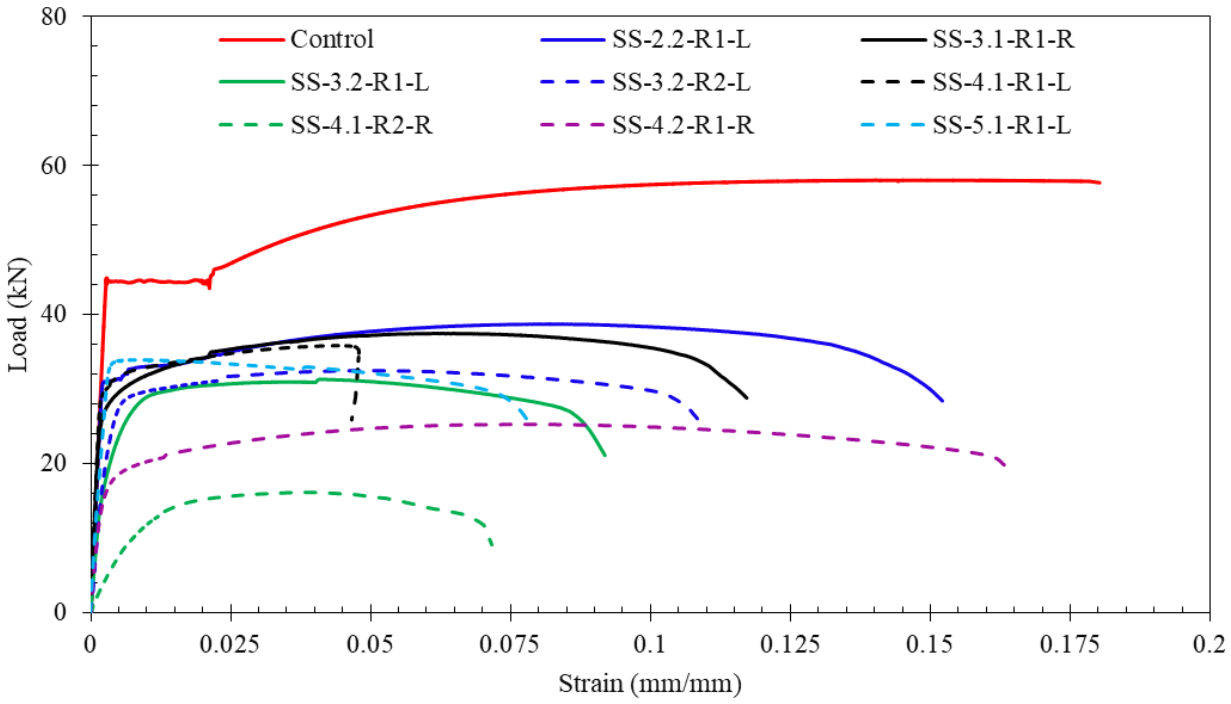

(a) 10M steel bars

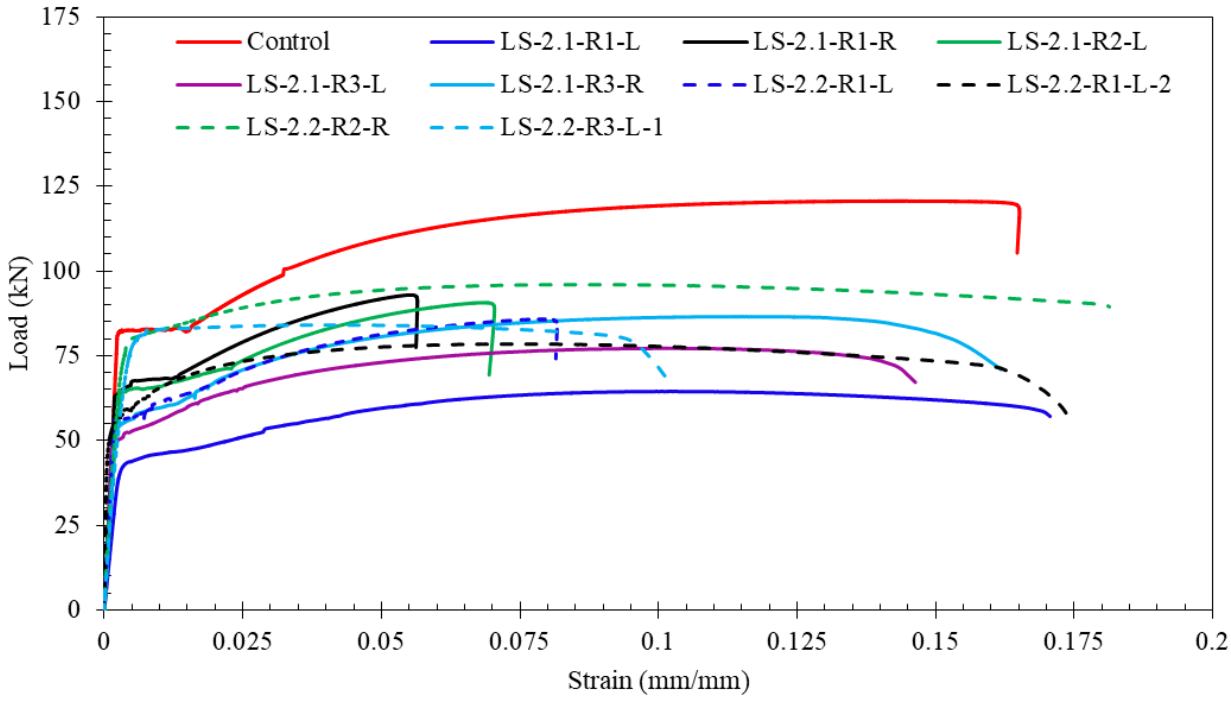

(b) 15M steel bars

Figure 5.14: Load-strain relationships of steel bars

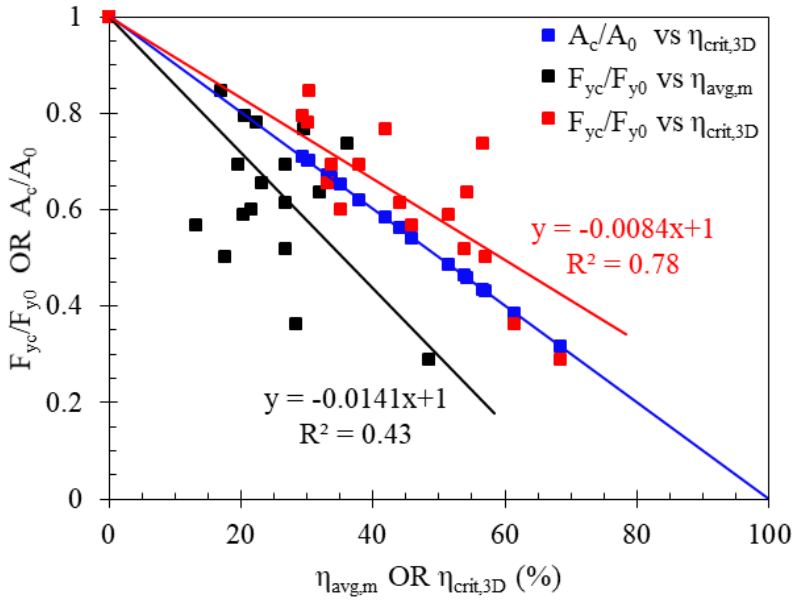

(a) At yield

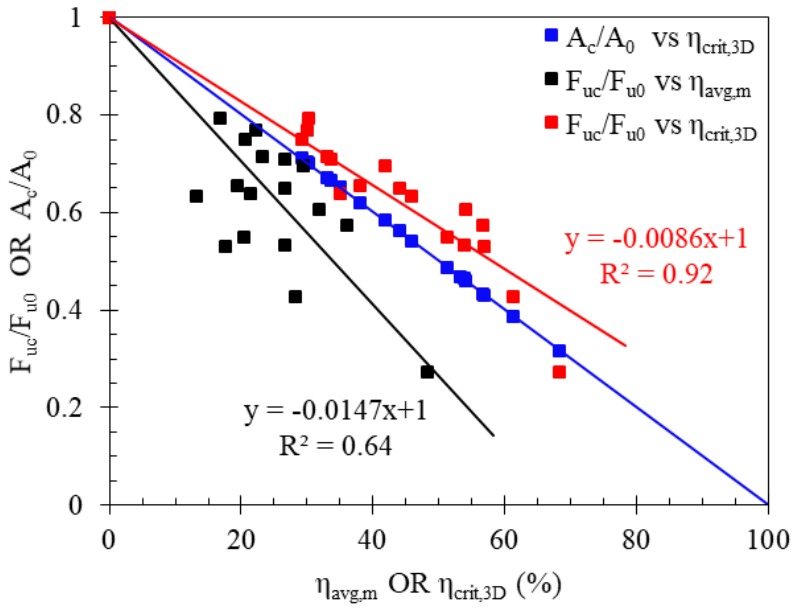

(b) At ultimate

Figure 5.15: Effect of corrosion on the load capacity of steel bars

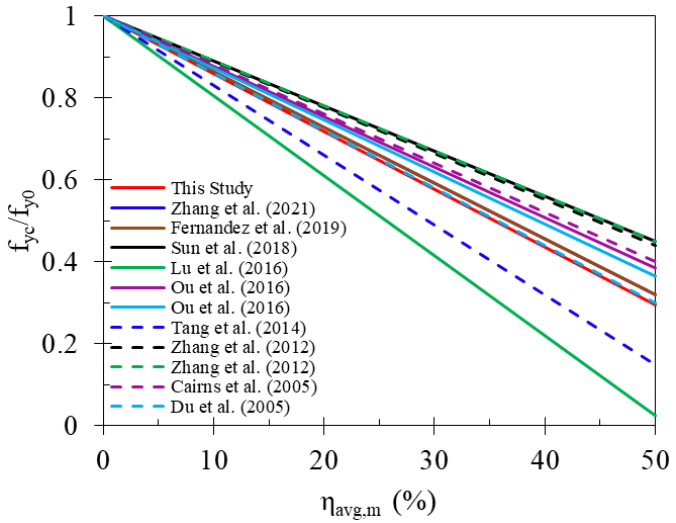

(a) At yield – based on mass loss

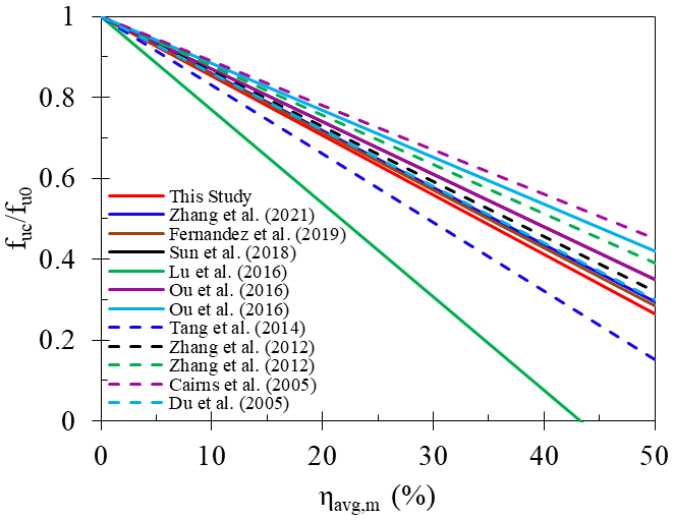

(b) At ultimate – based on mass loss

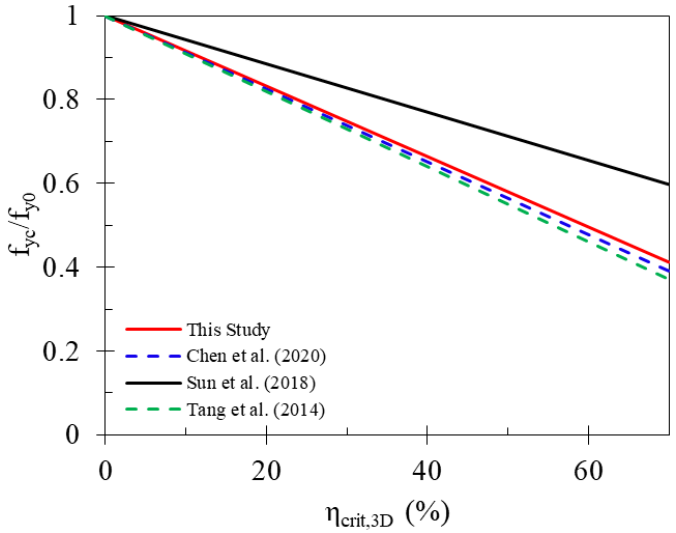

(c) At yield – based on critical area loss

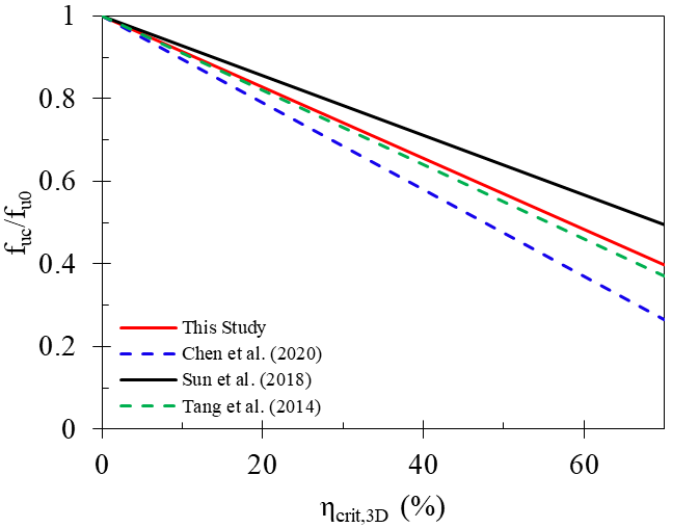

(d) At ultimate – based on critical area loss

Figure 5.16: Comparison of nominal strength reductions in the corroded steel bars with previous studies

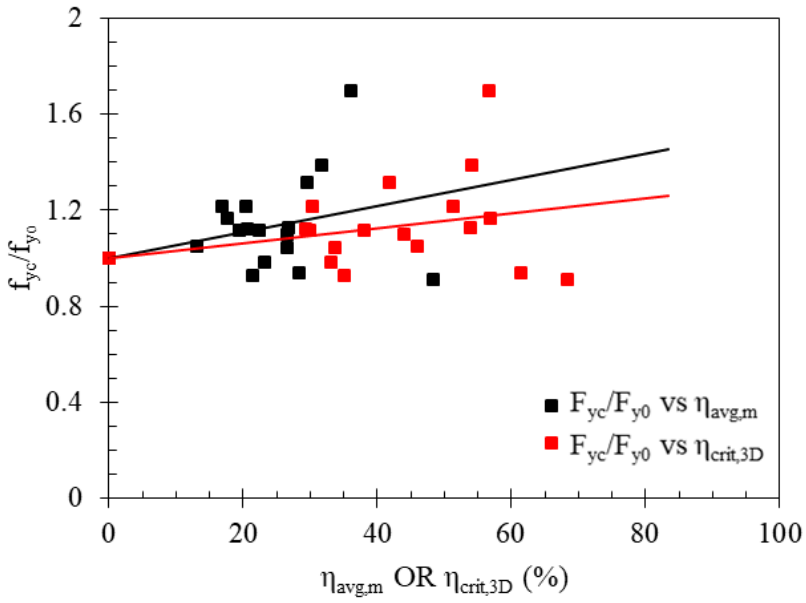

(a) At yield

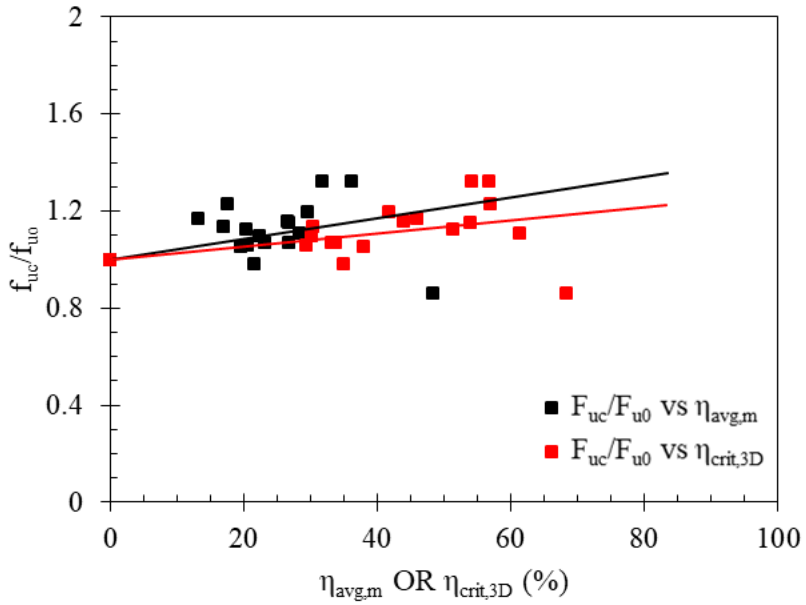

(b) At ultimate

Figure 5.17: Effect of corrosion on the effective strength of steel bars

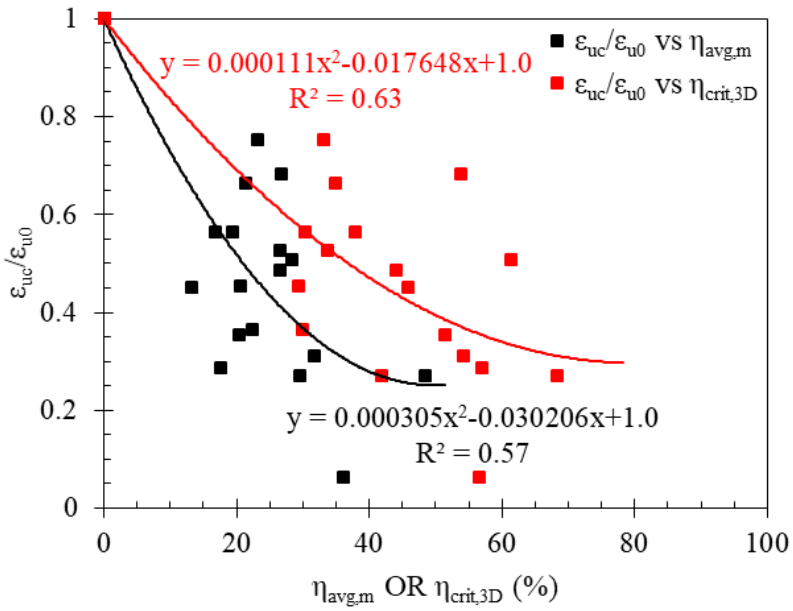

Figure 5.18: Effect of corrosion on the ultimate strain ratio of steel bars

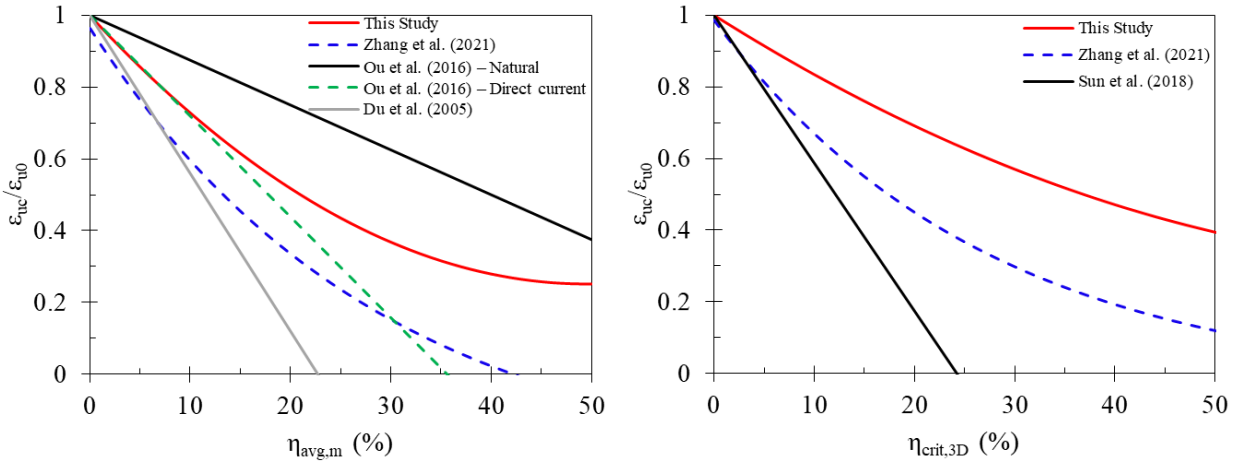

(a) Based on mass loss (b) Based on critical area loss

Figure 5.19: Comparison of ultimate strain reduction in the corroded steel bars with previous studies

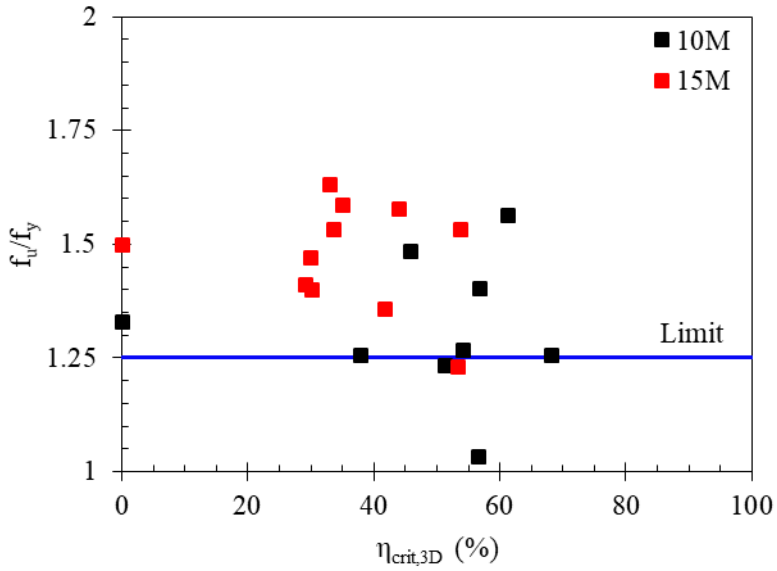

Figure 5.20: Effect of corrosion on the ratio between ultimate and yield strengths of steel bars

5.5 References

Al-Bayti, A., Almansour, H., Saatcioglu, M. (2022b). Tests Reinforced Concrete Beams under Coupled Effects of Variable Service Loads and Reinforcement Corrosion. To be submitted for publication.

Al-Bayti, A., Almansour, H., Saatcioglu, M. (2022c). Tests of Reinforced Concrete Beams under Coupled Effects of Maximum Service Loads and Reinforcement Corrosion. To be submitted for publication.

Almusallam, A. A. (2001). Effect of degree of corrosion on the properties of reinforcing steel bars. Construction and Building Materials, 15(8), 361-368.

ASTM G1-03. (2017)e1. Standard Practice for Preparing, Cleaning, and Evaluation Corrosion Test Specimens. ASTM International, West Conshohocken, Pennsylvania, USA.

Apostolopoulos, C. A., and Papadakis, V. G. (2008). Consequences of steel corrosion on the ductility properties of reinforcement bar. Construction and Building Materials, 22(12), 2316-2324.

ACI 318-14. (2014). Building Code Requirements for Structural Concrete (ACI 318-14) and Commentary on Building Code Requirements for Structural Concrete (ACI 318R-14). ACI Committee 318, American Concrete Institute, Farmington Hills, Michigan, USA.

Cairns, J., Plizzari, G. A., Du, Y., Law, D. W., and Franzoni, C. (2005). Mechanical properties of corrosion-damaged reinforcement. ACI Materials Journal, 102(4), 256-264.

Chen, E., Berrocal, C. G., Fernandez, I., Löfgren, I., and Lundgren, K. (2020). Assessment of the mechanical behaviour of reinforcement bars with localised pitting corrosion by Digital Image Correlation. Engineering Structures, 219, 110936.

Du, Y. G., Clark, L. A., and Chan A. H. C. (2005). Residual capacity of corroded reinforcing bars. Magazine of Concrete Research, 57(3), 135-147.

Du, Y. G., Clark, L. A., and Chan A. H. C. (2005). Effect of corrosion on ductility of reinforcing bars. Magazine of Concrete Research, 57(7), 407-419.

Fernandez, I., and Berrocal, C. G. (2019). Mechanical Properties of 30 year-old naturally corroded steel reinforcing bars. International Journal of Concrete Structures and Materials, 13, Article 9.

Fernandez, I., Lundgren, K., and Zandi, K. (2018). Evaluation of corrosion level of naturally corroded bars using different cleaning methods, computed tomography, and 3D optical scanning. Materials and Structures, 51, Article 78.

Lu, C., Yuan, S., Cheng, P., and Liu, R. (2016). Mechanical properties of corroded steel bars in pre-cracked concrete suffering from chloride attack. Construction and Building Materials, 123, 649-660.

Ou, Y.-C., Susanto, Y. T. T., and Roh, H. (2016). Tensile behavior of naturally and artificially corroded steel bars. Construction and Building Materials, 103, 93-104.

Palsson, R., and Mirza, M. S. (2002). Mechanical response of corroded steel reinforcement of abandoned concrete bridge. ACI Structural Journal, 99(2), 157-162.

Sun, X., Kong, H., Wang, H., and Zhang, Z. (2018). Evaluation of corrosion characteristics and corrosion effects on the mechanical properties of reinforcing steel bars based on three-dimensional scanning. Corrosion Science, 142, 284-294.

Tang, F., Lin, Z., Chen, G., and Yi, W. (2014). Three-dimensional corrosion pit measurement and statistical mechanical degradation analysis of deformed steel bars subjected to accelerated corrosion. Construction and Building Materials, 70, 104-117.

Tahershamsi, M., Fernandez, I., Lundgren, K., and Zandi, K. (2017). Investigating correlations between crack width, corrosion level and anchorage capacity. Structure and Infrastructure Engineering, 13(10), 1294-1307.

Xia, J., Jin, W. L., Zhao, Y. X., and Li, L. Y. (2013). Mechanical performance of corroded steel bars in concrete. Structures and Buildings, 166(5), 235-246.

Zhang, J., Huang, J., Fu, C., Huang, L., and Ye, H. (2021). Characterization of steel reinforcement corrosion in concrete using 3D laser scanning techniques. Construction and Building Materials, 270, 121402.

Zhang, W., Song, X., Gu, X., and Li, S. (2012). Tensile and fatigue behavior of corroded rebars. Construction and Building Materials, 34, 409-417.

Zhu, W., and François, R. (2013). Effect of corrosion pattern on the ductility of tensile reinforcement extracted from a 26-year-old corroded beam. Advances in Concrete Construction, 1(2), 121-136.

Chapter Six : Finite Element Analysis of Corroded Reinforced Concrete Beams Subjected to Service Loads

Abstract

This paper presents results of a numerical study that examined the flexural behavior of corroded reinforced concrete (RC) beams. Two-dimensional nonlinear finite element (FE) models were built and analyzed using DIANA finite element analysis software. A simplified approach was implemented in the FE models to simulate the damage induced by corrosion to reduce the computational efforts. The numerical analyses were validated with experimental tests of large-scale and small-scale RC beams subjected to the coupled effects of reinforcement corrosion and different levels of service loads. The predicted responses were in good agreement with test results in terms of failure modes, residual ultimate load capacity and ductility. The validated FE models were then used to conduct a parametric study for cases that were not covered in the experimental program, including the level of corrosion, level of service loads, strength of concrete, and tensile reinforcement ratio. This investigation showed that increasing service load levels of corroded beams caused further reductions in ultimate load capacity and ductility. Furthermore, increasing the tensile reinforcement ratio had a significant impact on improving the load-carrying capacity of corroded beams.

Keywords: FE analysis, DIANA, reinforcement corrosion, service loads, simplified approach, flexural behavior.

6.1 Introduction

Reinforced concrete (RC) is a composite material that is widely used in the construction of civil structures, including tunnels, buildings, and bridges. Initially, the embedded steel reinforcement is protected from corrosion by a thin passive film layer formed around the reinforcement during the early stages of cement hydration. High levels of chloride concentration, seeping through the voids and cracks of concrete, break down the passive film layer. For that reason, reinforcement corrosion initiates faster when RC structures are exposed to aggressive environmental conditions such as those in cold regions due to the use of de-icing salt. Typically, chloride contaminated concrete leads to the development of a localized pit corrosion. Furthermore, high levels of carbon dioxide caused by increased gas emissions reduce the alkalinity of concrete, which could break down the passive film layer. Typically, carbonation of concrete leads to the development of generalized corrosion attack. Nevertheless, both types of corrosion can be simultaneously present in RC structures. The consequences associated with the corrosion phenomena have detrimental influences on the load-carrying capacity, ductility, and service life of RC structures.

Over the past few decades, many experimental research studies examined the structural performance of damaged RC beams due to corrosion. At first, the response of corroded beams was investigated under no loads (Rodriguez et al., 1997; Mangat and Elgarf, 1999; Azad et al., 2007; Du et al., 2007; Torres-Acosta et al., 2007). In all these investigations, it was revealed that corrosion of steel reinforcement reduced the ultimate load capacity of beams. In some circumstances, the ductile behavior of beams was replaced by a premature rupture of corroded steel bars (Du et al., 2007). Afterward, the focus of research shifted towards corroding the beams under loads to simulate in-service conditions of RC beams/girders (Yoon et al., 2000; Ballim and Reid, 2003; El Maaddawy and Topper, 2005; Malumbela et al., 2009; Hariche et al., 2012; Du et al., 2013; Li et al., 2018; Zhang et al., 2018). Corroding RC beams under service loads is essential, particularly in the presence of load-induced cracks, which expose the embedded steel bars to chlorides more efficiently. Ballim and Reid (2003) indicated that deflections of corroded beams under loads were more than those which were corroded under no loads. Li et al. (2018) found that the ultimate load capacity of corroded beams was reduced with increased levels of loading.

Corrosion of steel reinforcement is a slow process that takes many years in natural environments. Simulating reinforcement corrosion in laboratory environments may also take a long period of

time to ensure proper reproduction of in-field corrosion. Recently, there was an increased demand to develop simplified approaches to predict the response of corroded RC beams and eliminate the need for experimental testing. Several researchers developed computational tools using finite element analyses to evaluate the behavior of corroded beams (Dekoster et al., 2003; Coronelli and Gambarova, 2004; Kallias and Rafiq, 2010, Hanjari et al., 2011; Ou and Nguyen 2014; Jnaid and Aboutaha, 2016).

Different techniques were implemented in the above-mentioned studies to include the damage induced by corrosion into the FE models. Generalized corrosion was modeled by reducing the sectional area along steel bars (Coronelli and Gambarova, 2004; Kallias and Rafiq, 2010; Hanjari et al., 2011; Ou and Nguyen 2014; Jnaid and Aboutaha, 2016). Localized pit corrosion was modeled by reducing the mechanical properties of corroded steel bars (Coronelli and Gambarova, 2004; Kallias and Rafiq, 2010; Hanjari et al., 2011; Ou and Nguyen 2014; Jnaid and Aboutaha, 2016) and/or by locally reducing the sectional area of steel bars (Hanjari et al., 2011). The development of corrosion cracks was modeled by reducing the strength of concrete in the affected region (Coronelli and Gambarova, 2004; Kallias and Rafiq, 2010; Hanjari et al., 2011). The characteristics of bond at the interface between the corroded reinforcement and concrete were also modified. The modification factors were derived from previous analytical and experimental research efforts devoted to understand the phenomena of corrosion in RC structures. Previous studies were focused on modeling the response of corroded beams without accounting for in-service conditions. In order to model the presence of service loads while corroding the beams, Shen et al. (2019) adopted a thermal expansion methodology to simulate the expansion of corrosion.

Clearly, there is a lack of research efforts to model the coupling effects of reinforcement corrosion and service loads, even though this effect was proven to cause more adverse effect on the ultimate load capacity of beams when compared to corroding the beams under no loads. The main objective of this paper is to develop a simplified approach to evaluate the flexural response of damaged RC beams due to corrosion. Finite element analysis is a powerful technique that can be used to simulate the response of RC beams with a reasonable accuracy. A simplified approach was implemented in DIANA FE analysis software by including the damage induced by corrosion into the FE models to predict the ultimate load capacity and ductility of corroded beams under service loads. The predictions were validated with corroded RC beams tested by Al-Bayti et al. (2022b, 2022c), which

included beams of different sizes subjected to the coupled effects of reinforcement corrosion and different levels of service loads. Subsequently, a parametric study was conducted to expand test data for cases that were not covered in the experimental program.

6.2 Reference Experimental Study

The reliability and accuracy of the proposed simplified FE approach was validated with corroded RC beams tested by Al-Bayti et al. (2022b, 2022c). As part of this experimental study, large-scale and small-scale beams were tested under the coupled effects of reinforcement corrosion and various service loads. All the beams were constructed with normal strength concrete and were reinforced with Grade 400 reinforcing bars. Large-scale "LS" beams had a larger cross-section and a longer span length than small-scale "SS" beams. Also, the tensile reinforcement ratio of large-scale beams (1.17%) was higher than that of small-scale beams (0.63%). The beams were designed to be under-reinforced with anticipated flexural failure. Figure 6.1 shows a schematic illustration of the beams, while Table 6.1 provides a summary of the dimension of beams along with reinforcement layout and detailing.

A four-point bending setup was used to conduct the mechanical testing of the simply-supported beams. Corrosion of steel reinforcement was accelerated by directly impressing current between the bottom longitudinal steel bars and an external cathode. The bottom middle portion of the beams was submerged into sodium chloride solution (5% NaCl) to help in depassivating the steel bars. The study was aimed to examine the pure flexural response of beams, and hence the bottom longitudinal steel bars were corroded within the constant moment region only. In addition, the beams were properly anchored at ends.

Table 6.2 presents a summary of the selected experimental large-scale and small-scale beams that were used to validate the FE models, along with the primary test parameters of beams. Control beams were loaded up until failure, to evaluate their ultimate load capacities. Corroded beams were tested either in the presence or absence of service loads. In the presence of loads, testing started by loading the beams to the desired service level. Then, this load was sustained while initiating the corrosion process of the bottom longitudinal steel bars. Beams LS-2.1, SS-3.1 and SS-4.2 were corroded under sustained service loads up until their failure, while beam LS-2.3 was corroded under sustained service loads for a certain duration of time before further increasing the loads up until the failure of the beam. In the absence of loads, testing started by corroding beams LS-2.4

and LS-5.1 under their self-weight for a certain duration of time. This was followed by loading the beams up until their failure.

All control beams exhibited a ductile response characterized by significant deformations before crushing of top concrete. In contrast, the response of corroded beams was either ductile or brittle. Large-scale beam LS-2.1 and small-scale beams SS-3.1, SS-4.2, and SS-5.1 failed due to the rupture of corroded steel bars, while large-scale beams LS-2.3 and LS-2.4 failed due to crushing of top concrete. For the beams that were corroded under service loads, the rupture of corroded steel bars occurred at the locations where flexural cracks were initiated, within the constant moment region of beams, as the open cracks allowed in further localization of corrosion and loss of reinforcement sectional area.

After the failure of RC beams, the corroded steel bars were carefully retrieved from the beams. Afterward, they were cleaned, weighed, and scanned to assess the level of corrosion in terms of average and localized sectional losses. Subsequently, direct tensile tests were conducted to evaluate the mechanical performance of corroded steel bars. Test data were then used to develop empirical expressions that correlate the properties of steel bars with the level of corrosion (discussed in the next section).

6.3 Corrosion-Induced Damage

There are several adverse effects associated with the initiation and propagation of reinforcement corrosion, influencing the load-carrying capacity and ductility of RC beams. This includes: (i) loss of reinforcement area, (ii) degradation of mechanical properties of steel reinforcement, (iii) deterioration of concrete, and (iv) impairment or complete loss of bond at the interface between the reinforcement and concrete.

6.3.1 Loss of Reinforcement Area

As mentioned previously, corrosion of steel reinforcement can be present in a generalized or localized form depending on the environmental exposure. Generalized corrosion causes a uniform loss of sectional area, influencing the entire surface of steel reinforcement, while localized pit corrosion is a local loss of steel that develops at random sites along the length of steel reinforcement. In the beams tested by Al-Bayti et al. (2022b, 2022c), the researchers observed another form of localized corrosion at the positions of flexural cracks within the corroded region

of beams. This type of corrosion developed as a result of chloride ingress through crack openings, causing a further loss of reinforcement area at the cracked sections of beams. In this study, loss of reinforcement area caused by localized corrosion was predicted using the empirical expression proposed by Al-Bayti et al. (2022a). The power-law function, shown in Figure 6.2, is expressed in the following:

$$\eta_{crit} = \begin{cases} 4.68\,{\eta_{avg,m}}^{0.69} & (\text{mean prediction "}\eta_{\text{crit,mean}}\text{"}) \\ 12.08\,{\eta_{avg,m}}^{0.50} & (\text{upper prediction "}\eta_{\text{crit,upper}}\text{"}) \end{cases} \quad (6.1)$$

where, η_{crit} is the maximum loss of reinforcement sectional area due to corrosion, and $\eta_{avg,m}$ is the average loss of reinforcement sectional area. The mean curve was established using the line of best fit of all data points, while the upper bound curve was established using the line of best fit of extreme points only. Predictions according to the upper bound curve ensure that the loss of reinforcement sectional area is not underestimated. It should be noted that predictions according to a lower bound curve gives a close representation of generalized corrosion, and hence it was not considered in this study. The residual area of corroded steel bars can be simply modeled using the following expression:

$$A_{c,avg} = (1 - \eta_{avg,m}) \times A_0 \quad (6.2)$$

$$A_{c,min} = (1 - \eta_{crit}) \times A_0 \quad (6.3)$$

where, $A_{c,avg}$ is the average area of corroded steel bars, $A_{c,min}$ is the minimum area of corroded steel bars, and A_0 is the area of non-corroded steel bars.

6.3.2 Degradation of Mechanical Properties of Reinforcement

Numerous research studies were carried out to examine the effect of corrosion on the mechanical performance of steel reinforcement (Almusallam, 2001; Palsson and Mirza, 2002; Cairns et al., 2005; Du et al., 2005; Apostolopoulos and Papadakis, 2008; Tang et al., 2014; Fernandez and Berrocal, 2019). Tensile strength of corroded steel bars was evaluated using either the nominal non-corroded sectional area, average corroded sectional area, or actual corroded sectional area. For that reason, there is a disagreement among researchers when it comes to modeling the influence of corrosion on the tensile strength of steel bars. This in turn, has a significant impact on the reliability and validity of previously developed approaches to predict the response of corroded RC beams.

Based on the tensile testing of the corroded steel bars retrieved from the beams tested by Al-Bayti et al. (2022a), it was demonstrated that the strength of steel bars, based on nominal sectional area, decreased significantly with the increase of corrosion levels. However, the tensile strength, based on actual corroded sectional area, increased slightly with the increase of corrosion levels. Therefore, the reduction in load capacity of corroded steel bars was primarily attributed to the localized loss of sectional area. In addition, the ductility of steel bars was significantly influenced by corrosion (Al-Bayti et al., 2022a). The non-uniform distribution of corrosion reduced the ultimate strain of steel bars with the increase of corrosion levels.

Accordingly, there are two approaches that can be implemented using FE analyses to model the effect of corrosion on the mechanical performance of steel bars. In the first approach, the reduction in strength of corroded steel bars can be modeled using empirical expressions established based on nominal sectional area. Likewise, the reduction in ductility can be modeled using empirical expressions that correlate the ultimate strain with the level of corrosion in steel bars. It is important to recognize that this approach accounts for the loss of reinforcement area, and hence modifying the geometrical properties of steel reinforcement is not needed. In the second approach, the residual sectional area of steel reinforcement is modeled while keeping its original material properties. This approach conservatively ignores the slight increase in strength of steel bars with the increase of corrosion levels. Also, since the smallest section and non-uniform distribution of reinforcement sectional areas are explicitly modeled, the reduction in ultimate strain was not considered. The latter approach was adopted in this study.

6.3.3 Deterioration of Concrete

Corrosion by-products have a lower density than steel. As a result, it occupies a larger volume when replacing the corroded portion of steel. The volumetric expansion of corrosion by-products generate radial stresses that lead to the development of cracks in the surrounding concrete. Cracking could be accompanied by spalling of the affected region if internal cracks extend to the outer surface of concrete. Previously, several researchers adopted a lower compressive strength to model the deterioration of corroded concrete (Coronelli and Gambarova, 2004; Kallias and Rafiq, 2010; Hanjari et al., 2011). The expression proposed by Coronelli and Gambarova (2004) for corroded compressed concrete was used for this purpose. This expression was derived based on a

previously developed model for cracked concrete elements by Vecchio and Collins (1986), as expressed in the following:

$$f_c^{c\prime} = \frac{f_c'}{1 + k\,\varepsilon_1/\varepsilon_o} \tag{6.4}$$

where, f_c' and $f_c^{c\prime}$ are the compressive strengths of non-corroded and corroded concrete, respectively, k is a coefficient related to the roughness and diameter of steel bars and was taken as 0.1 (Cape, 1999), ε_o is the strain of concrete at maximum compressive strength, and ε_1 is the average tensile strain of concrete perpendicular to compression, expressed in the following:

$$\varepsilon_1 = \frac{2\pi n(v_{rs} - 1)X}{b_o} \tag{6.5}$$

where, n is the number of longitudinal steel bars in compression, v_{rs} is the ratio of volume expansion of corrosion by-products relative to non-corroded steel and was taken as 2.0 (Molina et al., 1993), X is the penetration depth of corrosion, and b_o is the original width of the beam. In this study, the development of longitudinal corrosion cracks in the concrete cover of beams was modeled by reducing the tensile strength of the concrete elements in the affected region. The strength was reduced using the same proportion as the reduction in compressive strength of corroded cracked concrete, as expressed in the following:

$$f_t^c = \frac{f_c^{c\prime}}{f_c'} f_t \tag{6.6}$$

where, f_t and f_t^c are the tensile strengths of non-corroded and corroded concrete, respectively. This method was also employed by other researchers (Hanjari et al., 2011).

6.3.4 Bond Strength

Reinforcement corrosion has a significant influence on the bond characteristics at the interface between steel reinforcement and concrete. Previous research studies had shown that bond strength increased slightly at low levels of corrosion and prior to the development of corrosion cracks (Al-Sulaimani et al., 1990; Almusallam et al., 1996). This enhancement was primarily attributable to the increase in roughness of steel bars. However, there was a drastic reduction in bond strength with the increase of corrosion levels, owing to the worsening of interlock between steel reinforcement and concrete.

In the beams tested by Al-Bayti et al. (2022b, 2022c), the bottom longitudinal steel bars were corroded within the constant moment region of beams. As stated earlier, the localization of corrosion and additional loss of reinforcement area occurred at the locations of flexural cracking. This in turn, led to premature rupture of the corroded steel bars at the crack location before debonding of the concrete cover in the corroded portion of the beams. Strain measurements from gauges attached on the longitudinal steel bars and the surface of concrete showed that the increase in strains within the corroded portion of the beams had a slight impact on the redistribution of strains to the adjacent shear span regions. For that reason, the degradation of bond within the corroded portion of beams did not increase the demand at the ends of beams or significantly contribute to the flexural resistance of beams. It is also important to note that the available embedment length in the shear span regions and the provided hook anchorage at the beam ends were sufficient to prevent bond failures. For these reasons, the effect of corrosion on the bond strength at the interface between steel reinforcement and concrete was not considered in this study. Therefore, the results of the parametric study reported in this chapter are limited to beams and girders that are similar to those tested in the companion experimental program. This includes beams whose load-carrying capacity is not affected by the loss of bond between the corroded reinforcement and concrete in the positive moment region, and those that have sufficient anchorage of reinforcement so that the corrosion related reduction in bond would not lead to anchorage failure.

6.4 Finite Element Model

Nonlinear FE analysis using DIANA software was employed to simulate the behavior and failure mechanisms of corroded RC beams. The predictions of FE analyses were validated with experimental tests of non-corroded and corroded beams. Subsequently, a parametric study was conducted to examine the effect of various parameters, influencing the response of corroded beams.

6.4.1 Modeling Approach

6.4.1.1 Model Description

Two-dimensional FE models were developed using DIANA's graphical interface by replicating the experimental large-scale and small-scale beams in terms of geometry, location of longitudinal

and transverse reinforcement, along with the thickness of cover, as shown in Figure 6.3. The concrete section was modeled using eight-node quadrilateral regular plane stress elements (i.e., CQ16M elements), based on quadratic interpolation and Gauss integration. Steel reinforcement was modeled using an embedded approach, assuming a perfect bond between the reinforcement and concrete, as discussed previously. Embedded elements behave in a similar manner as truss elements (i.e., deforms in longitudinal direction only).

The dimension and location of support and loading plates were identical to those in the experimental setup. The plates were also modeled using eight-node quadrilateral regular plane stress elements, with elastic material properties. To simulate simply-supported boundaries, the center point of the left support was restrained from movements in the vertical and horizontal directions, while the center point of the right support was restrained from movement in the vertical direction only. Loads were applied at the center points of both loading plates using an incremental time-step approach. A regular Newton-Raphson iterative algorithm was adopted to solve the nonlinear system of equations.

6.4.1.2 Concrete Modeling

A smeared cracking approach using the total strain rotating crack model was adopted to define the constitutive behavior of concrete. In this approach, the direction of cracks is aligned with the principal strain direction, and so it rotates with the rotation of the principal strain direction. Compressive behavior of concrete was modeled using a parabolic stress-strain curve (DIANA, 2021), shown in Figure 6.4(a). In the hardening part of the curve, the strength of concrete increases linearly up to one-third of peak compressive strength, which is then followed by a nonlinear increase up to the peak compressive strength. In the softening part, the strength decreases in such a way that the area under the curve is equivalent to the ratio between the compressive fracture energy G_c and characteristic element length of concrete h. Compressive strength of concrete f_c' was obtained from the cylinder compression test. Compressive fracture energy G_c was taken as 250 times the tensile fracture energy (Nakamura and Higai, 2001). The strength of cracked concrete in compression was reduced due to lateral cracking according to the expression described in Vecchio and Collins (1993).

Tensile behavior of concrete was modeled according to the Japan Society of Civil Engineers (JSCE, 2010), shown Figure 6.4(b). This model accounts for the increase in concrete stiffness

caused by the transfer of stresses from the reinforcement to the surrounding concrete in-between cracks (i.e., tension stiffening effect). In the ascending branch of this curve, the tensile strength of concrete increases linearly up until cracking. Afterward, strength remains unchanged prior to descending nonlinearly. Tensile strength of concrete f_t was taken as $0.33\sqrt{f_c'}$ (f_c' in MPa). Tensile fracture energy G_t was estimated according to fib Model Code for Concrete Structures 2010 (CEB-FIP, 2013) and was taken as $73{f_c'}^{0.18}$ (f_c' in MPa). A summary of concrete properties used to model the beams is presented in Table 6.3.

6.4.1.3 Steel Reinforcement Modeling

Nonlinear behavior of steel reinforcement was modeled using Von Mises Plasticity model with isotropic strain hardening. Proper modeling of yield and strain hardening stages was ensured by directly using the stress-strain curves obtained from the direct tensile testing of steel bars into the software, as shown in Figure 6.4(c). A summary of steel reinforcement properties is presented in Table 6.4.

6.4.1.4 Corrosion and Load Modeling

The predicted response by FE analysis was validated with the experimental beams listed in Table 6.3. Analyses of control beams were performed by increasing loads incrementally up until failure, while analyses of corroded beams were performed by incorporating corrosion-induced damage and the applied service loads into the FE models. Longitudinal corrosion cracks in the cover of concrete were modeled by reducing the strength of concrete in the affected region according to the expressions presented in Section 6.3.3. Generalized corrosion was modeled by reducing the area of bottom longitudinal steel bars within the corroded portion of the beams, using the average loss of reinforcement area (i.e., mass loss) obtained from the experimental data. Non-uniform distribution of corrosion along the longitudinal steel bars was taken into consideration in the analyses. Localized corrosion was modeled by reducing the area of steel reinforcement at select positions within the corroded portion of beams, using the predictive empirical model presented in Section 6.3.1.

Considering the spatial distribution of localized corrosion is a complex phenomenon due to uncertainties and variabilities associated with the construction of RC structures as well as the nature of environmental exposures. Based on the findings by Al-Bayti et al. (2022b, 2022c), the

distribution of corrosion was strongly influenced by the presence of flexural cracks, resulting in a further loss of reinforcement area at the crack sections of beams. Such behavior was only observed in corroded beams with load-induced cracks. To model this behavior, localized elements were introduced in the FE models at the locations with flexural cracks, as illustrated for beams LS-2.1 and SS-3.1 in Figure 6.5. This simplified approach gives a close approximation of the variation of sectional losses of corroded steel reinforcement.

Accordingly, the analyses of beams LS-2.1, LS-2.3, SS-3.1, and SS-4.2, which were corroded under service loads, started by finding the location of flexural cracks using the FE analyses of control beams. Then, localized elements with a length equivalent to the mesh size of the model were introduced at the locations with cracks. The critical localized element was assigned to the cracked section that was closest to where the experimental failure of beams took place. In the absence of data, it is recommended to assume that the critical cracked section is located close or at the center of the beam. Loads were then incrementally increased to the desired service level. This load was equal to 80 kN, 60 kN, and 40 kN for beams LS-2.1/2.3, SS-3.1, and SS-4.2, respectively. Applied loads were sustained while reducing the strength of concrete and the area of the bottom longitudinal steel bars over time. The reduction rates of concrete strength and area of the longitudinal steel bars were assumed to be linear. A typical procedure employed for a beam that failed under service loads (i.e., beam LS-2.1) is shown in Figure 6.6(a), while that used for a beam that was loaded to failure at the end of the corrosion phase (i.e., beam LS-2.3) is shown in Figure 6.6(b).

In contrast, unlike corroded beams under loads, the distribution of corrosion in beams that were corroded under no loads (i.e., without flexural cracks) is subject to the randomness of localized pit corrosion. For that reason, the analyses of beams LS-2.4 and SS-5.1, which were corroded under no loads, started by randomly distributing localized elements along the longitudinal steel bars. Both beams were subjected to their self-weight only. This load was sustained while reducing the strength of concrete and the area of longitudinal steel bars linearly over time. At the end of the corrosion phase, loads were increased up until the failure of beams. Modeling the localized corrosion level in corroded beams without loads was slightly different from those which were corroded under loads. It is important to recognize that the cracked sections in corroded beams under loads allowed for simultaneous corrosion in all adjacent steel bars at the cracks. In contrast, the absence of transverse cracks causes uncertainty and randomness in the distribution of corrosion

along adjacent steel bars. In other words, it is less likely that localized pit corrosion will develop in all adjacent steel bars at a specific section of the beam. This effect was modeled by assuming that steel bars at the critical sections of the beams had a mixture of generalized and localized corrosion. Additional details on how this method was implemented for the corroded small-scale and large-scale beams with no loads are discussed in the next section.

6.4.2 Validation of Finite Element Model

The reliability and accuracy of the proposed procedure outlined in previous sections were ensured by validating the predicted responses using FE analysis with large-scale and small-scale RC beams tested by Al-Bayti et al. (2022b, 2022c). Test beams were divided into three main categories; (i) control (i.e., non-corroded) beams, (ii) corroded beams under loads, and (iii) corroded beams under no loads. Table 6.5 compares FE predictions and experimental test results of the beams in terms of ultimate displacements and loads.

6.4.2.1 Comparison with Control RC Beams

A comparison between FE analyses and the experimental load-displacement curves of control beams is shown in Figure 6.7. For the large-scale beam, the predicted response is in a good agreement with the experimental curves in terms of cracking, flexural stiffness, yield and ultimate load capacities. For example, the ratio between FE analysis and experimental findings at ultimate load (P_u^{EXP}/P_u^{FEA}) and ultimate displacement ($\Delta_u^{EXP}/\Delta_u^{FEA}$) were 1.04 and 0.99, respectively. Likewise, the response of the small-scale beam was well-captured by FE analysis in terms of cracking, flexural stiffness, and yield load capacity, however the ultimate load capacity was underestimated, even though a similar methodology was adopted to model the beams of different sizes. This is because FE analysis did not predict yielding of top longitudinal steel bars, which was measured experimentally. Consequently, the tensile resistance provided by yielding of top steel bars contributed to increasing the ultimate load capacity of the experimental beam when compared to the analysis. It is important to note that top steel bars were used to hold stirrups, and they were not included for resistance. Nevertheless, the top steel bars in the corroded beams (discussed in the next section) did not exhibit high increase in strains or yielding during the experimental tests, and hence the proposed modeling approach has good capabilities in predicting the response of beams.

To further validate the accuracy of the FE models, the predicted crack patterns are compared with those observed experimentally in Figure 6.8. Clearly, the crack patterns were representative of typical flexural behavior that are well-correlated with experimental cracks in terms of their distribution and number. Both beams exhibited a ductile response characterized by yielding of the bottom longitudinal steel bars before their failure caused by crushing of top concrete, similar to the experimental response.

A sensitivity analysis of the element size was carried out to verify and ensure the efficiency of the proposed FE models. The selected element sizes for the large-scale beam models were 60 mm, 30 mm, 15 mm, and 7.5 mm, while those for the small-scale beam models were 40 mm, 20 mm, 10 mm, and 5 mm. The result of FE analyses were compared in terms of load-displacement curves, as shown in Figure 6.9. It can be clearly seen that reducing the element size beyond 15 mm for the large-scale beam and 10 mm for the small-scale beam did not significantly influence the load-displacement curves of beams at all stages of loading. It is also important to recognize that reducing the size of elements increased the simulation time. For these reasons, large-scale and small-scale beams were modeled using element sizes of 15 mm and 10 mm, respectively.

6.4.2.2 Comparison with Corroded RC Beams under Loads

All corroded beams were analyzed using two localized corrosion levels (i.e., based on mean and upper bound predictions). A comparison between FE analyses and the experimental load-displacement curves of corroded beams under loads is shown in Figure 6.10. It is important to recognize that beams LS-2.1, SS-3.1, and SS-4.2 were corroded under sustained service loads until their failure, while beam LS-2.3 was corroded under sustained loads for a specific duration before increasing the loads to failure.

For the corroded large-scale beam under 60% of the beam ultimate load capacity (i.e., LS-2.1), the predicted localized corrosion levels using the mean and upper bound curves were 38.6% and 55.0%, respectively. The FE model with a localized sectional loss of 38.6% had a poor correlation with the experimental curve. This can be explained by underestimation in the loss of reinforcement area, resulting in a concrete crushing failure instead of the anticipated rupture of steel bars. In contrast, the predicted response using a localized sectional loss of 55.0%, based on the upper bound prediction, was in a good agreement with the experimental curve. The ratio between FE analysis and experimental load at failure (P_u^{EXP}/P_u^{FEA}) and displacement at failure ($\Delta_u^{EXP}/\Delta_u^{FEA}$) were 0.99

and 1.11, respectively. Furthermore, the crack pattern at failure, shown in Figure 6.11(a), had a good correlation with that observed experimentally. The failure of this beam occurred due to the rupture of bottom longitudinal steel bars through the cracked section close to the center, as shown in Figure 6.12(a). At failure, the strain of top concrete elements, shown in Figure 6.12(b), was equal to 0.0021 mm/mm, which is well below the crushing strain of 0.003–0.004 mm/mm. Likewise, the responses of corroded small-scale beams SS-3.1 (under 60% of the beam ultimate load capacity) and SS-4.2 (under 40% of the beam ultimate load capacity) were well-captured by the FE analyses when the localized sectional loss was predicted using the upper bound curve.

For the corroded large-scale beam under 60% of the beam ultimate load capacity (LS-2.3), the predicted response with a localized sectional loss of 31.1%, based on mean prediction, appears to be in a good agreement with the experimental curve at all stages of loading. The failure of this beam occurred due to crushing of top concrete at mid-span. This is confirmed in Figure 6.12(c-d). At failure, the strain in the bottom longitudinal steel bars, shown in Figure 6.12(c), was equal to 0.0443 mm/mm, which is well below the ultimate strain of 0.151 mm/mm for 15M steel bars. Minimum principal strain, shown in Figure 6.12(d), shows that top concrete elements had been crushed.

6.4.2.3 Comparison with Corroded RC Beams under no Loads

In this subsection, large-scale beam LS-2.4 and small-scale beam SS-5.1 were analyzed. For the large-scale beam, it was assumed that the randomized critical sections developed localized corrosion in two of the three longitudinal steel bars, while the remaining steel bar developed generalized corrosion. For the small-scale beam, it was assumed that localized corrosion developed in one steel bar and generalized corrosion developed in the other steel bar. The total contribution of both types of corrosion was used as input for the residual area of reinforcement in the two-dimensional FE models.

Figure 6.13 compares FE analyses and the experimental load-displacement curves of corroded beams under no loads. For large-scale beam LS-2.4, the predicted response was well-correlated with the experimental curve using either the mean prediction with a sectional area loss of 31.7% or upper bound prediction with a sectional area loss of 42.6%. However, the mean prediction gave a better approximation of the yield stage. At ultimate, the failure of this beam occurred due to crushing of top concrete, as anticipated. For small-scale beam SS-5.1, the predicted response

appears to be in a reasonable agreement with the experimental curve using the mean prediction with a sectional area loss of 42.7%. However, the stiffness of the beam, and load capacities at yield and ultimate were underestimated. The failure of this beam occurred due to the rupture of corroded steel bars.

6.5 Parametric Study

After validating the proposed FE models of the corroded large-scale and small-scale beams, a parametric study was conducted to examine the influence of parameters that were not covered in the experimental program. This includes: (i) level of corrosion, (ii) level of service loads (iii) strength of concrete, (iv) tensile reinforcement ratio, and (v) localized level of corrosion.

6.5.1 Influence of Corrosion Level

The first parameter that was examined is the influence of corrosion level (i.e., mass loss) on the behavior of beams under the coupled effects of reinforcement corrosion and service loads. For the large-scale beam under 60% of the beam ultimate load capacity, test data were validated at corrosion levels of 15.5% (LS-2.1) and 21.1% (LS-2.3). Accordingly, the parametric study was performed at incremental corrosion levels of 2.5%. For the small-scale beam under 40% of the beam ultimate load capacity, test data was validated at a corrosion level of 29.6% (SS-4.2). Thus, the parametric study was performed at incremental corrosion levels of 5.0%. For each corrosion level, FE models were modified with respect to the strength of concrete cover, generalized and localized corrosion levels, while keeping all other parameters the same.

Figure 6.14 displays the bounded predictions by FE analyses, which are expressed using the residual capacity and ductility ratios as a function of corrosion level. In this figure, the residual capacity and ductility ratios are defined as the ultimate load capacity and ultimate displacement of corroded beams relative to the predicted ultimate load capacity and ultimate displacement of the control beam, respectively. As shown in Figure 6.14(a), it is clear that the reduction in capacity of beam LS-2.1, based on mean prediction, is almost proportional to the level of corrosion. This is expected since the FE models did not exhibit a reduction in ductility before failure (i.e., typical flexural response), as demonstrated in Figure 6.14(b). However, according to the upper bound prediction, the reduction in capacity at corrosion levels exceeding 7.5%, was not proportional to the level of corrosion. This can be explained by the high localization of corrosion, reducing the

ductility of beams or causing rupture of the corroded steel bars in some cases. In contrast to beam LS-2.1, the predicted response of beam SS-4.2 was slightly different. It is clear that the reduction in capacity at corrosion levels exceeding 15%, based on mean prediction, was not proportional to the level of corrosion, as shown in Figure 6.14(c). This is primarily attributable to the drastic reduction in ductility, shown in Figure 6.14(d), caused by the low percentage of steel used in this beam when compared to large-scale beam LS-2.1. As demonstrated in this comparison, providing higher percentage of steel in reinforced concrete beams exposed to corrosion, can prevent the reduction in ductility and preserve the flexural response.

6.5.2 Influence of Service Loads

Small-scale beams were experimentally examined under the coupled effects of reinforcement corrosion and different levels of service loads, including 40% (SS-4.2) and 60% (SS-3.1) of the beam ultimate load capacity. For that reason, the parametric study was performed using service loads equivalent to 50% and 70% of the beam ultimate load capacity. In these FE models, the level of corrosion, causing failure under the applied service loads, was linearly interpolated or extrapolated from the validated FE models under 40% and 60% of the beam ultimate load capacity. For the large-scale beam (LS-2.1), the behavior was experimentally examined under the coupled effects of reinforcement corrosion and service loads equivalent to 60% of the beam ultimate load capacity. The parametric study was performed using service loads equivalent to 40%, 50%, and 70% of the beam ultimate load capacity. In these FE models, the level of corrosion, causing failure under the applied service loads, was found through trial and error. A summary of generalized and localized corrosion levels adopted to develop the FE models of large-scale and small-scale beams under different levels of service loads is presented in Table 6.6.

Figure 6.15 shows the influence of different service loads on the load-displacement relationships of corroded large-scale and small-scale beams. As expected, all beams had the same stiffness and failed at the desired level of service loading, however the displacements at failure were increased with the increase of service loads, due to the increase of corrosion levels that led to the failure of beams. To better understand the effect of reinforcement corrosion on the response of beams subjected to different levels of service loads, the residual capacity and ductility ratios of large-scale and small-scale beams are plotted as a function of the corrosion level in Figure 6.16. The residual capacity and ductility ratios were calculated relative to the experimental findings to ensure

consistency while comparing the effect of different service loading levels. As shown in Figure 6.16, increasing the levels of service loads increased the reduction rates of ultimate load capacity and ductility of corroded beams. This aligns with the conclusions drawn by Al-Bayti et al. (2022b) for corroded small-scale RC beams, which was attributed to the increase in flexural crack width, allowing in a further localization of corrosion at the location of cracks. Another important observation is that the reduction rates of ultimate load capacity and ductility of small-scale beams were more than that of large-scale beams. This also aligns with the conclusions drawn by Al-Bayti et al. (2022c) for corroded large-scale RC beams. Such behavior was explained by the increase in flexural crack width of small-scale beams since they were reinforced with a lower percentage of steel than large-scale beams.

6.5.3 Influence of Concrete Strength

The influence of concrete strength on the flexural behavior of corroded RC beams was examined in the presence and absence of service loads. Large-scale beams LS-2.1, LS-2.3, and LS-2.4, as well as small-scale beams SS-3.1, SS-4.2, and SS-5.1 were analyzed. All beams had a compressive strength of 51.7 MPa, except for beam SS-3.1 that had a compressive strength of 48.4 MPa. The parametric study was performed using various compressive strengths including 30 MPa, 40 MPa, and 60 MPa, while keeping other parameters of the FE models the same. The tensile strength and fracture energy were also modified based on the compressive strength of concrete.

Figure 6.17 shows the influence of concrete strength on the ultimate load capacity of all corroded beams. Clearly, the strength of concrete had a little to no impact on the ultimate load capacity of the heavily corroded beams LS-2.1, SS-3.1, SS-4.2, and SS-5.1. All these beams exhibited a brittle behavior characterized by rupture of longitudinal corroded steel bars, indicating that in such cases with high corrosion levels and/or service loads, the response of beams is mainly influenced by corrosion of the main flexural reinforcement and not the strength of concrete. In contrast, the ultimate load capacity of beams LS-2.3 and LS-2.4 increased with increasing strength of concrete. This was expected because both beams behaved in flexure and failed due to crushing of top concrete. It should be noted that FE models of beams LS-2.3 and LS-2.4 were terminated when top elements of concrete reached a strain value of 0.0035 mm/mm, to ensure consistency when comparing the analyses of beams.

6.5.4 Influence of Reinforcement Ratio

Tensile reinforcement area ratio is a key parameter that have a significant influence the flexural behavior of RC beams. This study investigated this parameter for the large-scale beam that had a tensile reinforcement ratio of 1.17%. The parametric study was performed using different tensile reinforcement ratios, including 0.80%, 1.60%, and 2.00% at different corrosion levels of either 10%, 15%, 20%, or 30%. The remaining parameters of FE models were kept the same, including the level of sustained loads (i.e., equal to 80 kN).

Figure 6.18 shows the effect of tensile reinforcement ratio on the ultimate load capacity of the large-scale beam using FE analysis, based on the mean and upper bound predictions. It was found that the beam with a tensile reinforcement ratio of 0.80% failed under its service capacity at an approximate corrosion level of 10%. However, increasing the tensile reinforcement ratio from 0.80% to 1.17%, 1.60%, or 2.00%, improved the ultimate load capacity of the corroded beam above the service level by more than 40%, 85%, or 125%, respectively. Furthermore, it increased the ability of the beam to undergo high levels of corrosion before failure. For example, the beam with a reinforcement ratio of 2.00% and corrosion level of 30%, had an excess capacity of 27 kN above the service level, as opposed to the beam with a reinforcement ratio of 1.17% that could not withstand this corrosion level. This increased ability to withstand high levels of corrosion is directly related to increasing the service life of beams.

6.5.5 Influence of Localized Corrosion Level at Non-Critical Sections of Beams

All corroded beam analyses completed in previous sections were conducted by assigning the maximum localized corrosion level η_{crit} to the crack at or close to the center of beams, where the experimental failure took place (i.e., critical crack/section). In the remaining transverse cracks within the constant moment region of beams (i.e., non-critical cracks), the localized corrosion level was assumed to be less than that in the critical crack. In this study, the loss of reinforcement area at these cracks was taken as 50% and 75% of η_{crit}. To validate this assumption and examine this parameter influence, a sensitively analysis was conducted for the large-scale beam LS-2.1 and small-scale beam SS-3.1. The parametric study was performed using six case scenarios, as described in Table 6.7. For Models 1, 2, 3 and 4, the non-critical cracked sections of beams had localized corrosion levels of 0%, 50%, 75%, and 90% of η_{crit}, respectively. In Model 5, it was assumed that some of the non-critical cracked sections had localized corrosion levels of 50% η_{crit}

while other sections had localized corrosion levels of 75% of η_{crit}. In Model 6, the localized corrosion levels in the non-critical cracked sections were obtained from the distribution of sectional area loss along steel bars using a three-dimensional laser scanner.

Figure 6.19 shows the influence of localized crack corrosion levels on the load-displacement relationships of beams LS-2.1 and SS-3.1. Note, the displacements of beams at failure are also reported on the figure for clarification. It can be seen that the level of corrosion in non-critical cracked sections had no influence on the ultimate load capacity of the beams considered in this parametric study, however its impact on the ductility of beams was clear. In the extreme cases, displacements at failure were either underestimated as in Model 1 with one localized element or overestimated as in Model 4 with multiple localized elements having an almost similar corrosion levels. Displacements at failure for the assumed profile in Model 5 were well-correlated with the actual sectional area loss in Model 6. For that reason, in the absence of experimental data, it could be assumed that the non-critical cracked sections of beams under service loads develop mixed localized corrosion levels of 50% and 75% of η_{crit}. Otherwise, it is safe to presume that the beams under service loads have one critical cracked section at or close to the center while keeping in mind that the ductility could be underestimated.

6.6 Conclusions

This paper investigated the flexural behavior of corroded RC beams under service loads. Corrosion-induced damage was introduced to FE models using a simplified approach implemented in DIANA FE analysis software. The predicted responses were validated with non-corroded and corroded large-scale and small-scale beams subjected to different levels of service loads. A parametric study was carried out to expand test data for cases that were not covered experimentally. The following conclusions can be drawn from the current investigation:

1) The proposed simplified approach introduced to FE models was able to simulate the response of flexural-dominant corroded RC beams under various service loads. FE analyses were reasonably accurate in predicting crack patterns, residual load capacity, residual ductility, and failure modes of corroded beams.
2) Simulating the flexural response of corroded RC beams under service loads was strongly influenced by the non-uniform distribution of corrosion, in particular the localization of corrosion at the critical cracked section of beams. Corrosion levels in non-critical cracked

sections of the beams, had an effect on the ductility of beams, while its impact on the ultimate load capacity was minimal for the beams considered in this study.

3) The decline of loading capacity in flexure dominant RC beams is directly proportional to the generalized form of corrosion. However, at a certain point during the service life of beams, the decline becomes more severe due to the severity of localized corrosion levels which reduces the ductility of beams.
4) The degradation rates of ultimate load capacity and ductility of corroded beams were increased with increasing the levels of service loads. In this study, such behavior was more pronounced in small-scale beams since they were reinforced with lower tensile reinforcement ratio than large-scale beams.
5) Strength of concrete had little to no impact on the ultimate load capacity of the heavily corroded beams since their response was governed by rupturing of longitudinal steel bars. However, the ultimate load capacity of corroded beams when governed by the crushing of concrete, increased with increasing the strength of concrete, as expected.
6) Tensile longitudinal reinforcement ratio had a significant influence on the flexural response of corroded beams. Increasing the reinforcement ratio, improved the ultimate load capacity of corroded beams, which in turn would contribute to increasing their service life. For example, increasing the reinforcement ratio from 0.8% to 2.0%, increased the ultimate capacity of the corroded large-scale beam by more than 125% above the service level.

Table 6.1: Dimension of beams and reinforcement detailing

Beam	Dimension (mm)		Longitudinal reinforcement		Transverse reinforcement	Cover thickness (mm)
	B x H x L	a	Tension	Compression		
Large-scale	200 x 300 x 3400	1000	3-15M	2-10M	10M @ 150 mm	25 mm
Small-scale	145 x 250 x 1800	500	2-10M	2-10M	10M @ 110 mm	15 mm

Table 6.2: Summary of selected beams for FE analysis validation

Beam size	Beam designation	Loading type (% of ultimate)	Corrosion density (μA/cm^2)	Duration (days)
Large-scale	LS-1.1/1.2	Monotonic to failure	NA	NA
	LS-2.1	60% ~80 kN	300/1000	135/15
	LS-2.3	60% ~80 kN	300	61
	LS-2.4	0%	300	103
Small-scale	SS-1.1/1.2	Monotonic to failure	NA	NA
	SS-3.1	60% ~60 kN	300	37
	SS-4.2	40% ~40 kN	300	167
	SS-5.1	0%	300	167

Table 6.3: Summary of FE model properties

Beam scale	Beam designation	Corrosion + Loads	f'_c (MPa)	f_t (MPa)	f_t^c (MPa)	$\eta_{avg,m}$ (%)	$\eta_{crit,upper}$ (%)	$\eta_{crit,mean}$ (%)
Large-scale	LS-1.1/1.2	Load to failure	51.70	2.37	2.37	0	0	0
	LS-2.1	Corrosion + 80 kN	51.70	2.37	0.75	21.13	54.96	38.68
	LS-2.3	Corrosion + 80 kN	51.70	2.37	0.93	15.45	47.04	31.13
	LS-2.4	Corrosion + 0 kN	51.70	2.37	0.78	20.21	42.58*	31.74*
Small-scale	SS-1.1/1.2	Load to failure	41.50	2.13	2.13	0	0	0
	SS-3.1	Corrosion + 60 kN	48.38	2.30	1.00	12.90	43.01	27.48
	SS-4.2	Corrosion + 40 kN	51.70	2.37	0.60	29.63	65.02	48.88
	SS-5.1	Corrosion + 0 kN	51.70	2.37	0.55	32.86	50.69**	42.73**

*For small-scale beam under no loads: it was assumed that one steel bar with $\eta_{avg,m}$ and one steel bar with η_{crit}.

**For large-scale beam under no loads: it was assumed one steel bar with $\eta_{avg,m}$ and two steel bars with η_{crit}.

Table 6.4: Material properties of steel bars

Property	10M	15M
Nominal diameter, D_o	11.3 mm	16.0 mm
Modulus of elasticity, E_s	190 GPa	190 GPa
Yield strength, f_y	445 MPa	404 MPa
Ultimate strength, f_u	591 MPa	605 MPa
Elongation at ultimate, ε_u (%)	14.3%	15.1%

Table 6.5: Comparison between FE predictions and experimental test results in terms of ultimate loads and displacements

	Beam designation	Failure Mode*	P_u (kN)**		P_u^{EXP}/P_u^{FEA}	Δ_u (mm)***		$\Delta_u^{EXP}/\Delta_u^{FEA}$
			P_u^{EXP}	P_u^{FEA}		Δ_u^{EXP}	Δ_u^{FEA}	
Large-scale	LS-1.1/1.2	Flexure	135.10	129.76	1.04	51.49	52.25	0.99
	LS-2.1	Brittle	82.10	83.27	0.99	20.00	17.95	1.11
	LS-2.3	Flexure	123.80	112.00	1.11	56.43	56.78	0.99
	LS-2.4	Flexure	120.50	104.88	1.15	44.73	46.04	0.97
Small-scale	SS-1.1/1.2	Flexure	106.92	86.61	1.23	27.22	30.47	0.89
	SS-3.1	Brittle	58.35	60.18	0.97	7.53	7.13	1.06
	SS-4.2	Brittle	38.25	40.40	0.95	5.27	4.90	1.08
	SS-5.1	Brittle	72.77	63.54	1.15	16.34	20.04	0.82

*Failure mode was either in flexure caused by crushing of concrete or brittle caused by rupture of steel bars.

**P_u is the ultimate load.

***Δ_u is the ultimate displacement.

Table 6.6: Properties of FE models under different service loads

Beam size	% of ultimate	Load (kN)	$\eta_{avg,m}$ (%)	$\eta_{crit,upper}$ (%)
Large-scale	LS-40%	53	37.00	72.61
	LS-50%	67	29.50	64.88
	LS-60%	80	21.13	54.96
	LS-70%	93	16.50	48.61
Small-scale	SS-40%	40	29.63	65.02
	SS-50%	50	20.40	54.01
	SS-60%	60	12.90	43.01
	SS-70%	70	7.12	32.01

Table 6.7: Localized corrosion levels in non-critical cracked sections of corroded beams

Model #	LS-2.1*	SS-3.1**
Model 1	0 η_{crit} = 0%	0 η_{crit} = 0%
Model 2	0.5 η_{crit} = 28%	0.5 η_{crit} = 22%
Model 3	0.75 η_{crit} = 41%	0.75 η_{crit} = 32%
Model 4	0.90 η_{crit} = 50%	0.90 η_{crit} = 39%
Model 5	0.5 η_{crit} and 0.75 η_{crit} = 28% and 41%	0.5 η_{crit} and 0.75 η_{crit} = 27% and 32%
Model 6	27%, 28%, 40%, 35%, 28%, 27%, and 33%	26% and 35%

* Critical section η_{crit} of beam LS-2.1 had a corrosion level of 54.96%

** Critical section η_{crit} of beam SS-3.1 had a corrosion level of 43.01%

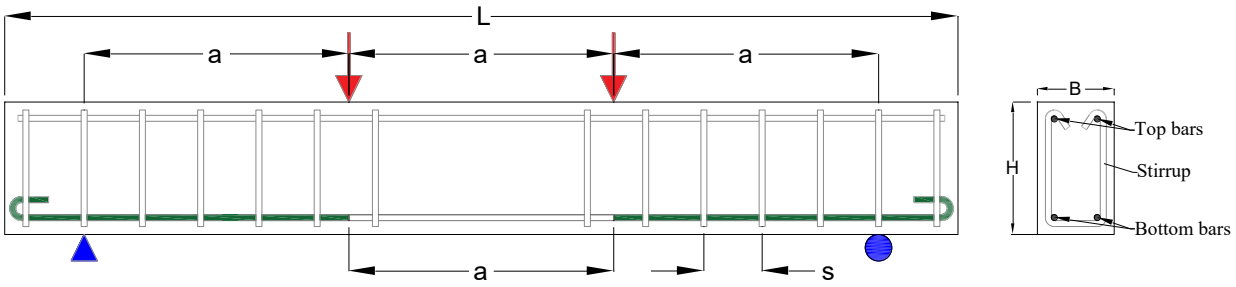

Figure 6.1: Schematic illustration of RC beams

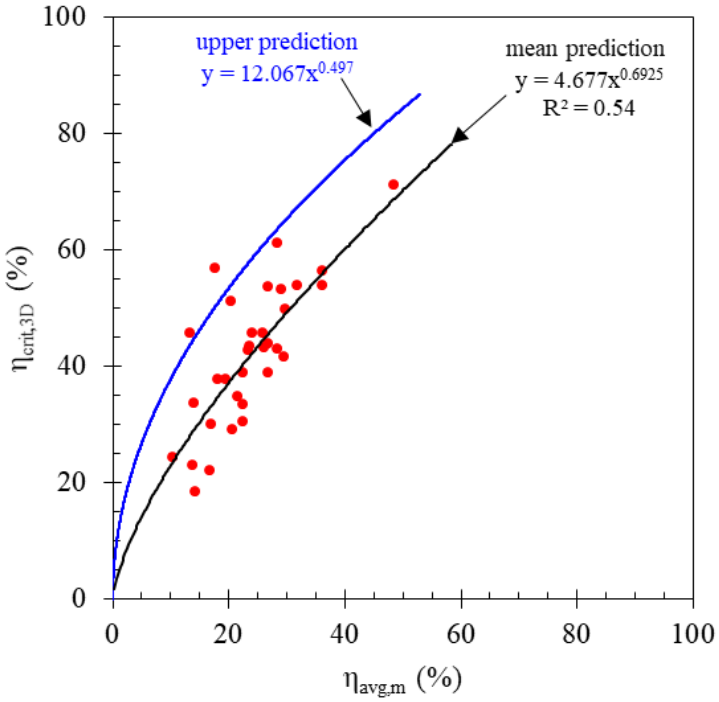

Figure 6.2: Relationship between maximum sectional loss and average sectional loss

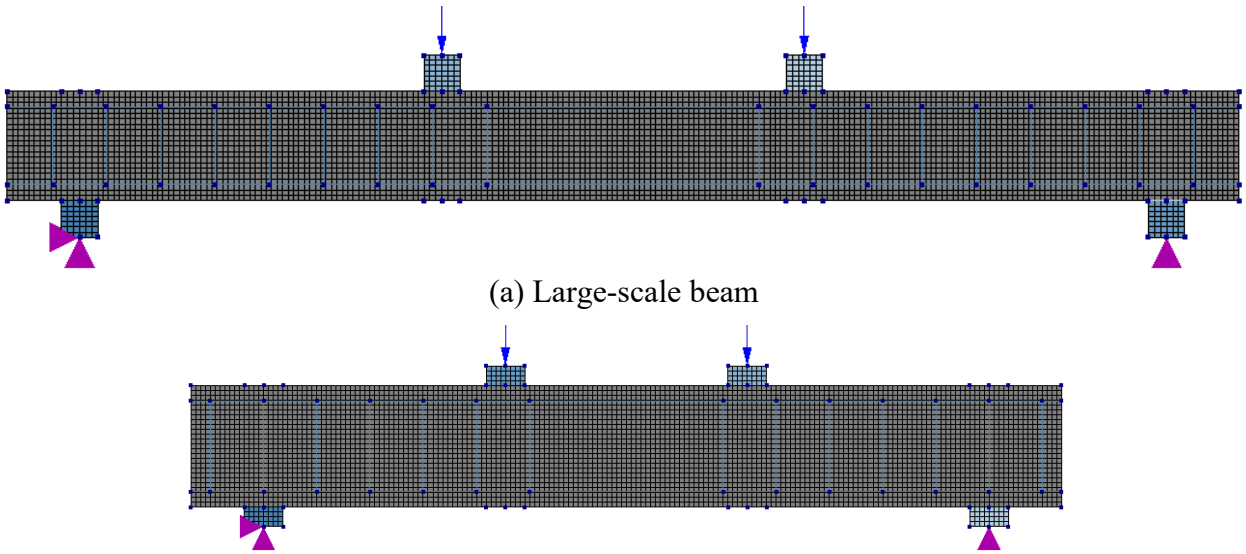

(a) Large-scale beam

(b) Small-scale beam

Figure 6.3: Discretized 2-D finite element model

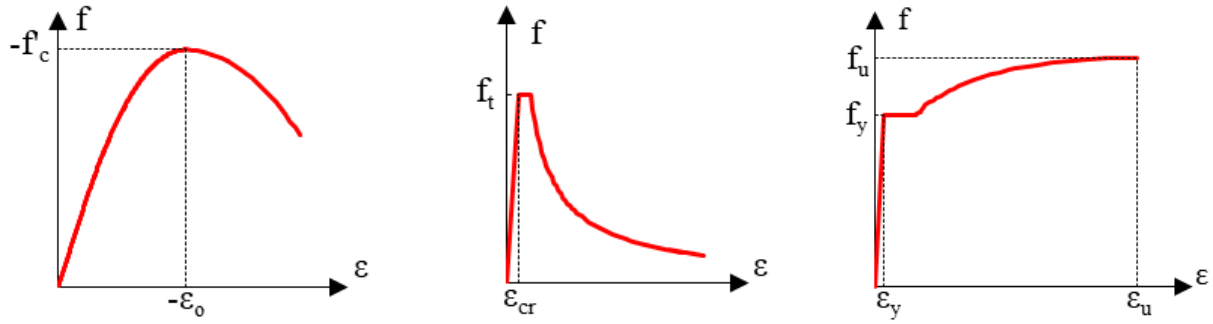

(a) Concrete in compression (b) Concrete in tension (c) Steel reinforcement

Figure 6.4: Stress-strain curves used in the FE models

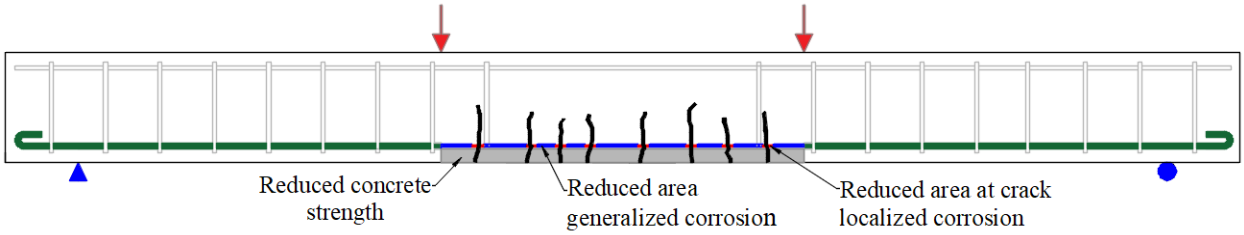

(a) Large-scale beam - LS-2.1

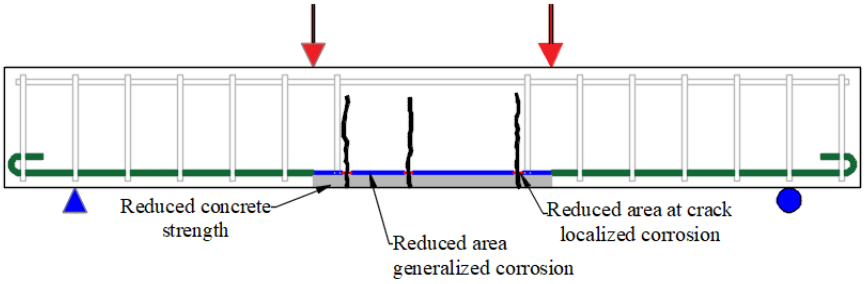

(b) Small-scale beam - SS-3.1

Figure 6.5: Illustration of the FE models of corroded beams

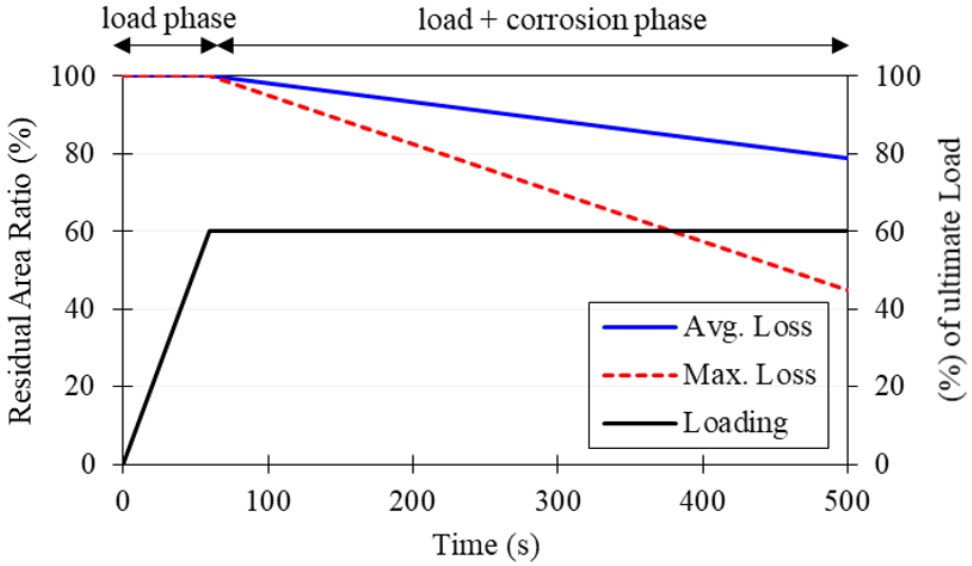

(a) Large-scale beam - LS-2.1

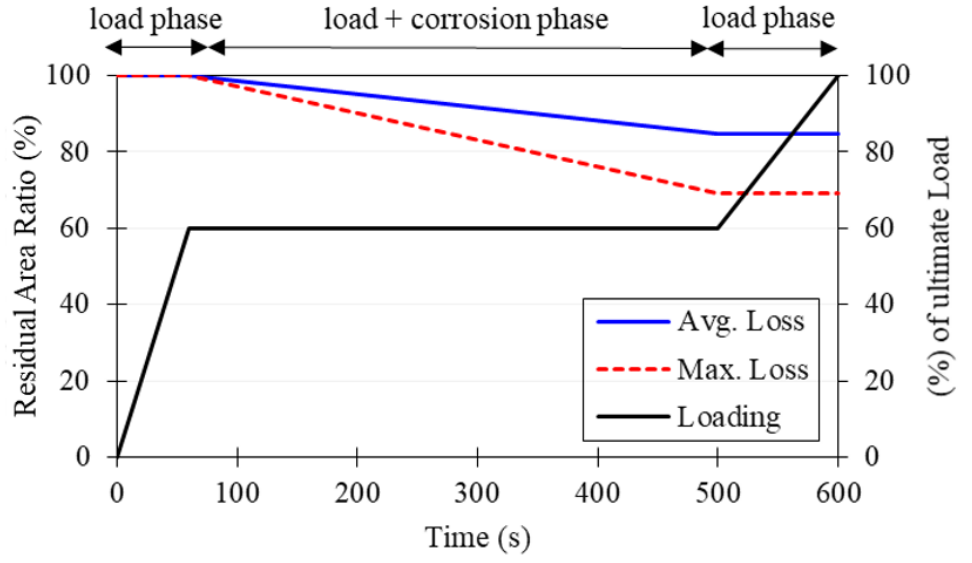

(b) Large-scale beam - LS-2.3

Figure 6.6: Incremental time-step approach for modeling beams under the coupled effects of corrosion and loads

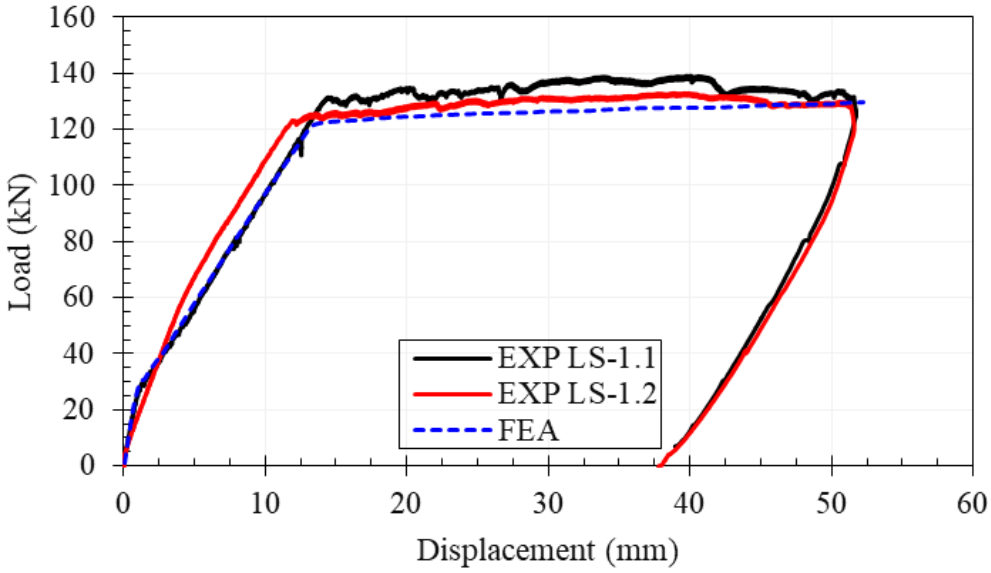

(a) Large-scale beam – LS-1.1/1.2

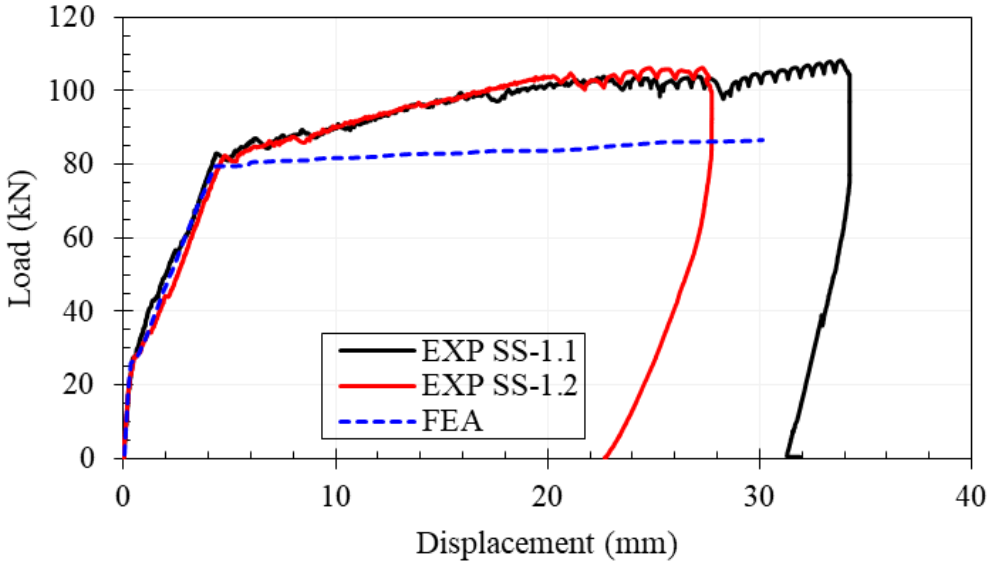

(b) Small-scale beam – SS-1.1/1.2

Figure 6.7: Comparison between FE predictions and experimental load-displacement relationships of control beams

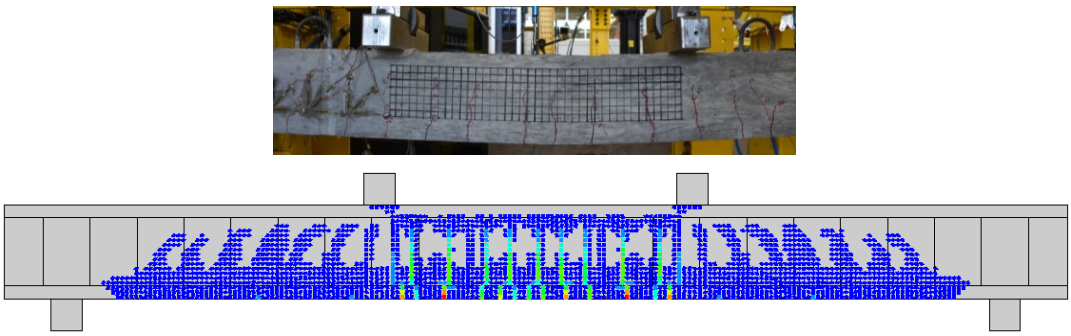

(a) Large-scale beam – LS-1.1

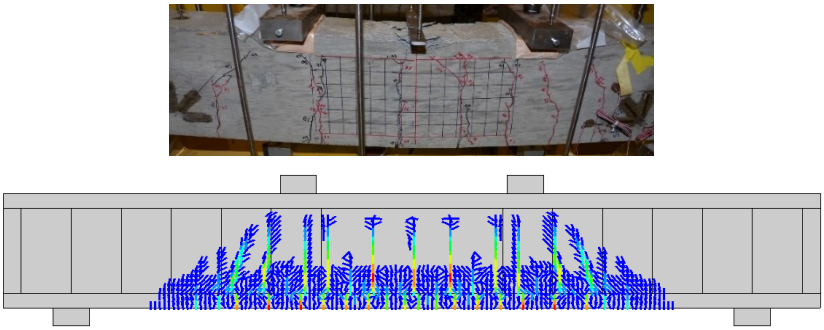

(b) Small-scale beam – SS-1.2

Figure 6.8: Comparison between FE predictions and experimental crack patterns of control beams at failure

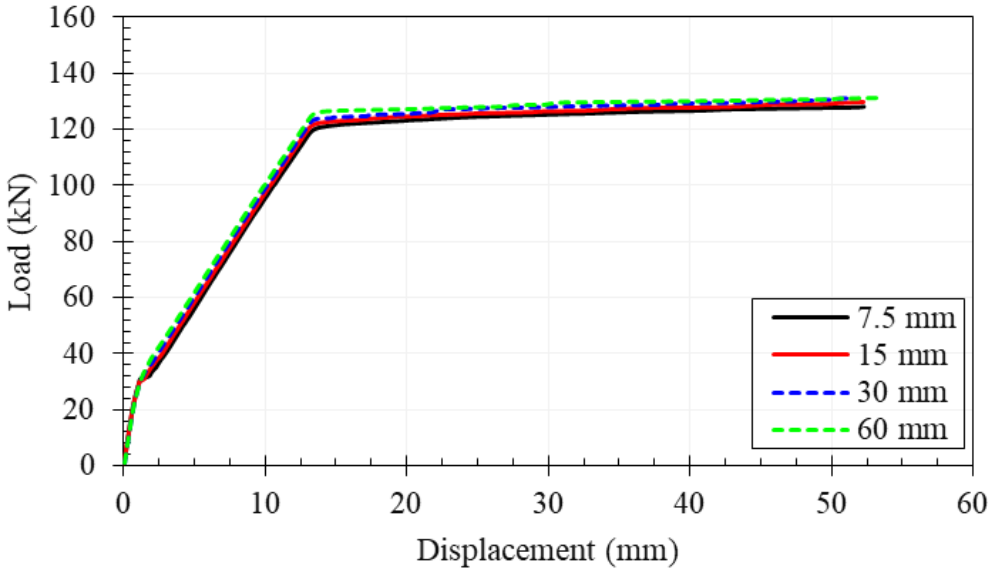

(a) Large-scale beam model

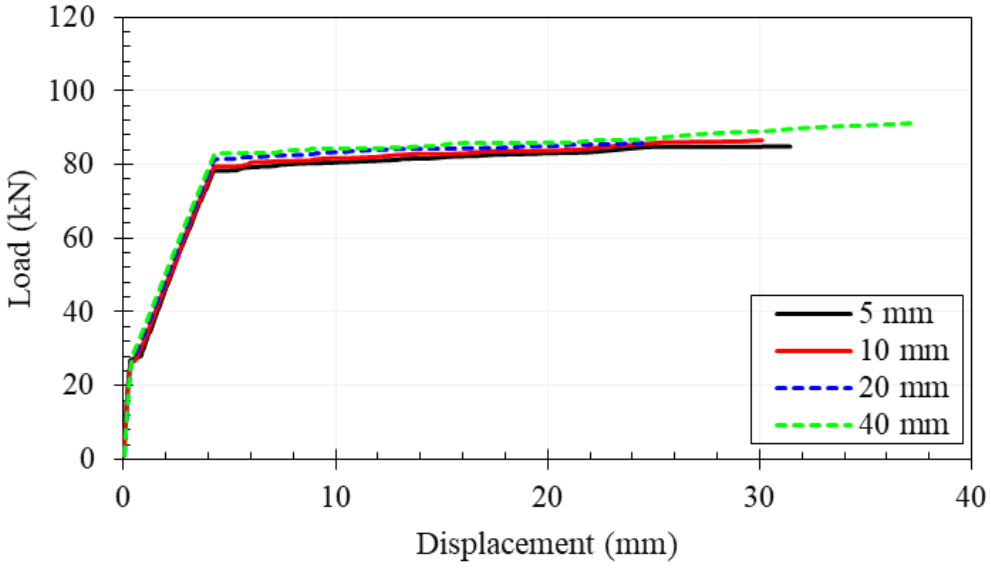

(b) Small-scale beam model

Figure 6.9: Sensitivity analysis of the element size of the FE models

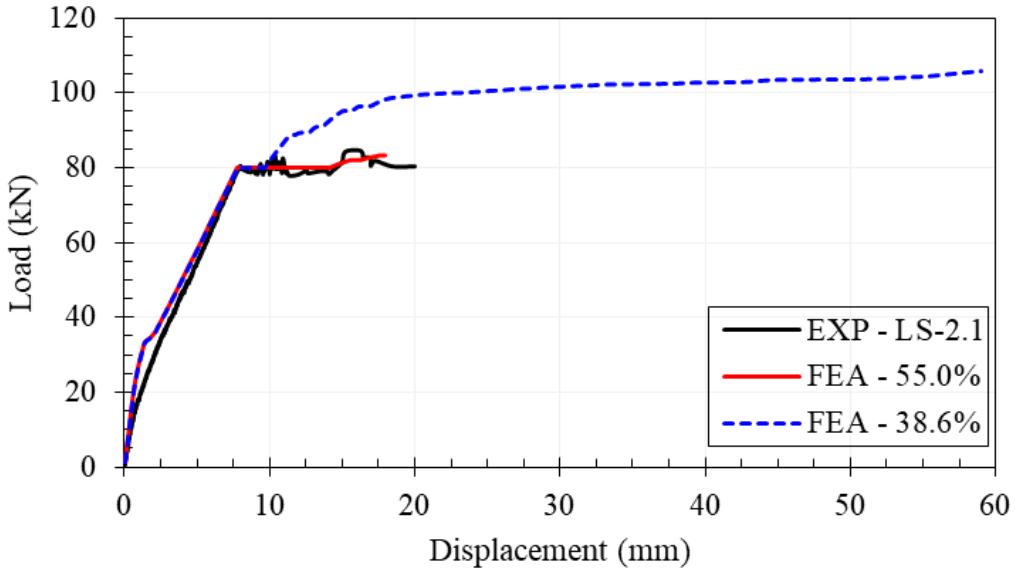

(a) Large-scale beam - LS-2.1

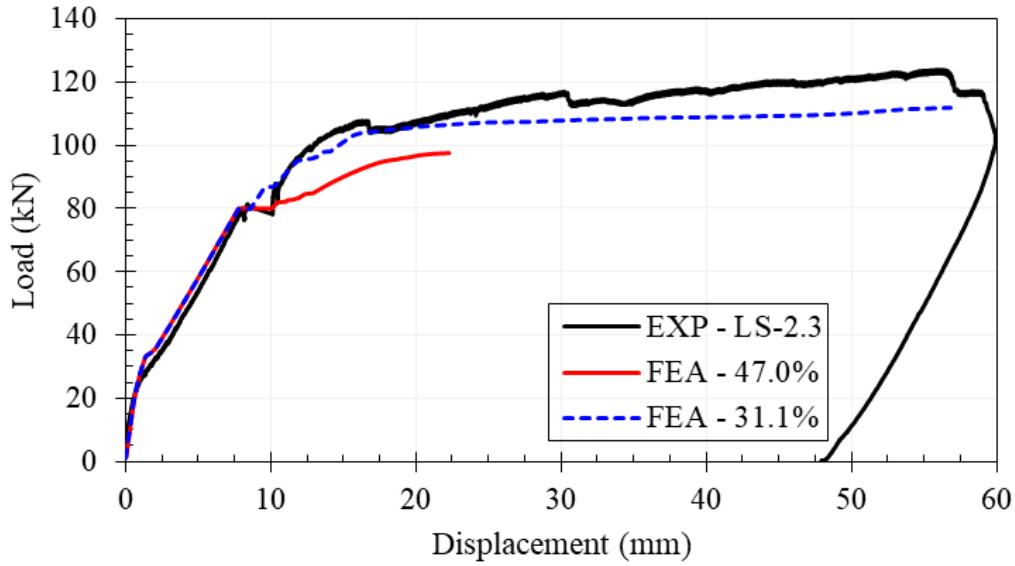

(b) Large-scale beam - LS-2.3

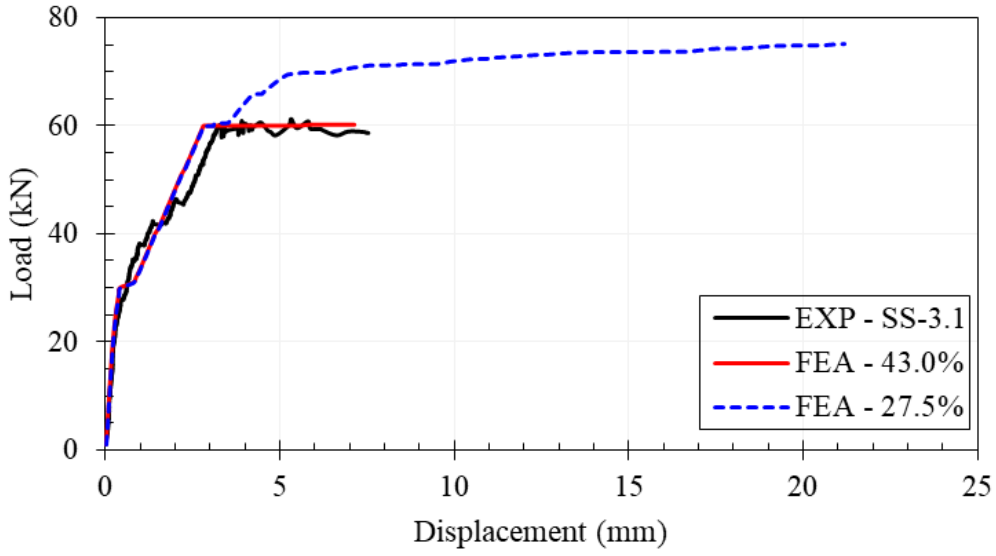

(c) Small-scale beam - SS-3.1

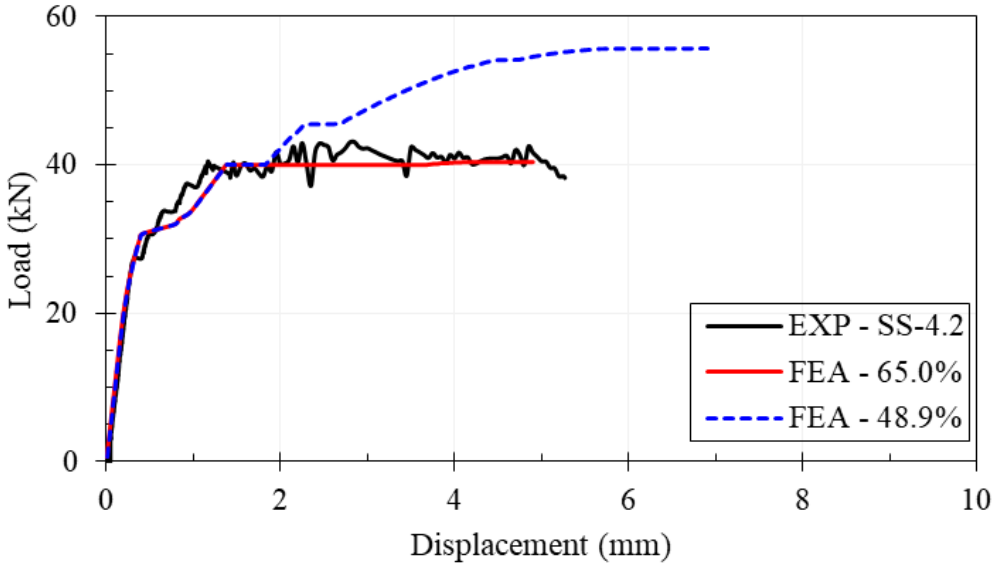

(d) Small-scale beam - SS-4.2

Figure 6.10: Comparison between FE predictions and experimental load-displacement relationships of corroded beams under loads

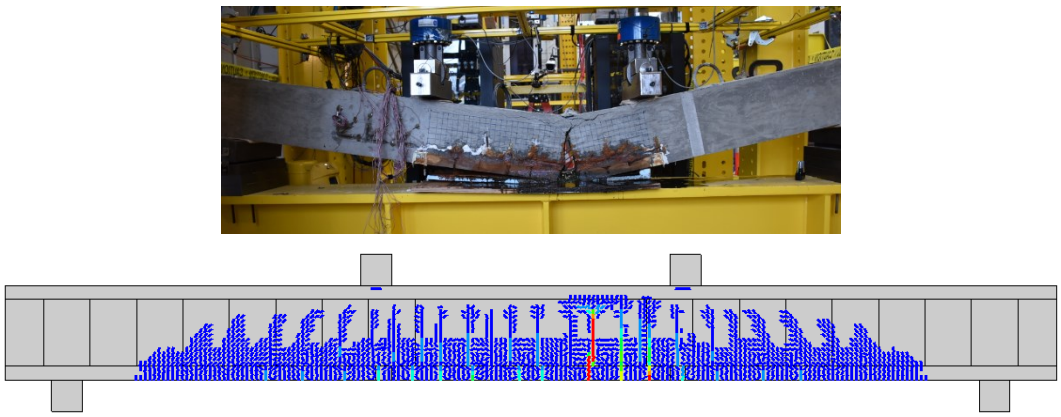

(a) Large-scale beam - LS-2.1

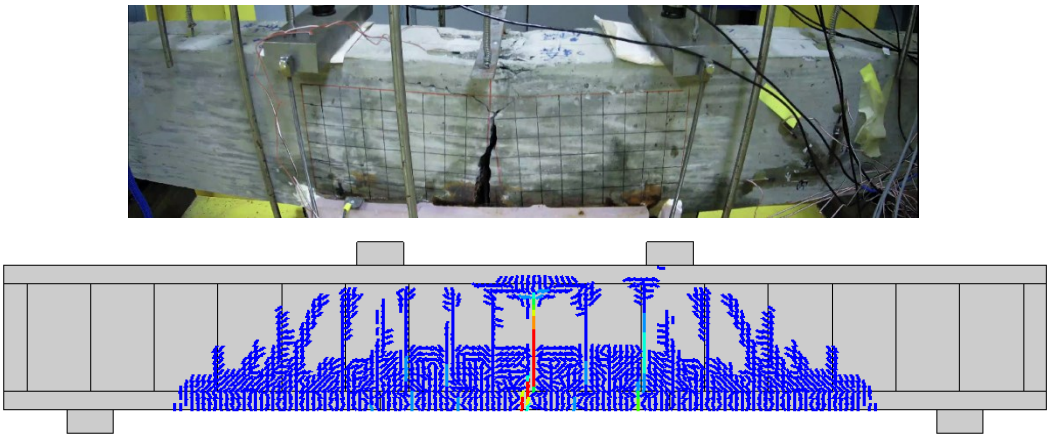

(b) Small-scale beam - SS-3.1

Figure 6.11: Comparison between FE predictions and experimental crack patterns of corroded beams at failure

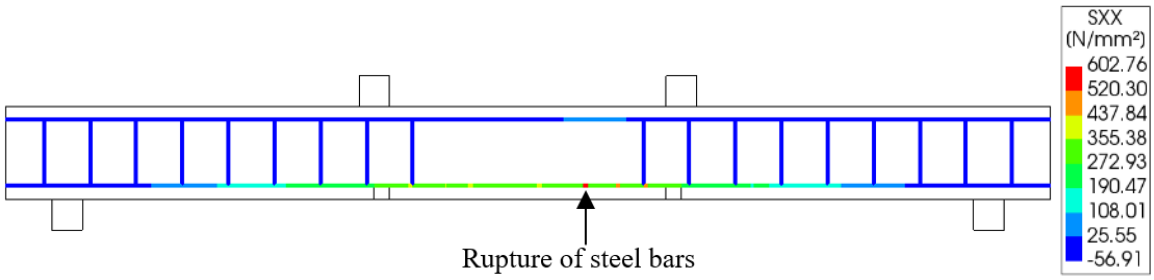

(a) Reinforcement stresses – beam LS-2.1

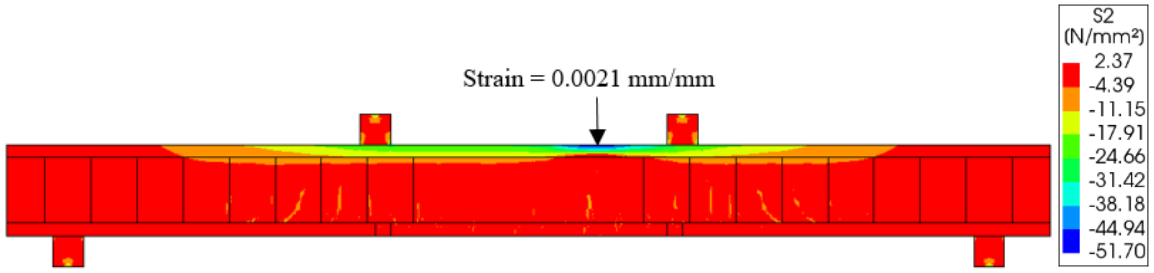

(b) Concrete minimum principal stresses – beam LS-2.1

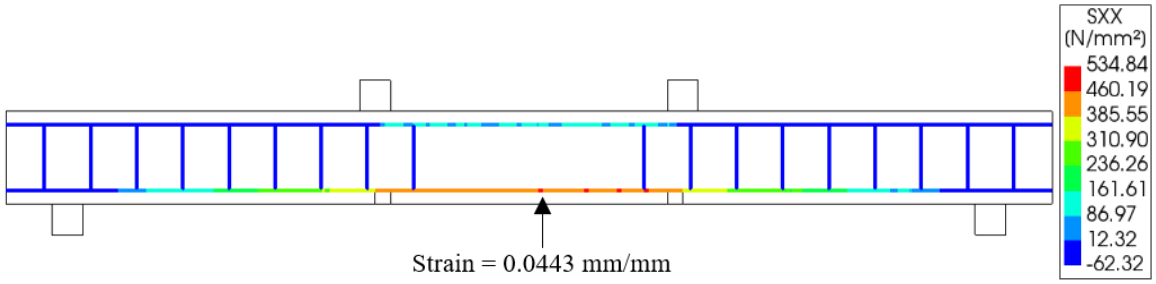

(c) Reinforcement stresses – beam LS-2.3

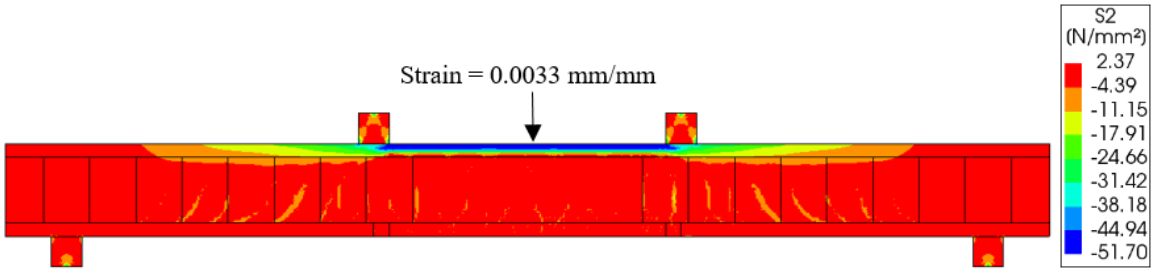

(d) Concrete minimum principal stresses – beam LS-2.3

Figure 6.12: Distribution of stresses in the corroded beams at failure

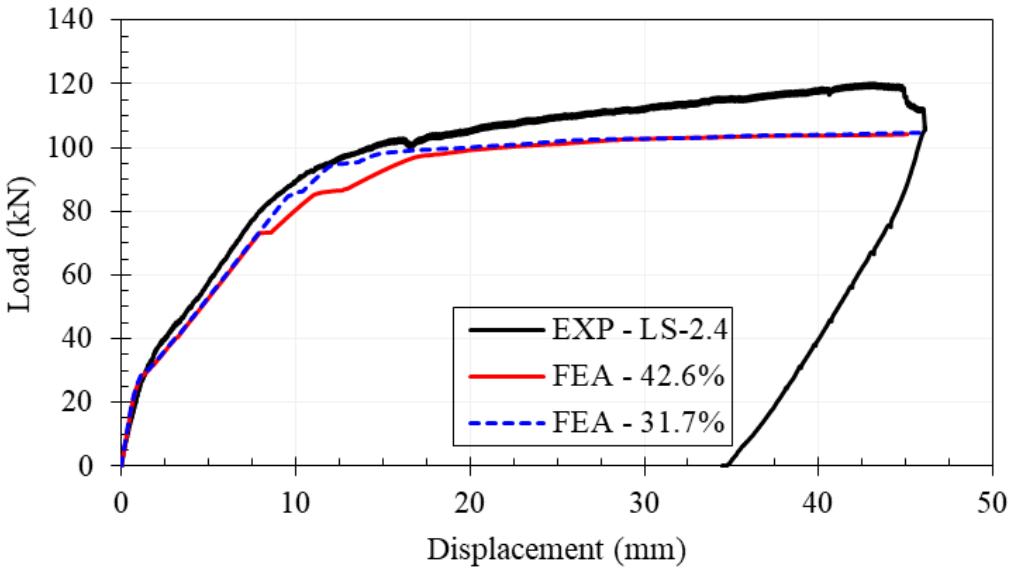

(a) Large-scale beam - LS-2.4

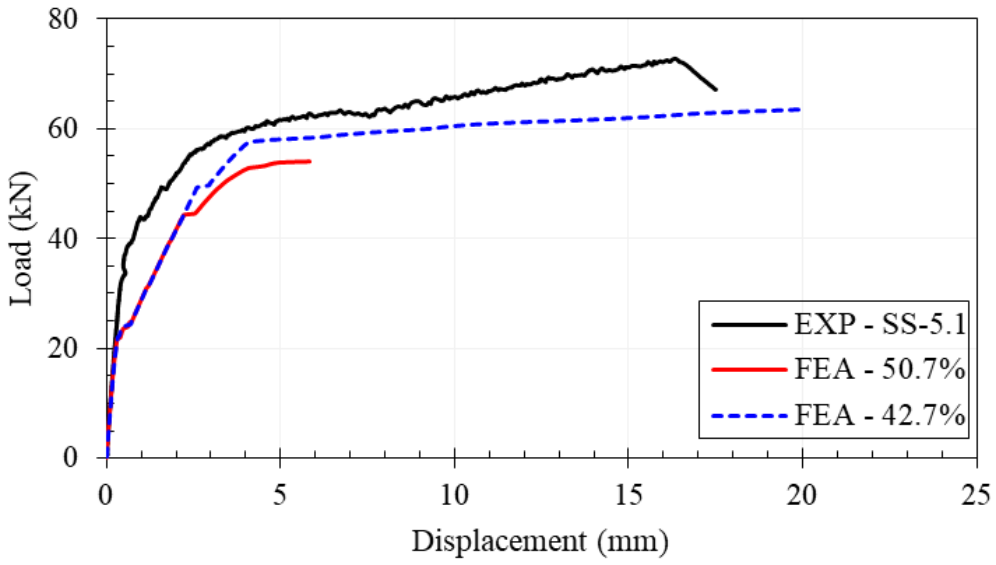

(b) Small-scale beam - SS-5.1

Figure 6.13: Comparison between FE predictions and experimental load-displacement relationships of corroded beams under no loads

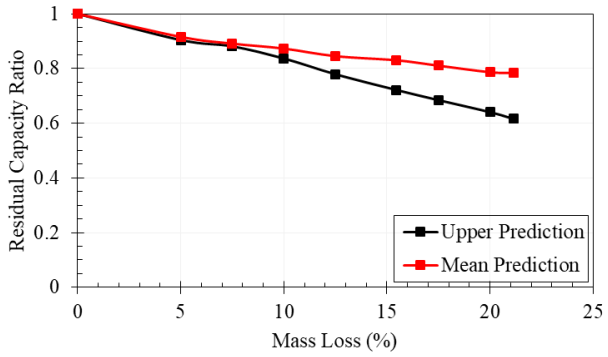

(a) Residual capacity ratio – beam LS-2.1

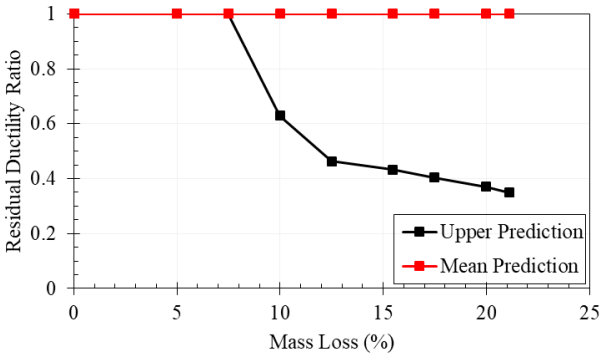

(b) Residual ductility ratio – beam LS-2.1

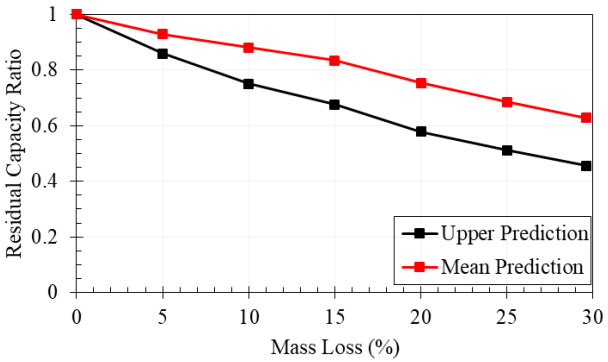

(c) Residual capacity ratio – beam SS-4.2

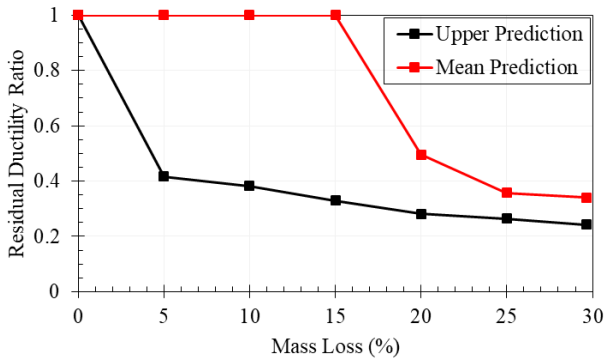

(d) Residual ductility ratio – beam SS-4.2

Figure 6.14: Influence of corrosion on residual capacity and ductility ratios of RC beams

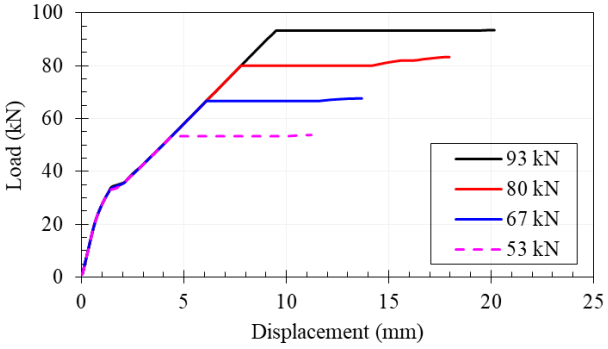

(a) Large-scale

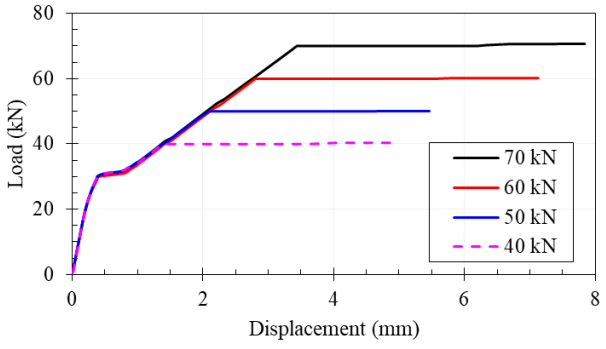

(b) Small-scale

Figure 6.15: Effect of service loads on the load-displacement relationships of corroded RC beams

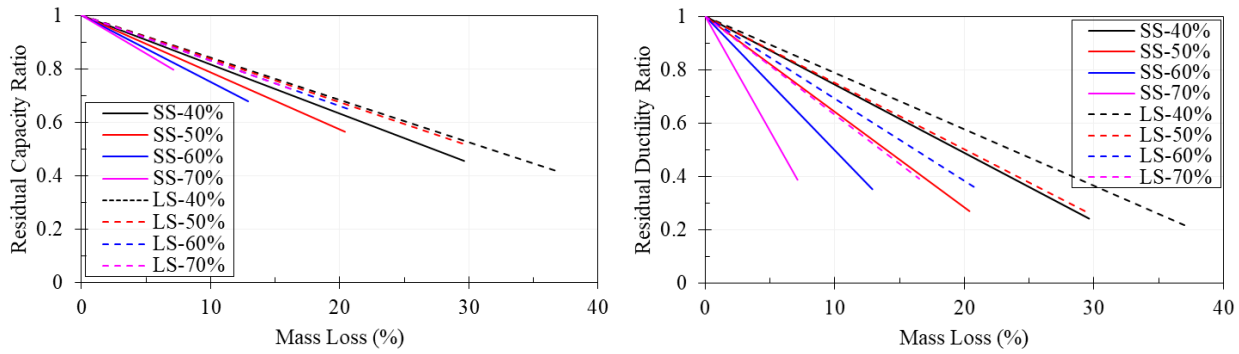

(a) Residual capacity ratio (b) Residual ductility ratio

Figure 6.16: Effect of different levels of service loads on the flexural behavior of corroded RC beams

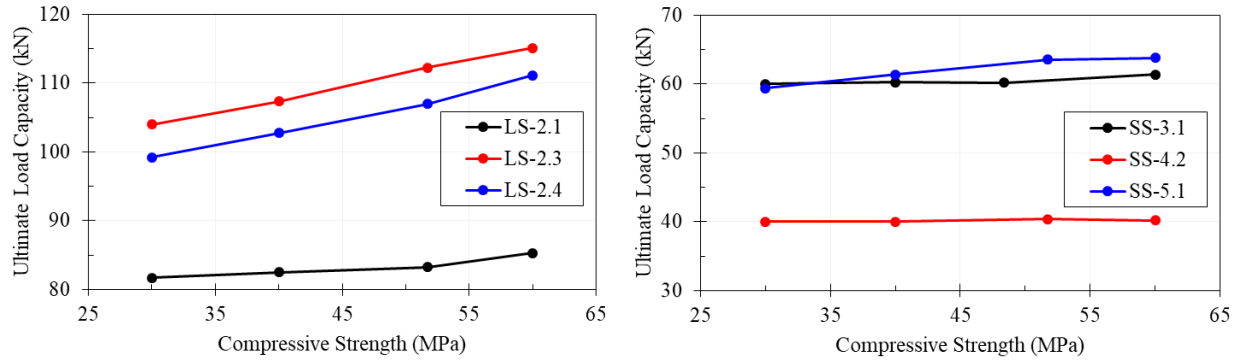

(a) Large-scale (b) Small-scale

Figure 6.17: Effect of concrete strength on the ultimate load capacity of corroded RC beams

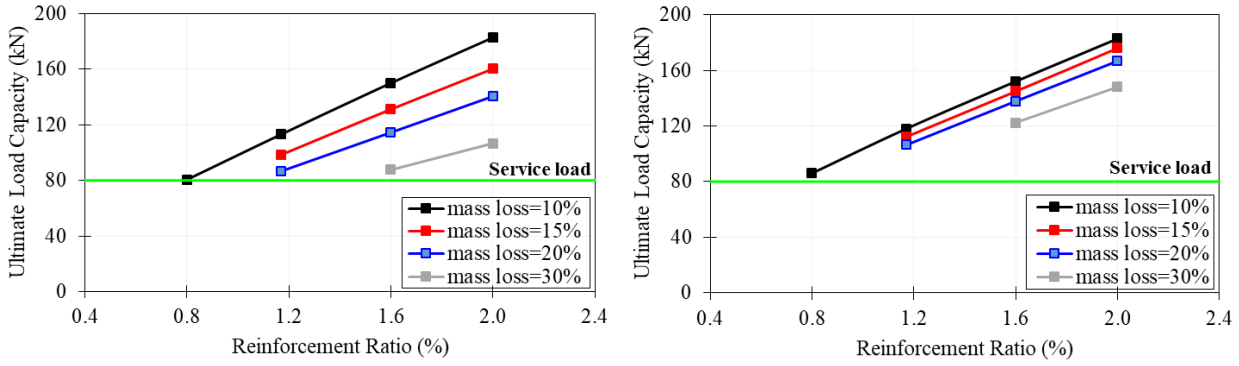

(a) Upper bound predictions (b) Mean predictions

Figure 6.18: Effect of tensile reinforcement ratio on the ultimate load capacity of corroded RC beams

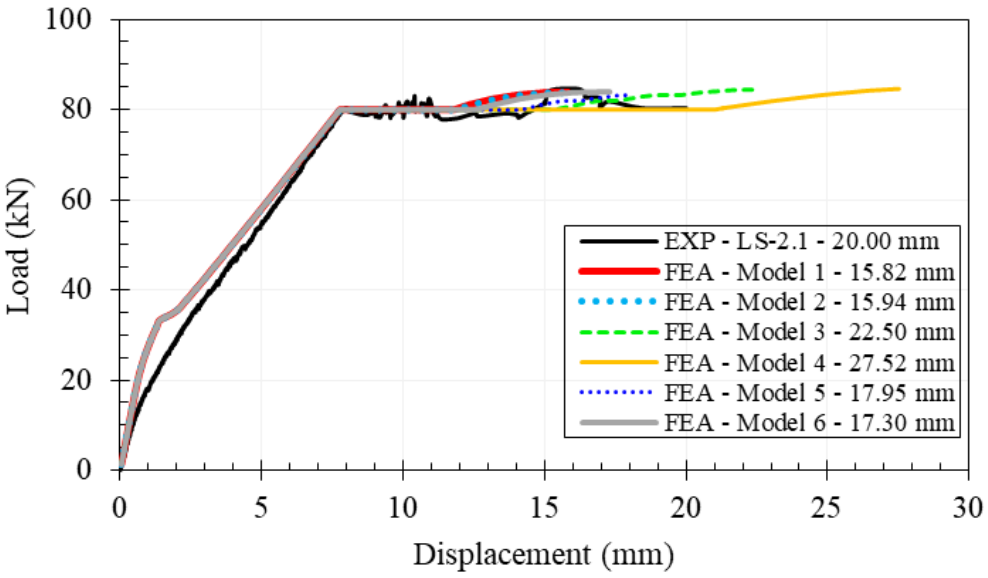

(a) Large-scale beam - LS-2.1

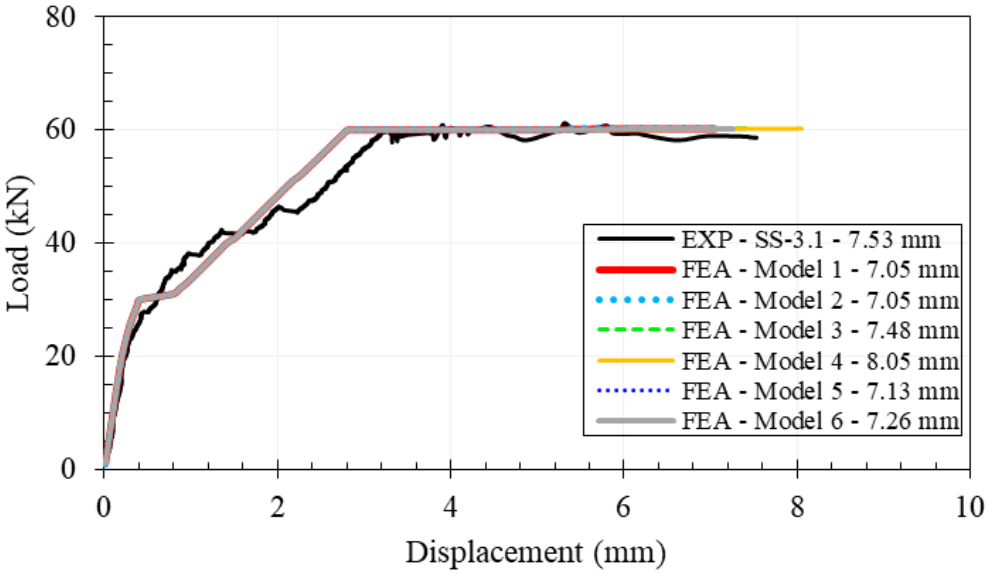

(b) Small-scale beam - SS-3.1

Figure 6.19: Effect of localized corrosion levels in non-critical cracked sections of RC beams

6.7 References

Al-Bayti, A., Almansour, H., Saatcioglu, M. (2022a). Influence of Corrosion on the Mechanical Performance of Steel Reinforcement. To be submitted for publication.

Al-Bayti, A., Almansour, H., Saatcioglu, M. (2022b). Tests Reinforced Concrete Beams under Coupled Effects of Variable Service Loads and Reinforcement Corrosion. To be submitted for publication.

Al-Bayti, A., Almansour, H., Saatcioglu, M. (2022c). Tests of Reinforced Concrete Beams under Coupled Effects of Maximum Service Loads and Reinforcement Corrosion. To be submitted for publication.

Almusallam, A. A. (2001). Effect of degree of corrosion on the properties of reinforcing steel bars. Construction and Building Materials, 15(8), 361-368.

Almusallam, A. A., Al-Gahtani, A. S., Aziz, A. R., and Rasheeduzzafar. (1996). Effect of reinforcement corrosion on bond strength. Construction and Building Materials, 10(2), 123-129.

Apostolopoulos, C. A., and Papadakis, V. G. (2008). Consequences of steel corrosion on the ductility properties of reinforcement bar. Construction and Building Materials, 22(12), 2316-2324.

Al-Sulaimani, G. J., Kaleemullah, M., Basunbul, I. A., and Rasheeduzzafar. (1990). Influence of corrosion and cracking on bond behavior and strength of reinforced concrete members. ACI Structural Journal, 87(2), 220-231.

Azad, A. K., Ahmad, S., and Azher, S. A. (2007). Residual strength of corrosion-damaged reinforced concrete beams. ACI Materials Journal, 104(1), 40-47.

Ballim, Y., and Reid, J. C. (2003). Reinforcement corrosion and the deflection of RC beams – an experimental critique of current test methods. Cement and Concrete Composites, 25(6), 625-632.

Cairns, J., Plizzari, G. A., Du, Y., Law, D. W., and Franzoni, C. (2005). Mechanical properties of corrosion-damaged reinforcement. ACI Materials Journal, 102(4), 256-264.

Cape`, M. (1999). Residual service-life assessment of existing R/C structures. MASc Thesis, Chalmers University of Technology, Göteborg, Sweden, and Milan University of Technology, Milan, Italy.

CEB-FIP (2013). fib Model Code for Concrete Structures 2010. International Federation for Structural Concrete, Ernst & Sohn, Lausanne, Switzerland.

Coronelli, D., and Gambarova, P. (2004). Structural assessment of corroded reinforced concrete beams: Modeling guidelines. ASCE Journal of Structural Engineering, 130(8), 1214-1224.

Dekoster, M., Buyle-Bodin, F., Maurel, O., and Delmas, Y. (2003). Modelling of the flexural behaviour of RC beams subjected to localised and uniform corrosion. Engineering Structures, 25(10), 1333-1341.

DIANA FEA BV. (2020). Finite Element Analysis - User's Manual Release 10.4. TNO Building and Construction Research Institute, Delft, Netherlands.

Du, Y. G., Clark, L. A., and Chan A. H. C. (2005). Residual capacity of corroded reinforcing bars. Magazine of Concrete Research, 57(3), 135-147.

Du, Y., Clark, L. A., and Chan, A. H. C. (2007). Impact of reinforcement corrosion on ductile behavior of reinforced concrete beams. ACI Structural Journal, 104(3), 285-293.

Du, Y., Cullen, M., and Li, C. (2013). Structural performance of RC beams under simultaneous loading and reinforcement corrosion. Construction and Building Materials, 38, 472-481.

El Maaddawy, T., Soudki, K., and Topper, T. (2005). Long-term performance of corrosion damaged reinforced concrete beams. ACI Structural Journal, 102(5), 649-656.

Fernandez, I., and Berrocal, C. G. (2019). Mechanical Properties of 30 year-old naturally corroded steel reinforcing bars. International Journal of Concrete Structures and Materials, 13, Article 9.

Hanjari, K. Z., Kettil, P., and Lundgren, K. (2011). Analysis of mechanical behavior of corroded reinforced concrete structures. ACI Structural Journal, 108(5), 532-541.

Hariche, L., Ballim, Y., Bouhicha, M., and Kenai, S. (2012). Effects of reinforcement configuration and sustained load on the behaviour of reinforced concrete beams affected by reinforcing steel corrosion. Cement and Concrete Composites, 34(10), 1202-1209.

JSCE. (2010). JSCE guidelines for concrete No. 15: Standard specifications for concrete structures - 2007 “Design”. Technical Report, Japan Society of Civil Engineers, Tokyo, Japan.

Jnaid, F., and Aboutaha, R. S. (2016). Residual flexural strength of corroded reinforced concrete beams. Engineering Structures, 119, 198-216.

Kallias, A. N., and Rafiq, M. I. (2010). Finite element investigation of the structural response of corroded RC beams. Engineering Structures, 32(9), 2984-2994.

Li, H., Li, B., Jin, R., Li, S., and Yu, J.-G. (2018). Effects of sustained loading and corrosion on the performance of reinforced concrete beams. Construction and Building Materials, 169, 179-187.

Malumbela, G., Moyo, P., and Alexander, M. (2009). Behaviour of RC beams corroded under sustained service loads. Construction and Building Materials, 23(11), 3346-3351.

Mangat, P. S., and Elgarf, M. S. (1999). Flexural strength of concrete beams with corroding reinforcement. ACI Structural Journal, 96(1), 149-158.

Molina, F. J., Alonso, C., and Andrade, C. (1993). Cover cracking as a function of rebar corrosion: Part 2 - Numerical model. Materials and Structures, 26, 532-548.

Nakamura, H., and Higai, T. (2001). Compressive fracture energy and fracture zone length of concrete. Part of Modeling of inelastic behavior of RC structures under seismic loads. American Society of Civil Engineers, 471-487.

Ou, Y.-C., and Nguyen, N. D. (2014). Plastic hinge length of corroded reinforced concrete beams. ACI Structural Journal, 111(5), 1049-1058.

Palsson, R., and Mirza, M. S. (2002). Mechanical response of corroded steel reinforcement of abandoned concrete bridge. ACI Structural Journal, 99(2), 157-162.

Rodriguez, J., Ortega, L. M., and Casal, J. (1997). Load carrying capacity of concrete structures with corroded reinforcement. Construction and Building Materials, 11(4), 239-248.

Shen, J., Gao, X., Li, B., Du, K., Jin, R., Chen, W., and Xu, Y. (2019). Damage evolution of RC beams under simultaneous reinforcement corrosion and sustained load. Materials, 12(4), 627.

Tang, F., Lin, Z., Chen, G., and Yi, W. (2014). Three-dimensional corrosion pit measurement and statistical mechanical degradation analysis of deformed steel bars subjected to accelerated corrosion. Construction and Building Materials, 70, 104-117.

Torres-Acosta, A. A., Navarro-Gutierrez, S., and Terán-Guillén, J. (2007). Residual flexure capacity of corroded reinforced concrete beams. Engineering Structures, 29(6), 1145-1152.

Vecchio, F. J., and Collins, M. P., 1986. The modified-compression field theory for reinforced concrete elements subjected to shear. ACI Journal Proceedings, 83(2), 219-231.

Vecchio, F. J., and Collins, M. P., 1993. Compression response of cracked reinforced concrete. ASCE Journal of Structural Engineering, 119(12), 3590-3610.

Yoon, S., Wang, K., Weiss, W. J., and Shah, S. P. (2000). Interaction between loading, corrosion, and serviceability of reinforced concrete. ACI Materials Journal, 97(6), 637-644.

Zhang, W., Zhang, H., Gu, X., and Liu, W. (2018). Structural behavior of corroded reinforced concrete beams under sustained loading. Construction and Building Materials, 174, 675-683.

Chapter Seven : Summary and Conclusions

7.1 Summary and Conclusions

This research project investigated the flexural behavior of reinforced concrete beams subjected to different levels of service loads coupled with corrosion of the main flexural tensile reinforcement. The project consisted of two main phases; i) experimental research, and ii) numerical research.

The experimental phase consisted of tests of 9 small-scale beams (145 x 250 x 1800 mm) and 6 large-scale beams (200 x 300 x 3400 mm). The beams were designed, constructed, instrumented, and loaded under a four-point load test setup. Two beams in each category served as control specimens without reinforcement corrosion. All control beams were monotonically loaded up until failure to establish their ultimate load capacities. The primary test variables of the remaining corroded beams were the applied corrosion current density, level of corrosion, and level of sustained load as percentage of beam ultimate load capacity (0% P_u, 40% P_u, and 60% P_u). The following conclusions are drawn from the experimental testing of small-scale and large-scale RC beams:

- The presence of flexural cracks in RC beams subjected to the coupled effects of reinforcement corrosion and service loads of either 40% and 60% of the beam ultimate load capacity, opened up a clear pathway for the chloride ions to reach the surface of embedded steel reinforcement, causing a localization of corrosion and significant loss of reinforcement area at the cracked sections of beams.
- The localized loss of reinforcement area at the cracked sections of beams subjected to service loads of either 40% and 60% of the beam ultimate load capacity combined with the non-uniform distribution of corrosion were the main contributing factors to degrading the load-carrying capacity and ductility of beams. The ductile behavior of non-corroded beams was replaced by a brittle failure caused by the rupture of corroded longitudinal tensile steel bars through transverse crack openings at the end of the service life of beams.

- Test results showed that the degradation of bond strength at the interface between the corroded reinforcement and concrete due to increased corrosion levels, had a minimal impact on the response of corroded beams, tested in this study. This was explained by the slight redistribution in strains/stresses from the corroded constant moment region of beams to the adjacent shear-dominant regions.
- The coupling effects of reinforcement corrosion and service loads is an important parameter that should be taken into consideration while evaluating the load-carrying capacity and ductility of damaged RC beams due to corrosion. According to the results of this study, the small-scale beam subjected to service loads equivalent to 40% of the beam ultimate load capacity, experienced further losses of 47% in ultimate load capacity and 68% in ductility when compared to the beam that was corroded under no loads. Likewise, the large scale beam subjected to service loads equivalent to 60% of the beam ultimate load capacity, experienced further losses of 32% in ultimate load capacity and 55% in ductility when compared to the beam that was corroded under no loads. This behavior is only expected in corroded RC beams with load-induced bending cracks.
- The degradation rates of ultimate load capacity and ductility were more drastic in corroded beams under high service loads. This could be attributed to the increase in crack width openings under higher service loads, allowing in further localizations of corrosion at the positions of cracks. This effect was clearly evident when examining small-scale beams which were corroded under 40% and 60% of the beam ultimate load capacity.
- Small-scale beams experienced more rapid decline of loading-carrying capacity than large-scale beams, which could be attributed to the increase in flexural crack width of small-scale beams because of the low percentage of steel used. Increasing the width of flexure cracks creates a clear and easy pathway for chloride ions to reach the embedded longitudinal tensile steel bars, and hence increasing the localized effect of corrosion in the corroded small-scale beams.
- The provided tensile reinforcement area ratio relative to minimum code requirements is a key parameter that contributes to the response of corroded beams of different sizes. It is recommended to provide a higher tensile reinforcement ratio and the use of multiple bars for enhanced redundancy to ensure that there are multiple paths for the beam to withstand service loads in the case where one steel bar ruptures due to corrosion.

- The use of an accelerated corrosion approach with a current density of 300 μA/cm^2 to corrode the longitudinal steel bars of small-scale beams instead of a staged approach with a slow rate of 100 μA/cm^2 for a portion of the test prior to further accelerating the rate to 300 μA/cm^2, had only a slight influence on damage induced by corrosion, and hence the effect of corrosion current density on the overall behavior of small-scale beams was concluded to be minimal for the range considered. However, the use of a very high current density (i.e., 1000 μA/cm^2) delayed the failure of the large-scale beam due to the fast build-up of corrosion by-products around the embedded steel bars, which filled up the voids and cracks of concrete, and hence the corrosion process of steel bars was slowed down. Nevertheless, the overall behavior of large-scale beams which were corroded using different current densities was almost identical at the end of the service life of beams.

After the failure of beams, the corroded steel bars were carefully retrieved from the beams. Afterward, they were cleaned and weighed to assess the corrosion level in terms of average mass loss. In addition, a three-dimensional laser scanner was used to assess the non-uniform distribution of corrosion along steel bars and the localized sectional area loss. Subsequently, direct tensile tests were used to evaluate the effect of corrosion on the mechanical performance of steel bars. The following conclusions are drawn from the corrosion level measurements and tensile tests of corroded steel bars:

- The non-uniform distribution of corrosion in cracked reinforced concrete beams was influenced by the presence of transverse cracks since crack openings allowed chloride ions to ingress to the exposed surface of steel bars, resulting in a further loss of reinforcement area. Pit corrosion at random sites along steel bars was the other contributor to the non-uniform distribution of corrosion.
- The loss of reinforcement area due to localized corrosion was increased with the increase of corrosion levels (i.e., mass loss). However, the rate of increase in the loss of reinforcement area was reduced with the increase of corrosion levels, for the corroded steel bars considered in this study. This was attributed to the reduction in flexural crack widths since the corroded steel bars were retrieved from beams subjected to lower levels of service loads or from beams with higher percentage of steel, and hence the access of chlorides to the surface of steel bars was limited.

- At the end of the tensile tests, all the corroded steel bars retrieved from the cracked reinforced concrete beams were ruptured at the location with the critical sectional loss, corresponding to the location where flexural cracks were present. For the corroded steel bar in un-cracked reinforced concrete beam, the location of reinforcement rupture was subjected to the spatial variability of pit corrosion.
- The majority of corroded steel bars did not exhibit plateauing of yield (i.e., no transition from yielding stage to strain hardening stage). However, few corroded steel bars exhibited a short yield plateau stage relative to that exhibited by the control steel bars.
- The tensile strength of steel bars, based on critical sectional area, was not influenced by the presence of localized corrosion attack. In fact, there was a slight increase in strength with increased corrosion levels. For that reason, the load capacity of corroded steel bars can be conservatively estimated using the maximum sectional loss of steel bars.
- The ductility of steel bars was strongly influenced by the non-uniform distribution of corrosion. There was a drastic reduction in ultimate strain of steel bars as the level of corrosion was increased. In addition, few corroded bars did not satisfy ACI 318-14 minimum code requirement for the ratio between ultimate and yield strengths.

The numerical research consisted of finite element analyses of beams using DIANA FE analysis software, which had superior modeling features for reinforced concrete. To simulate corrosion-induced damage, a simplified approach was implemented using two-dimensional nonlinear FE models, based on the experimental testing of the corroded beams and corroded steel bars. The analyses were validated with experimental large-scale and small-scale beams. Subsequently, a parametric study was conducted for cases that were not covered in the experimental program, including the level of corrosion, level of service loads, strength of concrete, and tensile reinforcement ratio. The following conclusions are drawn from the numerical research phase of the project:

- The proposed simplified approach introduced to FE models was able to simulate the response of flexural-dominant corroded RC beams under various service loads. FE analyses were reasonably accurate in predicting crack patterns, residual load capacity, residual ductility, and failure modes of corroded beams.

- Simulating the flexural response of corroded RC beams under service loads was strongly influenced by the non-uniform distribution of corrosion, in particular the localization of corrosion at the critical cracked section of beams. Corrosion levels in non-critical cracked sections of the beams, had an effect on the ductility of beams, while its impact on the ultimate load capacity was minimal for the beams considered in this study.
- The decline of loading capacity in flexure dominant RC beams is directly proportional to the generalized form of corrosion. However, at a certain point during the service life of beams, the decline becomes more severe due to the severity of localized corrosion levels which reduces the ductility of beams.
- The degradation rates of ultimate load capacity and ductility of corroded beams were increased with increasing the levels of service loads. In this study, such behavior was more pronounced in small-scale beams since they were reinforced with lower tensile reinforcement ratio than large-scale beams.
- Strength of concrete had little to no impact on the ultimate load capacity of the heavily corroded beams since their response was governed by rupturing of longitudinal steel bars. However, the ultimate load capacity of corroded beams when governed by the crushing of concrete, increased with increasing the strength of concrete, as expected.
- Tensile longitudinal reinforcement ratio had a significant influence on the flexural response of corroded beams. Increasing the reinforcement ratio, improved the ultimate load capacity of corroded beams, which in turn would contribute to increasing their service life. For example, increasing the reinforcement ratio from 0.8% to 2.0%, increased the ultimate capacity of the corroded large-scale beam by more than 125% above the service level.

7.2 Recommendations for Future Research

The following are recommended for further investigations:

1) Experimentally investigate the flexural behavior of reinforced concrete beams with different transverse crack widths due to either different tensile reinforcement ratios or strengths of concrete under the coupled effects of service loads and corrosion of the main flexural reinforcement.
2) Experimentally examine the size-effect of reinforced concrete beams under the coupled effects of service loads and corrosion of the main flexural reinforcement.

3) Experimentally compare the behavior of reinforced concrete beams subjected to sustained and fatigue loads when coupled with corrosion of the main flexural reinforcement.
4) Experimentally investigate the flexural behavior of reinforced concrete beams under the coupled effects of service loads and corrosion of the main flexural reinforcement across the entire length of beams.
5) Experimentally examine the response of reinforced concrete beams subjected to service loads when coupled with corrosion of the main flexural reinforcement, transverse reinforcement and end anchorage.
6) Expand the data for the empirical relationship between the average and maximum sectional area losses of steel reinforcement due to corrosion. A particular attention should be given to generate data for corrosion levels below than 10%.

Appendix A : Supplementary Material of Small-scale Beams

Appendix A provides supplementary materials for the experimental testing of small-scale RC beams. A brief presentation of these results and detailed discussions are presented in Chapter 3. This appendix includes images that were taken during the corrosion phase and at the failure of beams. It also presents the collected data during the corrosion and loading phases of the experimental testing. This includes: (i) voltage measurements, (ii) applied loads, (iii) displacements, and (iii) internal and external strains readings.

Voltage measurements were monitored during the corrosion phase of testing. The main objective of monitoring the voltage was to observe the change in the resistivity of concrete. The change of voltage measurements gives an indication of the development corrosion-induced cracks in the concrete surrounding the corroded steel reinforcement since the applied current was kept constant during the test. Each longitudinal tensile steel bar embedded in small-scale beams (i.e., labelled as Rebar 1 and Rebar 2) had its own power supply.

Applied loads were monitored using load cells that were connected to the pumps. Displacements were measured using linear variable differential transformers (LVDT). A total of ten LVDTs were placed at various positions along the top surface of small-scale beams, as illustrated in Figure A.1. All LVDTs were labelled according to their position away from the left support. For example, LVDT-1 was labelled as 0 mm, while the average of LVDT-7 and LVDT-8 was labelled as 1000 mm.

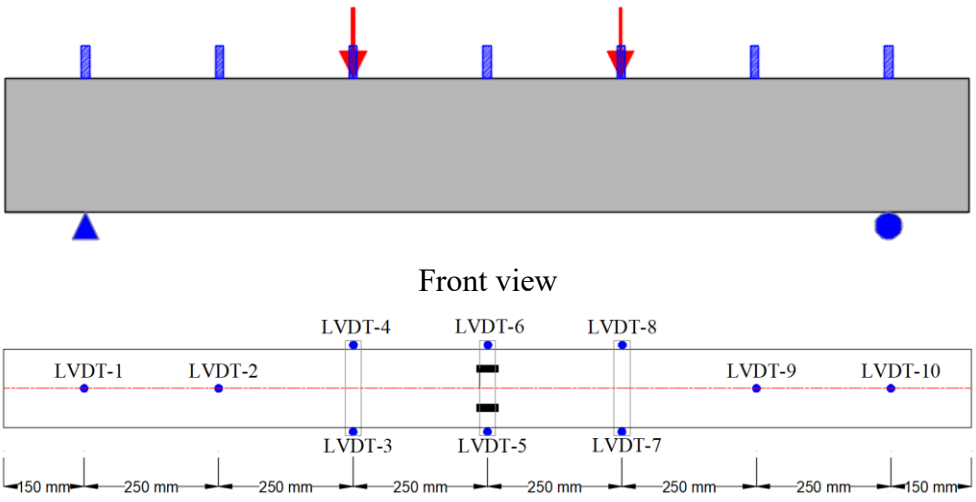

Figure A.1: Positions of LVDTs along the top surface of small-scale beams

A total of ten electrical strain gauges were attached at select positions on the tensile and compressive longitudinal steel bars. In addition, one internal concrete strain gauge was placed at the center of the beam between the top longitudinal steel bars. The location and labelling of all internal strain gauges are shown in Figure A.2. The position of internal strain gauges was carefully selected for a better understanding of the behavior of compression struts between loads and supports.

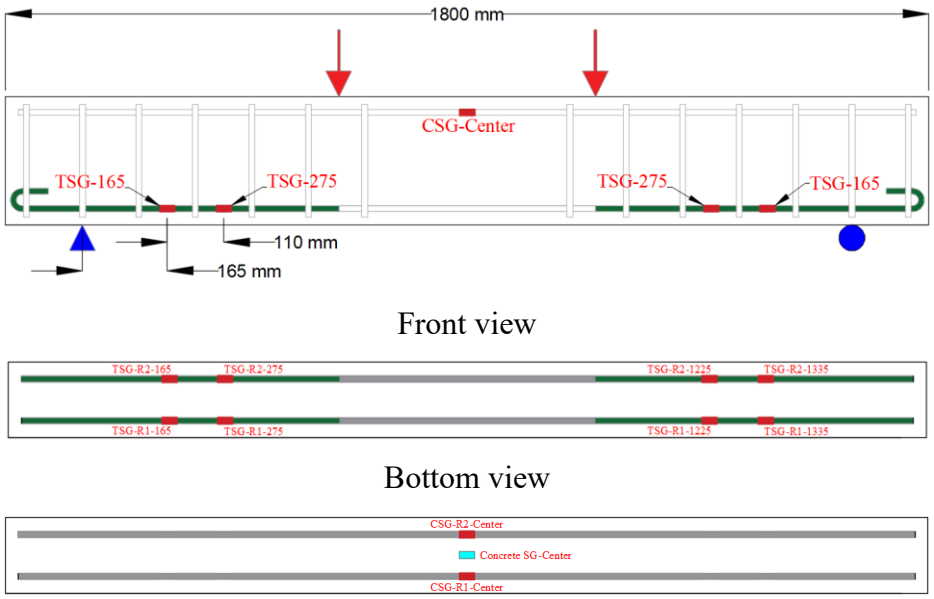

Figure A.2: Position of internal strain gauges – small-scale beams

External triaxial rosette strain gauges were attached on the side surface of concrete. One set of external triaxial rosette strain gauges was attached at each side of the beam, as illustrated in Figure A.3. The positions and number of external triaxial rosette strain gauges were selected to capture the change in the strut angle during the experimental testing. The horizontal gauge (H), inclined gauge (C), and vertical gauge (V) on the front face of the beam were labelled as EXT-SG-H1, EXT-SG-C1, and EXT-SG-V1. The gauges attached on the back face of the beam were labelled with the number 2 instead of 1. For example, the horizontal gauge on the back face of the beam was labelled as EXT-SG-H2.

After completing the experimental testing of the first four small-scale beams, it was felt necessary to add strain gauges to monitor the change of strains at the top surface of concrete. Accordingly, two external strain gauges were attached on the top surface of concrete at mid-span. These gauges were labelled as CSC-1-Center and CSC-2-Center.

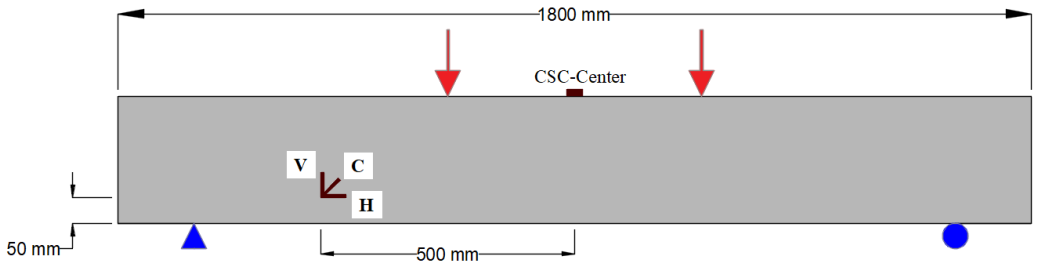

Figure A.3: Positions of external strain gauges – small-scale beams

A.1 Beam SS-1.1

Beam SS-1.1 served as a control specimen without reinforcement corrosion.

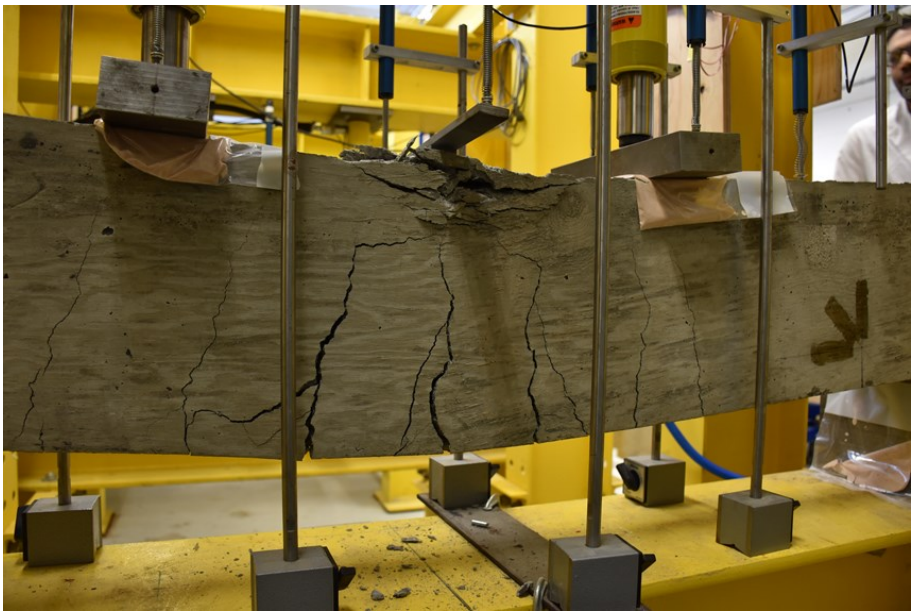

(a)

(b)

Figure A.4: Crack propagation and patterns at failure – beam SS-1.1

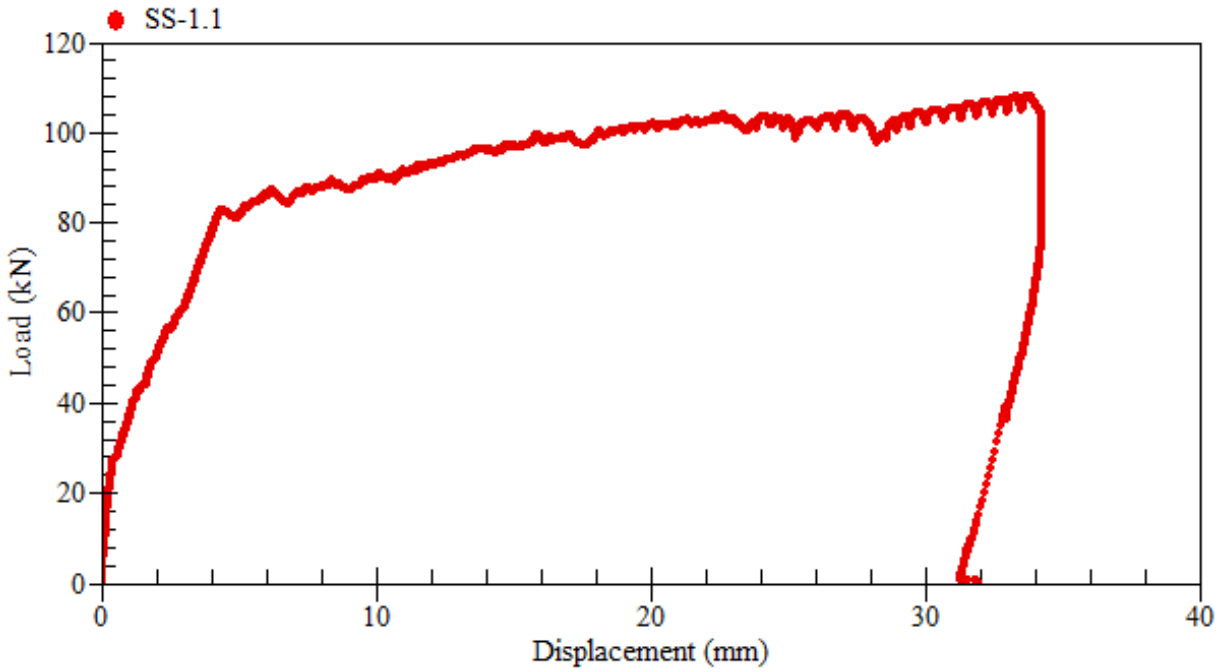

Figure A.5: Load-displacement relationship at mid-span – beam SS-1.1

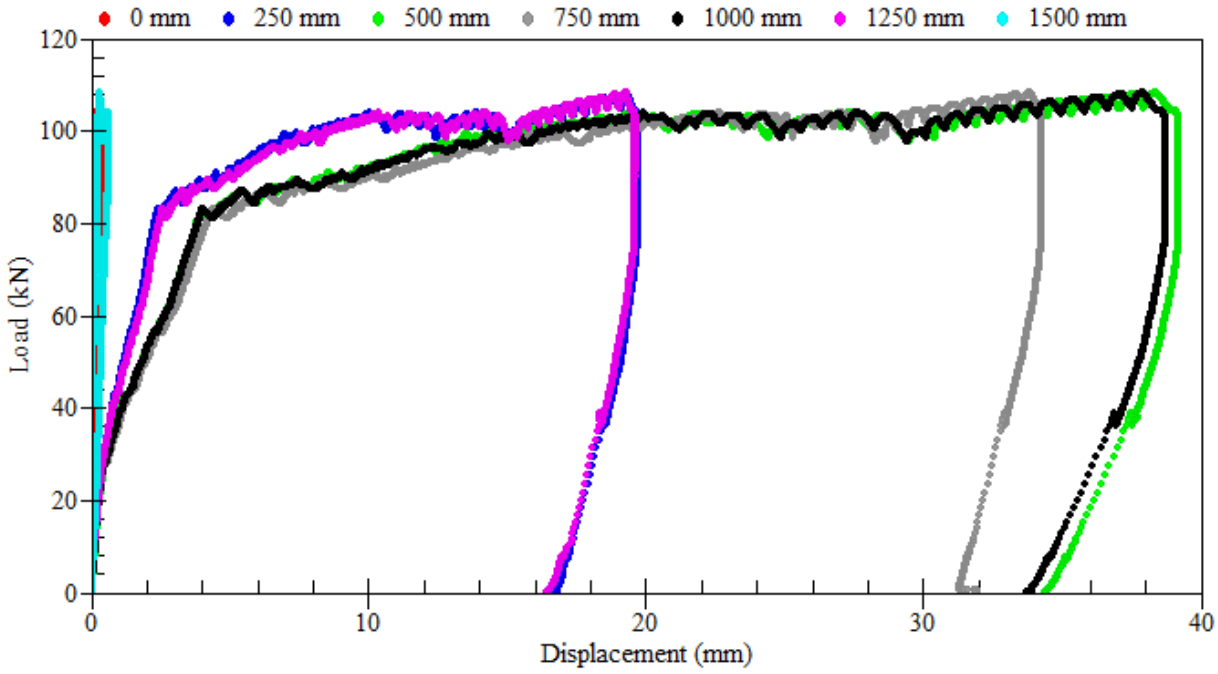

Figure A.6: Load-displacement relationships – beam SS-1.1

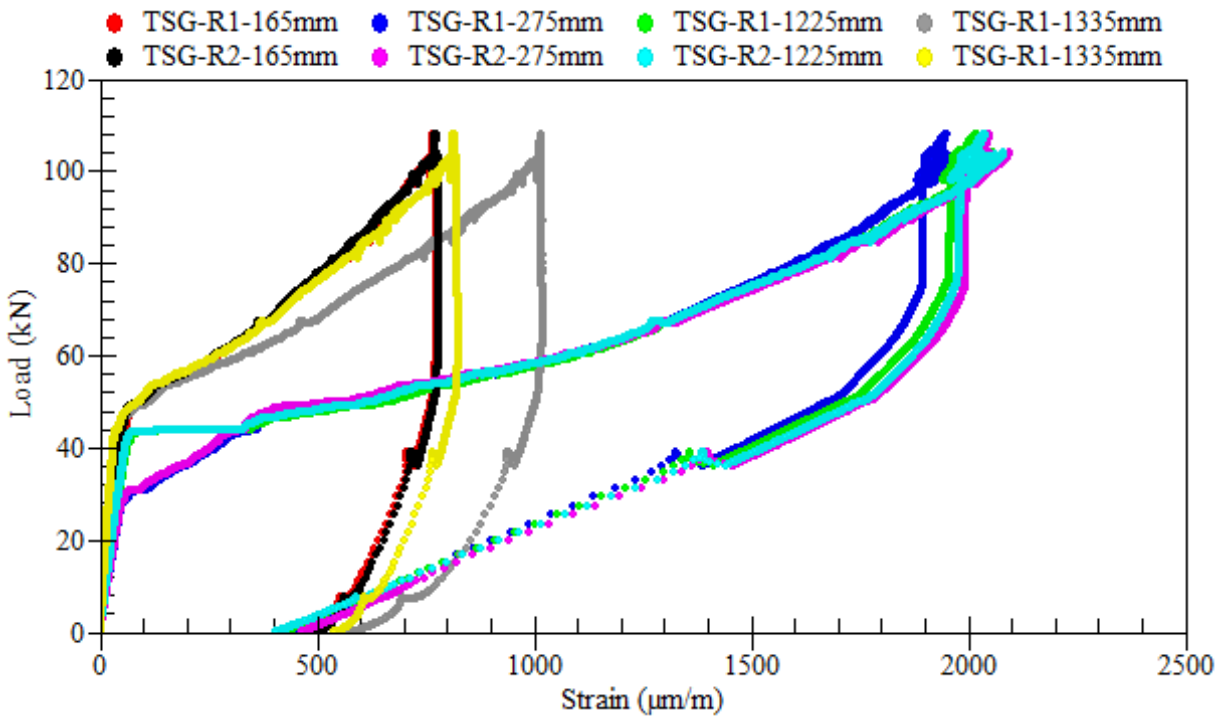

Figure A.7: Load-strain relationships of longitudinal tensile steel bars – beam SS-1.1

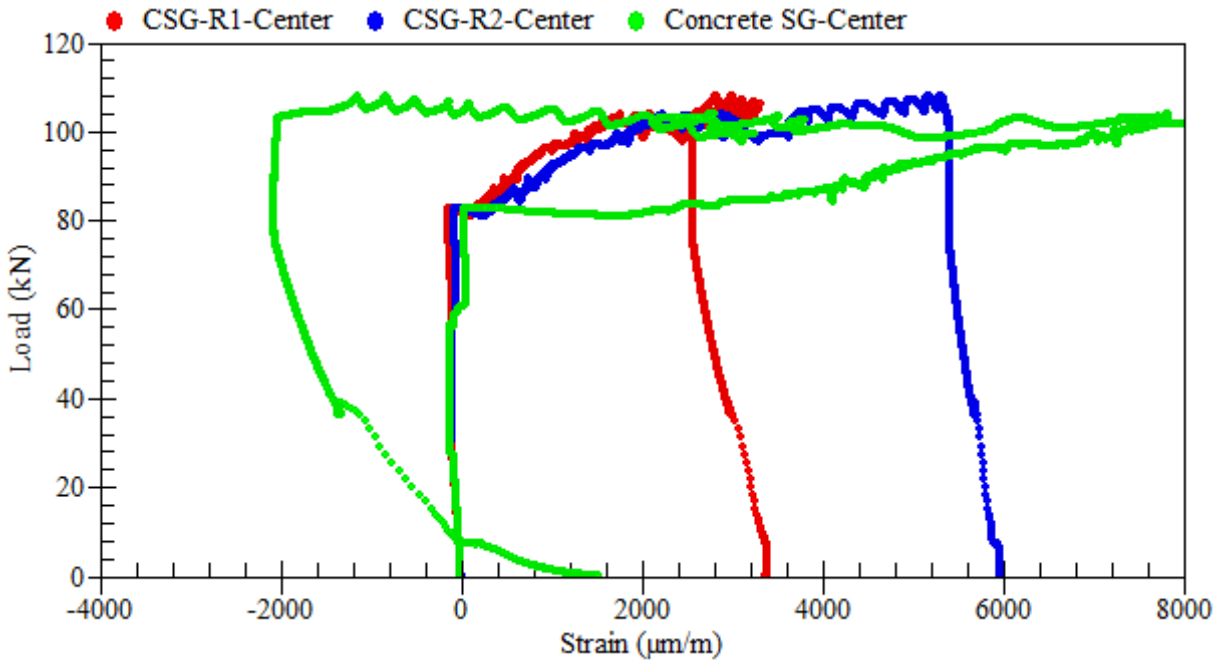

Figure A.8: Load-strain relationships of longitudinal compressive steel bars – beam SS-1.1

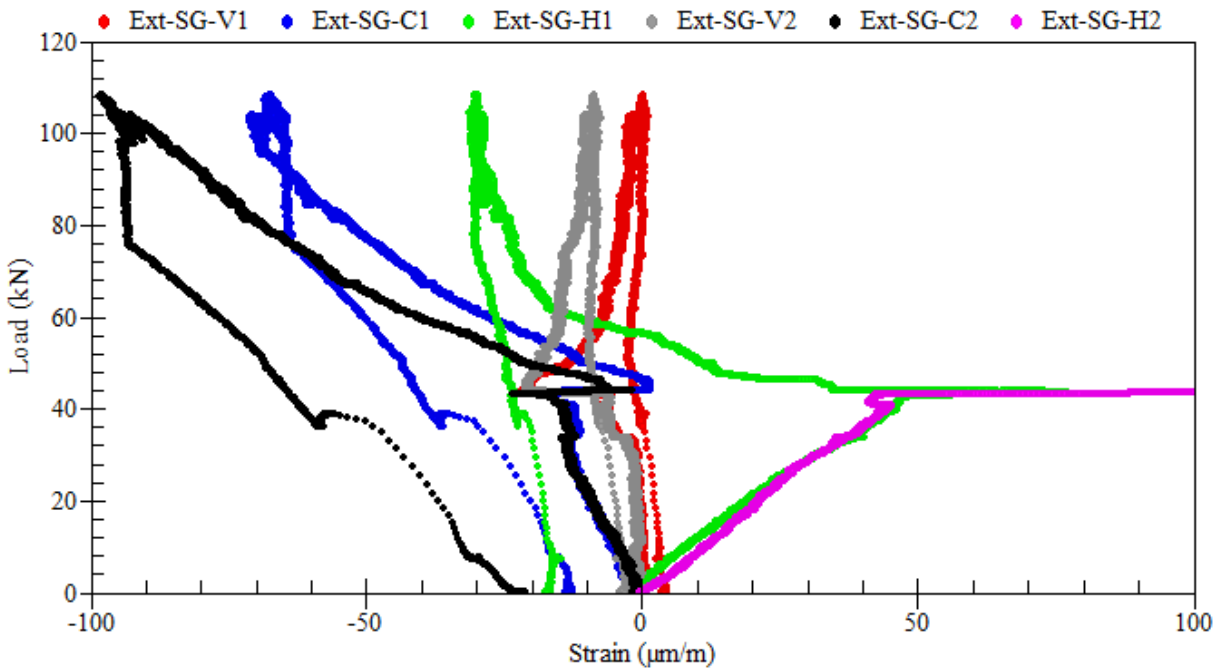

Figure A.9: Load-strain relationships of external rosettes on sides – beam SS-1.1

A.2 Beam SS-1.2

Beam SS-1.2 served as a control specimen without reinforcement corrosion.

(a)

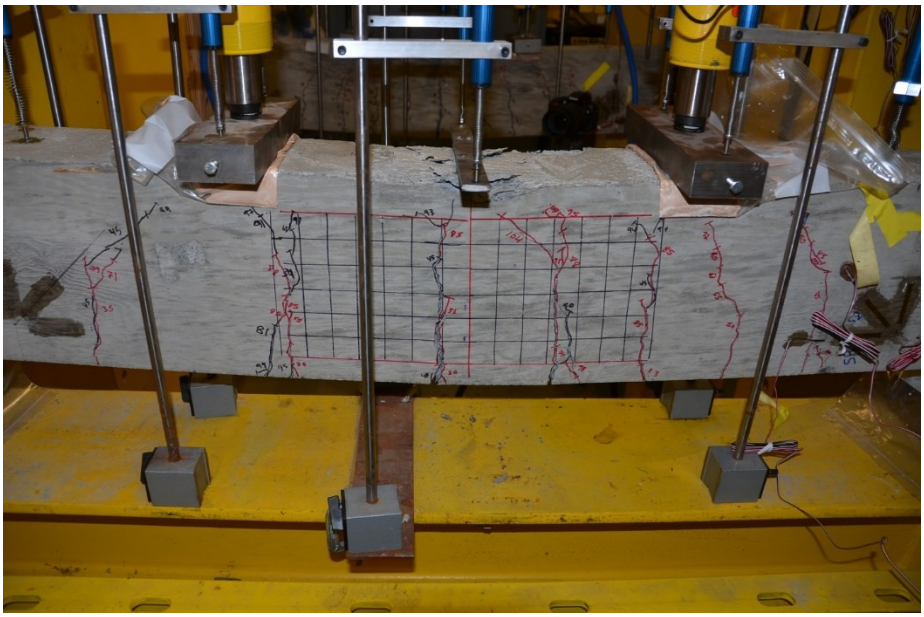

(b)

Figure A.10: Crack propagation and patterns at failure – beam SS-1.2

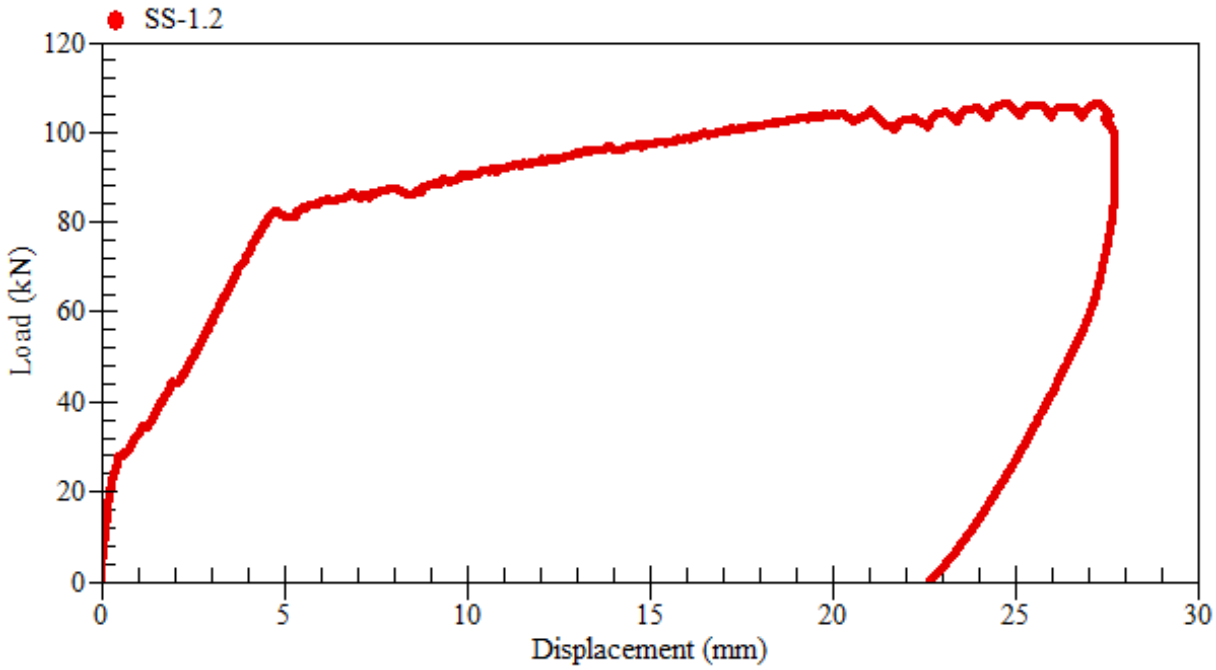

Figure A.11: Load-displacement relationship at mid-span – beam SS-1.2

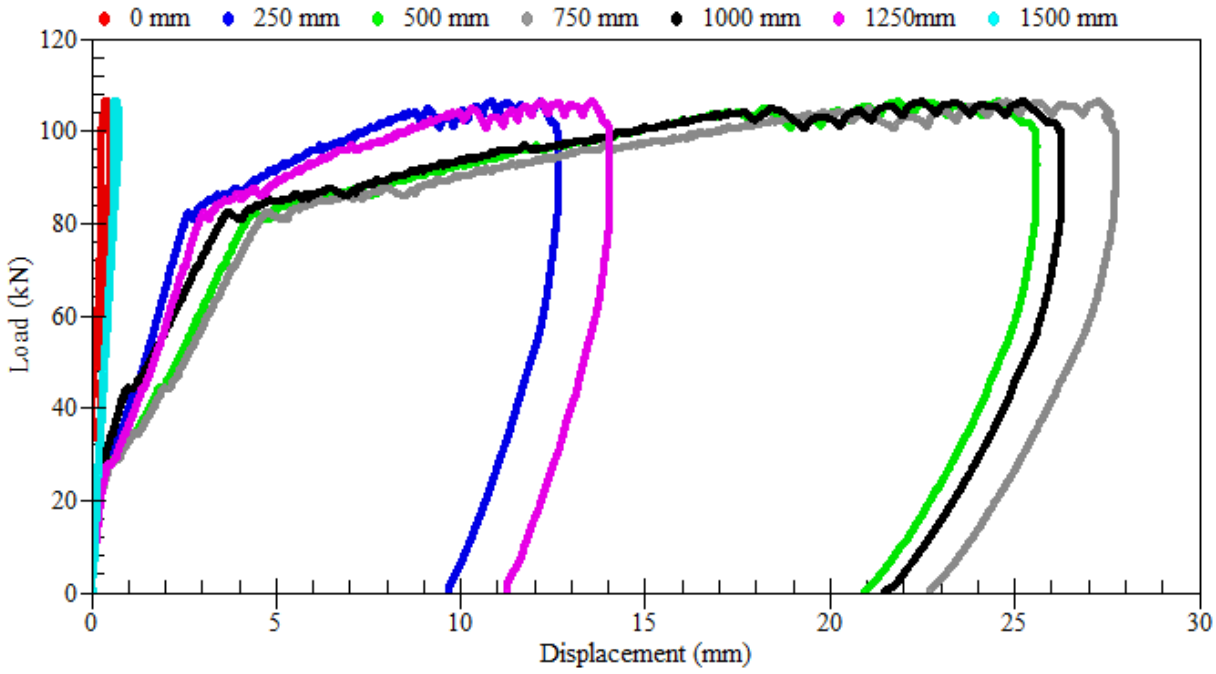

Figure A.12: Load-displacement relationships – beam SS-1.2

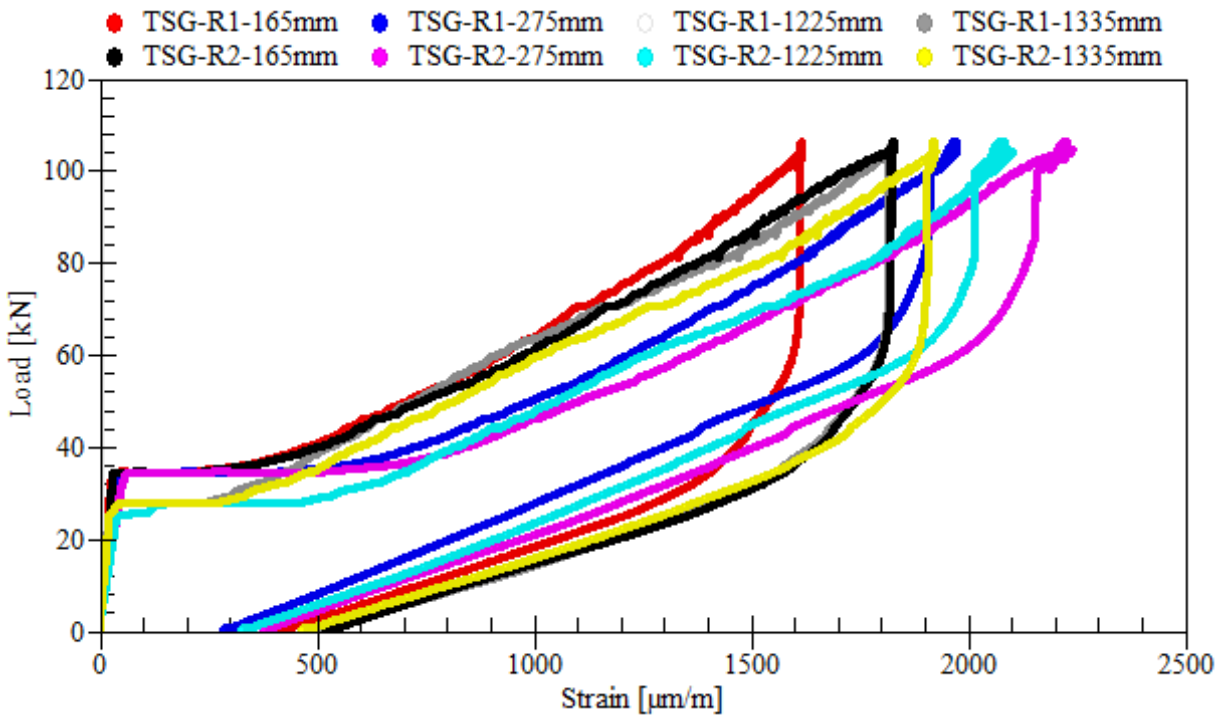

Figure A.13: Figure: Load-strain relationships of longitudinal tensile steel bars – beam SS-1.2

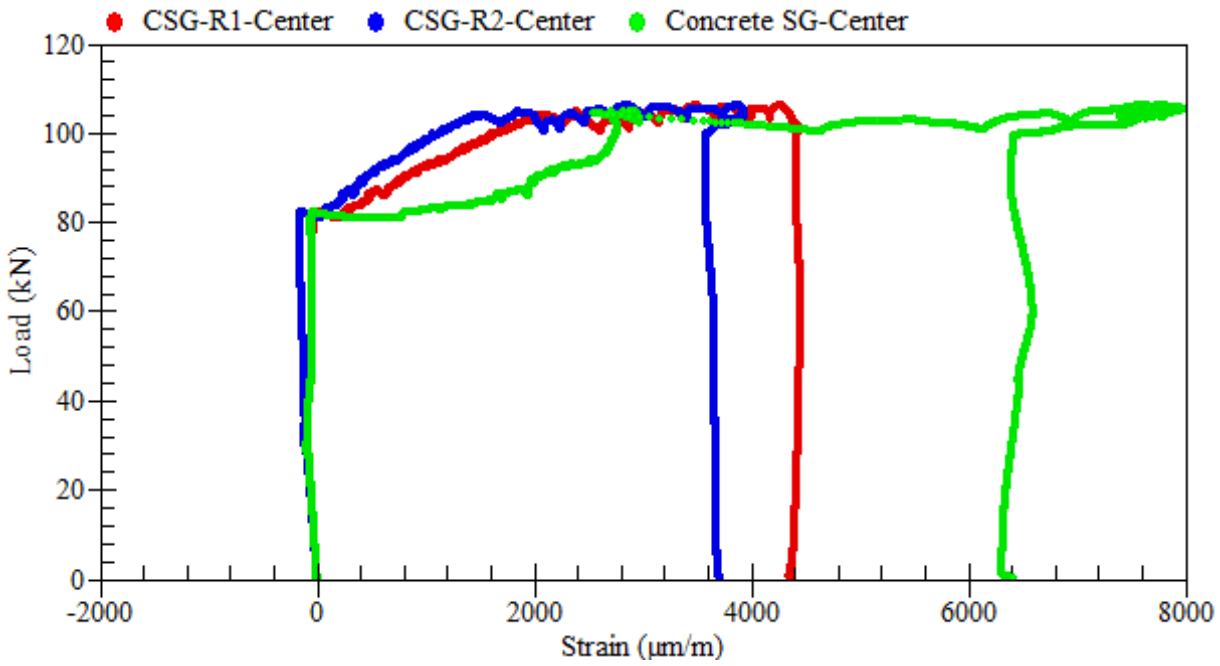

Figure A.14: Load-strain relationships of longitudinal compressive steel bars – beam SS-1.2

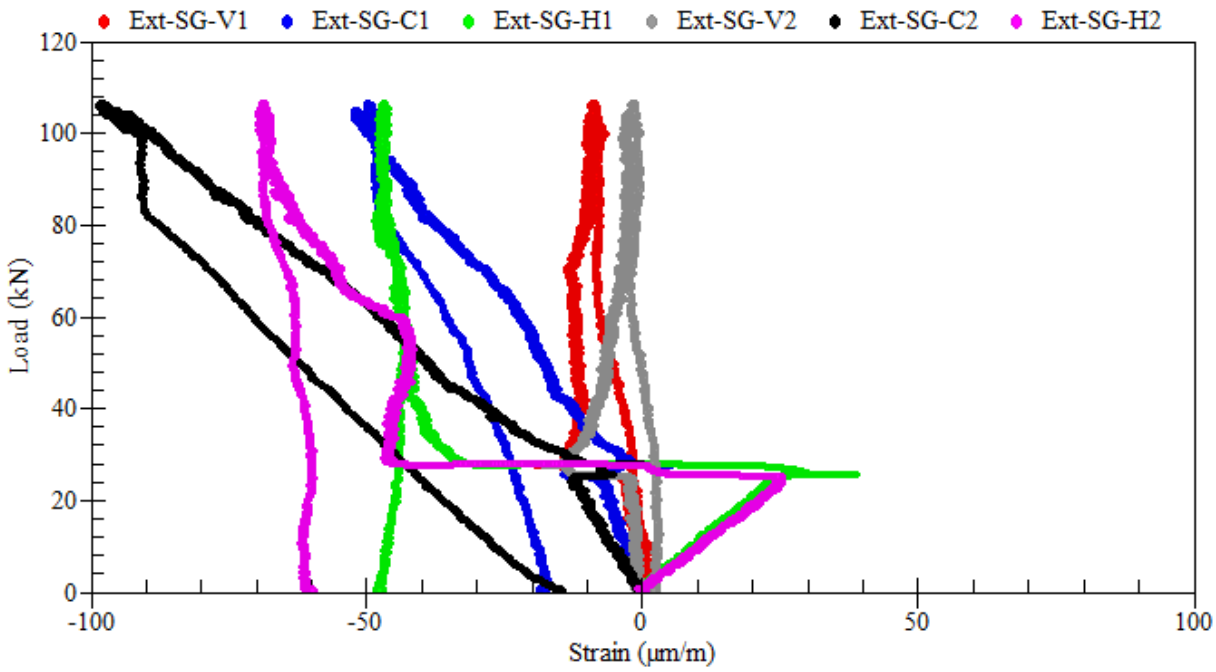

Figure A.15: Load-strain relationships of external rosettes on sides – beam SS-1.2

A.3 Beam SS-2.1

Beam SS-2.1 was tested under the coupled effects of reinforcement corrosion and service loads. The applied sustained load was equivalent to 60% of the beam ultimate load capacity (i.e., 60 kN). Reinforcement corrosion was accelerated using a current density of 100 μA/cm^2 over a duration of 35 days before increasing it to 300 μA/cm^2 up until the failure of the beam. The total duration of corrosion exposure was 73 days. The average mass loss of the beam was 13.7%. A summary of the gravimetric mass loss measurements of steel reinforcement is presented in Table A.1.

(a) during the test

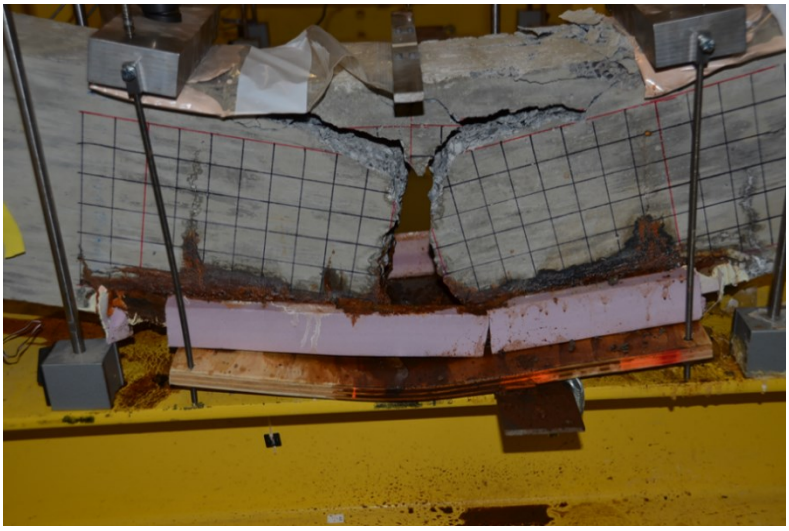

(b) at failure

Figure A.16: Crack propagation and failure of patterns – beam SS-2.1

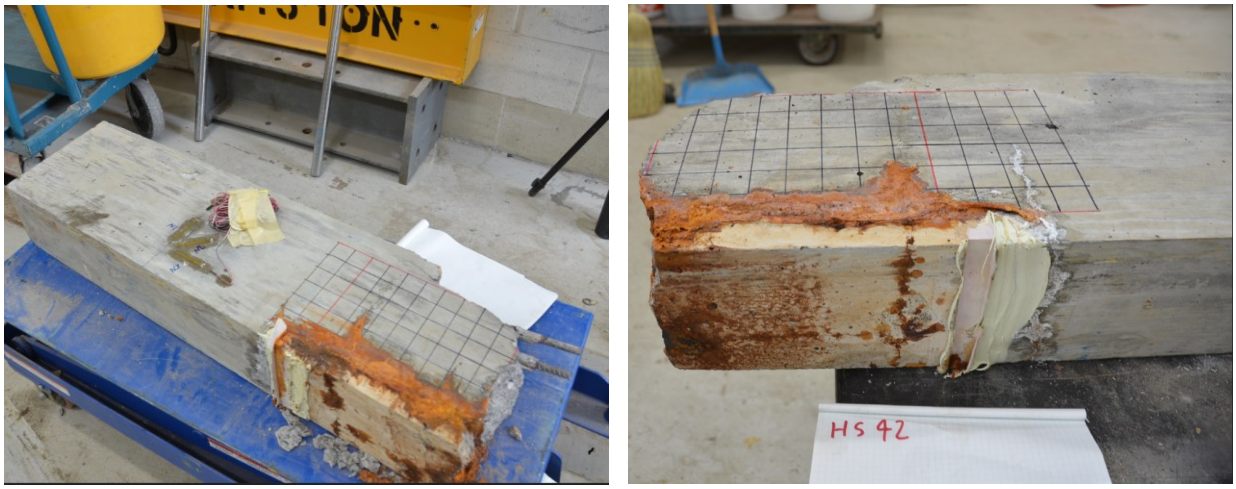

Figure A.17: Corrosion-induced damage in the cover of concrete – beam SS-2.1

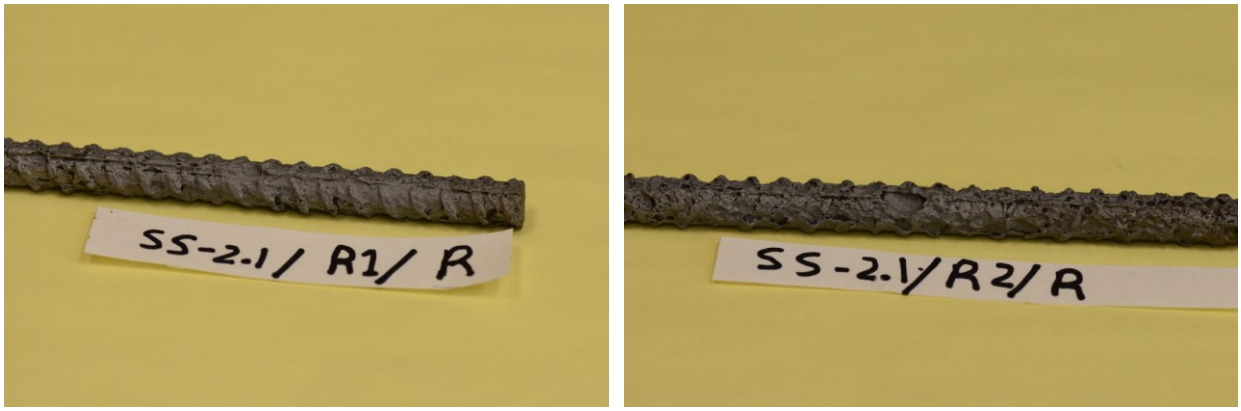

Figure A.18: Corrosion patterns on the clean surface of steel reinforcement – beam SS-2.1

Table A.1: Mass loss of corroded steel bars – beam SS-2.1

Rebar type	Rebar designation	Length (mm)	Mass (g)	Mass loss (%)	Rebar mass loss (%)
Control	R0	100.0	75.38	0.00	0.00
R1	R1-R	169.0	110.21	13.49	11.91
	R1-L	161.5	109.25	10.26	
R2	R2-R	168.0	106.86	15.62	15.50
	R2-L	154.0	98.23	15.38	

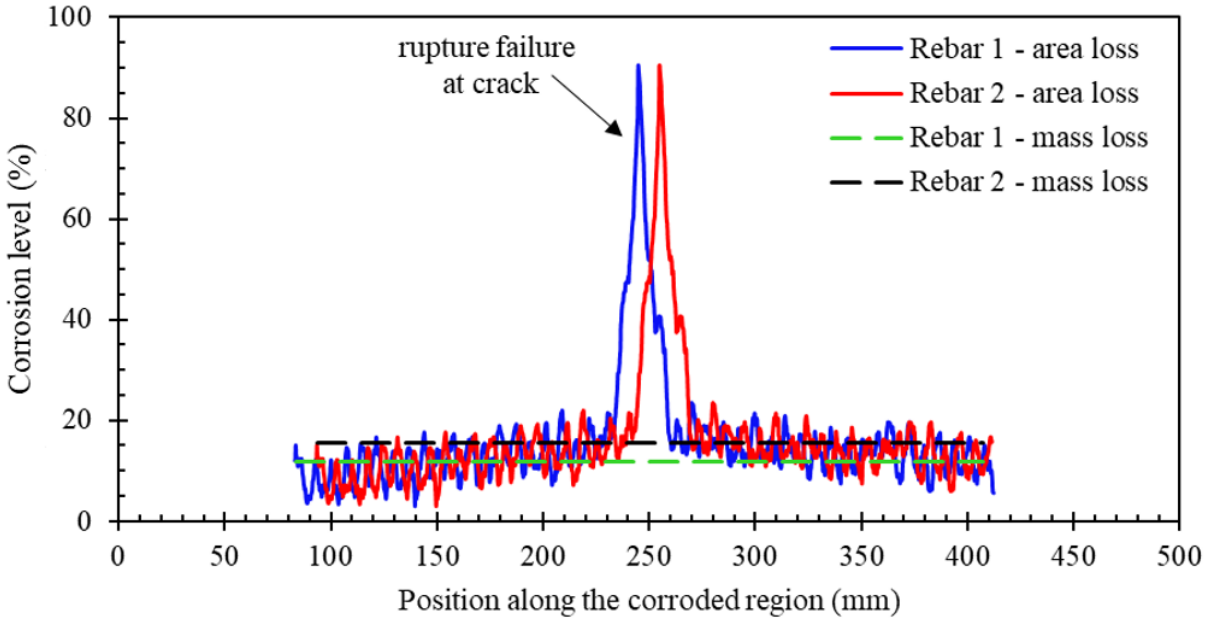

Figure A.19: Distribution of cross-sectional area loss along the corroded steel reinforcement – beam SS-2.1

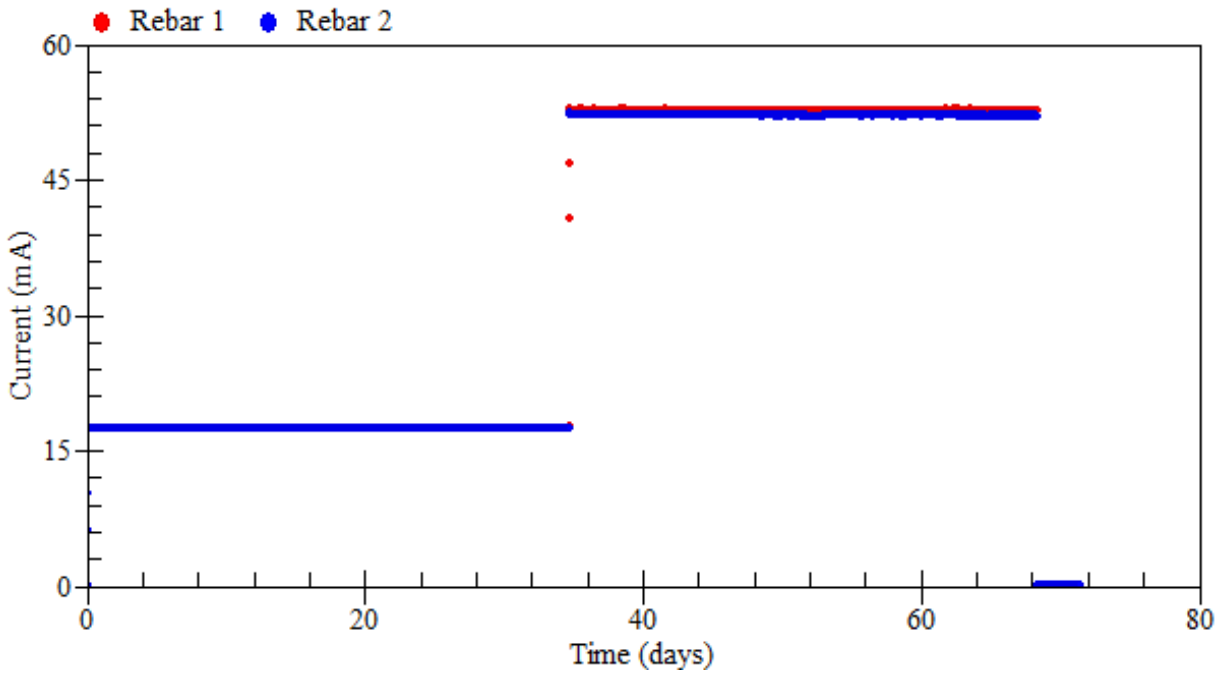

Figure A.20: Applied current – beam SS-2.1

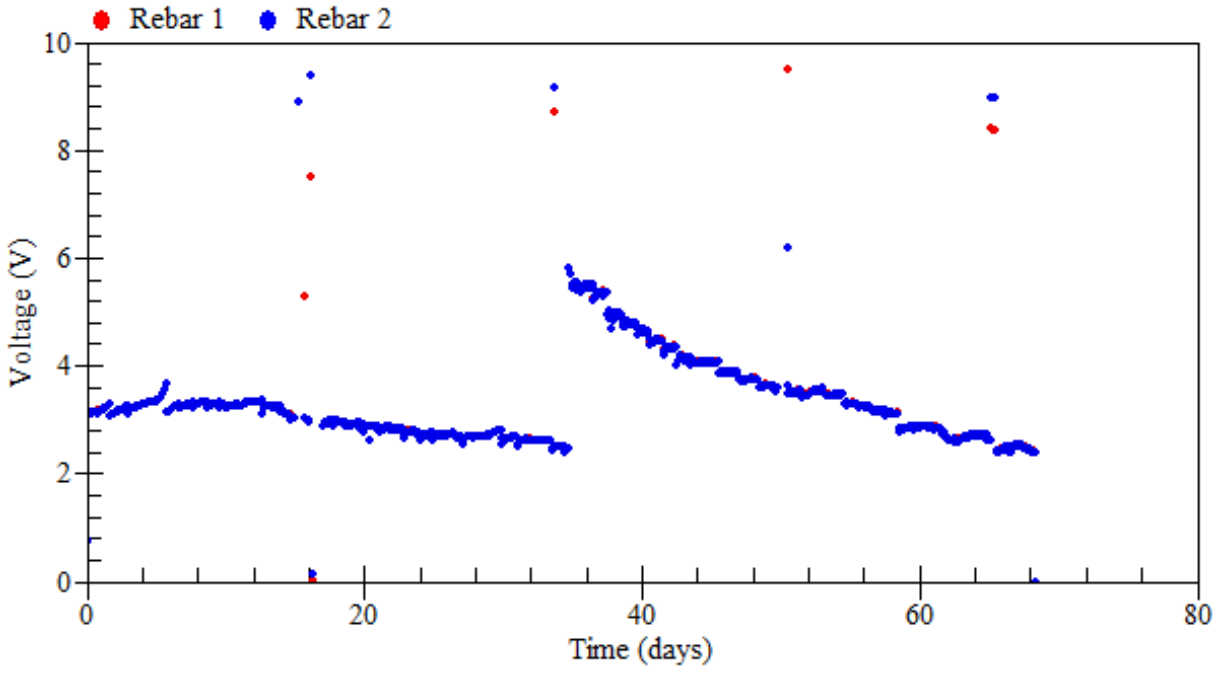

Figure A.21: Voltage measurements – beam SS-2.1

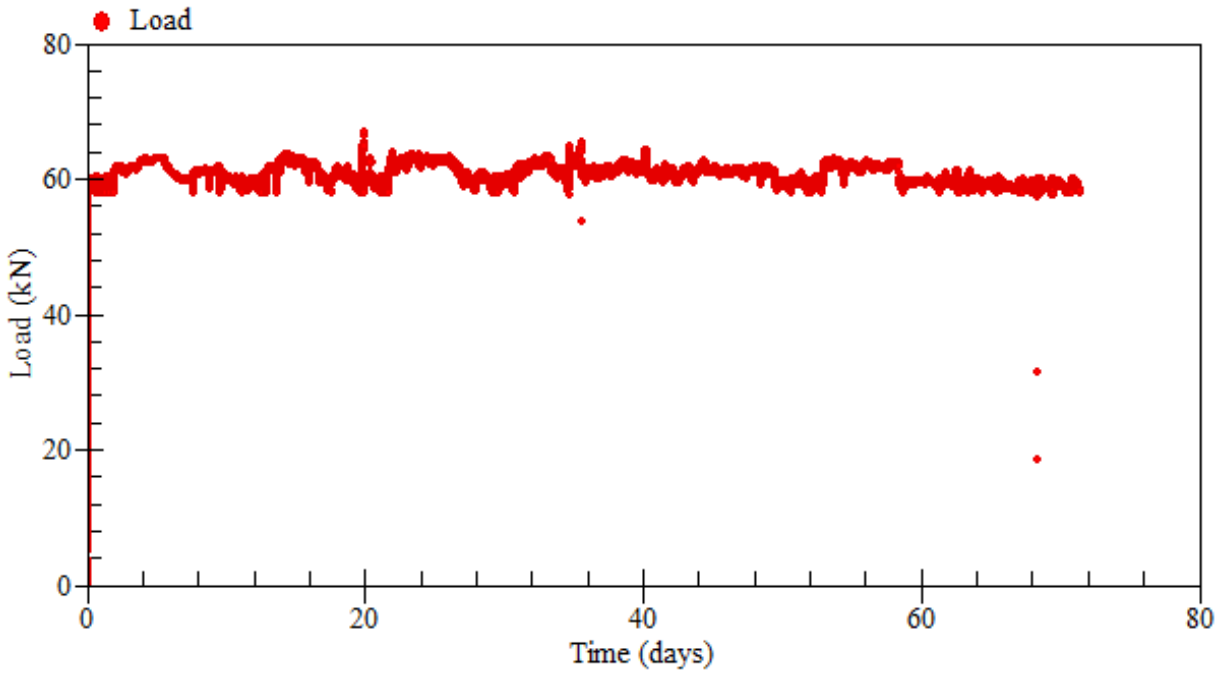

Figure A.22: Applied loads – beam SS-2.1

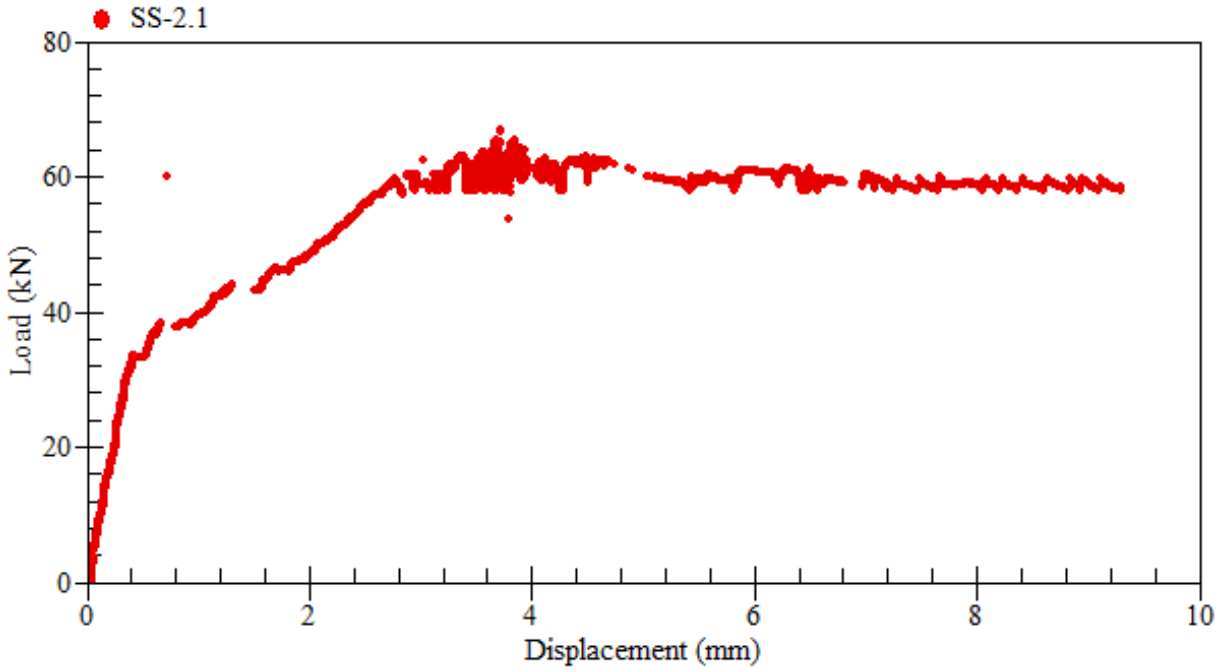

Figure A.23: Load-displacement relationship at mid-span – beam SS-2.1

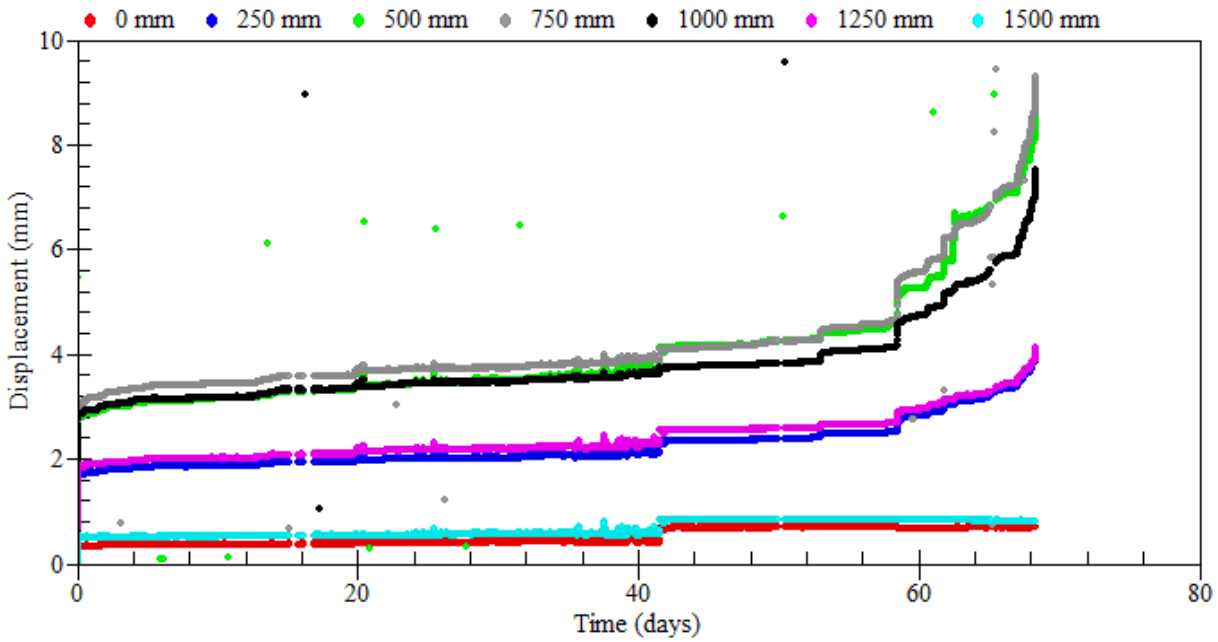

Figure A.24: Displacement measurements – beam SS-2.1

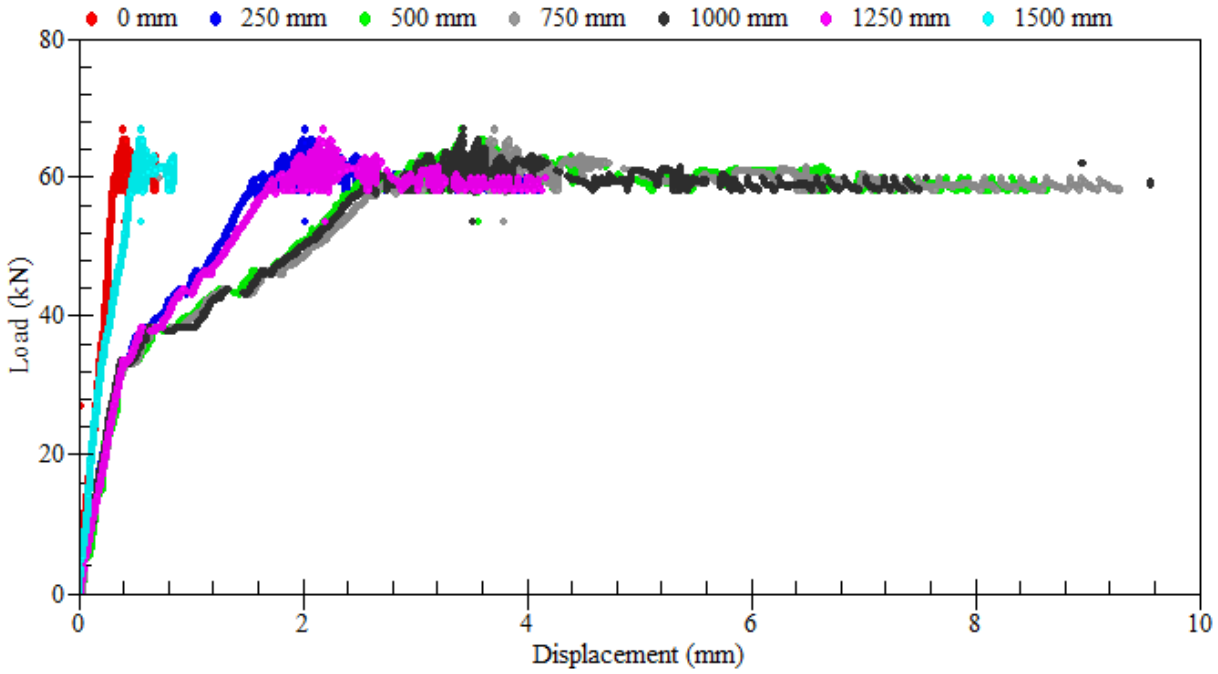

Figure A.25: Load-displacement relationships – beam SS-2.1

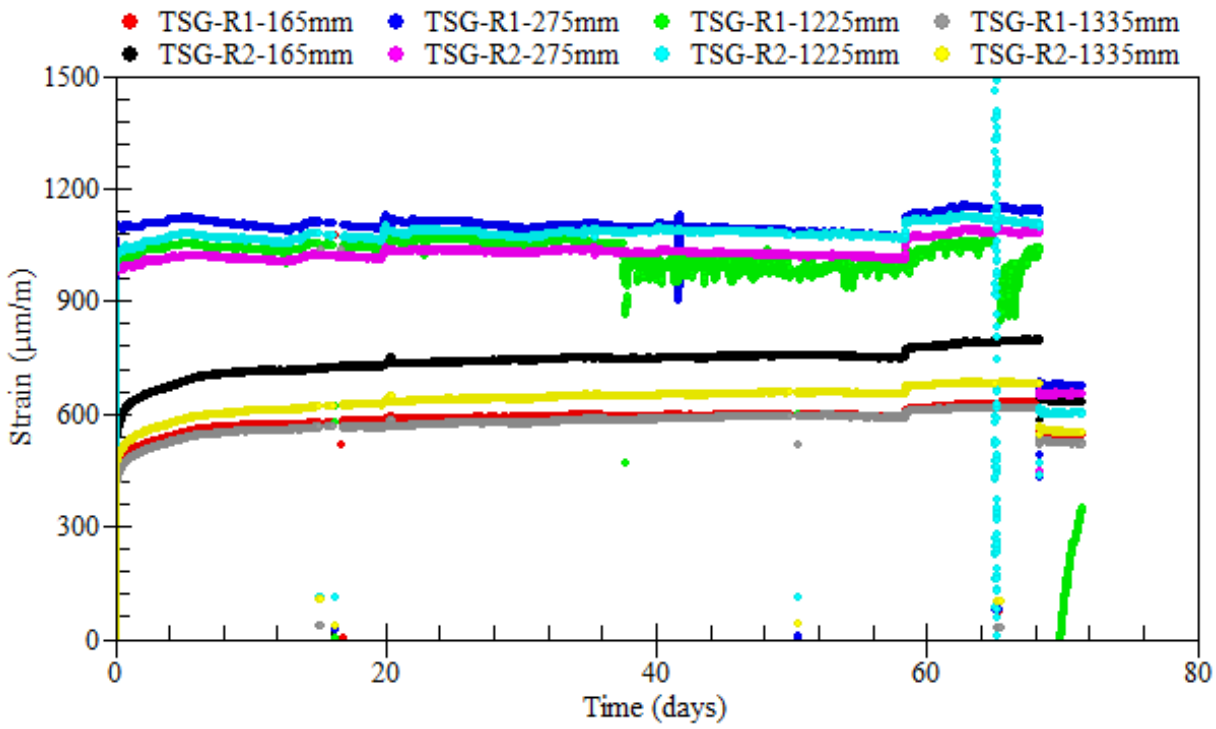

Figure A.26: Strain readings of longitudinal tensile steel bars – beam SS-2.1

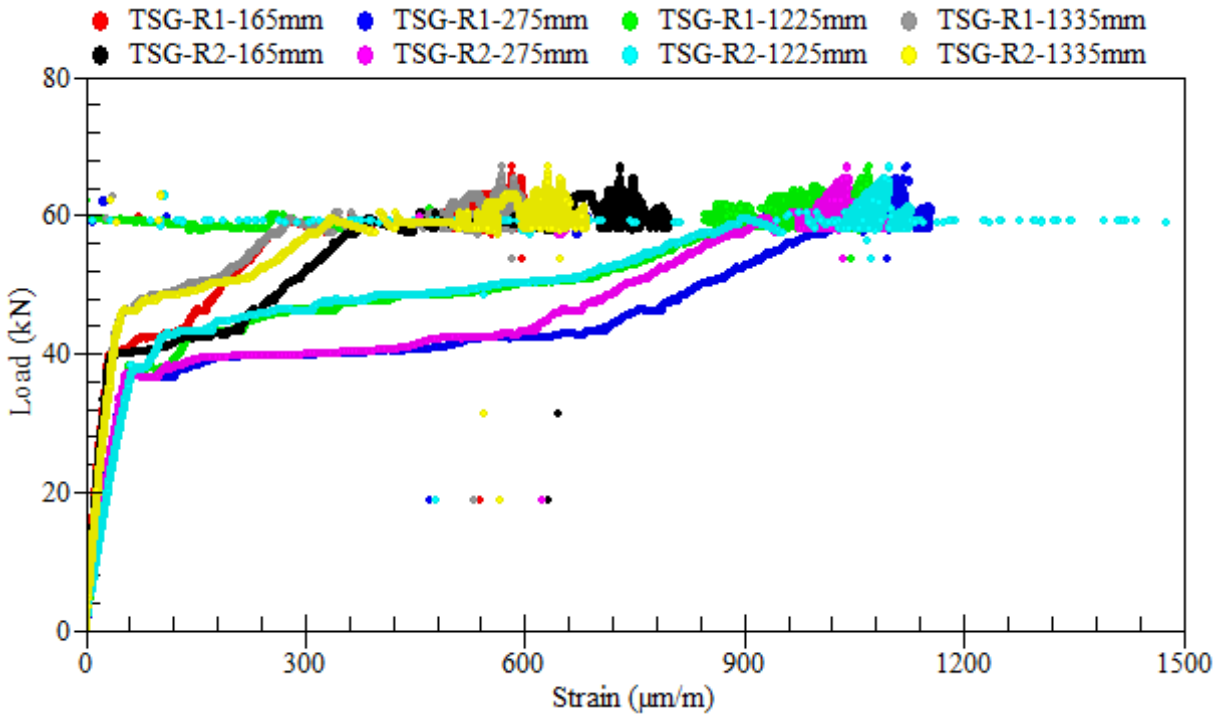

Figure A.27: Load-strain relationships of longitudinal tensile steel bars – beam SS-2.1

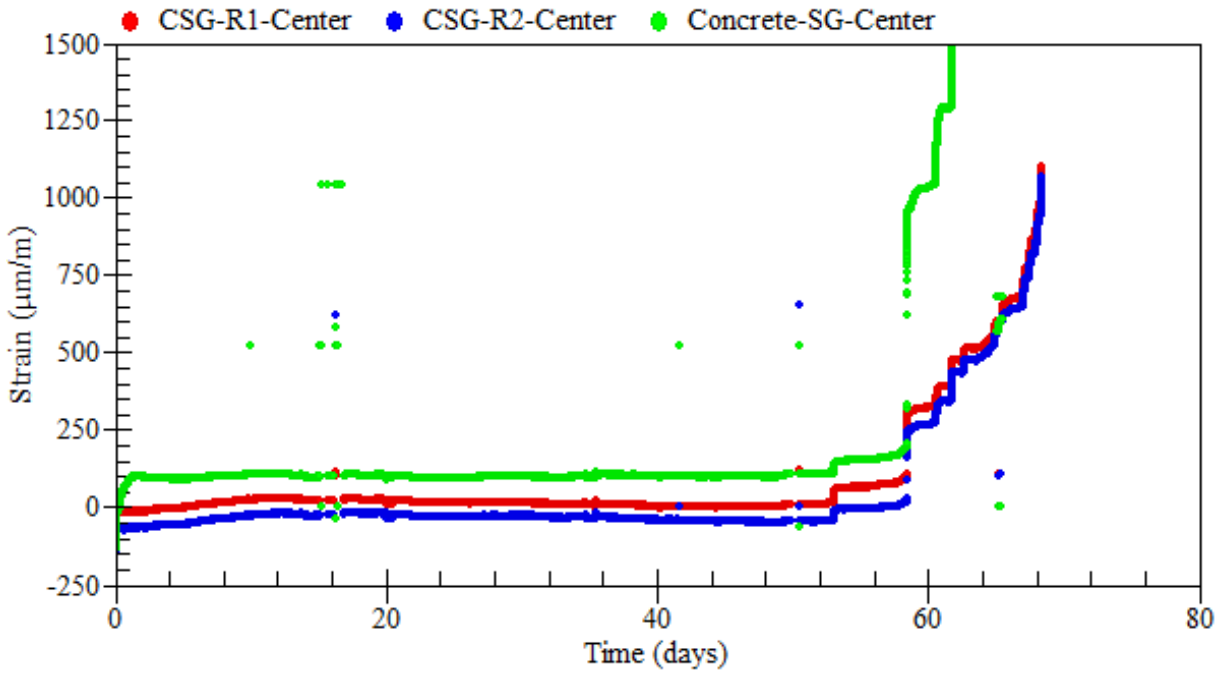

Figure A.28: Strain readings of longitudinal compressive steel bars – beam SS-2.1

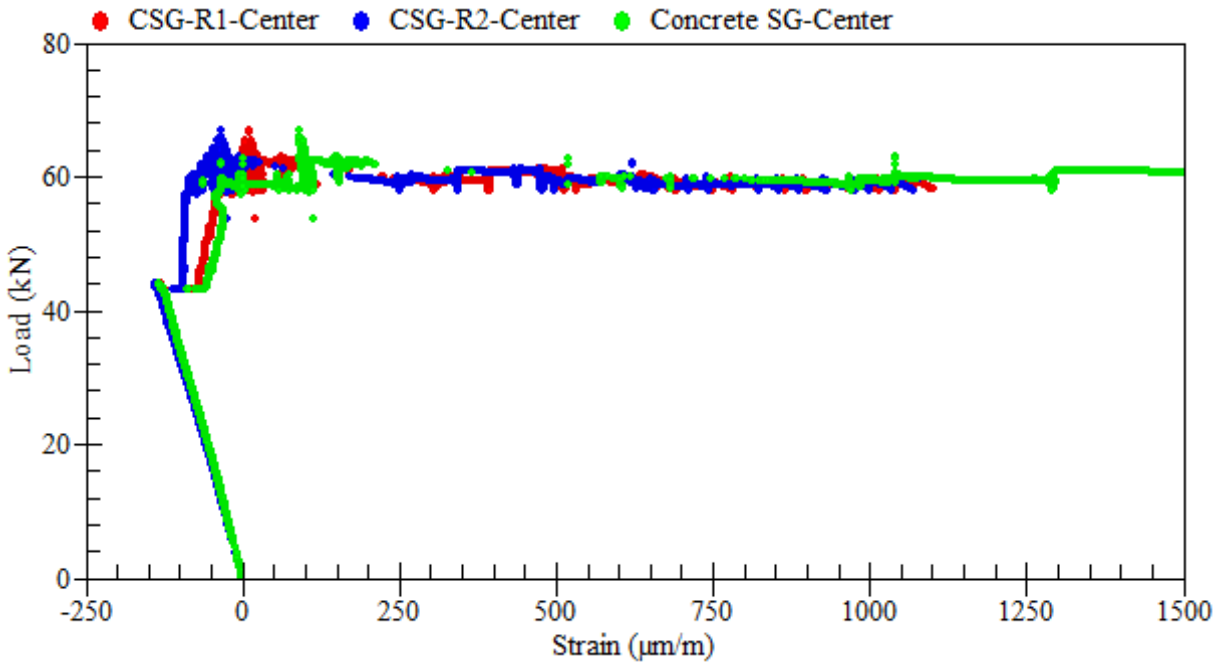

Figure A.29: Load-strain relationship of longitudinal compressive steel bars – beam SS-2.1

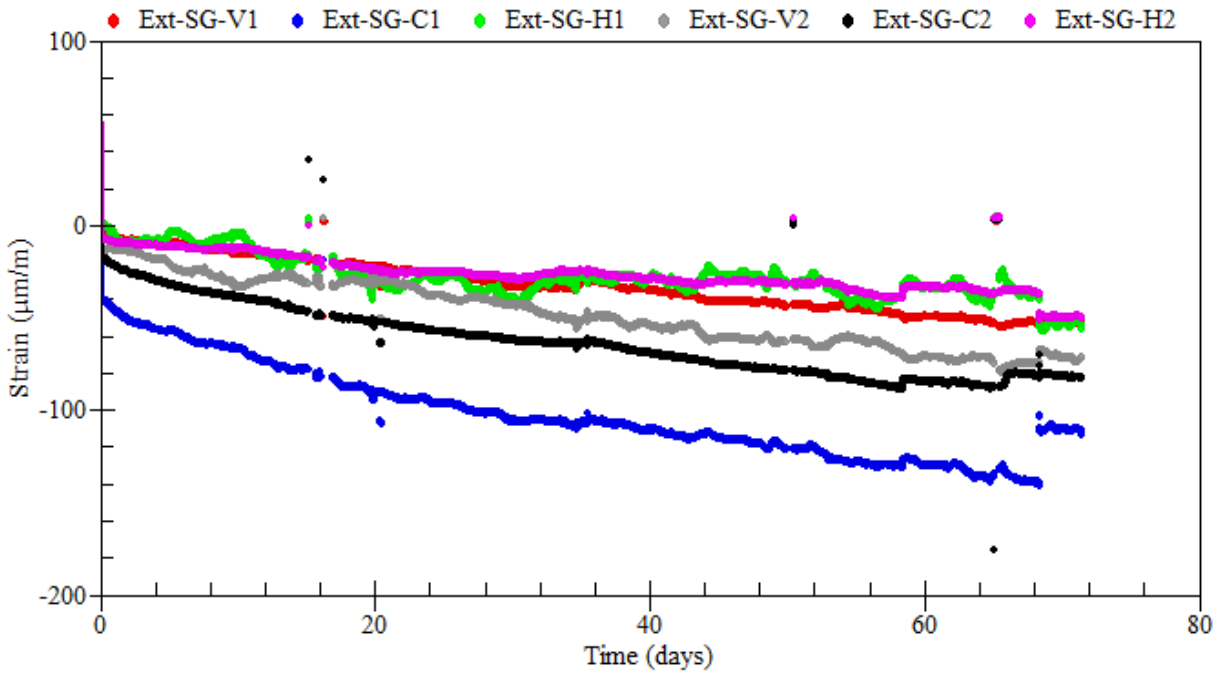

Figure A.30: Strain readings of external rosettes on sides – beam SS-2.1

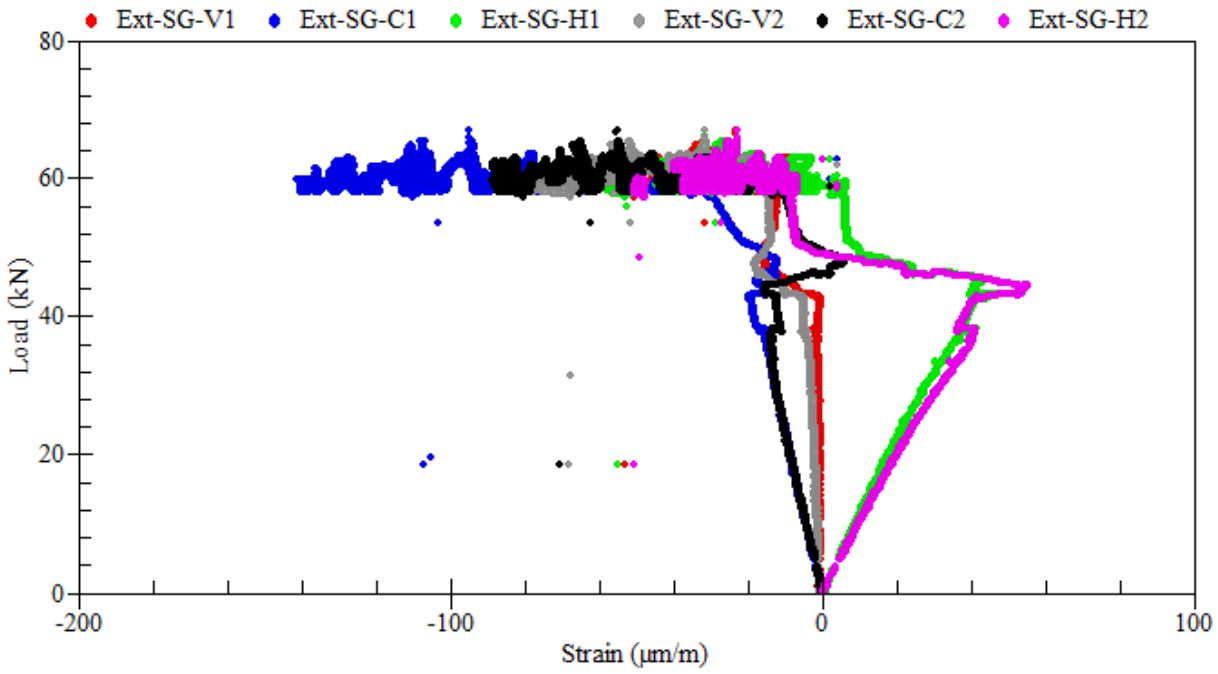

Figure A.31: Load-strain relationships of external rosettes on sides – beam SS-2.1

A.3 Beam SS-2.2

Beam SS-2.2 was tested under the coupled effects of reinforcement corrosion and service loads. The applied sustained load was equivalent to 60% of the beam ultimate load capacity (i.e., 60 kN). Reinforcement corrosion was accelerated using a current density of 100 μA/cm^2 over a duration of 35 days before increasing it to 300 μA/cm^2 up until the failure of the beam. The total duration of corrosion exposure was 82 days. The average mass loss of the beam was 18.7%. A summary of the gravimetric mass loss measurements of steel reinforcement is presented in Table A.2.

(a) during the test

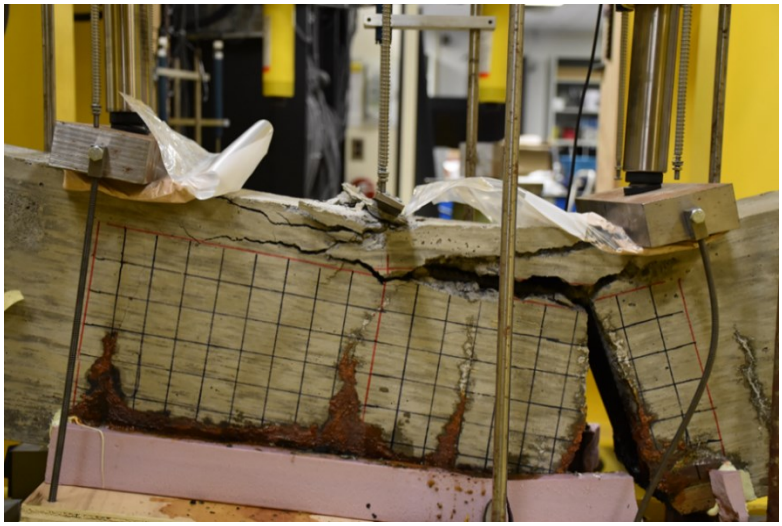

(b) at failue

Figure A.32: Crack propagation and patterns at failure – beam SS-2.2

Figure A.33: Corrosion-induced damage in the cover of concrete – beam SS-2.2

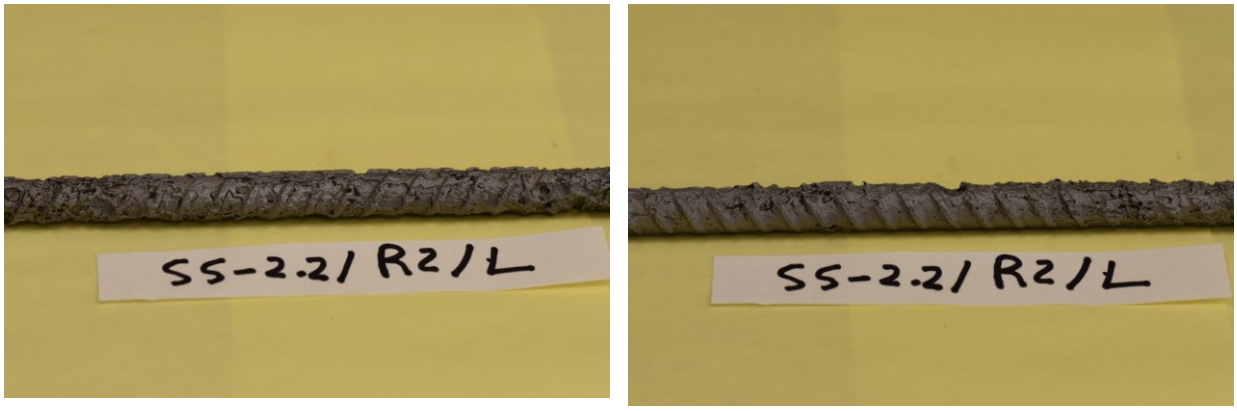

Figure A.34: Corrosion patterns on the clean surface of steel reinforcement – beam SS-2.2

Table A.2: Mass loss of corroded steel bars – beam SS-2.2

Rebar type	Rebar designation	Length (mm)	Mass (g)	Mass loss (%)
Control	R0	100.0	75.38	0.00
R1	R1-L	384.5	233.41	19.47
R2	R2-L	379.0	234.50	17.92

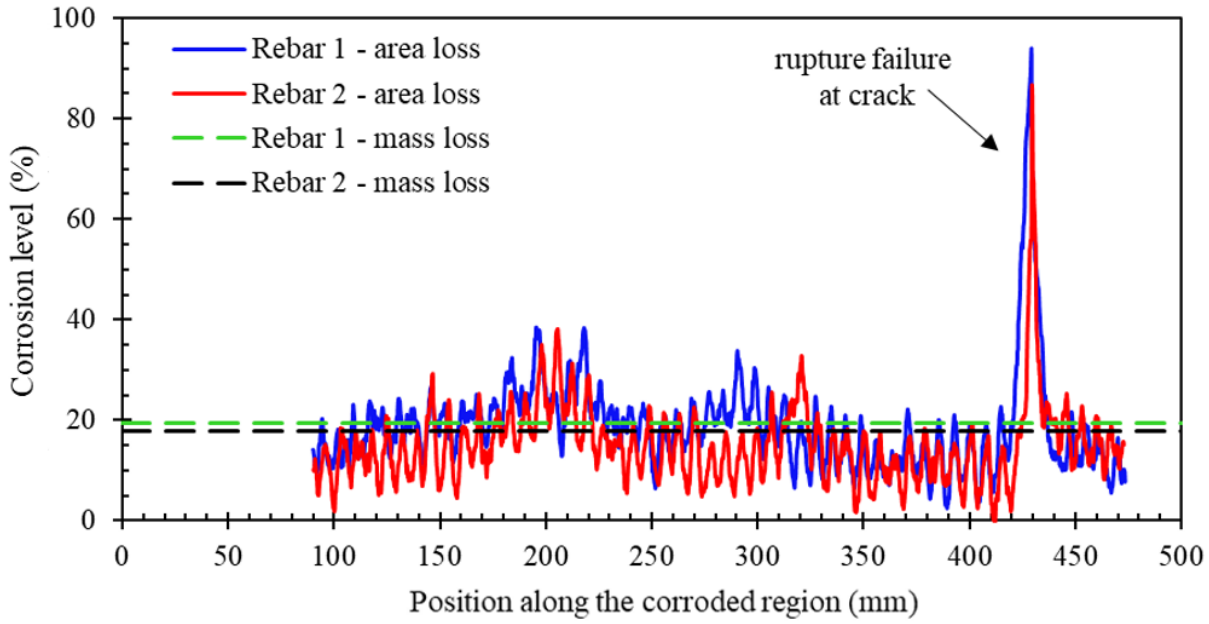

Figure A.35: Distribution of cross-sectional area loss along the corroded steel reinforcement – beam SS-2.2

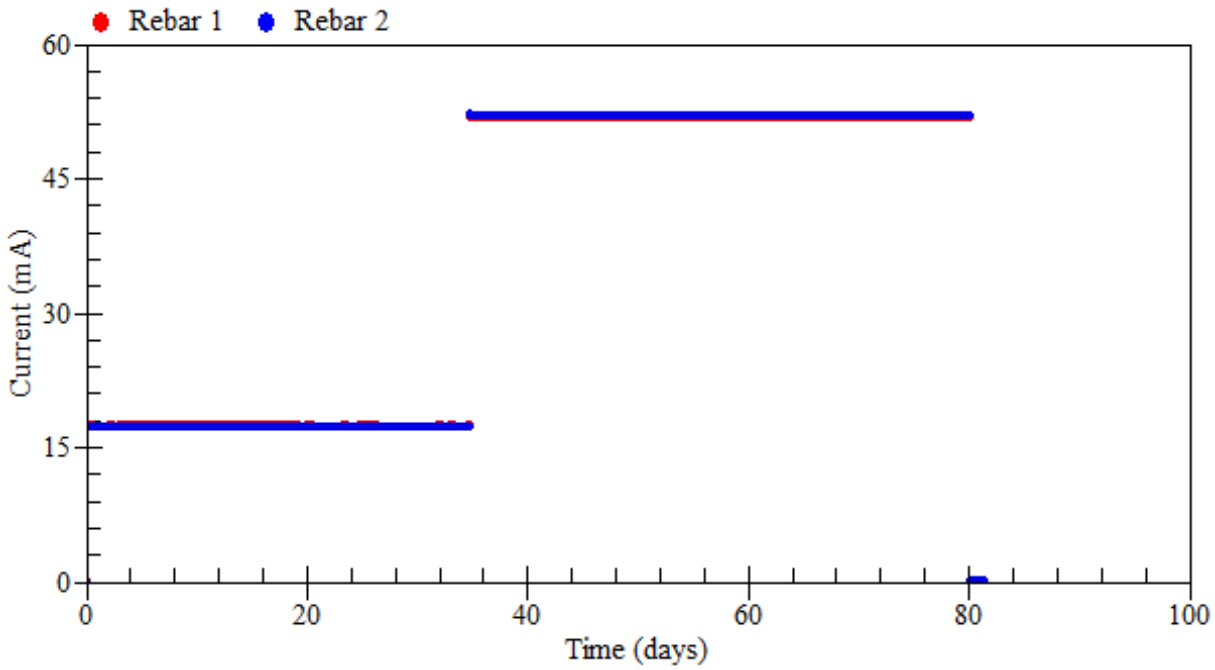

Figure A.36: Applied current – beam SS-2.2

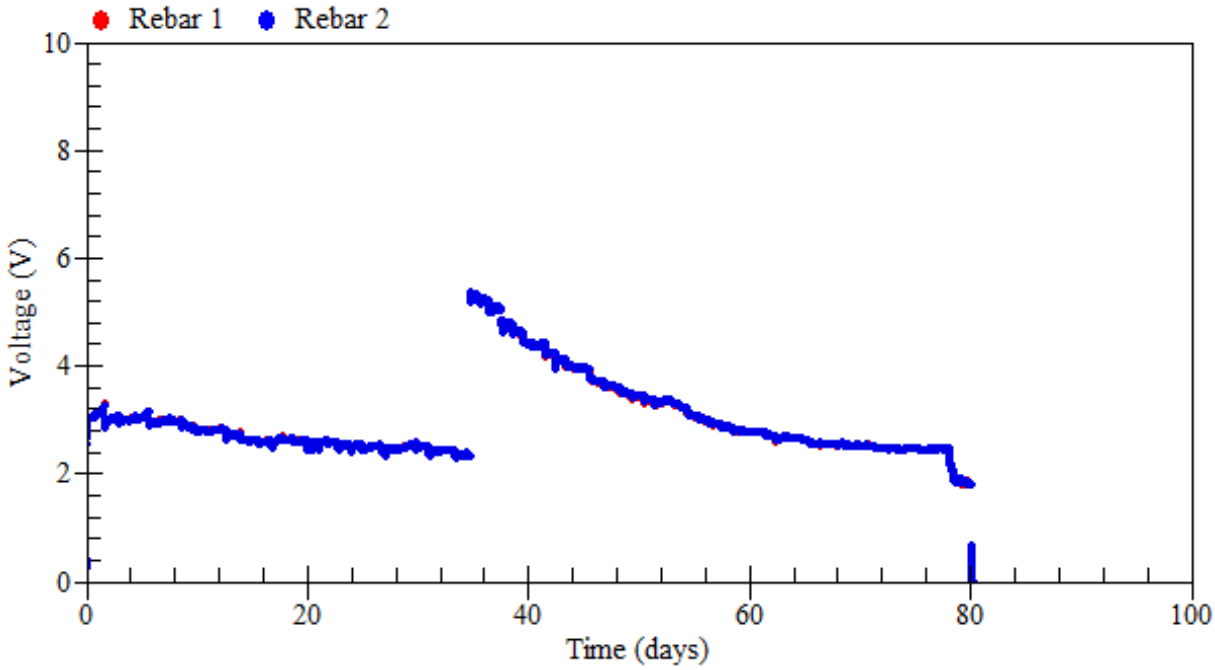

Figure A.37: Voltage measurements – beam SS-2.2

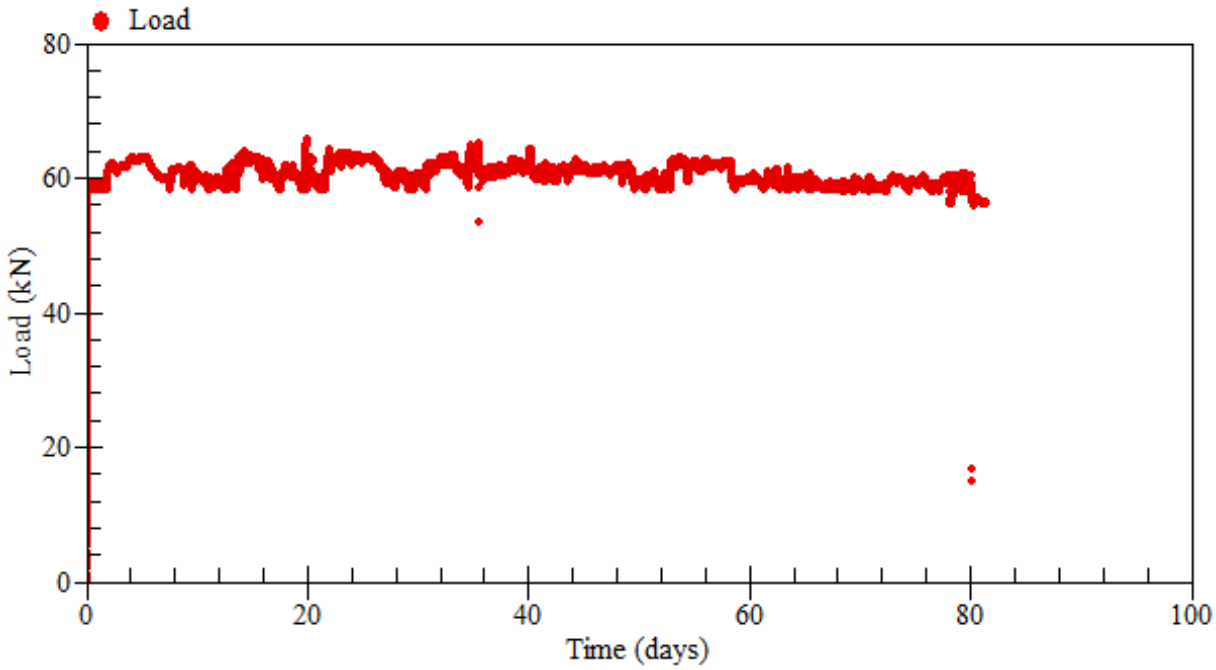

Figure A.38: Applied loads – beam SS-2.2

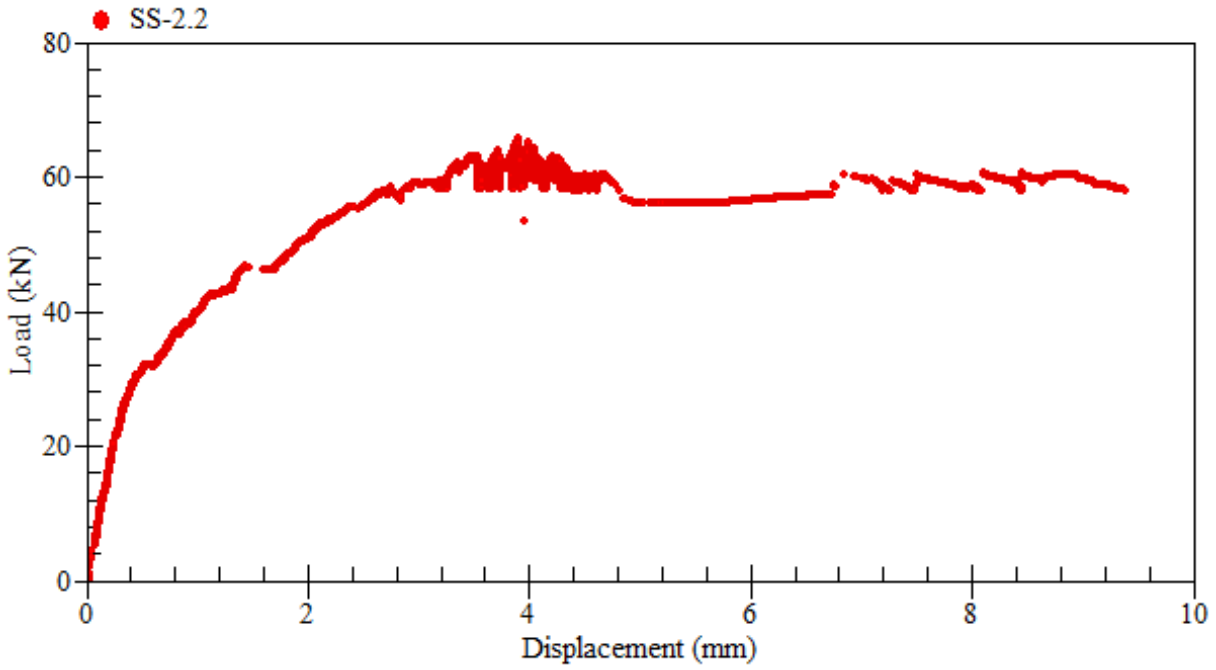

Figure A.39: Load-displacement relationship at mid-span – beam SS-2.2

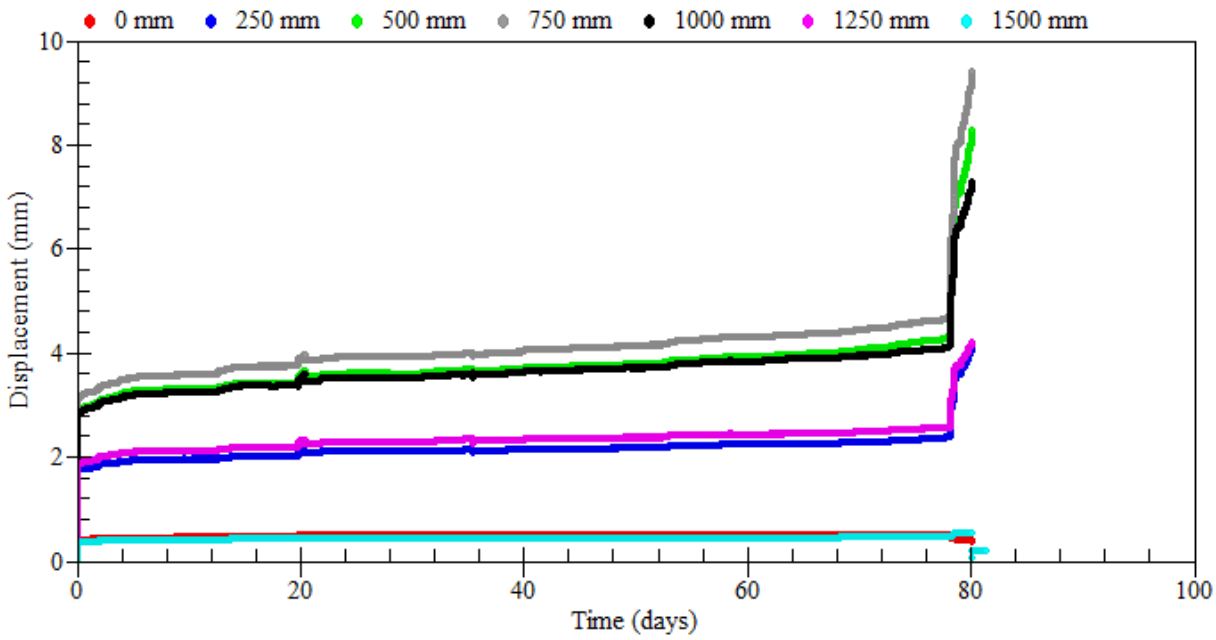

Figure A.40: **Displacement measurements – beam SS-2.2**

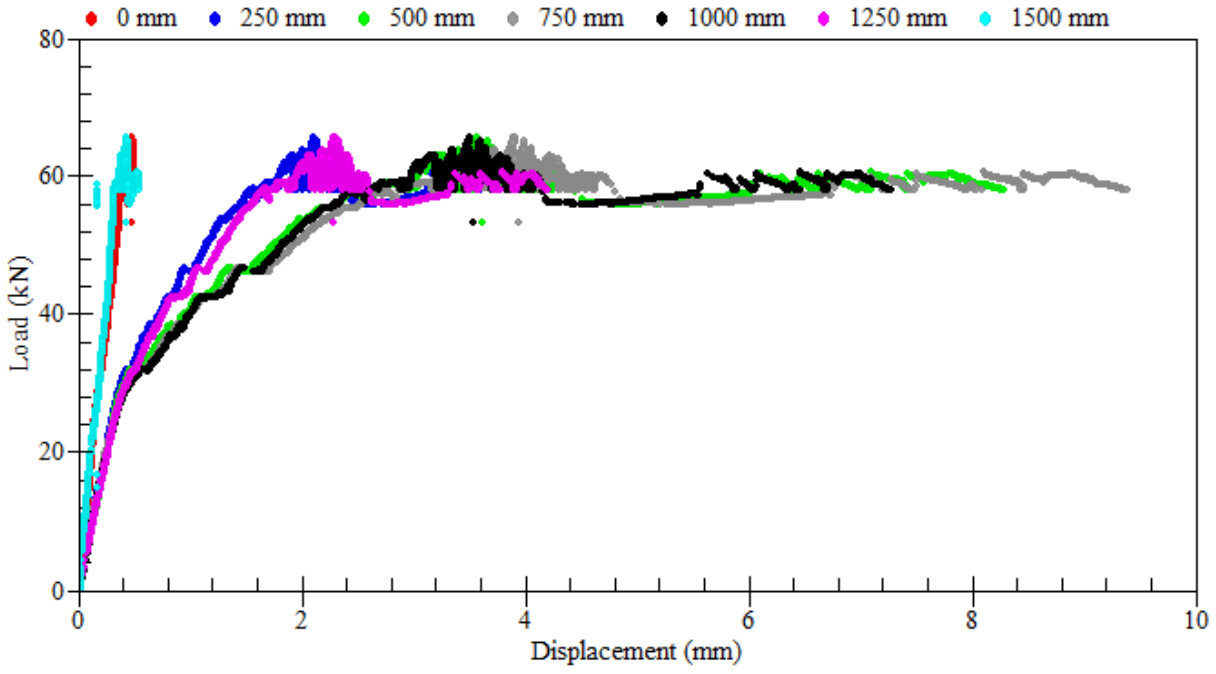

Figure A.41: **Load-displacement relationships at mid-span – beam SS-2.2**

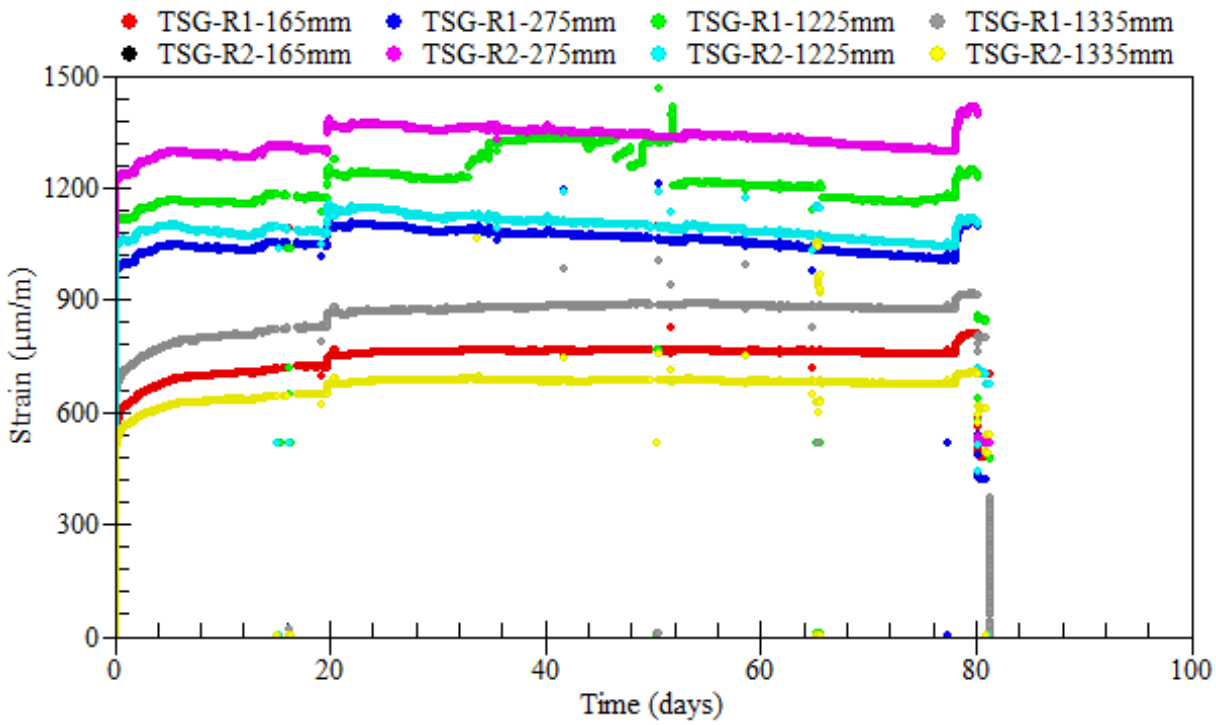

Figure A.42: Strain readings of longitudinal tensile steel bars – beam SS-2.2

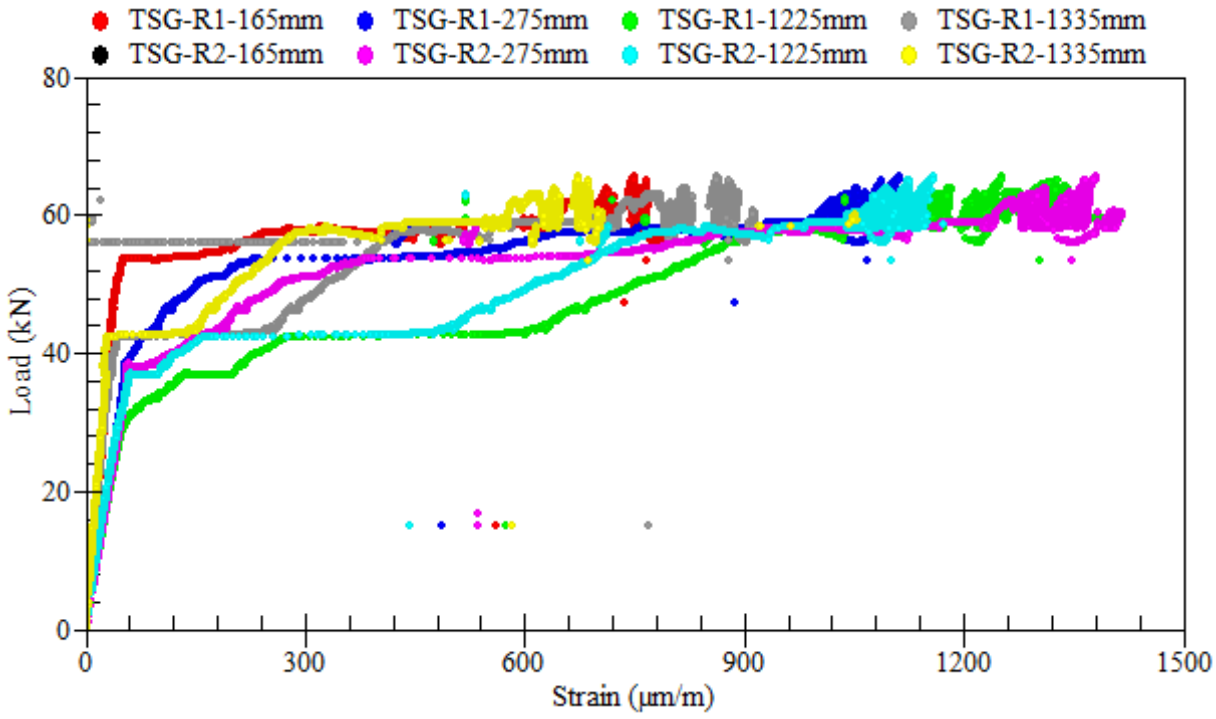

Figure A.43: Load-strain relationships of longitudinal tensile steel bars – beam SS-2.2

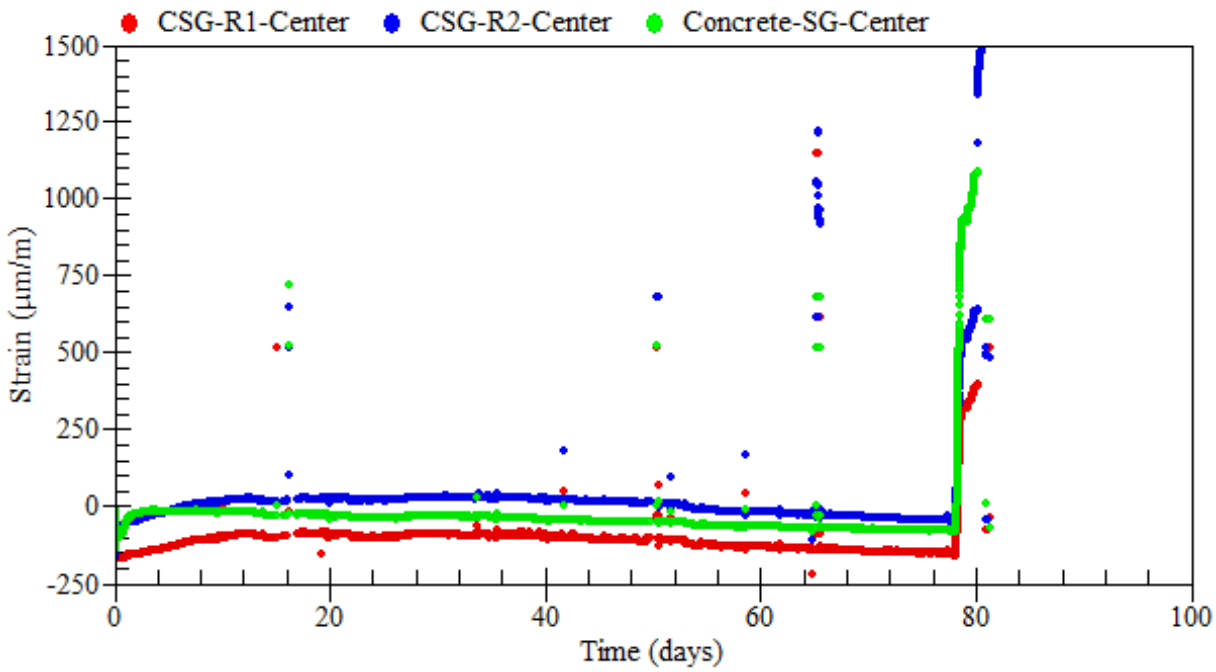

Figure A.44: Strain readings of longitudinal compressive steel bars – beam SS-2.2

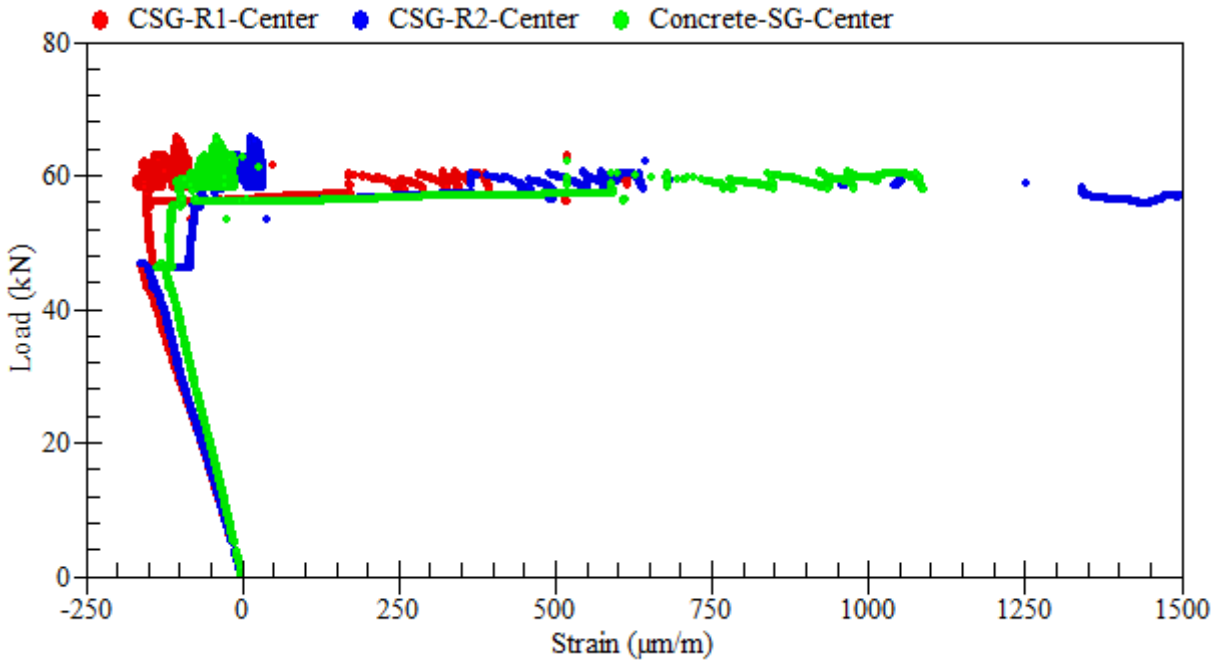

Figure A.45: Load-strain relationships of longitudinal compressive steel bars – beam SS-2.2

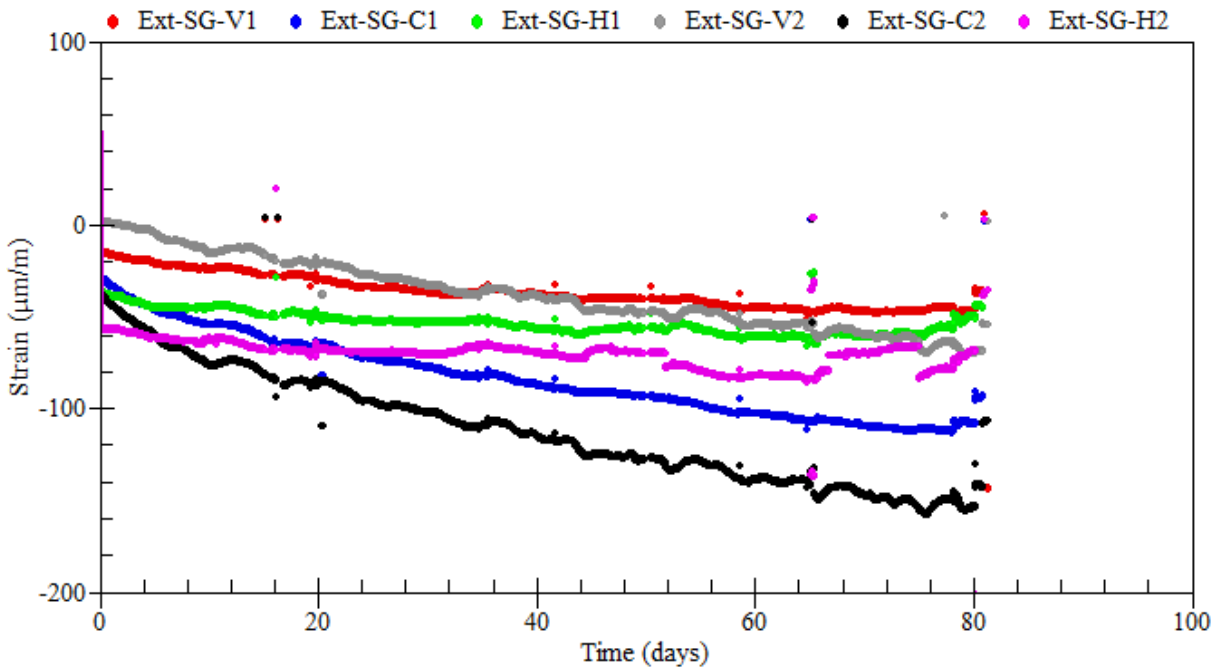

Figure A.46: Strain readings of external rosettes on sides – beam SS-2.2

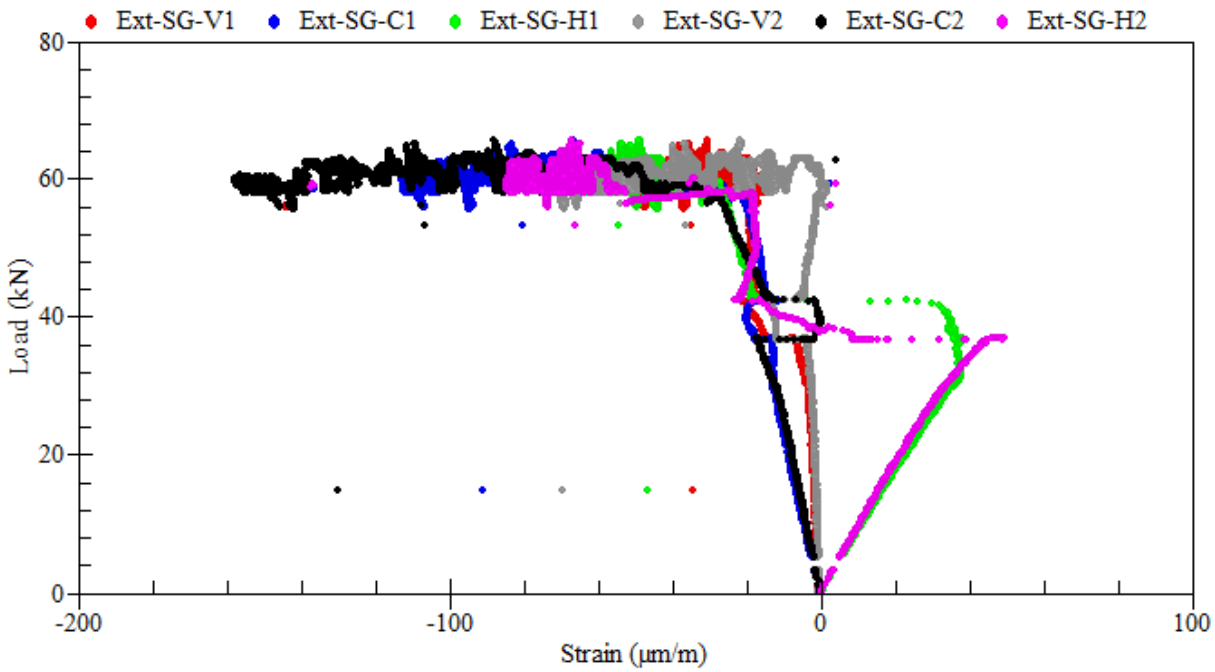

Figure A.47: Load-strain relationships of external rosettes on sides – beam SS-2.2

A.4 Beam SS-3.1

Beam SS-3.1 was tested under the coupled effects of reinforcement corrosion and service loads. The applied sustained load was equivalent to 60% of the beam ultimate load capacity (i.e., 60 kN). Reinforcement corrosion was accelerated using a current density of 300 $\mu A/cm^2$ up until the failure of the beam. The total duration of corrosion exposure was 37 days. The average mass loss of the beam was 12.9%. A summary of the gravimetric mass loss measurements of steel reinforcement is presented in Table A.3.

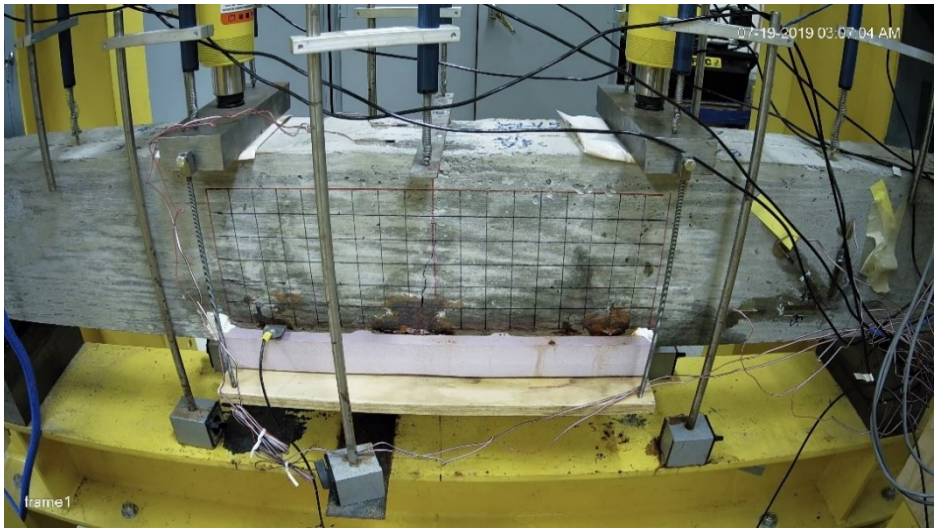

(a) during the test

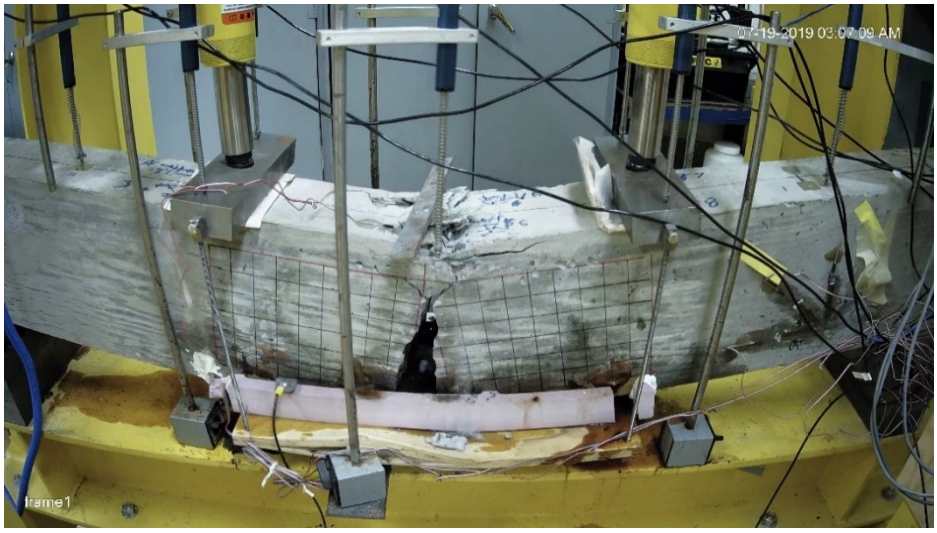

(b) at failure

Figure A.48: Crack propagation and patterns at failure – beam SS-3.1

Figure A.49: Corrosion-induced damage in the cover of concrete – beam SS-3.1

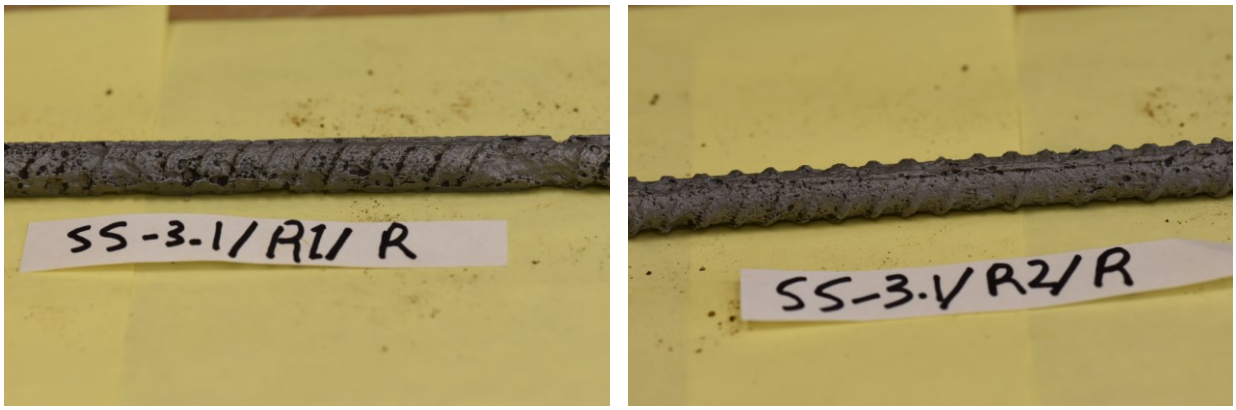

Figure A.50: Corrosion patterns on the clean surface of steel reinforcement – beam SS-3.1

Table A.3: Mass loss of corroded steel bars – beam SS-3.1

Rebar type	Rebar designation	Length (mm)	Mass (g)	Mass loss (%)	Rebar mass loss (%)
Control	R0	100.0	75.38	0.00	0.00
R1	R1-R	270	176.72	13.17	11.96
	R1-L	191	129.23	10.24	
R2	R2-R	268	174.2	13.77	13.84
	R2-L	199.5	129.43	13.93	

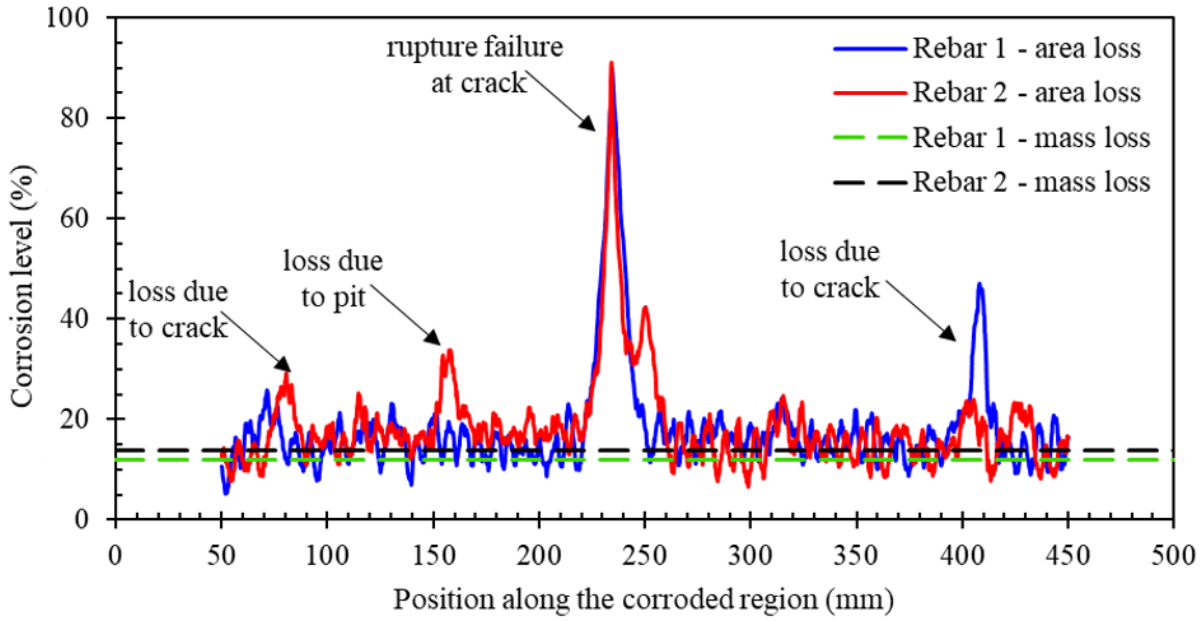

Figure A.51: Distribution of cross-sectional area loss along the corroded steel reinforcement – beam SS-3.1

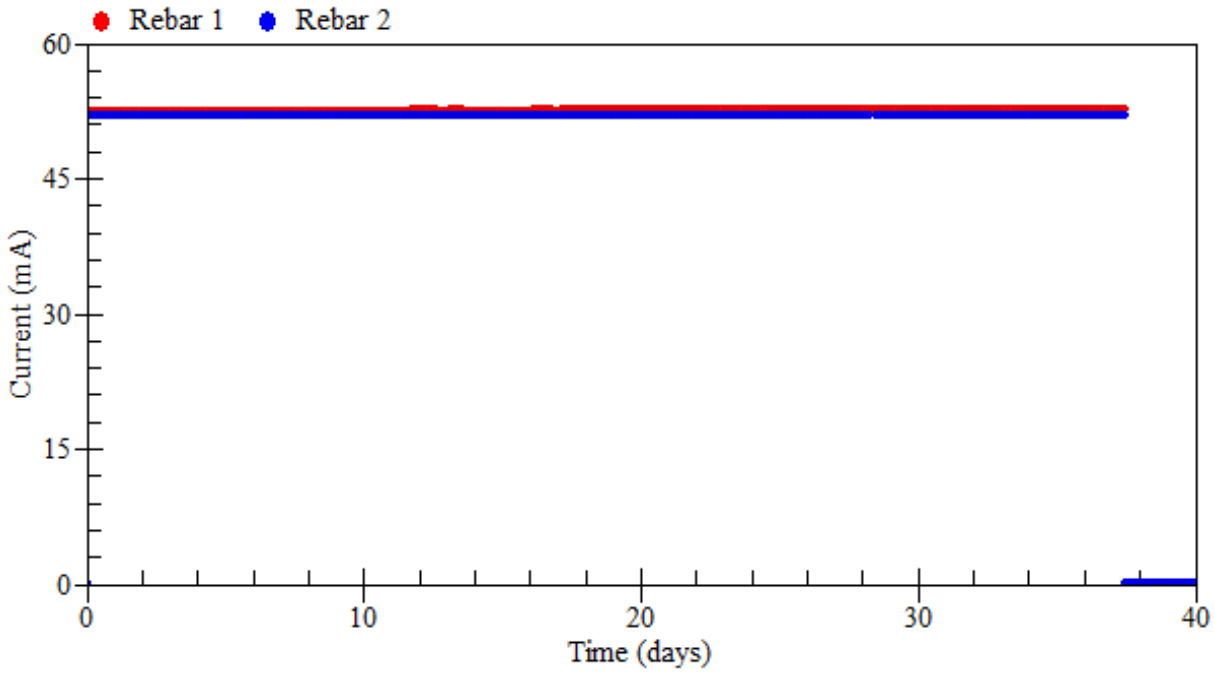

Figure A.52: Applied current – beam SS-3.1

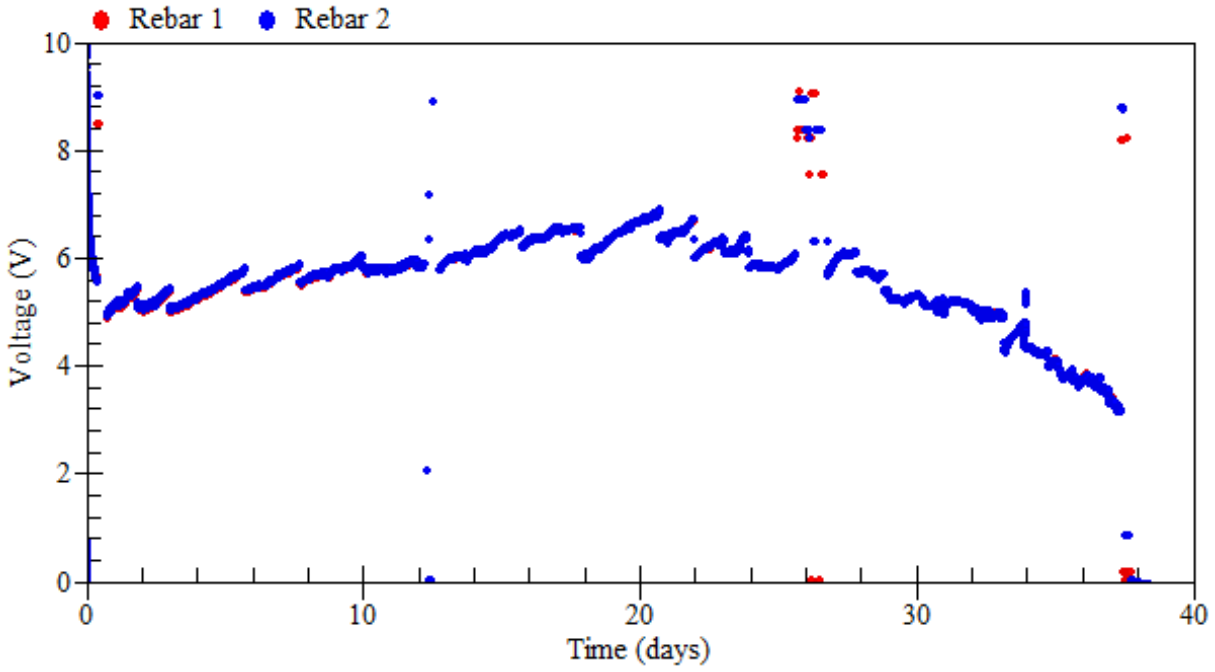

Figure A.53: Voltage measurements – beam SS-3.1

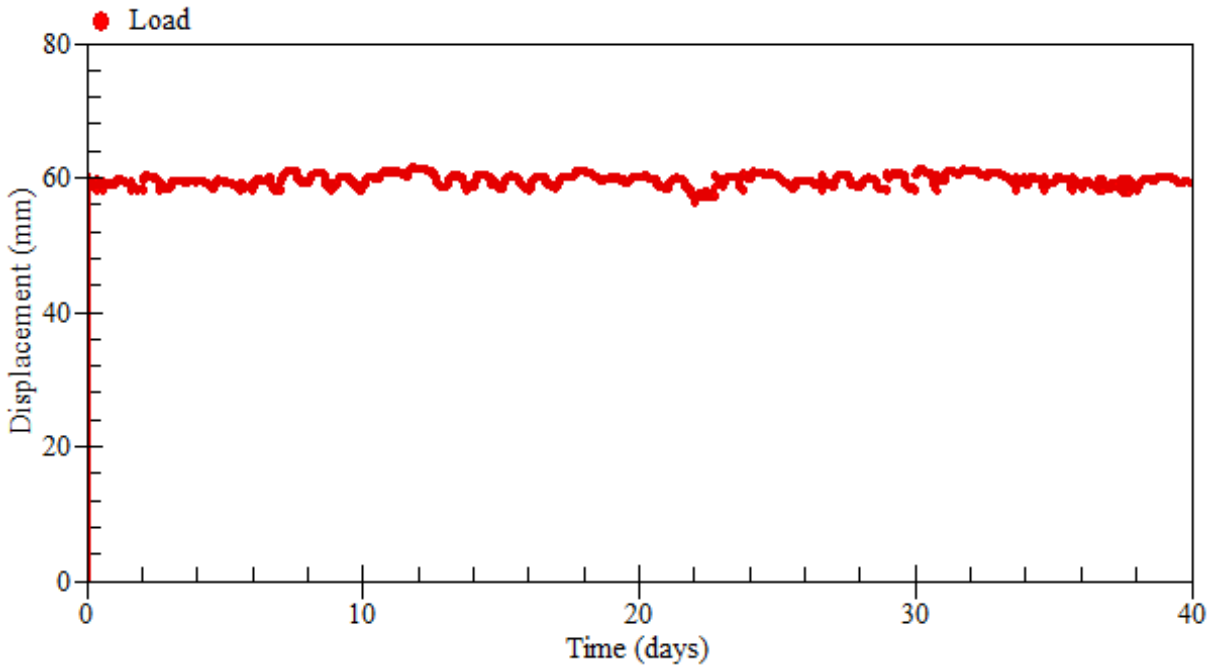

Figure A.54: Applied loads – beam SS-3.1

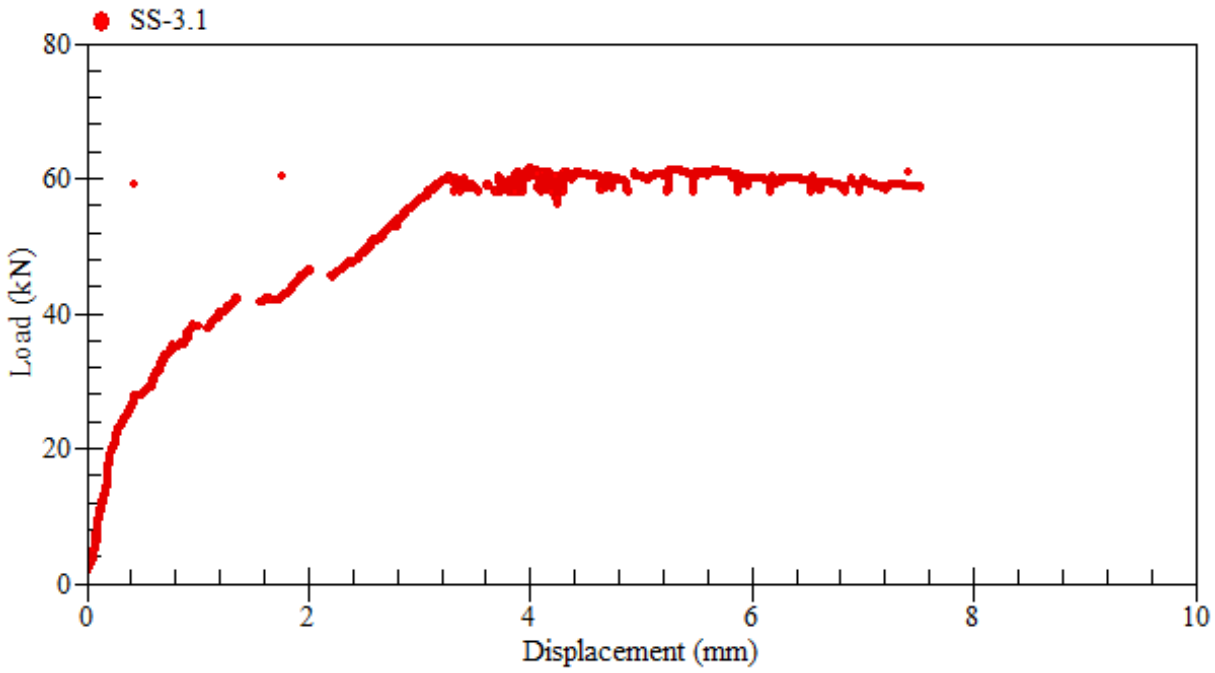

Figure A.55: Load-displacement relationship at mid-span – beam SS-3.1

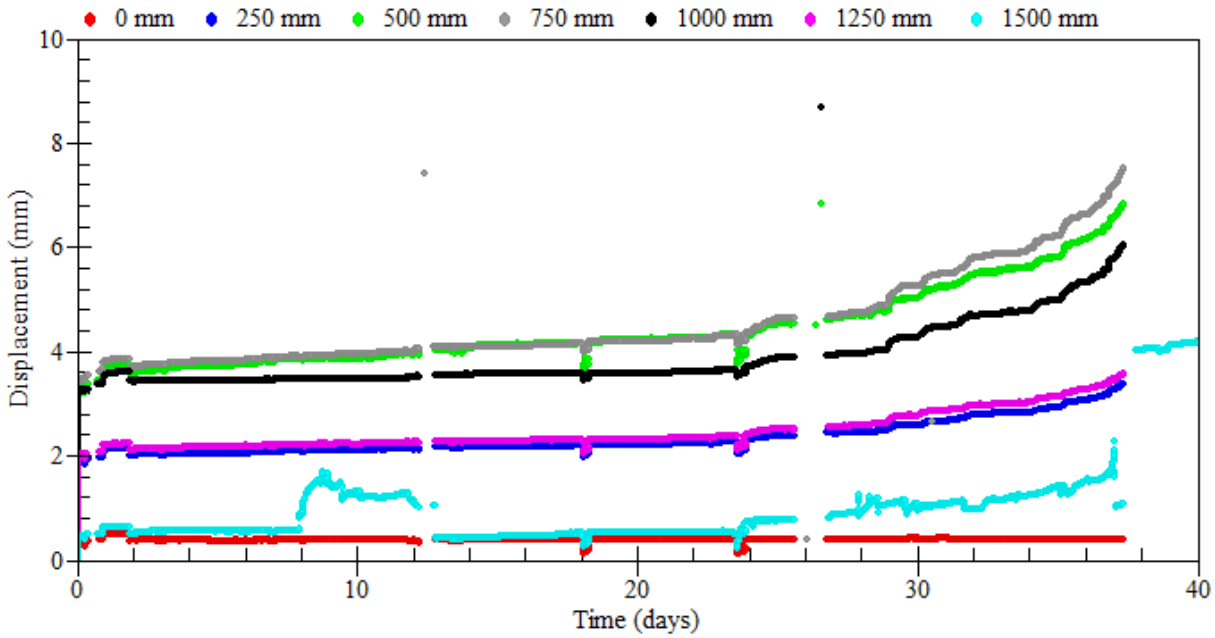

Figure A.56: Displacement measurements – beam SS-3.1

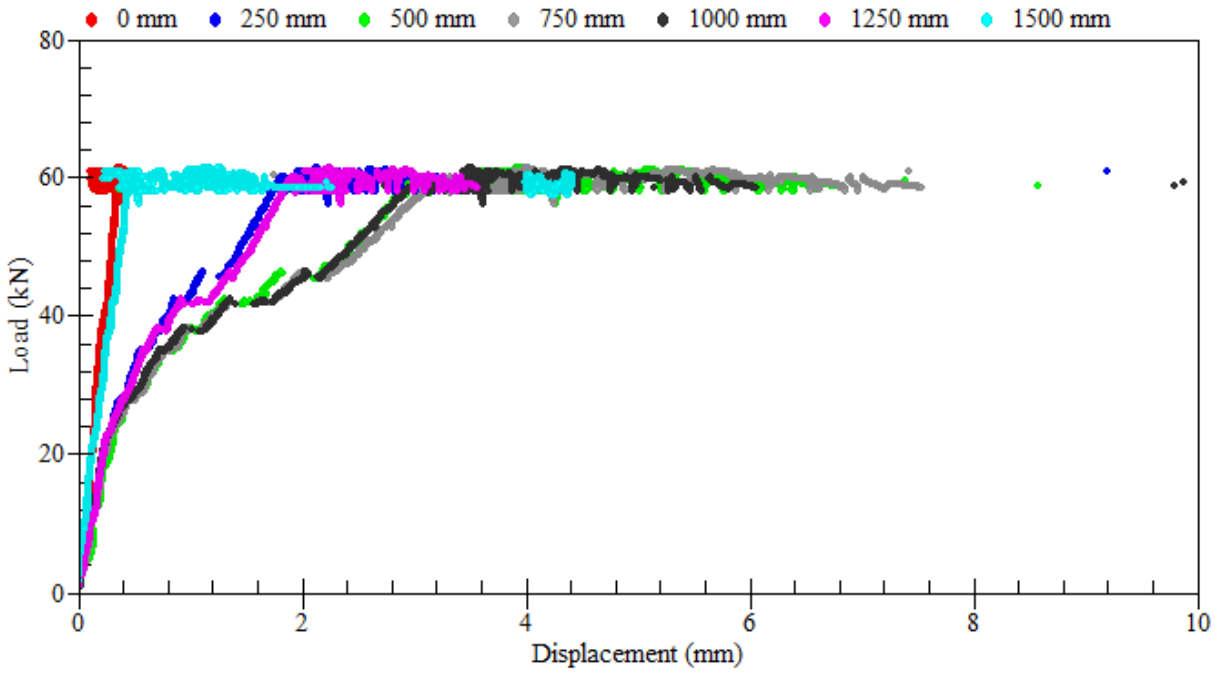

Figure A.57: Load-displacement relationships – beam SS-3.1

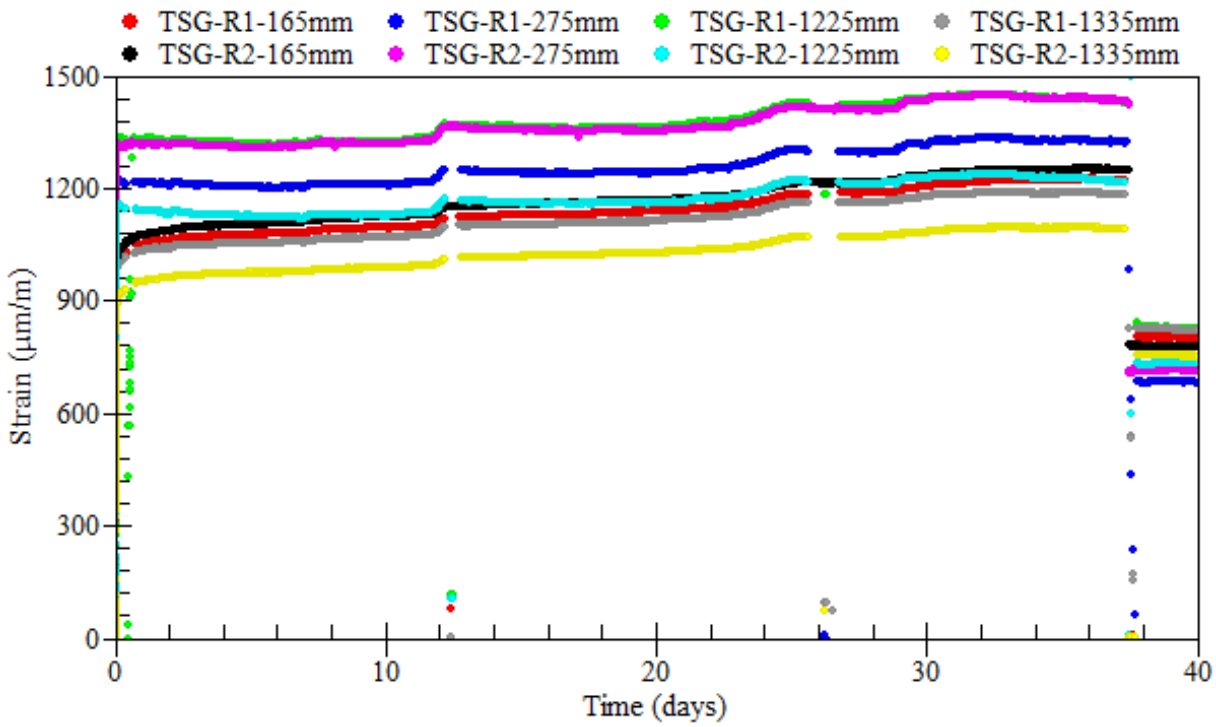

Figure A.58: Strain readings of longitudinal tensile steel bars – beam SS-3.1

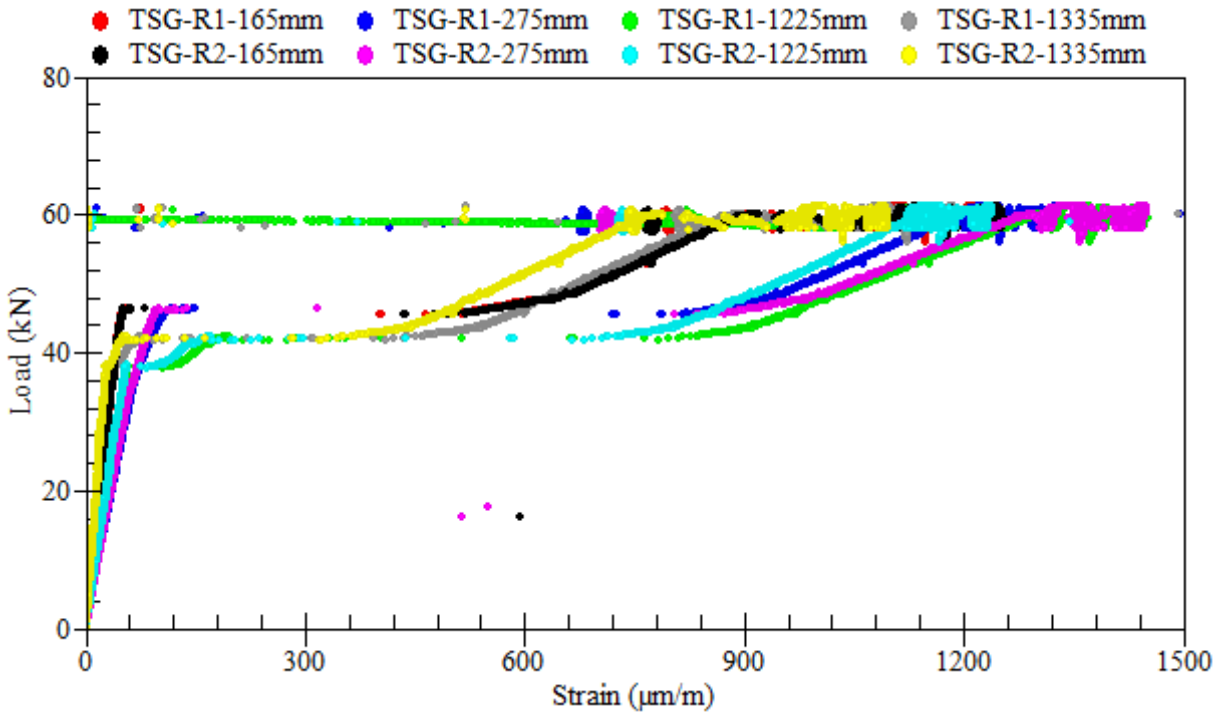

Figure A.59: Load-strain relationships of longitudinal tensile steel bars – beam SS-3.1

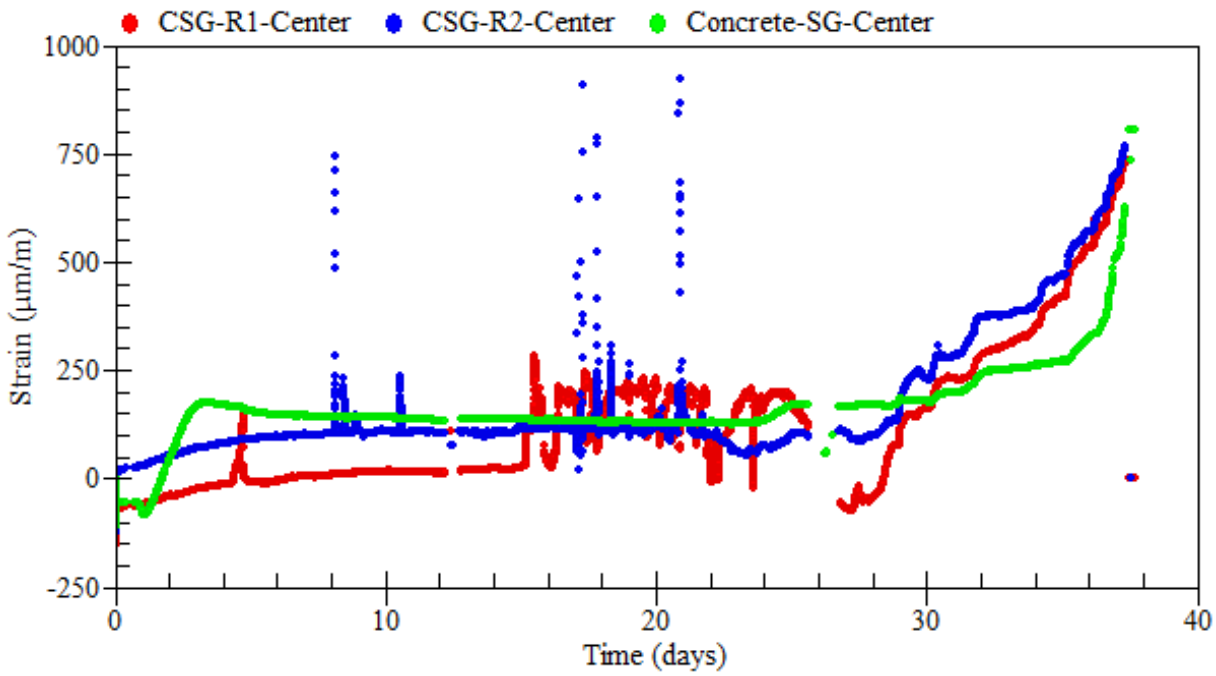

Figure A.60: Strain readings of longitudinal compressive steel bars – beam SS-3.1

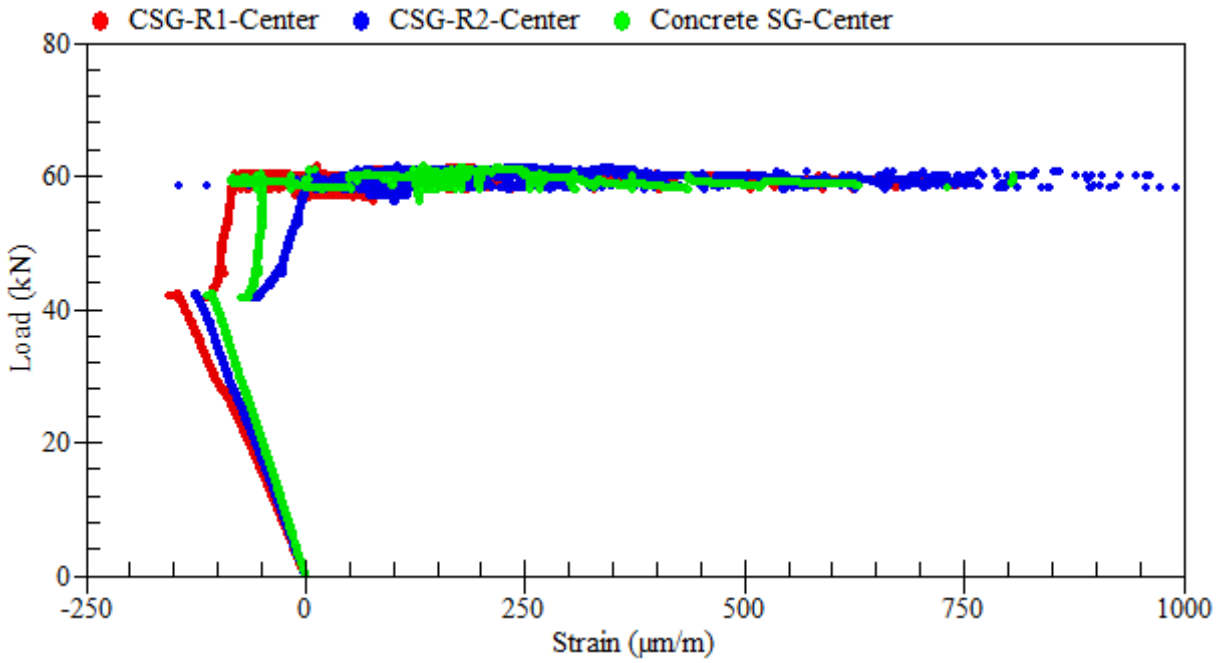

Figure A.61: Load-strain relationships of longitudinal compressive steel bars – beam SS-3.1

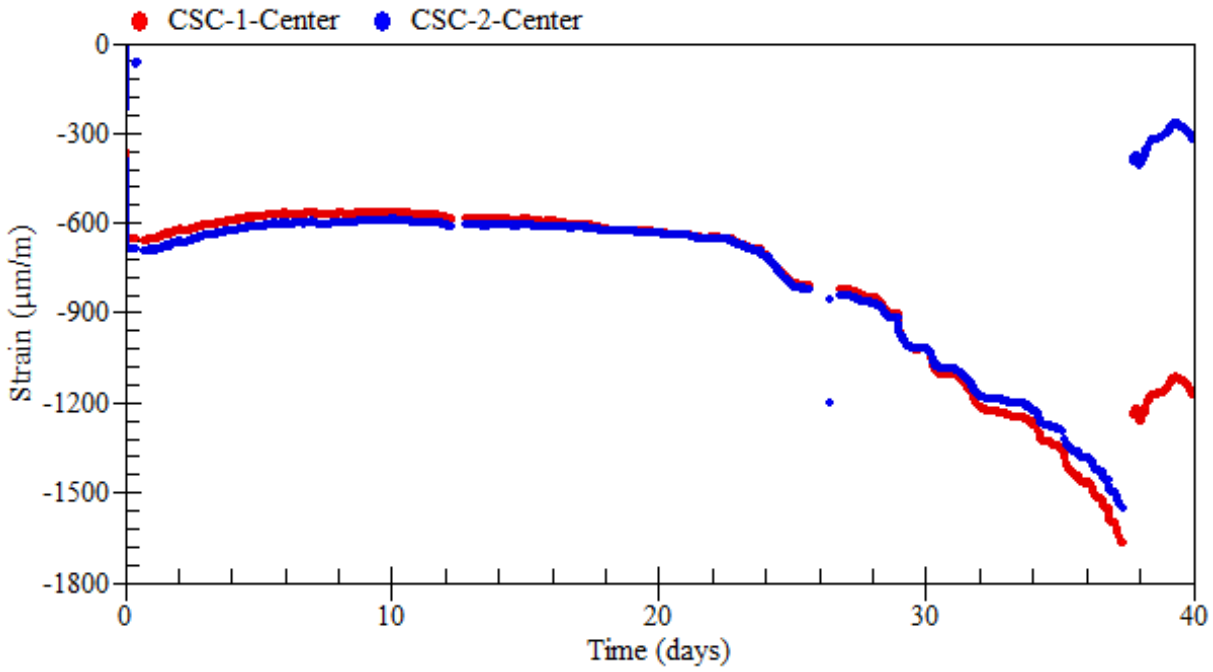

Figure A.62: Strain readings of external rosettes on top – beam SS-3.1

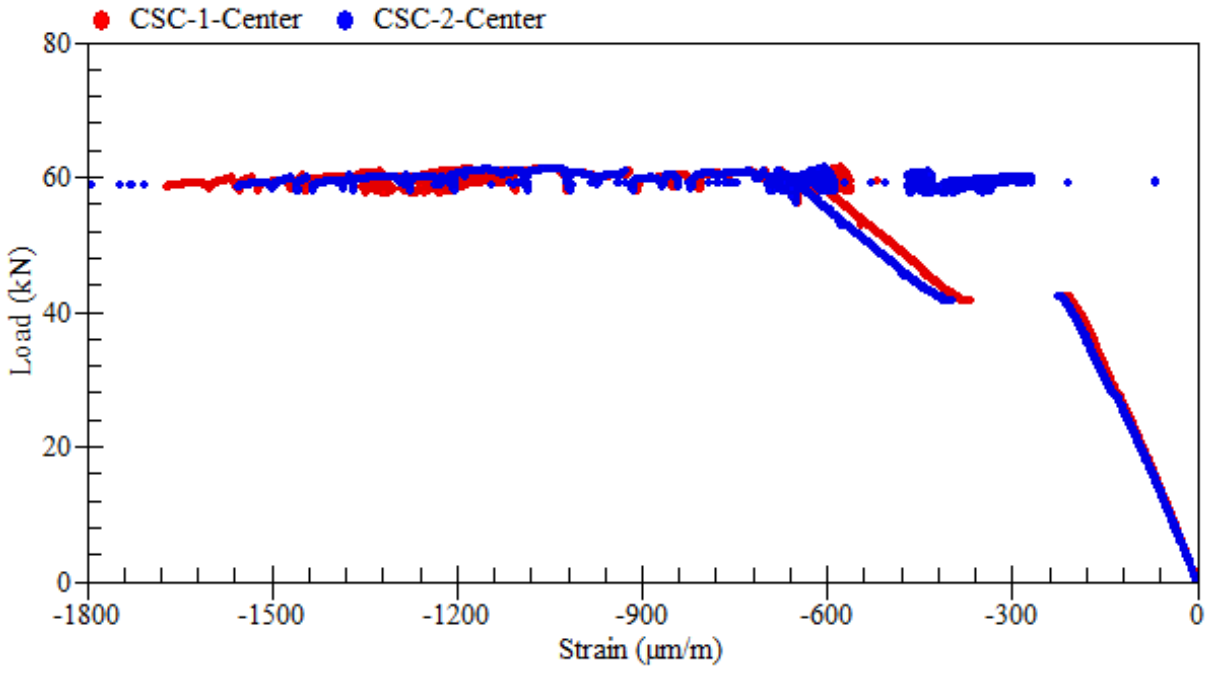

Figure A.63: Load-strain relationships of external rosettes on top – beam SS-3.1

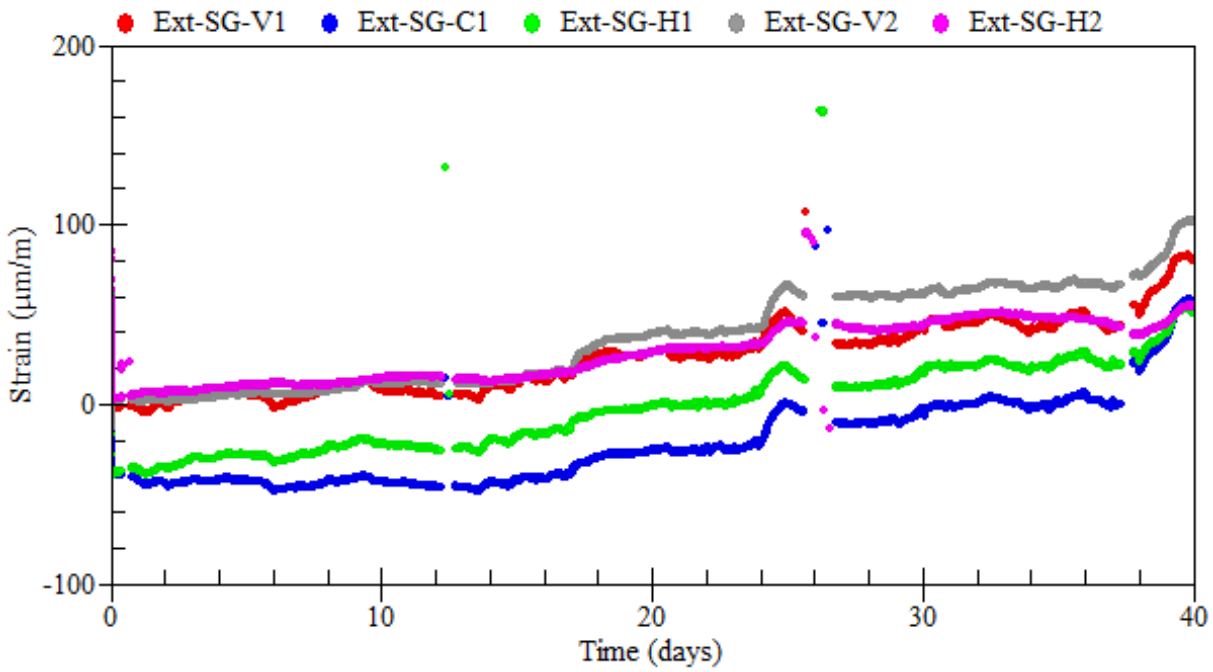

Figure A.64: Strain readings of external rosettes on sides – beam SS-3.1

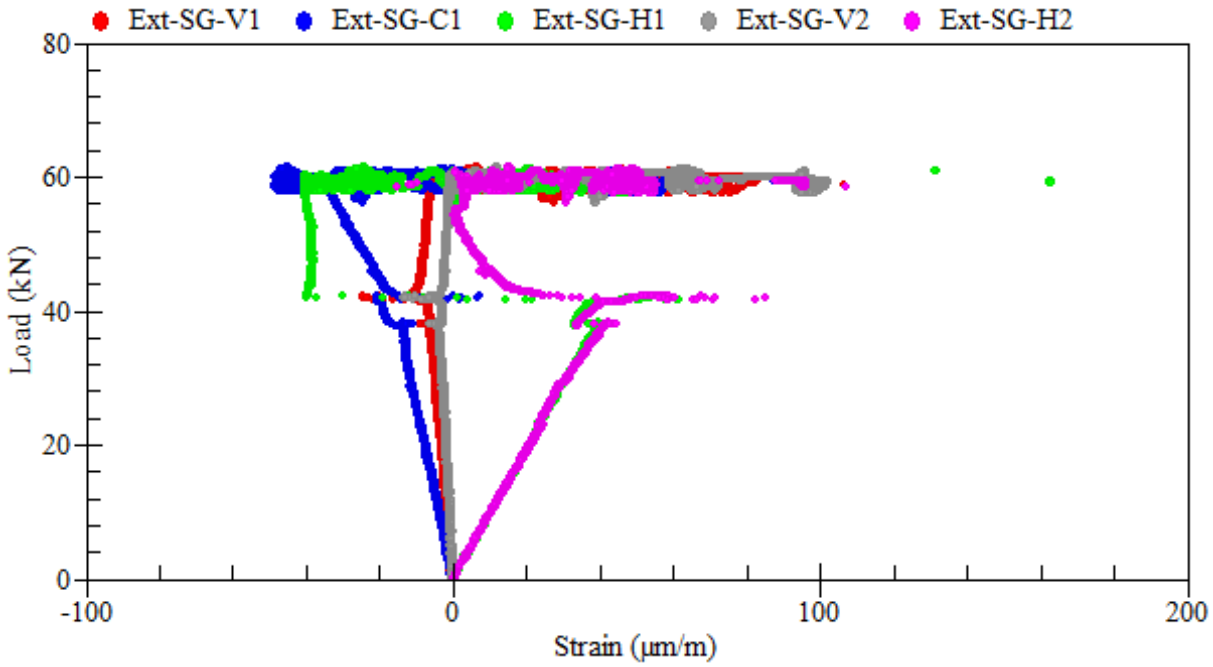

Figure A.65: Load-strain relationships of external rosettes on sides – beam SS-3.1

A.6 Beam SS-3.2

Beam SS-3.2 was tested under the coupled effects of reinforcement corrosion and service loads. The applied sustained load was equivalent to 60% of the beam ultimate load capacity (i.e., 60 kN). Reinforcement corrosion was accelerated using a current density of 300 μA/cm^2 up until the failure of the beam. The total duration of corrosion exposure was 52 days. The average mass loss of the beam was 19.0%. A summary of the gravimetric mass loss measurements of steel reinforcement is presented in Table A.4.

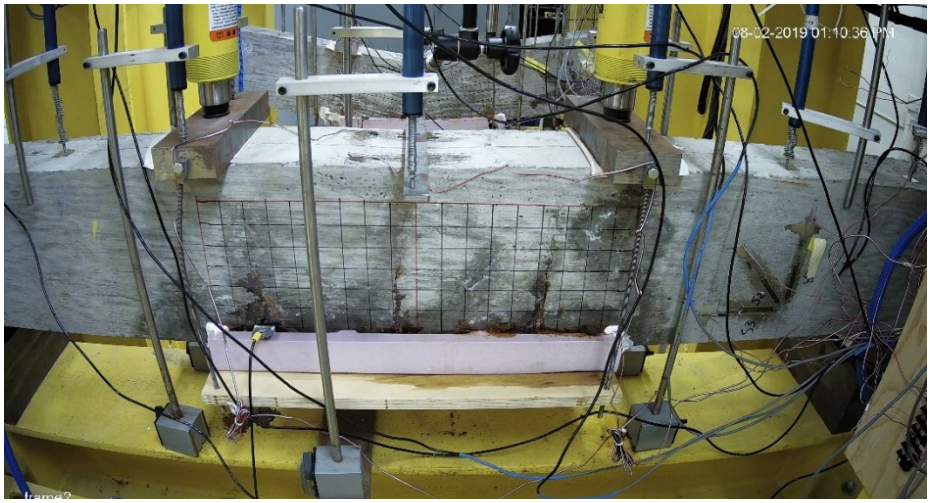

(a) during the test

(b) at failure

Figure A.66: Crack propagation and patterns at failure – beam SS-3.2

Figure A.67: Corrosion-induced damage in the cover of concrete – beam SS-3.2

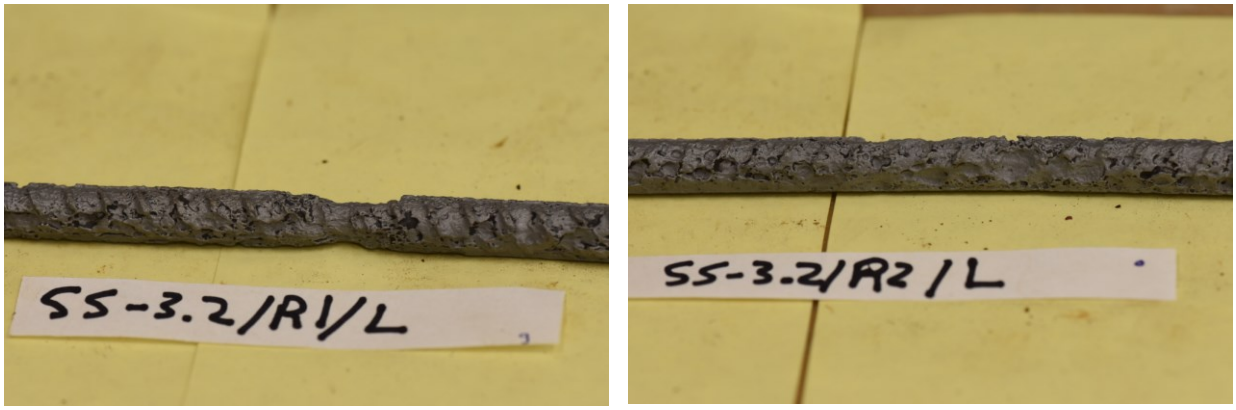

Figure A.68: Corrosion patterns on the clean surface of steel reinforcement – beam SS-3.2

Table A.4: Mass loss of corroded steel bars – beam SS-3.2

Rebar type	Rebar designation	Length (mm)	Mass (g)	Mass loss (%)
Control	R0	100.0	75.38	0.00
R1	R1-L	389.0	241.58	17.61
R2	R2-L	382.5	229.66	20.35

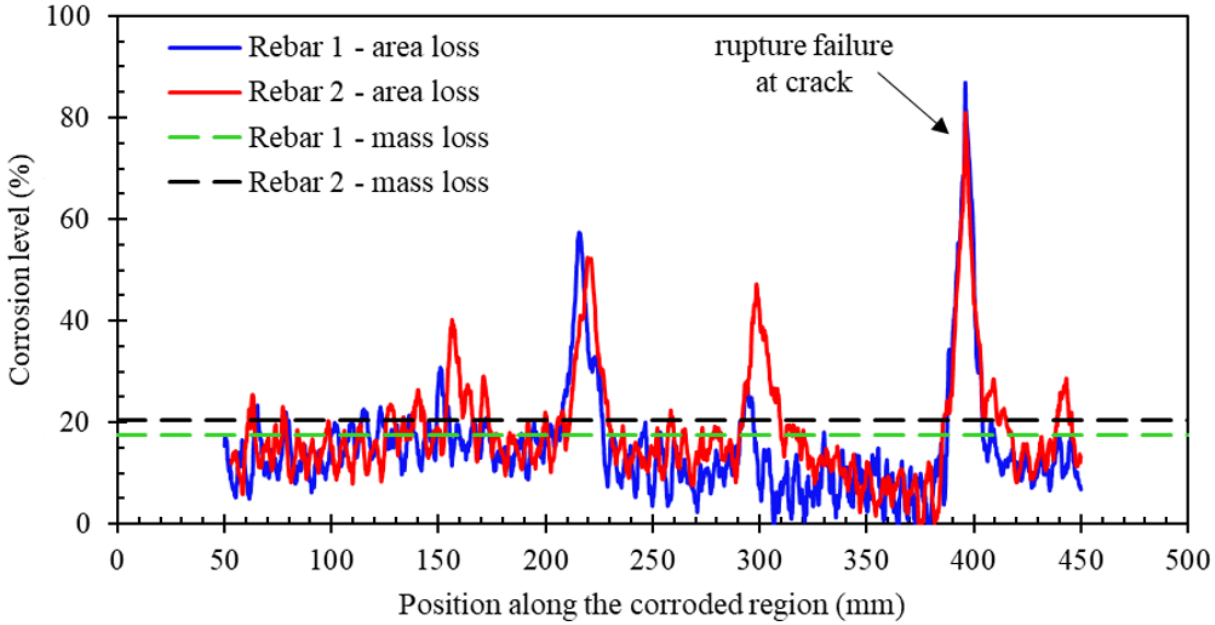

Figure A.69: Distribution of cross-sectional area loss along the corroded steel reinforcement – beam SS-3.2

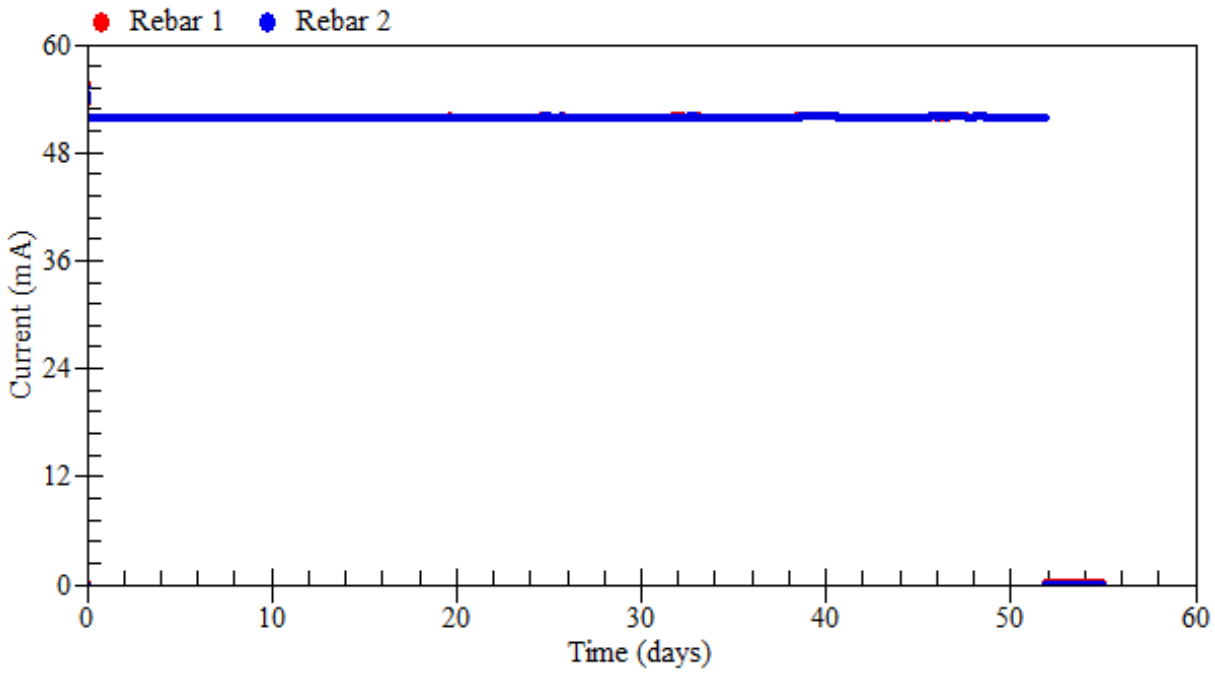

Figure A.70: Applied current – beam SS-3.2

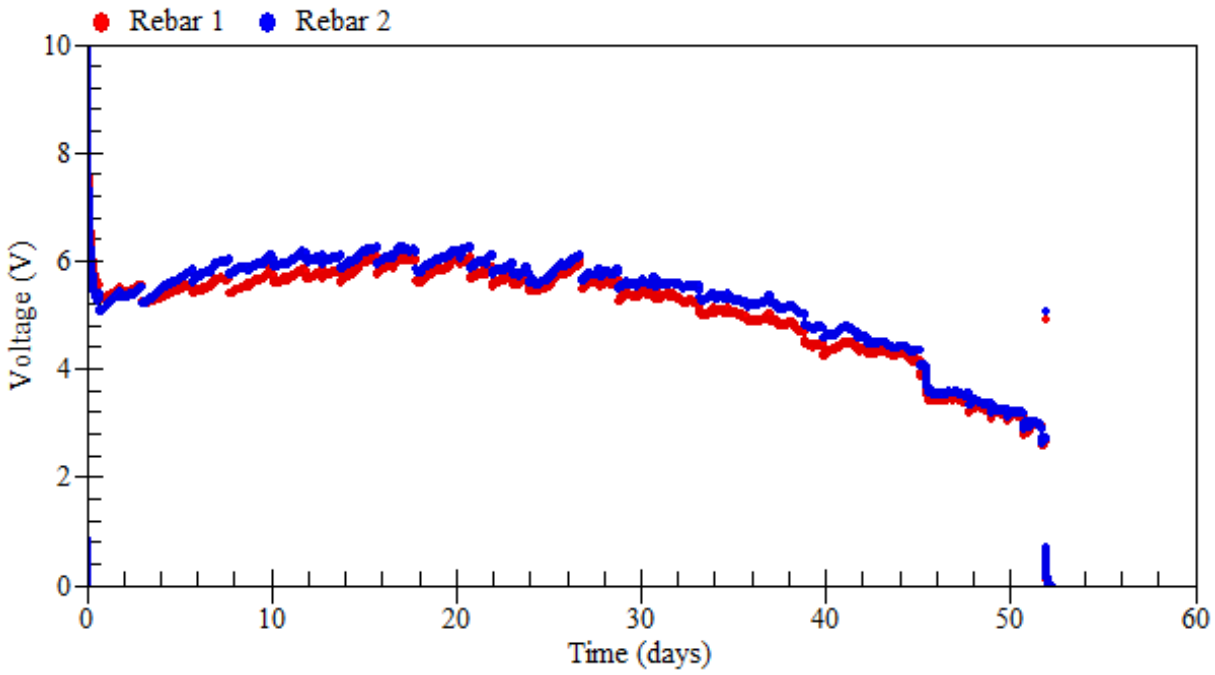

Figure A.71: Voltage measurements – beam SS-3.2

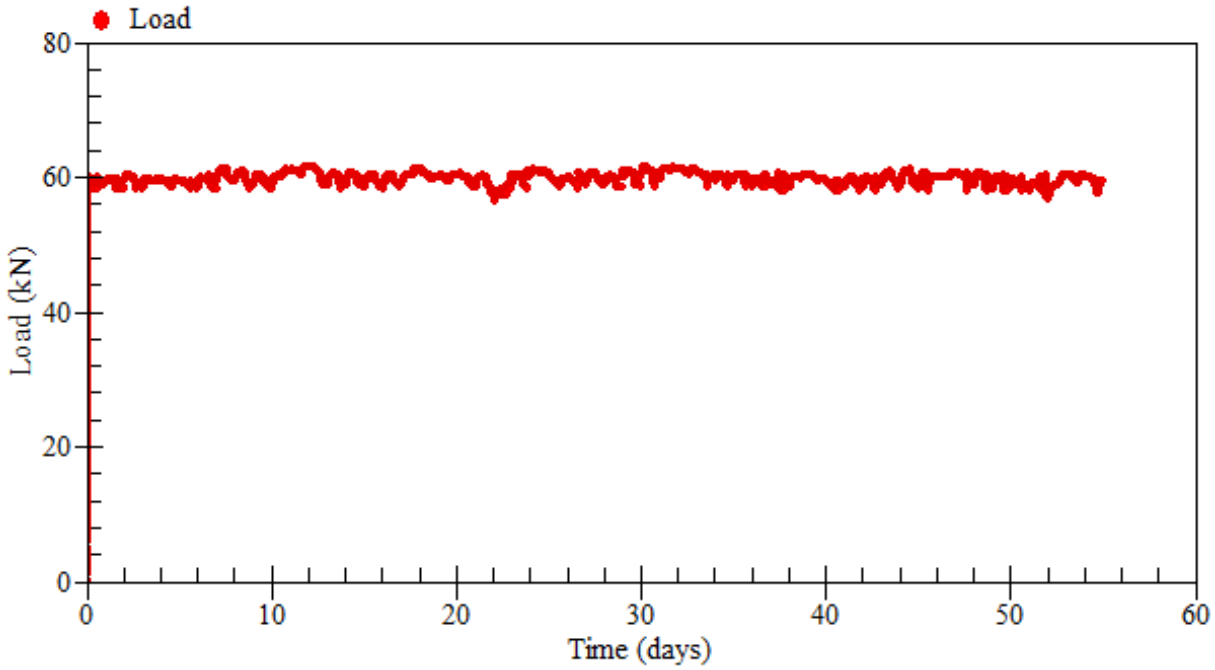

Figure A.72: Applied loads – beam SS-3.2

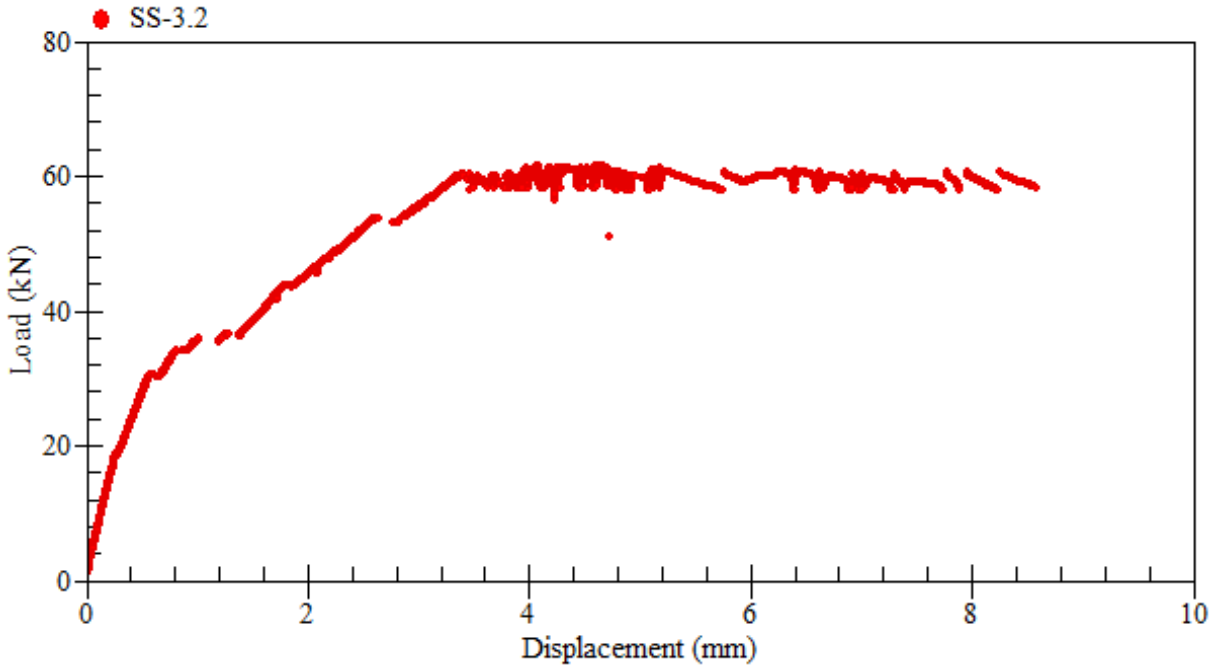

Figure A.73: Load-displacement relationship at mid-span – beam SS-3.2

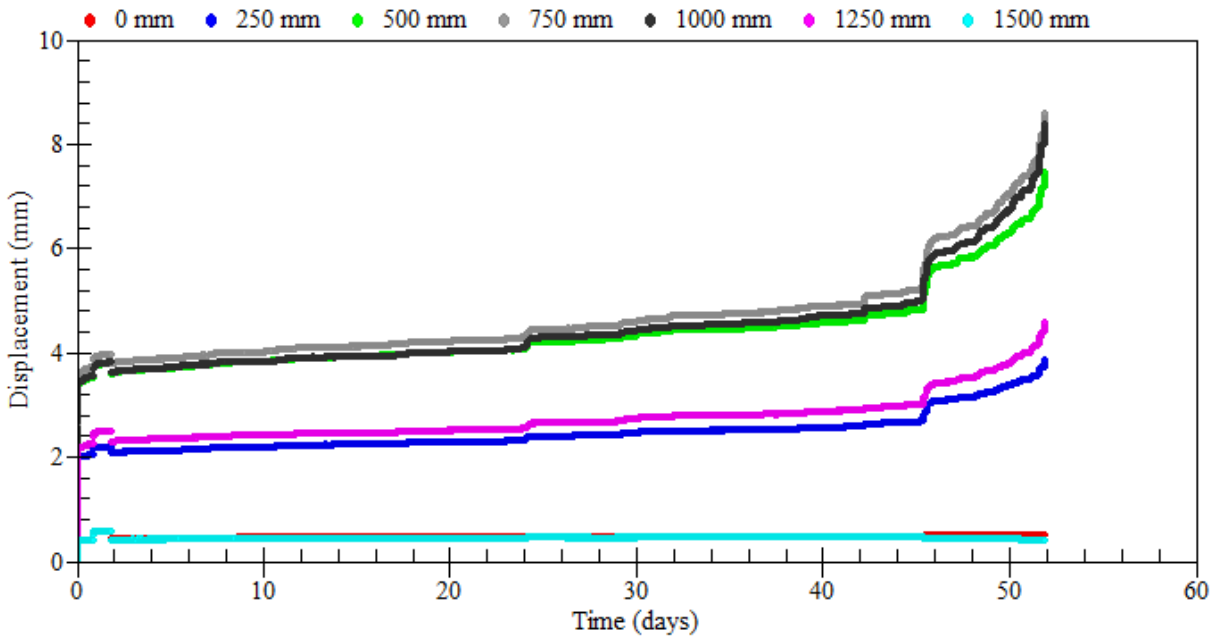

Figure A.74: Displacement measurements – beam SS-3.2

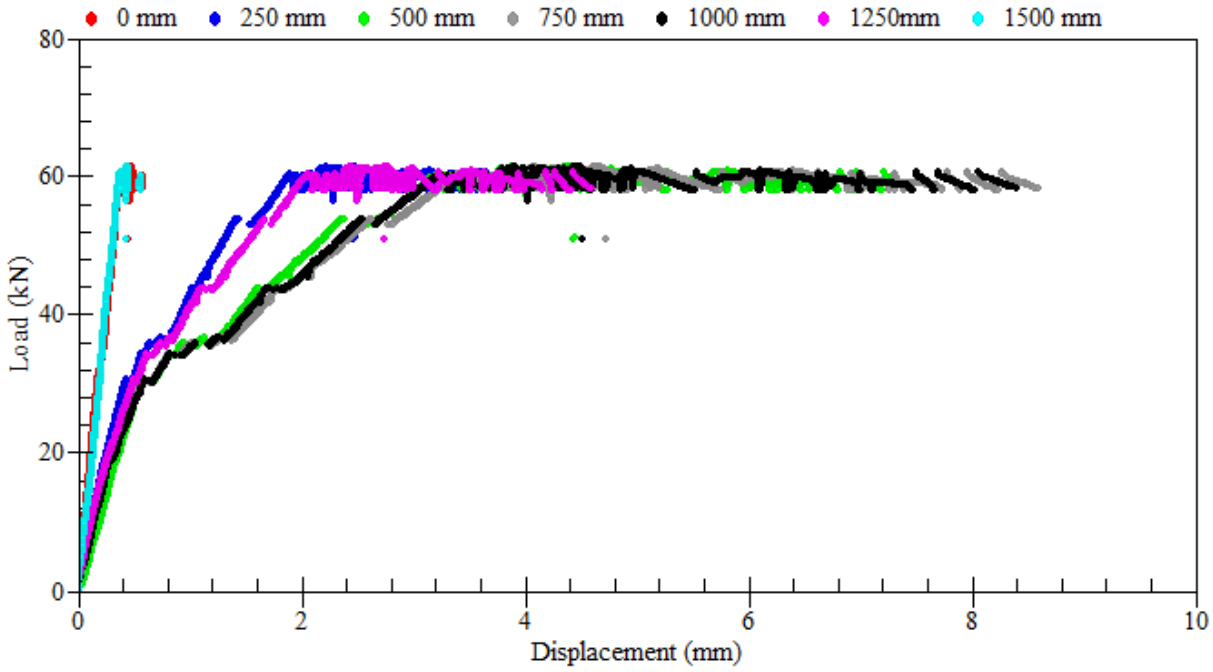

Figure A.75: Load-displacement relationships – beam SS-3.2

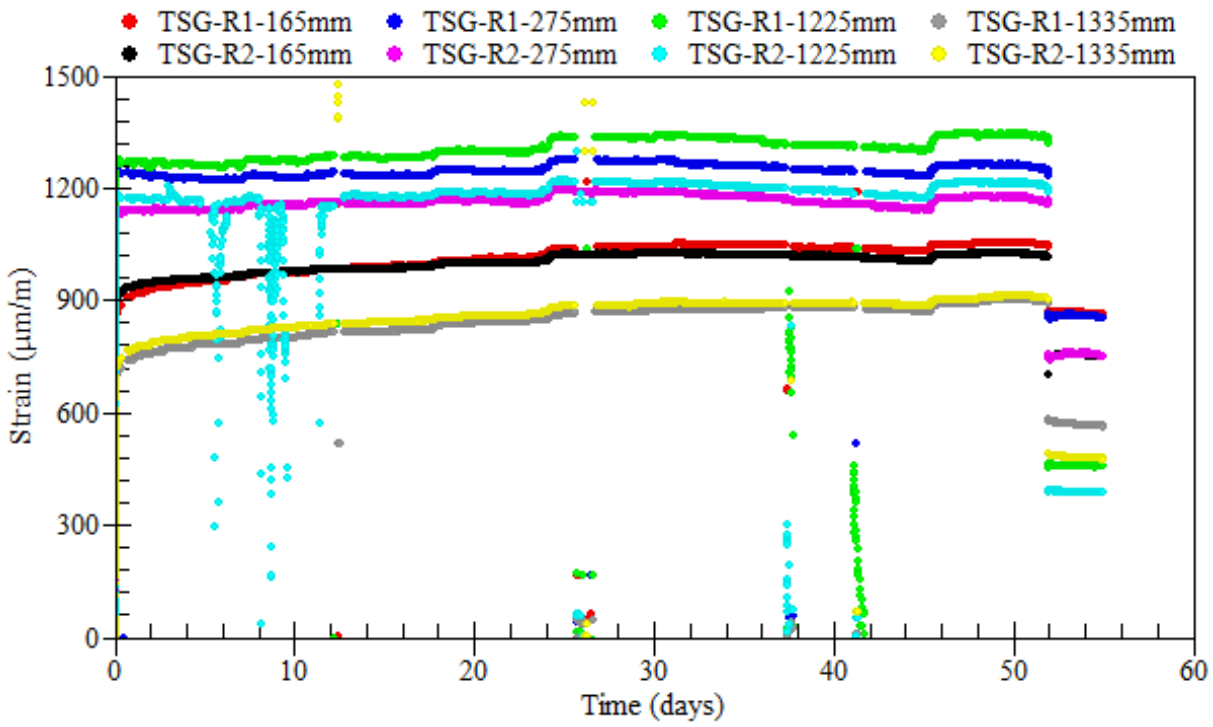

Figure A.76: Strain readings of longitudinal tensile steel bars – beam SS-3.2

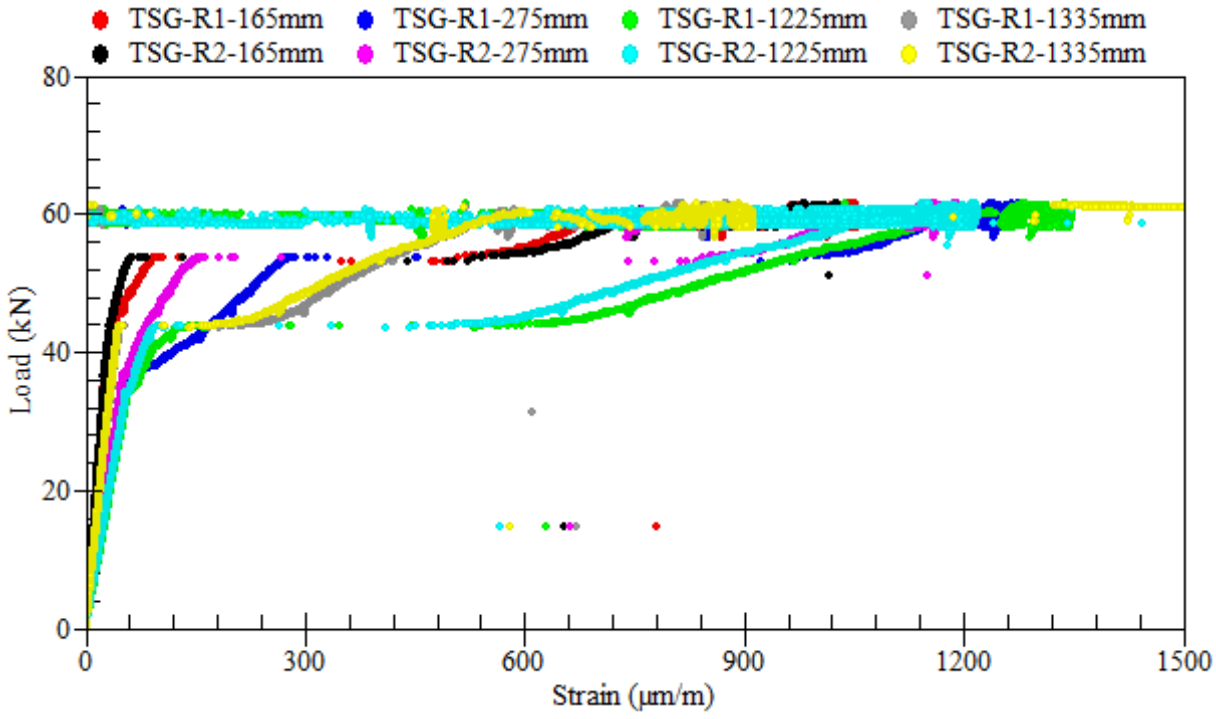

Figure A.77: Load-strain relationships of longitudinal tensile steel bars – beam SS-3.2

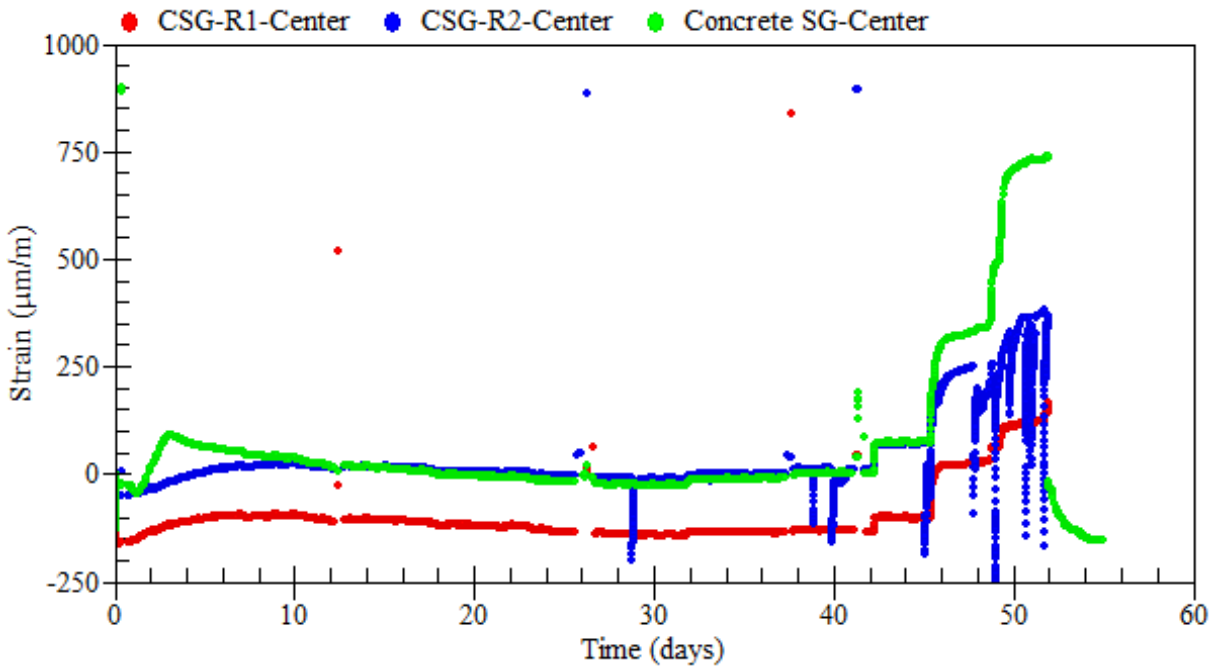

Figure A.78: Strain readings of longitudinal compressive steel bars – beam SS-3.2

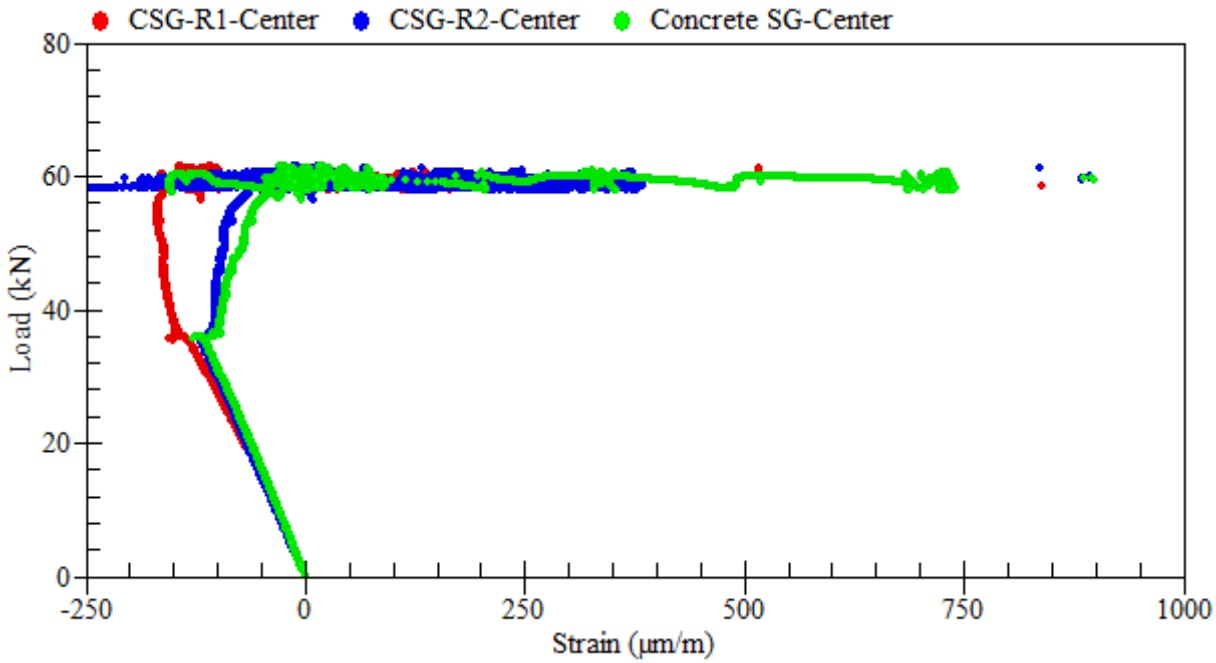

Figure A.79: Load-strain relationships of longitudinal compressive steel bars – beam SS-3.2

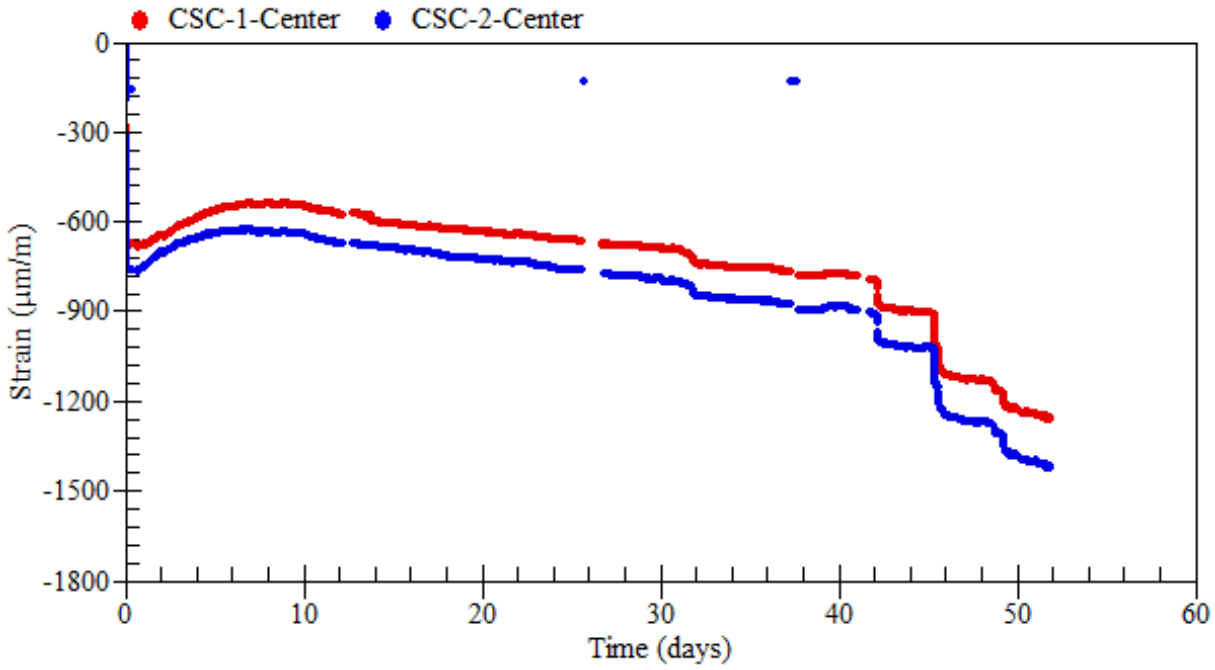

Figure A.80: Strain readings of external rosettes on top – beam SS-3.2

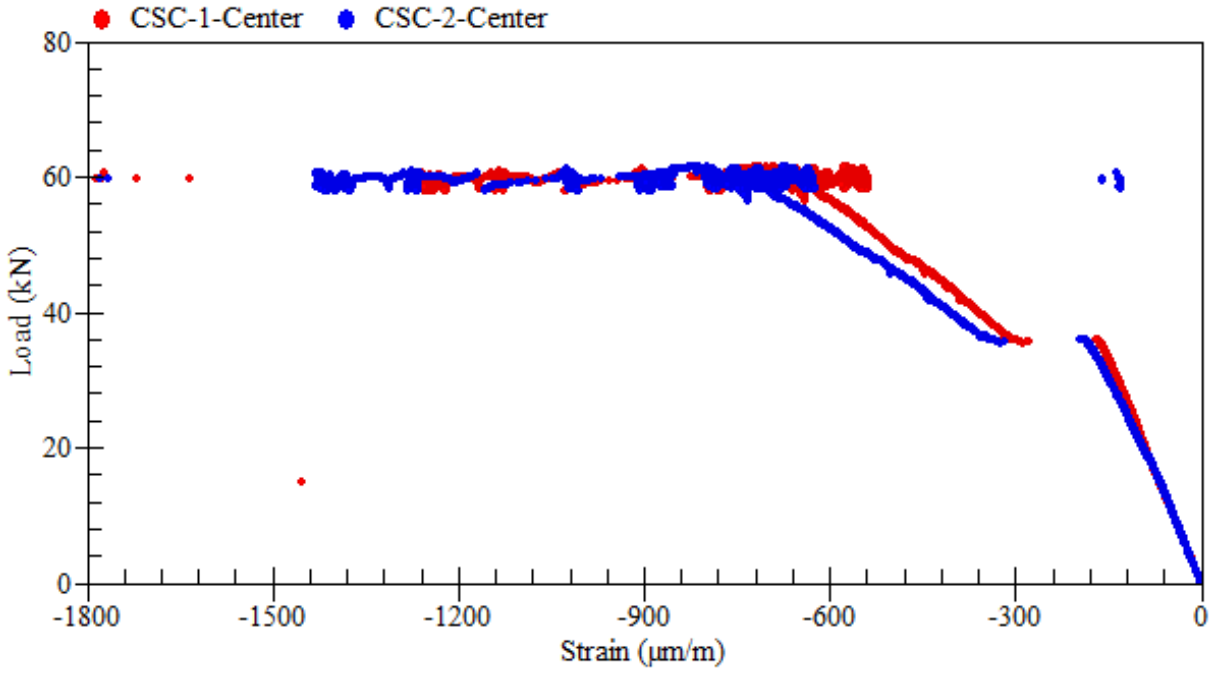

Figure A.81: Load-strain relationships of external rosettes on top – beam SS-3.2

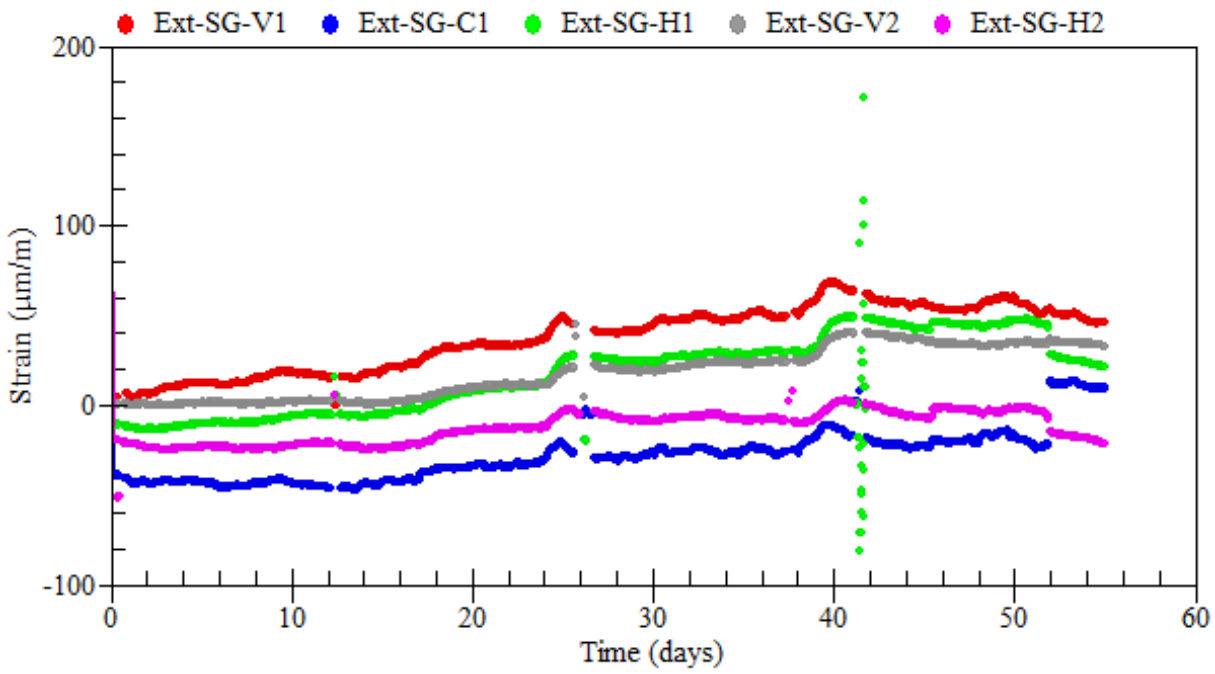

Figure A.82: Strain readings of external rosettes on sides – beam SS-3.2

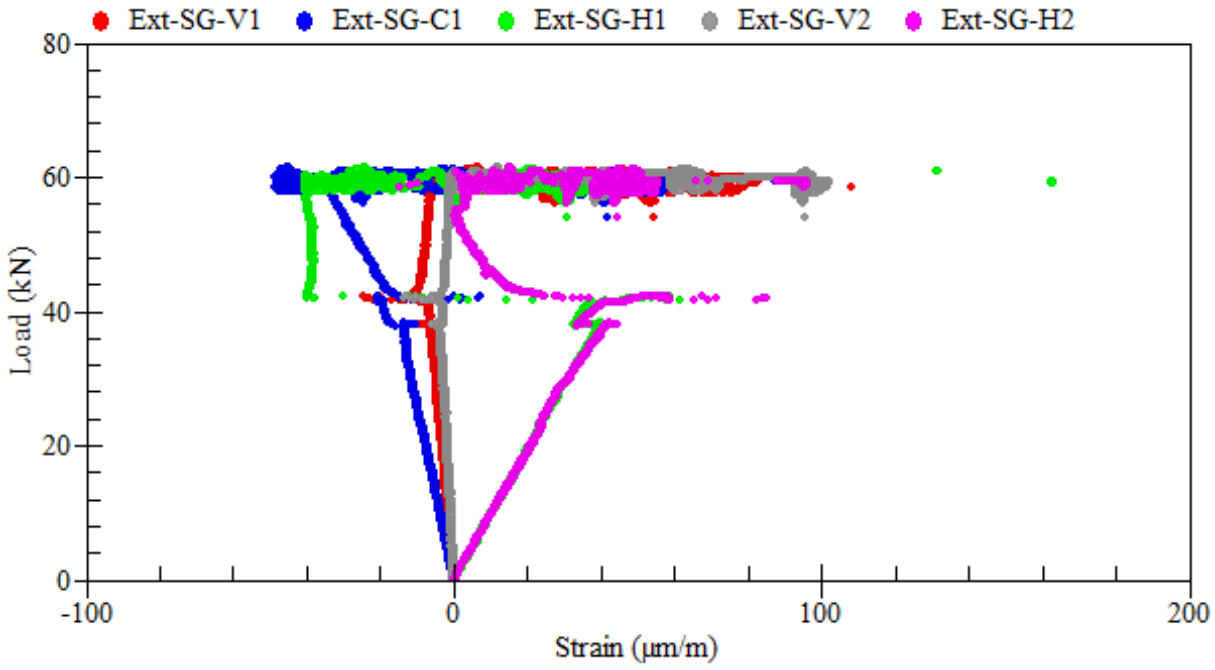

Figure A.83: Load-strain relationships of external rosettes on sides – beam SS-3.2

A.7 Beam SS-4.1

Beam SS-4.1 was tested under the coupled effects of reinforcement corrosion and service loads. The applied sustained load was equivalent to 40% of the beam ultimate load capacity (i.e., 40 kN). Reinforcement corrosion was accelerated using a current density of 300 $\mu A/cm^2$ up until the failure of the beam. The total duration of corrosion exposure was 152 days. The average mass loss of the beam was 40.1%. A summary of the gravimetric mass loss measurements of steel reinforcement is presented in Table A.5.

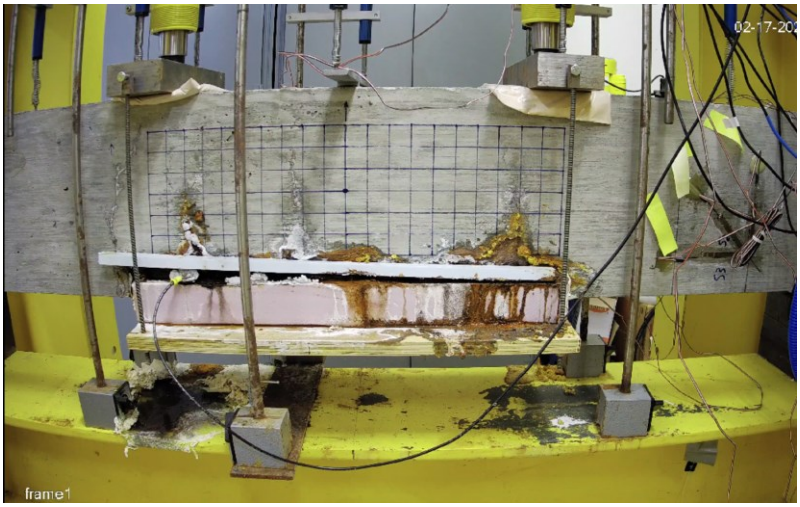

(a) during the test

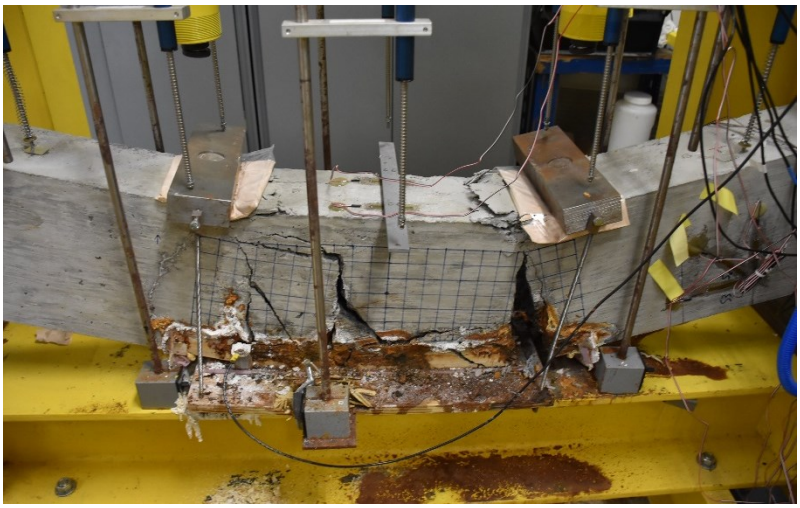

(b) at failure

Figure A.84: Crack propagation and patterns at failure – beam SS-4.1

Figure A.85: Corrosion-induced damage in the cover of concrete – beam SS-4.1

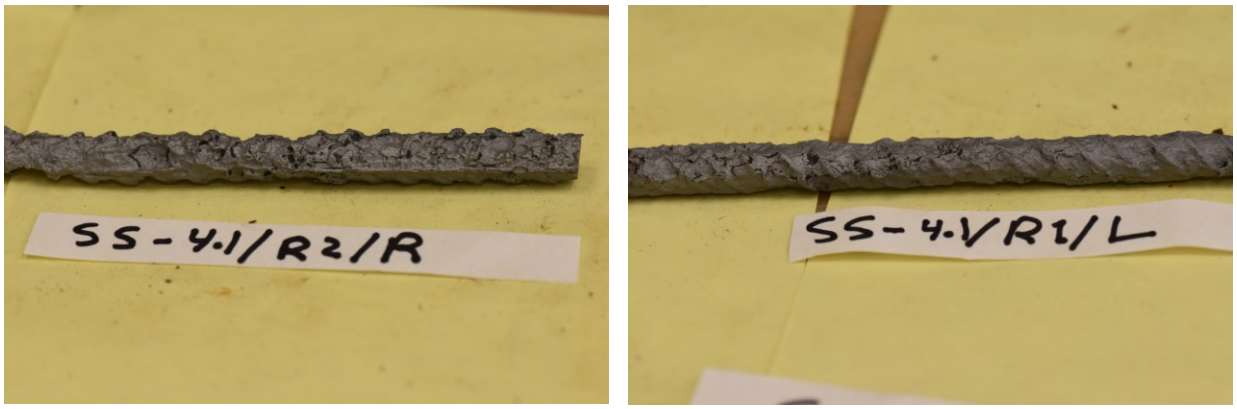

Figure A.86: Corrosion patterns on the clean surface of steel reinforcement – beam SS-4.1

Table A.5: Mass loss of corroded steel bars – beam SS-4.1

Rebar type	Rebar designation	Length (mm)	Mass (g)	Mass loss (%)
Control	R0	100.0	75.38	0.00
R1	R1-L	389.0	200.05	31.78
R2	R2-R	369.0	143.63	48.36

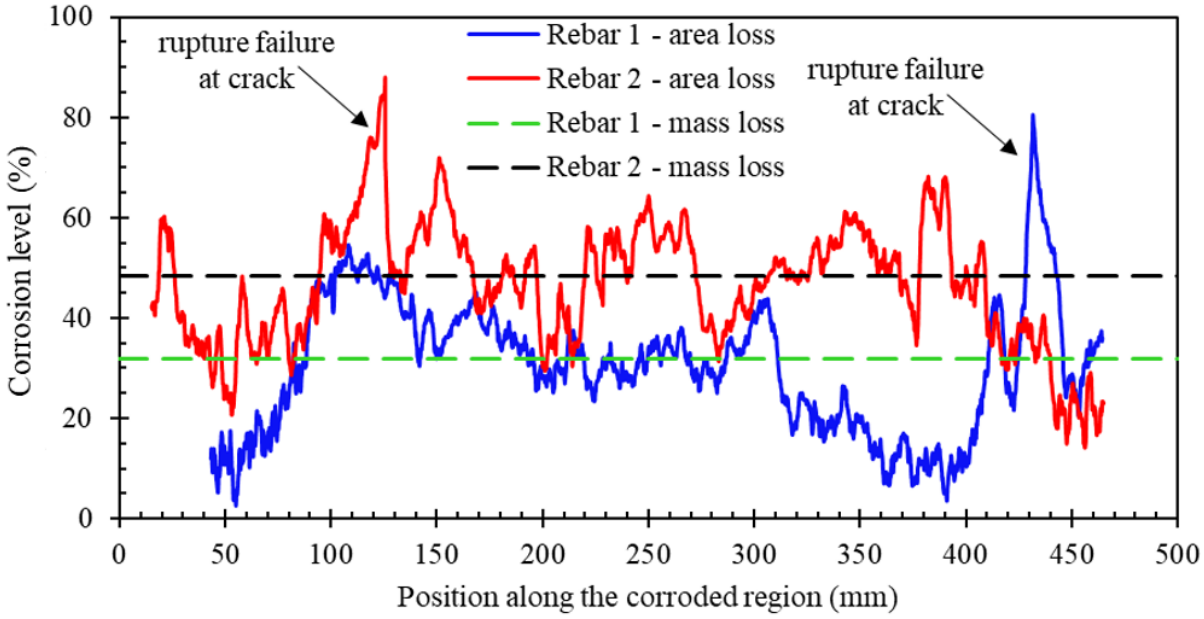

Figure A.87: Distribution of cross-sectional area loss along the corroded steel reinforcement – beam SS-4.1

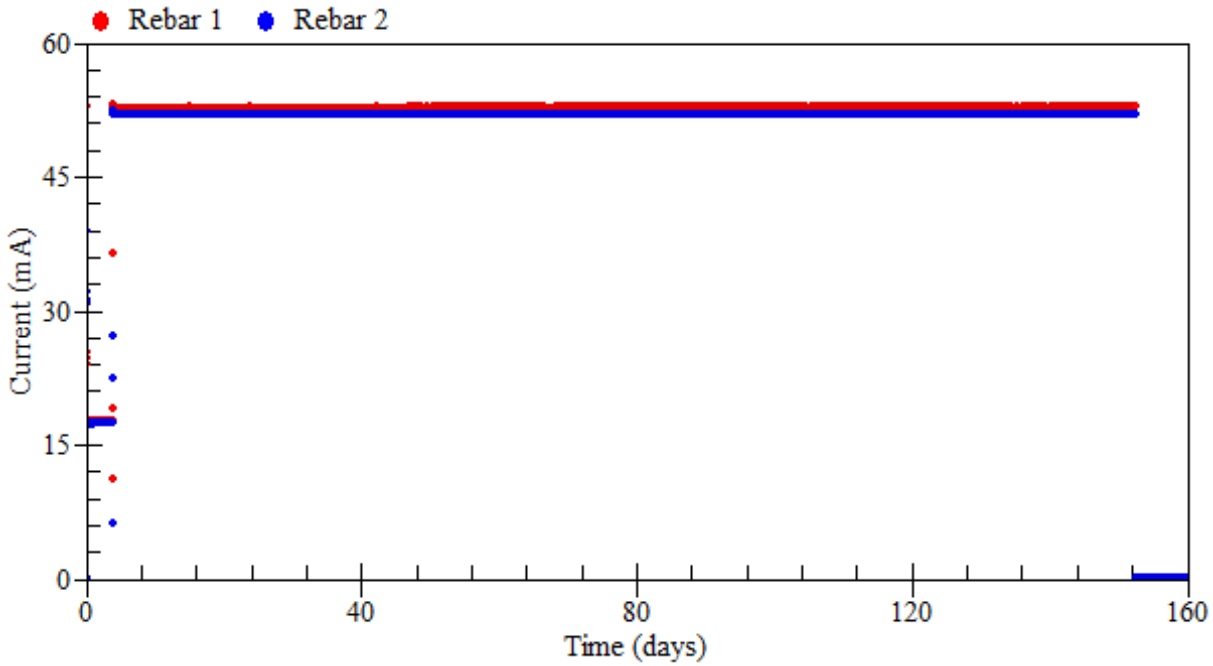

Figure A.88: Applied current – beam SS-4.1

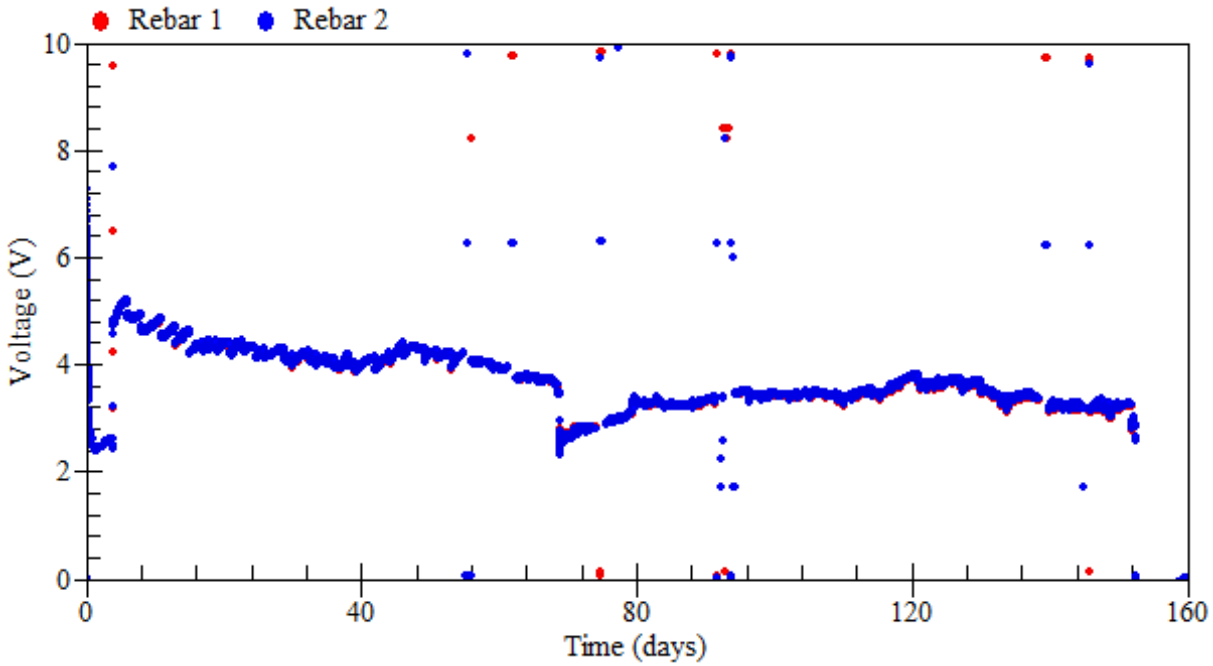

Figure A.89: Voltage measurements – beam SS-4.1

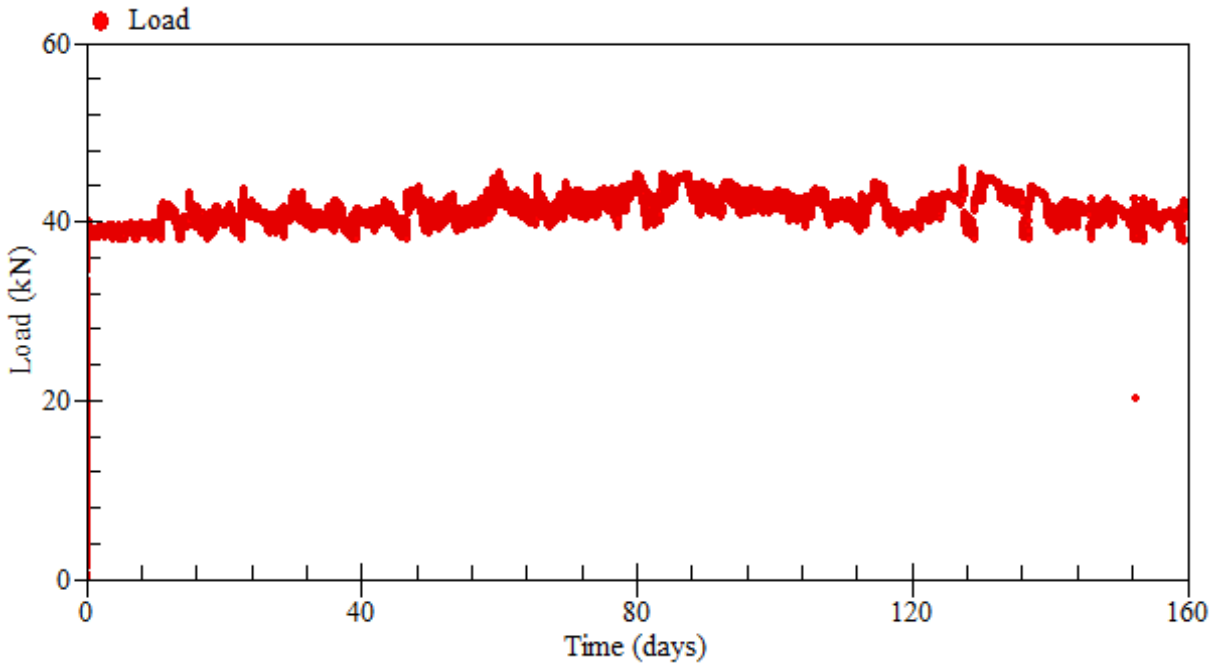

Figure A.90: Applied loads – beam SS-4.1

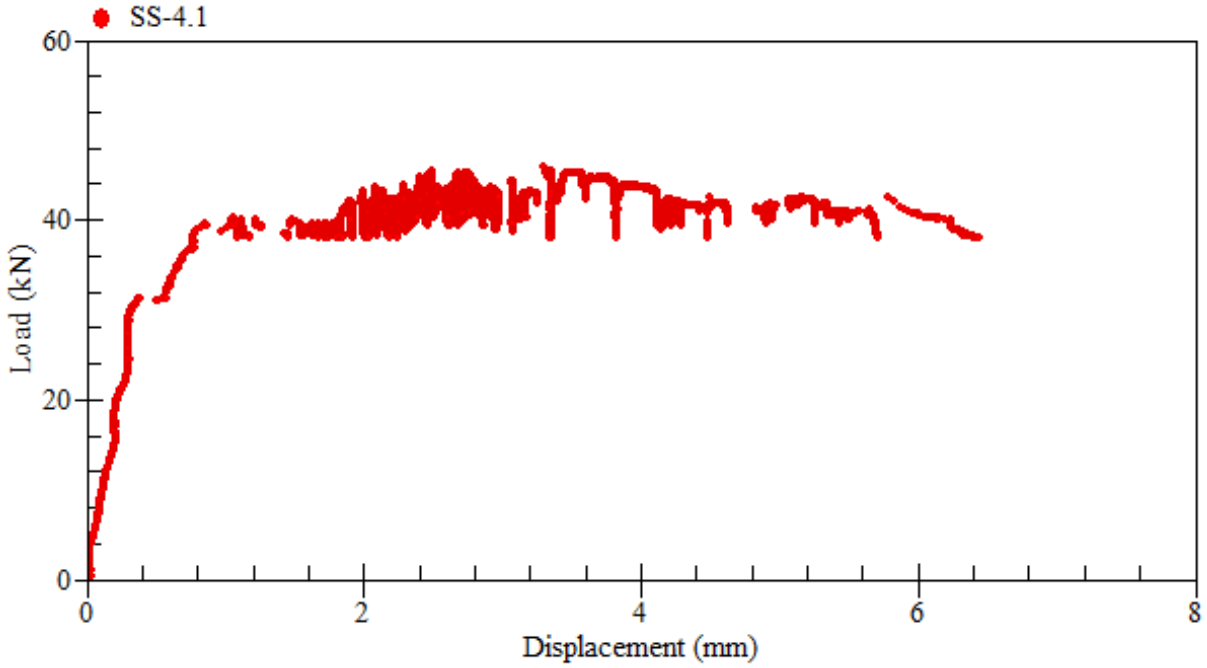

Figure A.91: Load-displacement relationship at mid-span – beam SS-4.1

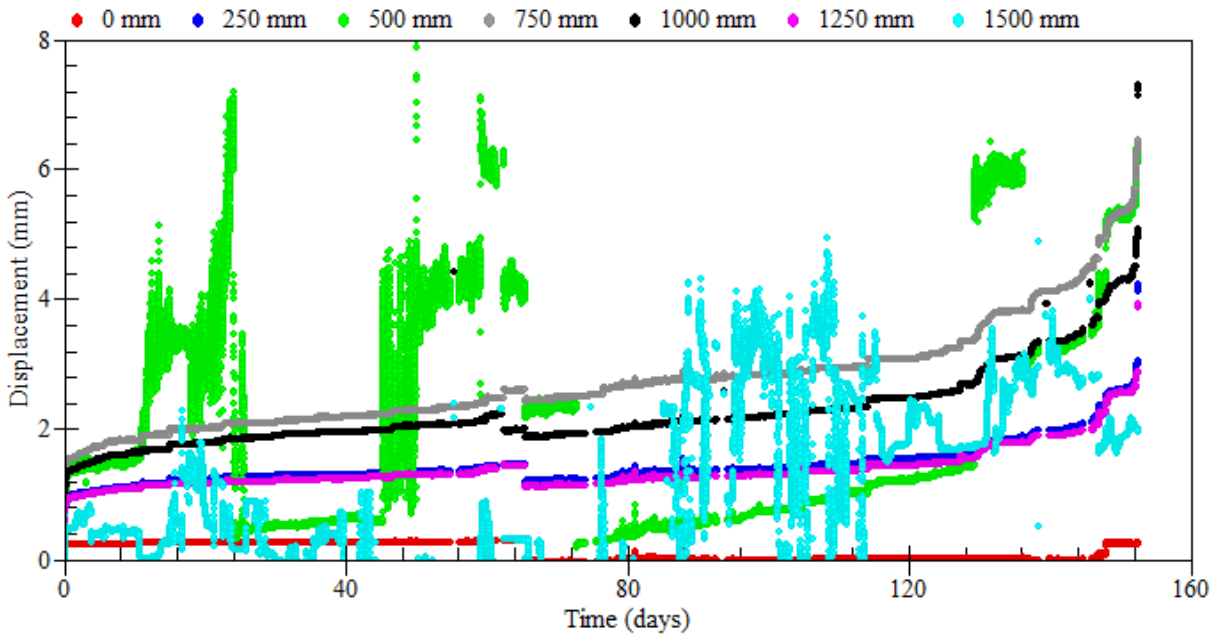

Figure A.92: Displacement measurements – beam SS-4.1

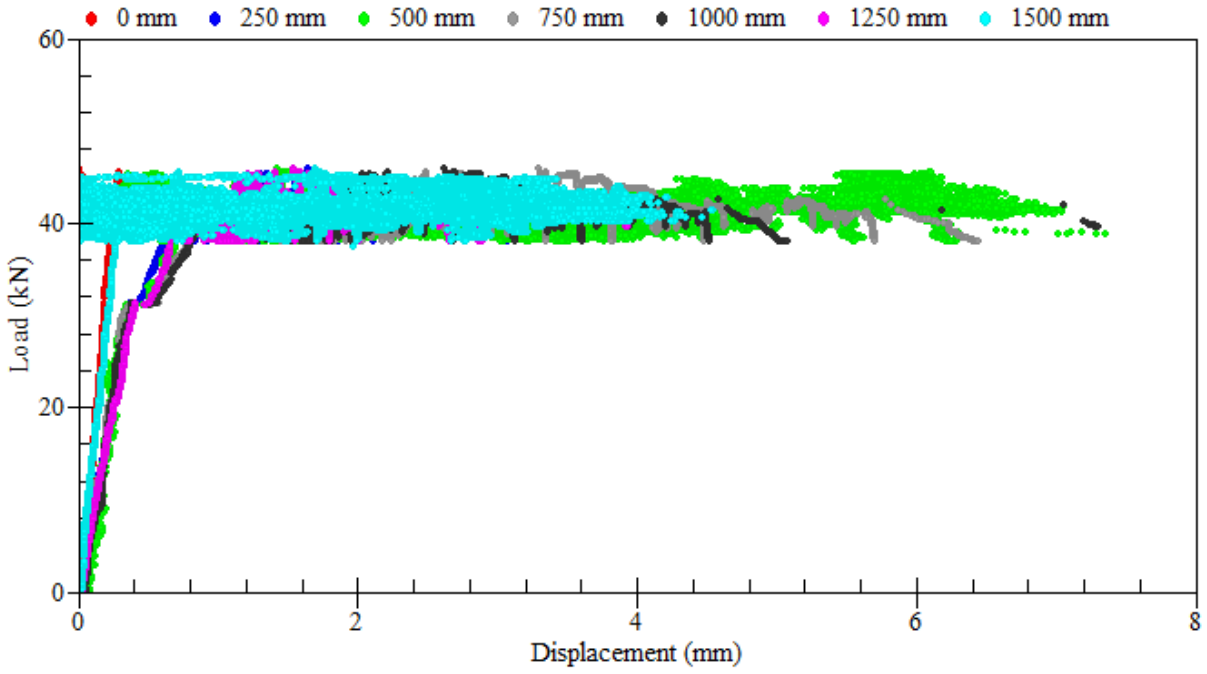

Figure A.93: Load-displacement relationships – beam SS-4.1

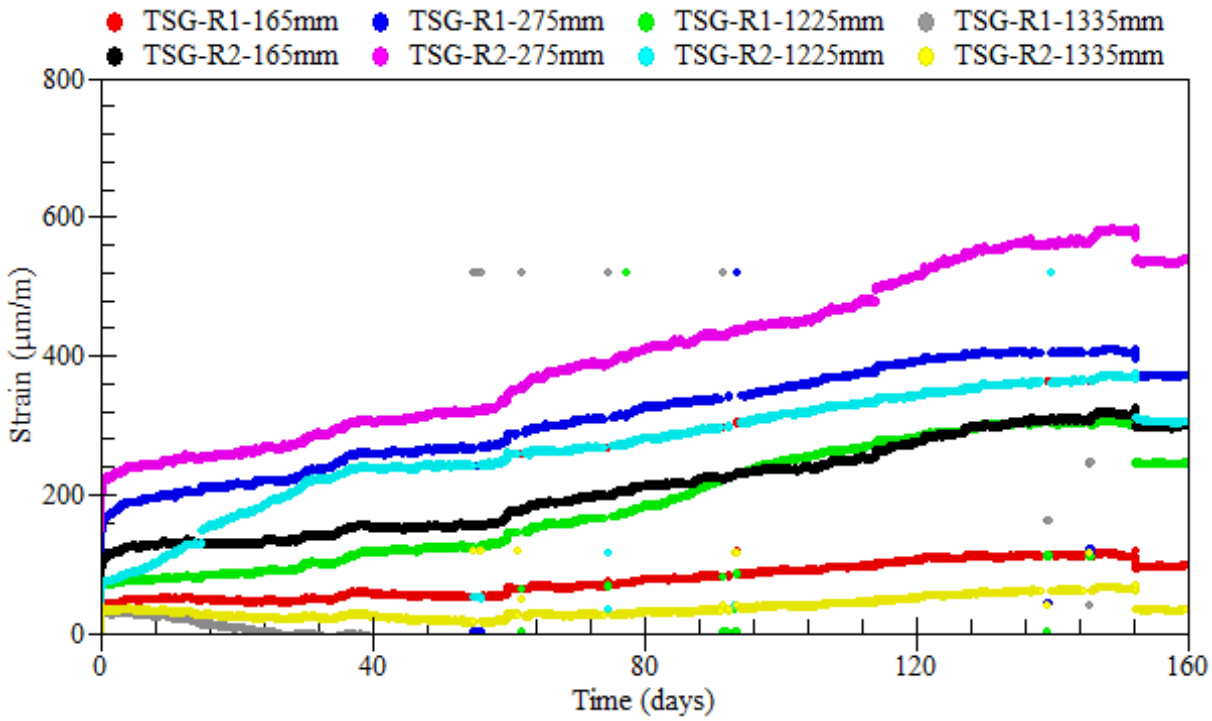

Figure A.94: Strain readings of longitudinal tensile steel bars – beam SS-4.1

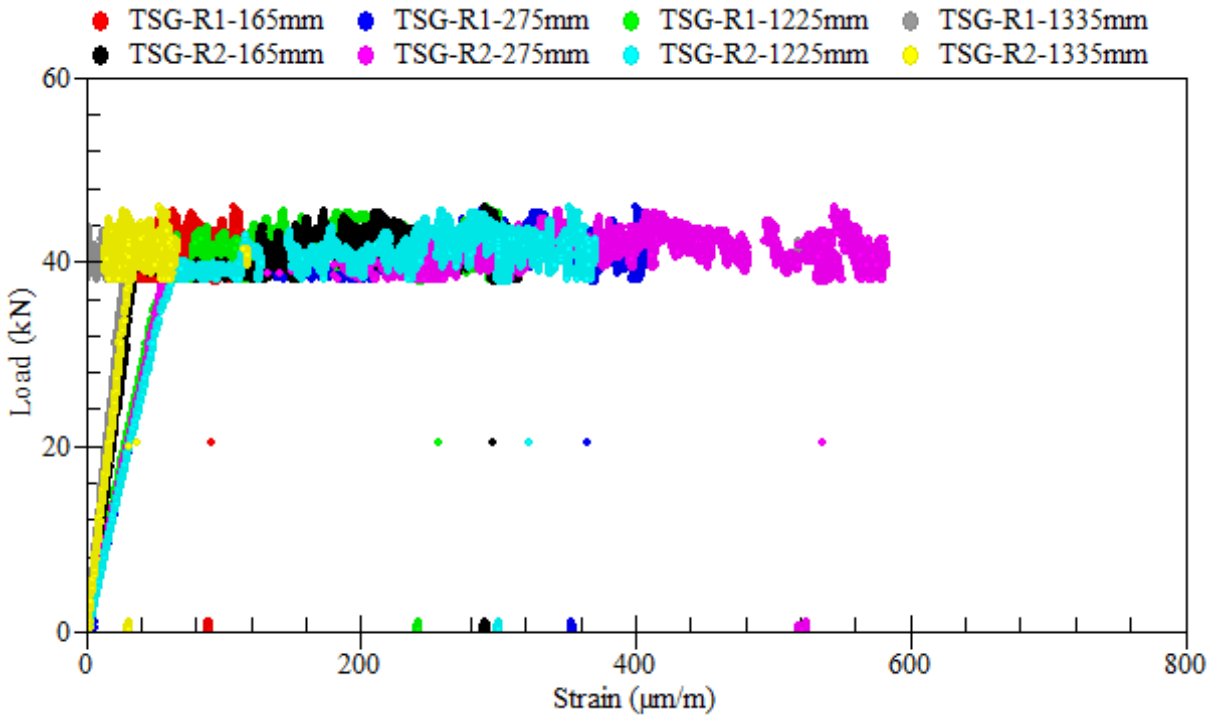

Figure A.95: Load-strain relationships of longitudinal tensile steel bars – beam SS-4.1

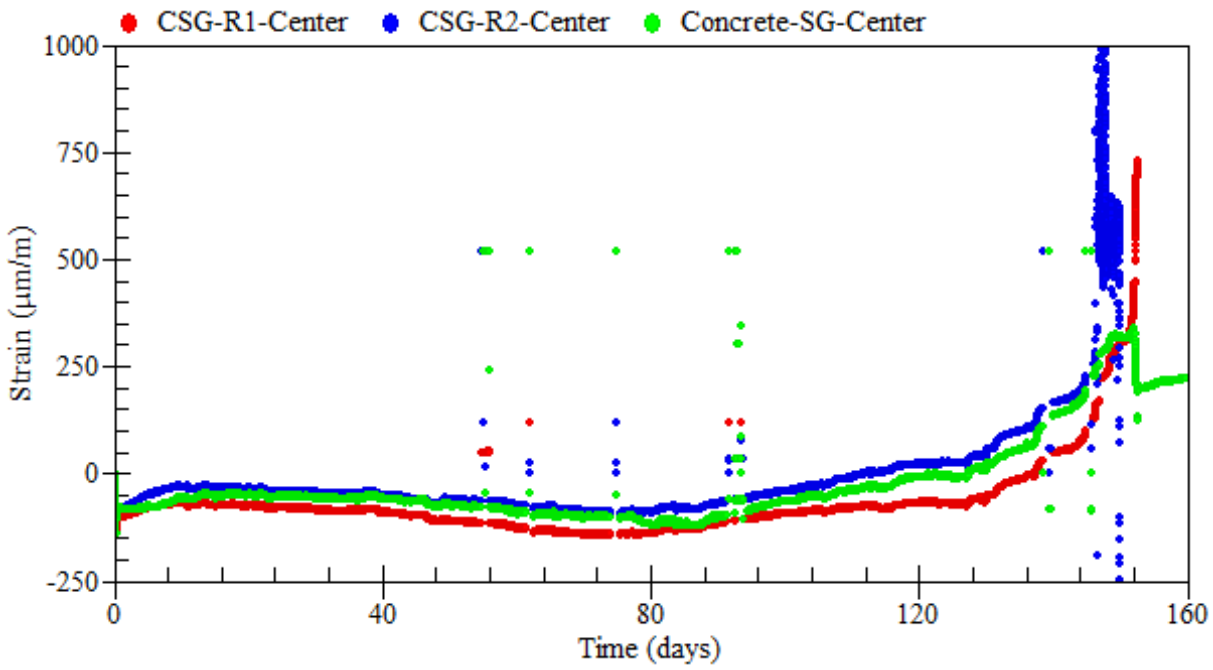

Figure A.96: Strain readings of longitudinal compressive steel bars – beam SS-4.1

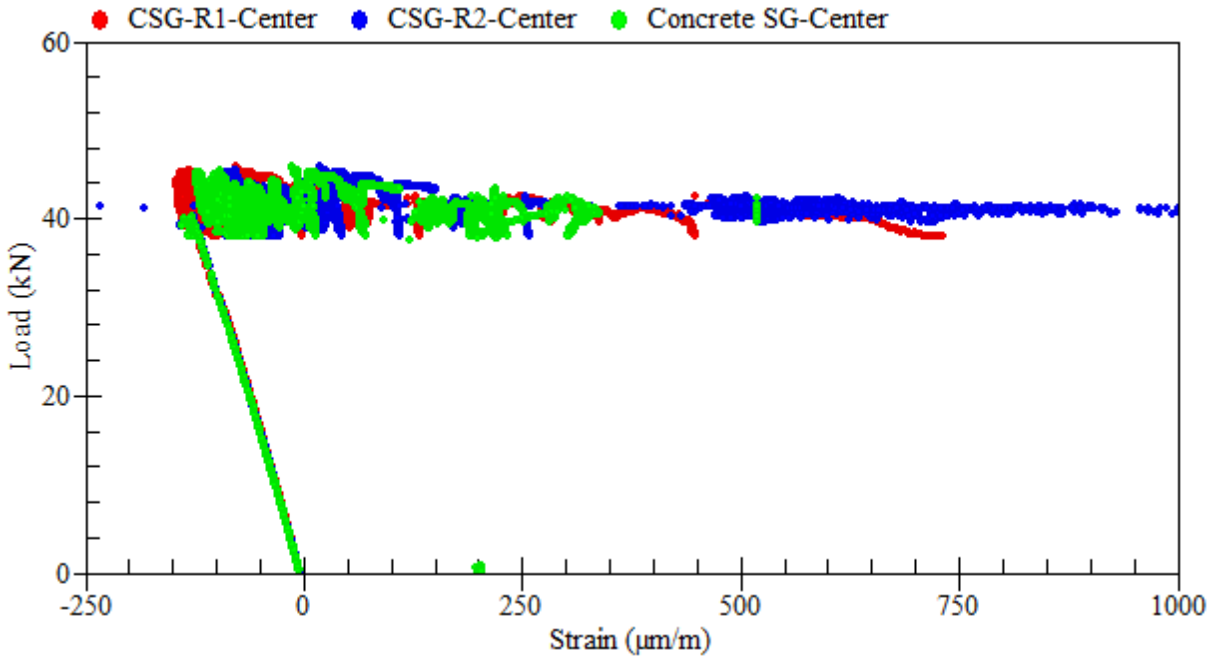

Figure A.97: Load-strain relationships of longitudinal compressive steel bars – beam SS-4.1

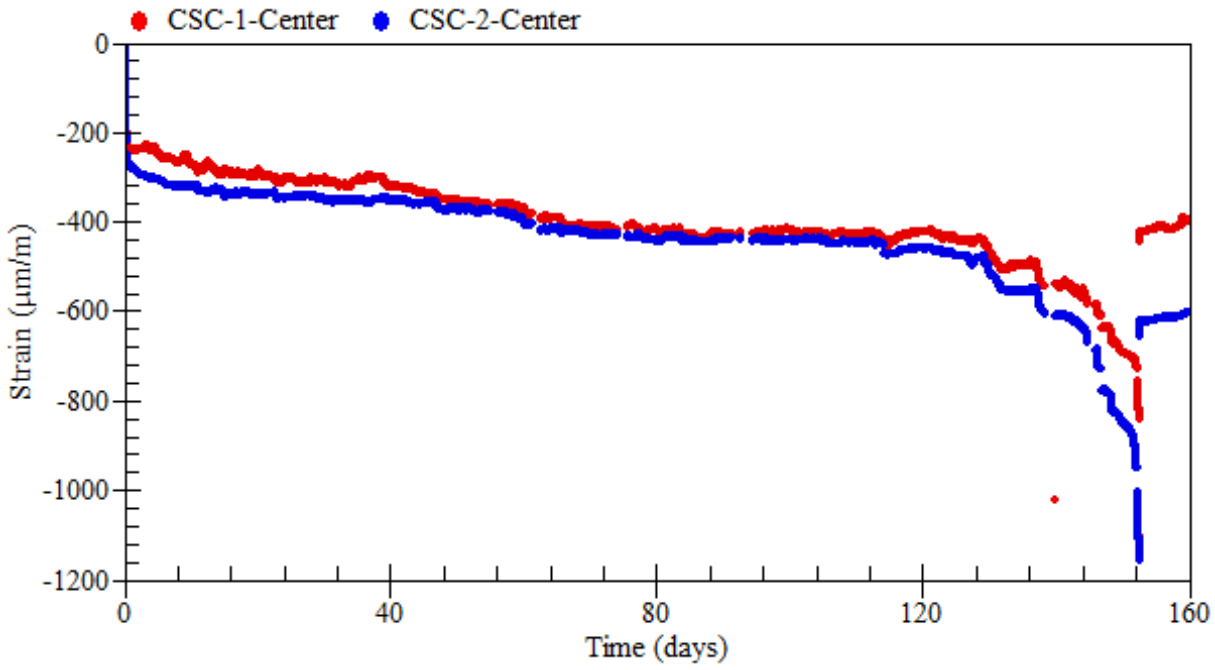

Figure A.98: Strain readings of external rosettes on top – beam SS-4.1

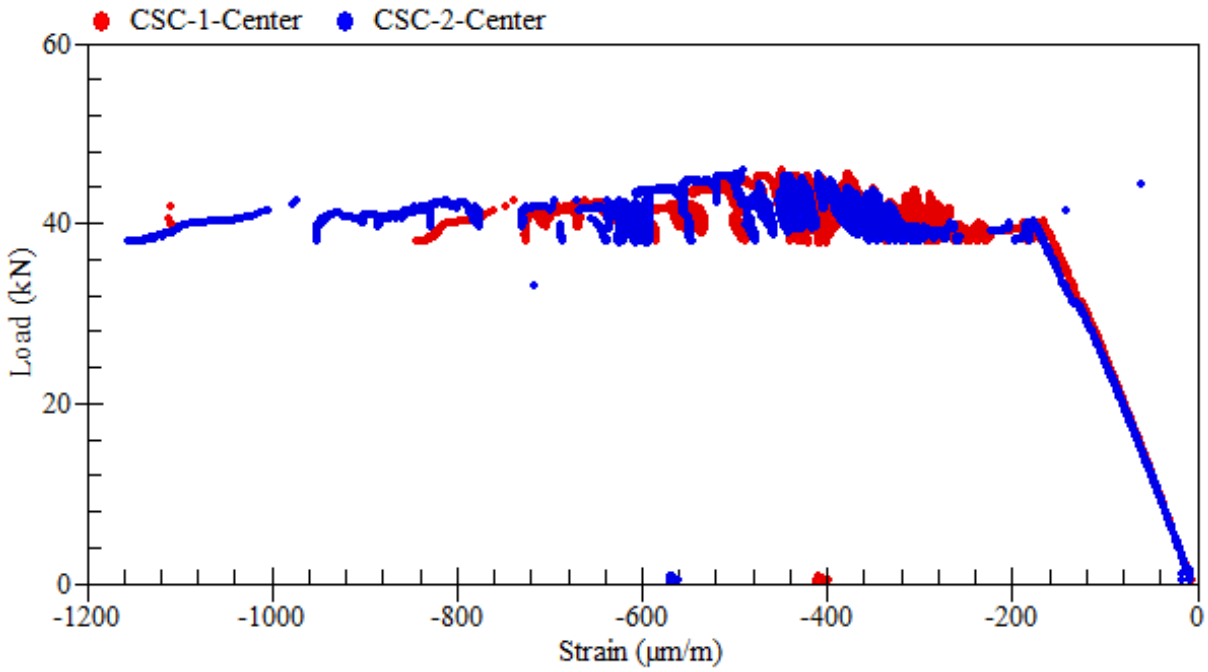

Figure A.99: Load-strain relationships of external rosettes on top – beam SS-4.1

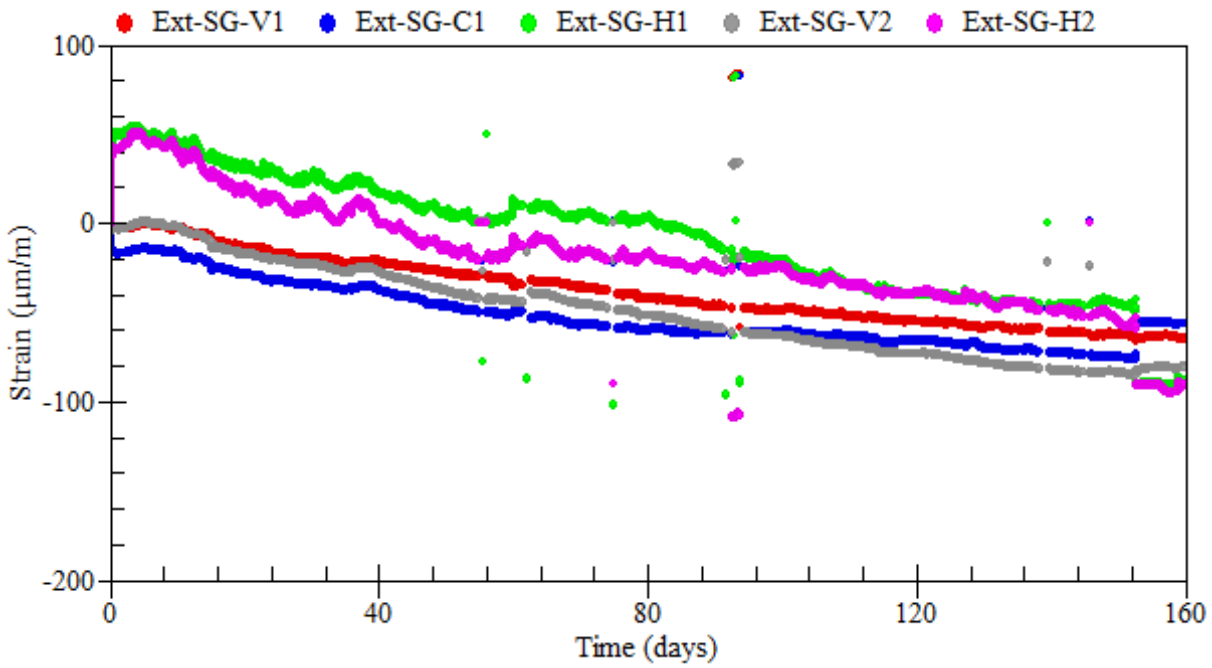

Figure A.100: Strain readings of external rosettes on sides – beam SS-4.1

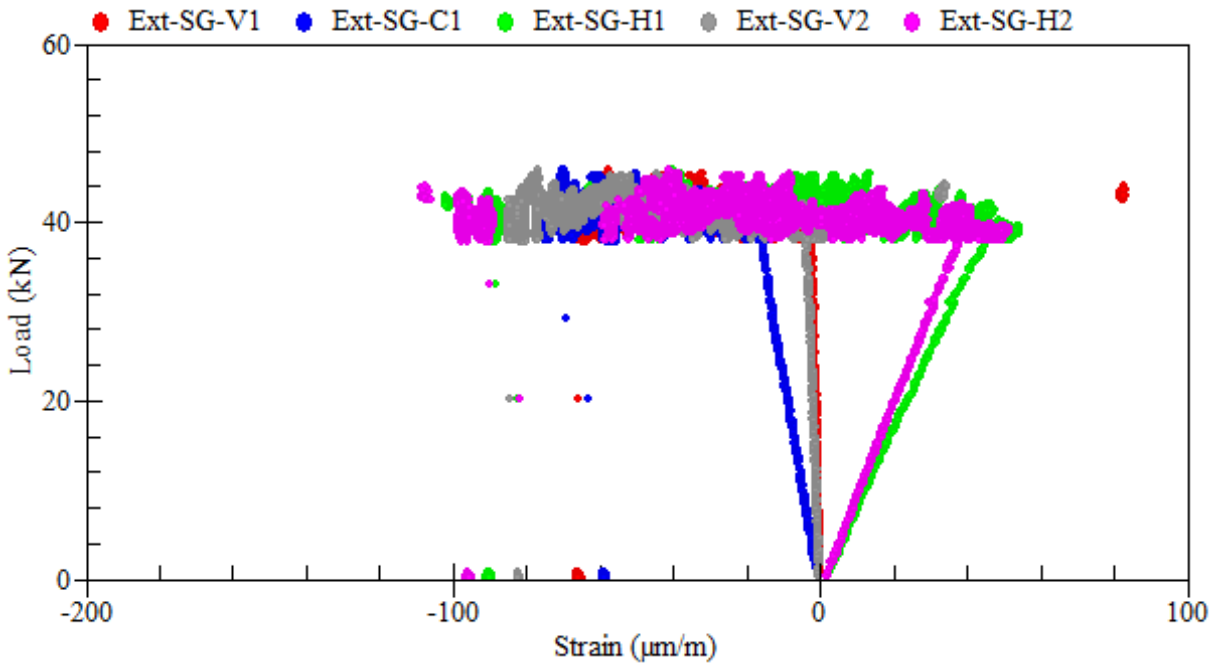

Figure A.101: Load-strain relationships of external rosettes on sides – beam SS-4.1

A.8 Beam SS-4.2

Beam SS-4.2 was tested under the coupled effects of reinforcement corrosion and service loads. The applied sustained load was equivalent to 40% of the beam ultimate load capacity (i.e., 40 kN). Reinforcement corrosion was accelerated using a current density of 300 $\mu A/cm^2$ up until the failure of the beam. The total duration of corrosion exposure was 167 days. The average mass loss of the beam was 29.6%. A summary of the gravimetric mass loss measurements of steel reinforcement is presented in Table A.6.

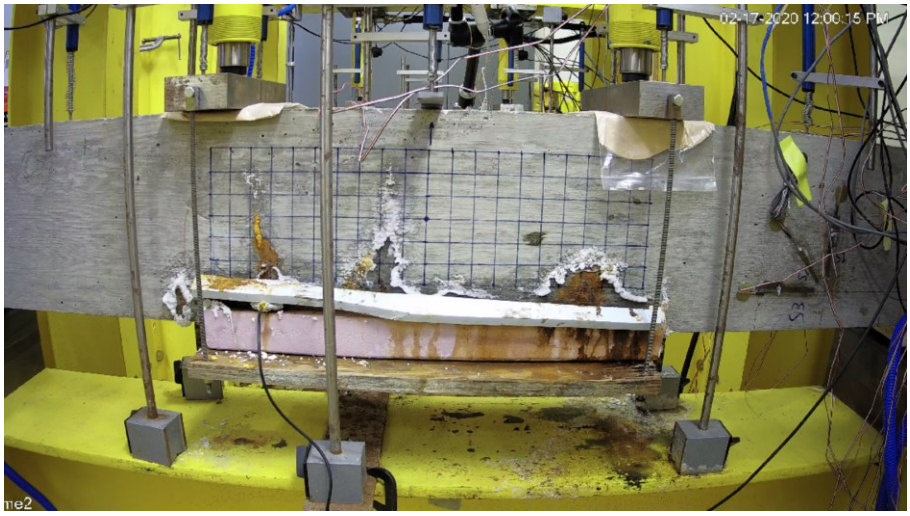

(a) during the test

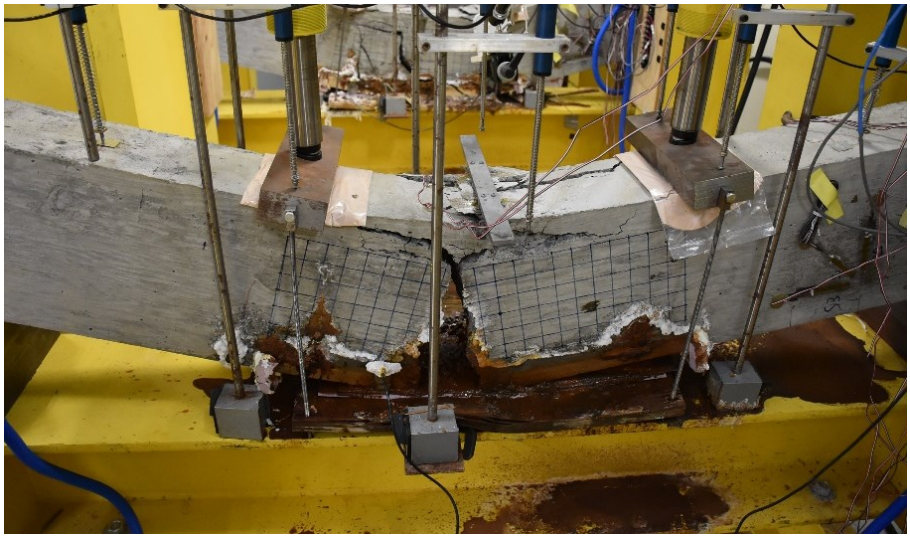

(b) at failure

Figure A.102: Crack propagation and patterns at failure – beam SS-4.2

Figure A.103: Corrosion-induced damage in the cover of concrete – beam SS-4.2

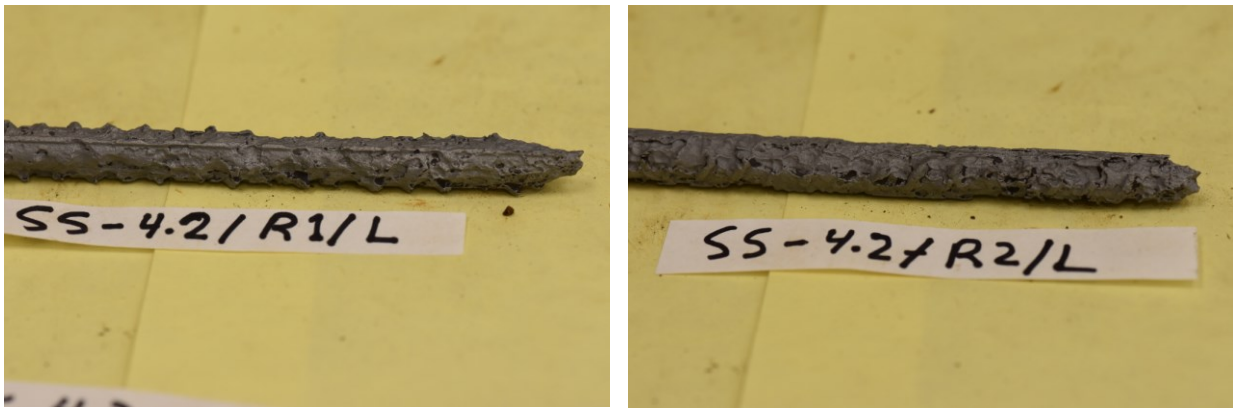

Figure A.104: Corrosion patterns on the clean surface of steel reinforcement – beam SS-4.2

Table A.6: Mass loss of corroded steel bars – beam SS-4.2

Rebar type	Rebar designation	Length (mm)	Mass (g)	Mass loss (%)	Rebar mass loss (%)
Control	R0	100.0	75.38	0.00	0.00
R1	R1-R	264.0	142.66	28.31	26.50
	R1-L	194.0	111.09	24.03	
R2	R2-R	267.0	128.64	36.08	32.77
	R2-L	201.0	108.55	28.36	

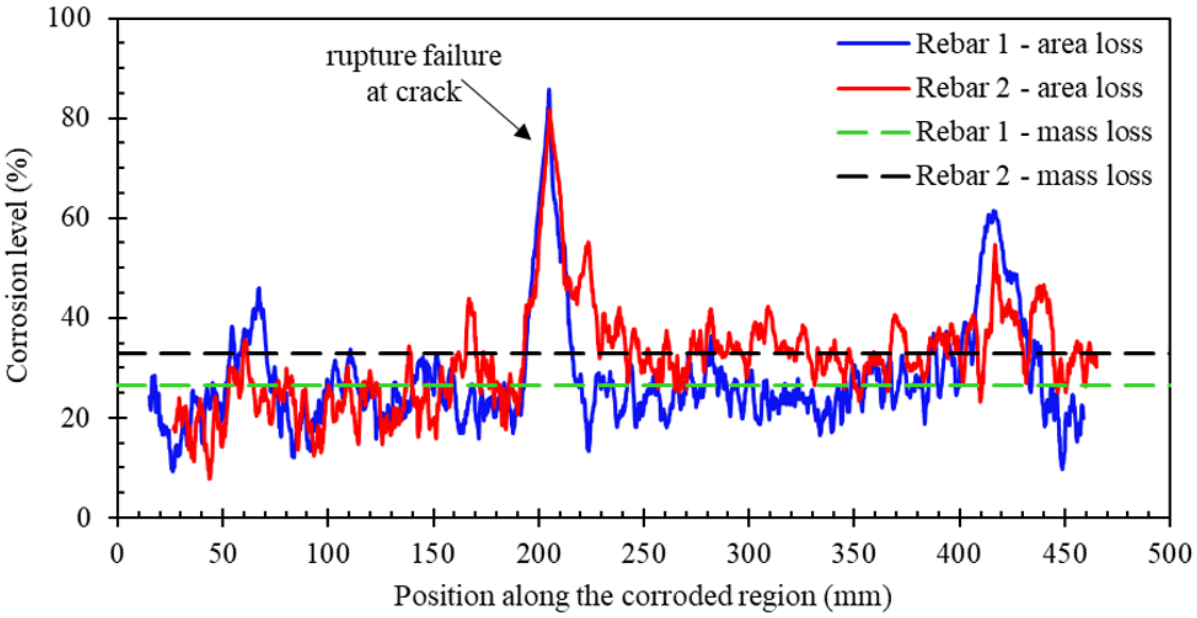

Figure A.105: Distribution of cross-sectional area loss along the corroded steel reinforcement – beam SS-4.2

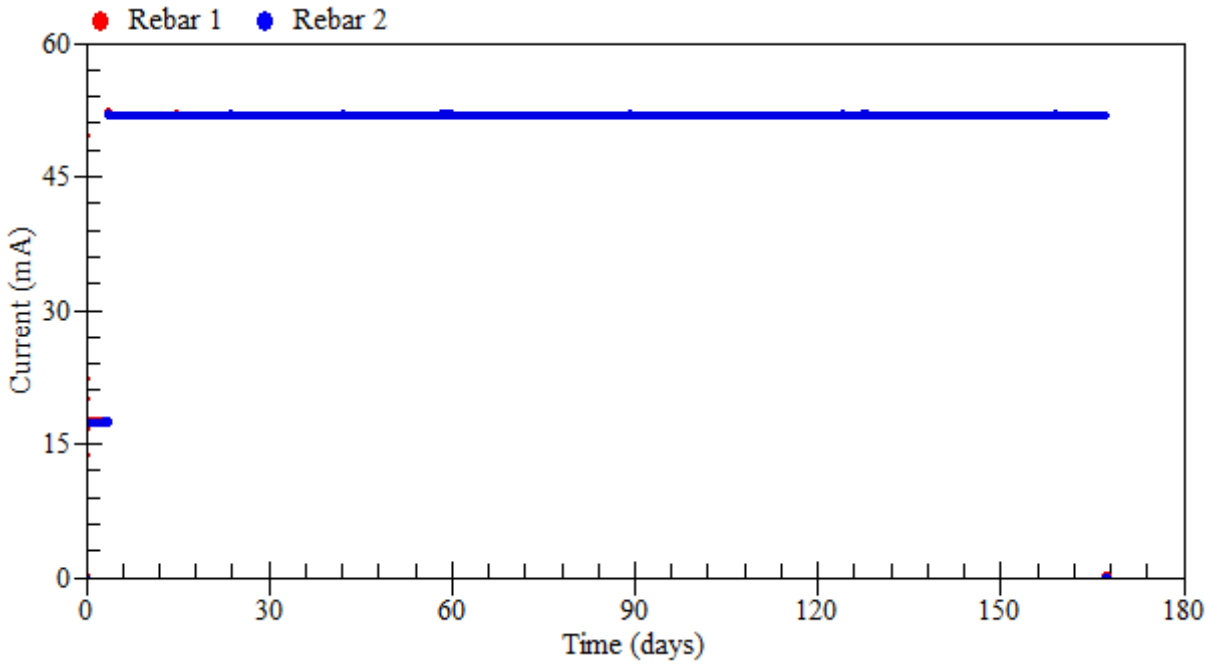

Figure A.106: Applied current – beam SS-4.2

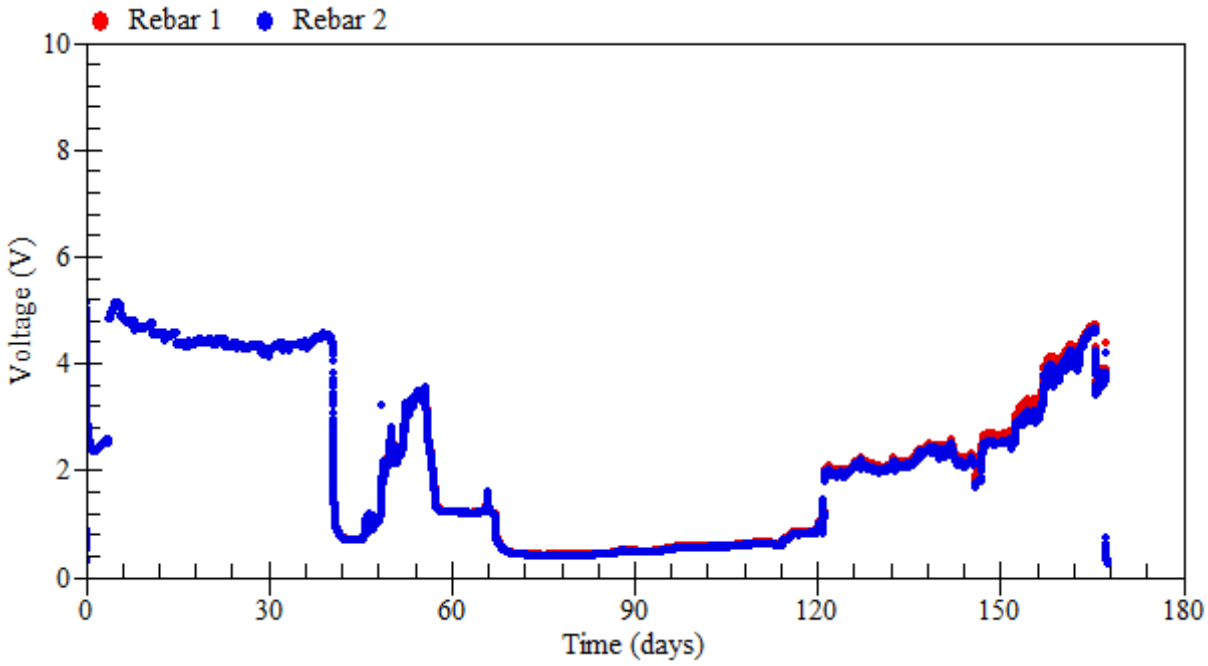

Figure A.107: Voltage measurements – beam SS-4.2

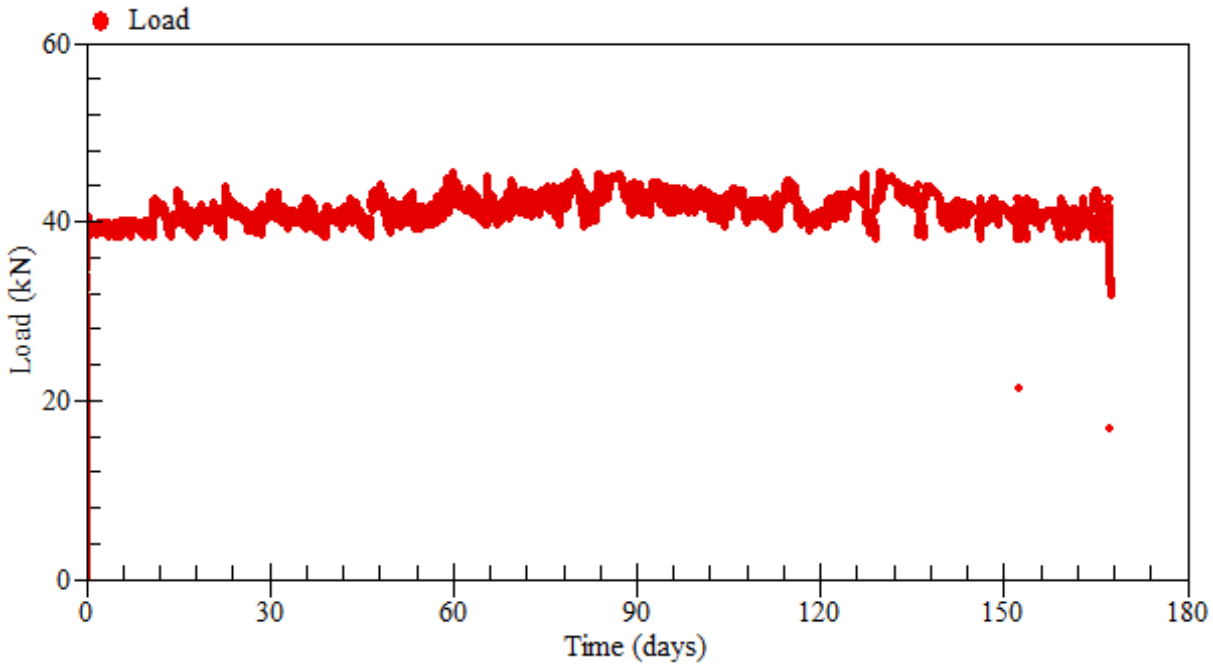

Figure A.108: Applied loads – beam SS-4.2

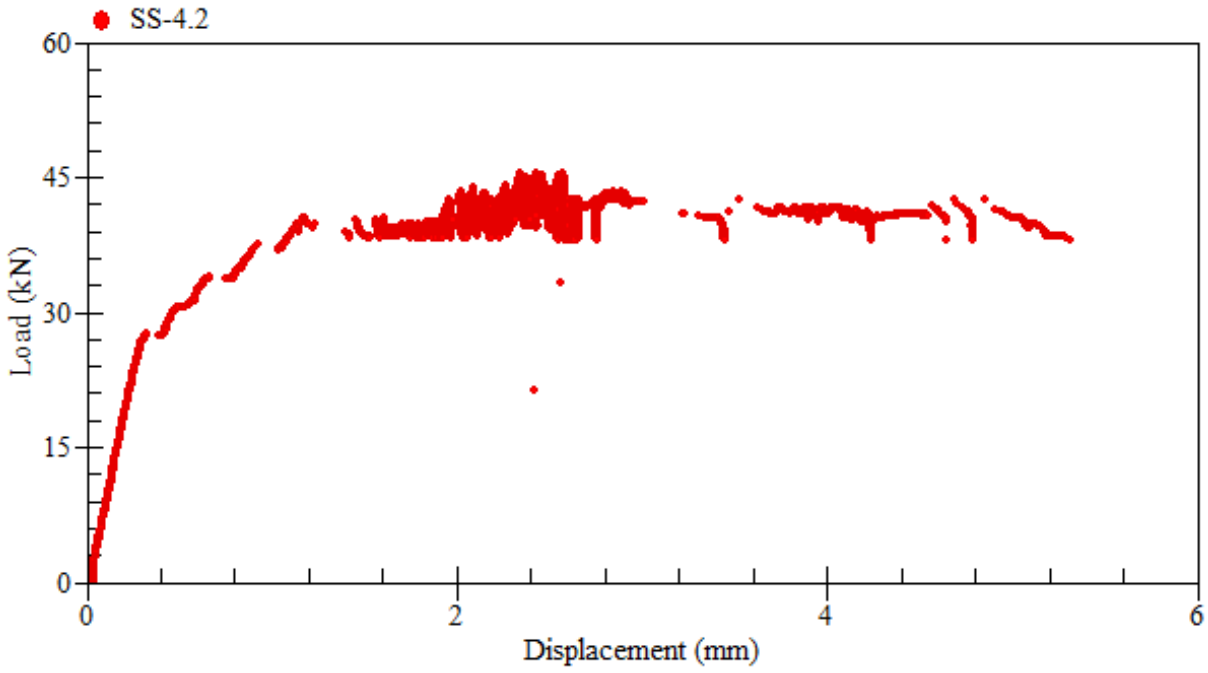

Figure A.109: Load-displacement relationship at mid-span – beam SS-4.2

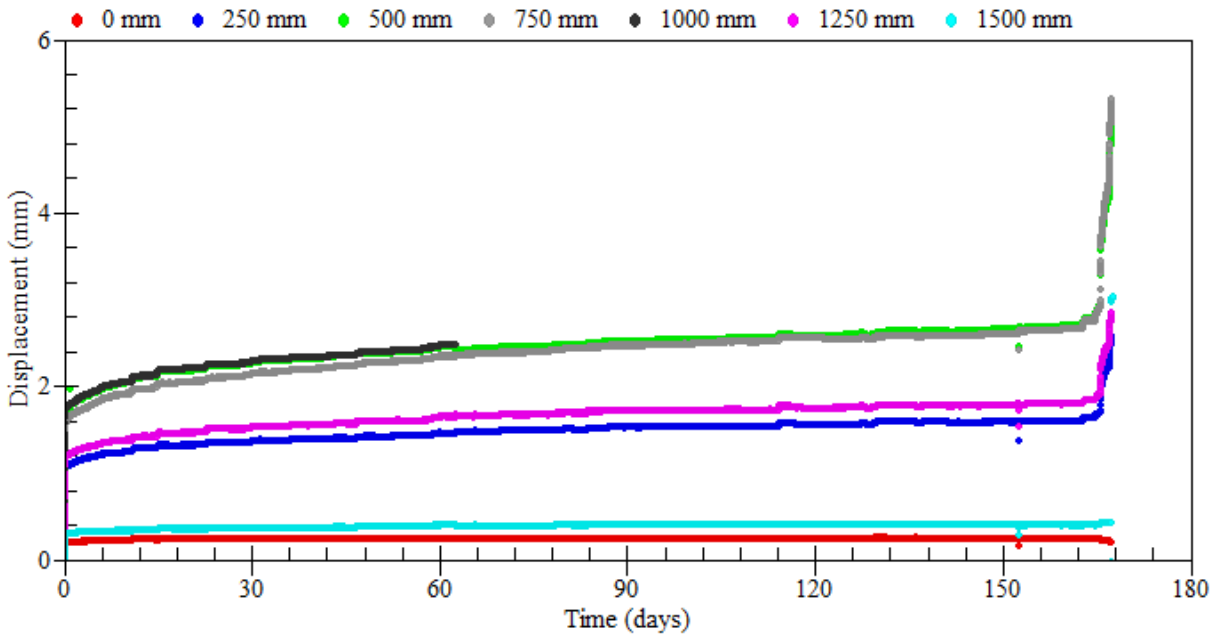

Figure A.110: Displacement measurements – beam SS-4.2

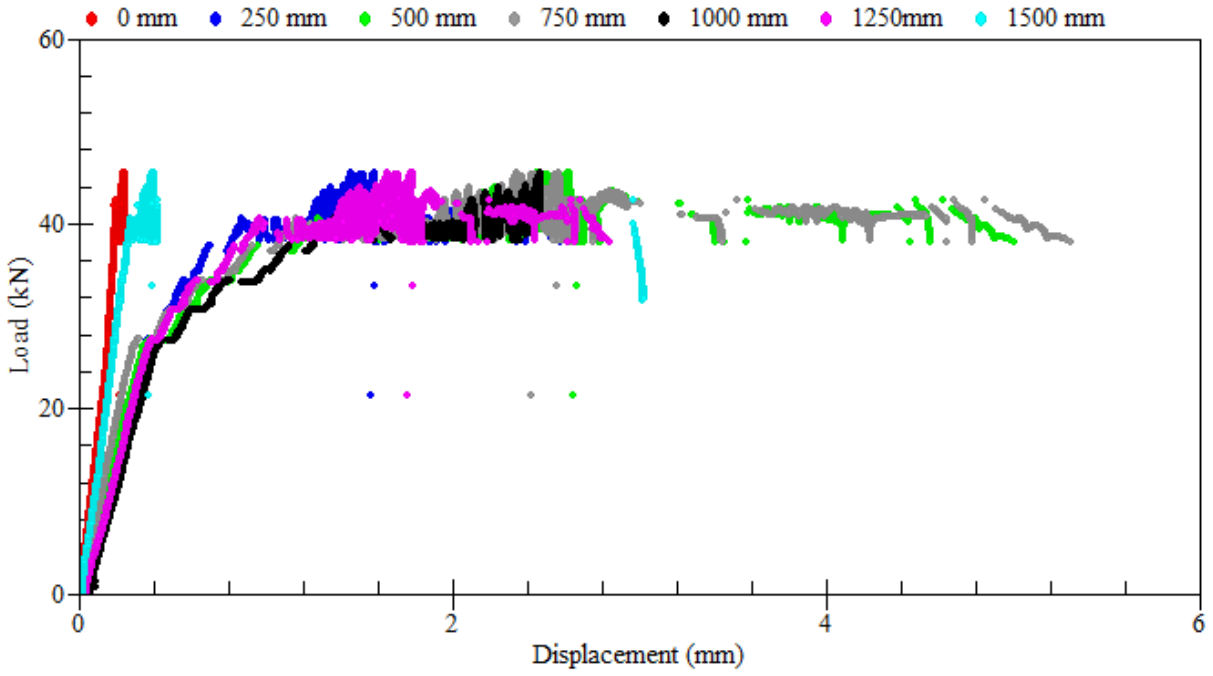

Figure A.111: Load-displacement relationships – beam SS-4.2

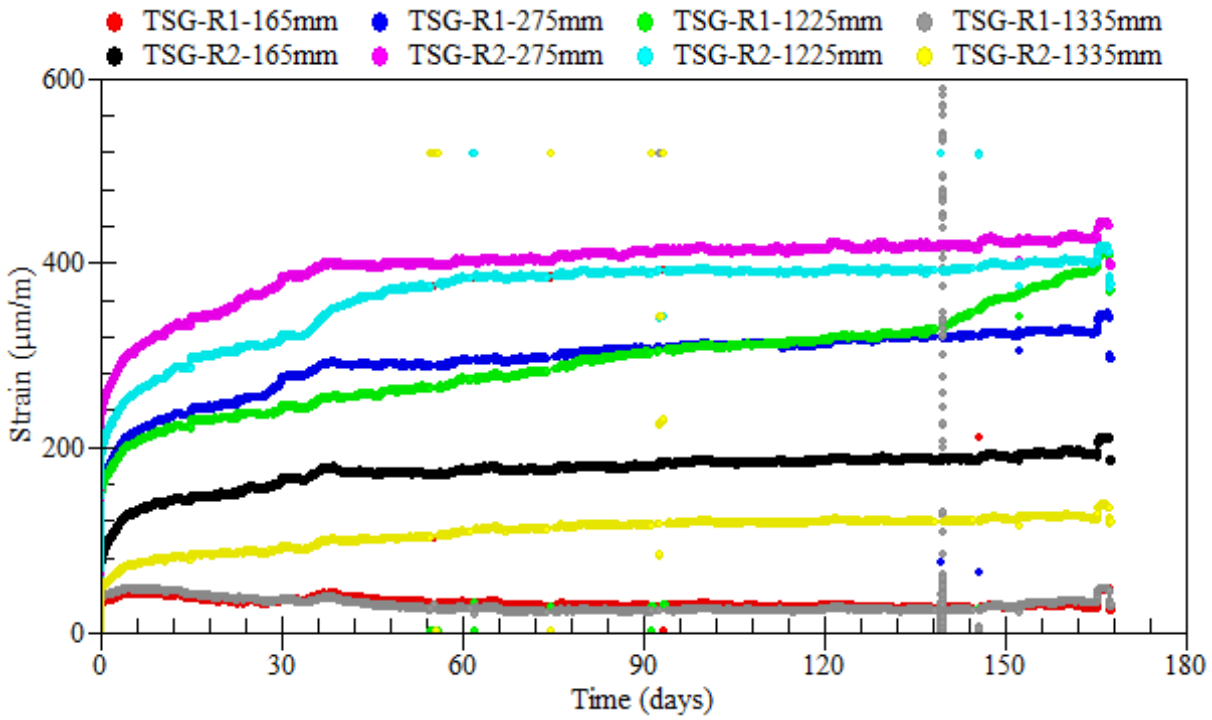

Figure A.112: Strain readings of longitudinal tensile steel bars – beam SS-4.2

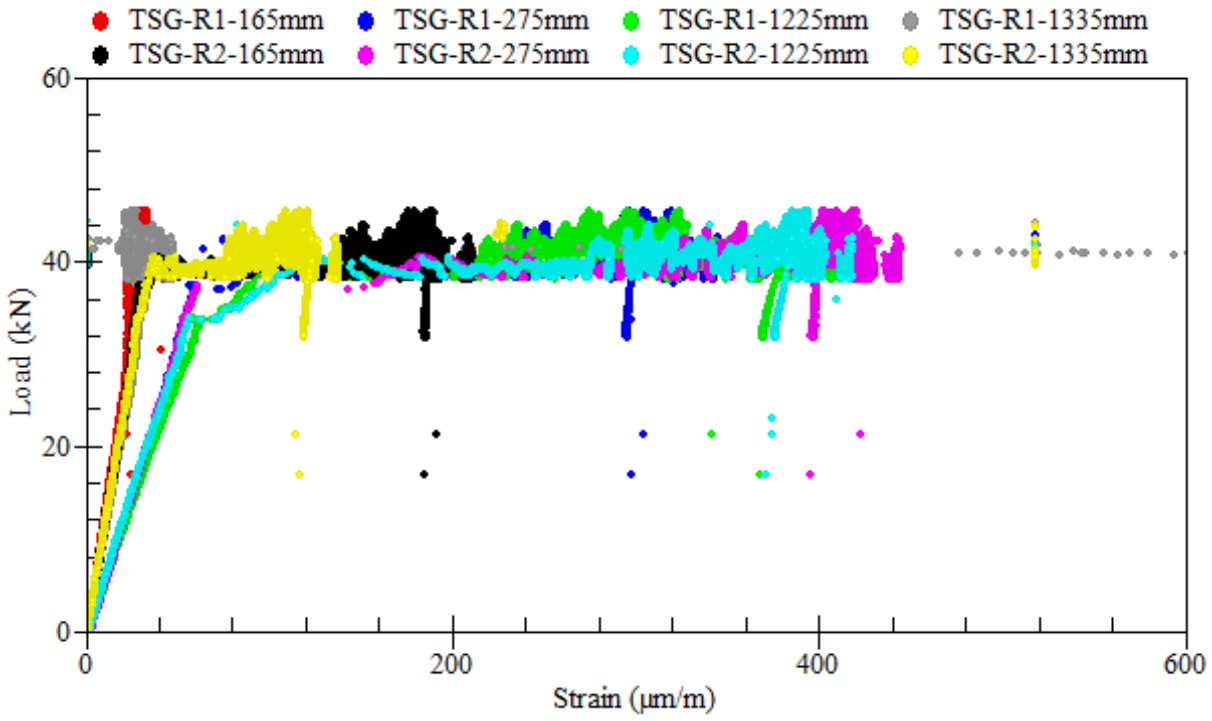

Figure A.113: Load-strain relationships of longitudinal tensile steel bars – beam SS-4.2

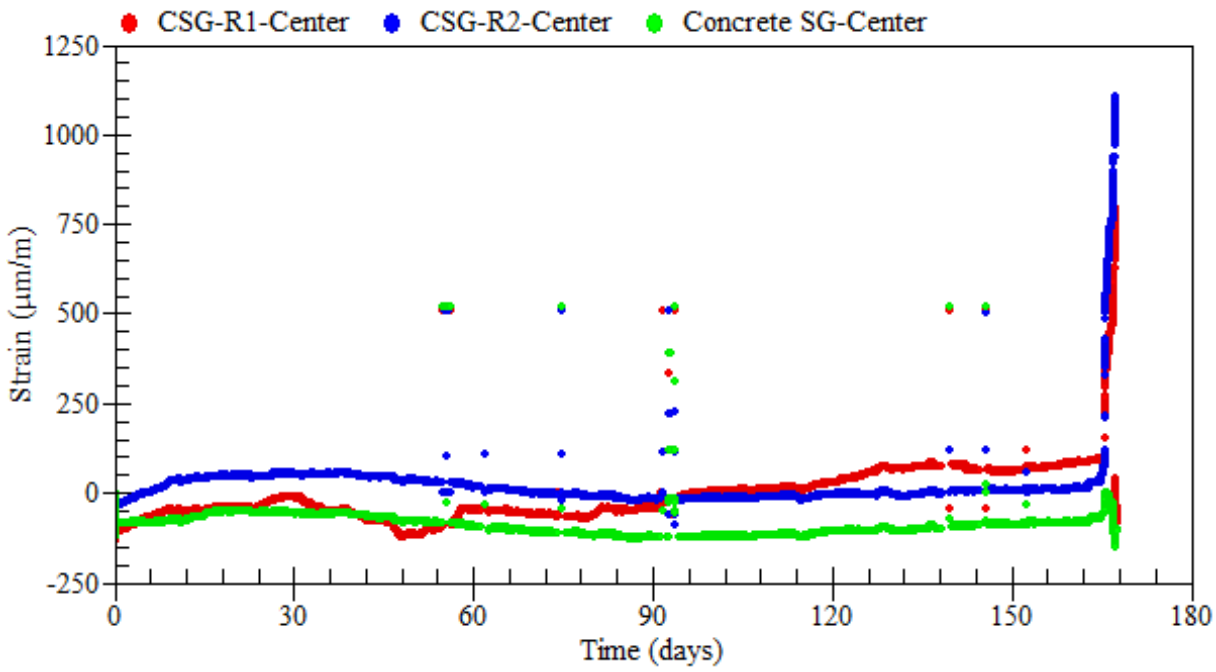

Figure A.114: Strain readings of longitudinal compressive steel bars – beam SS-4.2

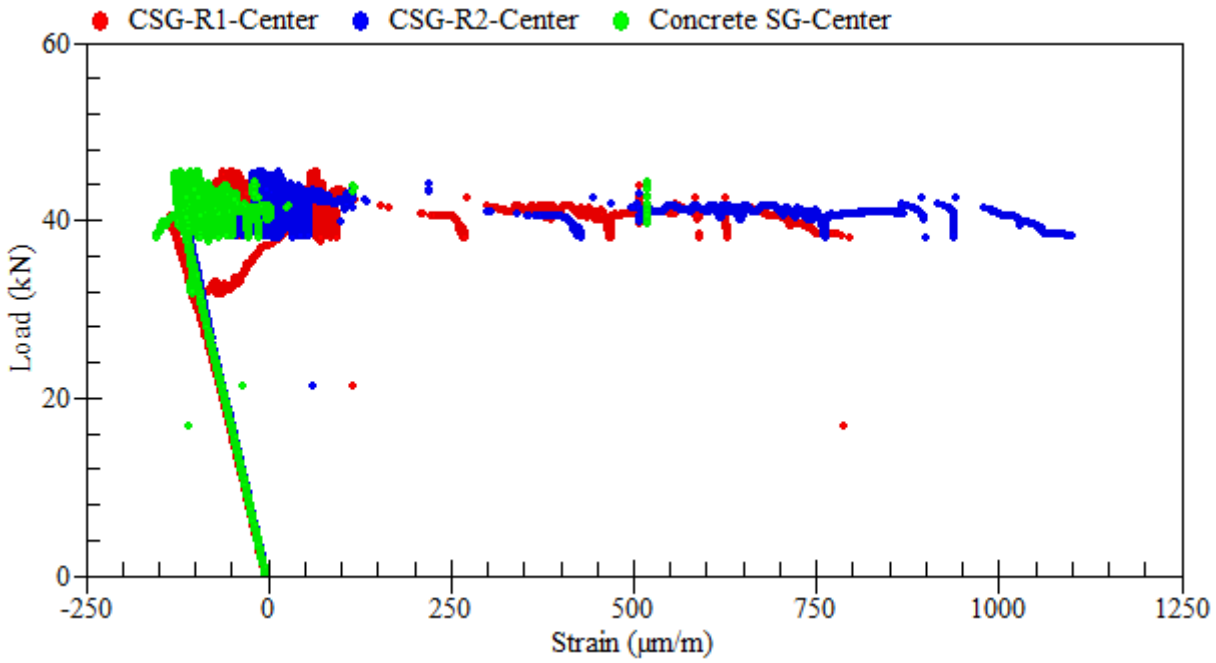

Figure A.115: Load-strain relationships of longitudinal compressive steel bars – beam SS-4.2

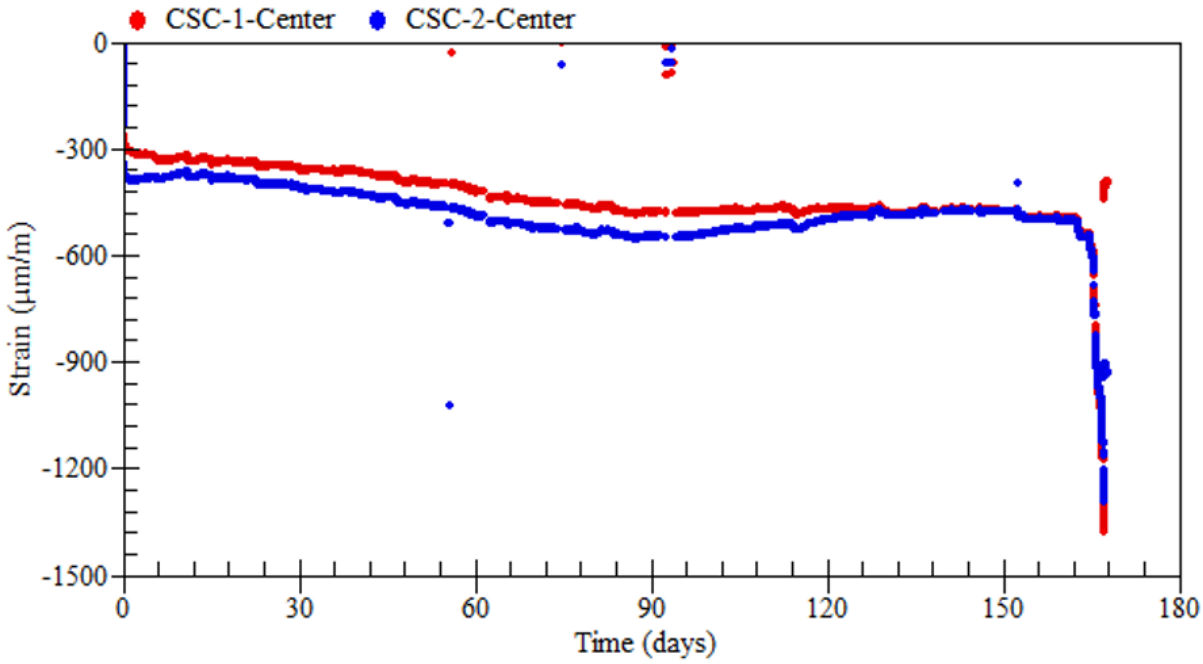

Figure A.116: Strain readings of external rosettes on top – beam SS-4.2

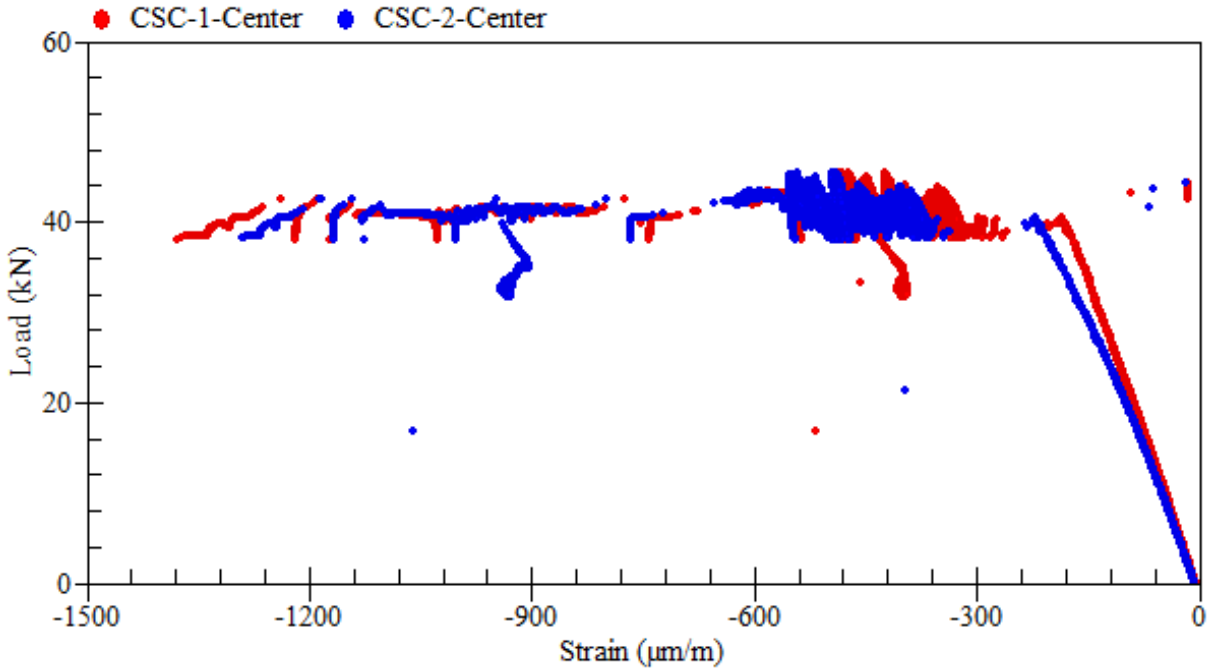

Figure A.117: Load-strain relationships of external rosettes on top – beam SS-4.2

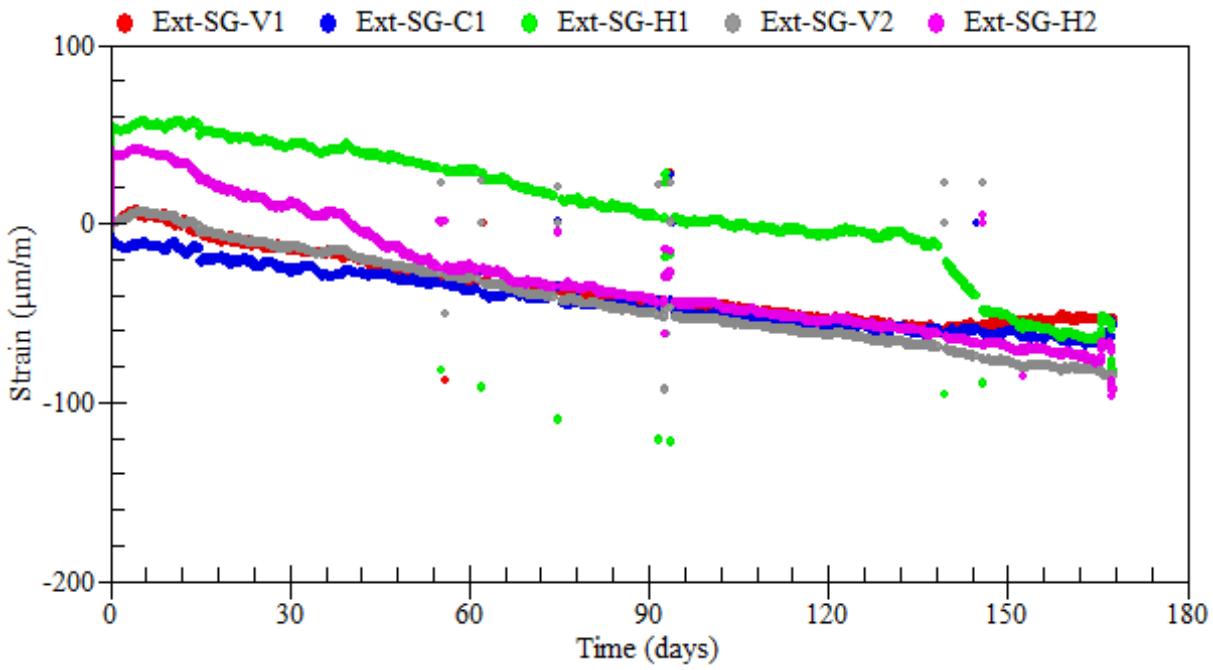

Figure A.118: Strain readings of external rosettes on sides – beam SS-4.2

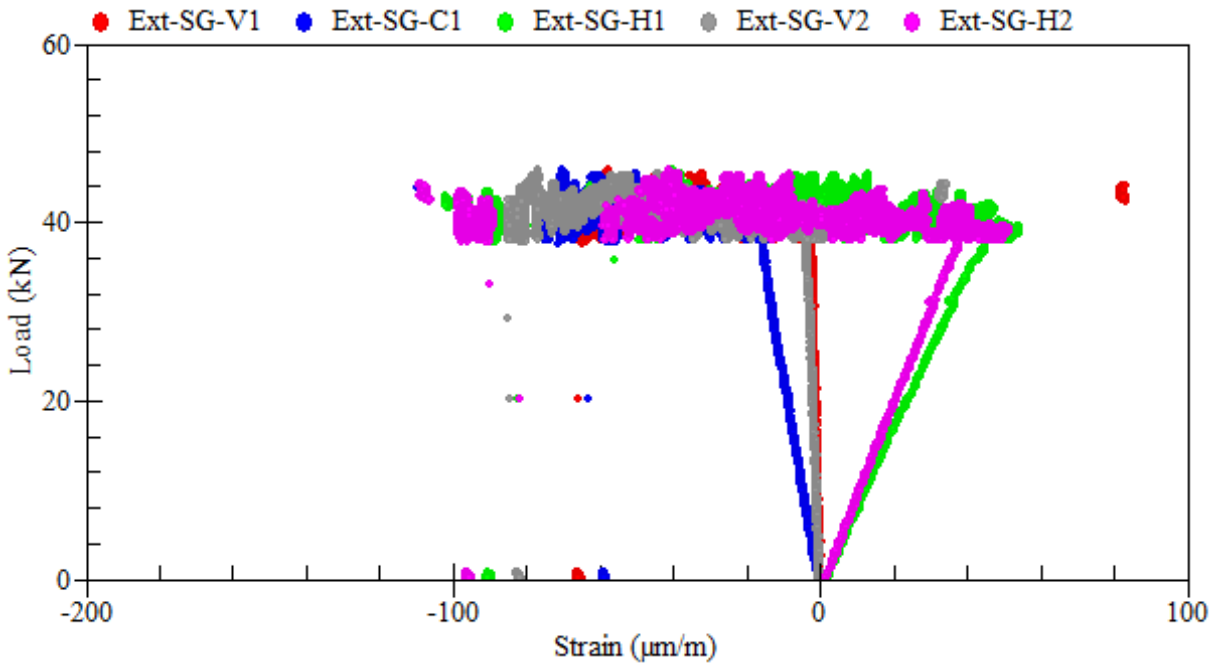

Figure A.119: Load-strain relationships of external rosettes on sides – beam SS-4.2

A.9 Beam SS-5.1

Beam SS-5.1 was corroded under its' self-weight only. Reinforcement corrosion was accelerated using a current density of 300 μA/cm^2 over a duration of 167 days. Then, the beam was loaded up until failure. The average mass loss of the beam was 32.9%. A summary of the gravimetric mass loss measurements of steel reinforcement is presented in Table A.7.

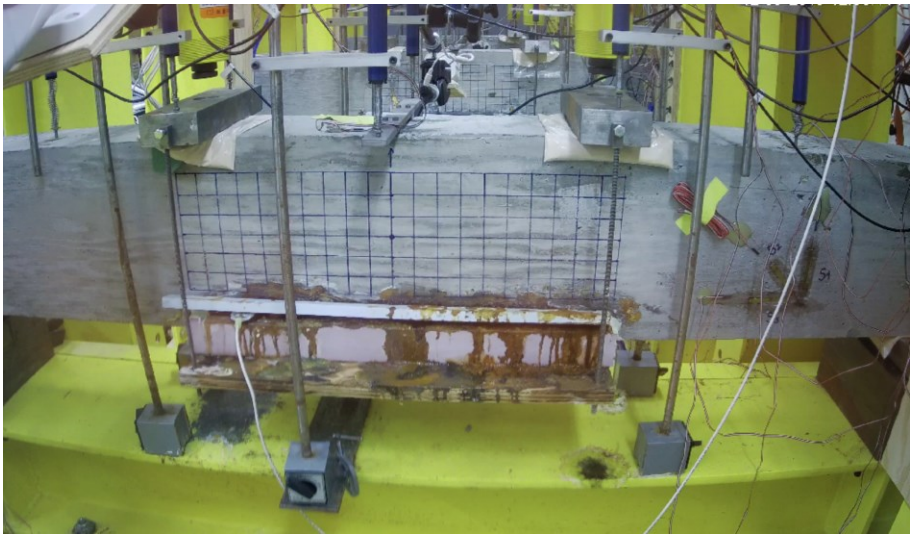

(a) during the test

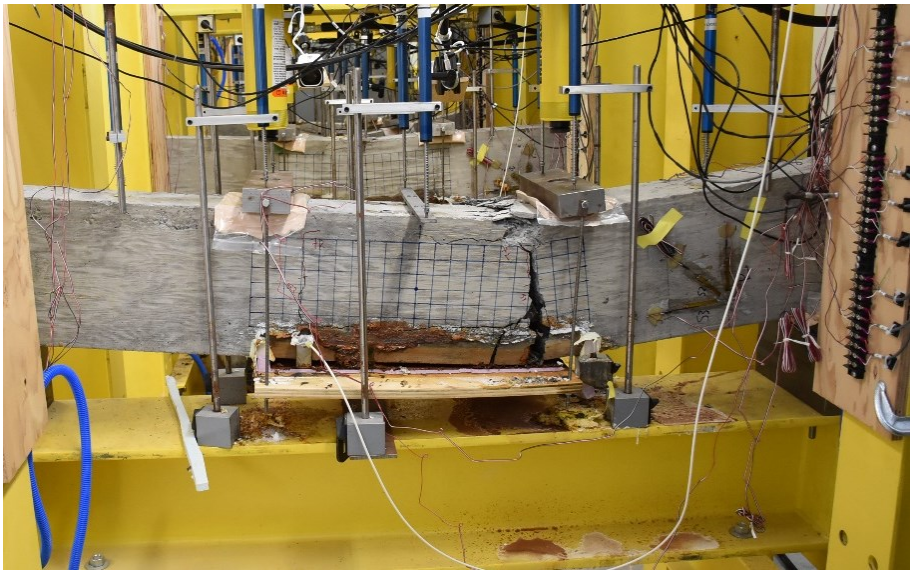

(b) at failure

Figure A.120: Crack propagation and patterns at failure – beam SS-5.1

Figure A.121: Corrosion-induced damage in the cover of concrete – beam SS-5.1

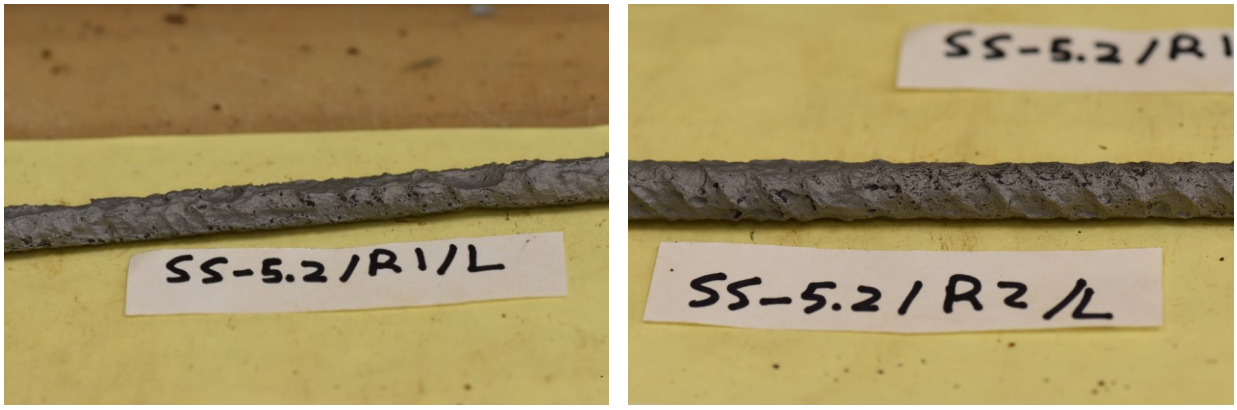

Figure A.122: Corrosion patterns on the clean surface of steel reinforcement – beam SS-5.1

Table A.7: Mass loss of corroded steel bars – beam SS-5.1

Rebar type	Rebar designation	Length (mm)	Mass (g)	Mass loss (%)
Control	R0	100.0	75.38	0.00
R1	R1-L	371.0	178.71	36.10
R2	R2-L	302.0	160.23	29.61

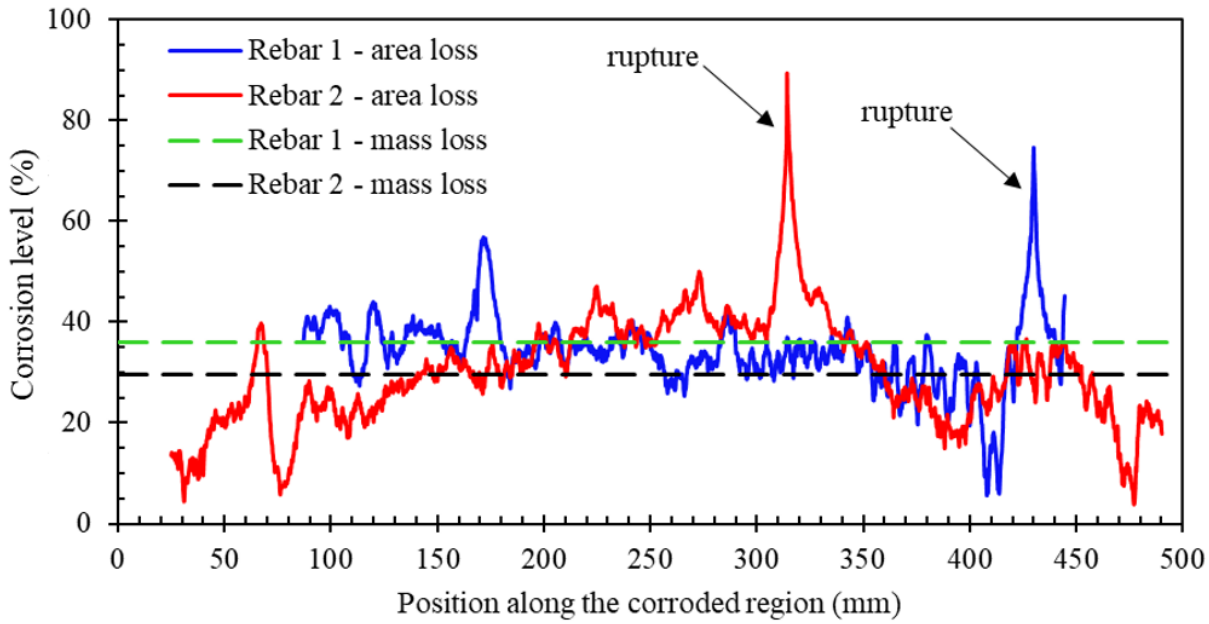

Figure A.123: Distribution of cross-sectional area loss along the corroded steel reinforcement – beam SS-5.1

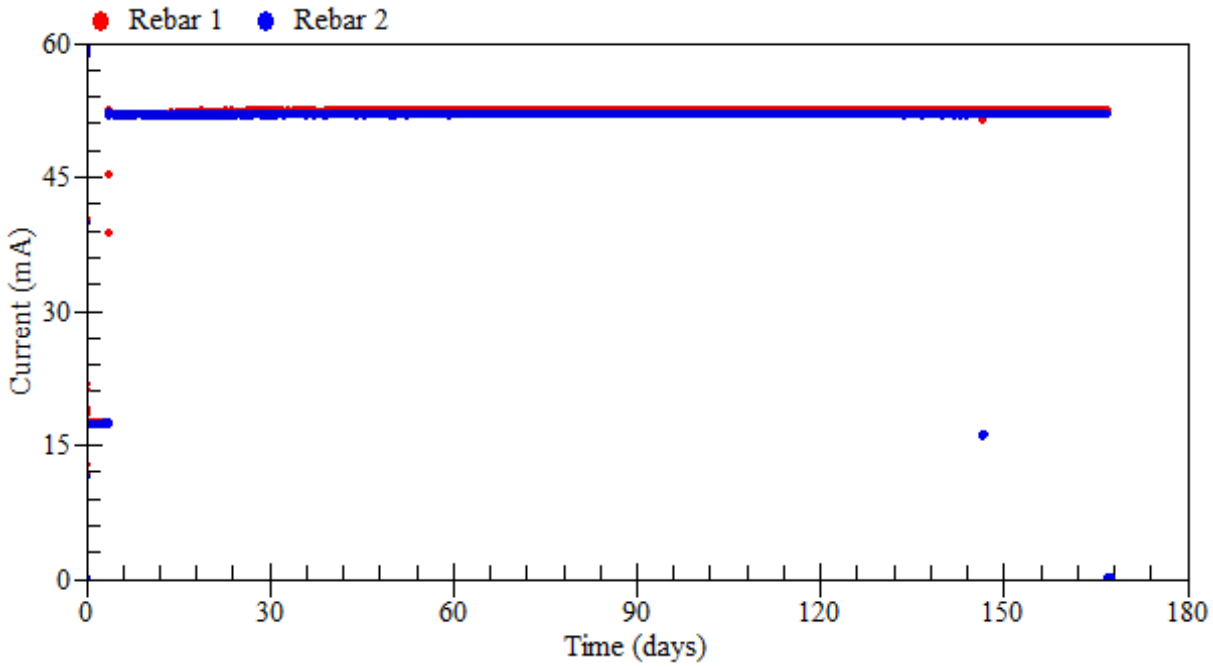

Figure A.124: Applied current – beam SS-5.1

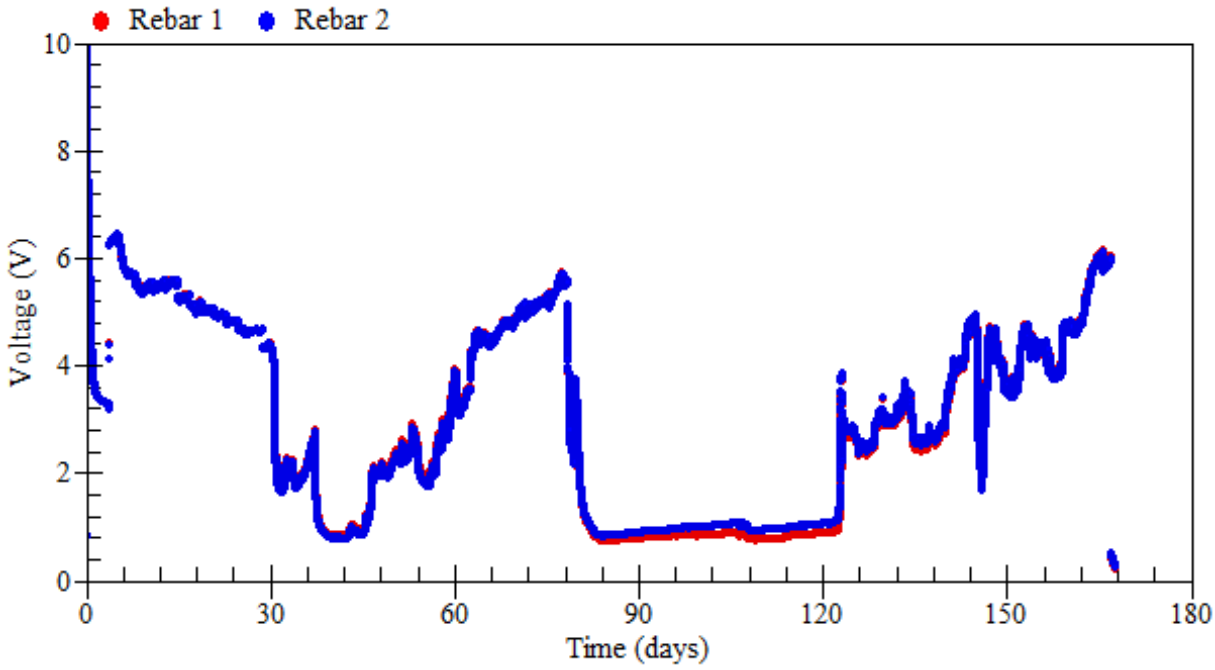

Figure A.125: Voltage measurements – beam SS-5.1

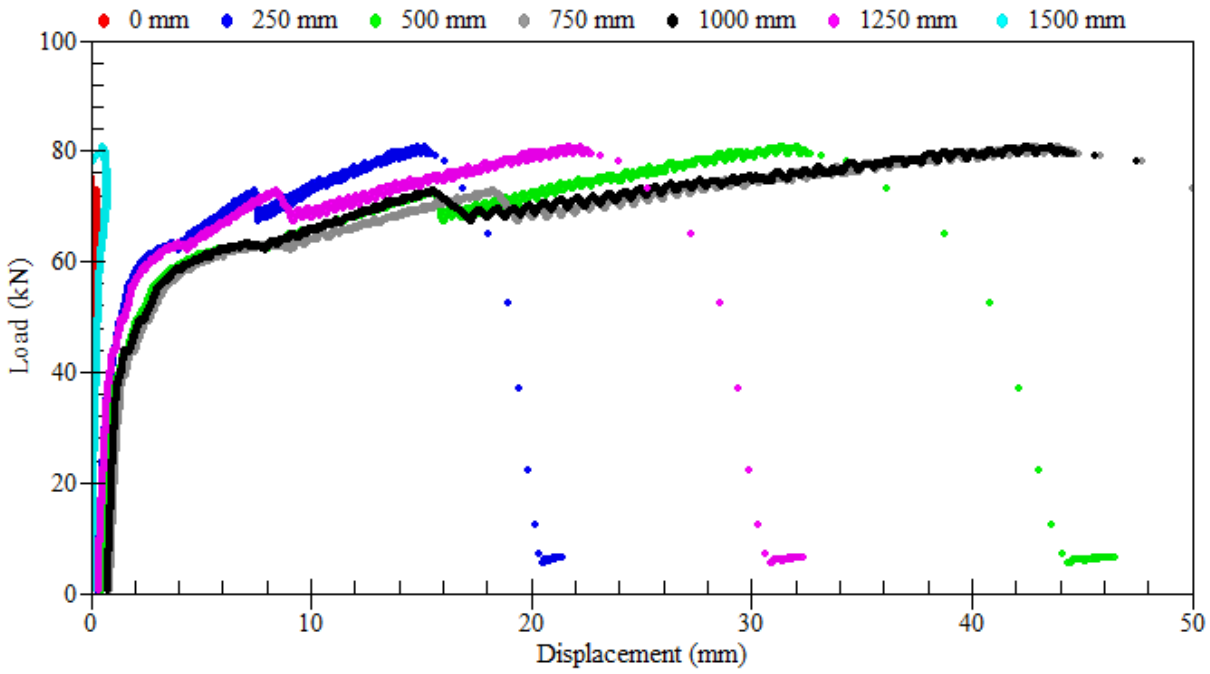

Figure A.126: Load-displacement relationships – beam SS-5.1

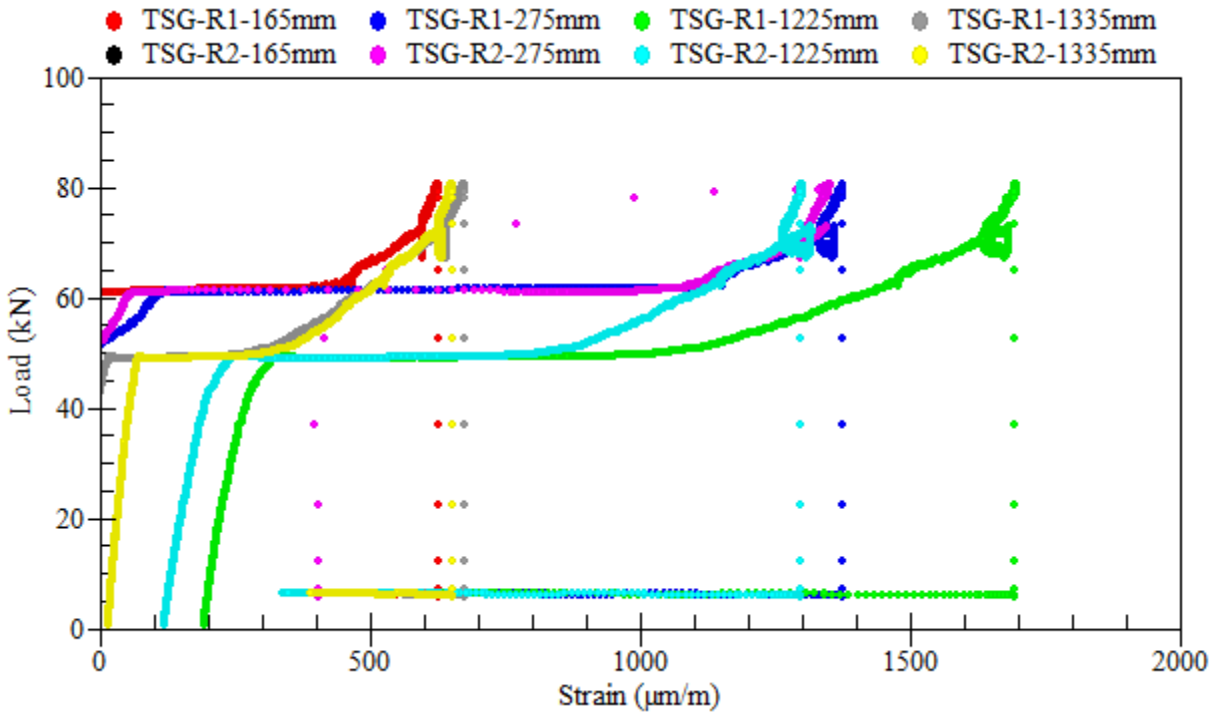

Figure A.127: Load-strain relationships of longitudinal tensile steel bars – beam SS-5.1

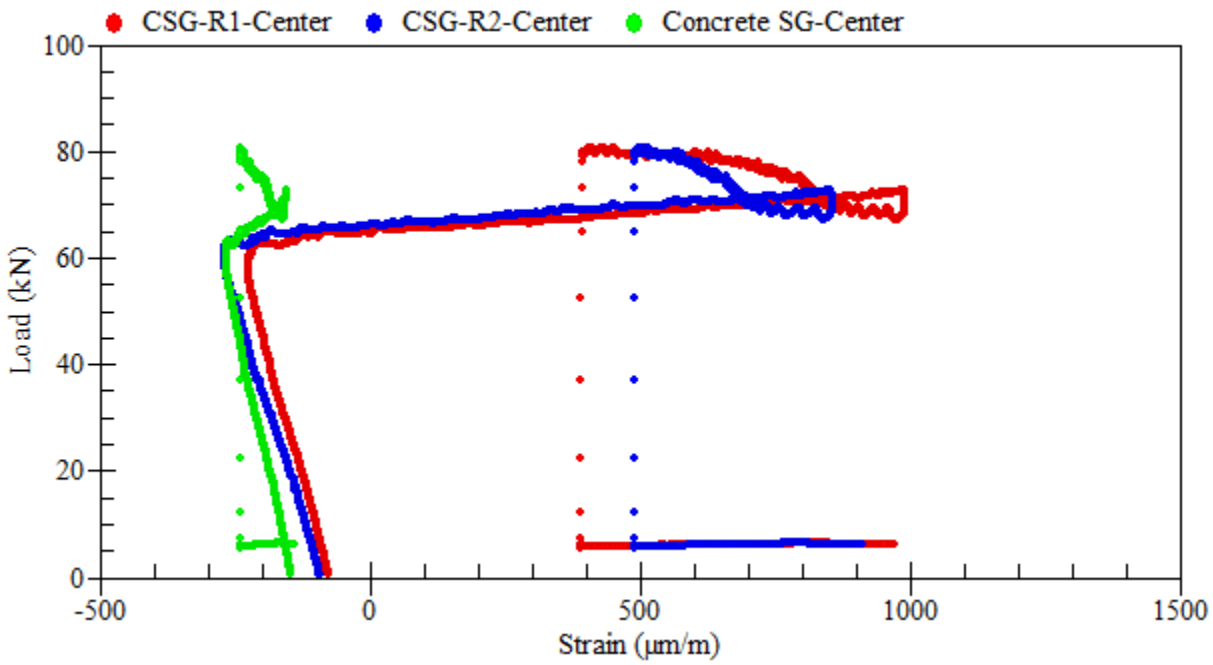

Figure A.128: Load-strain relationships of longitudinal compressive steel bars – beam SS-5.1

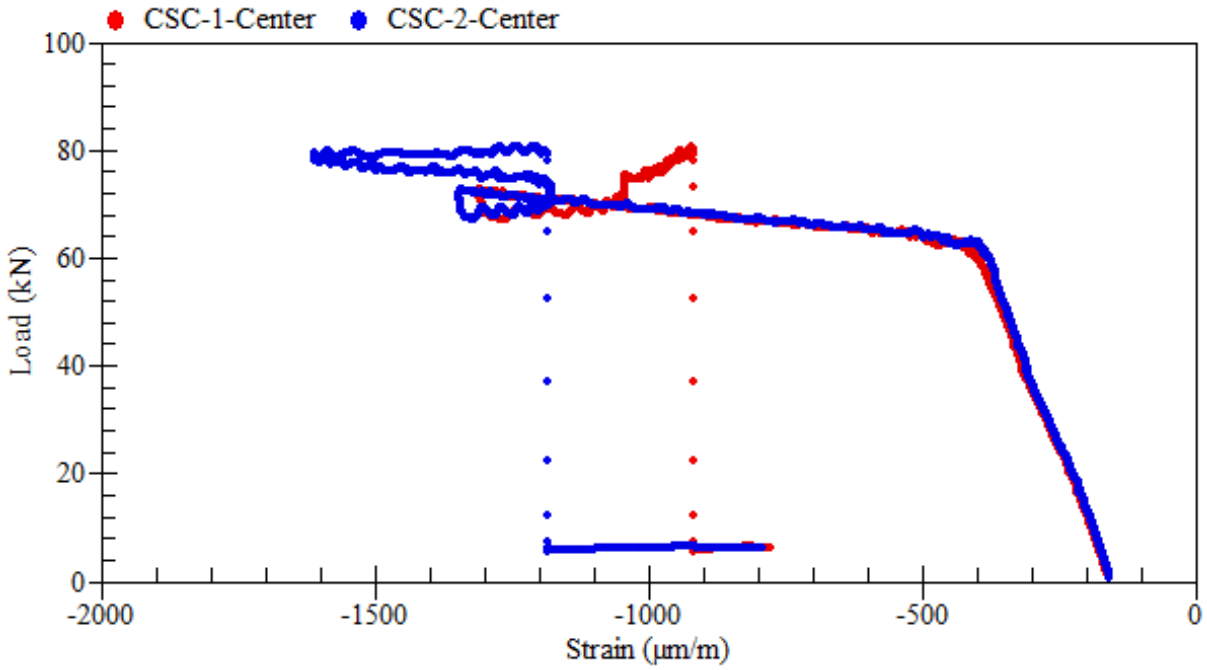

Figure A.129: Load-strain relationships of external rosettes on top – beam SS-5.1

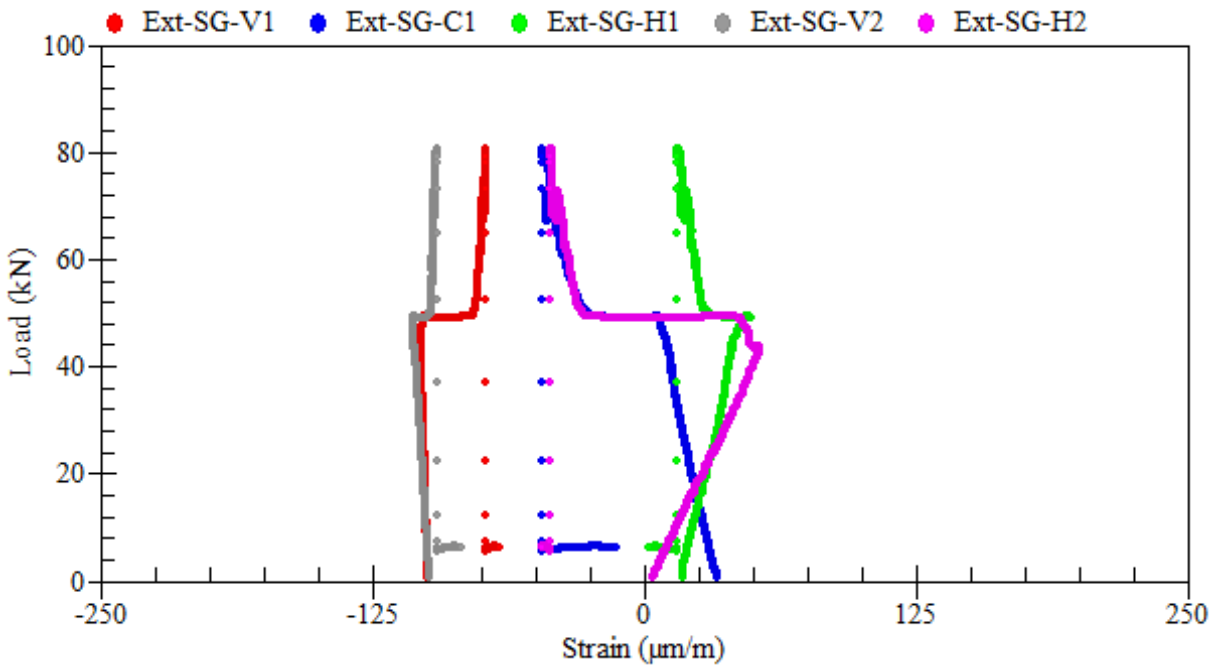

Figure A.130: Load-strain relationships of external rosettes on sides – beam SS-5.1

Appendix B : Supplementary Material of Large-scale Beams

Appendix B provides supplementary materials for the experimental testing of small-scale RC beams. A brief presentation of these results and detailed discussions are presented in Chapter 4. This appendix includes images that were taken during the corrosion phase and at the failure of beams. It also presents the collected data during the corrosion and loading phases of the experimental testing. This includes: (i) voltage measurements, (ii) applied loads, (iii) displacements, and (iii) internal and external strains readings.

Voltage measurements were monitored during the corrosion phase of testing. Each longitudinal tensile steel bar embedded in the large-scale beams (i.e., labelled as Rebar 1, Rebar 2 and Rebar 3) had its own power supply.

Applied loads were monitored using load cells that were connected to the pumps. Displacements were measured using linear variable differential transformers (LVDT). A total of six LVDTs were placed at various positions along the top surface of large-scale beams, as illustrated in Figure B.1. All LVDTs were labelled according to their position away from the left support. For example, LVDT-2 was labelled as 500 mm, while the average of LVDT-3 and LVDT-4 was labelled as 1500 mm.

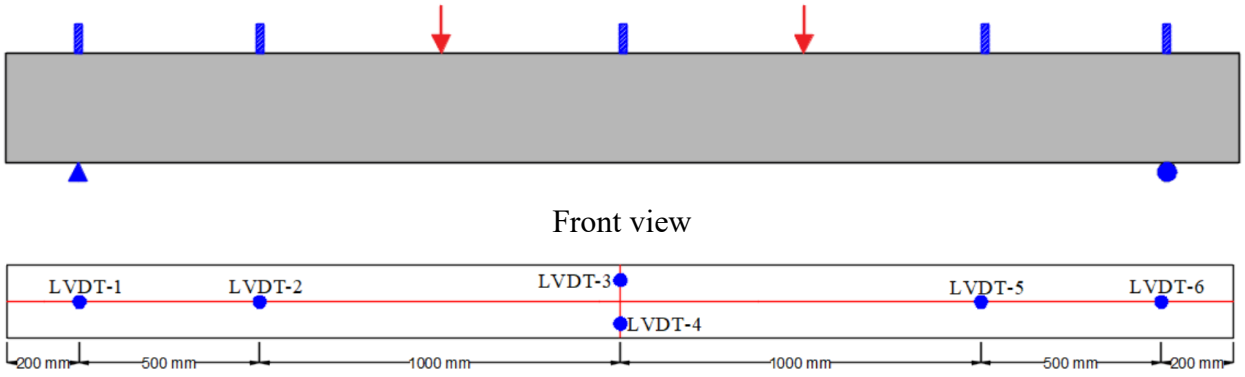

Figure B.1: Positions of LVDTs along the top surface of large-scale beams

A total of ten electrical strain gauges were attached at select positions on the tensile and compressive longitudinal steel bars. In addition, one internal concrete strain gauge was placed at the center of the beam between the top longitudinal steel bars. The location and labelling of all internal strain gauges are shown in Figure B.2. The position of internal strain gauges was carefully

selected for a better understanding of the behavior of compression struts between loads and supports.

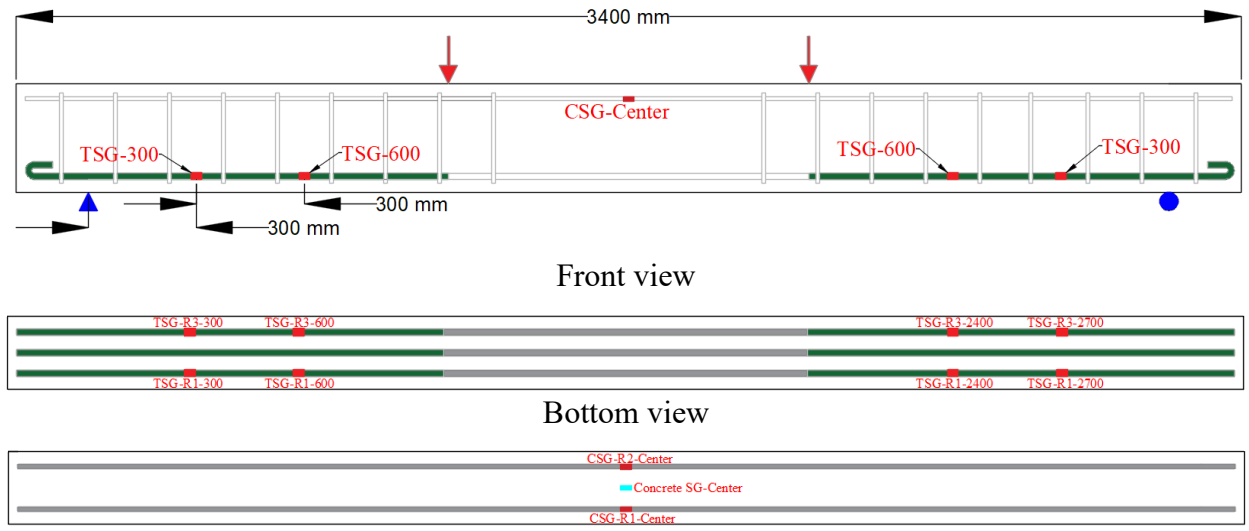

Figure B.2: Position of internal strain gauges – large-scale beams

External triaxial rosette strain gauges were attached on the side surface of concrete. Three sets of external triaxial rosette strain gauges were attached at each side of the beam, as illustrated in Figure B.3. The positions and number of external triaxial rosette strain gauges were selected to capture the change in the strut angle during the experimental testing. The horizontal gauge (H), inclined gauge (C), and vertical gauge (V) on the front face of the beam were labelled as EXT-SG-H1, EXT-SG-C1, and EXT-SG-V1. The gauges attached on the back face of the beam were labelled with the number 2 instead of 1. For example, the horizontal gauge on the back face of the beam was labelled as EXT-SG-H2. In addition, two external strain gauges were attached on the top surface of concrete at mid-span. These gauges were labelled as CSC-1-Center and CSC-2-Center.

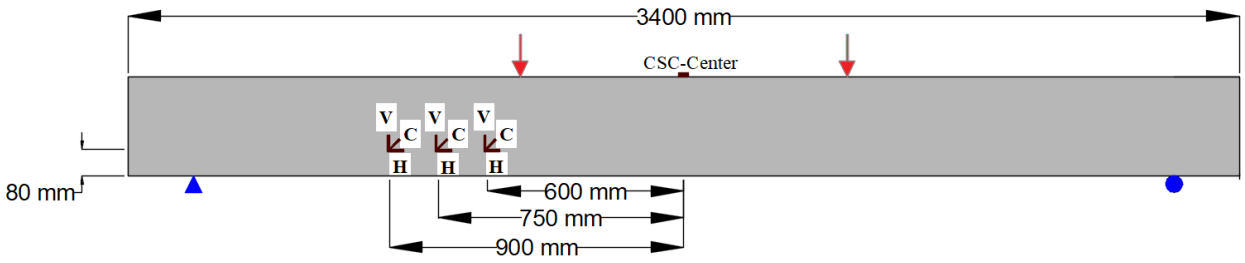

Figure B.3: Positions of external strain gauges – large-scale beams

B.1 Beam LS-1.1

Beam LS-1.1 served as a control specimen without reinforcement corrosion.

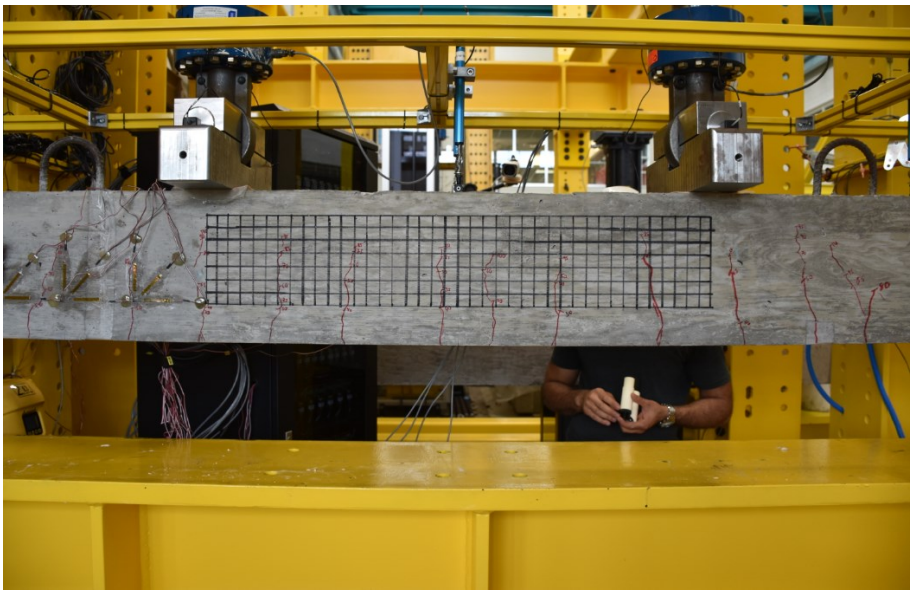

(a)

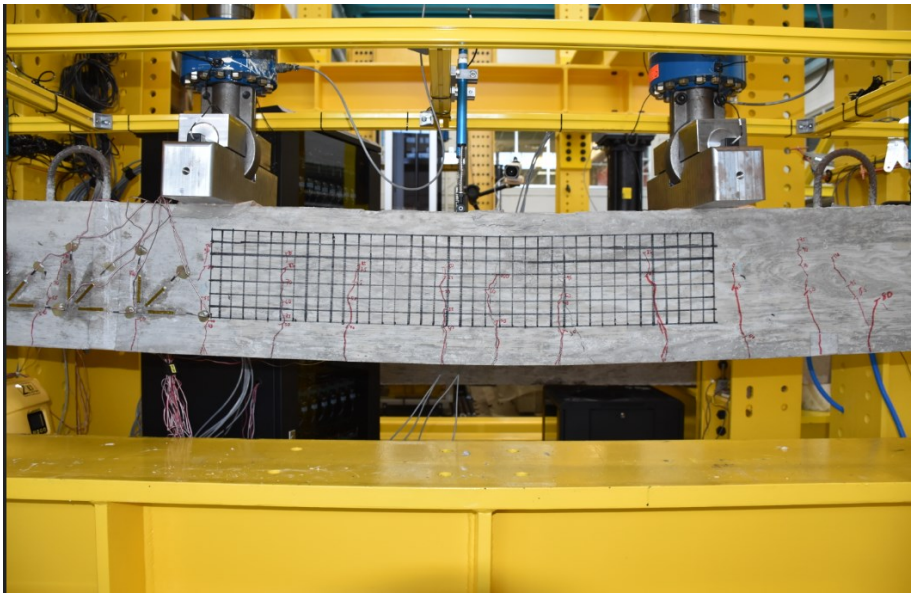

(b)

Figure B.4: Crack propagation and patterns at failure – beam LS-1.1

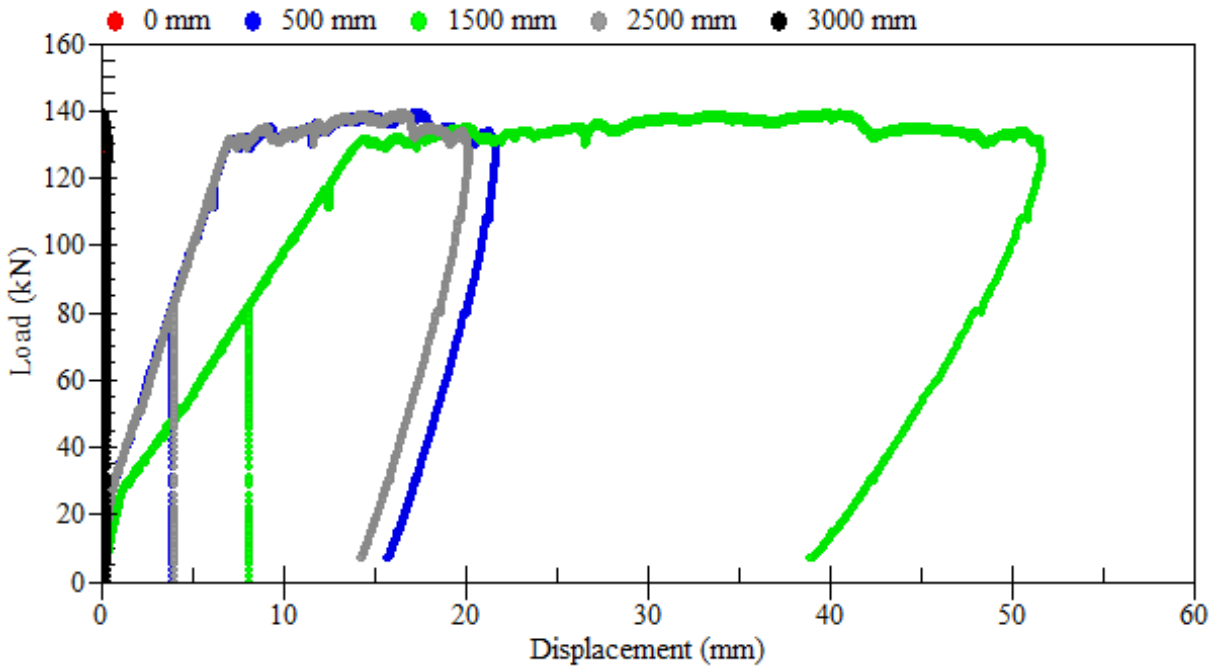

Figure B.5: Load-displacement relationships – beam LS-1.1

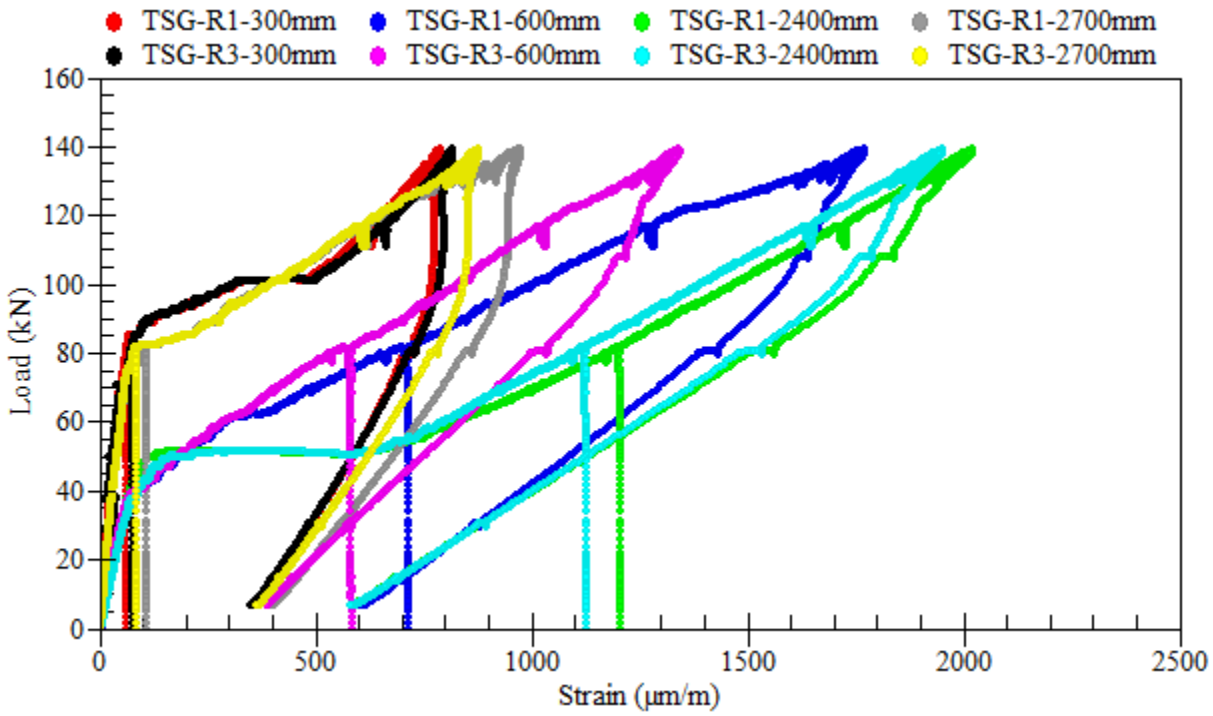

Figure B.6: Load-strain relationships of longitudinal tensile steel bars – beam LS-1.1

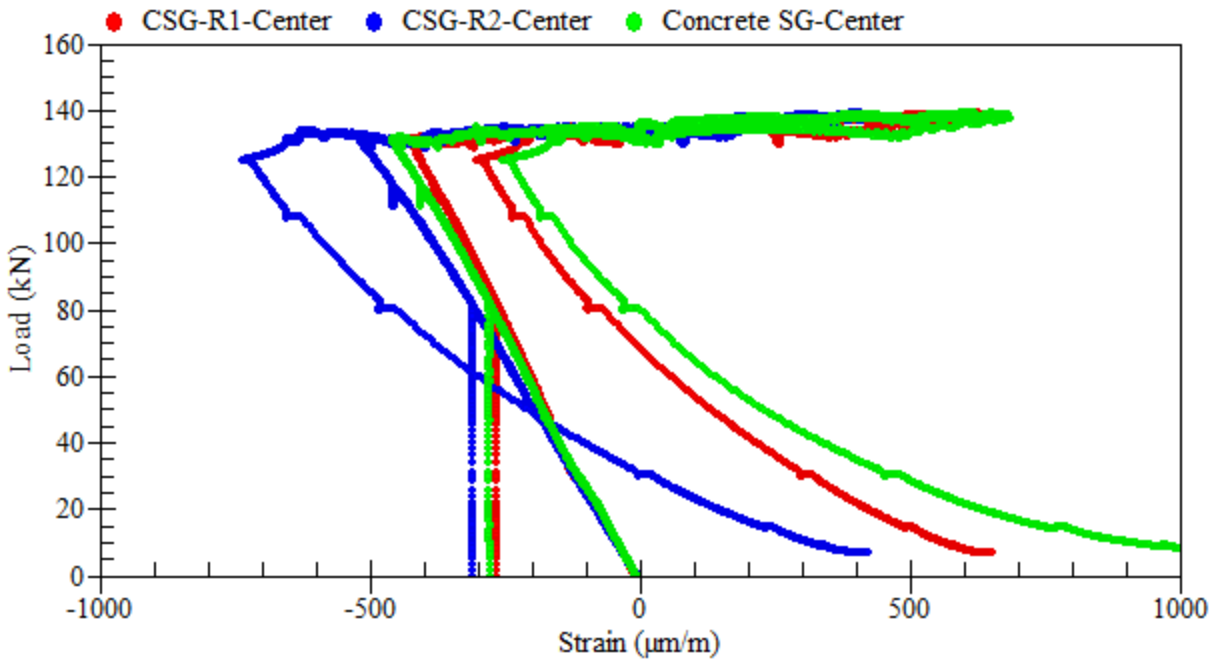

Figure B.7: Load-strain relationships of longitudinal compressive steel bars – beam LS-1.1

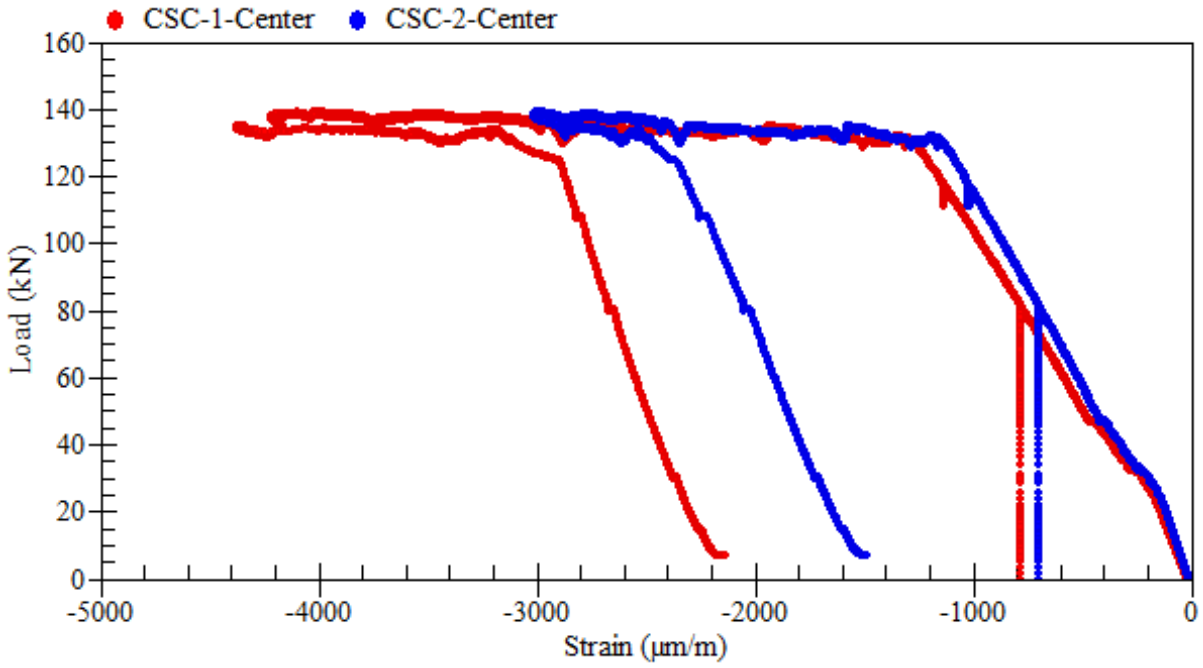

Figure B.8: Load-strain relationships of external rosettes on top – beam LS-1.1

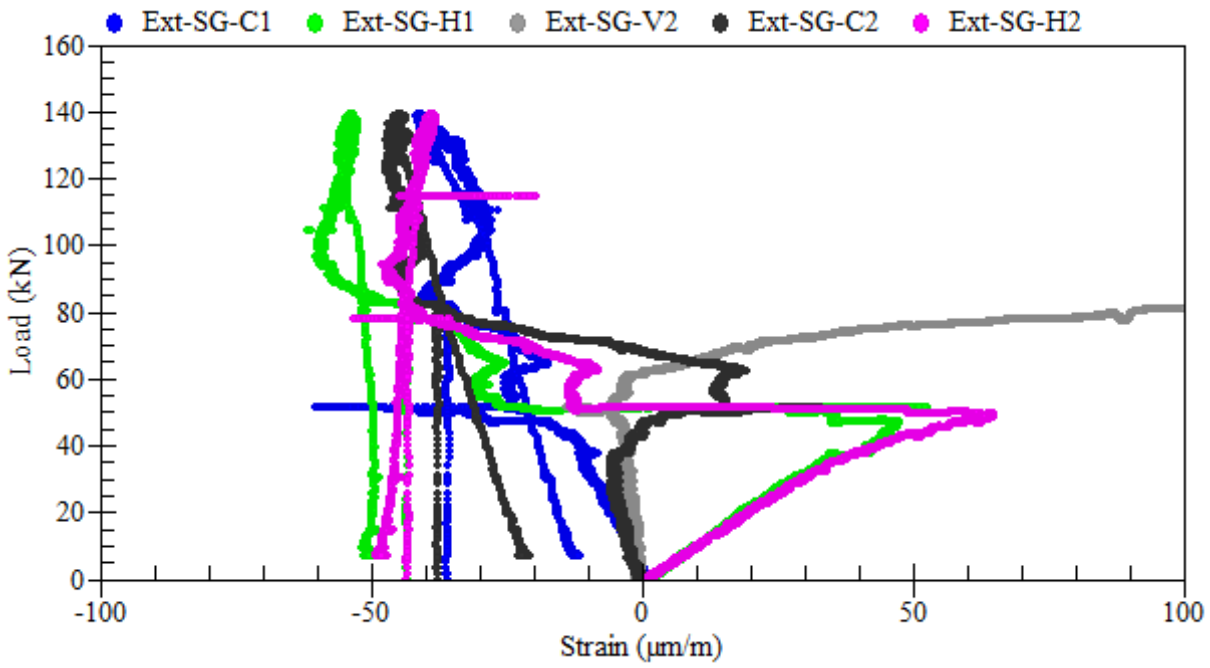

Figure B.9: Load-strain relationships of external rosettes on sides at 600 mm away from center – beam LS-1.1

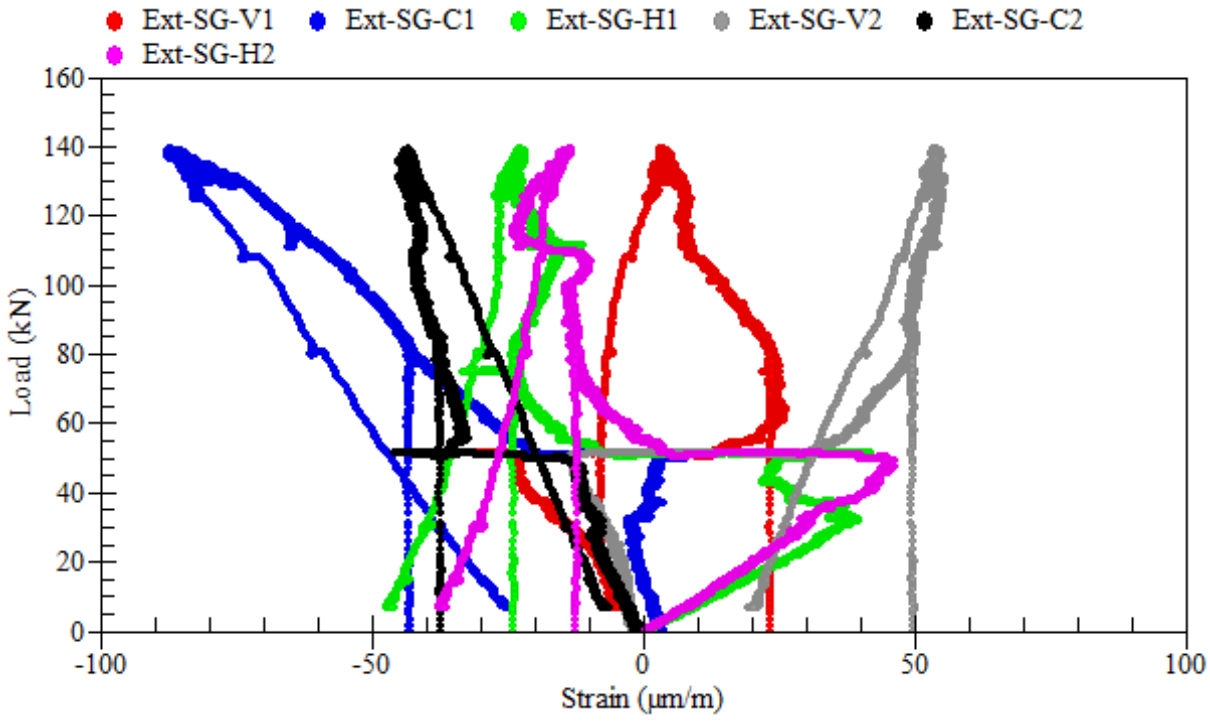

Figure B.10: Load-strain relationships of external rosettes on sides at 750 mm away from center – beam LS-1.1

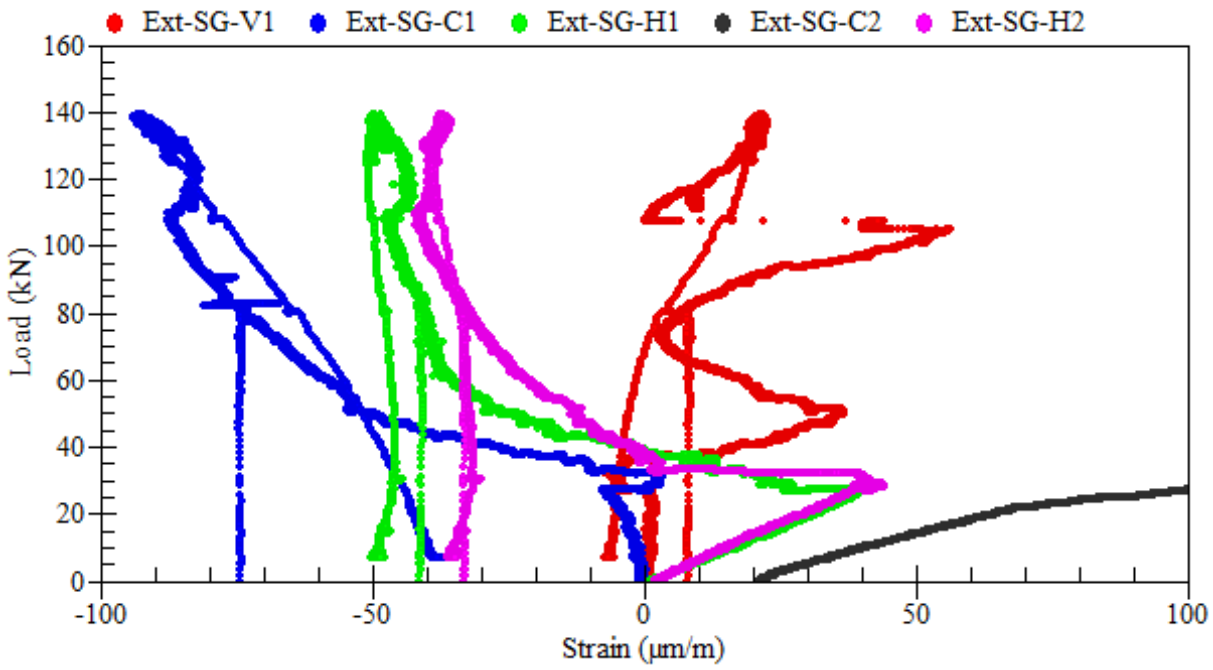

Figure B.11: Load-strain relationships of external rosettes on sides at 900 mm away from center – beam LS-1.1

B.2 Beam LS-1.2

Beam LS-1.2 served as a control specimen without reinforcement corrosion.

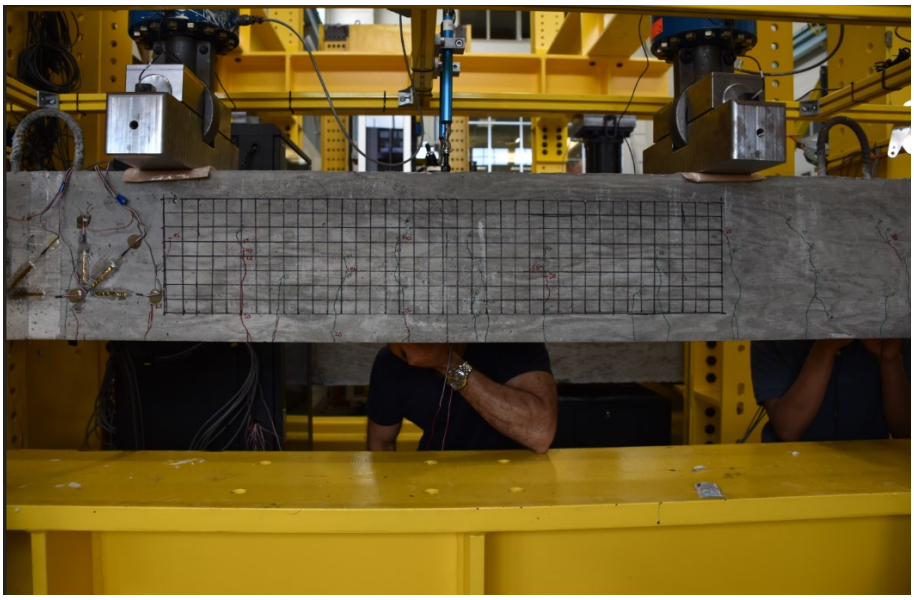

(a)

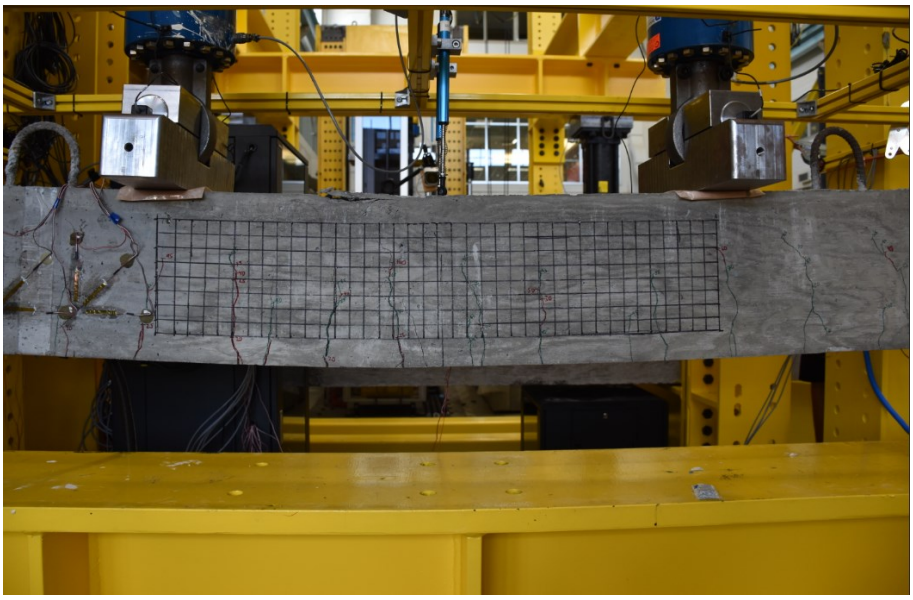

(b)

Figure B.12: Crack propagation and patterns at failure – beam LS-1.2

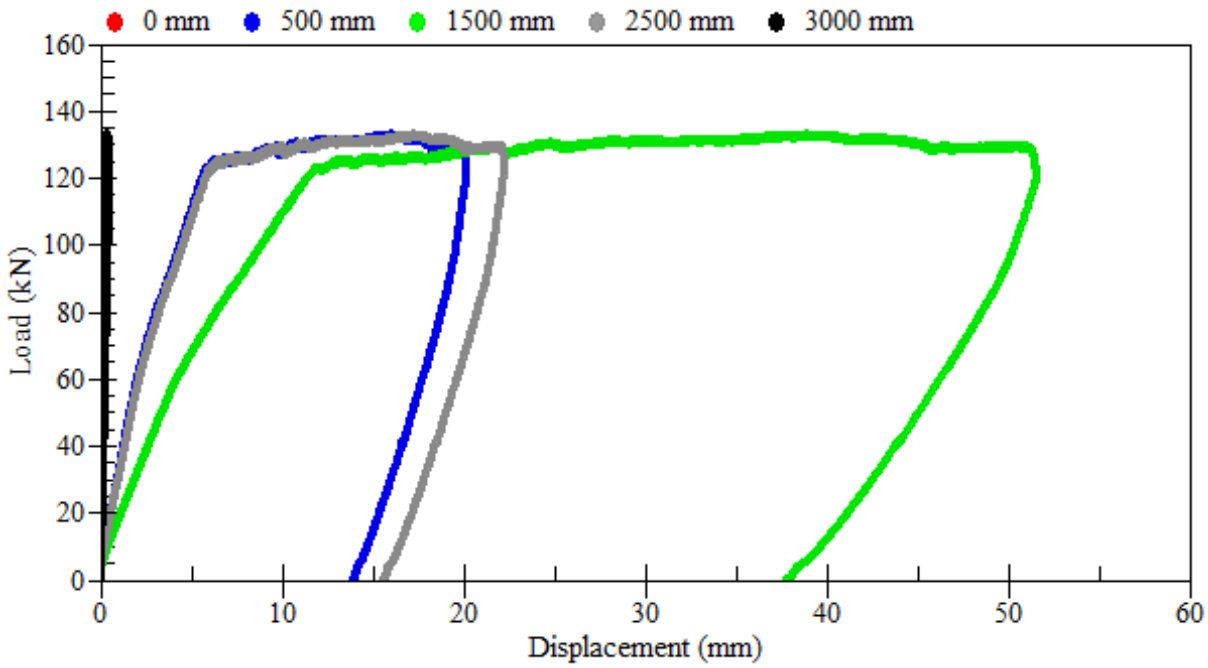

Figure B.13: Load-displacement relationships – beam LS-1.2

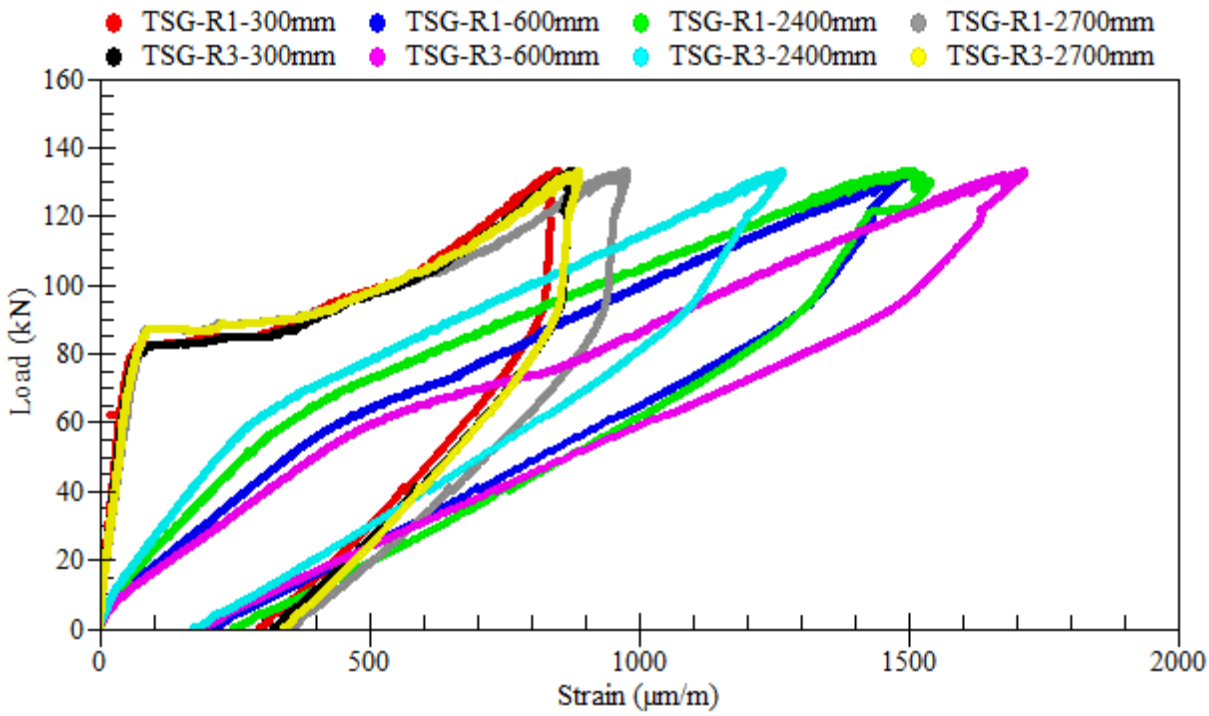

Figure B.14: Load-strain relationships of longitudinal tensile steel bars – beam LS-1.2

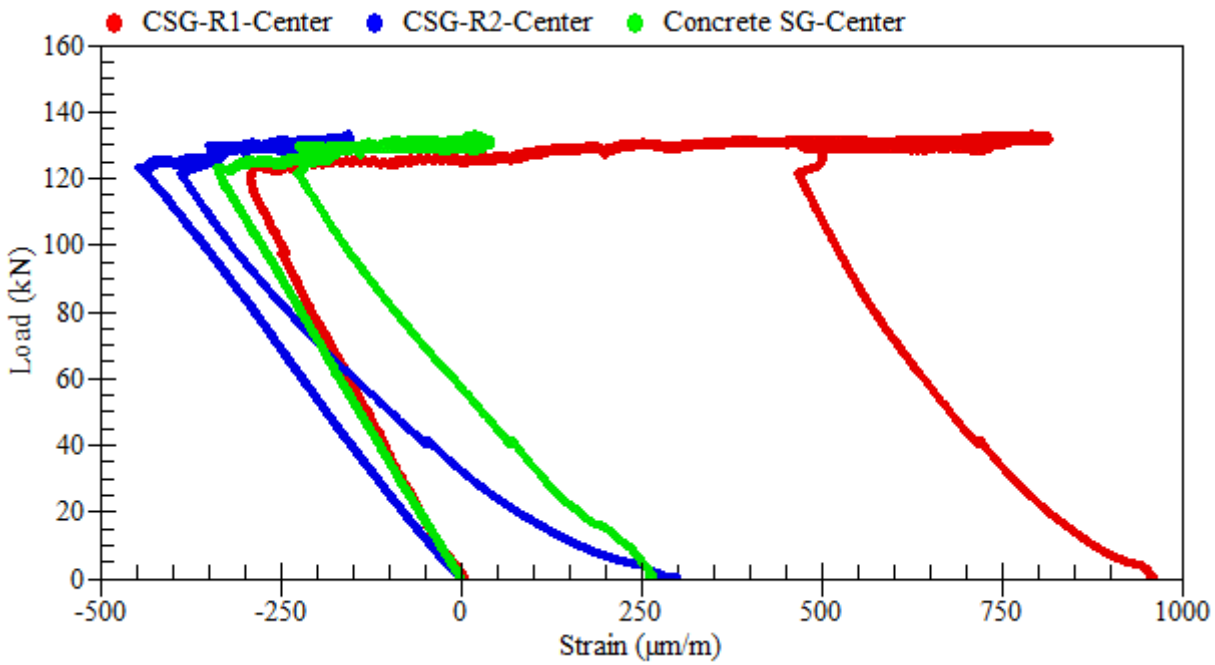

Figure B.15: Load-strain relationships of longitudinal compressive steel bars – beam LS-1.2

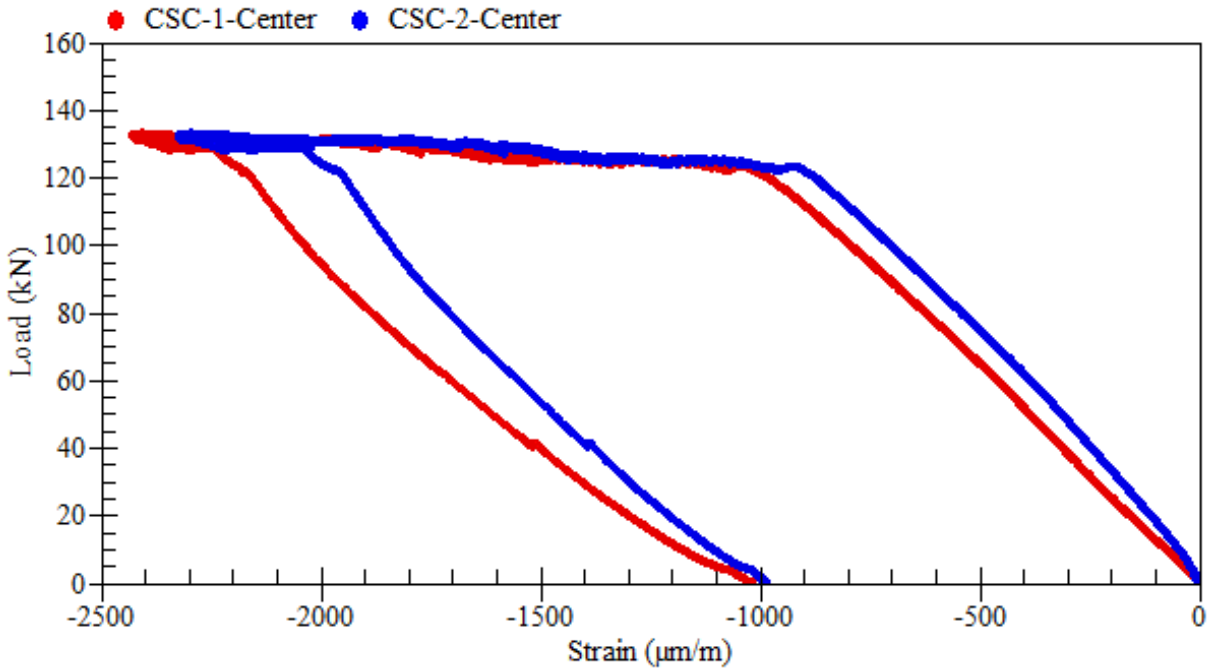

Figure B.16: Load-strain relationships of external rosettes on top – beam LS-1.2

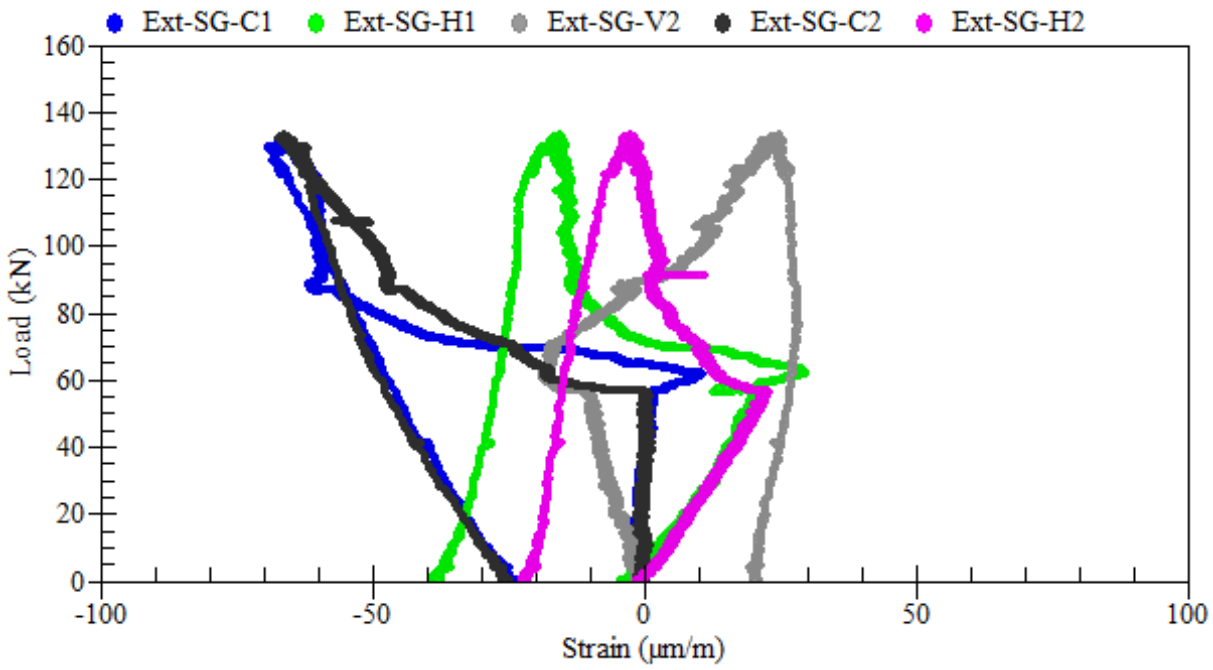

Figure B.17: Load-strain relationships of external rosettes on sides at 600 mm away from center – beam LS-1.2

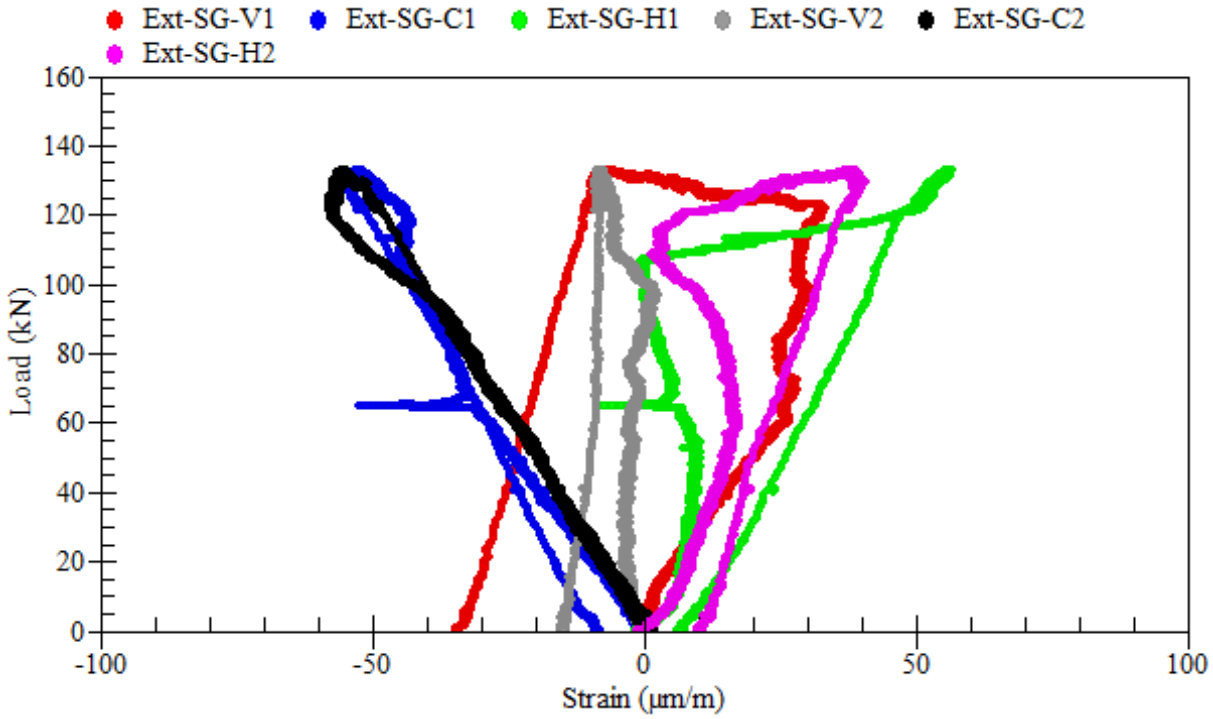

Figure B.18: Load-strain relationships of external rosettes on sides at 750 mm away from center – beam LS-1.2

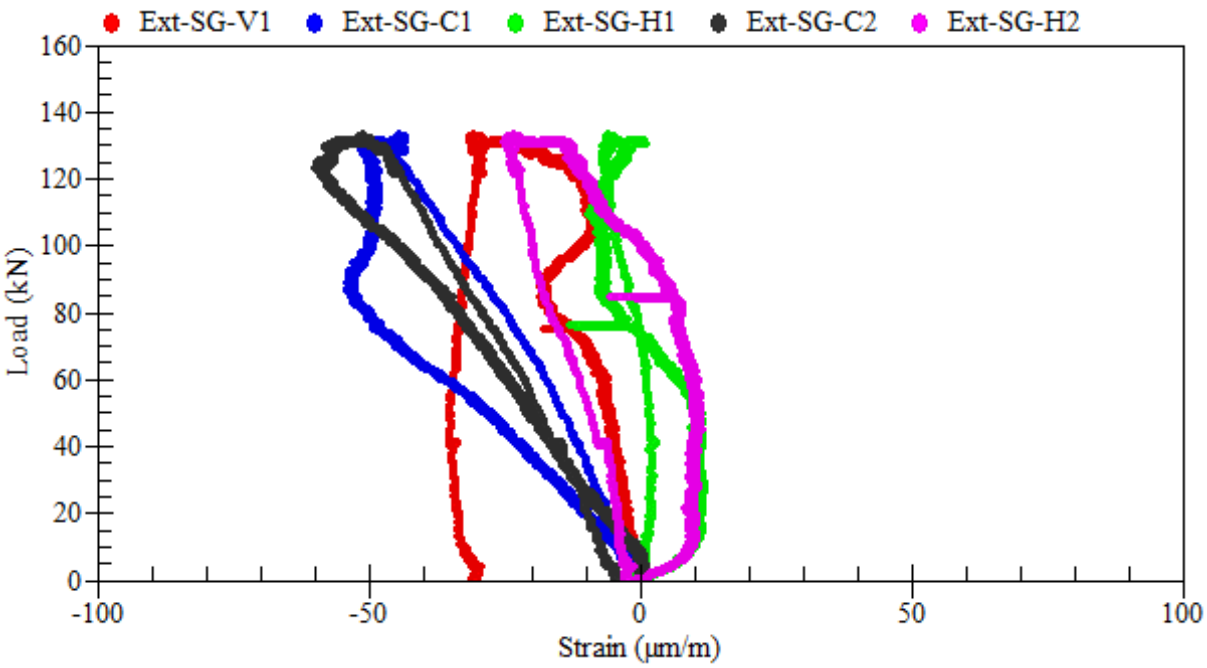

Figure B.19: Load-strain relationships of external rosettes on sides at 900 mm away from center – beam LS-1.2

B.3 Beam LS-2.1

Beam LS-2.1 was tested under the coupled effects of reinforcement corrosion and service loads. The applied sustained load was equivalent to 60% of the beam ultimate load capacity (i.e., 80 kN). Reinforcement corrosion was accelerated using a current density of 300 $\mu A/cm^2$ over a duration of 135 days before increasing it to 1000 $\mu A/cm^2$ up until the failure of the beam. The total duration of corrosion exposure was 150 days. The average mass loss of the beam was 21.1%. A summary of the gravimetric mass loss measurements of steel reinforcement is presented in Table B.1.

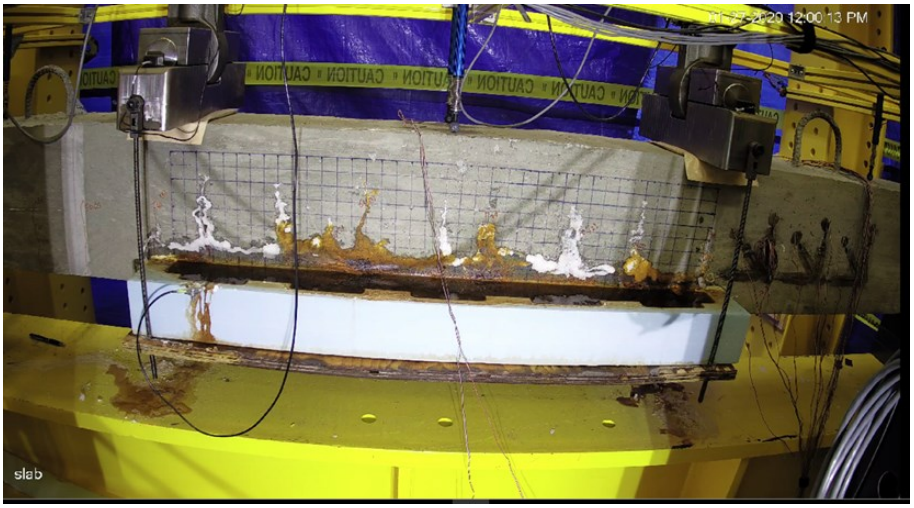

(a) during the test

(b) at failure

Figure B.20: Crack propagation and patterns at failure– beam LS-2.1

Figure B.21: Corrosion-induced damage in the cover of concrete – beam LS-2.1

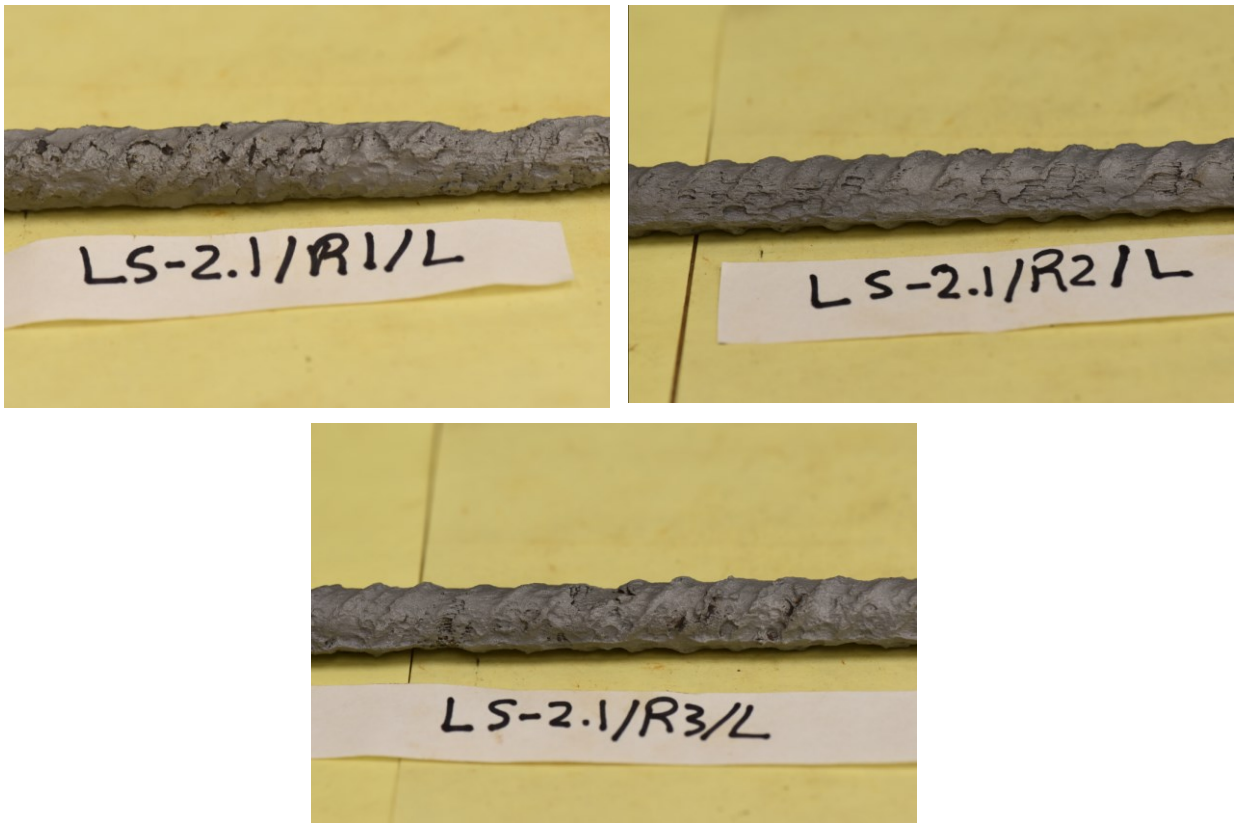

Figure B.22: Corrosion patterns on the clean surface of steel reinforcement – beam LS-2.1

Table B.1: Mass loss of corroded steel bars – beam LS-2.1

Rebar type	Rebar designation	Length (mm)	Mass (g)	Mass loss (%)	Rebar mass loss (%)
Control	R0	99	152.96	0	0
R1	R1-R	319	382.99	22.29	23.97
	R1-L-1	333	377.07	26.71	
	R1-L-2	250	299.56	22.45	
R2	R2-R	328	435.4	14.08	17.12
	R2-L-1	325	398.91	20.56	
	R2-L-2	250	322.06	16.62	
R3	R3-R	323	383.38	23.18	22.31
	R3-L-1	326	395.78	21.42	
	R3-L-2	249	298.72	22.35	

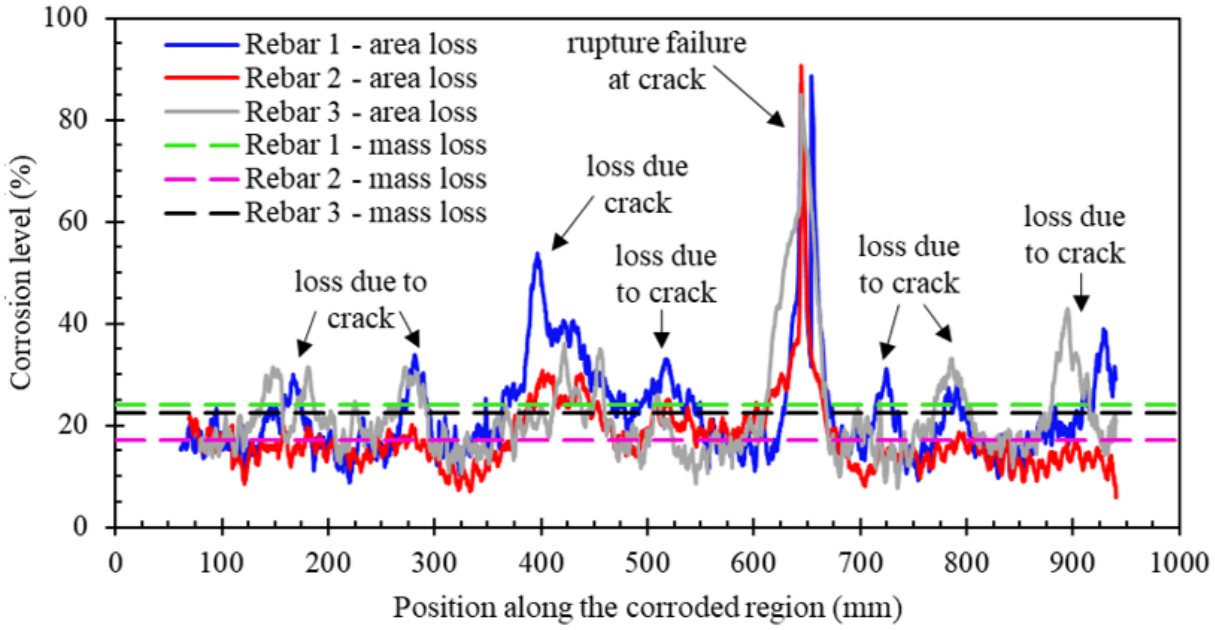

Figure B.23: Distribution of cross-sectional area loss along the corroded steel reinforcement – beam LS-2.1

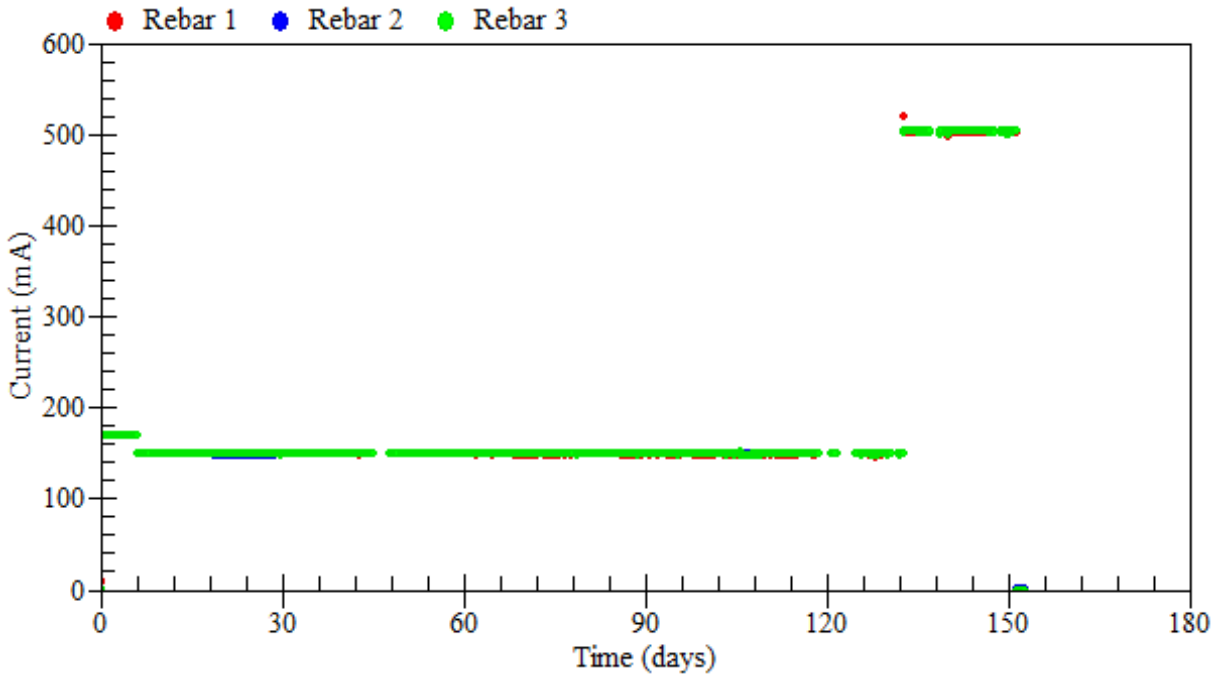

Figure B.24: Applied current – beam LS-2.1

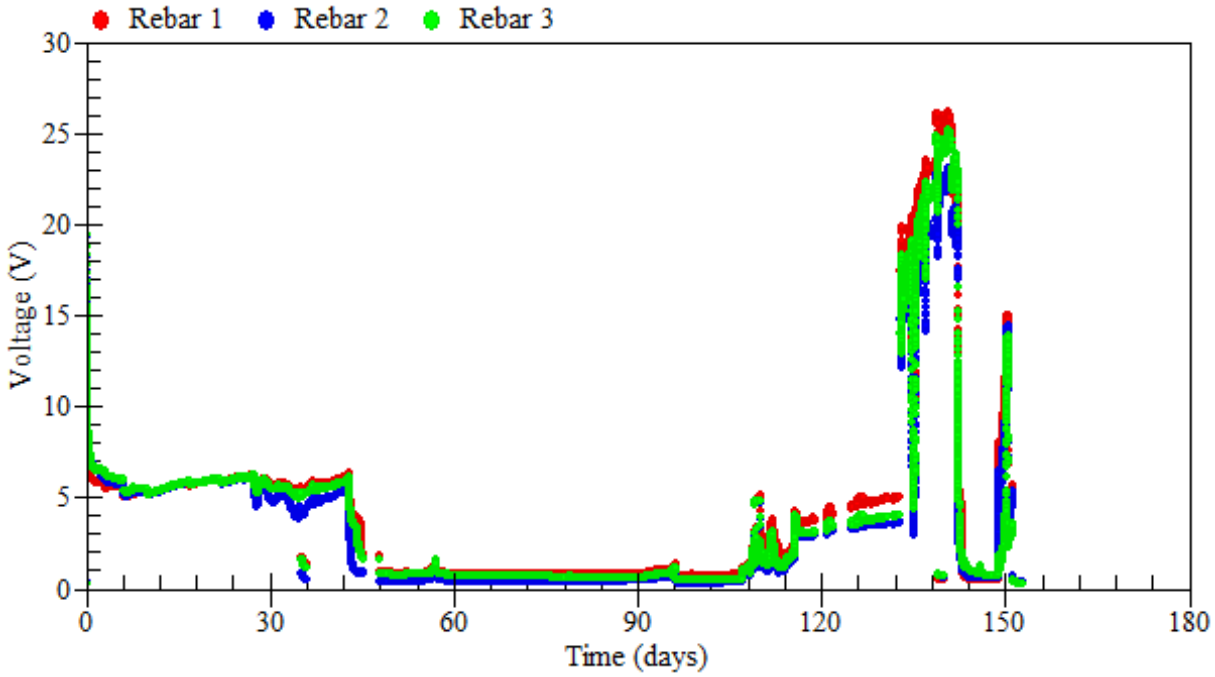

Figure B.25: Voltage measurements – beam LS-2.1

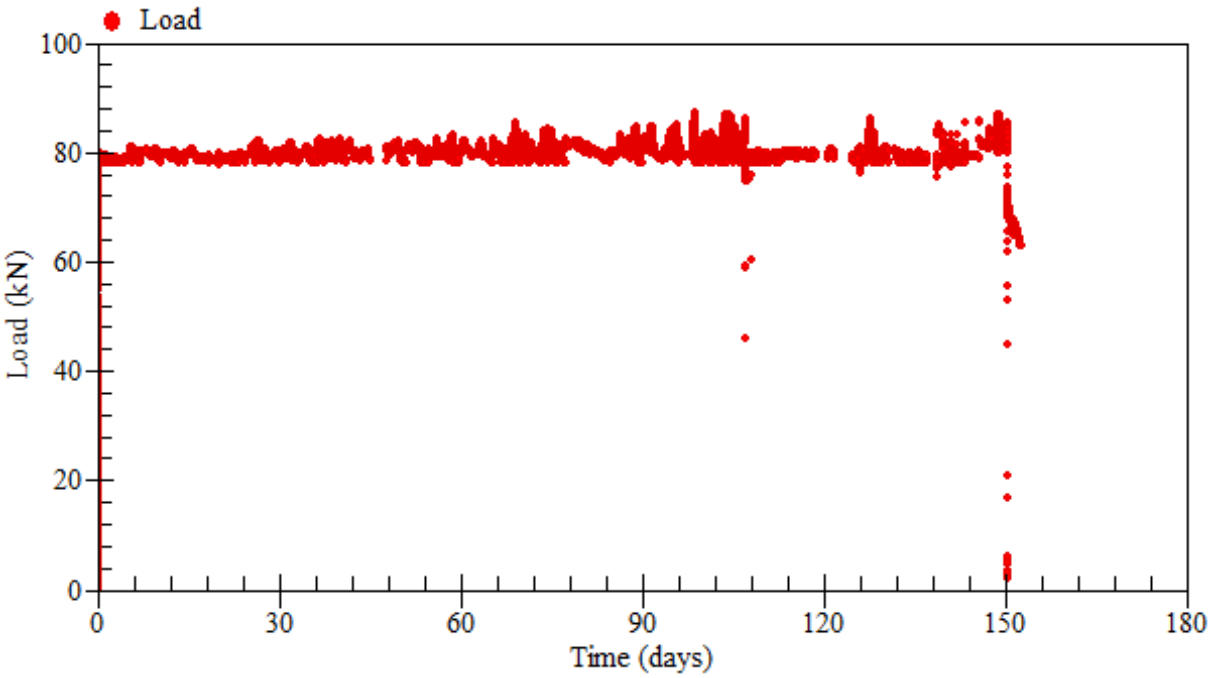

Figure B.26: Applied loads – beam LS-2.1

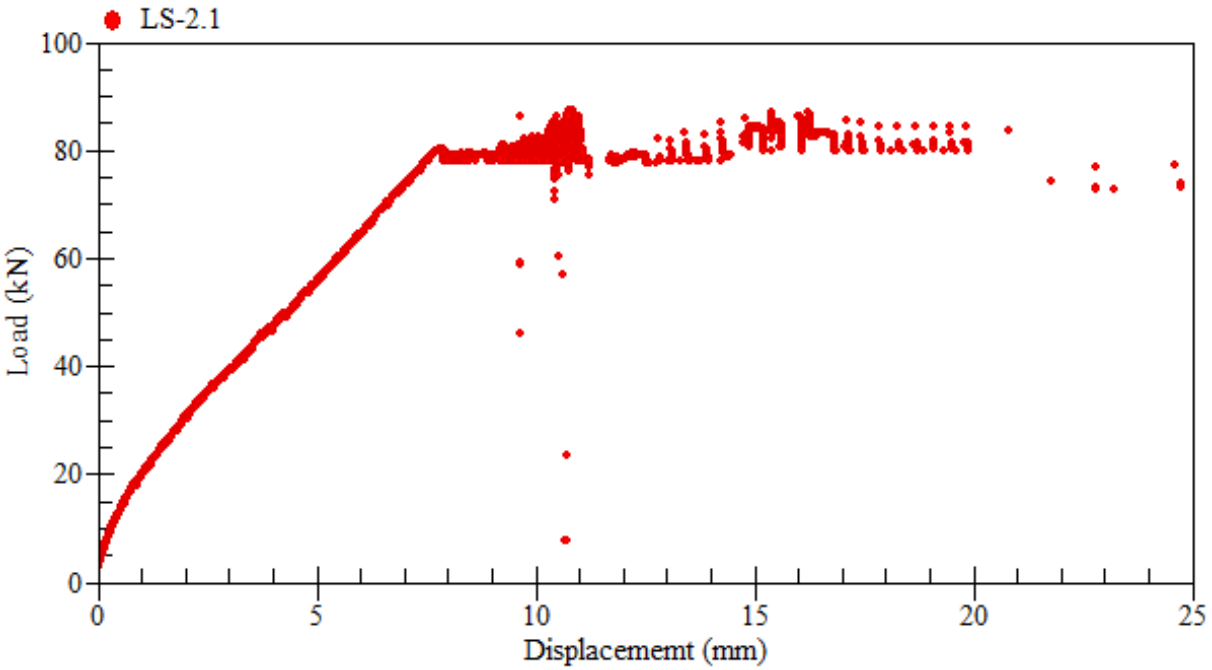

Figure B.27: Load-displacement relationship at mid-span – beam LS-2.1

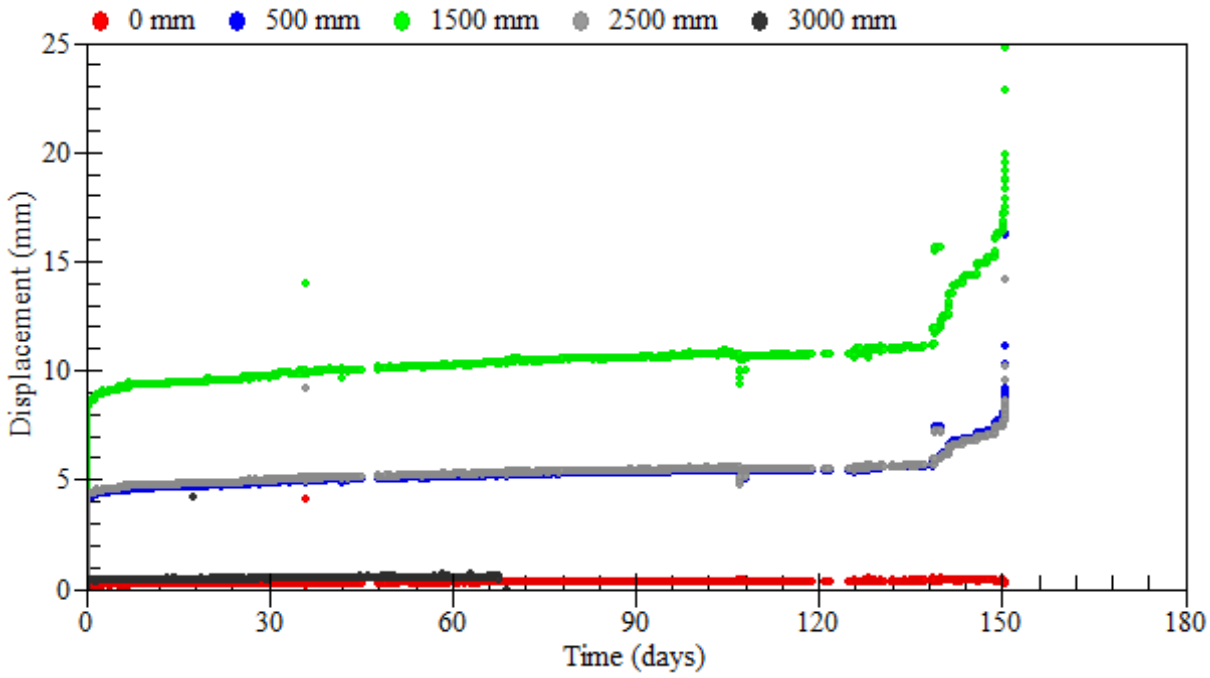

Figure B.28: Displacement measurements – beam LS-2.1

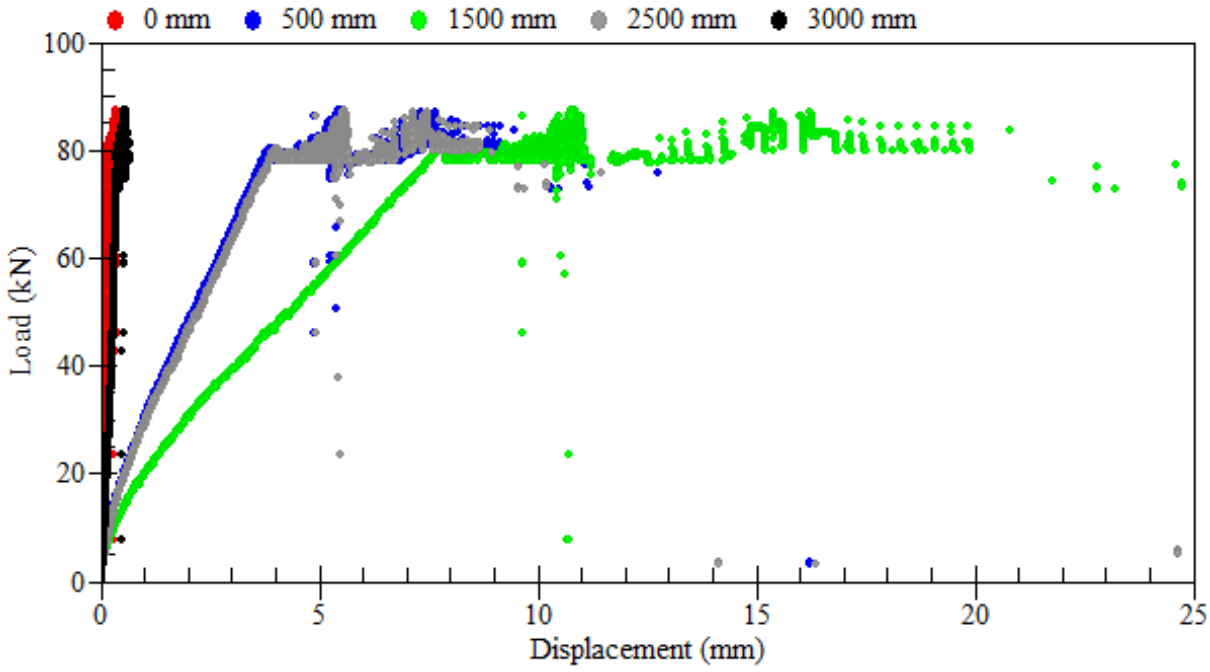

Figure B.29: Load-displacement relationships – beam LS-2.1

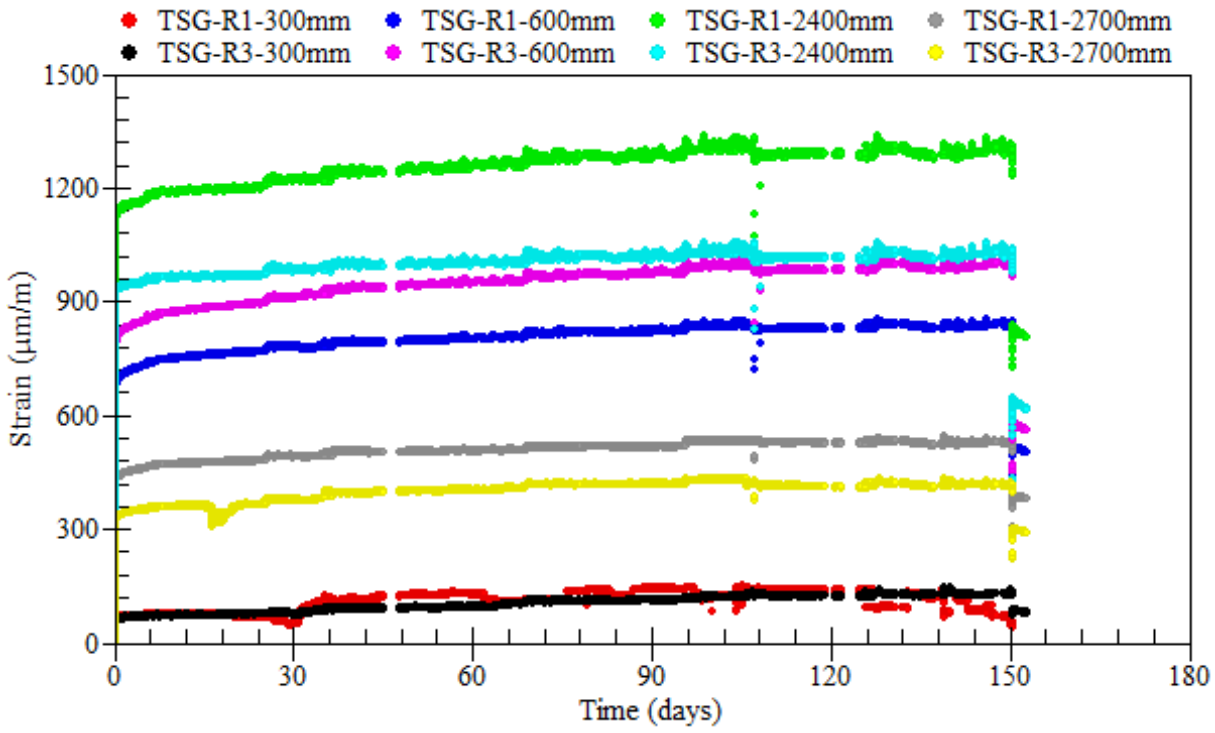

Figure B.30: Strain readings of longitudinal tensile steel bars – beam LS-2.1

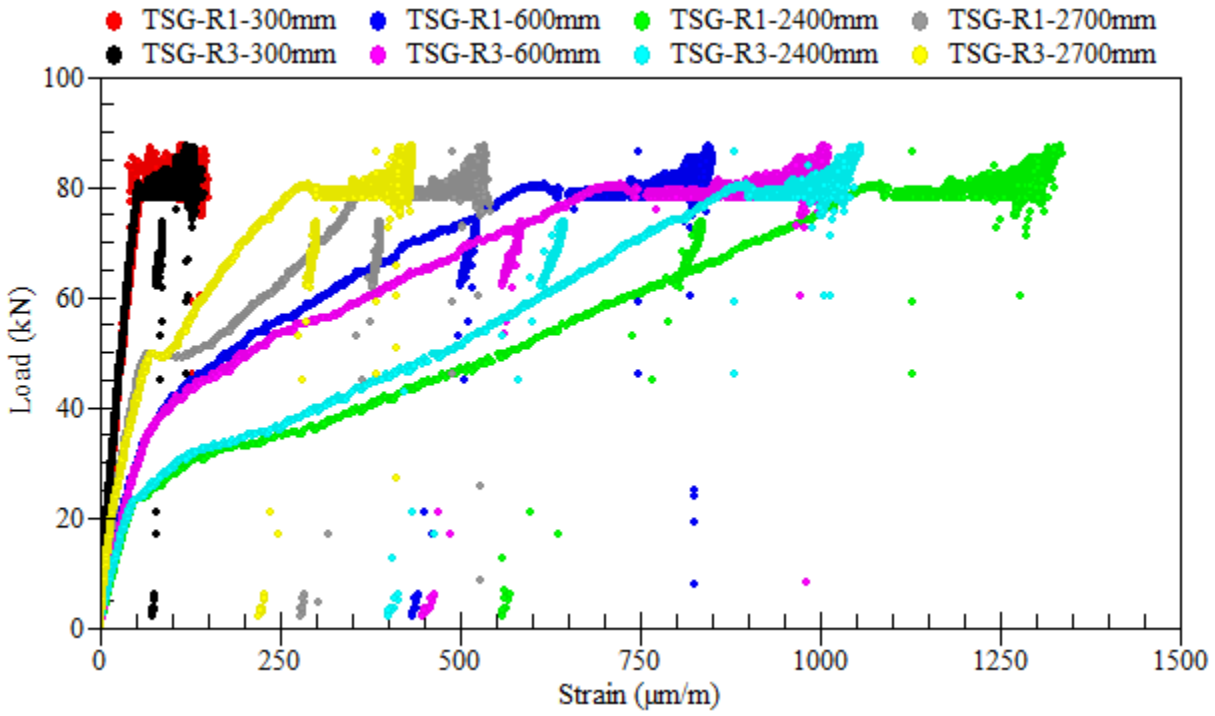

Figure B.31: Load-strain relationships of longitudinal tensile steel bars – beam LS-2.1

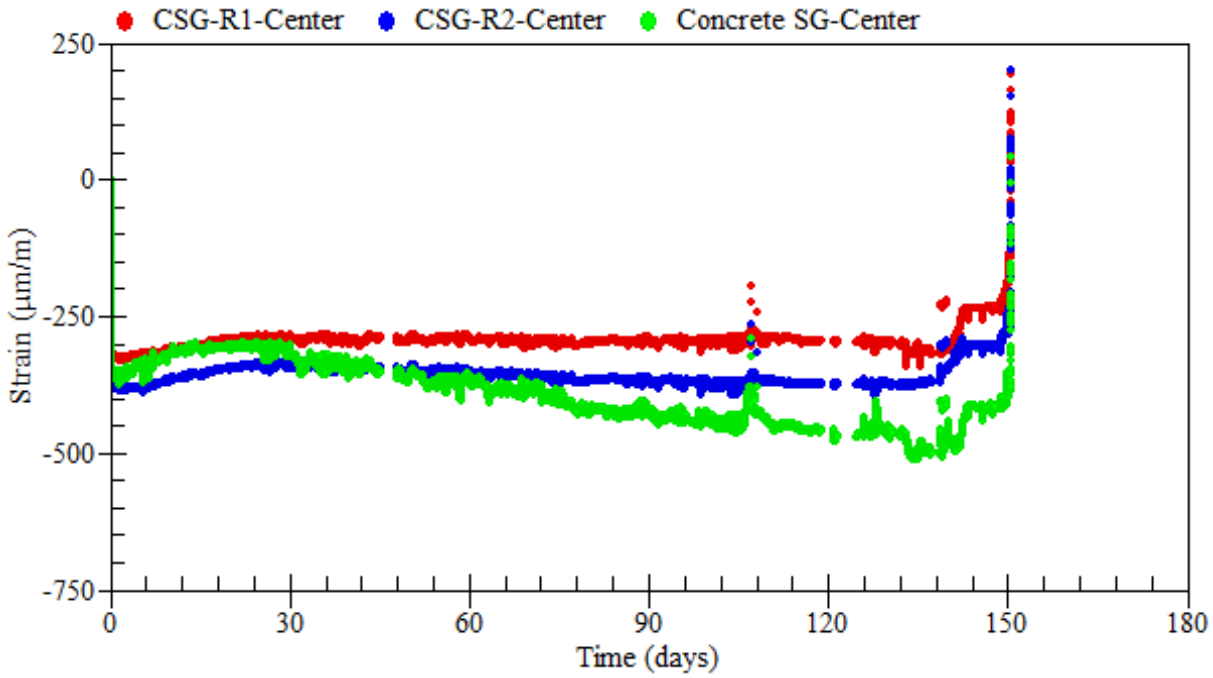

Figure B.32: Strain readings of longitudinal compressive steel bars – beam LS-2.1

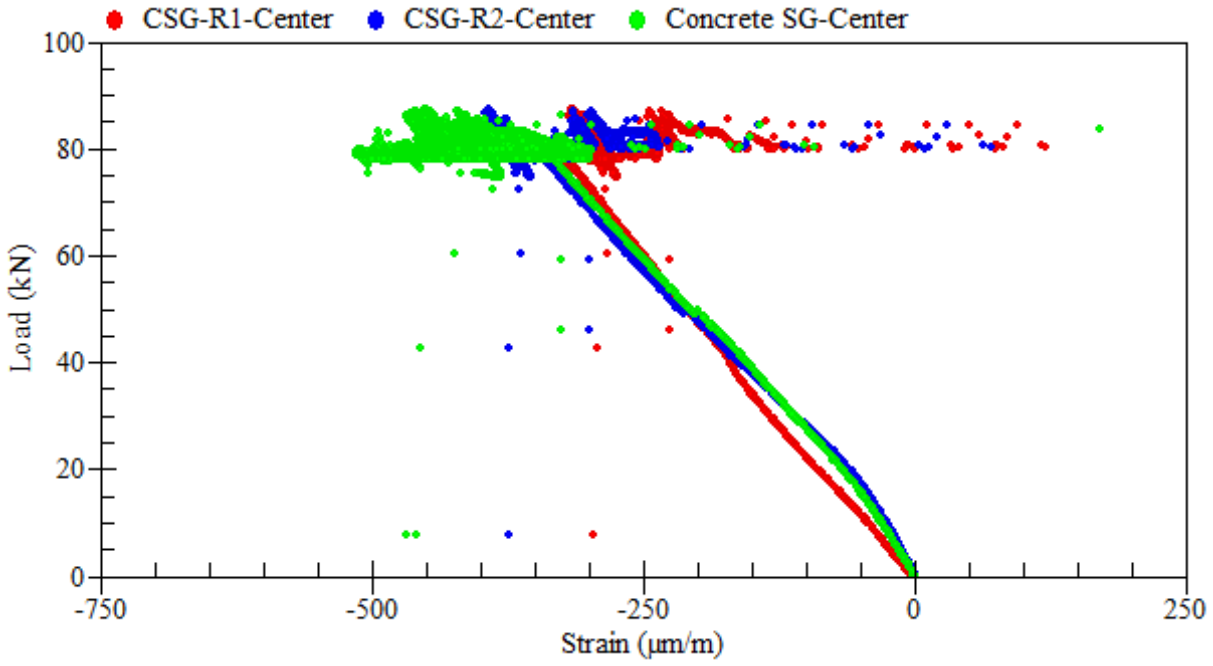

Figure B.33: Load-strain relationships of longitudinal compressive steel bars – beam LS-2.1

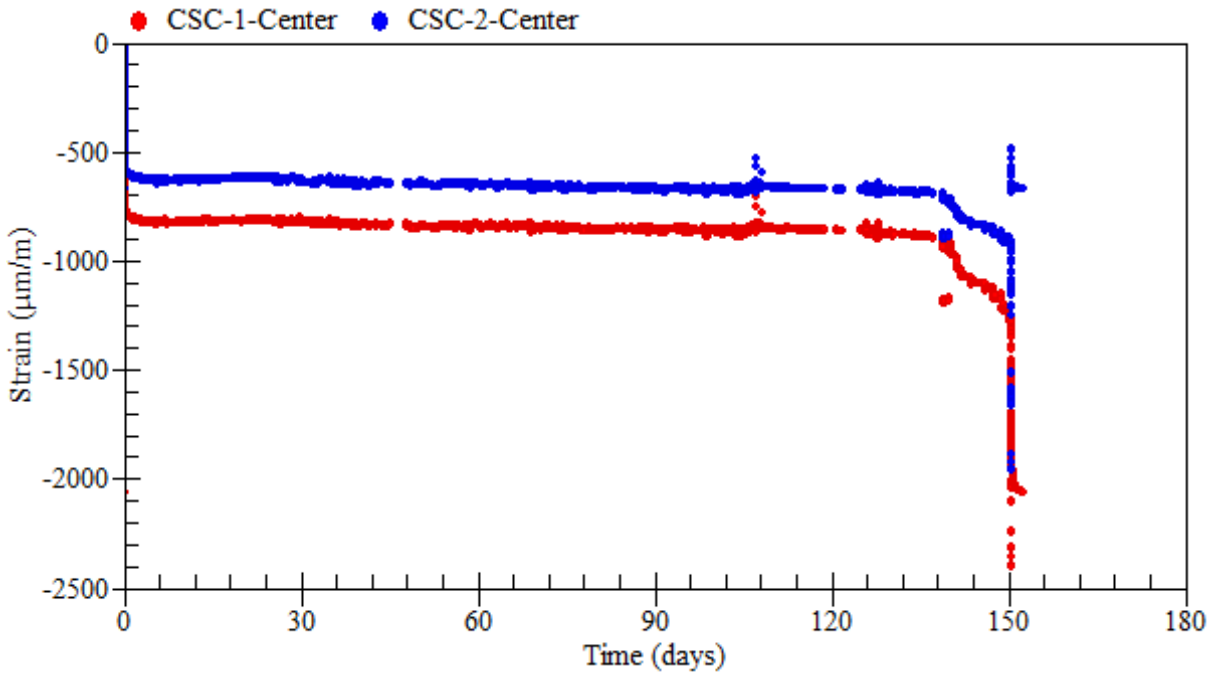

Figure B.34: Strain readings of external rosettes on top – beam LS-2.1

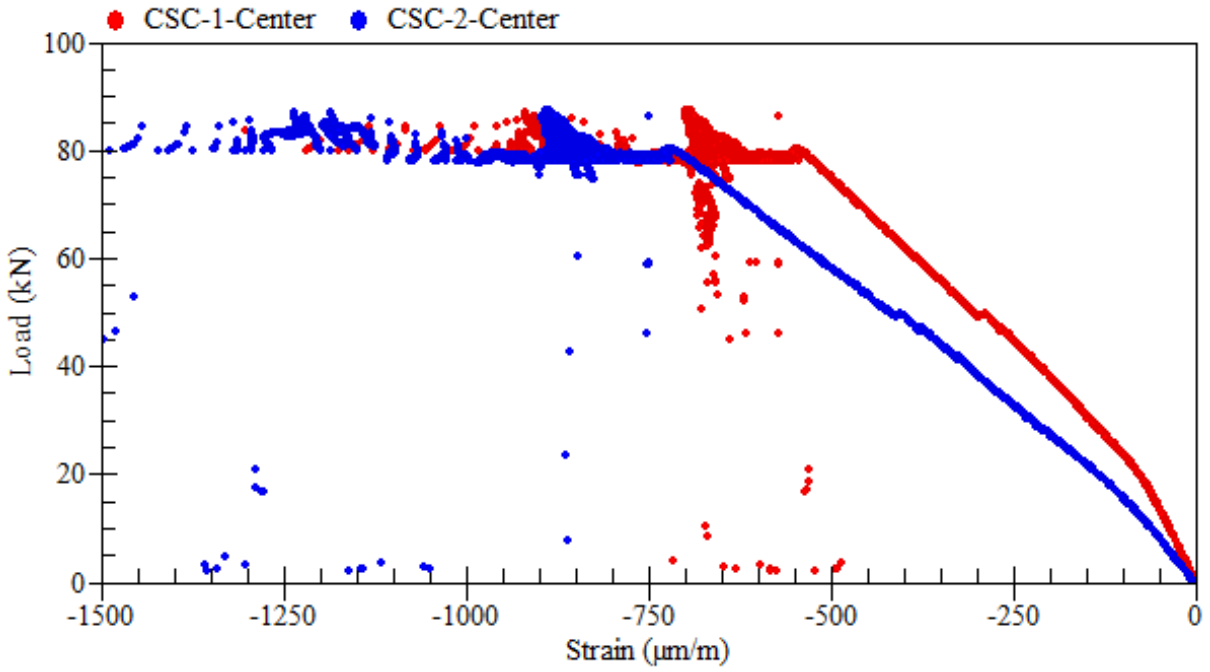

Figure B.35: Load-strain relationships of external rosettes on top – beam LS-2.1

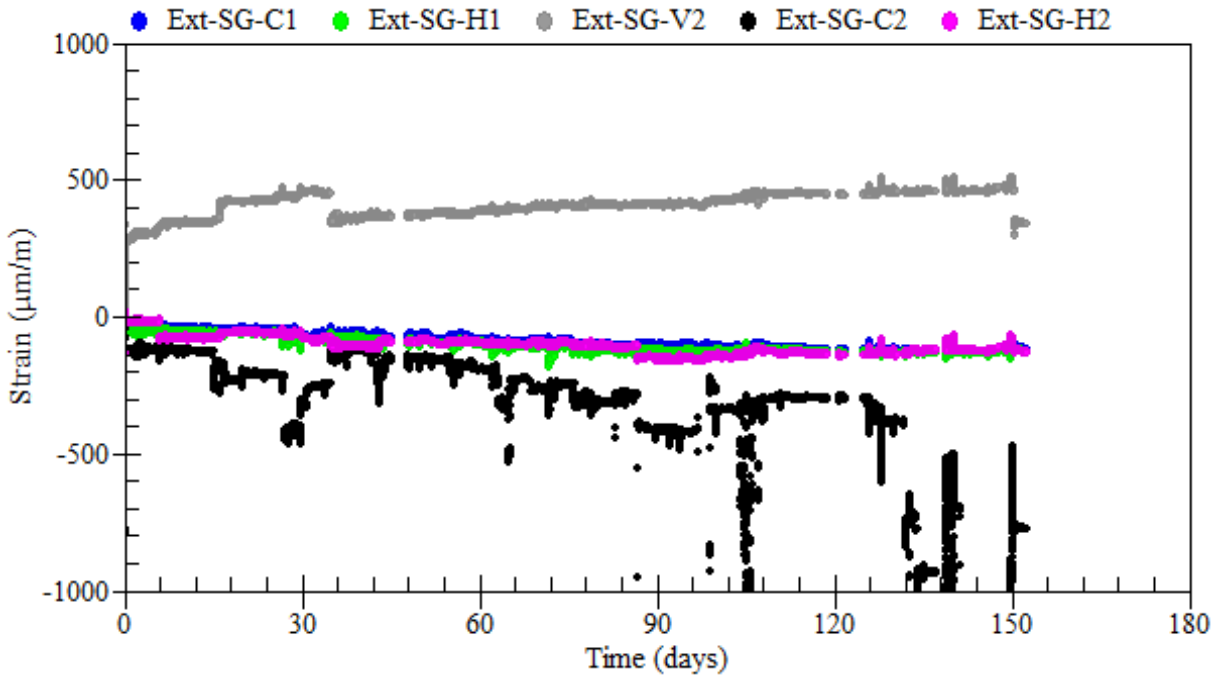

Figure B.36: Strain readings of external rosettes on sides at 600 mm away from center – beam LS-2.1

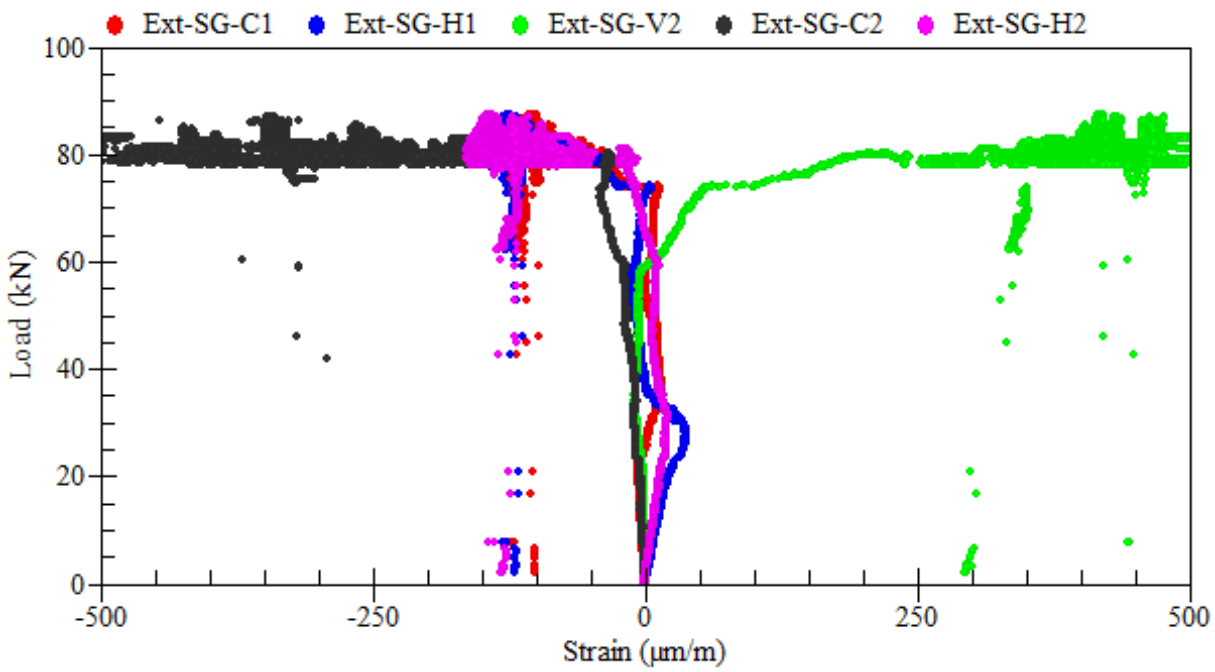

Figure B.37: Load-strain relationships of external rosettes on sides at 600 mm away from center – beam LS-2.1

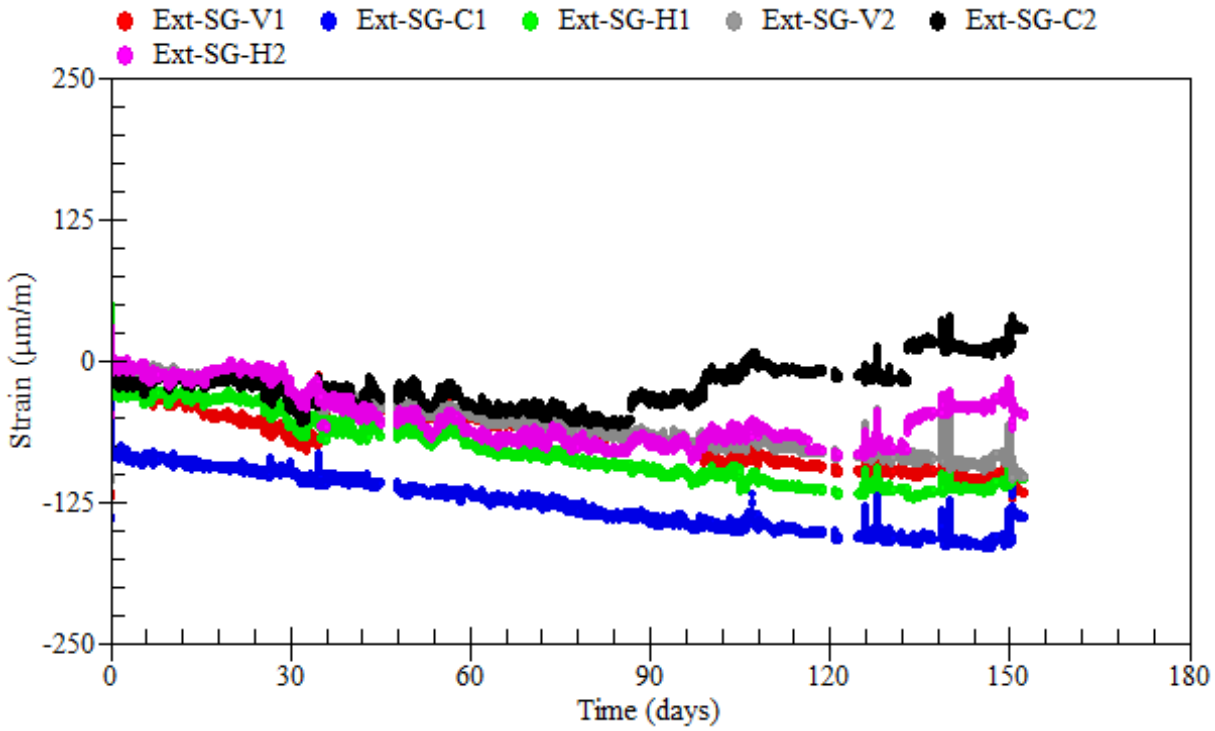

Figure B.38: Strain readings of external rosettes on sides at 750 mm away from center – beam LS-2.1

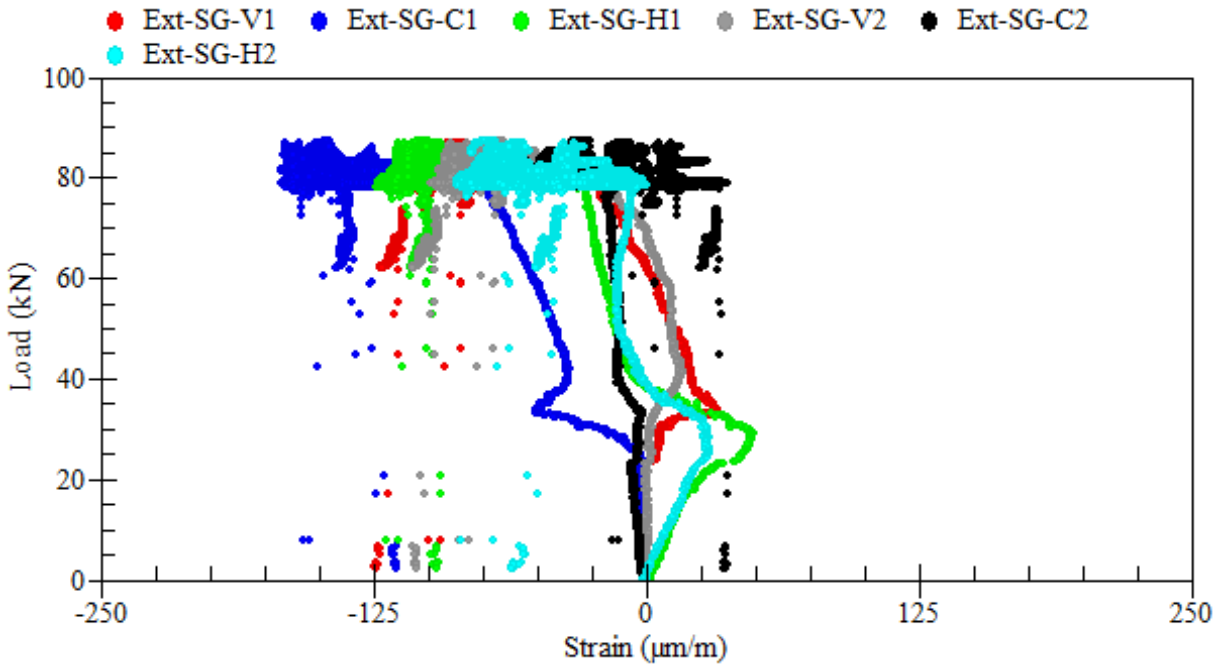

Figure B.39: Load-strain relationships of external rosettes on sides at 750 mm away from center – beam LS-2.1

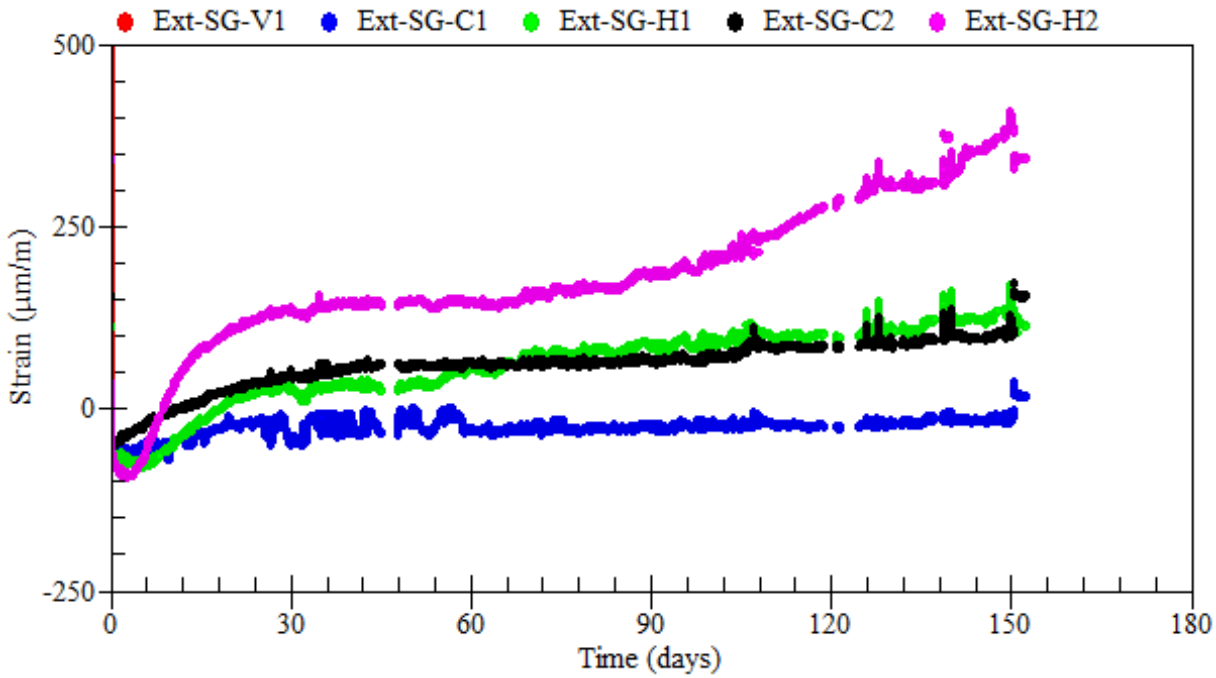

Figure B.40: Strain readings of external rosettes on sides at 900 mm away from center – beam LS-2.1

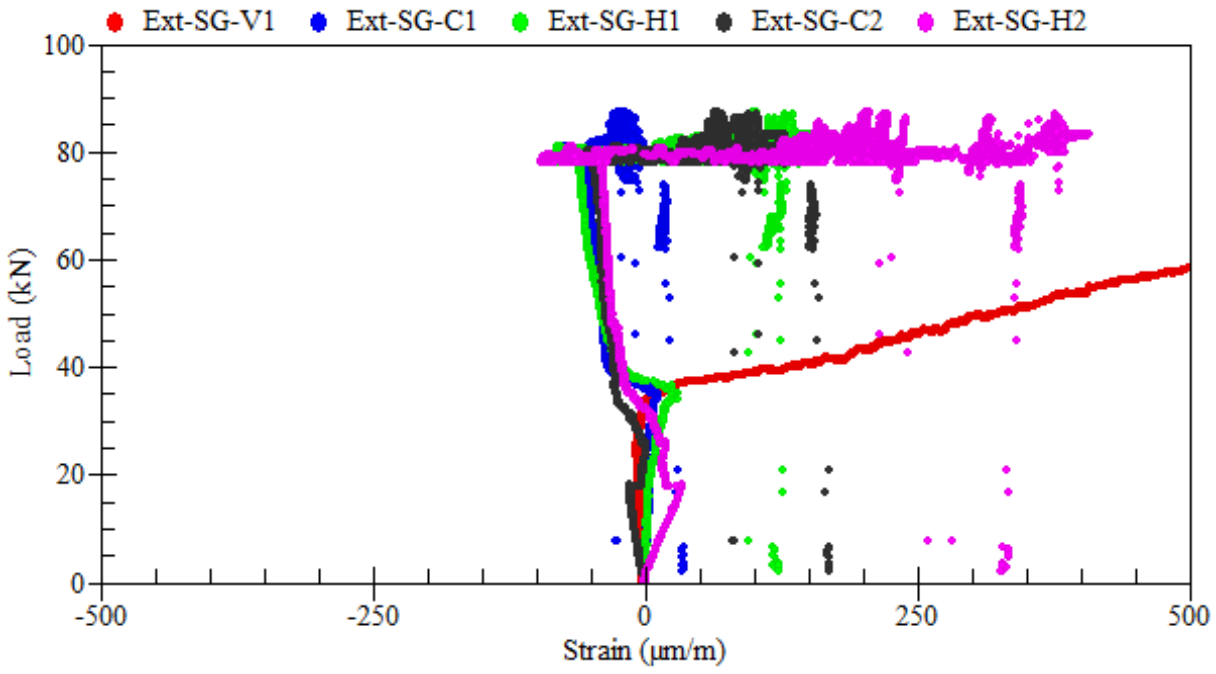

Figure B.41: Load-strain relationships of external rosettes on sides at 900 mm away from center – beam LS-2.1

B.4 Beam LS-2.2

Beam LS-2.2 was tested under the coupled effects of reinforcement corrosion and service loads. The applied sustained load was equivalent to 60% of the beam ultimate load capacity (i.e., 80 kN). Reinforcement corrosion was accelerated using a current density of 500 $\mu A/cm^2$ over a duration of 33 days before increasing it to 1000 $\mu A/cm^2$ up until the failure of the beam. The total duration of corrosion exposure was 191 days. The average mass loss of the beam was 25.1%. A summary of the gravimetric mass loss measurements of steel reinforcement is presented in Table B.2.

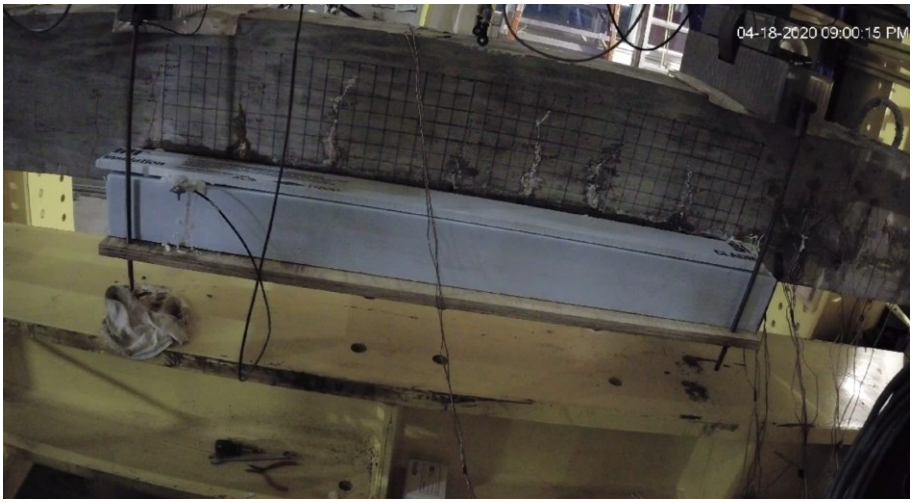

(a) during the test

(b) at failure

Figure B.42: Crack propagation and patterns at failure – beam LS-2.2

Figure B.43: Corrosion-induced damage in the cover of concrete – beam LS-2.2

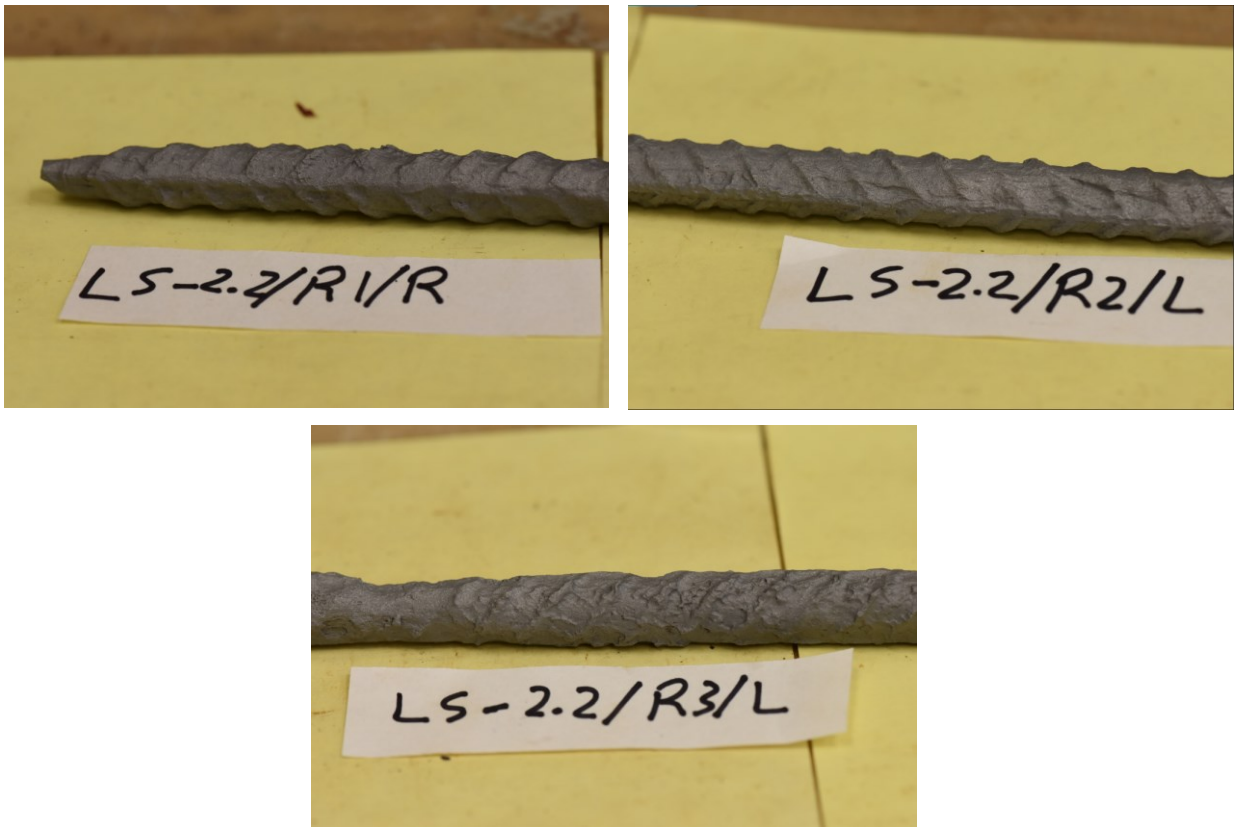

Figure B.44: Corrosion patterns on the clean surface of steel reinforcement – beam LS-2.2

Table B.2: Mass loss of corroded steel bars – beam LS-2.2

Rebar type	Rebar designation	Length (mm)	Mass (g)	Mass loss (%)	Rebar mass loss (%)
Control	R0	99	152.96	0	0
R1	R1-R	210	240.36	25.92	26.45
	R1-L-1	355	402.39	26.64	
	R1-L-2	287	325.47	26.60	
R2	R2-R-1	319	409.65	16.88	20.34
	R2-R-2	118	139.44	23.52	
	R2-L-1	371	438.22	23.55	
	R2-L-2	83	109.27	14.79	
R3	R3-R	217	248.60	25.85	28.38
	R3-L-1	300	326.84	29.49	
	R3-L-2	389	427.10	28.94	

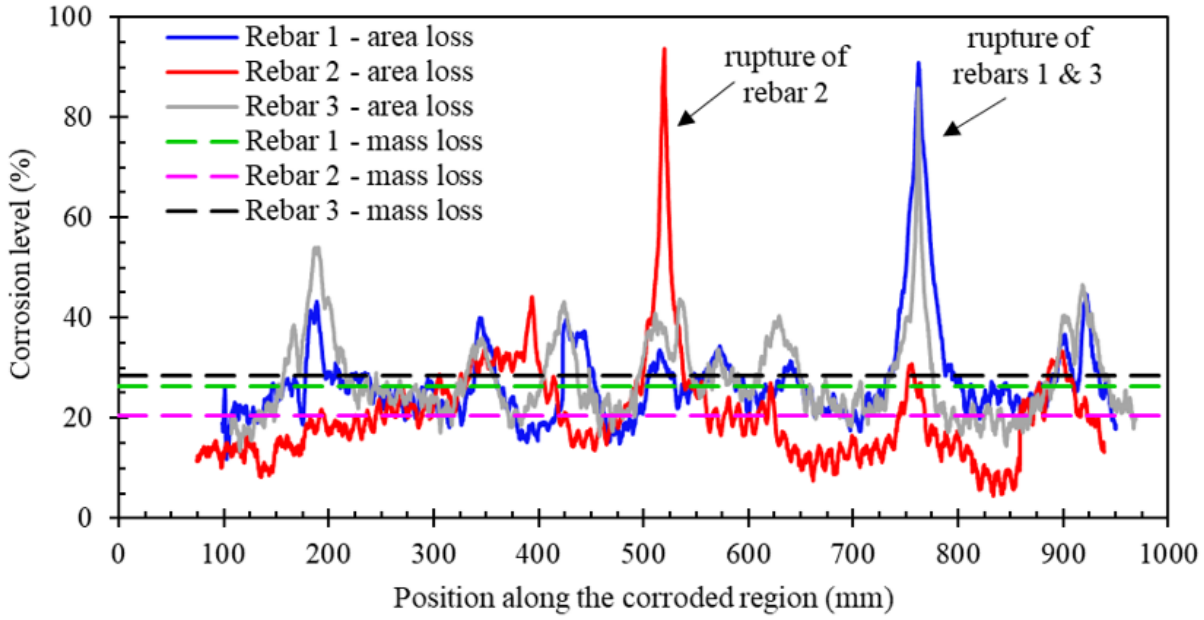

Figure B.45: Distribution of cross-sectional area loss along the corroded steel reinforcement – beam LS-2.2

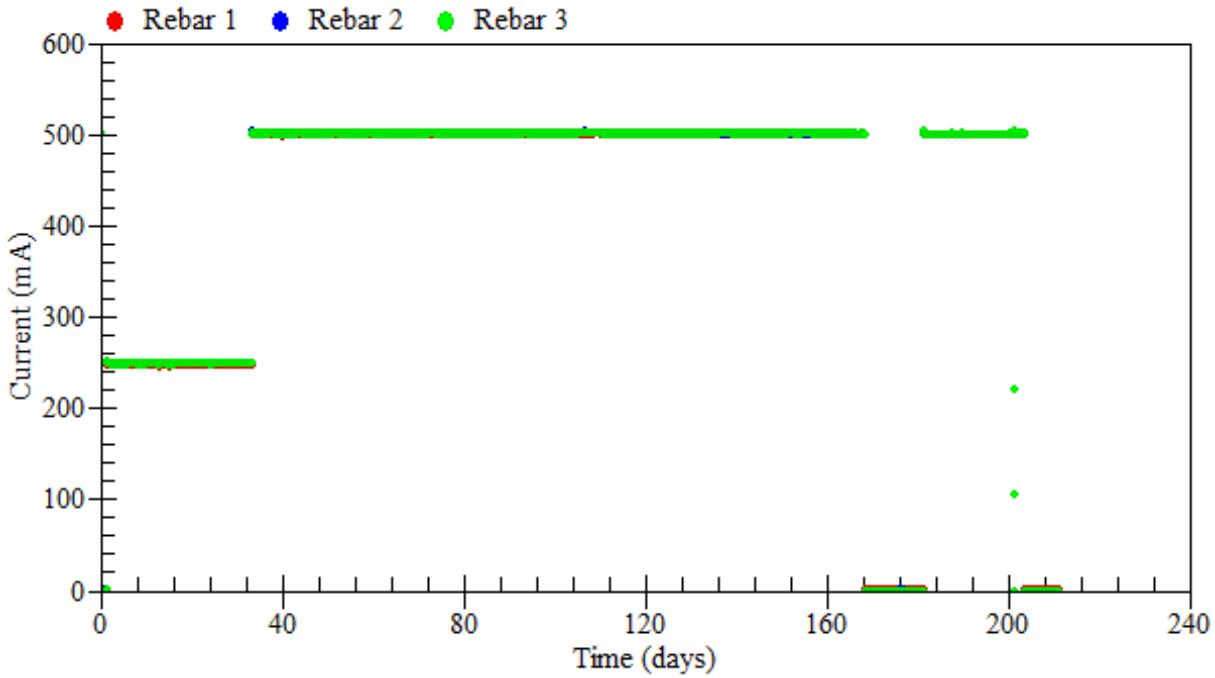

Figure B.46: Applied current – beam LS-2.2

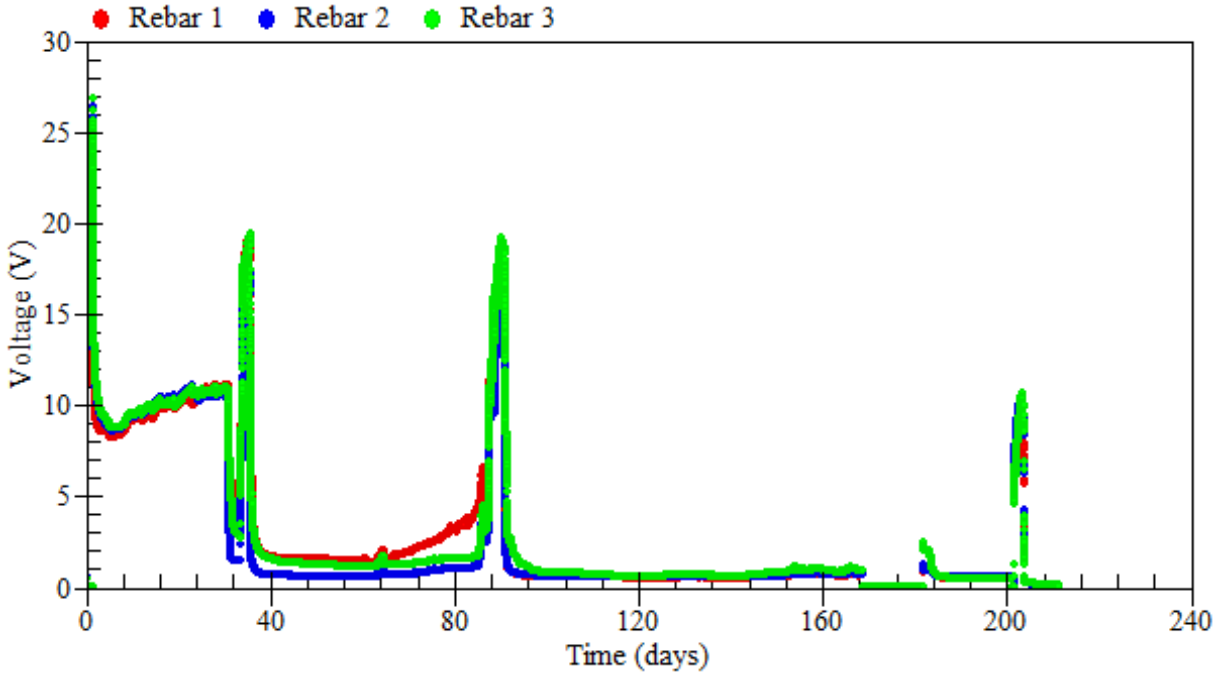

Figure B.47: Voltage measurements – beam LS-2.2

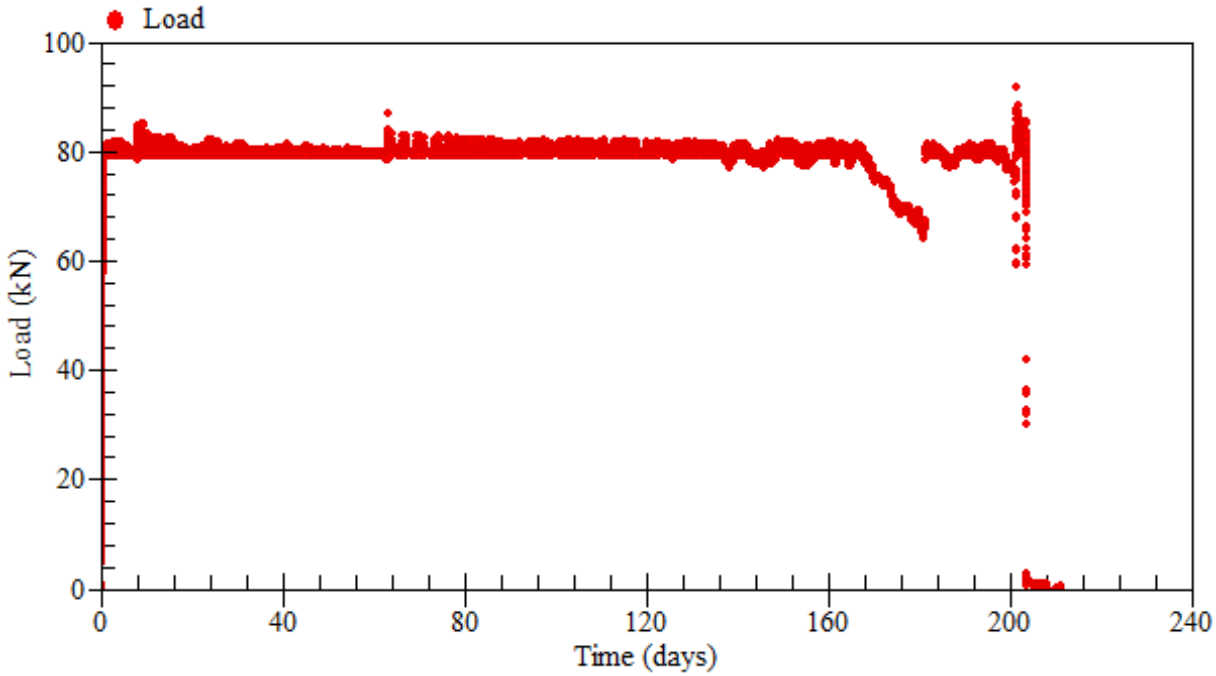

Figure B.48: Applied loads – beam LS-2.2

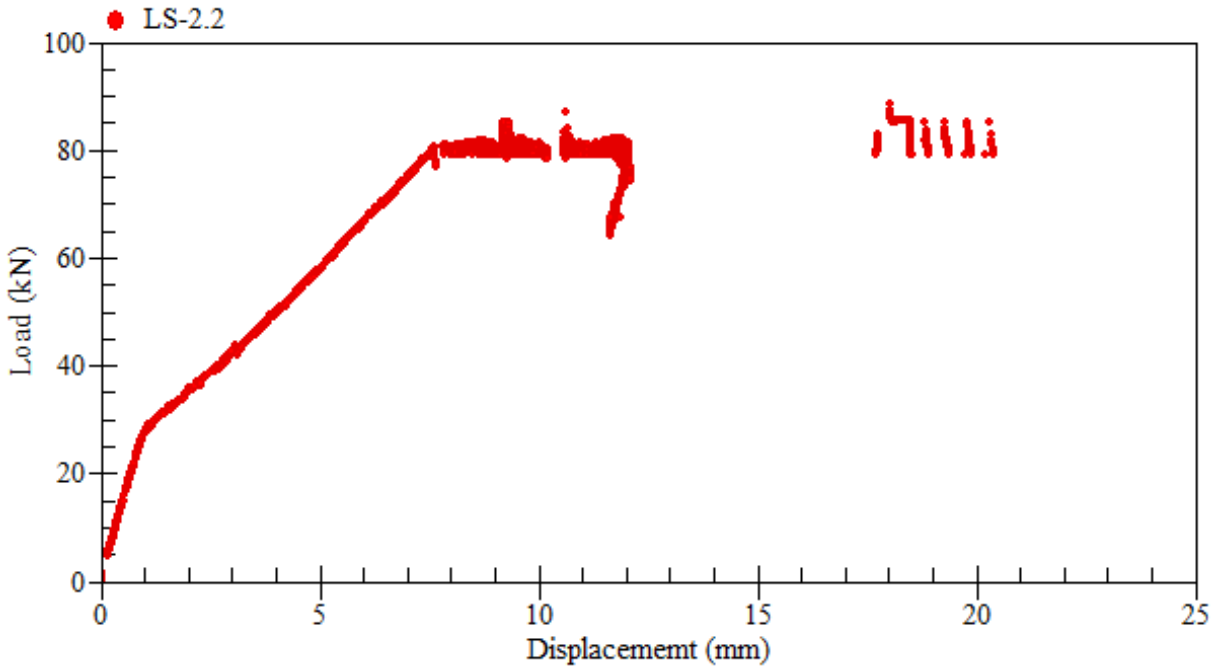

Figure B.49: Load-displacement relationship at mid-span – beam LS-2.2

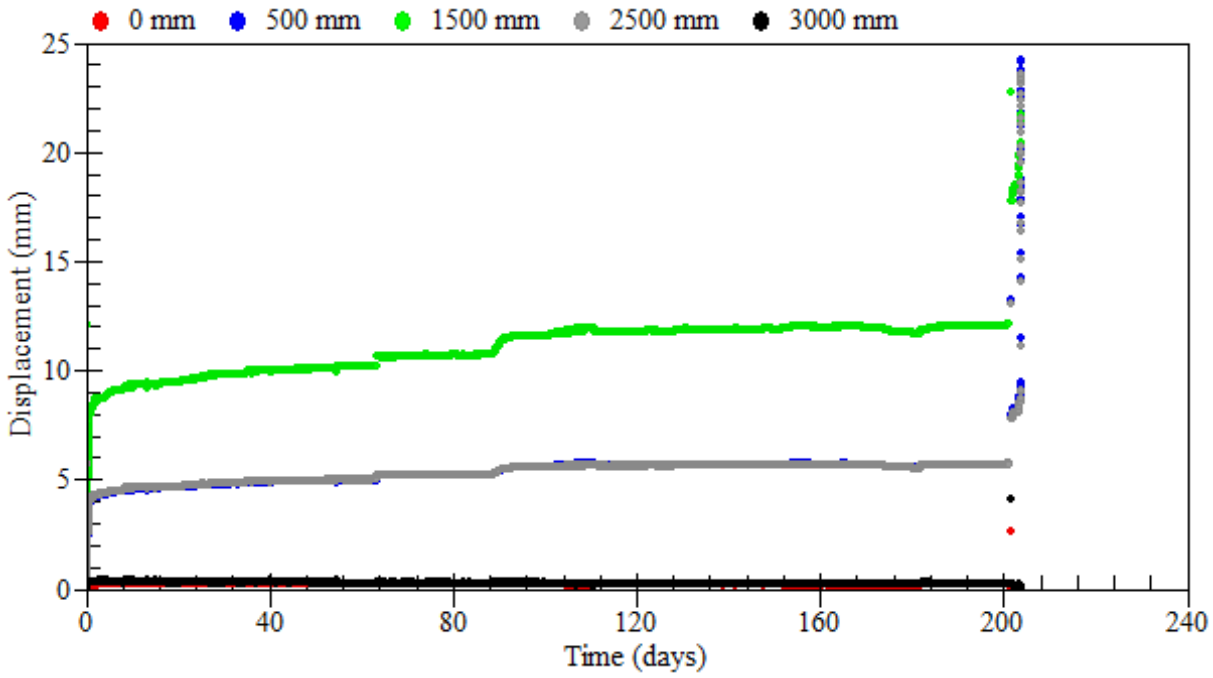

Figure B.50: Displacement measurements – beam LS-2.2

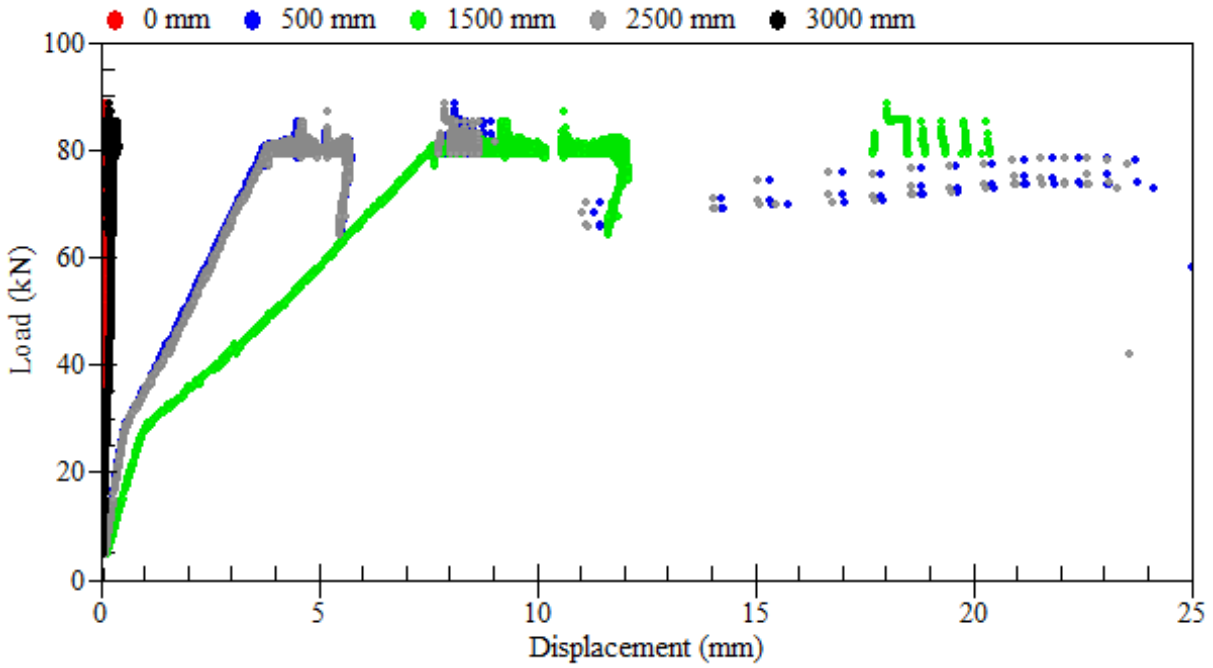

Figure B.51: Load-displacement relationships – beam LS-2.2

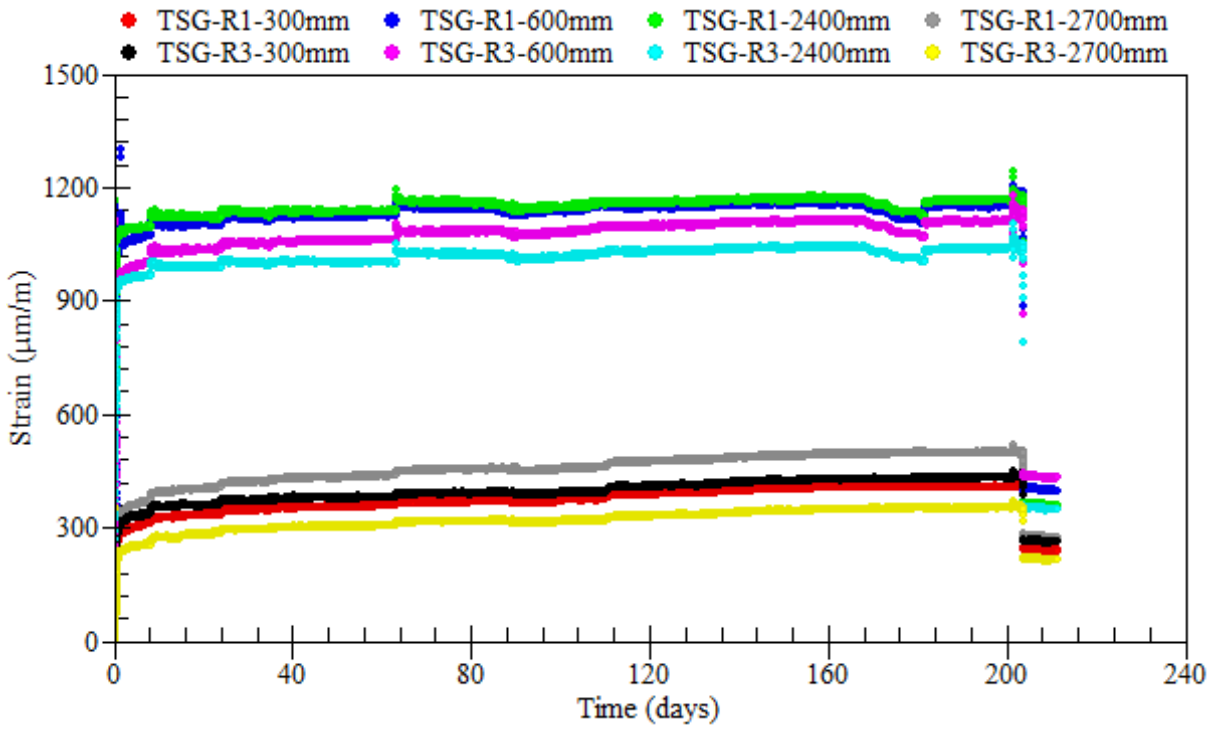

Figure B.52: Strain readings of longitudinal tensile steel bars – beam LS-2.2

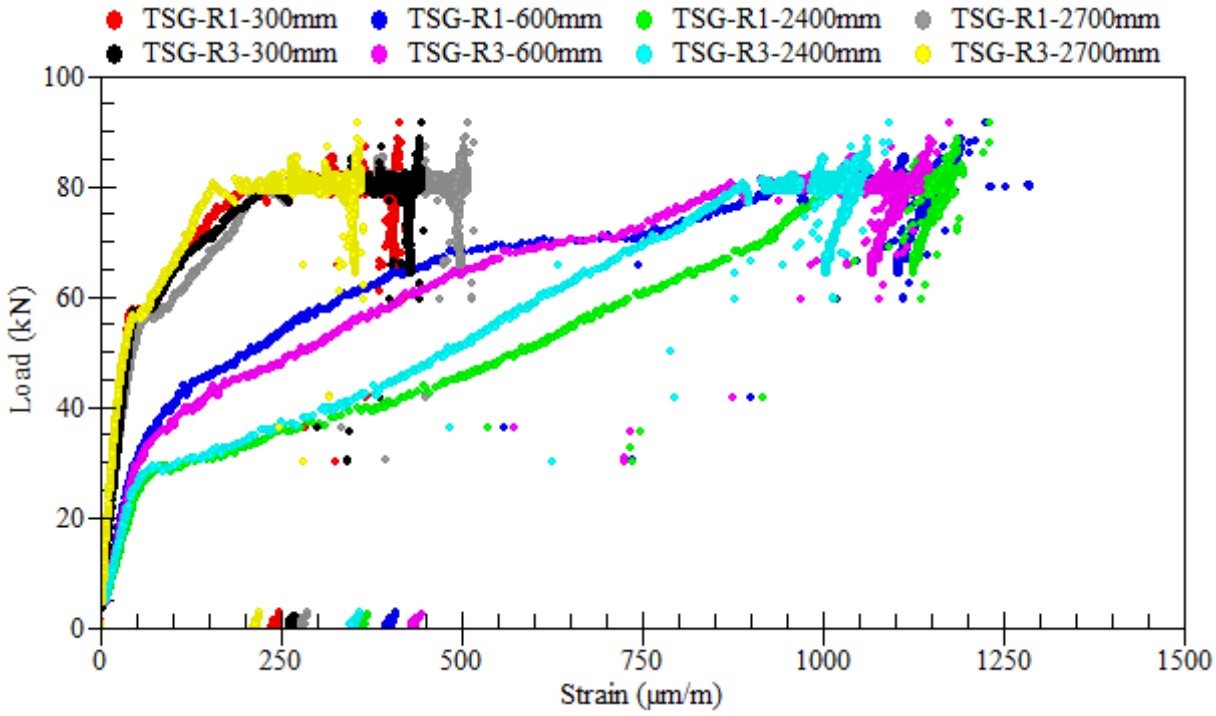

Figure B.53: Load-strain relationships of longitudinal tensile steel bars – beam LS-2.2

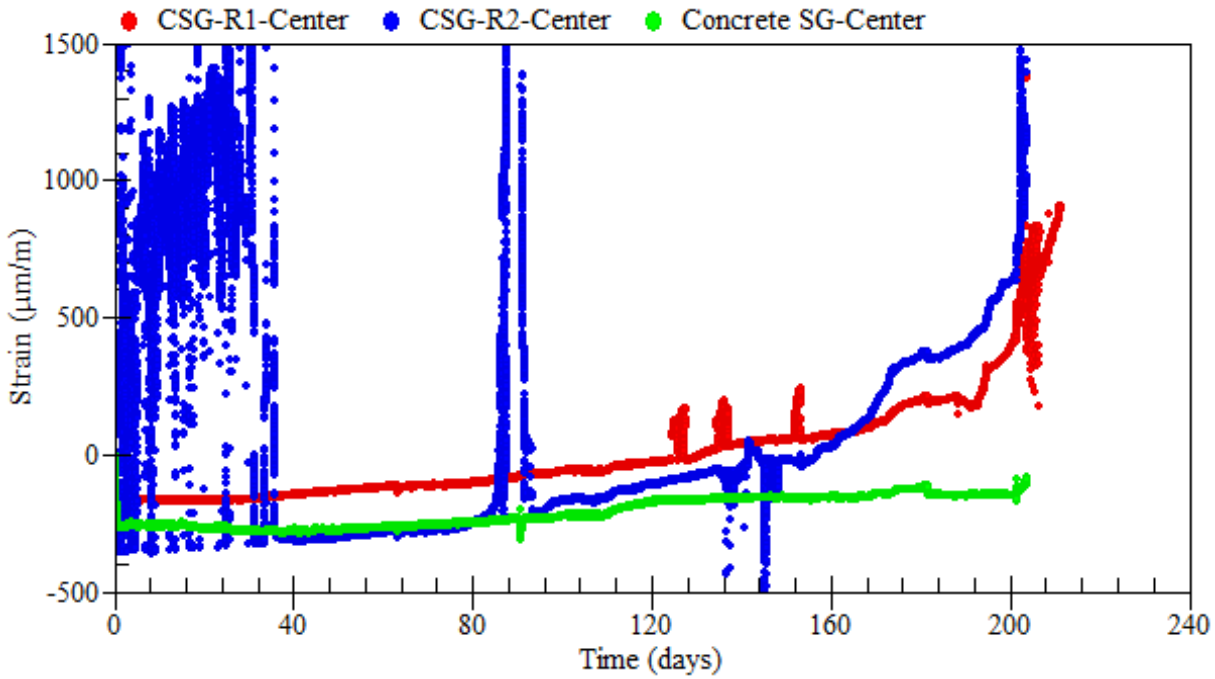

Figure B.54: Strain readings of longitudinal compressive steel bars – beam LS-2.2

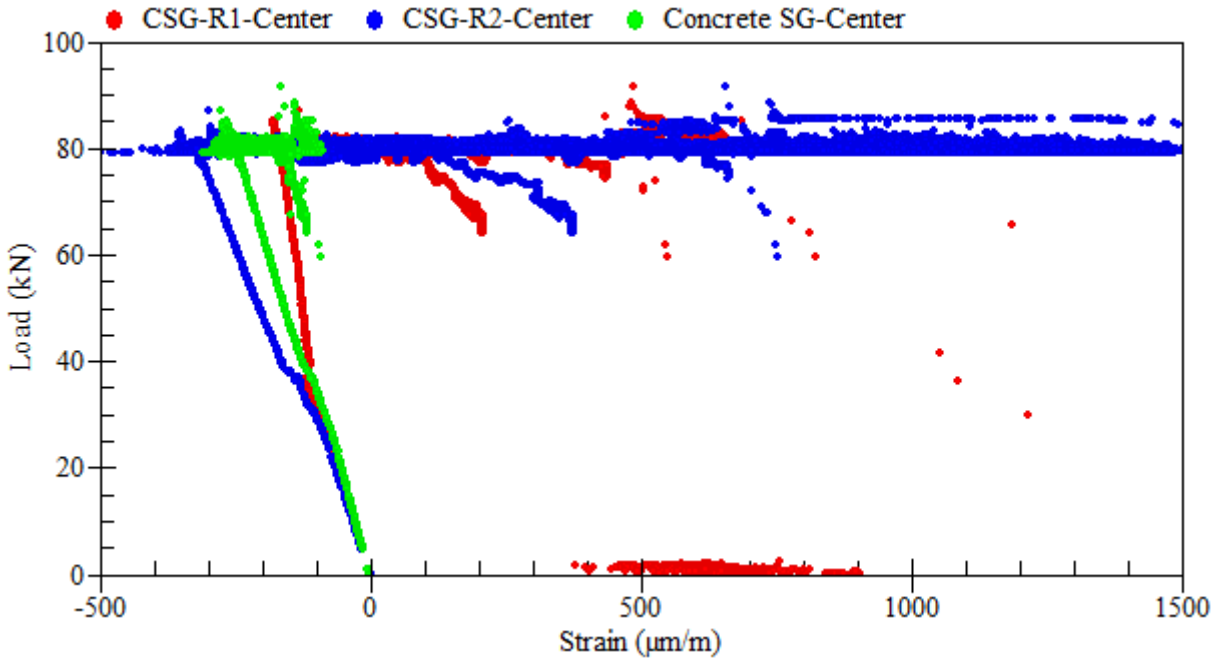

Figure B.55: Load-strain relationships of longitudinal compressive steel bars – beam LS-2.2

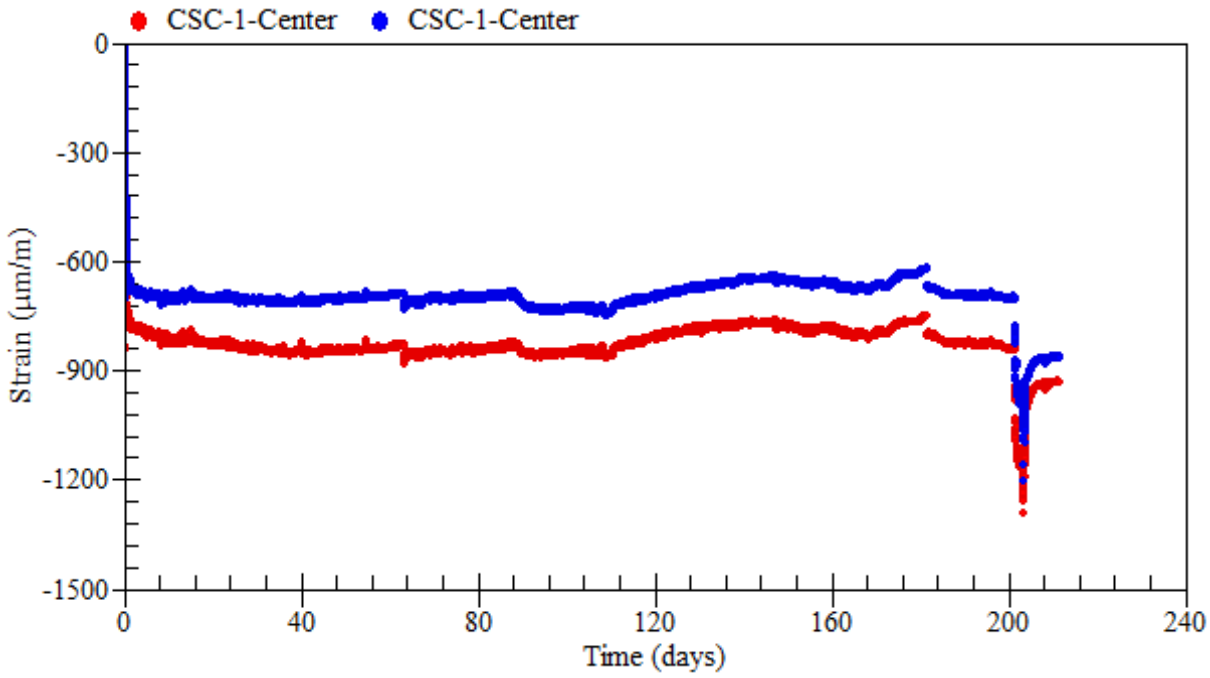

Figure B.56: Strain readings of external rosettes on top – beam LS-2.2

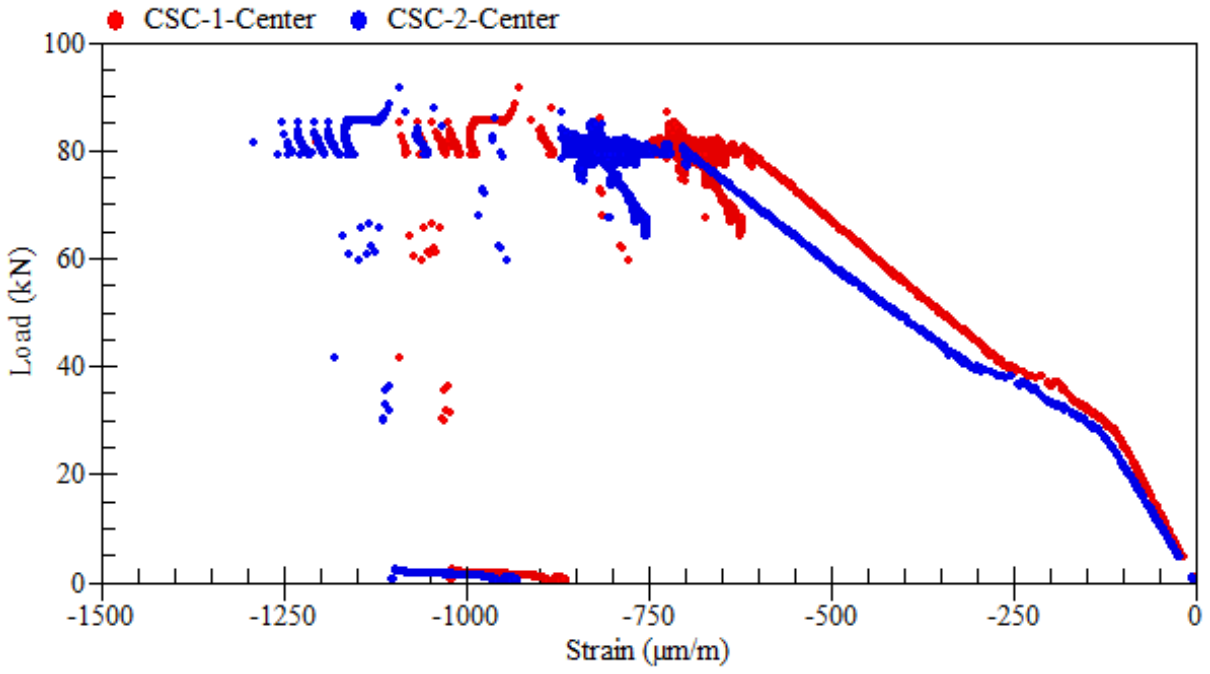

Figure B.57: Load-strain relationships of external rosettes on top – beam LS-2.2

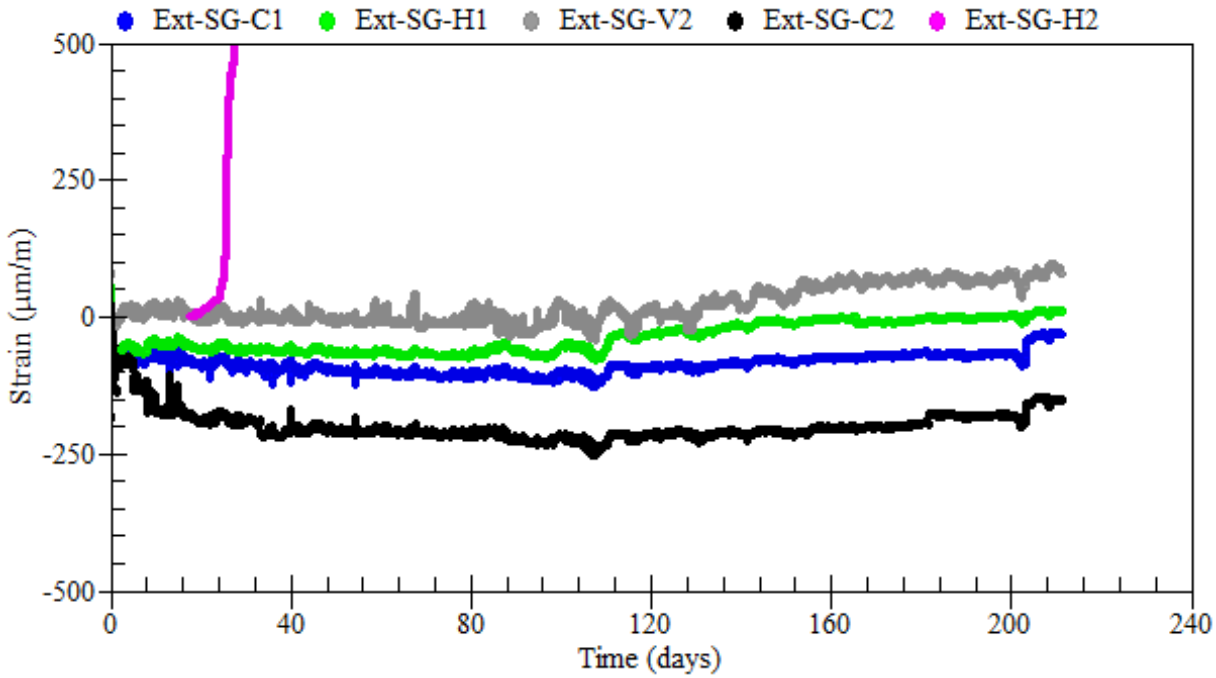

Figure B.58: Strain readings of external rosettes on sides at 600 mm away from center – beam LS-2.1

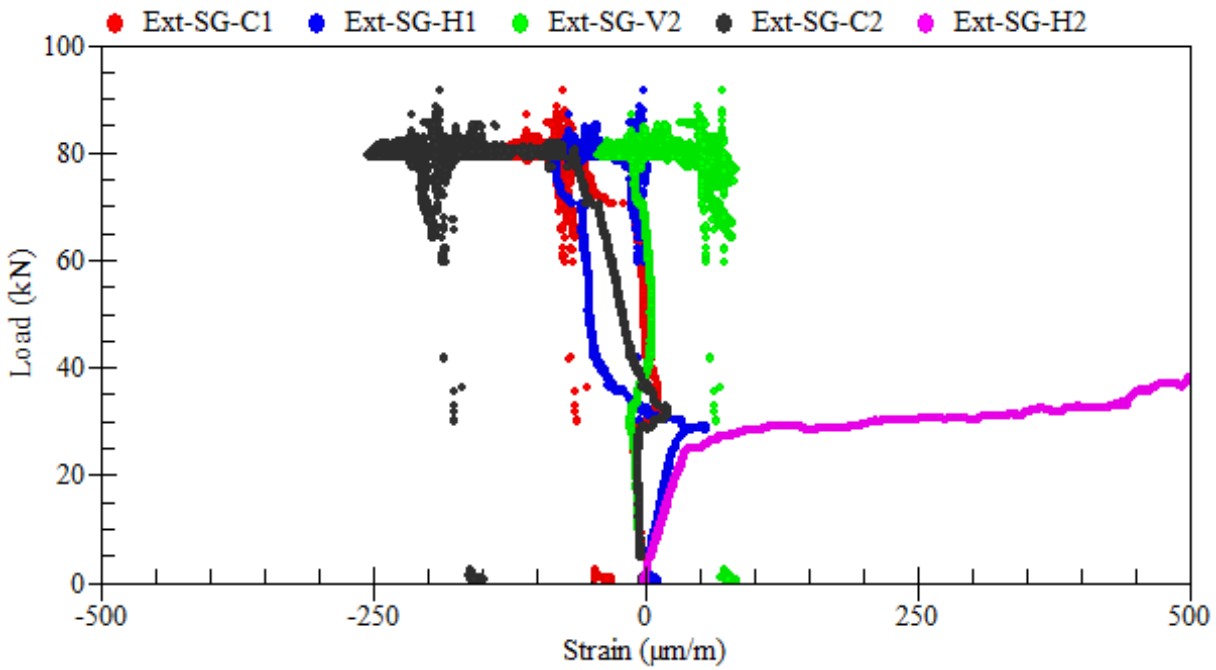

Figure B.59: Load-strain relationships of external rosettes on sides at 600 mm away from center – beam LS-2.2

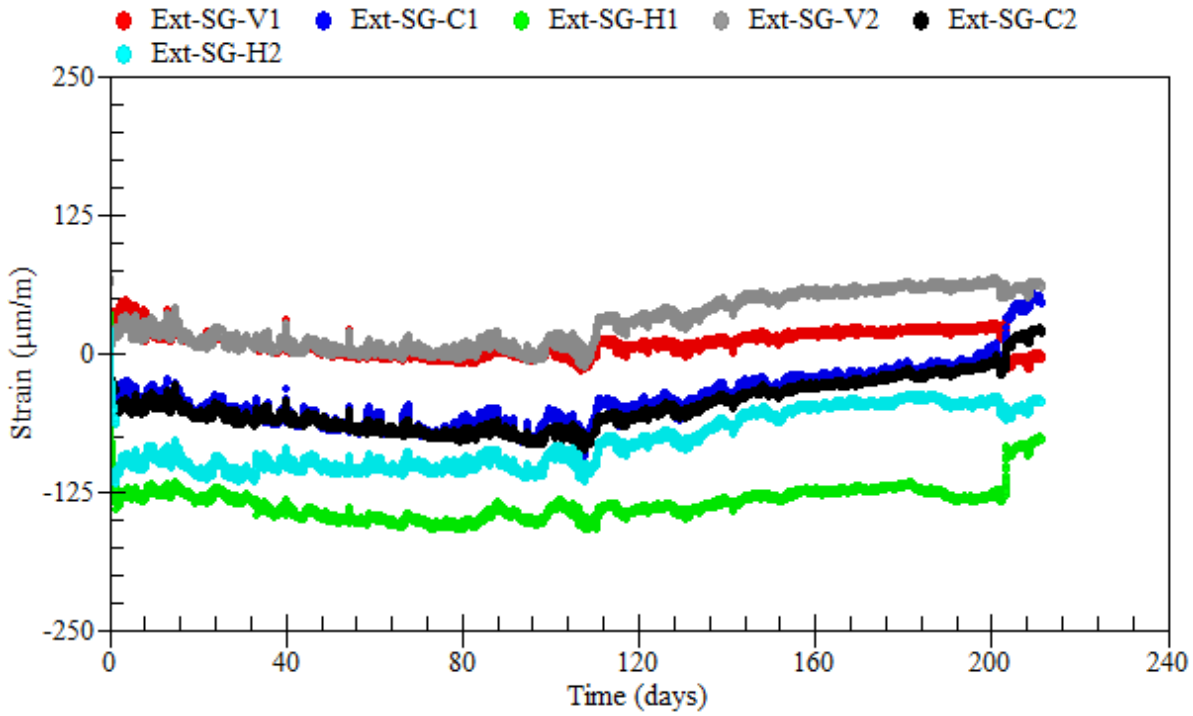

Figure B.60: Strain readings of external rosettes on sides at 750 mm away from center – beam LS-2.2

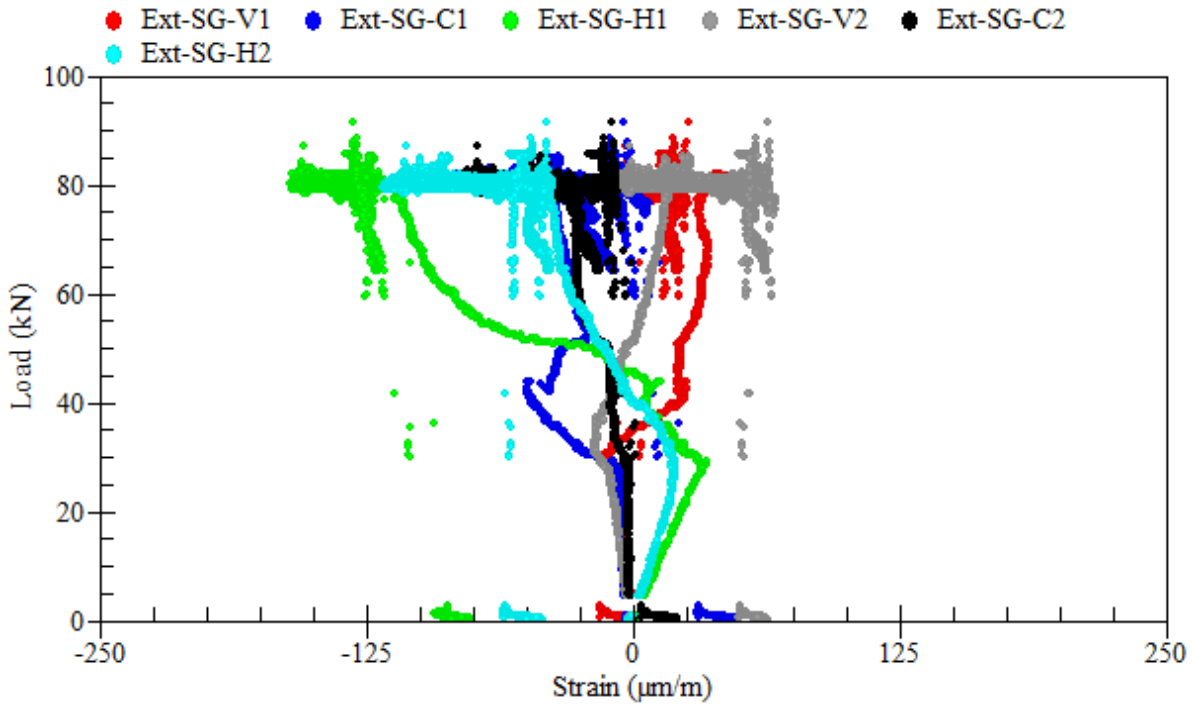

Figure B.61: Load-strain relationships of external rosettes on sides at 750 mm away from center – beam LS-2.2

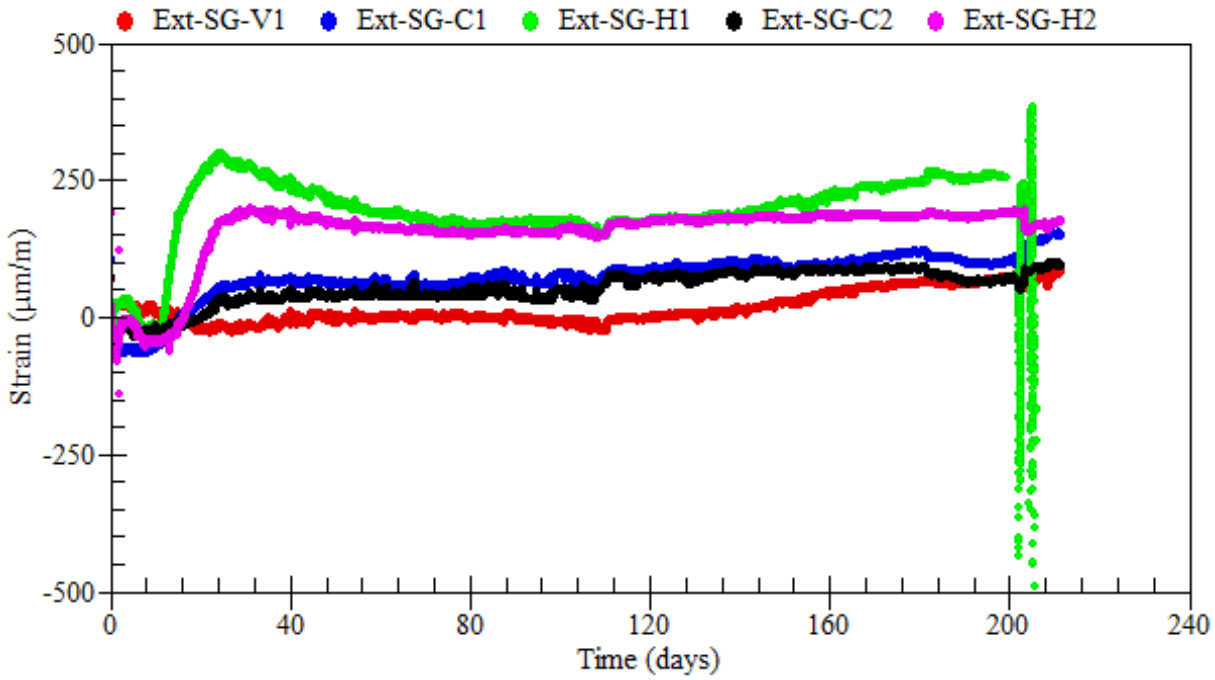

Figure B.62: Strain readings of external rosettes on sides at 900 mm away from center – beam LS-2.2

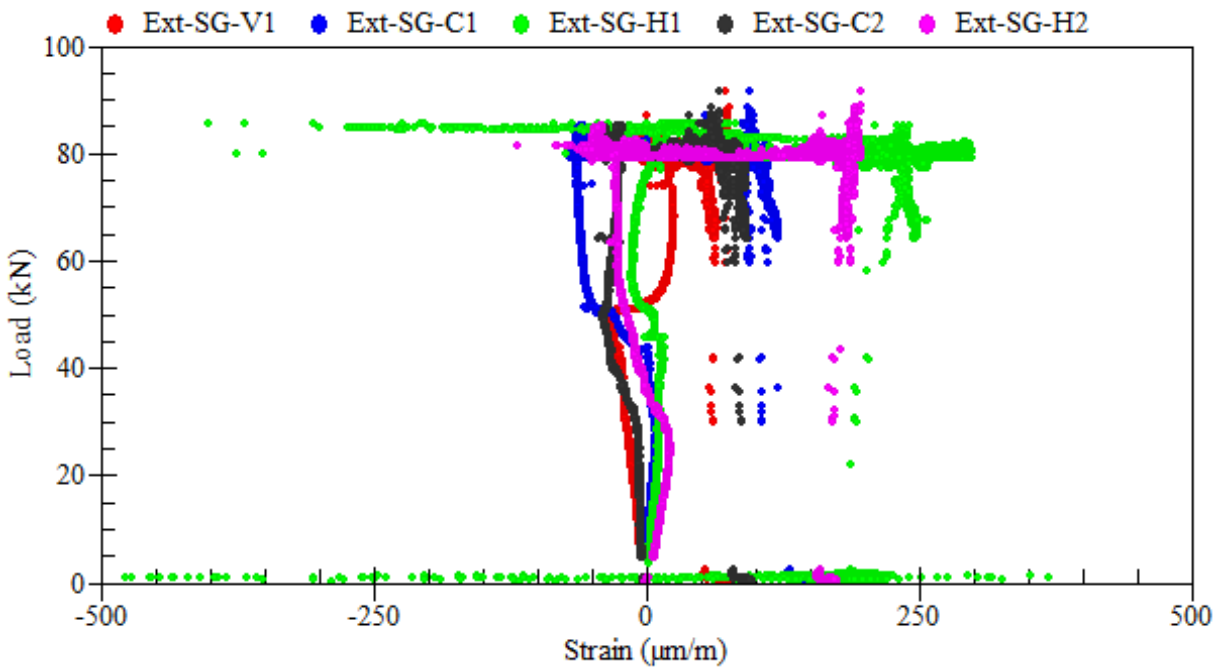

Figure B.63: Load-strain relationships of external rosettes on sides at 900 mm away from center – beam LS-2.2

B.5 Beam LS-2.3

Beam LS-2.3 was tested under the coupled effects of reinforcement corrosion and service loads. The applied sustained load was equivalent to 60% of the beam ultimate load capacity (i.e., 80 kN). Reinforcement corrosion was accelerated using a current density of 300 $\mu A/cm^2$ over a duration of 61 days. Then, the beam was loaded up until failure. The average mass loss of the beam was 15.5%. A summary of the gravimetric mass loss measurements of steel reinforcement is presented in Table B.3.

(a) at the end of the corrosion phase

(b) at failure

Figure B.64: Crack propagation and patterns at failure – beam LS-2.3

(a)

(b)

Figure B.65: Corrosion-induced damage in the cover of concrete – beam LS-2.3

Table B.3: Mass loss of corroded steel bars – beam LS-2.3

Rebar type	Rebar designation	Length (mm)	Mass (g)	Mass loss (%)
Control	R0	99	152.96	0.00
R1	R1	325	416.06	17.14
R2	R2	290	377.84	15.67
R3	R3	328	438.16	13.54

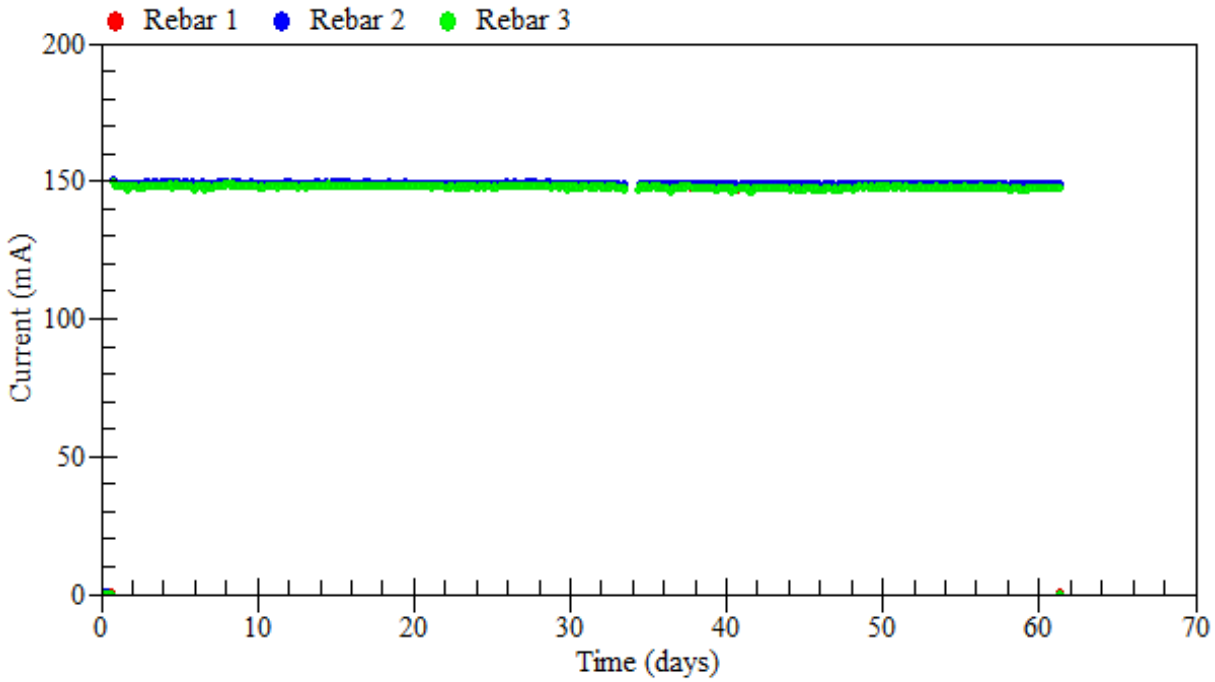

Figure B.66: Applied current – beam LS-2.3

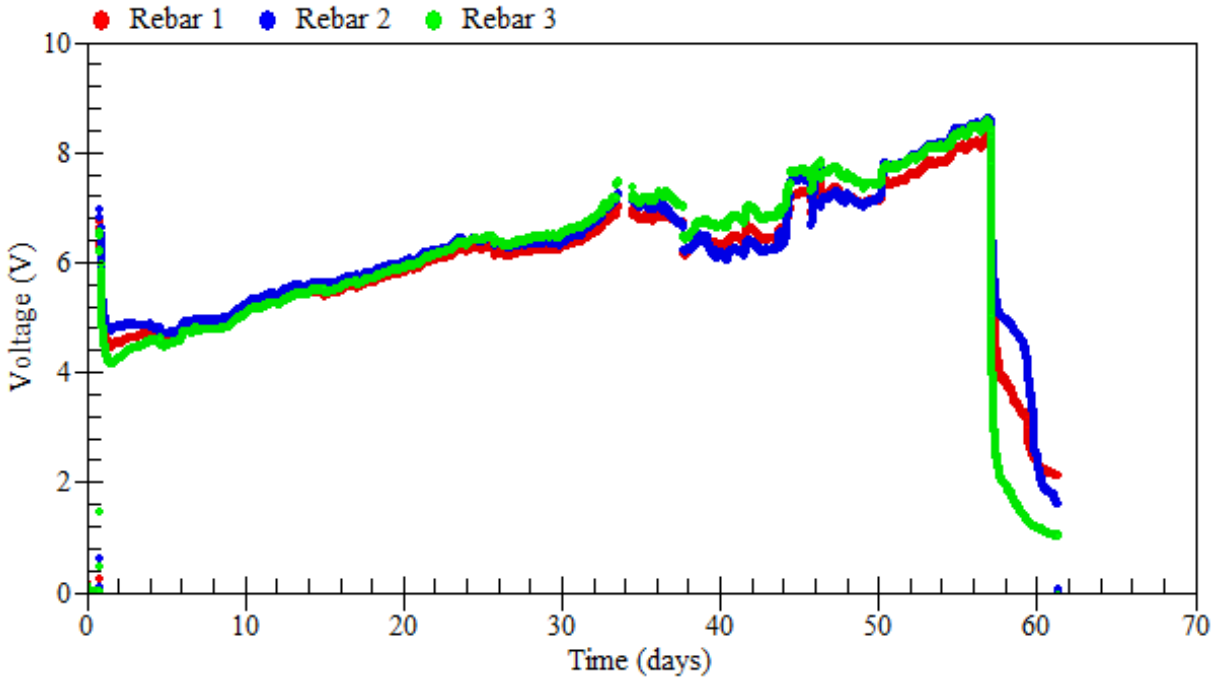

Figure B.67: Voltage measurements – beam LS-2.3

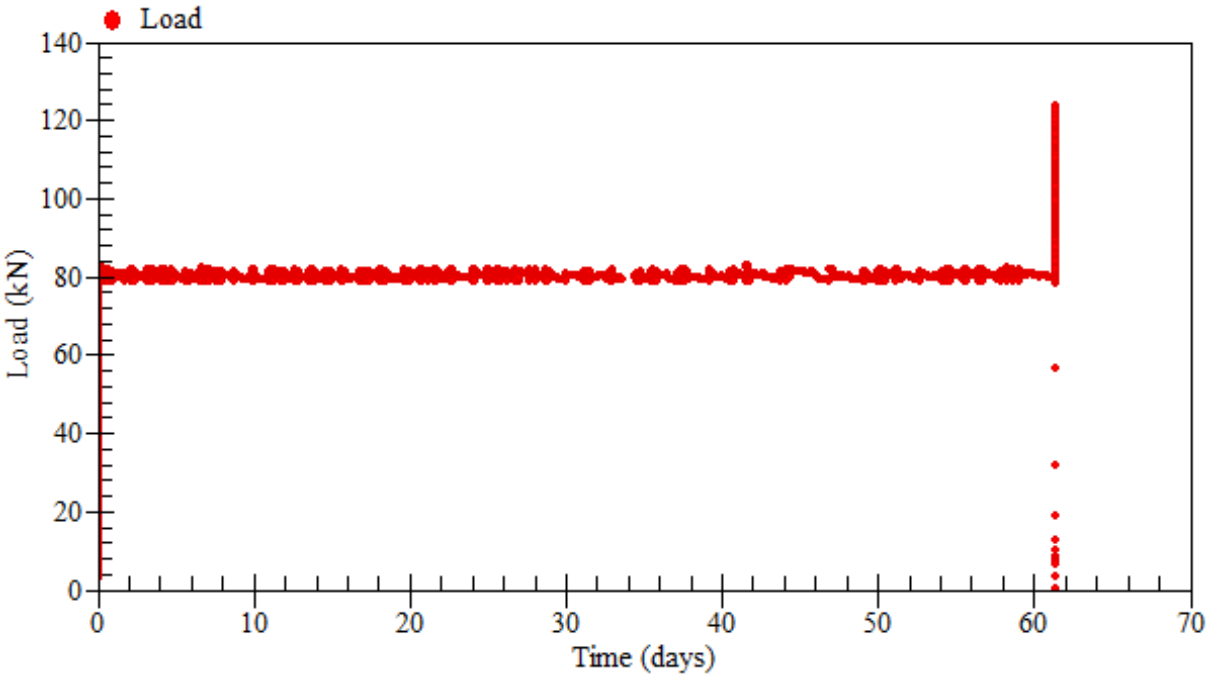

Figure B.68: Applied loads – beam LS-2.3

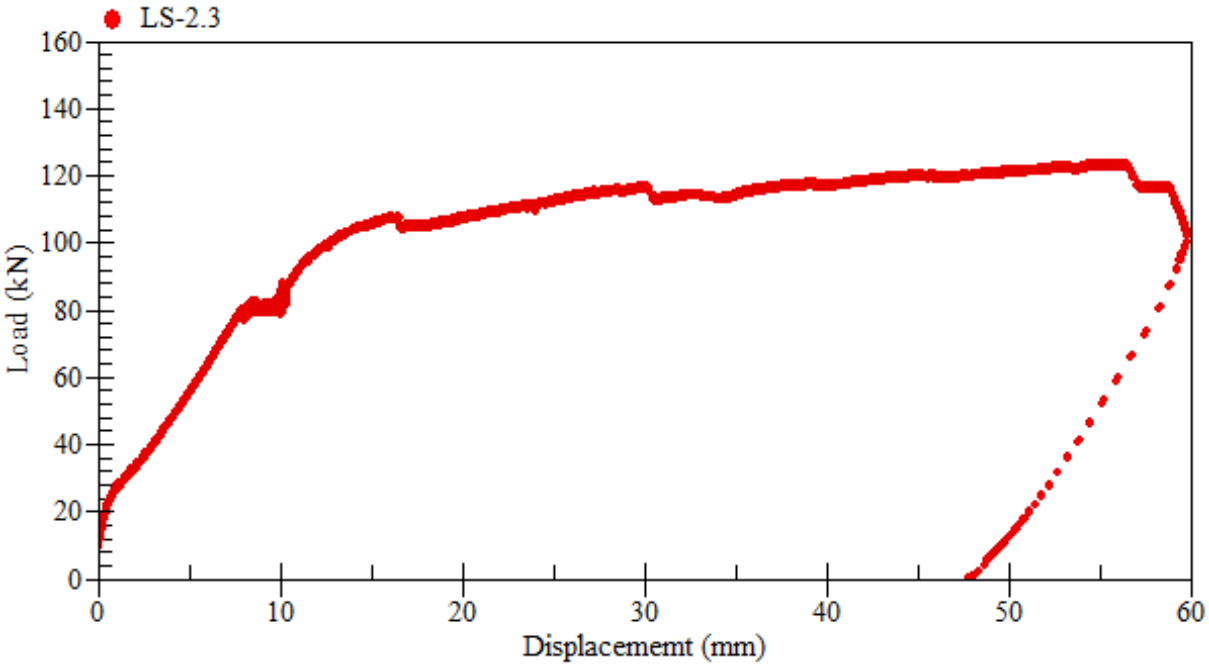

Figure B.69: Load-displacement relationship at mid-span – beam LS-2.3

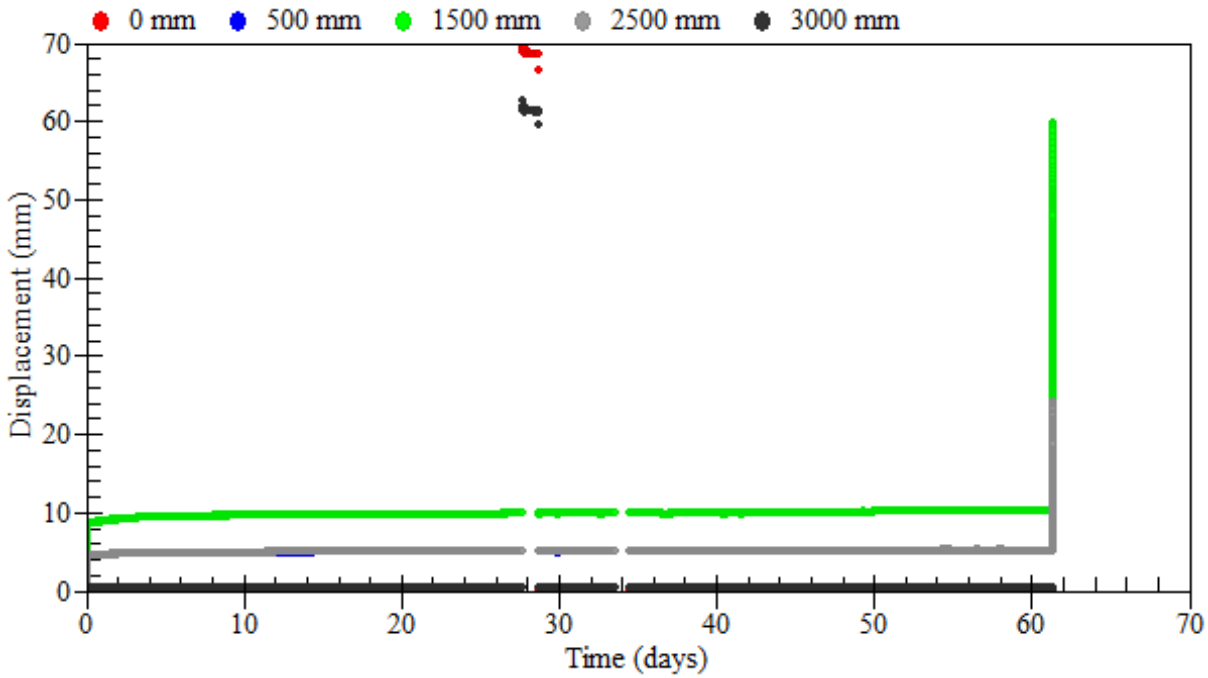

Figure B.70: Displacement measurements – beam LS-2.3

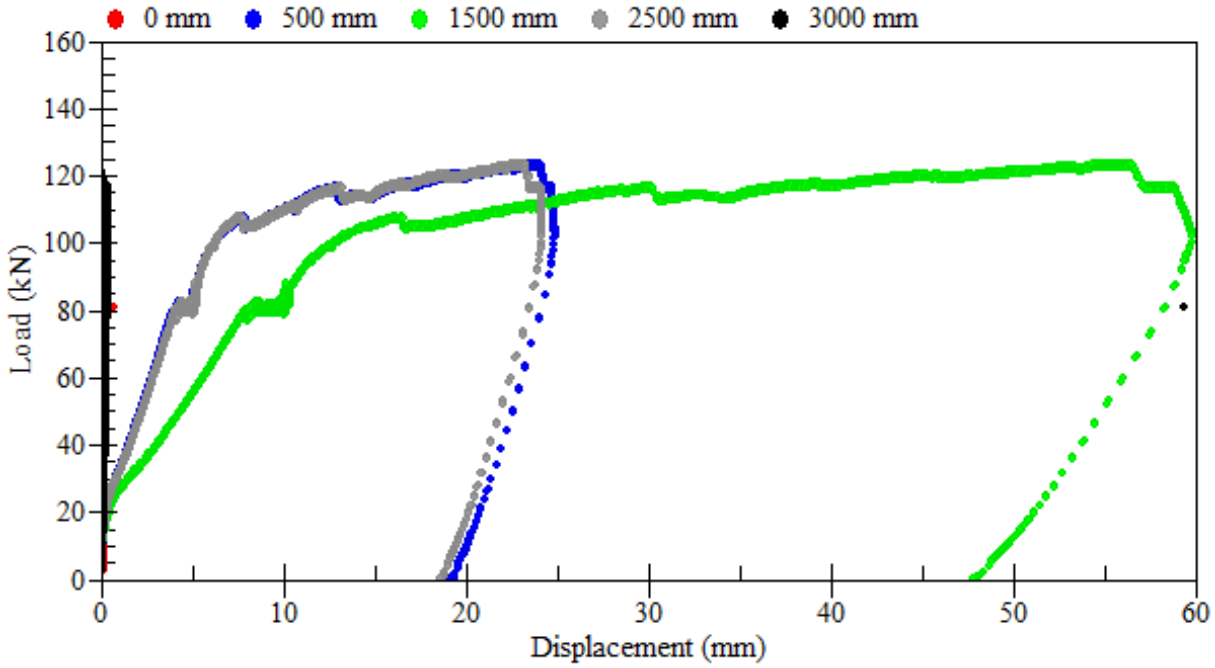

Figure B.71: Load-displacement relationships – beam LS-2.3

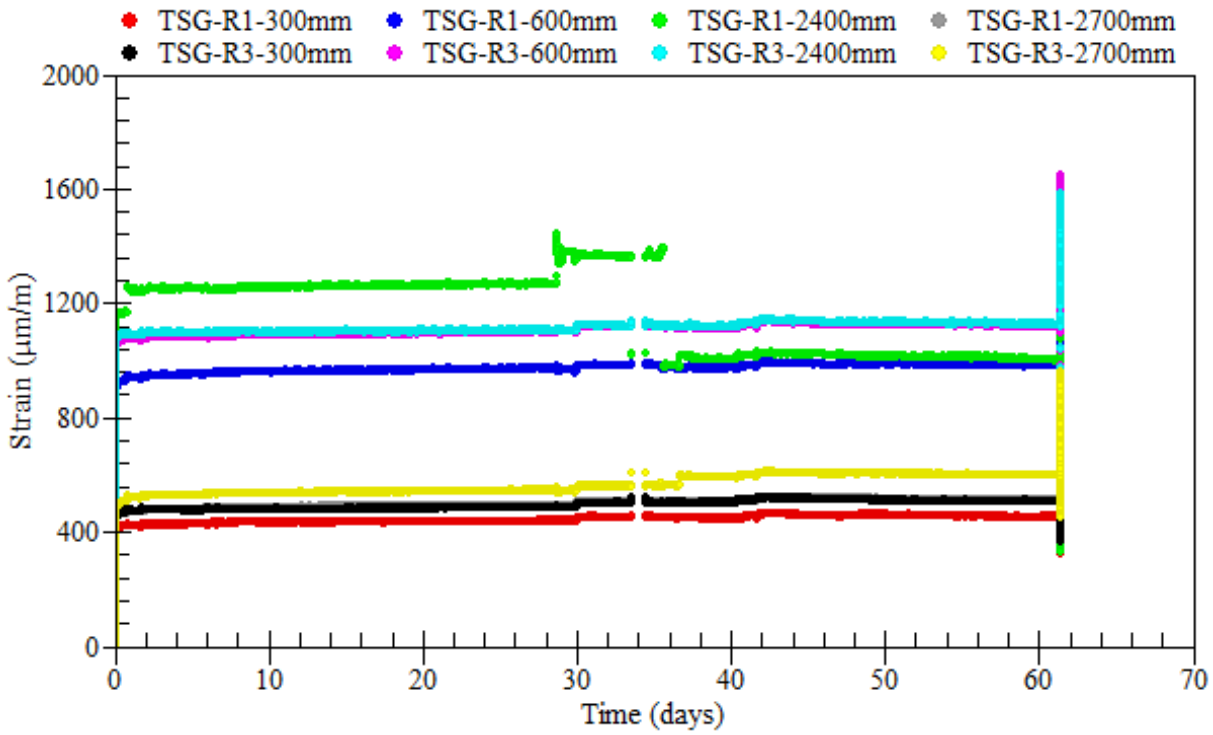

Figure B.72: Strain readings of longitudinal tensile steel bars – beam LS-2.3

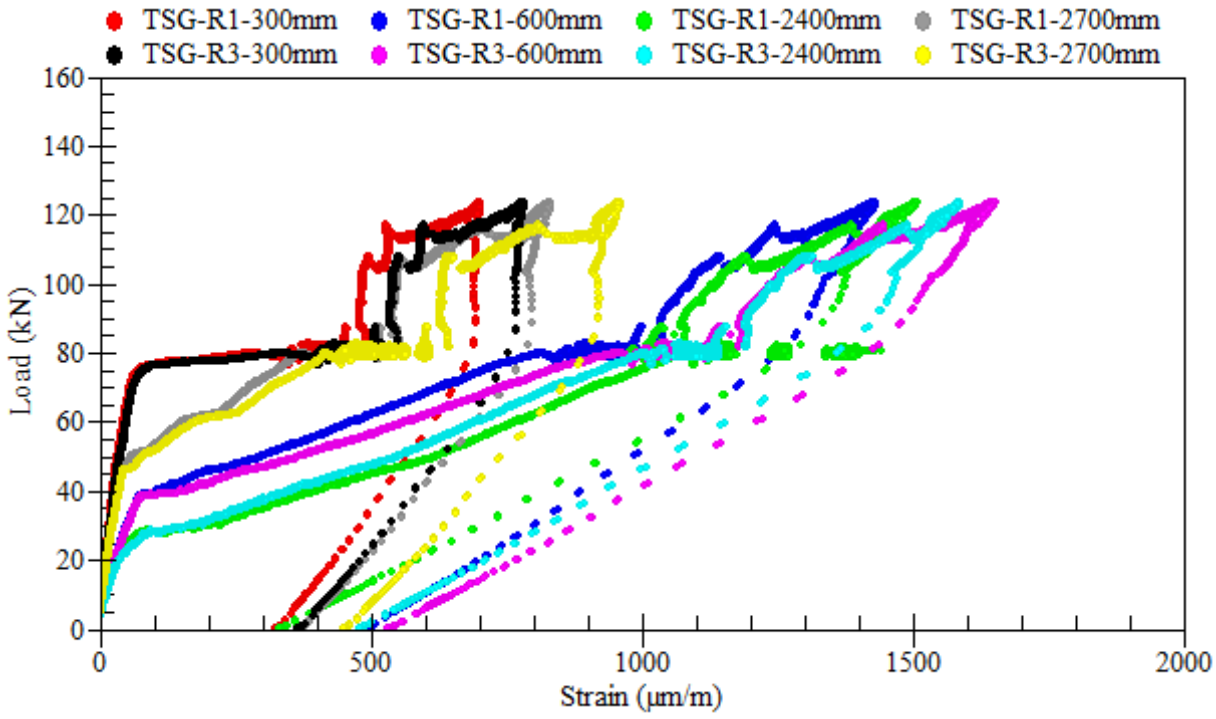

Figure B.73: Load-strain relationships of longitudinal tensile steel bars – beam LS-2.3

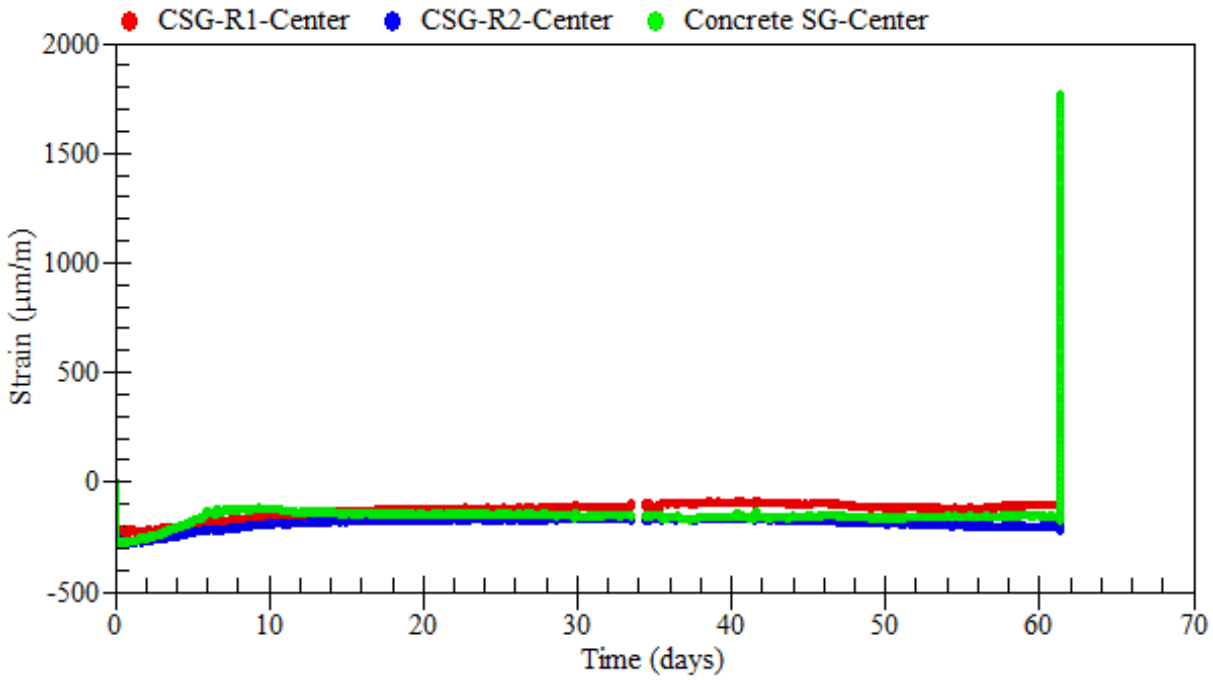

Figure B.74: Strain readings of longitudinal compressive steel bars – beam LS-2.3

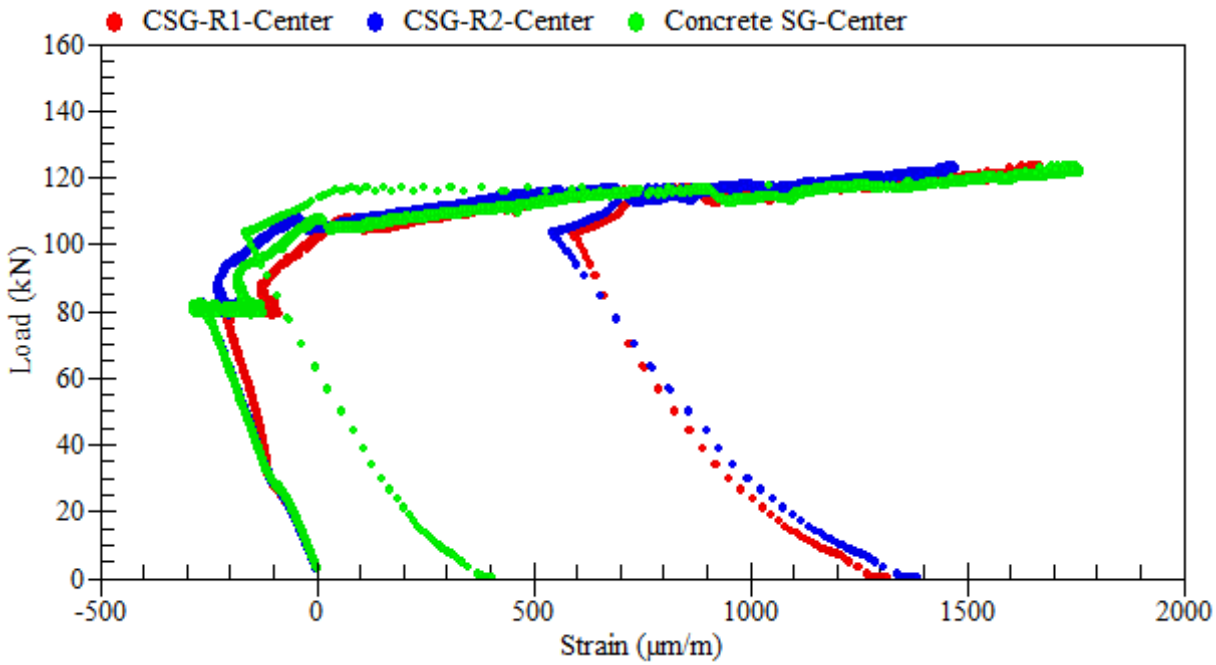

Figure B.75: Load-strain relationships of longitudinal compressive steel bars – beam LS-2.3

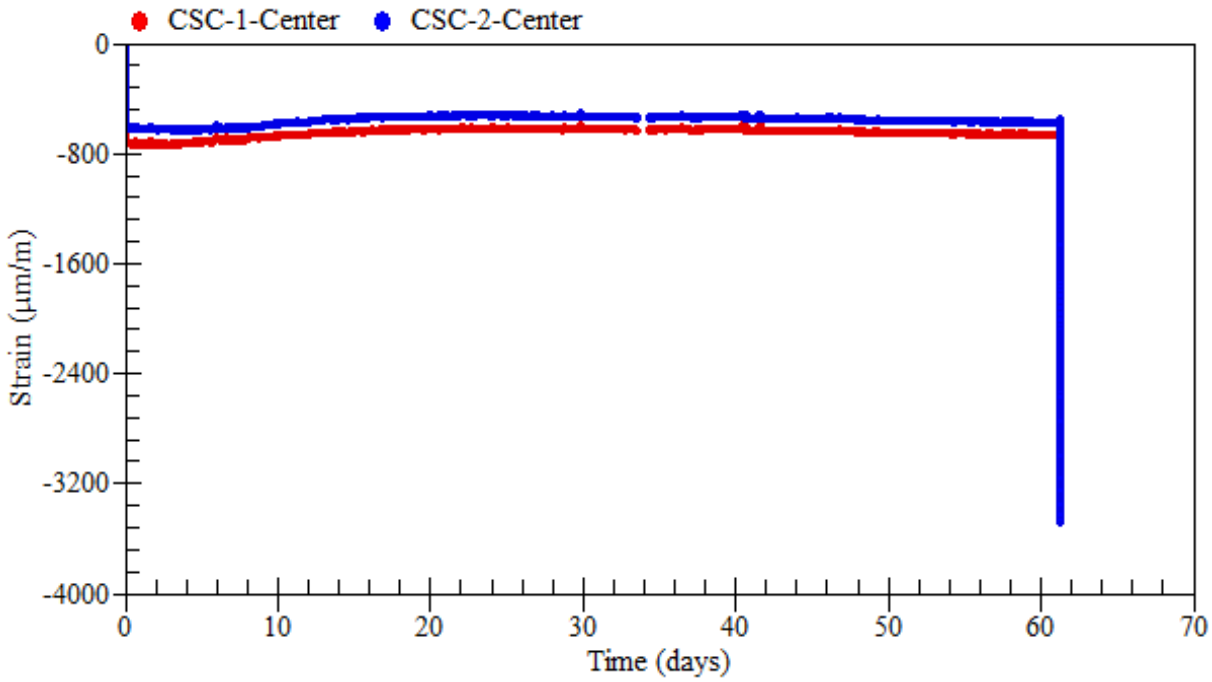

Figure B.76: Strain readings of external rosettes on top – beam LS-2.3

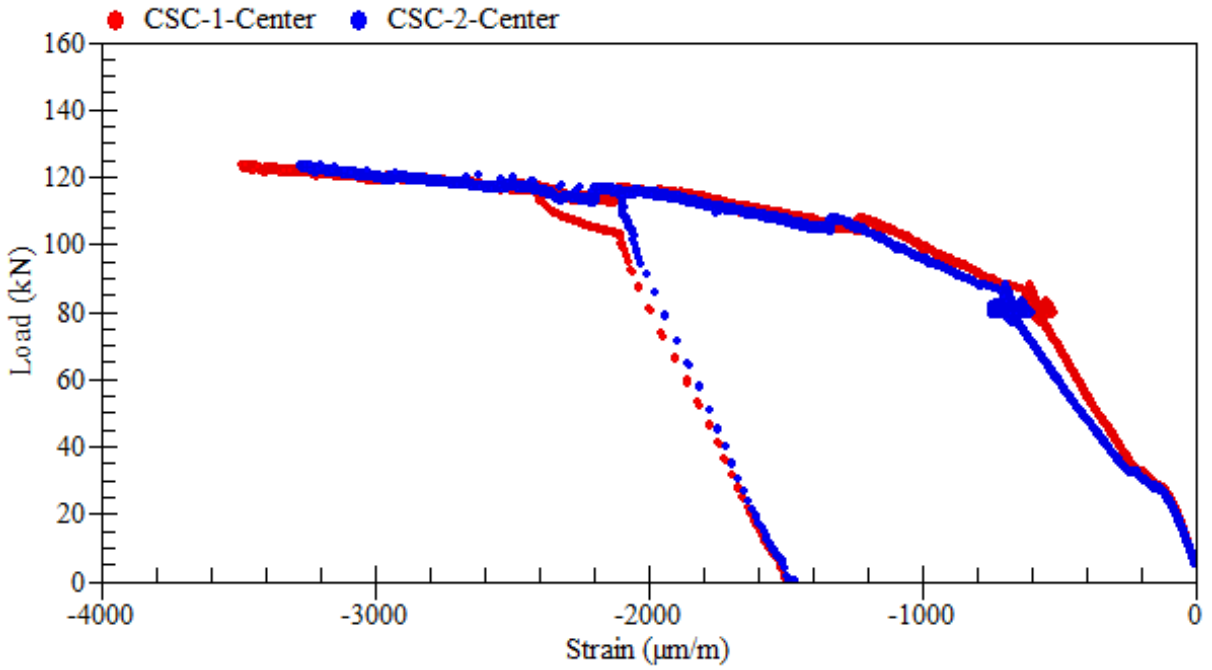

Figure B.77: Load-strain relationships of external rosettes on top – beam LS-2.3

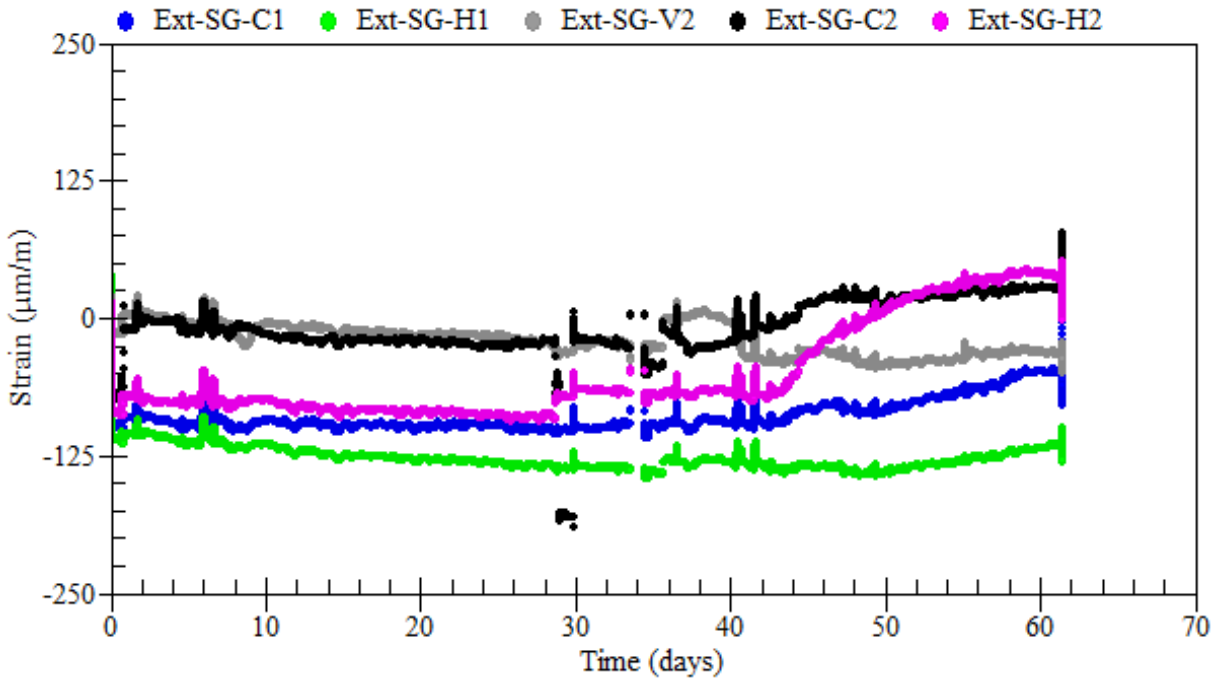

Figure B.78: Strain readings of external rosettes on sides at 600 mm away from center – beam LS-2.3

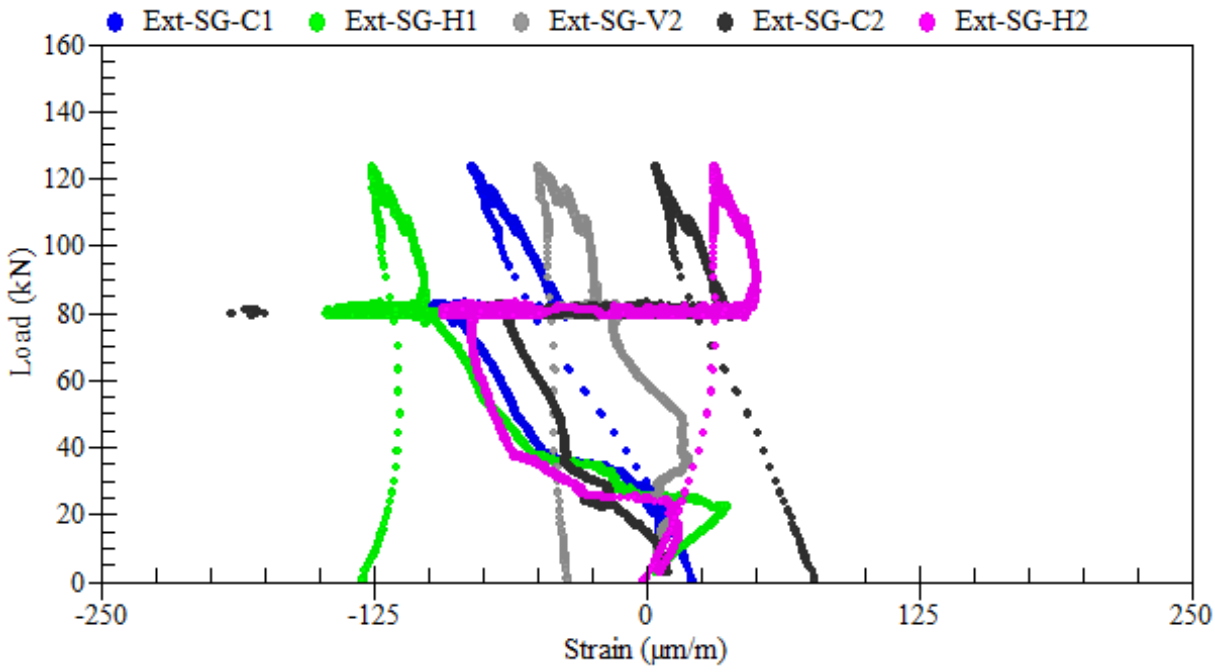

Figure B.79: Load-strain relationships of external rosettes on sides at 600 mm away from center – beam LS-2.3

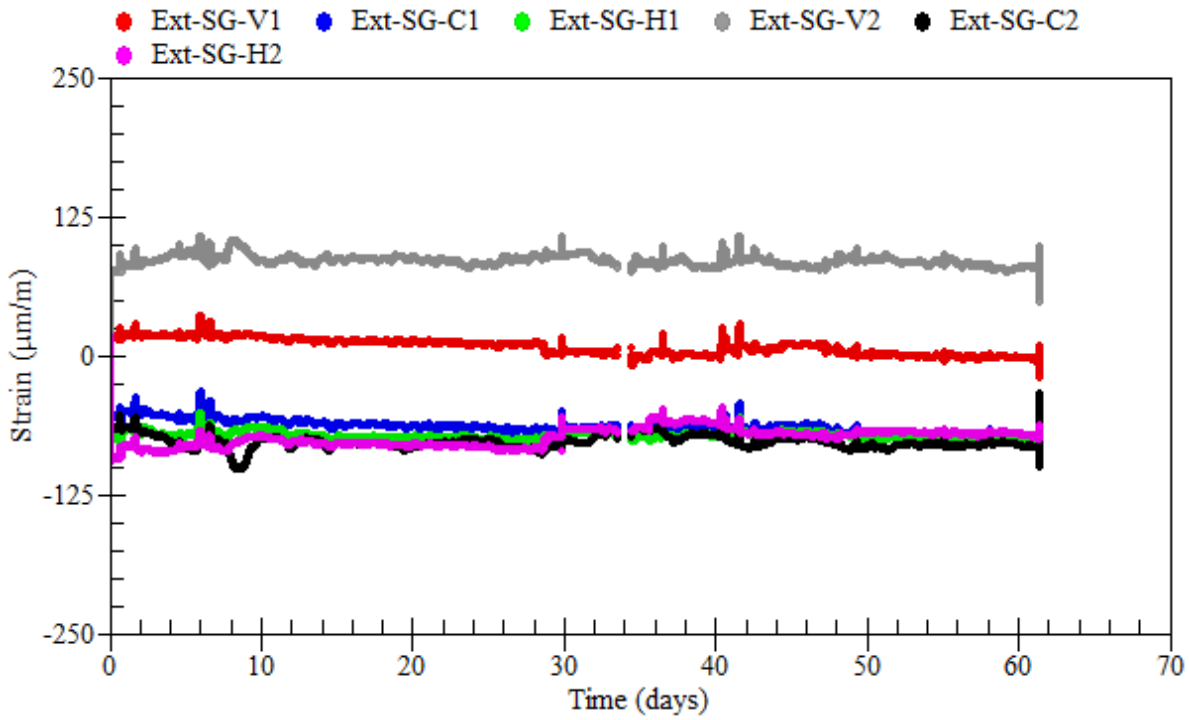

Figure B.80: Strain readings of external rosettes on sides at 750 mm away from center – beam LS-2.3

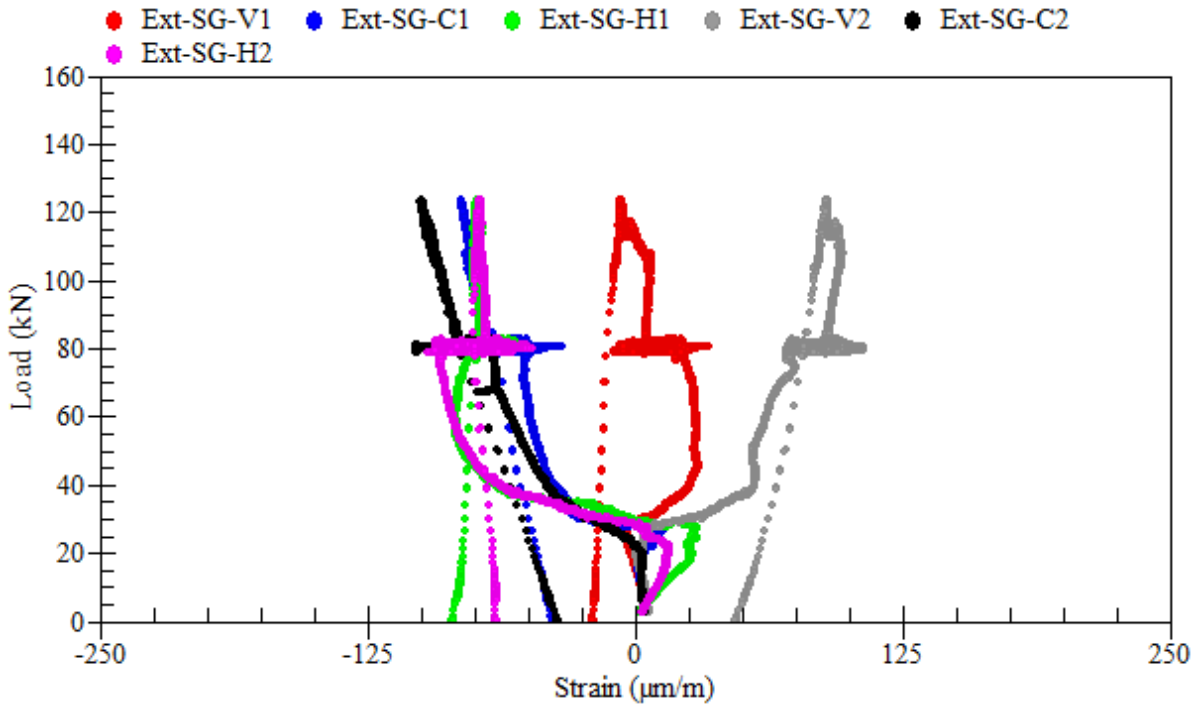

Figure B.81: Load-strain relationships of external rosettes on sides at 750 mm away from center – beam LS-2.3

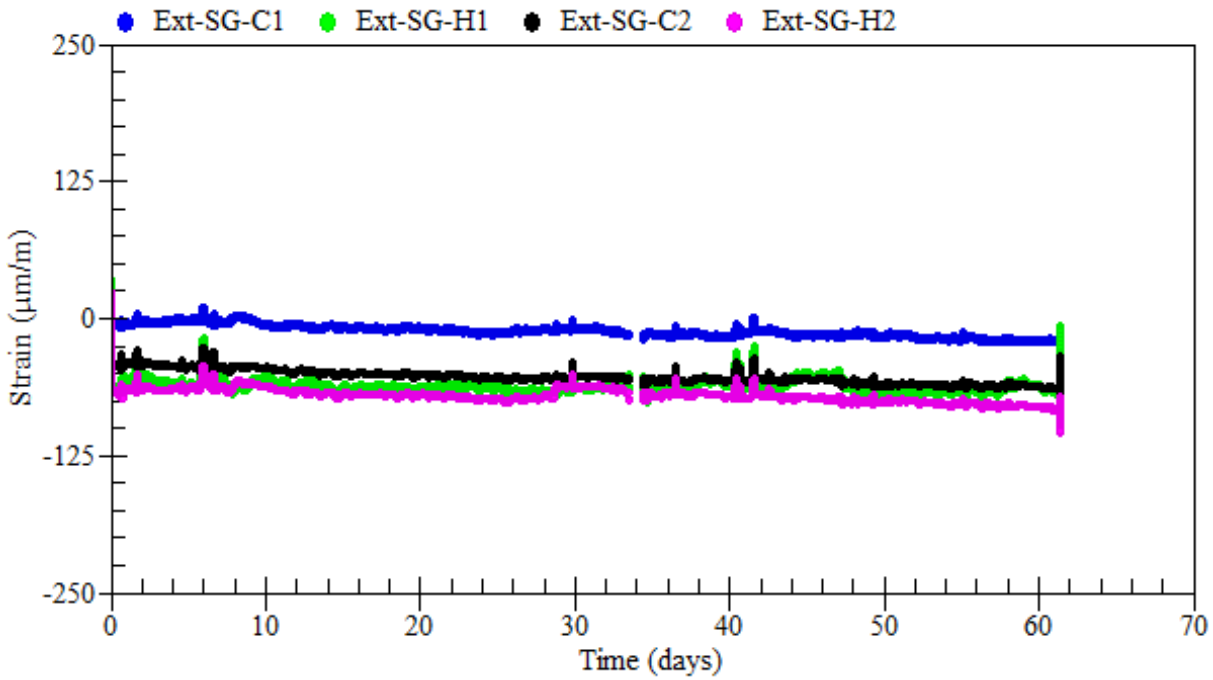

Figure B.82: Strain readings of external rosettes on sides at 900 mm away from center – beam LS-2.3

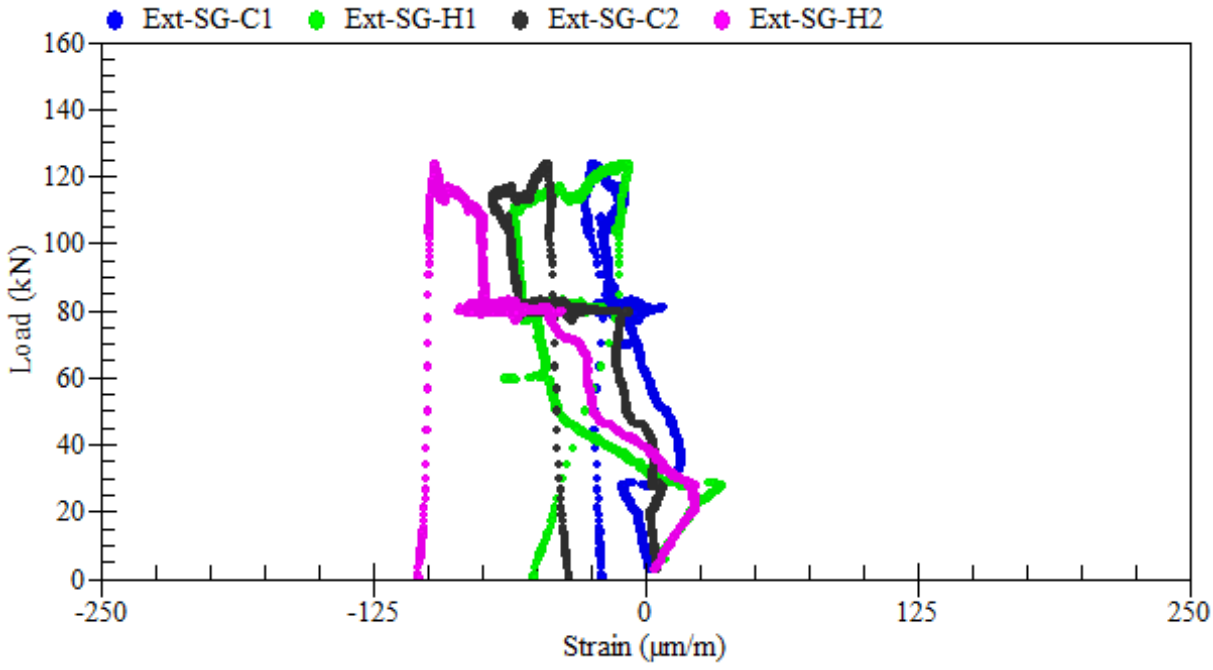

Figure B. 83: Load-strain relationships of external rosettes on sides at 900 mm away from center – beam LS-2.3

B.6 Beam LS-2.4

Beam LS-2.4 was corroded under its' self-weight only. Reinforcement corrosion was accelerated using a current density of 300 $\mu A/cm^2$ over a duration of 103 days. Then, the beam was loaded up until failure. The average mass loss of the beam was 20.2%. A summary of the gravimetric mass loss measurements of steel reinforcement is presented in Table B.4.

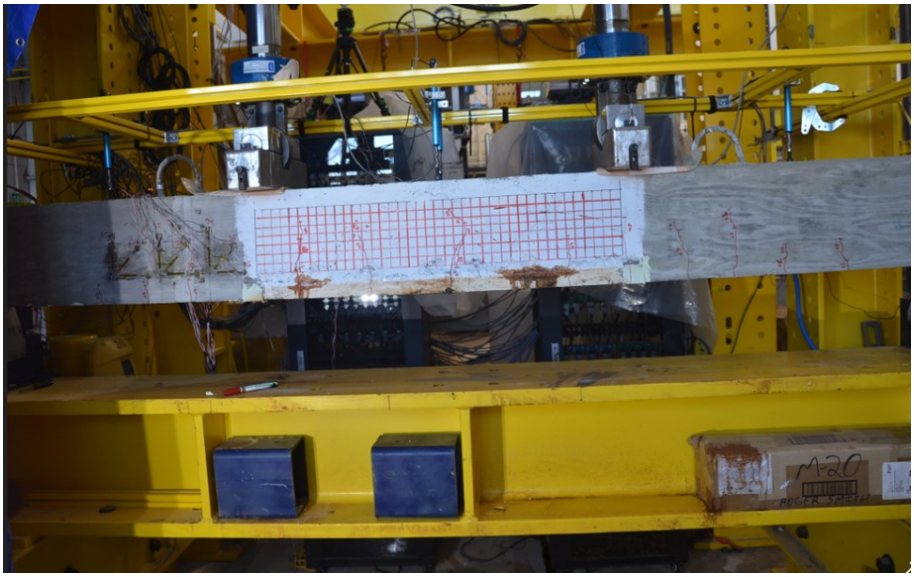

(a) at the end of the corrosion phase

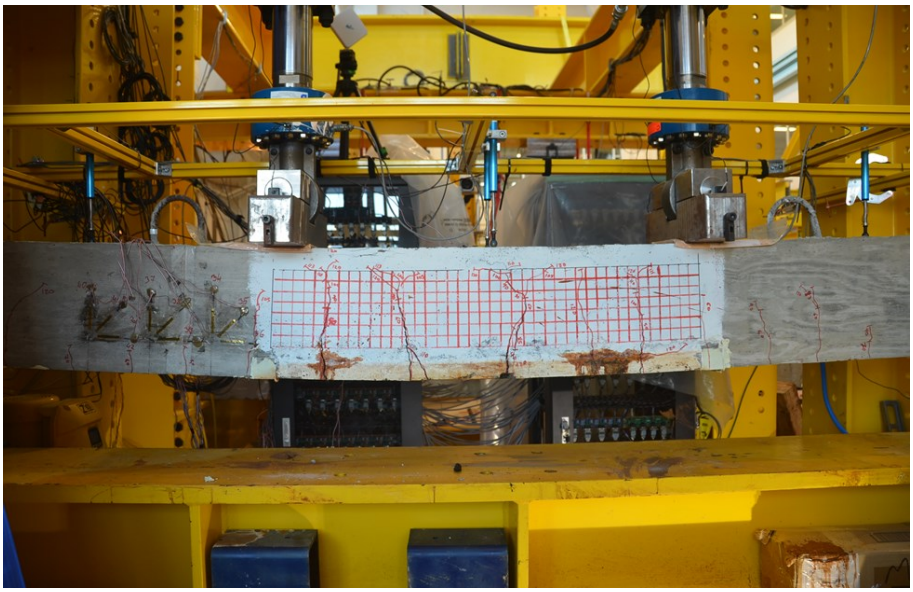

(b) at failure

Figure B.84: Crack propagation and patterns at failure – beam LS-2.4

(a)

(b)

Figure B.85: Corrosion-induced damage in the cover of concrete – beam LS-2.4

Table B.4: Mass loss of corroded steel bars – beam LS-2.4

Rebar type	Rebar designation	Length (mm)	Mass (g)	Mass loss (%)	Rebar mass loss (%)
Control	R0	99	152.96	0.00	0.00
R1	R1-R	392	479.44	20.84	22.12
	R1-L	398	471.11	23.39	
R2	R2-R	398	500.27	18.65	19.25
	R2-L	405	501.56	19.85	
R3	R3-R	396	510.73	16.53	19.25
	R3-L	400	482.43	21.94	

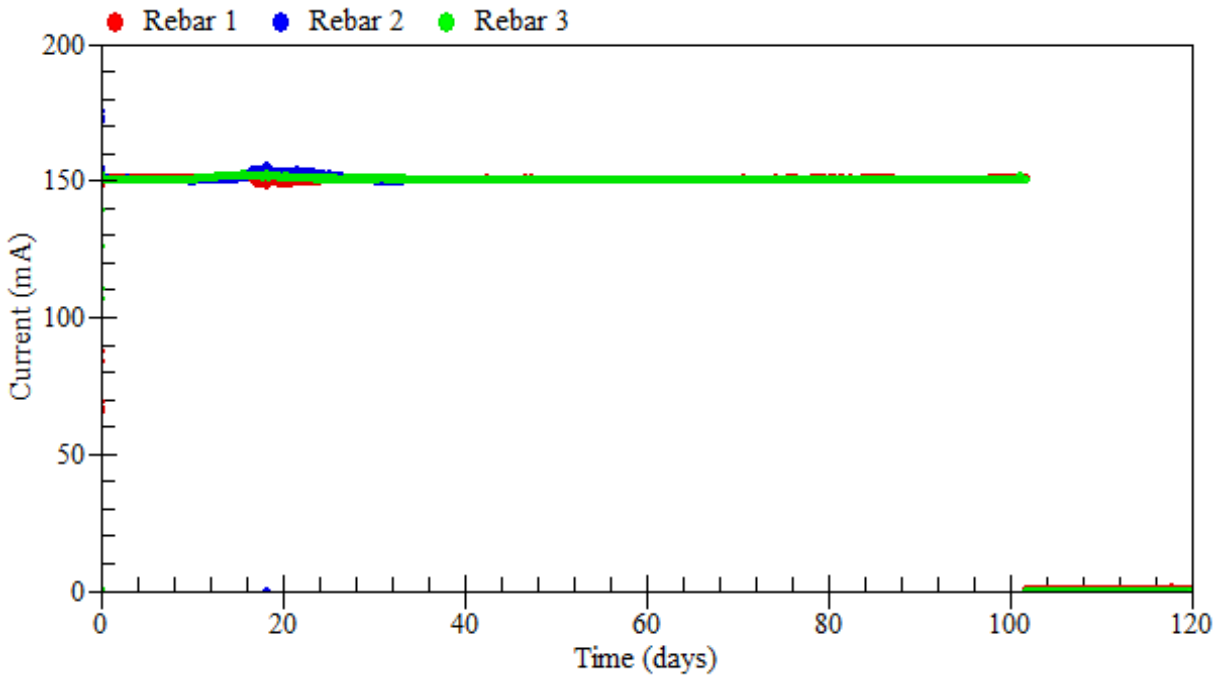

Figure B.86: Applied current – beam LS-2.4

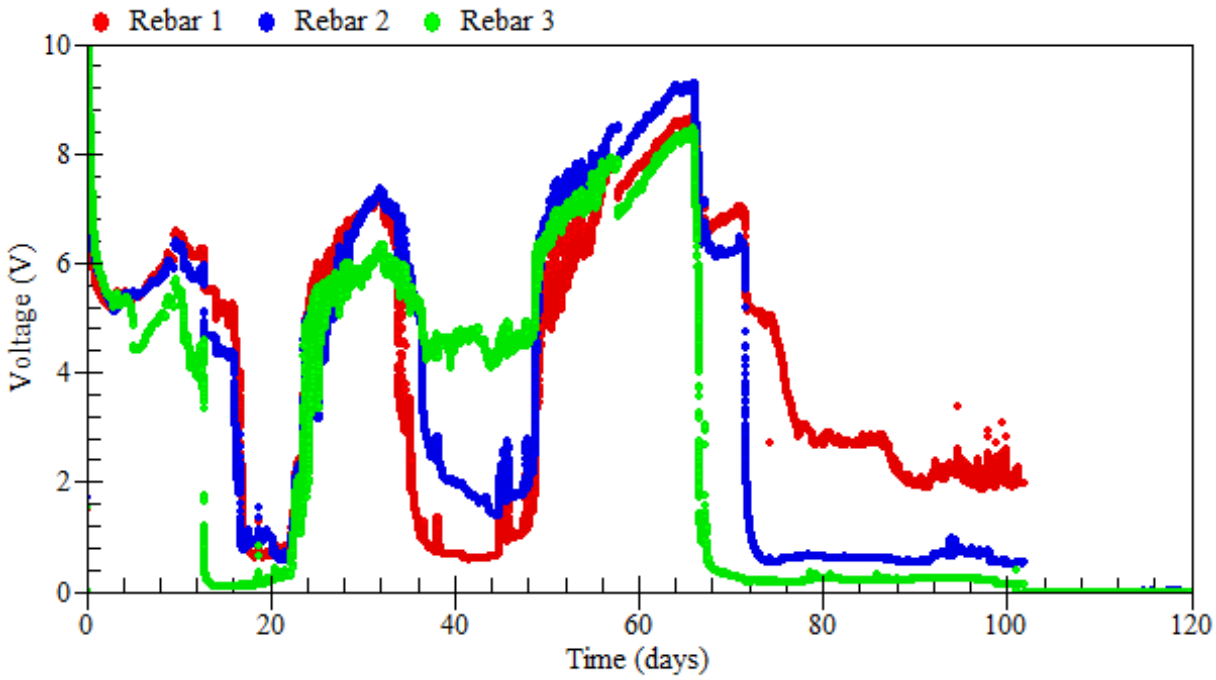

Figure B.87: Voltage measurements – beam LS-2.4

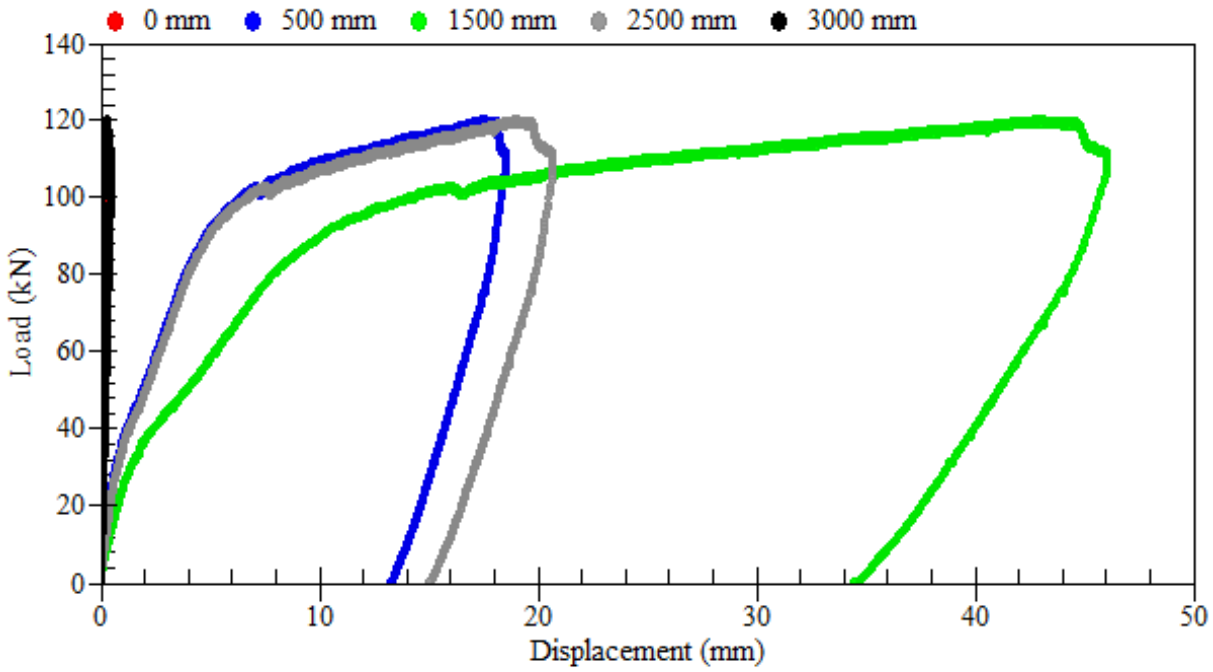

Figure B.88: Load-displacement relationships – beam LS-2.4

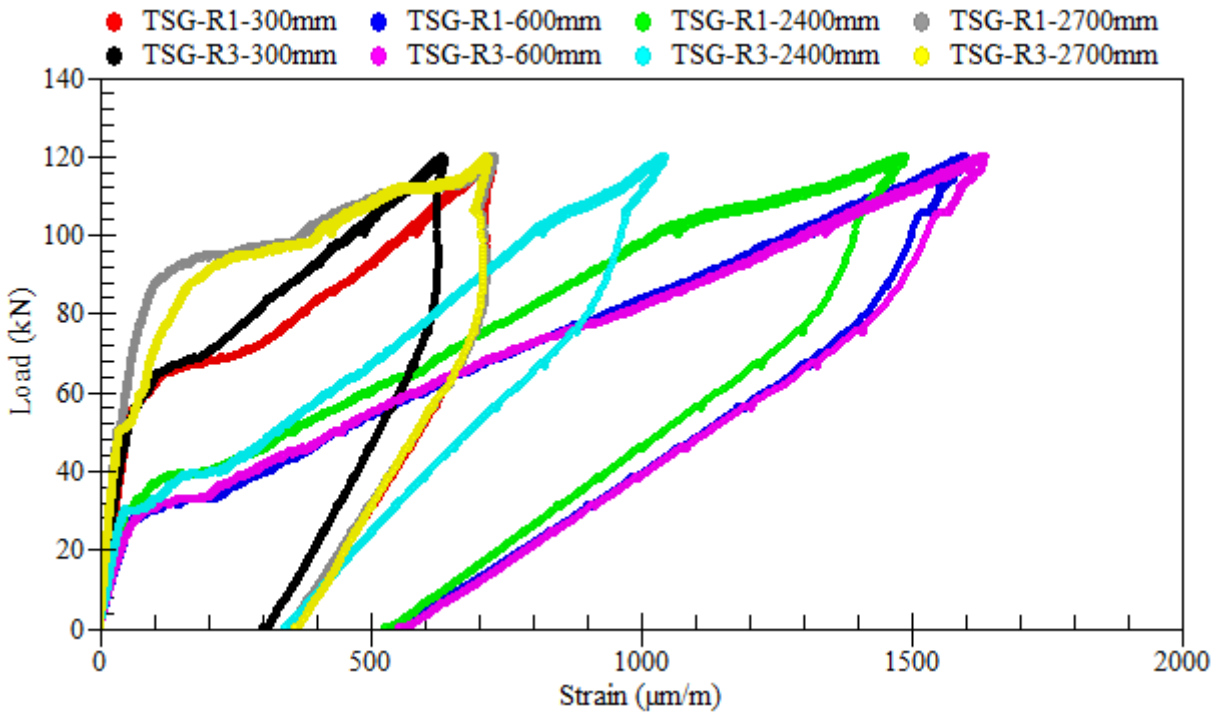

Figure B.89: Load-strain relationships of longitudinal tensile steel bars – beam LS-2.4

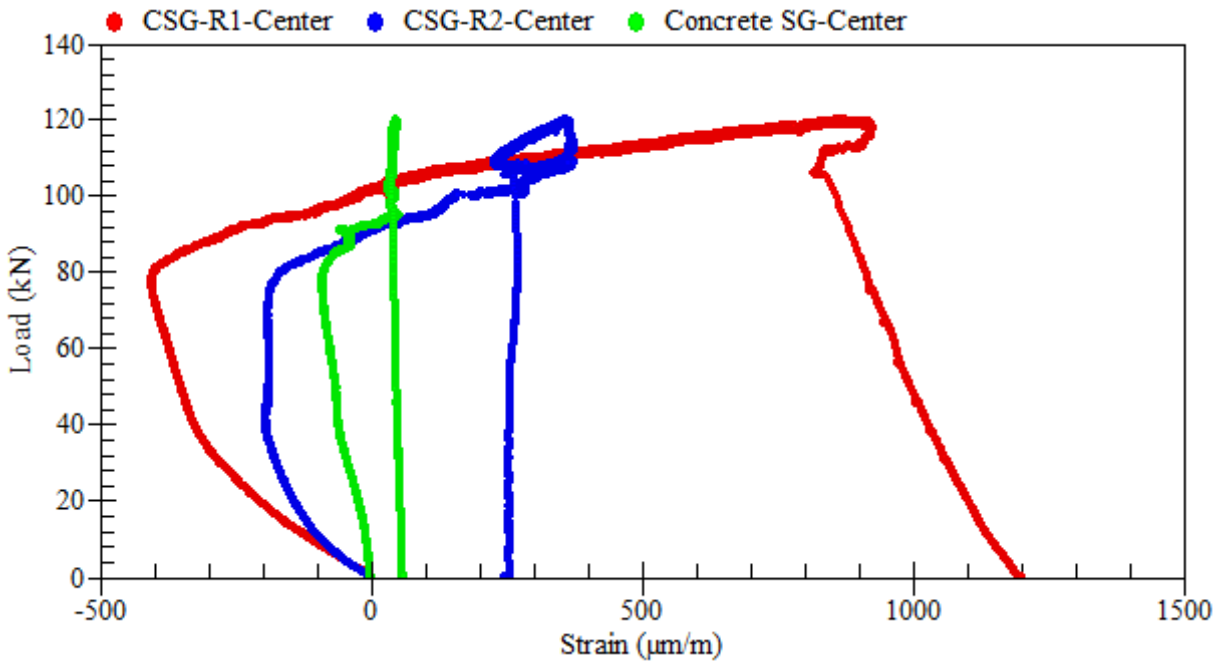

Figure B.90: Load-strain relationships of longitudinal compressive steel bars – beam LS-2.4

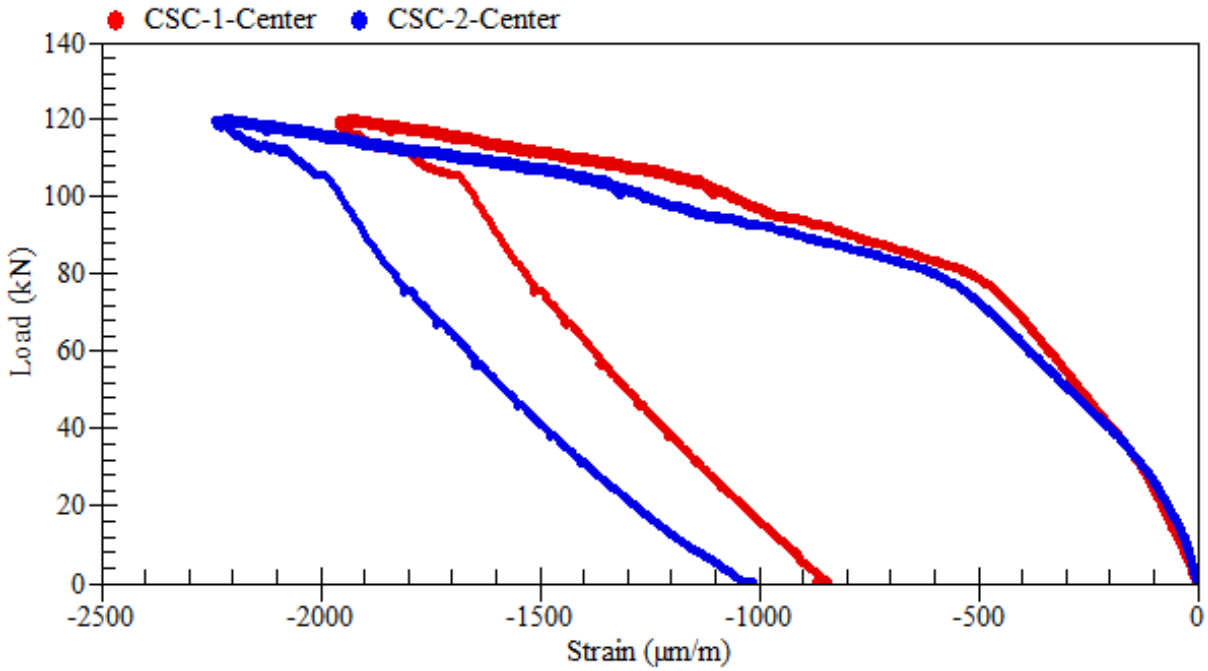

Figure B.91: Strain readings of external rosettes on top – beam LS-2.4

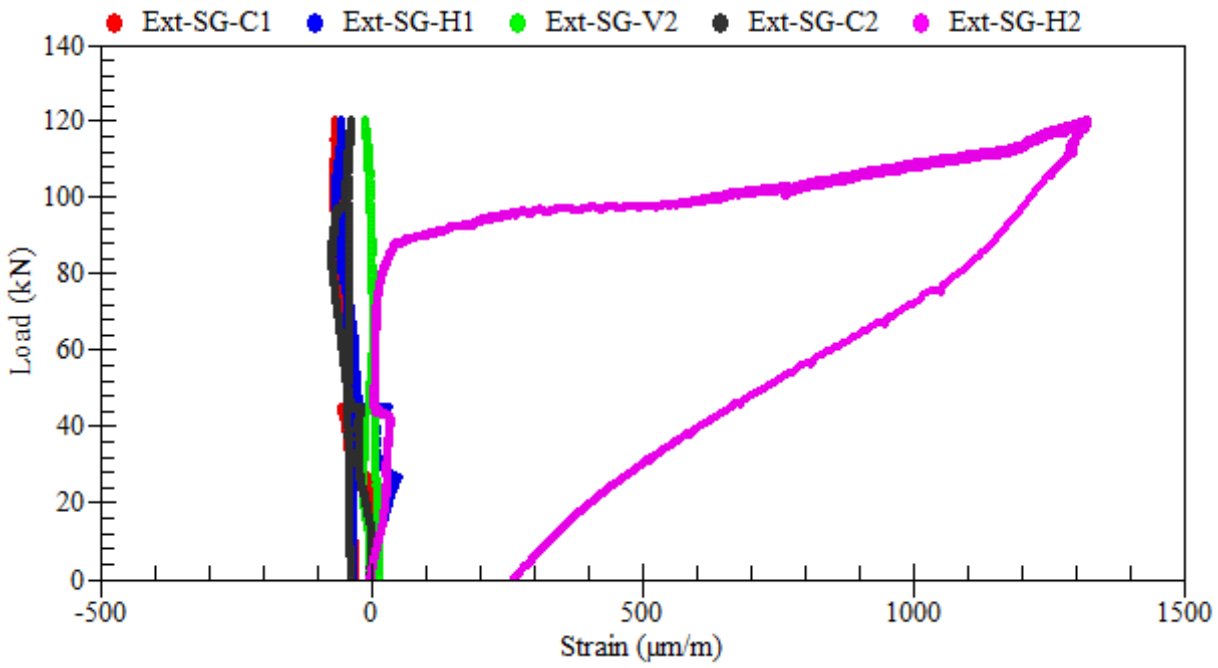

Figure B.92: Load-strain relationships of external rosettes on sides at 600 mm away from center – beam LS-2.4

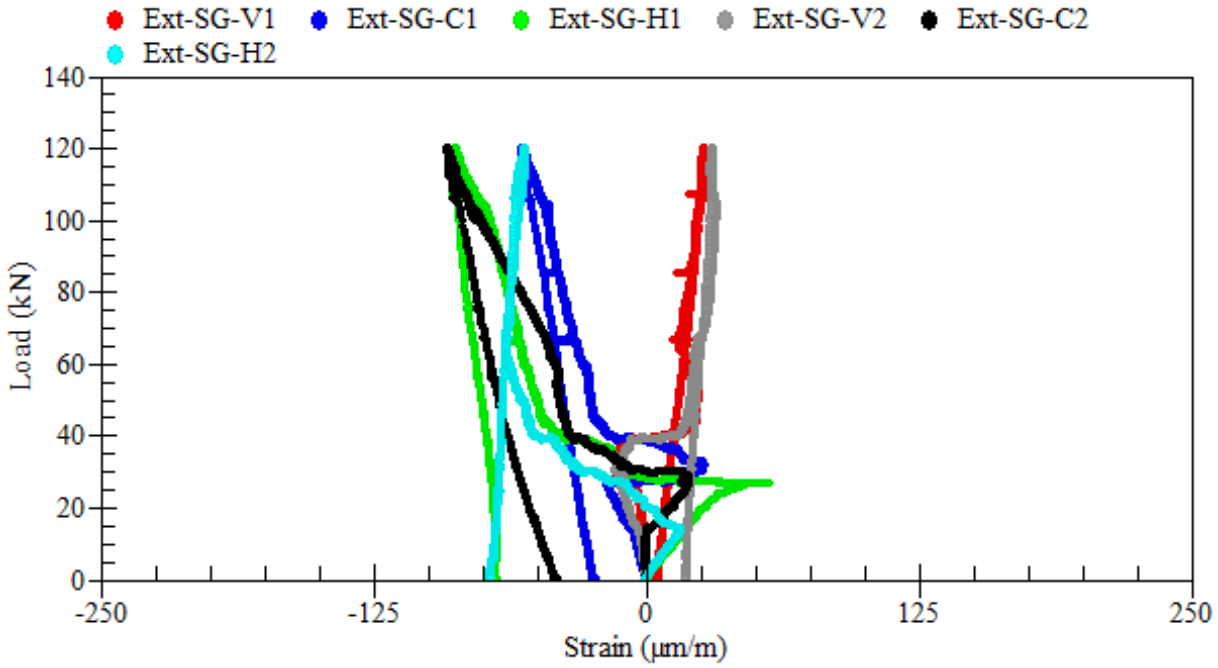

Figure B.93: Load-strain relationships of external rosettes on sides at 750 mm away from center – beam LS-2.4

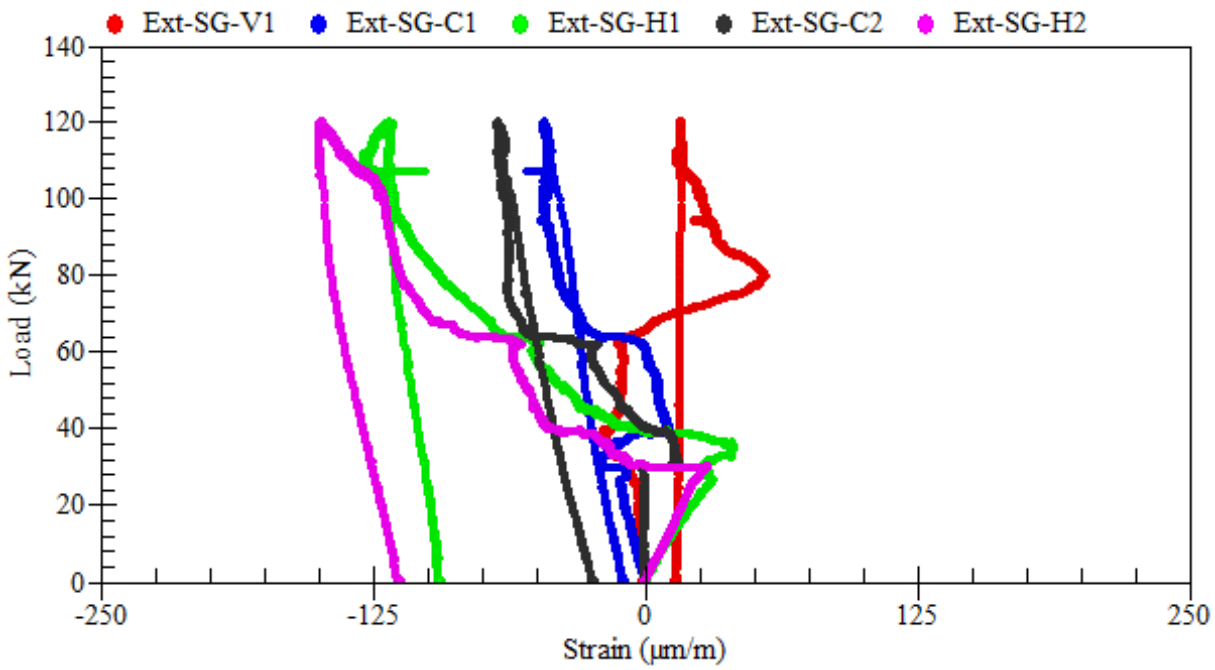

Figure B.94: Load-strain relationships of external rosettes on sides at 900 mm away from center – beam LS-2.4